

AD-A059 900

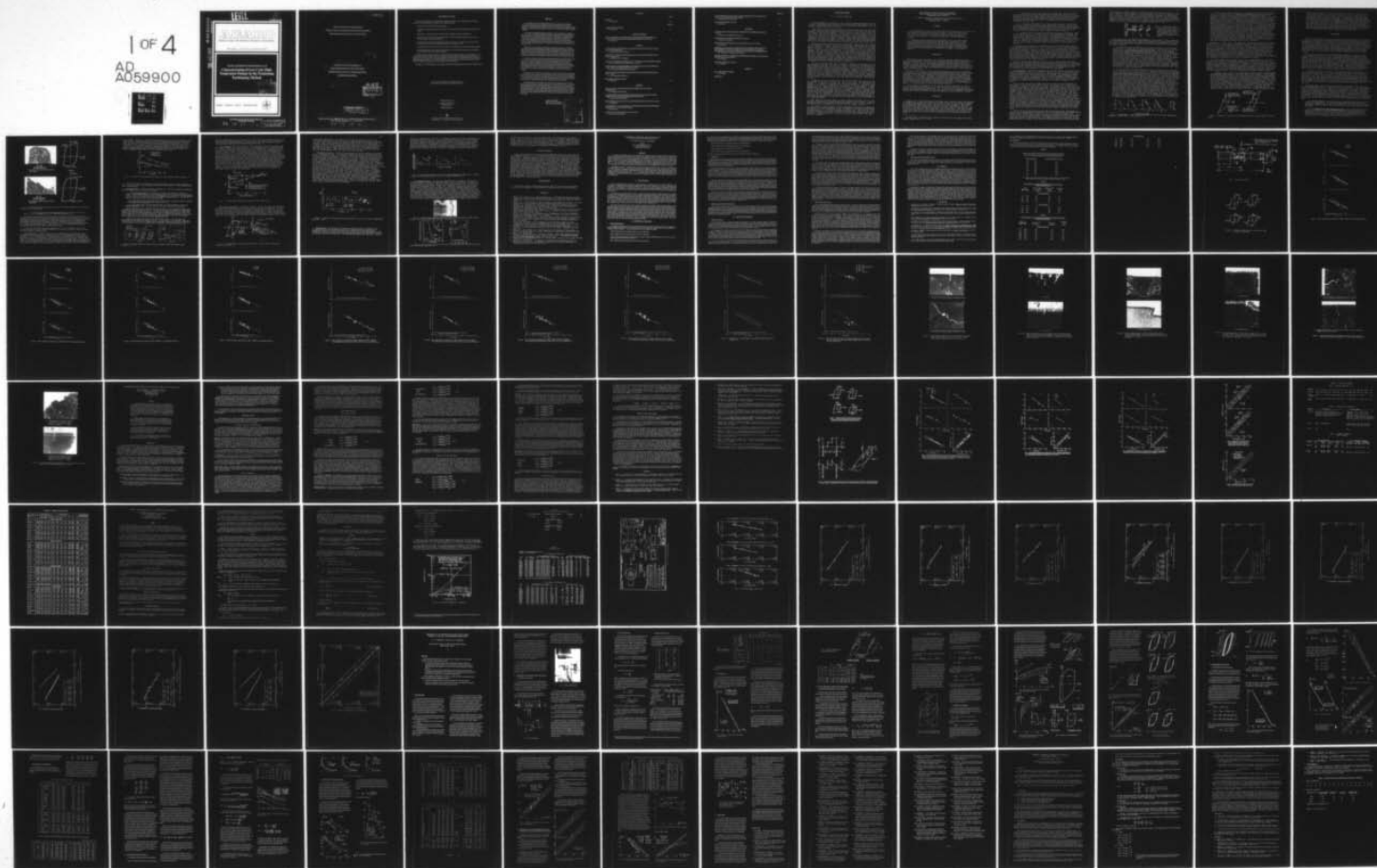
ADVISORY GROUP FOR AEROSPACE RESEARCH AND DEVELOPMENT--ETC F/G 11/6
CHARACTERIZATION OF LOW CYCLE HIGH TEMPERATURE FATIGUE BY THE S--ETC(U)
AUG 78

UNCLASSIFIED

AGARD-CP-243

NL

1 of 4
AD
A059900



LEVEL

AGARD-CP-243

AD A059900

AGARD-CP-243

DDC FILE COPY

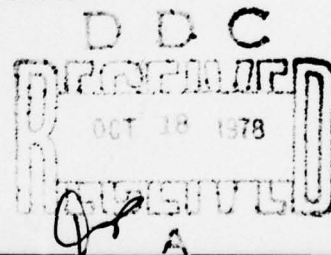
AGARD

ADVISORY GROUP FOR AEROSPACE RESEARCH & DEVELOPMENT

7 RUE ANCELLE 92200 NEUILLY SUR SEINE FRANCE

AGARD CONFERENCE PROCEEDINGS No. 243

Characterization of Low Cycle High Temperature Fatigue by the Strainrange Partitioning Method



NORTH ATLANTIC TREATY ORGANIZATION



DISTRIBUTION AND AVAILABILITY
ON BACK COVER

78 10 17 081

DISTRIBUTION STATEMENT A

Approved for public release
Distribution Unlimited

NORTH ATLANTIC TREATY ORGANIZATION
ADVISORY GROUP FOR AEROSPACE RESEARCH AND DEVELOPMENT
(ORGANISATION DU TRAITE DE L'ATLANTIQUE NORD)

AGARD Conference Proceedings No.243

CHARACTERIZATION OF LOW CYCLE HIGH
TEMPERATURE FATIGUE BY THE STRAINRANGE
PARTITIONING METHOD

DDC
RECEIVED
OCT 18 1978
A

DISTRIBUTION STATEMENT A

Approved for public release
Distribution Unlimited

Papers presented at the 46th Meeting of the AGARD Structures and Materials Panel
held in Aalborg, Denmark on 11-12 April 1978.

78 10 17 081 400 043
mt

THE MISSION OF AGARD

The mission of AGARD is to bring together the leading personalities of the NATO nations in the fields of science and technology relating to aerospace for the following purposes:

- Exchanging of scientific and technical information;
- Continuously stimulating advances in the aerospace sciences relevant to strengthening the common defence posture;
- Improving the co-operation among member nations in aerospace research and development;
- Providing scientific and technical advice and assistance to the North Atlantic Military Committee in the field of aerospace research and development;
- Rendering scientific and technical assistance, as requested, to other NATO bodies and to member nations in connection with research and development problems in the aerospace field;
- Providing assistance to member nations for the purpose of increasing their scientific and technical potential;
- Recommending effective ways for the member nations to use their research and development capabilities for the common benefit of the NATO community.

The highest authority within AGARD is the National Delegates Board consisting of officially appointed senior representatives from each member nation. The mission of AGARD is carried out through the Panels which are composed of experts appointed by the National Delegates, the Consultant and Exchange Program and the Aerospace Applications Studies Program. The results of AGARD work are reported to the member nations and the NATO Authorities through the AGARD series of publications of which this is one.

Participation in AGARD activities is by invitation only and is normally limited to citizens of the NATO nations.

The content of this publication has been reproduced directly from material supplied by AGARD or the authors.

Published August 1978

Copyright © AGARD 1978
All Rights Reserved

ISBN 92-835-0220-5



*Printed by Technical Editing and Reproduction Ltd
Harford House, 7-9 Charlotte St, London, W1P 1HD*

PREFACE

The AGARD Structures and Materials Panel has had a long and active interest in researching subjects that are of a critical nature and of common interest to the NATO community. In keeping with this tradition, the Panel, in the Spring of 1971 deemed it highly advisable to initiate some specific activities in the area of low cycle high temperature fatigue (LCHTF).

At the Fall 1972 S&M Panel Meeting, Mr Drapier, who was charged by AGARD with the coordination of the various activities on this subject, submitted a document entitled "Ad Hoc Group on Low Cycle High Temperature Fatigue - Status Report" (AGARD R-604), which reviewed the LCHTF work being carried out by the laboratories interested in this problem and belonging to the various NATO nations. In the fall of 1973, Mr Drapier presented to the S&M Panel his in-depth report entitled "Survey of Activities in the Field of Low Cycle High Temperature Fatigue". This document was published as AGARD R-618 in February 1974.

Through the continuing efforts of Mr Drapier, supported by this Panel, AGARD has published a volume containing the papers presented at the Specialists' Meeting on Low Cycle High Temperature Fatigue (AGARD-CP-155) held in Washington D.C. in April of 1974. At this meeting, experts were invited to provide replies to a number of questions raised by the organizers; each subject was introduced by a paper, the purpose of which was to survey the problem areas associated with that subject and to orient and focus the subsequent discussion.

One of the conclusions of the above noted Specialists Meeting was the recognition of the need for more reliable life prediction methods that are applicable to LCHTF gas turbine components. It was in the spring of 1975 that Mr Hirschberg presented a pilot paper suggesting a cooperative testing program aimed at evaluating the ability of the Strainrange Partitioning Method to predict life in the creep-fatigue range. Messrs Hirschberg and Drapier were designated coordinators for this evaluation program. The laboratories surveyed in AGARD R-618 were then contacted by the coordinators and invited to participate in the program.

During the period in which this test program was being conducted, several mini-symposia were organized by the coordinators for the participants. There were three such meetings held on the continent for the European participants and three held in the US for their participants. It was felt that these meetings were very effective in getting the program organized, resolving many questions, exchanging information, and keeping the activity on schedule.

The Panel is pleased to acknowledge and express its sincere appreciation to the many groups and individuals who contributed so much to the success of this meeting: to the Danish National Delegates who hosted this Specialists' Meeting; to Messrs Drapier and Hirschberg who planned the content of this cooperative program, coordinated the activity, and organized the Specialists' Meeting; to Mr John M.N. Willis, the Executive of the S&M Panel; to the staff who so ably provided support throughout the meeting; and especially to the authors, session chairmen, recorders, and participants whose combined efforts contributed to the success of this meeting.

George C. DEUTSCH
Chairman, Sub-Committee on
High Temperature Materials

APPROVED BY	
DATE	DATE REVIEWED
BY	BY
UNANNOUNCED	
JUSTIFICATION	
BY	
DISTRIBUTION/AVAILABILITY CODES	
DIR.	AVAIL. FOR SPECIAL
A	

CONTENTS

	Page
PREFACE by G.C.Deutsch	iii
	Reference
INTRODUCTORY REMARKS by G.C.Deutsch	I
 <u>KEYNOTE ADDRESS</u>	
THE DEVELOPMENT AND APPLICATION OF STRAINRANGE PARTITIONING AS A TOOL IN THE TREATMENT OF HIGH TEMPERATURE METAL FATIGUE by S.S.Manson	K
 <u>SESSION I</u>	
A STRAINRANGE PARTITIONING ANALYSIS OF LOW CYCLE FATIGUE OF COATED AND UNCOATED RENE' 80 by C.S.Kortovich and A.A.Sheinker	1
STRAINRANGE PARTITIONING BEHAVIOR OF THE NICKEL-BASE SUPERALLOYS, RENE' 80 AND IN 100 by G.R.Halford and A.J.Nachtigall	2
LOW CYCLE FATIGUE BEHAVIOR OF IN-100: STRAINRANGE PARTITIONING METHOD by M.C.VanWanderham, R.M.Wallace and C.G.Annis, Jr	3
APPLICABILITY OF THE SRP METHOD AND CREEP-FATIGUE DAMAGE APPROACH TO THE LCHTF LIFE PREDICTION OF IN-100 ALLOY by J.L.Chaboche, H.Policella and H.Kaczmarek	4
STRAINRANGE PARTITIONING OF MARMOO2 OVER THE TEMPERATURE RANGE 750°C – 1040°C by V.T.A.Antunes and P.Hancock	5
DISCUSSION SUMMARY, Session I by H.R.Tipler	D1
 <u>SESSION II</u>	
THE LOW CYCLE FATIGUE BEHAVIOUR OF NIMONIC 90 AT ELEVATED TEMPERATURE by G.F.Harrison and M.J.Weaver	6
AN APPLICATION OF STRAINRANGE PARTITIONING TO THE LOW CYCLE-HIGH TEMPERATURE FATIGUE LIFE PREDICTION OF WASPALOY by G.Asquith and S.H.Sprinthal	7
HIGH TEMPERATURE LOW CYCLE FATIGUE BEHAVIOUR OF CAST IN738LC ALLOY by L.Massarelli	8
CONTRIBUTION A L'EVAULATION DE LA METHODE STRAINRANGE PARTITIONING APPLICATION A L'ALLIAGE BASE NICKEL par C.Perruchet	9
CREEP-FATIGUE INTERACTION IN ALLOY IN738LC by M.F.Day and G.B.Thomas	10

	Reference
AN ANALYSIS OF THE LOW CYCLE FATIGUE BEHAVIOR OF THE SUPERALLOY RENE' 95 BY STRAINRANGE PARTITIONING by J.M.Hyzak and H.L.Bernstein	11
DISCUSSION SUMMARY, Session II by H.Zenner	D2
<u>SESSION III</u>	
AN APPLICATION OF STRAINRANGE PARTITIONING TO COPPER-BASE ALLOYS AT 538°C by R.H.Stentz, J.T.Berling and J.B.Conway	12
STRAINRANGE PARTITIONING APPLIED TO Ti-6Al-4V by H.Nowack and J.Vreke	13
STRAINRANGE PARTITIONING IN CYCLIC CREEP OF Al Cr Mo V STEEL by E.G.Ellison	14
EXPERIENCES IN THE USE OF STRAINRANGE PARTITIONING FOR PREDICTING TIME DEPENDENT STRAIN-CONTROLLED CYCLIC LIFETIMES OF UNIAXIAL SPECIMENS OF 2¼Cr-1Mo STEEL, TYPE 316 STAINLESS STEEL AND HASTELLOY X by C.R.Brinkman, J.P.Strizak and M.K.Booker	15
THE APPLICATION OF "STRAINRANGE PARTITIONING METHOD" TO MULTIAXIAL CREEP-FATIGUE INTERACTION by S.Y.Zamrik	16
DISCUSSION SUMMARY, Session III by G.R.Halford	D3
<u>SESSION IV</u>	
FINAL DISCUSSION SUMMARY by J.M.Drapier	D4
APPENDIX A1	A1

INTRODUCTORY REMARKS

by G. C. DEUTSCH (NASA-USA)

I am very pleased to welcome you to this Specialist Meeting on Characterization of Low-Cycle High-Temperature Fatigue by the Strainrange Partitioning Method. This is a highly specialized meeting involving both participants and observers who are carefully selected specialists in the field.

Since advanced turbine engine materials for military applications are being used to a high fraction of their ultimate capabilities, there is thus a great need for more meaningful high temperature mechanical property tests on these materials as well as for improved analytical techniques for the prediction of their service life. One particularly vexing problem has been the difficulty in describing and predicting the behavior of materials at high temperatures and in real environments, such as creep-fatigue interactions present in low-cycle high-temperature fatigue of engine components. The panel has made an attempt to address this problem by supporting a cooperative testing program aimed at the evaluation of the Strainrange Partitioning approach for the analysis and prediction of low-cycle high-temperature fatigue life.

Nineteen laboratories in five countries participated in this program, each testing its own materials of interest under its own laboratory conditions so that the results obtained will provide validation for a wide range of materials and to insure maximum usefulness to each of the participating laboratories. What we have taken here is the first, very necessary step in the evaluation of a life prediction approach - the evaluation of the ability of this method to predict the life of specimens subjected to complex loading from specimen data obtained from simple tests. One could not hope to obtain reliable life predictions for engine components if it were not possible to reliably predict the lives of well controlled laboratory specimens. The culmination of this evaluation program is the Specialist meeting you are now attending, which brings together these investigators for the purpose of sharing their laboratory testing experiences, permitting an in-depth evaluation of the Strainrange Partitioning method, and providing maximum exposure to the findings and recommendations of this distinguished body of specialists.

It is now my distinct honor and privilege to introduce to you a dear friend of long standing. Since 1974, Stan Manson has been a Professor of Engineering at Case Western Reserve University. For the prior 18 years, he was chief of the Materials & Structures Division at NASA's Lewis Research Center. In this capacity, he directed a broad effort of more than 100 scientists and engineers devoted to the development of advanced materials, methods of characterizing material behavior, and the application of materials to sophisticated aeronautical, space, and industrial structures. Included within the list of subjects covered by this group of experts are superalloys, composites including eutectics, structural high temperature ceramics, refractory metals, corrosion and oxidation, low- and high-cycle fatigue, creep and creep-rupture, fracture mechanics, stress-analysis, and other aspects of materials and structural mechanics.

In addition to his role as director of this large effort, he has personally participated in individual research for over thirty years, specializing in the analysis of structures in the creep and plastic flow range, in time-temperature parameters for creep and creep-rupture, in low-cycle fatigue and cumulative fatigue damage, in thermal shock parameters, and most notably in creep-fatigue at elevated temperatures. His research has led to over 100 technical publications, a book, "Thermal Stress and Low-Cycle Fatigue", and to a number of chapters in other books. For his pioneering work in metal fatigue, he received in 1967 the NASA Medal for Exceptional Scientific Achievement, and in 1972 the Distinguished Contributions Award from the Society for Experimental Stress Analysis. In 1974 he was awarded a Von Karman prize by the TRE Corporation to honor the most significant contributions in structural-material technology in the decade since the death of Theodore Von Karman. The prize was awarded in recognition of his contributions in the development of life-prediction methods.

Stan Manson is an active member of several technical societies. He is a past president of the Society for Experimental Stress Analysis. He was elected in 1971 to Honorary membership in the Society of Materials Science, Japan - the only scientist in the western world so recognized. He is also a Fellow of the Royal Society.

Most recently Professor Manson has been pioneering along with his co-developers Gary Halford and Marvin Hirschberg, in the development of the method of Strainrange Partitioning. It is this activity that brings us together here in this beautiful city of Aalborg, Denmark. In presenting Professor Manson to you, I must tell you that I have both good news and bad news. The bad news is that Stan is almost never a man of few words. The good news is that his words are usually worth hearing. With that, I give you Stan Manson.

THE DEVELOPMENT AND APPLICATION OF STRAINRANGE
PARTITIONING AS A TOOL IN THE TREATMENT OF HIGH
TEMPERATURE METAL FATIGUE*

S. S. Manson, Professor of Mechanical and Aerospace Engineering
Case Western Reserve University
Cleveland, Ohio 44106

ABSTRACT

The background and basis of the Strainrange Partitioning Method is described, and the results of a number of investigations applying the method to high temperature metal fatigue problems are briefly reviewed. Among the subjects thus far studied are the effects of frequency, stress and strain hold periods, stress and strain ramping, creep-fatigue interspersions, and thermomechanical cycling.

Of special interest has been the establishment of a set of universalized life relations which are normalized by the ductility of the material. These relations together with a set of rules that have been devised for treating multiaxiality by the method, have, for example, been useful in predicting torsion behavior, and in particular in establishing a new relationship between torsion and tension that had previously not been considered. They have also been useful in the development of a framework for treatment of environmental effects.

INTRODUCTION

Strainrange Partitioning (SRP), as a tool for treating high temperature fatigue, was conceived just about 7 years ago. The underlying concept of partitioning the total inelastic strainrange into its four generic components developed because alternative approaches in use at that time led to perplexing questions that could not readily be answered by existing methods. In the intervening years we have attempted to resolve many of these questions and are making a dedicated effort to apply the SRP concept to many types of problems, both to learn of its potential and to become alerted to limitations that require further inquiries.

While the effort has been intense the main investigators have been the originators of the method. It is only now, as the method passes from infancy to a more advanced early development stage, that other investigators have become encouraged to make inquiries of their own. This Specialists' Meeting is the culmination of the first phase of outside participation. It is indeed a privilege to join with this eminent international group of investigators in a mutual exchange of experiences in the application of Strainrange Partitioning. I expect that much good will come of this meeting - some of it gratifying in that successes will be reported in applications of interest to the investigators, some of it pointing to areas that need further development before it can be successfully applied. All contributions are useful, and completely welcome.

It is my special privilege not only to join Mr. Deutsch in welcoming you, but to express the keynote of the meeting. I shall not attempt to add new data; that will be the role of the international specialists. But I do think that it is appropriate for me to provide some background information of the logic that led to the development of the method, together with a brief overview of the types of problems that have already been treated.

BACKGROUND

Genesis. The concept underlying the SRP Method came to fruition during the preparation of another report the purpose of which was to refine the Time-and-Cycle Fraction approach for treating high temperature fatigue. Our goal was to point out that two major changes in the application of the method would improve its accuracy considerably. The first was to use cyclic creep rupture data in place of the static data then (and now) used; the second was to eliminate the double accounting of the "creep effect": once when we summed the time fractions based on creep rupture data, and then again when we included this same creep strain within the total strainrange in evaluating the fatigue cycle fraction. In attempting to work out the details of such improvements several dilemmas presented themselves:

* Keynote paper to AGARD Specialist Meeting on Evaluation of Strainrange Partitioning, AALBORG, Denmark, April 11, 12, 1978.

1. How should the cyclic creep rupture data be generated? We had been using constant load testing in tension and compression, allowing the specimen to strain about 1% in each direction before reversal, but how critical was the strain amplitude? Furthermore, since we were summing only the tensile portions of the test time, did we really need to waste the time allowing the specimen to creep during the strain reversal, or could we compress it back to the starting point of strain rapidly, and thereby save test time?

2. In a symmetrical loading test it might be easy to separate out that part of each half of the cycle that was "creep", and therefore remove it from the total strainrange involved in the cycle when considering the fatigue effect, using the basis that its damaging effect had already been accounted for in the time fraction summation. But in considering unsymmetrical cycles, wherein the creep strain in tension was different from that in compression, which component should we subtract?

3. Of special interest in resolving issue 2 above was the case when the creep was in compression only, as frequently occurs during thermomechanical loading. Not only was there a question as to how to correct the strainrange for calculating the fatigue effect, but the whole issue of how to treat compressive creep, even in the time-fraction calculation, required attention. Should compressive creep be regarded to be as damaging as tensile creep? Should we use the cyclic creep rupture results based on tension creep to estimate compressive creep damage. What, in fact, is the true role of compression, whether creep or plasticity, in elevated temperature fatigue?

It is inappropriate to dwell on the deliberations that led from the above questions to the formulation of the SRP concept. But it is clear that once the total strainrange is regarded as a synthesis of $\Delta\epsilon_{pp}$, $\Delta\epsilon_{cc}$ and $\Delta\epsilon_{cp}$ (or $\Delta\epsilon_{pc}$), the questions become resolved, or they vanish altogether. There is no longer the issue of how to generate a cyclic creep rupture curve because SRP does not require one; the four generic life relationships take their place. There is no longer a need to separate that part of the total strainrange due to the already accounted for creep from the strainrange causing pure fatigue; a true creep-fatigue interaction emerges, and the net effect depends on which types of strainranges are involved, and in what proportion. And finally, there is no need to deliberate over the role of compression because compression, just like tension, governs which of the strainranges will be present, and in what proportion.

That some questions were answered or negated does not mean that SRP could answer all questions, nor that new questions were not raised by its substitution. But it did mean that we had a fresh starting point and a new basis on which to frame a logic to seek answers and to point to new potential relationships not as clearly evident without this new tool. Before proceeding to outline some of the consequences of the implementation of SRP, it is helpful to discuss some physical aspects underlying the method.

Basic Mechanism. Although the implementation of the method does not require a knowledge of the mechanistic basis, it is certainly instructive to seek an understanding of the physics involved in the creep-fatigue process. Thus we undertook very early to provide a simplified model of the process based on the SRP framework. We recognized the extreme complexity of the process; all the intricacies of the room temperature mechanism, plus the complications added by superimposing creep, plus the environmental factors aggravated by addition of an aggressive atmosphere. However, we felt that a start could be made by considering the simplest model that contained some of the important elements of the problem.

Figure 1 shows the simplified model we adopted in which (B) is an enlargement of a small region in the vicinity of the surface in (A). We consider first a strain cycle designated cp. During the tensile half, the stress is presumed to be too low to activate slip in the slip plane EF. But given enough time, sliding is presumed to take place along the grain boundary GH, displacing the upper half of the crystal relative to the lower half, as shown in (C). Cavitation can also occur in the grain boundary as shown. During the compressive half of the cycle, when the loading is assumed to be very rapid, the total strain is assumed to be returned to its initial condition. But the time is short and in order to accomplish the effect in short time, a high stress level develops. The reverse sliding takes place along the family of slip planes parallel to EF, but no grain boundary sliding occurs because the time is too short. The final condition is as shown in (D). Although upon completion of the cycle there is no net strain as measured by an extensometer, internally there is left a considerable disruption on a localized structural scale. Net internal strains remain in both the slip planes and grain boundaries, and cavities may exist in the grain boundaries. Moreover, if the cycle is repeated similar strains will be superimposed on the strains accumulated from all previous cycles. Every cycle causes a ratcheting of tensile grain boundary strain, balanced by a ratcheting of compressive slip plane strain. Each type of strain is essentially accumulated, cycle by cycle, until the capacity of the material to deform in one or the other of the two modes is exhausted, and failure ensues.

Similar models have been constructed for each of the other generic strainrange components. For pc approximately the same localized structural features develop, except perhaps for the absence of grain boundary cavitation. For pp straining we envision cyclic reversal within the slip planes. However, although some "healing" may take place by compensating slip during the compressive half, which exactly reverses the slip in a particular slip plane occurring in the tensile half, a net damage per cycle still persists. All the mechanisms drawn on to explain room temperature fatigue, wherein pp is the principal mode

for most materials, become relevant: intrusions and extrusions, subgrain formation, cracking of subgrain boundaries, agglomeration of dislocations, and others too numerous to discuss at this time. And finally, for cc straining mechanisms analogous to pp deformation occur, except that grain boundaries replace slip planes in the model, and grain boundary cavitation becomes an additional source of damage. In all cases, of course, environmental attack is an important factor, being both of general nature on the complete surface of the material, and of particular intensity in the region where clean nascent surface has become exposed by the reversed deformation, for example the region E'G' in Fig. 1.

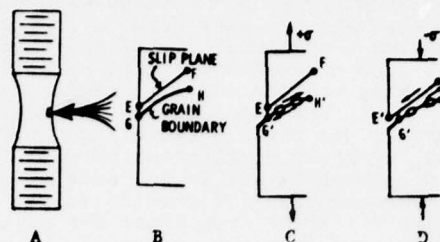


Figure 1. Simplified schematic illustration of the creep-fatigue interaction occurring when tensile creep along grain boundaries is reversed by compressive plasticity along crystallographic slip planes.

Some Implications of the Hypothesized Mechanism - While reduced to almost simplistic terms (recognizing that the process is much more complicated) the model nevertheless leads us to some natural consequences that simplify the treatment of high temperature fatigue. In addition it provides us with a framework of logic for attacking aspects of the process not directly resolved.

a) Once we differentiate between only two types of deformation, grain boundary sliding (call it "creep") and slip plane sliding (call it "plasticity"), it follows that there are only four generic permutations possible. Thus all the problems, involving any complicated loading pattern whatever, reduce to the determination of which of three basic strainranges develop during the cycle ($\Delta\epsilon_{pc}$ and $\Delta\epsilon_{cp}$ cannot exist concurrently, by definition). Where in the cycle any particular element of strain occurs becomes of secondary importance to the net strain within the complete cycle, and the strain reversal pattern. We no longer think in terms of whether the problem is one of stress-hold, strain-hold, variable frequency, variable temperature, or any of the many complicated types of loadings that are of practical interest. Rather, we think in terms of the type of strainranges it generates. Problems, therefore, are assumed to reduce to a consideration of one or more of four possible generic strainranges, not more than three in any one hysteresis loop. Furthermore, material characterization becomes a matter of establishing four life relationships, and their determination is accomplished under experimentally convenient conditions, while their use extends to complex loading as well.

b) Once we identify the mechanism with inelastic strainrange, and in particular view it (at least for the pc and cp modes) as a ratchet causing essentially monotonic strain accumulation until straining capacity is exhausted, we recognize the importance of ductility in governing fatigue life. However, we now are led to draw an important distinction between "plastic" ductility and "creep" ductility. For practical purposes we are led to consider as the most important ductility, for a particular life relation, that type which is associated with the tensile portion of the cycle. Thus for pp and pc we would regard the ordinary tensile ductility as governing, while for the cc and cp strains the "creep" ductility is of primary importance. While it is difficult to obtain a true measure of "creep ductility", a first approximation of its measure is the ductility determined in the creep rupture test of approximately the same duration as the fatigue test required. These considerations led us to propose some tentative life relationships for each of the four generic strainranges in Ref. 2 in which strainrange was related to cyclic life through the ductility associated with the tensile component of the strainrange involved. More recently, Halford, Saltzman and Hirschberg (Ref. 3) have refined these relationships based on additional data. The form of their equations differ somewhat from the earlier ones, but again the basic ductility identification is the same: pp and pc relate to tensile ductility; cp and cc relate to creep ductility. The equations are of immense value in obtaining life estimates for which fatigue data are scarce, or for temperatures and environments not yet studied, or in transferring information on one lot of material to the estimation of fatigue data on another lot.

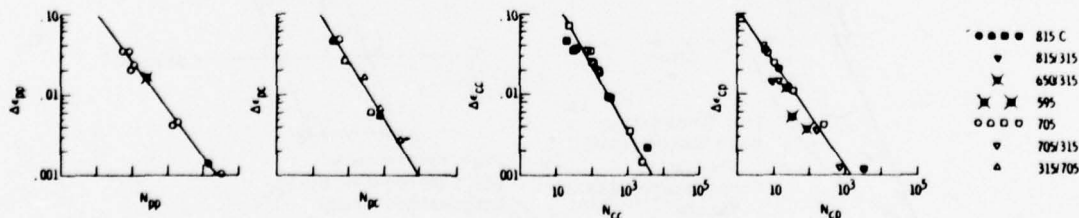


Fig. 2. Strainrange vs. cyclic life relationships for 316 SS at various temperatures, including bi-thermal tests. (Data from Ref. 4)

c) Once we relate life to the type of strainrange present, and to the monotonic ductility, we automatically put temperature and temperature variations during the cycle into a perspective not previously employed. Fatigue life is known to be extremely sensitive to temperature, and as a result estimation of life at a particular temperature, or transfer of knowledge of behavior at another temperature, is very difficult, particularly when fluctuations occur during the cycle. The SRP framework regards temperature as important primarily in determining the type of strainranges that develop when a given set of external loading conditions are applied. If the temperatures are all very low, pp strainrange may develop because no creep is possible at such low temperatures. Or if they are all very high, a cc strainrange component may predominate under similar loading conditions. Or if the tensile period has high temperature while the compressive period low temperatures, cp strainrange may develop. Correspondingly low temperature during tension and high temperature during compression tends to produce pc strain. Thus, the major burden of providing information for quantitative treatment of temperature effects is shifted to the structural analyst, requiring him to make an important distinction between inelastic plastic strain and inelastic creep strain. Actually, it is not much of an additional burden to him because he must calculate the required information anyway since the constitutive equations for creep strain are different from those for plastic flow, and the two types of strain are easily retrieved from the memory of required analysis. In fact, the SRP framework makes more complete use of his analysis than if the major requirement were merely to supply total inelastic strainrange.

Reasoning such as the above - that temperature significantly influences the loading system required to produce a given strainrange, but does not necessarily influence the cyclic life once a given type of strainrange is induced, - led us to make the study (Ref. 4) of the effect of temperature on the life relationships for 316 stainless steel and 2 1/4 Cr-1 Mo steel. Fig. 2 shows the results for 316 stainless steel indicating essential independence of temperature for all the four strainranges; similar results were obtained for 2 1/4 Cr - 1 Mo steel. Even bithermal tests, wherein half the range was conducted at low temperature to insure absence of creep, while the other half was conducted at high temperature to insure predominance of creep, showed the same life relationship to strainrange as did the isothermal tests at various temperatures. Thus the conclusion must be reached that, for these two materials the fatigue life relationships are independent of temperature in the range of temperatures studied.

It should be emphasized, of course, that it is not a requirement of the SRP method that the life relations be independent of temperature. In fact, it is not even to be expected, since we have already pointed out the importance of ductility on life, and have alluded to the significance of environmental interaction. Since ductility and environmental attack may depend strongly on temperature, variations in fatigue life with temperature could be expected for those temperature ranges where the effects are strong. For the 316 SS and the 2 1/4 Cr-1 Mo steel in the temperature and time ranges tested these effects were secondary. In any case, the SRP Method separates the rheological effects of temperature from the temperature effects on ductility and oxidation (or other chemical effects).

d) Relating life to the type of strainrange involved also adds a new perspective to the effect of mean stress not similarly viewed by other methods. At room temperature the mean stress relaxes to zero when large inelastic strainranges are applied. But at high temperatures mean stresses can develop even at high strainranges because of the creep-plasticity interaction. Certain types of mean stress naturally develop during the generation of the desired strainranges for SRP purposes. They are, therefore, already accounted for in the life relations for those strainranges. Consider, for instance, the generation of cp and pc loops under isothermal conditions. The cp loop, as discussed in connection with Fig. 1, can be generated by slow straining at low stress in tension and fast straining in compression. A typical hysteresis loop is as shown in Fig. 3A. The peak compressive stress is higher than the peak tensile stress, so that the mean stress is compressive. Correspondingly a pc loop produces a mean tensile stress, as shown in Fig. 3B. One might be tempted to argue

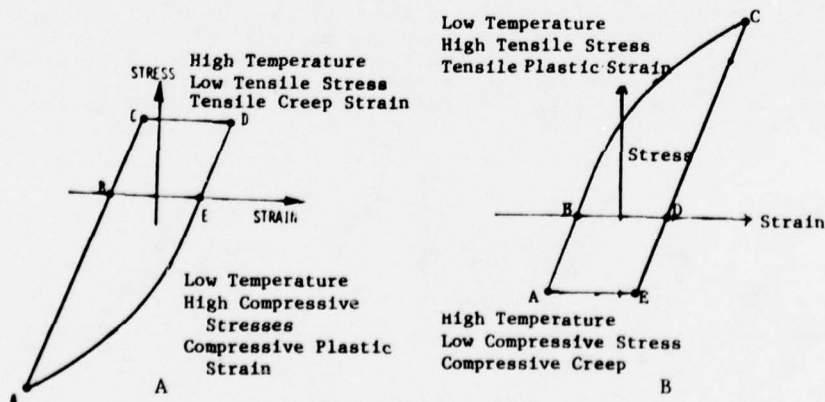


Fig. 3. Schematic illustration of hysteresis loops for cp and pc types of strainranges.

that the mean compressive stress of cp loop should be beneficial, while the mean tensile stress of the pc loop should be detrimental. Yet, for a material like 316 Stainless Steel, the life associated with the loop having tensile mean stress could be twenty times as high as that for the loop having compressive mean stress, temperature and strainrange both being equal. No careful tests have been conducted to determine whether the same cp strainrange, generated under conditions that result in a mean tensile stress would be more damaging than a similar strainrange conducted under conditions resulting in a mean compressive stress. Nor have careful tests been conducted to ascertain the mean stress-effect for small strain oscillations. These are subjects yet to be studied. But it is clear from the SRP framework, and from the life relationships we already know for several materials, that our concepts regarding mean stress effects gained from experience at room temperature must be revised to embrace high temperature creep-plasticity interactions.

APPLICATIONS

Before reviewing some of the specific studies that have been conducted we should point out that some of our efforts have been directed toward the development of techniques for implementation of procedure. For example, it has been necessary to establish a procedure for separating the total inelastic strainrange into its generic strainrange components. This can be done analytically if the constitutive equations used in the structural analysis are sufficiently accurate. However, in the absence of the required accuracy, we can use a semi-experimental approach we have developed wherein the loading cycle is duplicated on a uniaxial specimen, and the stabilized hysteresis loop observed. It requires only a small fraction of the cyclic fatigue life to accomplish stabilization; thus the time saving efficiency of the approach is high relative to conducting the test to complete fracture.

The procedure for separation of the strainrange components is described in Ref. 5. Basically what is required is a determination of the second stage creep rate at each instant of time during the cycle. This is accomplished either by actually stopping the loading at each of several stress levels during the test, and measuring the creep rate which is approached asymptotically with time, or by an analytical approach using the power law relation between stress and creep rate. The experimental method is especially valuable when both temperature and stress change during the cycle, as in thermomechanical loading (Ref. 6), but is useful for isothermal loading as well. Once the total creep strain in each half of the cycle has been determined, the plastic components are determined by subtraction from the known total inelastic strainrange. The strainrange components are then calculated from knowledge of the individual creep and plasticity strains in each half of the cycle. I shall illustrate the approach later in connection with Fig. 8.

A second general aspect that relates to all problems treated is the method of combining the cumulative damage of resulting strainrange components when more than one is present during a single cycle. The Interaction Damage Rule (Ref. 2) has served this purpose well. The rule uses the cyclic life that would be associated with each of the partitioned strainranges as if the entire inelastic strainrange involved in the cycle were of that type. For example if the total inelastic strainrange were 1%, and only 0.1% were cp strain, we would not need to know the cp life for 0.1% strainrange, only for 1% strainrange. The advantage is that we are not forced into a need for accurate knowledge of the life relationships at low strainranges where experimental determinations are difficult.

Stress-Hold Tests. One of the most interesting and revealing critical tests that have been conducted within the SRP framework related to stress-hold at elevated temperature on 316 Stainless Steel (Ref. 1). These tests were analogous to our cyclic creep-rupture tests in that the load was held constant until a fixed strain was reached. However, the reversal was accomplished by first reducing the temperature to a low value, below where creep would be expected, and rapidly returning the strain to its initial value. In one test the load-hold was imposed in tension at 704 C and the compression at 316 C, while in the other case the load hold occurred in compression at 704 C while the tension return was at 316 C. The hysteresis loops and the failure modes are shown in Fig. 4. On several scores one might have expected the tensile hold to be less damaging than the compressive hold:

a) The mean stress for the tensile-hold was compressive while that for the compressive-hold was tensile. This mean stress difference between the two types of loading was exaggerated by the fact the reversal strain in each case was at a low temperature, causing a high or flow stress relative to the stress required to cause the creep.

b) The time per cycle was considerably longer for the compressive-hold test because the compressive creep rate was much lower than the tensile creep rate. Considering the total test time to cause failure, the compressive-hold test was subjected to an exposure time 50 times longer than the tensile-hold test. If ordinary oxidation was a major factor in governing life the compressive-hold test would have had to be regarded as the much more vulnerable one.

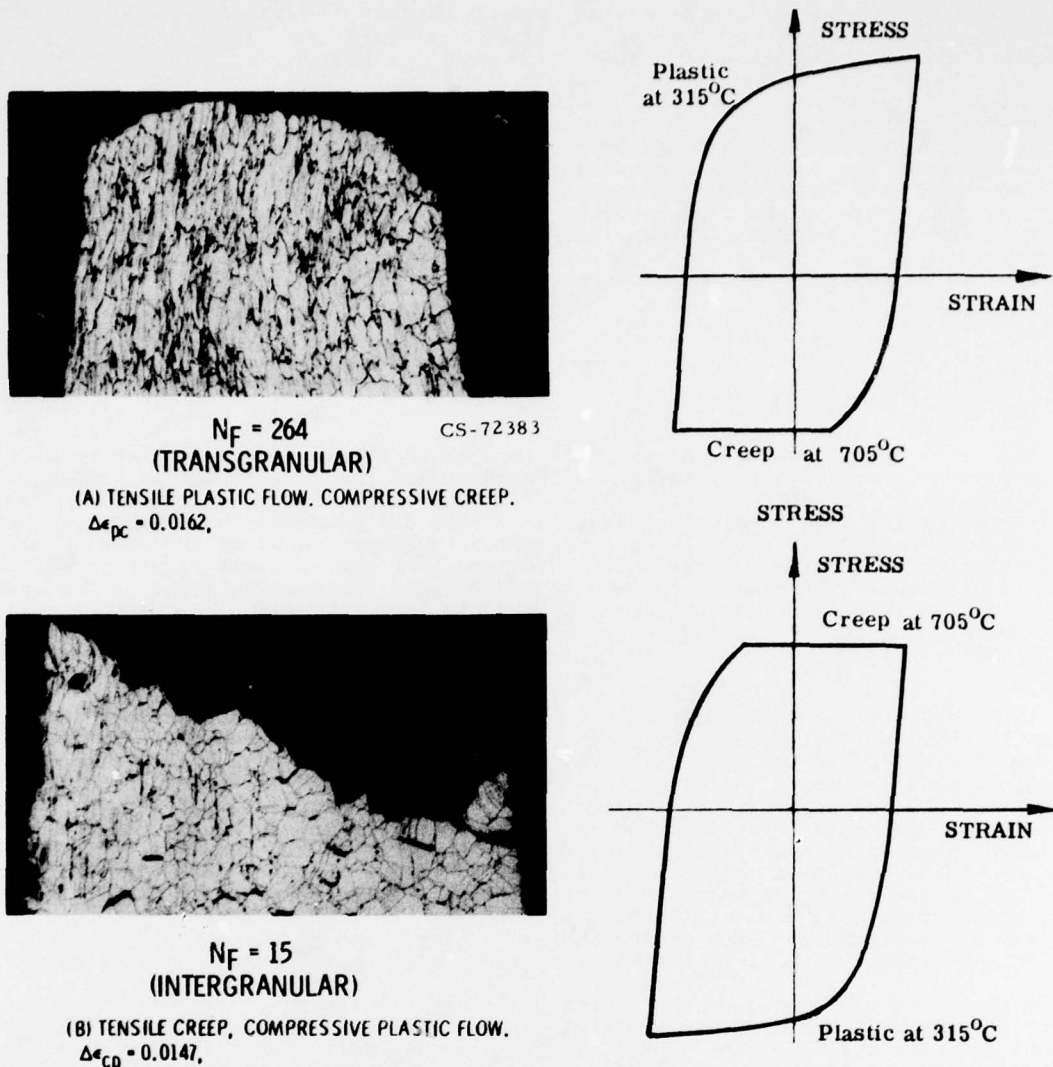


Fig. 4. Photomicrographs and hysteresis loops of fractured specimens of 316 stainless steel tested in creep-fatigue.

c) The SRP inelastic strainrange was somewhat lower for the tensile hold, being $\Delta\epsilon_{cp} = 1.47\%$ compared to $\Delta\epsilon_{pc} = 1.62\%$ for compressive hold.

Yet, with all the positive factors operating in behalf of the tensile-hold test, its life was shorter than that for the compressive-hold test by a factor of nearly 18. The explanation in this case is simply that, according to the SRP life relations, the cp strainrange induced during the tensile-hold is much more damaging than the corresponding pc strainrange associated with the compressive-hold. Note also that the tensile-hold tests resulted in a highly intercrystalline failure, while the compressive-hold resulted in a transcrystalline failure mode. Quantitatively, the life values associated with each of the tests are very close to predictions by SRP.

Similar load-hold tests have been conducted on 2 1/4 Cr-1Mo Steel which, at low strains, happens to be more severely damaged by pc than by cp straining. The lives were still as predicted by SRP analysis.

Strain-Hold Tests. Since strain-hold, and accompanying stress relaxation is so important in nuclear and aerospace applications, it is not surprising that this subject has been studied so extensively. From an SRP viewpoint the phenomenon is simply one of inducing cp, pc, or cc strainranges. During tensile strain-hold, the stress causes creep which in turn reduces the stress, trading elastic strain for creep strain. Tensile-hold induces cp strainrange, compressive-hold pc strainrange, and combined-tensile and compressive-hold induces cc strainrange. Many such laboratory tests have been analyzed quantitatively within the SRP framework. A typical result is shown in Fig. 5 (Ref. 2) for 304 stainless

steel at 650C. The loss in life with increased hold-time is greater for the lower strain-ranges because a larger percentage of the total strainrange can be converted to the cp type. For a 0.5% total strainrange varying the hold-period from 10^{-2} min. to 10^3 min. can reduce life by a factor of 40, but at a 2% strainrange the reduction is by only a factor of 6. For compressive-hold in 304 and 316 Stainless Steel the reduction factor is not nearly as high as for tensile-hold because pc damage is not as severe as cp damage. Combined tensile-and compressive-hold produces cc strain which reduces life more than compressive-hold alone, but not as much as tensile-hold.

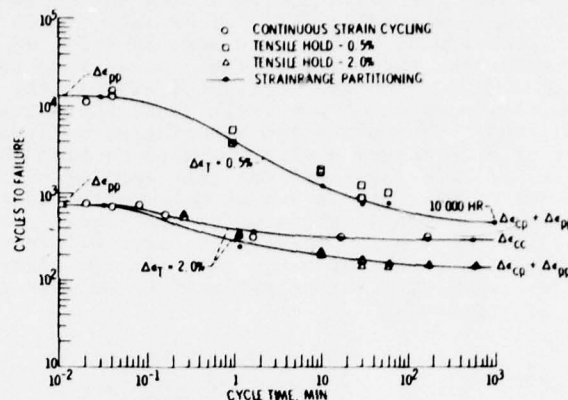


Fig. 5. Effect of strain-hold time on cycles life for 304 SS at 650C (From Ref. 2)

For 2 1/4 Cr-1 Mo steel opposite results were observed, and are readily predicted by SRP. Compressive-hold is more damaging than tensile-hold because pc is more damaging than cp for this material.

Frequency Effects. Applying a given strainrange at a series of different frequencies produces differences in life for three reasons:

- The type of strain that develops is different for different frequencies. Slower cycling tends to induce cc strainranges, while fast cycling features pp strainranges. Thus, as frequency is varied under symmetrical cycling (i.e., no hold-periods) the mix of pp and cc strainranges varies, generally decreasing cyclic life for the lower frequencies wherein cc strains predominate.
- The longer cycle times associated with the lower frequencies may be conducive to metallurgical transformations that reduce ductility.
- The longer cycle times associated with the lower frequencies allow more surface oxidation, which may also reflect itself as a reduction in ductility.

Figure 6 shows results of some SRP calculations (Ref. 2) for frequency effect, and a comparison with experimental results. In Fig. 6A are shown the results for symmetrical cycling 316 stainless steel at 815C. At the lowest frequency shown, 10^{-5} Hz, the strainrange is expected to be absorbed almost entirely as cc, whereas at frequencies for 1 to 10 Hz, almost all the strainrange becomes pp. Thus the lower shelf of life is the cc life, and the upper shelf is the pp life for the imposed strainrange. This is true, however, only if ductility is not seriously altered by exposure time.

In Fig. 6B are shown calculations for A286 Steel at 595 C. For this material metallurgical transformations reduce ductility for the longer cycle periods. That such transformations are involved is deduced from the progressively lower ductilities observed in creep-rupture tests as the rupture time is increased. Calculations based on the

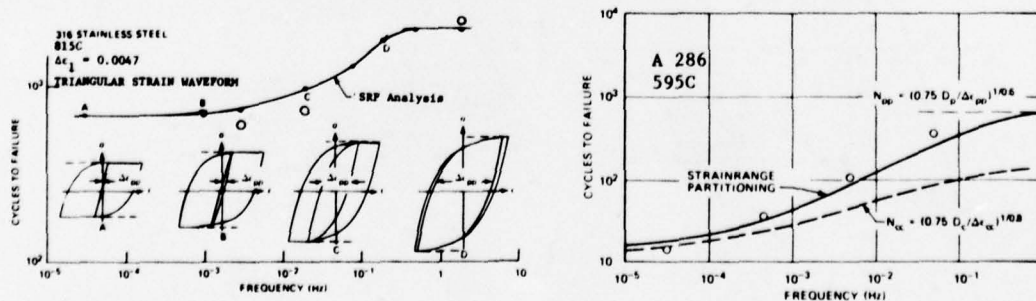


Fig. 6. Frequency effects on cyclic life for 316 SS at 815C and A-286 at 595C (From Ref. 2).

ductility degradation for the cc component (the dotted curve in the figure) produce good comparison with experimental results. In this case a lower shelf of life does not occur in the frequency range investigated, because progressively lower frequencies produce lower and lower creep ductilities, which reduce the cc life.

Strain ramping. When the strain rate is slow during the rising strain period, and fast during the period of strain reduction, a cp strainrange tends to be induced because the stress is tensile for a longer period than it is compressive. Conversely, when the strain rate is slow during the rising period, and fast during the declining period, pc strain is induced. Figure 7 shows some results (Ref. 5) of such strain ramping tests on 316 Stainless Steel at 704C, together with predictions made by SRP. On the vertical axis is shown the ratio of life for the ramping condition, normalized to the pp life for the same inelastic strain range at 704C. On the horizontal axis is the rate at which the ramping was imposed during the slow portion of the cycle (the return rate being as rapid as could be experimentally achieved). The predicted lines agree well with the experimental points. Note that severe loss of life occurs during the slow ramping while strain is increasing, but very little loss of life occurs if the slow ramping occurs while the strain is decreasing. As already noted, this is due to detrimental cp strain developing under the first condition, while pc strain develops under the second condition for the 316 Stainless Steel. The calculations are in general agreement with the experimental results. For 2 1/4 Cr-1 Mo Steel, on the other hand, the opposite effect might be expected: slow decreasing strain ramping might be expected to be more damaging than slow ramping while the strain is increasing.

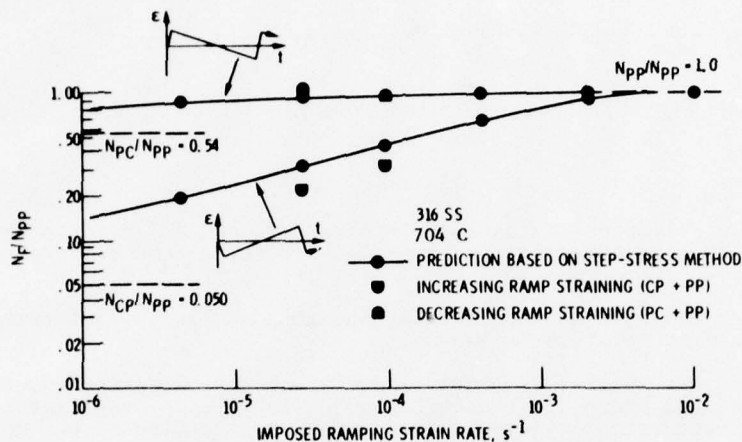


Fig. 7. Strain ramping experiments analyzed by SRP. (From Ref. 5).

Thermomechanical Loading. Simultaneous change in strain (or stress) and temperature provides a severe challenge to any predictive method. SRP has been applied to the study of several such types of loading, one of which is shown in Fig. 8 (Ref. 6). Fig. 8A shows the hysteresis loop for a test in which the temperature was ramped in phase with the strain. As strain was increased temperature was increased; as strain was decreased temperature was decreased. Note the complex shape of the hysteresis loop. Stress actually decreases along FGH even though the strain is increasing, because of reduced yield stress

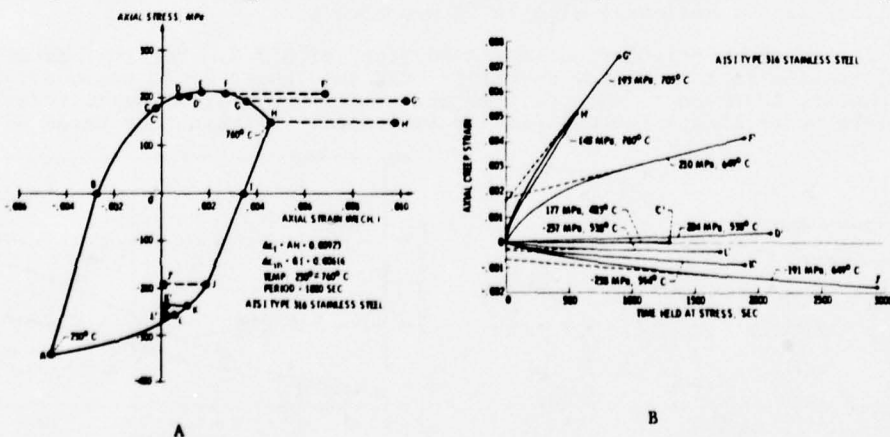


Fig. 8. Thermomechanical loading analyzed by SRP. 316 SS ramped in phase with temperature (From Ref. 6).

at the higher temperatures. The analysis in this case was made by observing the stabilized steady-state creep rate at each of a number of points where the test was put into load-control, and the stress and temperature held steady until a minimum creep rate developed. That is the significance of the lines FF', GG', etc. The time patterns of strain variation for each of the points where temperature and stress were held constant are shown in Fig. 8B. From these measured steady-state creep rates, the strain range components were computed, and a life predicted as 334 cycles. The observed life for this case was 307 cycles. While this is a single case of a very successful prediction, many more thermomechanical tests are needed to provide confidence.

Interspersion Loading. Another very interesting type of test available for analysis was the "Interspersion" test. It consisted of applying a tensile load and allowing the metal to creep under constant load and temperature for approximately 24 hours, after which a reversed higher load induced in a relatively short time a compressive (plastic) strain of magnitude equal to the tensile creep strain. After the creep strain was reversed, a series of rapidly applied fatigue cycles were also imposed. It will be recognized that 24 hour creep period, and its rapid reversal, define what is essentially a cp strain in SRP terminology. Thus, Saltsman and Halford (Ref. 8) have analyzed these tests within the SRP framework using the cp life relationship we initially obtained on 2 1/4 Cr - 1 Mo Steel in Ref. 1. Although the tests were initially conceived as a check on the validity of the time-and-cycle fraction approach to high temperature fatigue analysis, the data provided an opportunity to check long-time data with predictions based on SRP life relations obtained in relatively short time. Fig. 9 shows the results for 2 1/4 Cr-1 Mo Steel. The plot shows the ratio of experimental life to life predicted according to cp analysis. This ratio is plotted against test time. Note that the data fall within a scatterband of a factor of 2 in life, which is very acceptable. Note also that the scatterband is almost independent of time. In other words, the long-time tests (up to about 1 year) agree almost as well as the short time tests when predicted from cp life data obtained in relatively short time tests (less than 100 hours). There does seem to be a tendency for the longest time tests, to fall into the lower range of the scatterband, possibly reflecting oxidation effects at the long times. However, this question requires further study. What is of special significance here is that a very complex test has lent itself to very simple analysis within the SRP framework.

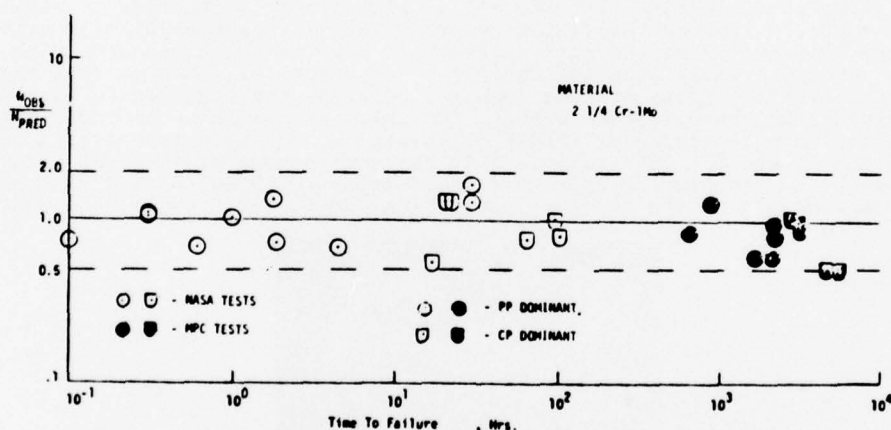


Fig. 9. Analysis of Interspersion tests by SRP for 2 1/4 Cr-1 Mo Steel in temperature range 482 - 593C.

Multiaxiality. The question of multiaxiality required special treatment by SRP. Initially we started with a Von Mises criterion for combining the stress and strain components in order to provide "effective" values to use in the life relationships. But because SRP draws such an important distinction between tension and compression, questions of algebraic sign had to be resolved. The approach developed is described in Ref. 9 and 10

with special application to torsion. In addition we took into account that multiaxiality can cause an effect on ductility, and we accordingly modified the life relationships to account for this factor as well. Typical results (Ref. 10) are shown in Fig. 10 where the torsion results of 304 Stainless Steel are predicted from uniaxial fatigue results at RT, 538, and 649C. The agreement is excellent. It is interesting that the new approach, correcting for ductility alterations associated with multiaxiality, explained for the first time why in the past it has been so difficult to correlate torsion and uniaxial tension fatigue simply on the basis of octahedral shear strain theory even at R.T.

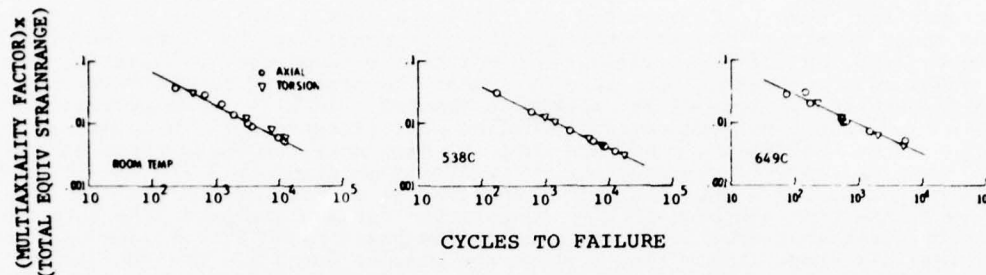


Fig. 10. Application of SRP to analysis of high temperature torsion tests. Special account is taken of multiaxiality effects on ductility (From Ref. 10).

Environmental Effects. We have long recognized that environment is important in fatigue, especially at elevated temperature where oxidation is enhanced. In particular we note from Fig. 1 that nascent surface is more prone to appear at the intersection of grain boundaries with surfaces. These sites are therefore likely to be more severely attacked, as illustrated in Fig. 11 (Ref. 11). Oxidation at such sites is very rapid, and therefore exposure time and available reactant (usually oxygen) display critical values: at the critical value the surface reaction occurs, but given more time or more reactant does not appreciably increase the amount of reaction. Thus we feel that cycle time, beyond the critical value of time required to allow the reaction to take place, does not appreciably change the oxidation effect. On this basis we have provided a rationale (Ref. 12) for including environment in SRP calculations. The main emphasis is placed on the determination of the SRP life relations in the environment of interest using relatively short time tests, and tracking further effects of exposure by estimating what happens to ductility as a result of the exposure. Fig. 12A shows, for example, how ductility of



Fig. 11. Attack of grain boundary region at surface during thermal fatigue cycling. Udiment 700 cycled between 1088C and 316C. (From Ref. 11).

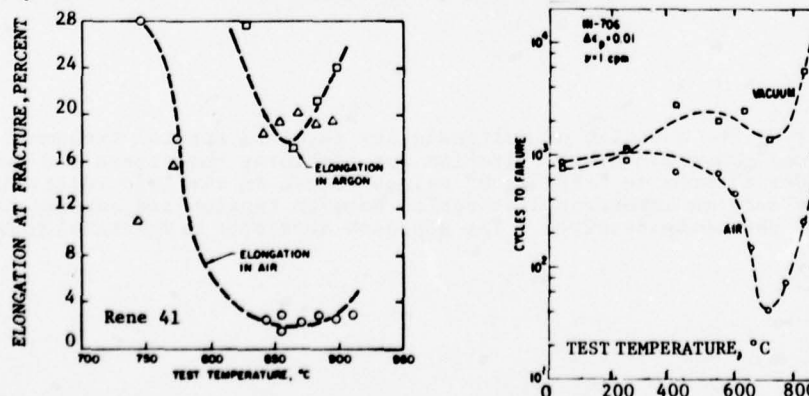


Fig. 12. Reflection of ductility variation on fatigue properties in reactive and in inert environment (From Ref. 12).

a nickel-base alloy Rene 41 varies with temperature in air and the inert environment argon. Since no fatigue data were available on this alloy we sought information on other alloys to demonstrate the relationship between ductility and fatigue. Figure 12B shows fatigue results for another nickel-base alloy, IN-706. It can be seen that a minimum in fatigue life occurs at some critical temperature, just as a minimum of ductility occurs for Rene 41 (Each alloy has its own individual temperature at which the minimum occurs). Further discussion on SRP aspects of environment can be found in Ref. 12.

CONCLUDING REMARKS

I have outlined some of the major efforts expended during the first seven years of the development of SRP as a tool in creep-fatigue analysis. Although much has been done more remains. The major need is an extension to the treatment of low strains and long service times. Cumulative damage associated with complex cycles, multiaxiality (particularly under variable loading history and phase relation among the components), and special environmental effects are additional factors. Metallurgical instabilities will no doubt require special considerations. The list can be proliferated. The close scrutiny given by objective, concerned, and interested investigators will serve an invaluable purpose in the years ahead to evaluate the method and to improve it for direct utility to those whose needs can be served by its application. This Specialists Meeting is the first of such objective interchanges of experiences that will do much to add the proper perspective towards its value and its limitations. Much of the information to be presented may be satisfying in that the results observed are in agreement with expectations based on the method; other results may be perplexing because they do not fall in line with such expectations. Perhaps we can help each other to apply the method in a more useful manner; perhaps we can apprise each other of genuine needs for further developments, or limitations that are insurmountable. In any case I know this will be an exciting experience for us all. My best wishes for a fruitful meeting.

ACKNOWLEDGEMENT

The financial support of NASA under Grant No. NSG-7035 is gratefully acknowledged. The author is also grateful to Frieda Mosby for typing and layout of the manuscript.

REFERENCES

1. Manson, S.S., Halford, G.R., and Hirschberg, M.H., "Creep-Fatigue Analysis by Strain-range Partitioning", Proceedings of First Symposium, on Design for Elevated Temperature Environment, San Francisco, California, May 10-12, 1971, pp. 12-24; disc. pp. 25-28 (1971).
2. Manson, S.S., "The Challenge of Unify Treatment of High-Temperature Fatigue: A Partisan Proposal Based on Strainrange Partitioning ASTM-ASME, STP 520, pp. 744-775, 1973.
3. Halford, G.R., Saltsman, J.F., Hirschberg, M.H., "Ductility Normalized-Strainrange Partitioning Life Relations for Creep-Fatigue Life Predictions", Environmental Degradation of Engineering Materials, pp. 599-612, 1977.
4. Halford, G.R., Hirschberg, M.H., Manson, S.S., "Temperature Effects on the Strainrange Partitioning Approach for Creep-Fatigue Analysis", Fatigue at Elevated Temperatures, ASTM, STP-529, pp. 658-667, 1973.
5. Manson, S.S., Halford, G.R., Nachtigal, A.J., "Separation of the Strain Components for Use in Strain Range Partitioning", published in Advances in Design for Elevated Temperature Environment, ASME, pp. 17-28, 1975.
6. Halford, G.R., and Manson, S.S., "Life Prediction of Thermal-Mechanical Fatigue Using Strainrange Partitioning", Thermal Fatigue of Materials and Components, ASTM STP 612, D.A. Spera and D.F. Mowbray, Eds., American Society for Testing and Materials, 1976, pp. 239-254.
7. Curran, R.M. and Wundt, B.M., "A Program to Study Low-Cycle Fatigue and Creep Interaction in Steels at Elevated Temperatures," Current Evaluation of 2 1/4 Chrome 1 Molybdenum Steel in Pressure Vessels and Piping, pp. 49-82, ASME, 1972.
8. Saltsman, J.F., and Halford, G.R., "Application of Strainrange Partitioning to the Prediction of MPC Creep-Fatigue Data for 2 1/4 Cr-1 Mo Steel". ASME-MPC-3, pp. 283-298, 1976.
9. Manson, S.S. and Halford, G.R., "Multiaxial Rules for Treatment of Creep-Fatigue Problems by Strain-range Partitioning", Symposium on Creep-Fatigue Interaction, ASME-MPC-3, pp. 299-318, 1976.
10. Manson, S.S. and Halford, G.R., Discussion to paper: "Multiaxial Low-Cycle Fatigue of Type 304 Stainless Steel" by J.J. Blass and S.Y. Zamrik, 1976 ASME-MPC Symposium on Creep-Fatigue Interaction, ASME, 1976, pp. 129-159.
11. Howes, M.A.H., "Thermal Fatigue Data on 15 Nickel- and Cobalt-Base Alloys" NASA CR-72738, IITRI-B-6-78-38, May 1970.
12. Manson, S.S., and Zab, R., "A Framework for Estimation of Environmental Effect in High Temperature Fatigue", Proceedings of Conference Environmental Degradation of Engineering Materials, October 10-12, 1977.

A STRAINRANGE PARTITIONING ANALYSIS OF LOW CYCLE FATIGUE OF COATED AND UNCOATED RENE' 80

C. S. KORTOVICH AND A. A. SHEINKER

TRW Inc.
Materials Technology Laboratory
23555 Euclid Avenue
Cleveland, Ohio 44117, USA

ABSTRACT

A strainrange partitioning analysis was conducted on ultrahigh vacuum, strain-controlled, low cycle fatigue behavior of uncoated and aluminide coated Rene' 80 nickel-base superalloy at 1000°C (1832°F) and 871°C (1600°F). The results indicated little effect of coating or temperature on the fatigue resistance. There was, however, a significant effect on fatigue life when creep was introduced into the strain cycles. The effect of this creep component was analyzed in terms of the method of strainrange partitioning. The longest lives were obtained with $\Delta\epsilon_{pp}$ type cycling, while the $\Delta\epsilon_{cc}$ cycle caused a reduction of fatigue life of about 1/2 order of magnitude with respect to the $\Delta\epsilon_{pp}$ life. The $\Delta\epsilon_{pc}$ type cycle caused a life reduction of slightly less than 1 order of magnitude with respect to the $\Delta\epsilon_{pp}$ life, while the $\Delta\epsilon_{pc}$ type cycle provided a fatigue life approximately 1 order of magnitude below that of the $\Delta\epsilon_{pp}$ life.

Metallographic evaluation indicated that microstructural damage varied with cycle type and test temperature. Specimens tested with the $\Delta\epsilon_{pp}$ type deformation exhibited a transgranular fracture mode. Specimens tested with the $\Delta\epsilon_{cc}$ type deformation exhibited an intergranular fracture mode with extensive grain boundary sliding resulting in steps or grain extrusions, particularly at 1000°C (1832°F). Specimens tested with the $\Delta\epsilon_{pc}$ type deformation exhibited an intergranular fracture mode, while the $\Delta\epsilon_{cc}$ specimens exhibited different fracture modes depending on test temperature. At 1000°C (1832°F), the fracture mode was intergranular, while at 871°C (1600°F), the fracture mode was transgranular.

I INTRODUCTION

The use of diffusion aluminide protective coating systems on superalloys in gas turbine engines for the improvement of oxidation and hot corrosion resistance has become quite widespread as a result of increasing cycle temperatures. Although they accomplish this purpose, there is concern that such coatings may degrade the mechanical properties of coated hardware. Of particular concern is a reduction of fatigue resistance in complex geometry hot section components such as turbine blades and vanes which experience severe thermal-mechanical strain cycling during engine service.

The application of a coating to the surface of a material can have a number of effects relevant to the fatigue properties of the coating-substrate system (1). For example, the deformation behavior of the substrate may be changed by the presence of a surface layer having a different elastic modulus and yield strength from that of the substrate. If the fatigue properties of the coating are better than those of the substrate, increased life may be expected. On the other hand, if the fatigue properties of the coating are poorer than those of the substrate, cracks in the coating will serve as surface notches and as paths for the hostile environment to reach the substrate, resulting in reduced fatigue life. In general, the effect that a coating has on the fatigue properties depends on the strainrange, the maximum tensile and compressive strain, temperature, frequency and the nature of the coating itself (1).

The present study was undertaken to provide further insight into the thermal-mechanical fatigue behavior of the nickel-base superalloy Rene' 80 in the coated (CODEP B-1) and uncoated condition. This involved closed-loop, servo-controlled fatigue testing with independently programmed temperature control and strain cycling to develop baseline data for the analysis of thermal fatigue behavior by the method of strainrange partitioning (2). Tests were performed in air and in vacuum to separate the effects of environmental interactions from mechanical effects of the coating on fatigue behavior. Interpretation was made of the influence of thermal cycling on fatigue life within the framework of the strainrange partitioning concept by correlating microstructural damage with various types of reversed inelastic strain cycles involving reversed and unreversed tensile and compressive creep deformation. The work was a cooperative effort between the Materials Technology Laboratory of TRW Inc. and the Materials and Structures Division of the NASA-Lewis Research Center, with vacuum tests being performed at TRW and air testing at NASA. This paper presents the results of the vacuum fatigue tests performed at TRW.

II EXPERIMENTAL PROCEDURE

A. Material and Specimens

The chemical composition of the Rene' 80 material used in this study is presented in Table I of Appendix 1. Tubular, hourglass-shaped specimens with threaded ends were individually cast as solid round bars and machined to the configuration shown in Figure 1. The uncoated specimens were heat treated as follows:

1218°C (2225°F)/2 hours vacuum/argon quench to room temperature

1093°C (2000°F)/4 hours vacuum/argon quench to room temperature

1052°C (1925°F)/4 hours vacuum, furnace cool in vacuum to 649°C (1200°F) within 1 hour, air cool to room temperature (this simulates the coating cycle)

843°C (1550°F)/16 hours vacuum/furnace cool to room temperature.

The coated specimens were prepared with a CODEP B-1 aluminide coating. The alumina precoat was deposited on both the internal and external surfaces of the specimens by the electrophoresis technique. All other aspects of the coating application process conformed to General Electric Company Specification No. F50T58-S1. The resulting coating thickness was approximately 0.05mm (0.002 inch). The coated specimens were given the following heat treatment:

1218°C (2225°F)/2 hours vacuum/argon quench to room temperature

1093°C (2000°F)/4 hours vacuum/argon quench to room temperature

Coating cycle as per G.E. Specification No. F50T58-S1

843°C (1550°F)/16 hours vacuum/furnace cool to room temperature.

The specimen processing and heat treatment are also summarized in Table II of Appendix 1.

B. Fatigue Tests

The fatigue test program involved isothermal strain cycling to establish the four basic types of creep-fatigue life relationships defined by the strainrange partitioning method (2). In this paper, the four basic types of reversed inelastic strain, $\Delta\epsilon_{PP}$, $\Delta\epsilon_{PC}$, $\Delta\epsilon_{CP}$, and $\Delta\epsilon_{CC}$, are referred to as PP, PC, CP, and CC, respectively. The idealized stress-strain hysteresis loops for these four basic types of deformation are illustrated in Figure 2. The PP, PC, CP, and CC types of strainrange-fatigue life relationships were obtained by conducting HRSC, CCCR, TCCR, and UCCR types of tests, respectively, which are defined in Appendix 1.

The basic test program for the present study was conducted at 1000°C (1832°F) and in an ultrahigh vacuum environment below 10^{-7} torr. On the basis of the results obtained from this basic program, similar tests were conducted at 871°C (1600°F) in a poorer vacuum (approximately 10^{-6} torr) to determine the effect of the variation of these parameters on the four basic types of creep-fatigue life relationships defined by the strainrange partitioning method. In order to more completely define the effect of temperature on low cycle fatigue life, a series of HRSC tests was conducted on uncoated material at a range of temperatures from the ambient to 1000°C (1832°F) in the poorer vacuum. Values of the modulus of elasticity used to calculate the elastic strains at each test temperature are presented in Table 1.

Equipment and procedures used for the vacuum thermal fatigue tests in this program have been described in detail previously (3,4). Briefly, the test apparatus was designed to perform completely reversed push-pull fatigue tests on hourglass-shaped specimens using independently programmable temperature and strain control. Temperature was programmed using a thyatron-controlled 50 KV AC transformer for direct resistance heating of the specimen, while diametral strain was controlled directly using an LVDT-type extensometer coupled to a programmable, closed-loop, electrohydraulic servosystem. The measured specimen diameter was compensated electronically for thermal expansion so that net mechanical strain was controlled directly. Load, diameter and temperature were recorded continuously, with load-diameter hysteresis loops being obtained at periodic intervals during each test.

Tests were conducted over a range of strain amplitudes (as measured by the width of the hysteresis loop at zero load) versus cycles to failure. All HRSC tests were conducted at approximately 1.0 Hz. For the CCCR and TCCR tests, the time required to reverse the creep portion of the cycle by plastic strain and then initiate the creep portion again was one second or less. For the UCCR tests, the time required to initiate creep in the reversed direction was also one second or less. Fatigue failure was defined in all cases as complete separation of the specimens into two pieces. Fractured specimens were sectioned longitudinally and examined metallographically to evaluate the character of the microstructural damage associated with each of the applied cycles.

C. Supplementary Mechanical Property Tests

The mechanical properties of the Rene' 80 material used in this program are presented in Table III of Appendix 1. Supplementary vacuum tensile and creep-rupture tests were also conducted in this study to provide baseline characterization data. All of the supplementary tests were conducted in ultrahigh vacuum (below 10^{-7} torr) at 871°C (1600°F) and 1000°C (1832°F) using tubular hourglass-shaped specimens identical to those used for the fatigue tests. The tensile tests were conducted on both coated and uncoated specimens using a crosshead extension rate approximately equivalent to the frequency of the HRSC fatigue tests (1.0 Hz). The creep-rupture tests were conducted at constant load on coated and uncoated specimens.

III RESULTS AND DISCUSSION

A. Fatigue Test Results

The fatigue test results are presented in Table IV of Appendix 1. Note that in Table IV, eight CCCR tests were conducted on uncoated material at 1000°C (1832°F) instead of the usual five. Three extra tests (89U-PC-1, 94U-PC-14 and 97U-PC-15) were conducted here because analysis of the data for the first five tests indicated that drift may have occurred in the zero point for the load and strain control settings, resulting in erroneous readings. Thus, the values of total, inelastic, and partitioned inelastic strainrange for these five tests may be in error.

The ultrahigh vacuum fatigue test results from Table IV of Appendix 1 are plotted against longitudinal strainrange in Figures 3 through 6. For the remainder of the discussion, the term strainrange always refers to longitudinal strainrange. Each figure contains three different graphs including a plot and a least squares fit of total strainrange versus observed cycles to failure, inelastic strainrange versus observed cycles to failure, and partitioned inelastic strainrange versus life relationships computed using the interaction damage rule (5). Figures 3 and 4 contain the results of tests conducted at 1000°C (1832°F) on uncoated and coated material, respectively, while Figures 5 and 6 contain the results of tests conducted at 871°C (1600°F) on uncoated and coated material, respectively.

For the tests conducted at 1000°C (1832°F), Figures 3 and 4, the results indicate that the relative positions of the failure lives for the four basic types of strainrange components (PP, PC, CP and CC) change little as a result of the presence of the aluminide coating. In all instances, PP deformation was the least damaging, while PC deformation was

the most damaging by approximately an order of magnitude difference in number of cycles to failure. The CP and CC lines were quite close together and fell between the PC and PP lines, ranging from 2/3 to 1/2 order of magnitude below the PP line. A difference was observed between the coated and uncoated materials, however, in that for the values of inelastic and partitioned inelastic strainrange included in this study for uncoated material, the lines for CP and CC approached the PP line at the low strainrange values, Figures 3b and 3c.

The results of the tests conducted at 871°C (1600°F), Figures 5 and 6, were consistent with those conducted at 1000°C (1832°F) in that the aluminide coating had little effect on the relative positions of the failure lives for the four basic types of strainrange components. In all cases, PP deformation was the least damaging. Unlike the 1000°C (1832°F) results, however, the PC and CP lines were both comparable, ranging from 1/2 to 1 order of magnitude below the PP line. In terms of total and inelastic strainrange, the CC results were somewhat comparable to those for PC and CP, but the partitioned inelastic strainrange results indicated that CC was less damaging than PC and CP by approximately 1/2 order of magnitude at the higher strainrange values. Manson and Halford (6) have made an analysis utilizing strainrange partitioning of the low cycle fatigue data generated independently by Lord and Coffin on uncoated Rene' 80 at 871°C (1600°F). They determined that the partitioned lives for the 0.0032 strainrange at this temperature were $N_{PP} = 600$, $N_{CP} = 450$, $N_{PC} = 190$ and $N_{CC} = 80$. With the exception of the N_{CC} results, these values agree quite closely with the data presented in Figure 5c. This indicates that the method of strainrange partitioning has potential as a unifying framework around which the many factors concerning fatigue at elevated temperatures can be coherently structured.

The results for each of the basic types of deformation have been plotted separately in Figures 7 through 10 in terms of total strainrange versus observed cycles to failure and partitioned inelastic strainrange versus life relationship computed using the interaction damage rule (5). For each of these plots, a least squares fit was made of all of the data. These least squares lines suggest that, for all four basic types of deformation, there was little difference between coated and uncoated material at 1000°C (1832°F) and 871°C (1600°F) and further, there was little effect of temperature on the fatigue results. These results were not unexpected in that the ultrahigh vacuum test atmosphere nullified the effect of oxidation behavior, thus minimizing possible differences in fatigue behavior.

To summarize these fatigue results more clearly, the least squares lines shown in Figures 7 through 10 are included in the composite plot of Figure 11. These results indicate that PP deformation resulted in the least damaging type of cycling. When a time-dependent creep component was introduced into the cycle, however, an effect was observed which was dependent upon which portion of the cycle contained the creep component. The PC type of deformation, in which creep was introduced in the compressive portion of the cycle, was most damaging, resulting in failure lives one order of magnitude below those for PP deformation. The CP type deformation, in which creep was introduced in the tensile portion of the cycle, resulted in failure lives slightly higher than those for PC, i.e., slightly less than an order of magnitude below those for PP. The least damaging of the creep type cycling was CC, in which creep occurred both in the tensile and compressive portions of the cycle. It resulted in failure lives approximately 1/2 an order of magnitude below those for PP.

The results for the HRSC tests conducted at a number of different temperatures on uncoated material in a poorer vacuum (approximately 10^{-6} torr) are shown in Figure 12. This figure contains a plot of total strainrange versus observed cycles to failure and a plot of inelastic strainrange versus observed cycles to failure. No tests were conducted under these conditions at 871°C (1600°F), but the least squares lines from Figure 5 for the ultrahigh vacuum tests have been included for comparative purposes. The results for inelastic strainrange indicate a decrease in fatigue life as temperature is reduced. It has been generally acknowledged that, in the absence of time-dependent deformation (creep), a material's ductility will be an indicator of its relative fatigue resistance, with a decrease in ductility usually resulting in a decrease in fatigue life (7). Ductility results for cast Rene' 80 indicate a decrease with temperature from 1000°C (1832°F) (8). Thus, the inelastic strainrange results for Rene' 80 do reflect the decrease in fatigue life with decreasing ductility.

B. Microstructural Observations

All the fatigue specimens failed within the hourglass areas. There was no evidence of the specimen geometry change known as "barrelling," which is characterized by an increase in specimen diameter adjacent to the center of the original hourglass configuration. This effect has been observed in 304 stainless steel (9,10) and tantalum-base materials (3,4). Metallographic examination was conducted on selected specimens and included light and scanning electron microscopy to aid in the interpretation of the fatigue results. The results indicated that microstructural damage varied with cycle type, test temperature and surface condition (coated versus uncoated), Figures 13 through 18.

Specimens tested with the PP type deformation (HRSC tests) exhibited primarily a transgranular fracture mode for all test temperatures and surface conditions. This is a common fracture mode for materials tested at high frequencies where creep deformation is negligible. This fracture mode reflects the fact that the PP deformation resulted in the highest fatigue lives. Transgranular crack propagation in a highly alloyed cast nickel-base superalloy such as Rene' 80 is retarded by the heavy matrix precipitation of the gamma-prime strengthening phase. For uncoated specimens, grain boundary areas at the specimen surface were common crack initiation sites, with the cracks becoming transgranular after a short distance, Figure 13a. Crack initiation was also observed at grain boundary microporosity, Figure 13b. After initiation in the grain boundary region, these cracks become transgranular. For coated specimens, considerable numbers of coating cracks were observed leading to transgranular crack propagation, Figure 14. Since the fatigue results for the PP type tests, Figure 7, indicated no appreciable differences in failure times as a function of surface condition, the presence of the aluminide coating and its attendant cracks did not degrade the PP fatigue life of this alloy.

Specimens tested with the PC type deformation (CCCR tests) exhibited a predominantly intergranular fracture mode. In general, intergranular crack initiation and propagation occur at a faster rate than transgranular cracking in nickel-base superalloys, and the presence of this fracture mode in PC specimens suggests why this type of strain cycling resulted in lower fatigue lives than the PP type. At 1000°C (1832°F), there was considerable evidence of grain boundary sliding which took place during the compressive (creep) portion of the cycle resulting in steps or grain extrusions along the sides of the specimens. Examples of these extrusions are shown in Figure 15 for the uncoated material and Figure 16 for the coated material. Specimens tested at 871°C (1600°F) did not exhibit the extent of grain boundary sliding seen at 1000°C (1832°F). Considerable numbers of surface cracks were observed in the coated specimens, but the presence of the aluminide coating and its attendant cracks did not degrade the PC fatigue life of this alloy (Figure 8).

Specimens tested with the CP type deformation (TCCR tests) exhibited primarily an intergranular type of fracture mode both at 1000°C (1832°F) and 871°C (1600°F), Figure 17. Unlike materials such as iron base alloy A-286 and 304 stainless steel, which exhibit intergranular fracture resulting from internal grain boundary "decohesion" as a consequence of CP cycling (9,10), specimens of Rene' 80 studied in the present investigation usually exhibited some form of surface grain boundary cracking into the specimen. High magnification SEM analyses of Rene' 80 specimens revealed no internal grain boundary "decohesion" or cavitation in this alloy. In addition, the CP specimens did not exhibit the grain boundary sliding observed in the PC specimens, and this may explain why the CP failure lives were slightly higher. The presence of numerous coating cracks did not result in an appreciable degradation in CP fatigue life, Figure 9.

Specimens tested with the CC type deformation (UCCR tests) exhibited different fracture modes depending on the test temperature. At 1000°C (1832°F), the fracture mode was primarily intergranular, while at 871°C (1600°F) the fracture mode was transgranular. Examples of these various modes are shown in Figure 18. There was no evidence of grain boundary extrusion at the specimen surface or of internal grain boundary decohesion or cavitation in these specimens.

C. Supplementary Mechanical Property Tests

The results of the supplemental vacuum tensile and creep rupture tests are presented in Tables 2 and 3. The ultimate tensile strengths obtained in the supplementary tests at 1000°C (1832°F) were much higher than that shown for this material in Table III of Appendix 1 because of the considerably higher strain rate (equivalent to 1.0 Hz) used in the supplementary tests.

VI SUMMARY

The results of ultrahigh vacuum, low cycle fatigue tests conducted on uncoated and CODEP B-1 aluminide coated specimens of Rene' 80 nickel-base superalloy at 1000°C (1832°F) and 871°C (1600°F) indicated little effect of coating or temperature on the fatigue properties. There was, however, a significant effect on fatigue life as a function of strain cycle type. The method of strainrange partitioning offers an appropriate framework around which to correlate the effects of these strain cycle types. In terms of partitioned inelastic strainrange, the completely reversed plasticity type of strain cycling (PP) resulted in the highest fatigue lives. When a time-dependent creep component was introduced into the cycle, an effect was observed which was dependent upon which portion of the cycle contained the creep component. When creep was introduced in the compressive portion of the cycle (PC), failure lives were approximately one order of magnitude below those for PP deformation. When creep was introduced in the tensile portion of the cycle (CP), failure lives were slightly higher than those for the PC deformation, i.e., slightly less than an order of magnitude below those for PP. The least damaging of the creep type cycling was CC, in which creep occurred both in the tensile and compressive portions of the cycle resulting in failure lives approximately 1/2 order of magnitude below those for PP.

Metallographic evaluation indicated that microstructural damage varied with cycle type and test temperature. Specimens tested with the PP type deformation exhibited primarily a transgranular fracture mode. Specimens tested with the PC type deformation exhibited a predominantly intergranular fracture mode. At 1000°C (1832°F), there was considerable evidence of grain boundary sliding which took place during the compressive (creep) portion of the cycle resulting in steps or grain extrusions along the sides of the specimens. Specimens tested at 871°C (1600°F) did not evidence the same extent of grain boundary extrusion. Specimens tested with the CP type deformation exhibited an intergranular type of fracture mode at both test temperatures. Specimens tested with the CC type deformation exhibited different fracture modes depending on the test temperature. At 1000°C (1832°F), the fracture mode was intergranular, while at 871°C (1600°F), the fracture mode was transgranular. At both test temperatures, considerable evidence of surface cracking was observed in coated specimens for all the types of strain cycling.

V REFERENCES

1. M. Gell and G. R. Leverant, "Mechanisms of High-Temperature Fatigue," Fatigue at Elevated Temperatures, ASTM STP 520, ASTM, 1973, pp. 37-67.
2. S. S. Manson, G. R. Halford, and M. H. Hirschberg, "Creep-Fatigue Analysis by Strainrange Partitioning," Design for Elevated Temperature Environment, American Society of Mechanical Engineers, 1971, pp. 12-24.
3. K. D. Sheffler and G. S. Doble, TRW Inc., "Influence of Creep Damage on the Low Cycle Thermal-Mechanical Fatigue Behavior of Two Tantalum Base Alloys," 1972, NASA Report No. NAS-CR-121001, TRW Report No. ER-7592.
4. K. D. Sheffler and G. S. Doble, "Thermal Fatigue Behavior of T-111 and ASTAR 811C in Ultrahigh Vacuum," Fatigue at Elevated Temperatures, ASTM STP 520, ASTM, 1973, pp. 491-499.
5. S. S. Manson, "The Challenge to Unify Treatment of High Temperature Fatigue - A Partisan Proposal Based on Strainrange Partitioning," Fatigue at Elevated Temperatures, ASTM STP 520, ASTM, 1973, pp. 744-782.
6. S. S. Manson and G. R. Halford, Discussion appearing in Journal of Pressure Vessel Technology, Trans. ASME, February 1976, p. 83, of paper by J. T. Fong, "Energy Approach for Creep-Fatigue Interactions in Metals at High Temperature," Journal of Pressure Vessel Technology, Trans. ASME, Vol. 96, Series J, No. 3, August 1975, p. 214.
7. S. S. Manson, "Fatigue: A Complex Subject-Some Simple Approximations," Experimental Mechanics, Vol. 5, No. 7, July 1965, pp. 193-226.
8. L. J. Fritz, Metcut Research Associates, Inc., "Tensile and Creep-Rupture Properties of Engineering Alloys at Elevated Temperatures," Report prepared under Contract NAS-3-18911 for NASA-Lewis Research Center, Cleveland Ohio 44135.
9. K. D. Sheffler, TRW Inc., "Vacuum Thermal-Mechanical Fatigue Testing of Two Iron Base High Temperature Alloys," 1974, NASA Report No. NAS-CR-13424, TRW Report No. ER-7696.

10. K. D. Sheffler, "Vacuum Thermal-Mechanical Fatigue Behavior of Two Iron-Base Alloys," Thermal Fatigue of Materials and Components, ASTM STP 612, D. A. Spera and D. F. Mowbray, eds., ASTM, 1976, pp. 214-226.

Acknowledgments

This work was performed in the Materials Technology Laboratory of TRW Inc. under the financial sponsorship of the U.S. Army Air Mobility Research and Development Laboratory for the National Aeronautics and Space Administration, Contract NAS-3-17830. The project manager for NASA was Dr. G. R. Halford of the Lewis Research Center. The experimental work was performed by Mr. J. W. Sweeney of TRW Inc.

TABLE 1

MODULUS OF ELASTICITY USED TO CALCULATE ELASTIC STRAIN IN
LOW CYCLE FATIGUE TESTS CONDUCTED IN THIS PROGRAM (1)

<u>Test Temperature</u>		<u>Modulus of Elasticity, 10³ MPa</u>
<u>°C</u>	<u>°F</u>	
Room	Room	206.7
204	400	198.4
538	1000	181.1
649	1200	174.4
760	1400	166.5
871	1600	156.9
1000	1832	144.1

- (1) Modulus of elasticity data obtained from General Electric Co. Aircraft Engine Group, Materials Data Unit, Cincinnati, Ohio 45215, October 8, 1974.

TABLE 2

SUPPLEMENTARY TENSILE PROPERTIES OF RENE' 80 MATERIAL
USED IN THIS PROGRAM

<u>Test Temperature</u>		<u>Yield Strength at 0.2% Offset</u>	<u>Ultimate Tensile Strength</u>	<u>Reduction of Area</u>
<u>°C</u>	<u>°F</u>	<u>MPa</u>	<u>MPa</u>	<u>%</u>
<u>Uncoated Specimens</u>				
871	1600	547	736	27.5
871	1600	530	768	30.1
1000	1832	236	429	33.5
1000	1832	230	423	32.8
<u>Coated Specimens</u>				
871	1600	575	761	27.8
871	1600	552	786	20.8
1000	1832	230	465	29.7
1000	1832	234	483	31.2

TABLE 3

SUPPLEMENTARY CREEP RUPTURE PROPERTIES OF RENE' 80 MATERIAL
USED IN THIS PROGRAM

<u>Test Temperature</u>		<u>Applied Stress</u>	<u>Rupture Life</u>	<u>Reduction of Area</u>
<u>°C</u>	<u>°F</u>	<u>MPa</u>	<u>Hours</u>	<u>%</u>
<u>Uncoated Specimens</u>				
871	1600	345	2.1	31.0
871	1600	241	84.8	23.0
1000	1832	207	0.7	29.7
1000	1832	172	1.0	31.1
1000	1832	103	48.7	29.5
1000	1832	103	52.6	32.1

Coated Specimens

871	1600	345	9.4	28.3
871	1600	310	66.6	20.6
1000	1832	159	15.4	29.6
1000	1832	103	60.0	31.1
1000	1832	103	21.6	35.1

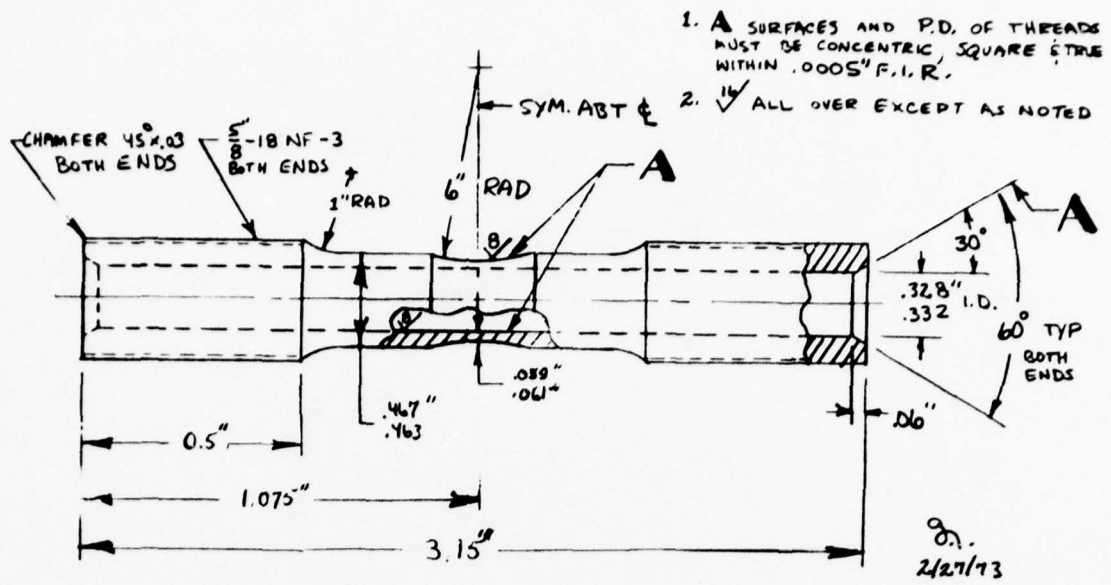


Figure 1. Fatigue test specimen

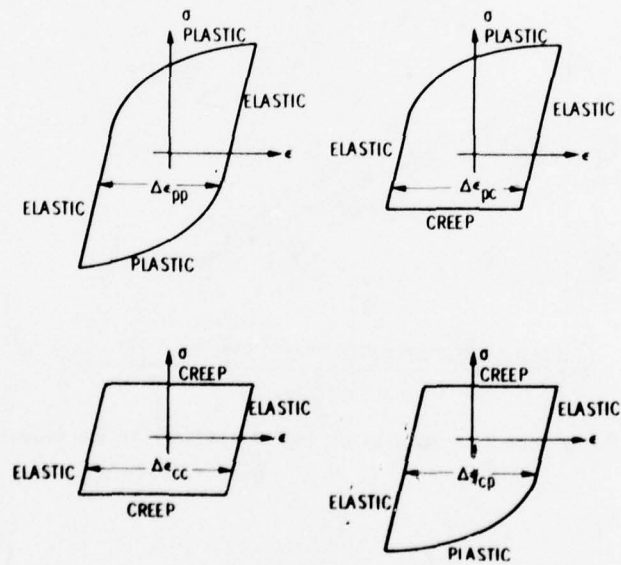


Figure 2. Idealized hysteresis loops for the four basic types of inelastic strainrange.

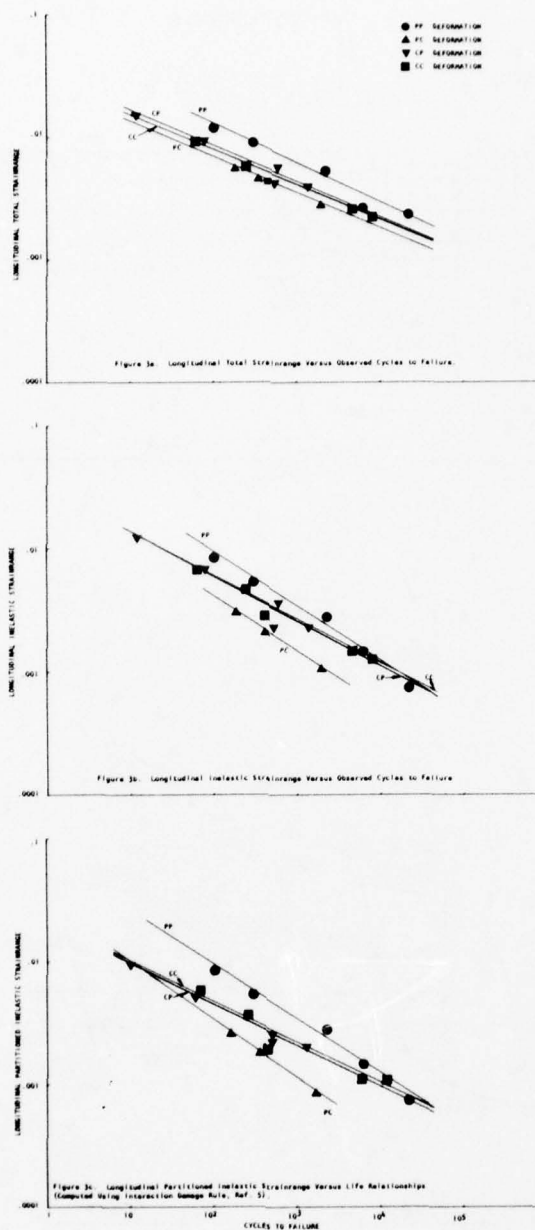


Figure 3. Rene' 80 Fatigue Test Results at 1000°C (1832°F) In the Uncoated Condition.

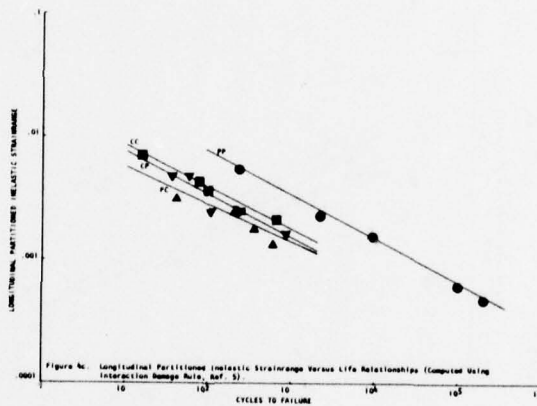
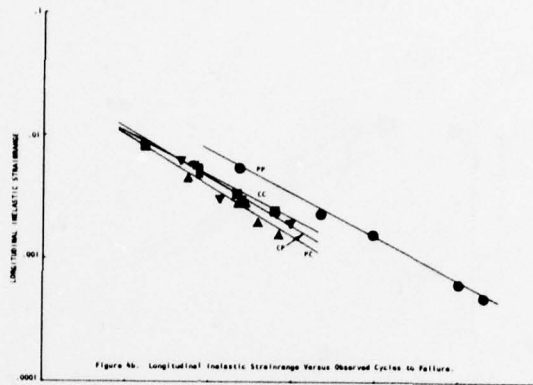
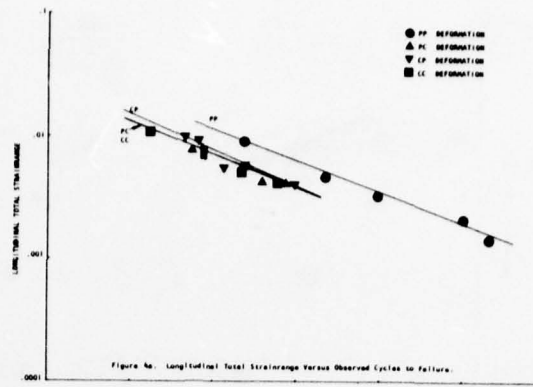


Figure 4. Rene' 80 Fatigue Test Results at 1000°C (1832°F) In the Coated Condition.

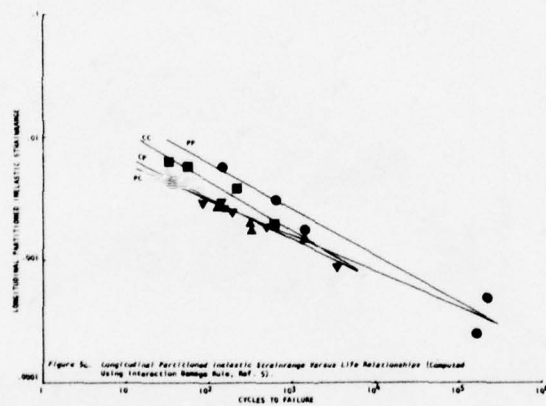
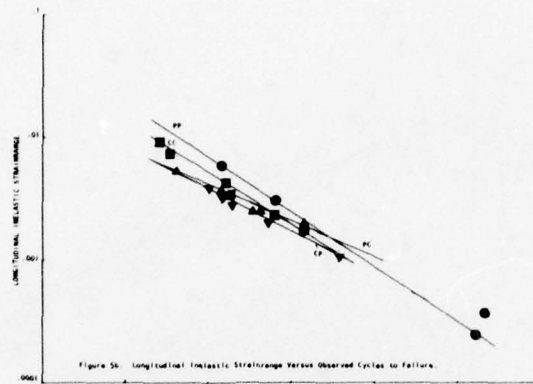
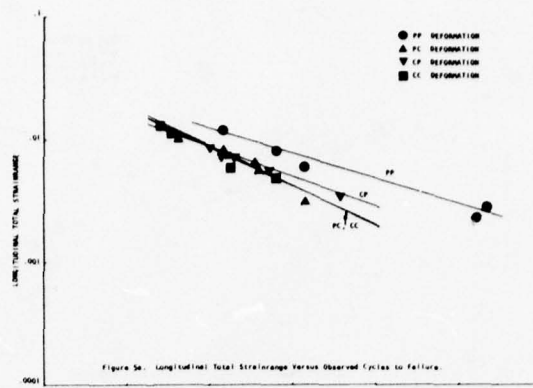


Figure 5. Rene' 80 Fatigue Test Results at 871°C (1600°F) in the Uncoated Condition.

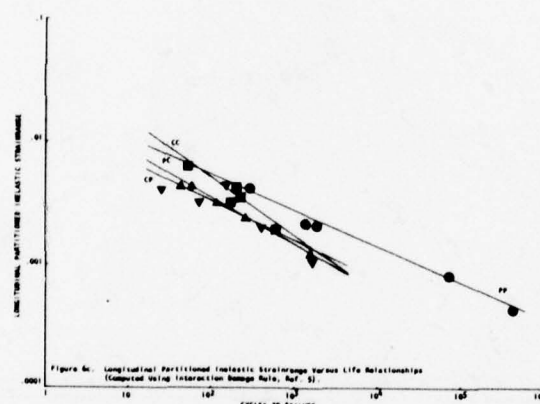
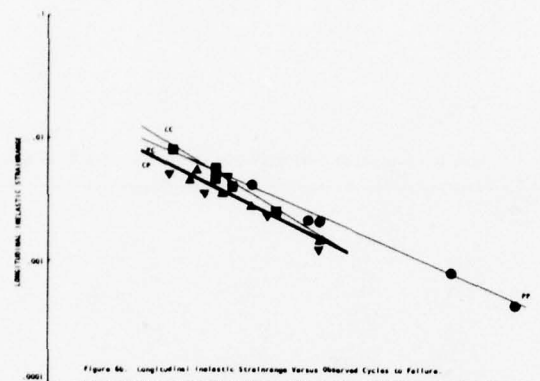
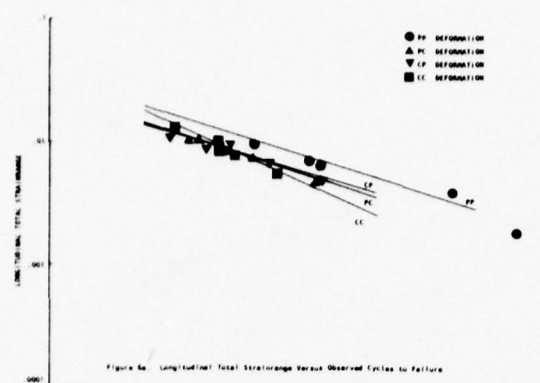


Figure 6. Rene' 80 Fatigue Test Results at 871°C (1600°F) In the Coated Condition.

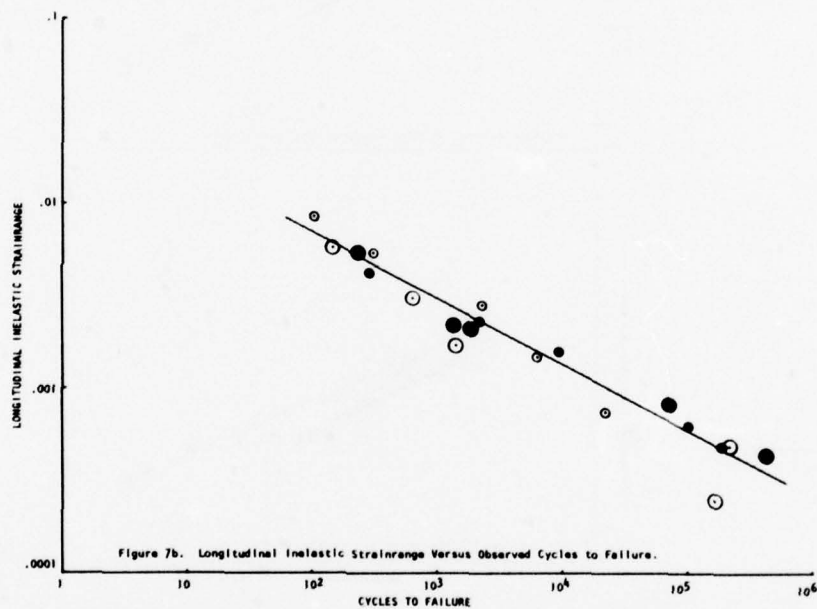
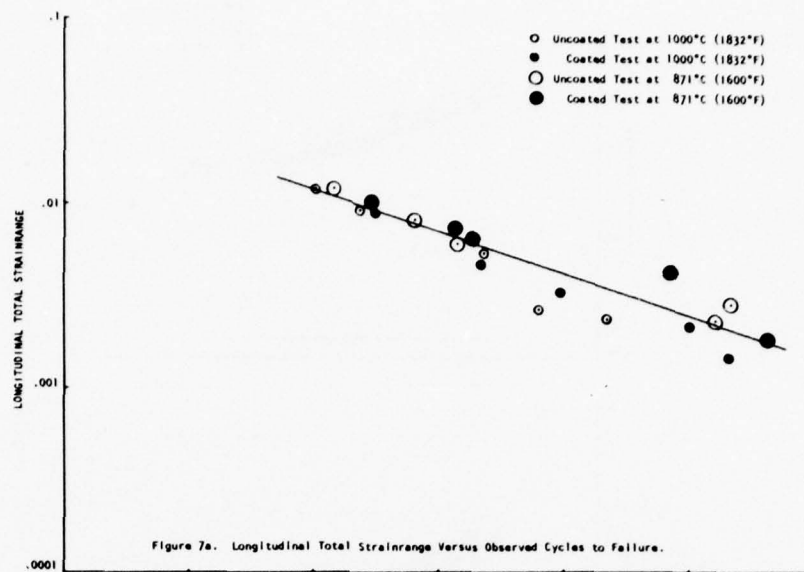


Figure 7. Rene' 80 Fatigue Test Results at 1000°C (1832°F) and 871°C (1600°F) for Uncoated and Coated Specimens Tested with the $\Delta\epsilon_{pp}$ Type Deformation.

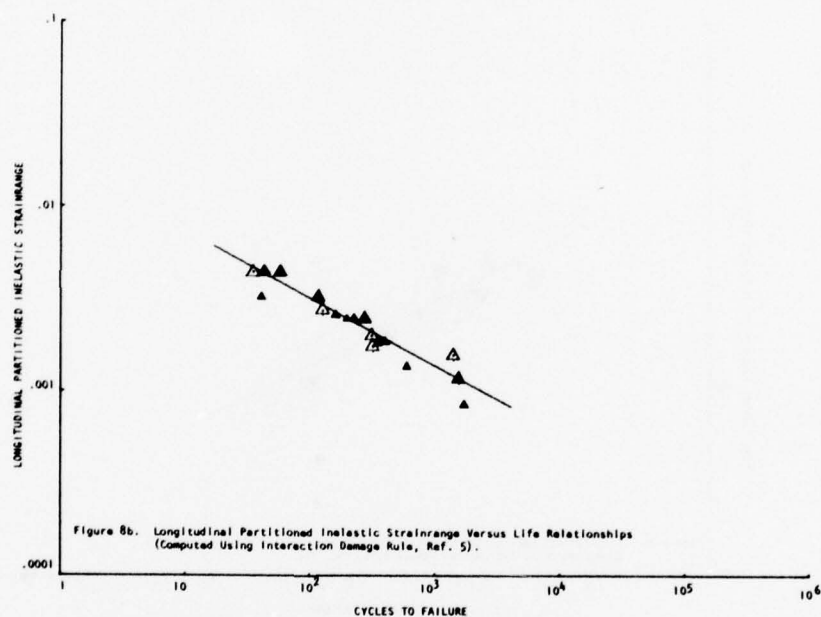
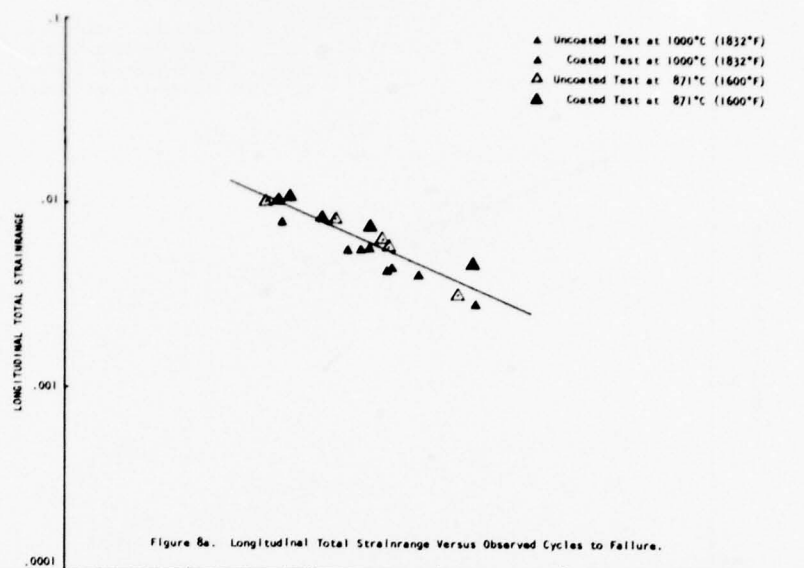


Figure 8. Rene' 80 Fatigue Test Results at 1000°C (1832°F) and 871°C (1600°F) for Uncoated and Coated Specimens Tested with the $\Delta\epsilon_{pc}$ Type Deformation.

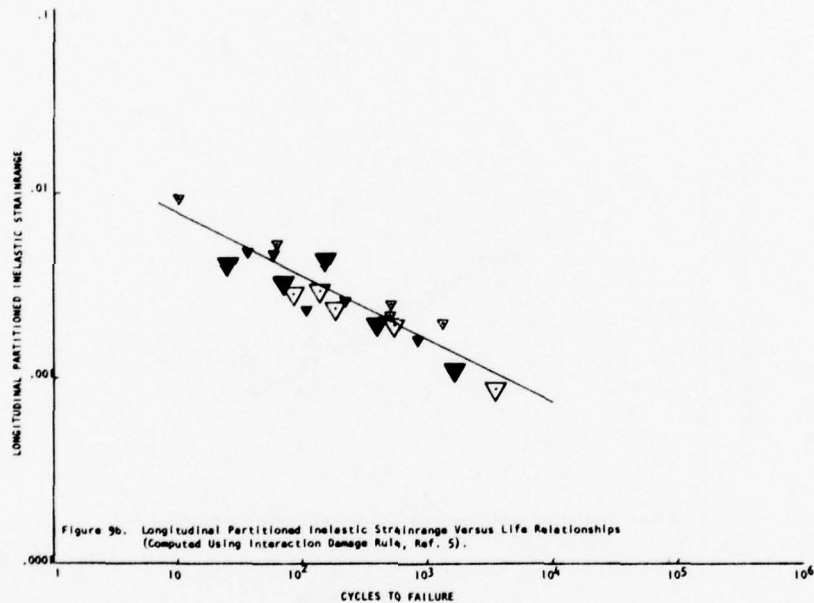
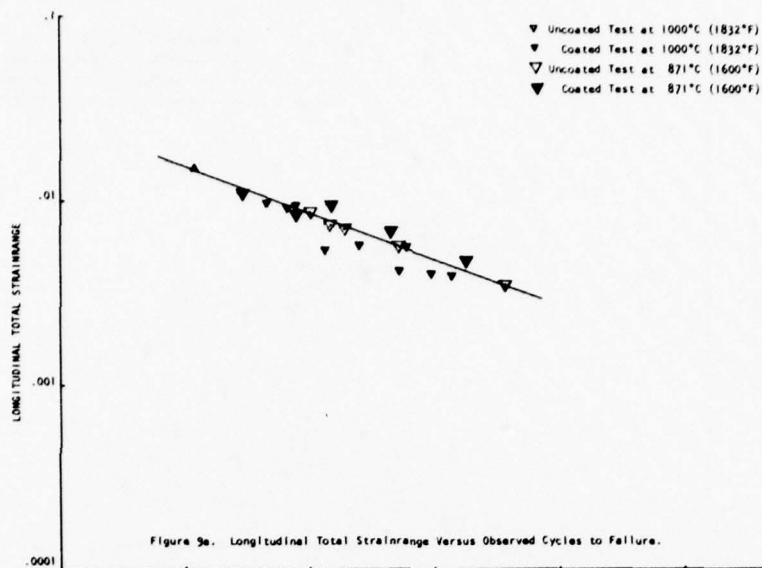


Figure 9. Rene' 80 Fatigue Test Results at 1000°C (1832°F) and 871°C (1600°F) for Uncoated and Coated Specimens Tested with the $\Delta\epsilon_{cp}$ Type Deformation

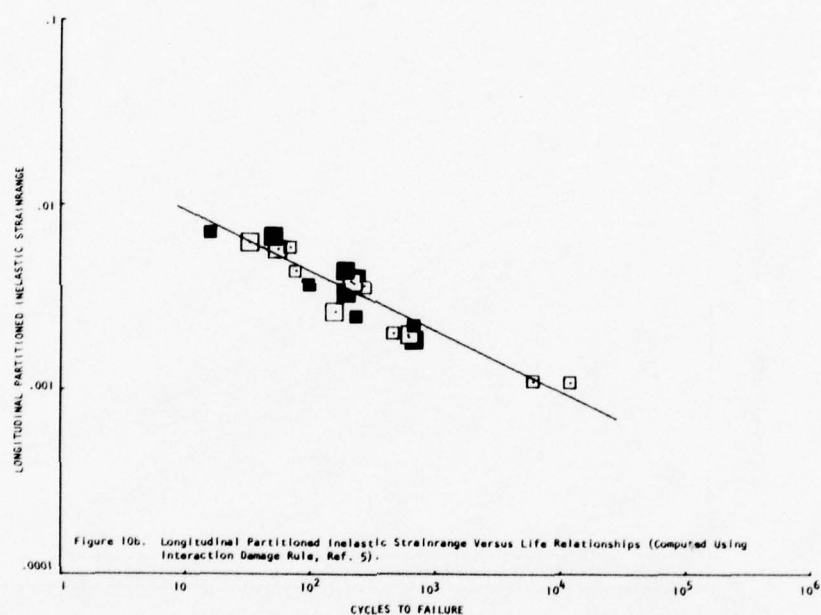
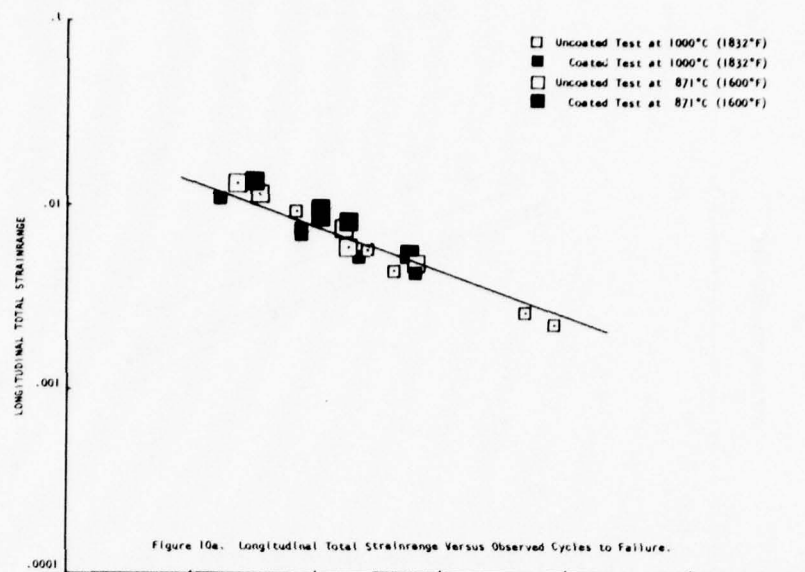


Figure 10. Rene' 80 Fatigue Test Results at 1000°C (1832°F) and 871°C (1600°F) for Uncoated and Coated Specimens Tested with the $\Delta\epsilon_{CC}$ Type Deformation.

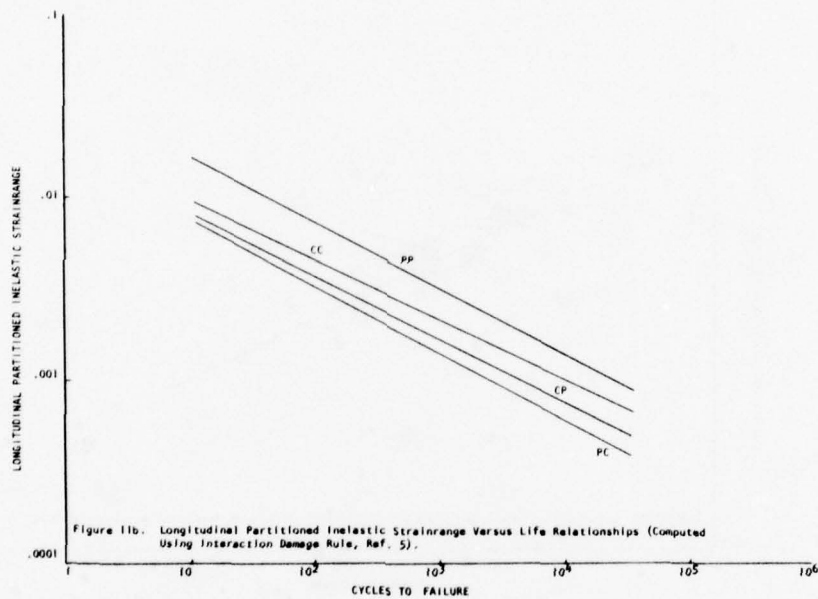
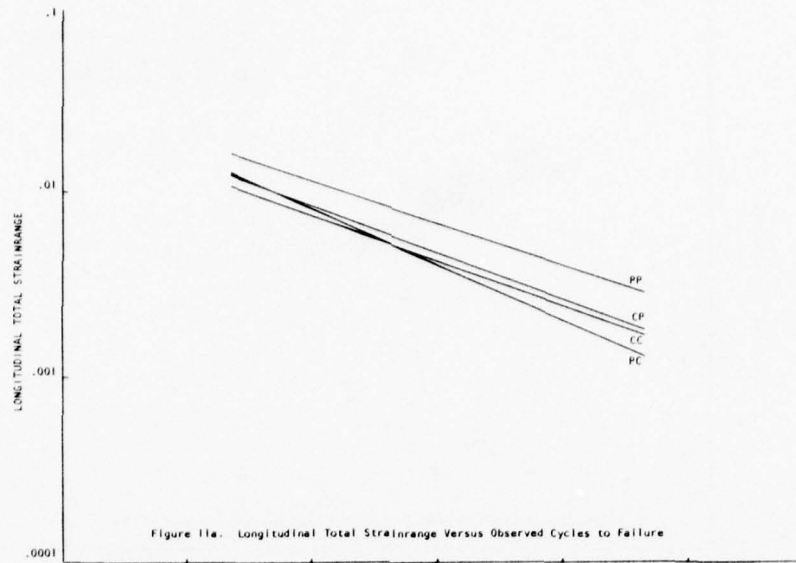


Figure 11. Composite Plot of Least Squares Lines Through Fatigue Data Shown in Figures 7-10.

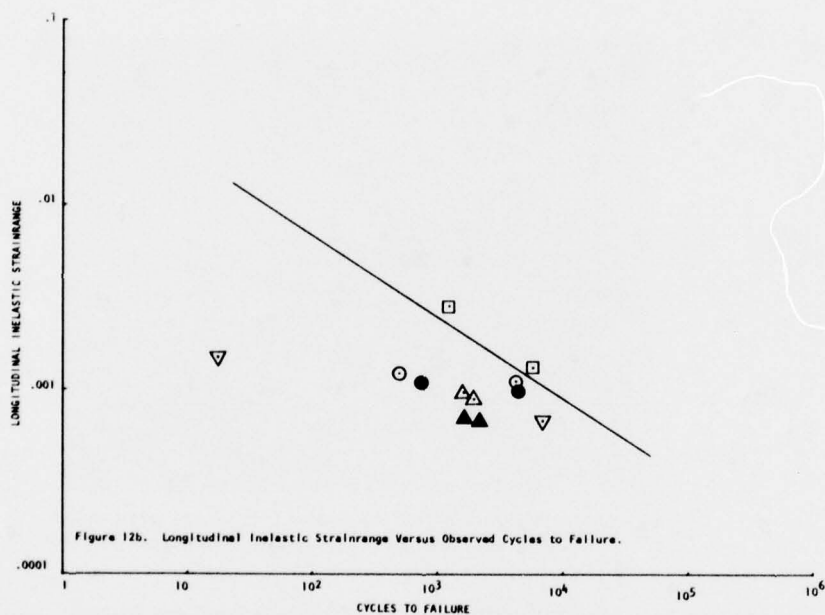
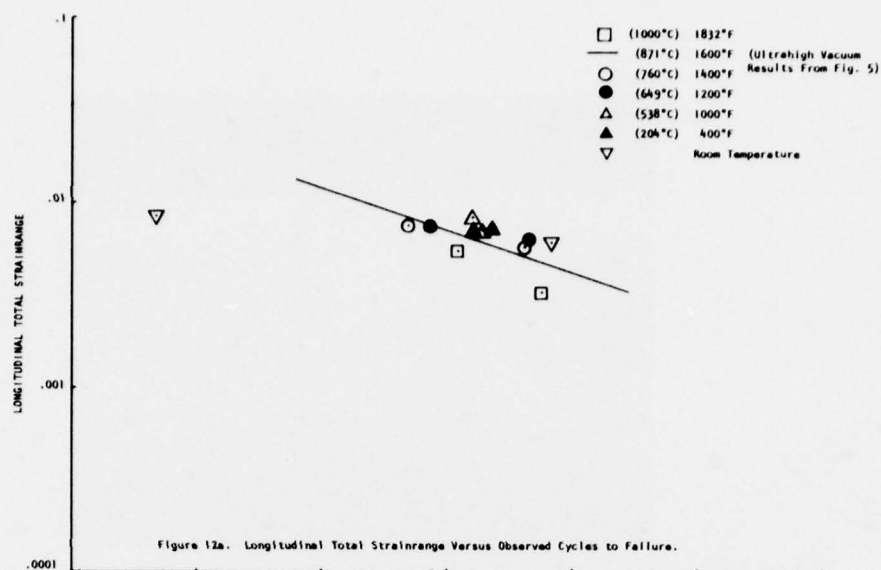
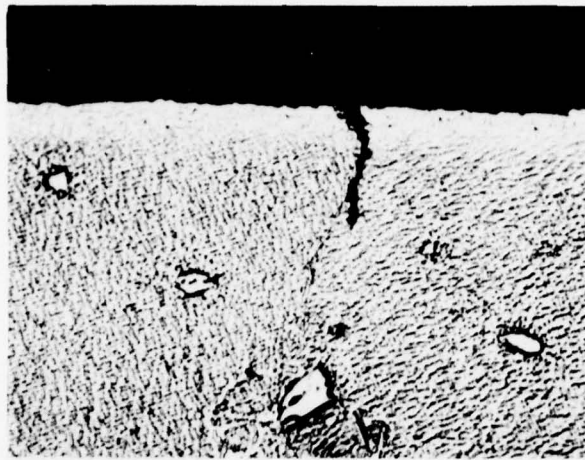
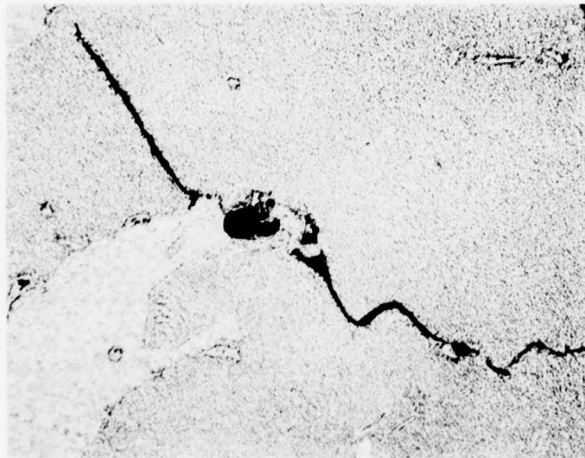


Figure 12. Rene' 80 Fatigue Test Results at Various Temperatures for Uncoated Material Tested in Poorer Vacuum (Approximately 10^{-6} Torr) with the $\Delta\epsilon_{pp}$ Type Deformation.



a) Surface Grain Boundary Crack Initiation with Crack Branching Off Into Matrix Region, 800X Magnification.



b) Grain Boundary Porosity Crack Initiation with Crack Branching Off Into Matrix Region, 400X Magnification.

Figure 13. Light photomicrographs of fatigue specimen 8U-PP-7, tested at 1000°C (1832°F), 1.033 Hz, total strainrange of 0.00247. Failure occurred after 22,115 cycles. Fry's etch.

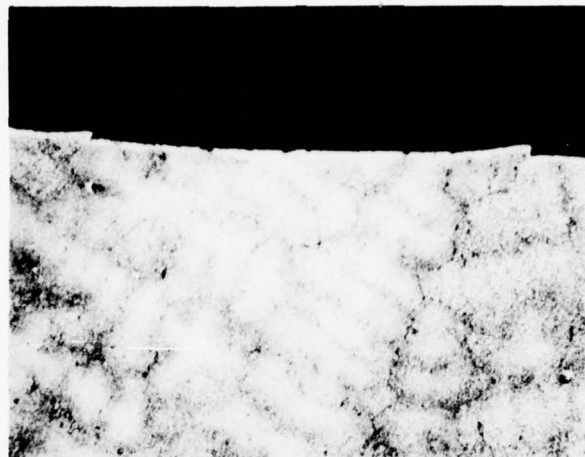


a) Unetched

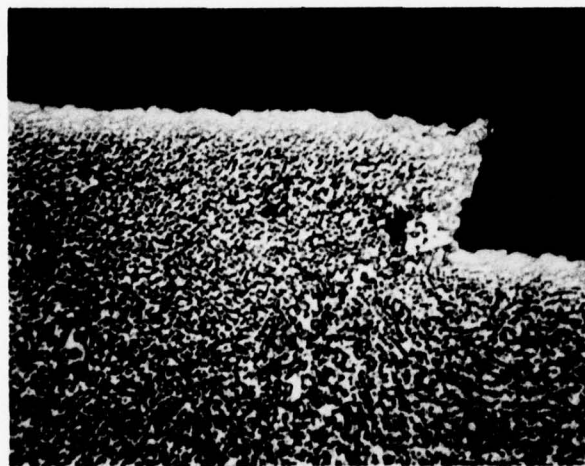


b) Fry's etch

Figure 14. Light photomicrographs of fatigue specimen 51C-PP-6, tested at 871°C (1600°F), total strainrange of 0.00672. Failure occurred after 1860 cycles. Note coating cracks propagating transgranularly into specimen, 500X magnification.

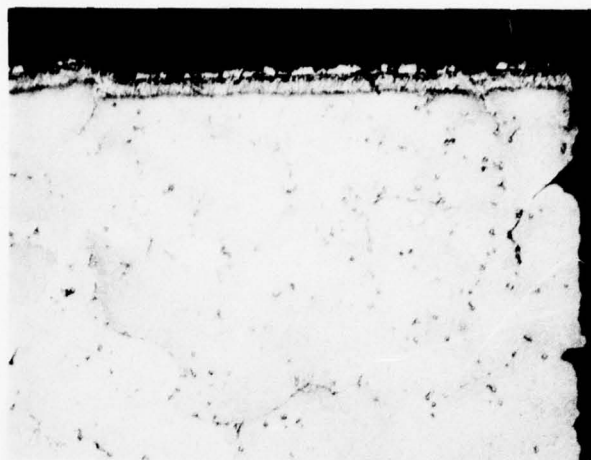


a) 80X Magnification

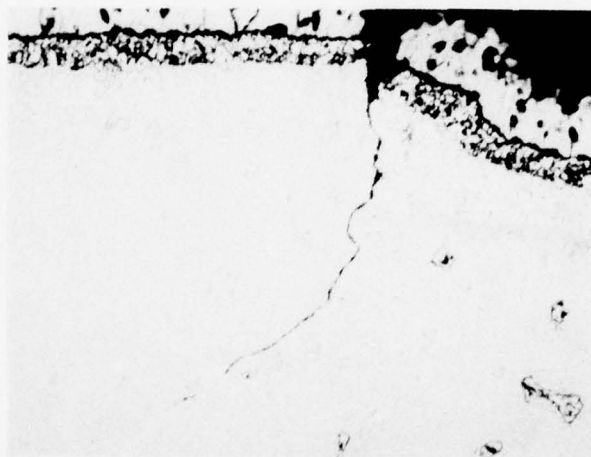


b) 800X Magnification

Figure 15. Light photomicrographs of uncoated fatigue specimen 10U-PC-2, tested at 1000°C (1832°F), total strainrange of 0.01999. Failure occurred after 19 cycles. Note grain extrusion as a result of PC deformation. Fry's etch.

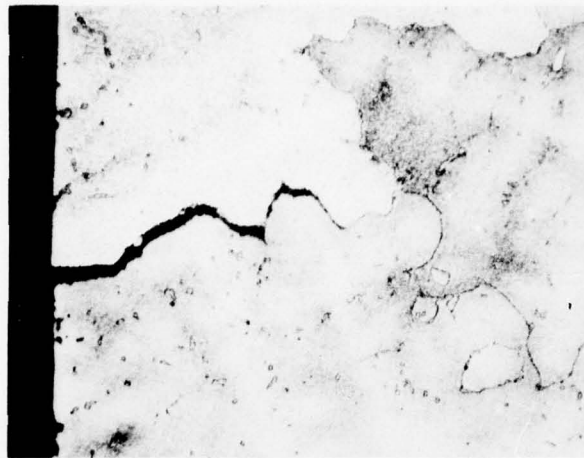


a) 100X Magnification

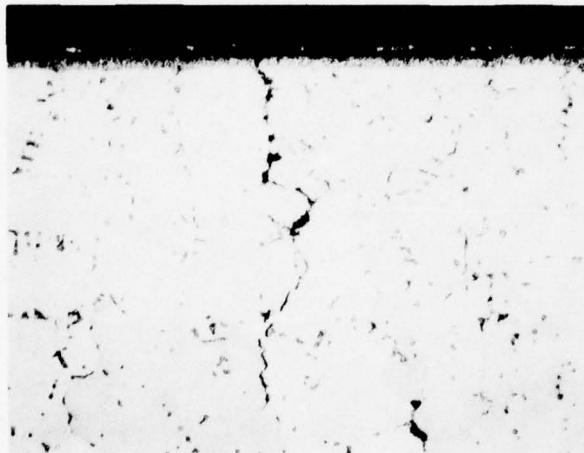


b) 500X Magnification

Figure 16. Light photomicrographs of coated fatigue specimen 57C-PC-2, tested at 1000°C (1832°F), total strainrange of 0.00450. Failure occurred after 386 cycles. Note grain extrusion and intergranular cracking as a result of PC deformation. Fry's etch.

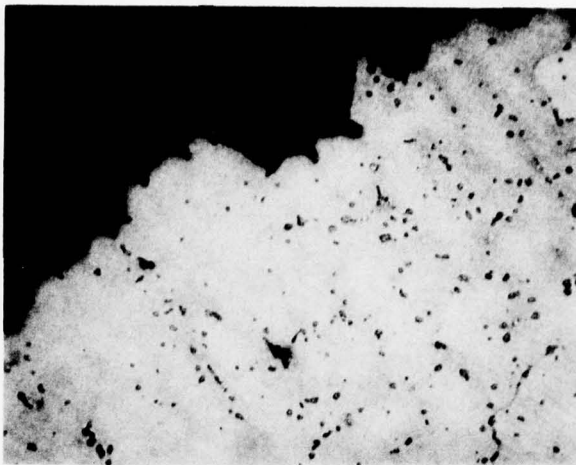


a) Uncoated specimen 31U-CP-6, tested at 871°C (1600°F), total strainrange of 0.00586, 530 cycles to failure.

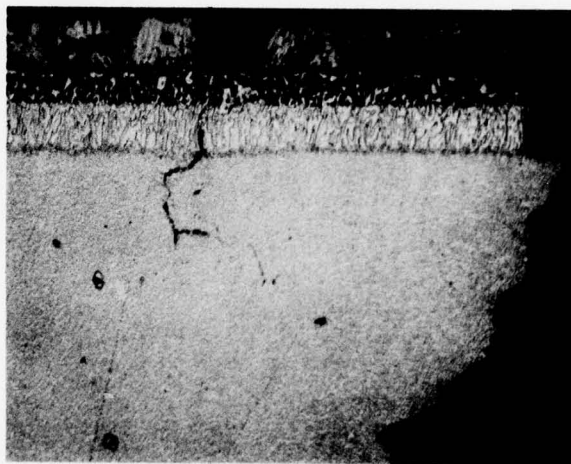


b) Coated specimen 62C-CP-1, tested at 871°C (1600°F), total strainrange of 0.00995, 150 cycles to failure.

Figure 17. Light photomicrographs of intergranular fracture mode in specimens tested with the CP type deformation. Fry's etch. 100X magnification.



a) Intergranular Fracture Mode in Coated Specimen 68C-CC-1, Tested at 1000°C (1832°F), .01135 Total Strainrange, 17 Cycles to Failure 100X



b) Transgranular Fracture Mode in Coated Specimen 69C-CC-2, Tested at 871°C (1600°F), .01005 Total Strainrange, 108 Cycles to Failure. 500X

Figure 18. Light Photomicrographs Showing Examples of Fracture Modes for Specimens Tested with the CC Type Deformation. Fry's etch.

STRAINRANGE PARTITIONING BEHAVIOR OF THE NICKEL-BASE SUPERALLOYS, RENE' 80 AND IN 100

G. R. Halford and A. J. Nachtigall, Engineers
 National Aeronautics & Space Administration
 Lewis Research Center
 21000 Brookpark Road
 Cleveland, OH 44135
 USA

ABSTRACT

A study has been made to assess the ability of the method of Strainrange Partitioning (SRP) to both correlate and predict high-temperature, low-cycle fatigue lives of nickel-base superalloys for gas turbine applications. Baseline data from strain-controlled, low-cycle fatigue tests are expressed in terms of the PP, PC, CP, and CC partitioned inelastic strainrange versus life relationships for coated and uncoated Rene' 80 at 1000°C, Gatorized (creep-formed) IN 100 at 760°C, and cast IN 100 at 925°C. SRP is shown to correlate the cyclic lives of the baseline tests to within factors of nearly two.

The partitioned strainrange versus life relationships for uncoated Rene' 80 and cast IN 100 have also been determined from the Ductility Normalized-Strainrange Partitioning (DN-SRP) equations. These were used to predict the cyclic lives of the baseline tests. Predicted and observed cyclic lives agreed to within factors of nearly three.

The life predictability of the method is also verified for cast IN 100 by applying the baseline results to the cyclic life prediction of a series of complex strain-cycling tests with multiple hold periods at constant strain. Predictions were within factors of two in cyclic life.

It is concluded that the method of SRP can correlate and predict the cyclic lives of laboratory specimens of the nickel-base superalloys evaluated in this program.

INTRODUCTION

Strainrange Partitioning (SRP) is a method for dealing with high-temperature low-cycle fatigue failures of metallic materials. Introduced in 1971 by Manson, Halford, and Hirschberg (Ref. 1) of the NASA-Lewis Research Center, it has been undergoing continual development since then. To-date, over 50 technical papers have been written on various aspects of the method. As a result, new dimensions in understanding, refinement of procedures, extension to new applications, or simply more laboratory specimen data for a variety of important engineering alloys have been added. Professor Manson, in his introductory paper (Ref. 2) to this Specialists Meeting, reviews the highlights of many of these past achievements and points to worthy areas for future exploration.

Although considerable experience has been gained with the use of the method of SRP at the laboratory level over the past 7 years, it seems likely that more will be required before the method can be used with confidence in the design of aeronautical gas turbine hardware and other high-temperature, high performance equipment. This AGARD Specialists Meeting thus represents a significant milestone in the development of the method because of the large number of independent laboratories that are reporting on their experiences with its use at the laboratory level of evaluation.

Owing to the nature of this Specialists Meeting, it is assumed that the reader is familiar enough with the basic concepts and terminology associated with the method of SRP that a review is not required herein. If additional background is needed, references 1 to 5 should be consulted. However, certain words are used frequently throughout this paper which are best defined at the outset so that the reader has a better understanding of the context in which they are used.

Baseline - Refers to the high-temperature, low-cycle fatigue tests and results used directly in the establishment of the four SRP inelastic strainrange versus life relationships.

Verification - Refers to the non-baseline high-temperature, low-cycle fatigue tests and results used to check how well the established SRP life relationships can be used to predict cyclic lives.

Correlation - Refers to how well the equations of the established SRP life relationships represent the individual baseline data. The smaller the deviation of the baseline data from the equations, the better the correlation.

Prediction - Refers to how well the equations of the established SRP life relationships represent the verification test results. The smaller the deviation of the verification data from the equations, the better the predictability. Since the Ductility Normalized-Strainrange Partitioning (DN-SRP) life relationships (Ref.6) did not use any information from the baseline tests, it is considered that predictions of the baseline results are being made when using the DN-SRP equations. These equations can also be used to predict the verification results.

The objectives of this paper were to determine how well the method of SRP can both correlate and predict the high-temperature, low-cycle fatigue lives of specimens of advanced gas turbine alloys. Two nickel-base superalloys were selected for this purpose: Rene' 80 with and without an aluminide (Codep B-1) coating, and IN 100 in the Gatorized (creep-formed) and cast conditions. The four partitioned inelastic strainrange versus life relationships (PP, PC, CP, and CC) were established for each alloy condition using a series of baseline stress-hold, strain-limited tests to introduce creep strains into the cycles. In addition, an evaluation was made of how well the life relations could be determined by the recently proposed DN-SRP equations.

A limited number of verification tests were also performed with specimens of cast IN 100 using a series of complex strain cycles involving multiple periods of constant strain hold which introduced creep through the process of relaxation. The verification tests were used to evaluate the predictability of the SRP method.

EXPERIMENTAL DETAILS

The high-temperature, low-cycle fatigue test results were obtained in the fatigue laboratory of the NASA-Lewis Research Center using closed-loop, servo-controlled, electro-hydraulic testing machines. Hirschberg has described this facility in detail in Ref. 7. Testing was performed in a still air environment using axially loaded specimens with diametral extensometry.

Specimens, Materials, and Temperatures

Two specimen geometries were employed, the tubular, hour-glass shaped specimens described in Ref. 7, and a smaller, solid hour-glass shaped specimen with a minimum test section diameter of 5 mm and a 40 mm hour-glass radius. Threaded ends were provided for gripping. Overall length was 75 mm. Two nickel-base superalloys were studied, each in two different conditions; cast Rene' 80 with and without an aluminide coating, and IN 100 in the Gatorized and cast conditions. The chemical compositions, processing and heat treatment, and mechanical properties at room temperature and the elevated temperature of interest for each alloy are presented in Tables I, II, and III respectively of Appendix 1.

Rene' 80 - The Rene' 80 specimens were supplied by TRW, Inc. under contract to NASA (Ref. 8). Enough specimens were prepared at the time for the testing program conducted in air and reported in this paper, and for the vacuum program conducted at TRW, Inc. and reported upon at this Specialists Meeting by Kortovich and Sheinker (Ref. 9). The intent of the air and vacuum programs was to establish a data base for assessing the effects of environment and protective coatings on the high-temperature low-cycle fatigue behavior of Rene' 80. The specimens were cast as individual solid bars and were subsequently machined to the tubular hour-glass shape. Half of the specimens were left uncoated and the remainder coated with an aluminide (Codep B-1) coating. Details of the coating process can be found in Ref. 8.

The coating thickness was approximately 0.05 mm. The stress and strain calculations for the coated specimens were based upon their room temperature dimensions prior to the application of the coating, i.e., it was assumed that the coating carried none of the applied load at the test temperature of 1000°C.

Gatorized IN 100 - IN 100 was tested in the Gatorized (creep-formed) condition. Small solid specimens of this alloy were machined from a segment of a gas turbine disk (provided by Pratt & Whitney Aircraft, Florida) that had been creepformed by the Gatorizing process.

The exact chemical composition, processing heat treatment, and mechanical properties are not known, although this batch of material would be expected to be similar to the Gatorized IN 100 material reported on at this Specialists Meeting by VanWanderham, Wallace, and Annis (Ref. 10) of Pratt & Whitney Aircraft, Florida. Tests were conducted at 760°C.

Cast IN 100 - Tubular, hour-glass shaped specimens of IN 100 were individually cast to near final dimensions. Approximately 0.2 mm thickness of material was machined from the inside and outside diameters to produce the finished test section dimensions. No heat treatment was applied to the cast specimens. Tests were conducted at 925°C.

SRP Test Procedures

The high-temperature, low-cycle fatigue tests were performed using the procedures recommended by Hirschberg and Halford (Ref. 5). Schematic stress-strain hysteresis loops are shown in Figs. 1(a)-(d) for the types of cycles used in conducting the baseline tests to establish the four SRP life relationships. The strain-controlled PP type test cycles (Fig. 1(a)) were applied using either a triangular or sinusoidal strain versus time waveform at a frequency of 0.5 to 1.0 Hz. In analyzing the results of the PP type tests, it was assumed that the imposed strain rates were high enough to preclude the occurrence of creep strain, thus producing inelastic strains that could be classified as plasticity. For the PC, CP, and CC type cycles, the creep strain was imposed by controlling the load on the specimen at a constant value until the desired creep strain limit was reached, whereupon, the loading direction was reversed and the other half of the cycle was imposed. If it was desired to impose creep strain in this portion of the cycle, the load was again held at a constant value until the desired opposite creep strain limit was attained, or if plasticity was desired, the specimen was rapidly loaded until the opposite strain limit was reached. The time required for the plasticity portion of the cycle was on the order of 0.5 to 2.0 seconds.

Since one of the objectives of the program was to verify the predictive capability of SRP, a series of verification tests was performed which featured test cycles quite different from those used in the baseline tests for establishing the SRP life relations. The type of cycle selected contained periods of constant strain during which creep strain accumulated through the process of stress relaxation. Stress relaxation is, of course, a frequently encountered condition in many high-temperature thermal fatigue problems. From the point of view of interpretation by SRP, creep strain accumulated either by stress relaxation or by direct constant stress creep is equally damaging.

A schematic representation of the verification test cycle is shown in Fig. 2 for the case of the multiple tensile relaxation cycle (MTRC). A duplicate series of tests, but with a multiple compressive relaxation cycle (MCRC) was also performed. The essential advantage of this type of cycle is that a considerable amount of creep strain can be accumulated for a fixed time per cycle. For the present case, the total amount of creep strain encountered with three hold periods of nearly two minutes each was about twice that which could have been obtained with a single hold period of six minutes at the peak strain. The short hold period of a few seconds at the one extreme of the strain cycle was introduced as a matter of testing convenience only. The fact that a component of completely reversed creep strain (CC) was introduced was taken into account when partitioning the inelastic strainranges and predicting the lives of these tests.

RESULTS AND DISCUSSION

Baseline SRP Evaluation

A complete listing of the baseline high-temperature, low-cycle fatigue data generated in this program is given in Table IV of Appendix 1 for each of the alloy conditions investigated. Sufficient information is included to perform a thorough SRP evaluation, or if so desired, an interpretation of the results in terms of other high-temperature, low-cycle fatigue approaches such as those described in Refs. 11-17. The four SRP life relationships for each alloy condition were established following the procedures described in Ref. 5. Each life relationship was expressed in terms of a power law equation relating the inelastic strainrange and cyclic life. The coefficients and exponents were determined using a least squares curve fit technique. The resultant life relationships are presented in Figs. 3, 4, and 5 for Rene' 80, Gatorized IN 100, and cast IN 100, respectively.

Rene' 80 - cursory examination of the data for coated Rene' 80 and comparison with the uncoated results did not reveal significant differences. Hence, the PP, PC, CP, and CC life relationships were established for the combined data set. The least squares curve fit SRP life relationships for Rene' 80 at 1000°C are presented in Figs. 3(a)-(e) and are listed below:

$$\begin{array}{ll}
 \Delta \epsilon_{PP} = 0.062(N_{PP})^{-0.51} \\
 \Delta \epsilon_{PC} = 0.116(N_{PC})^{-0.64} \\
 \Delta \epsilon_{CP} = 0.034(N_{CP})^{-0.45} \\
 \Delta \epsilon_{CC} = 0.051(N_{CC})^{-0.49}
 \end{array}
 \quad \text{EQ(1)}$$

Rene' 80
1000°C
Least Squares Fit

Because the scatter in the data is nearly a factor of two in life (see for example, the PP results in Fig. 3(a)), the least squares curve fits should not be extrapolated much beyond the current range of data. The assumption that the coated and uncoated data could be considered to be of the same population is borne out in Fig. 3(f) where it can be seen that coated and uncoated results are evenly distributed above and below the central 45 degree perfect agreement line. Life differences between coated and uncoated specimens, however, may become important when the life times become significantly greater than those involved in the current program. Techniques for anticipating potential differences will be discussed in a later section.

As seen from Fig. 3(e), the four SRP life relationships for Rene' 80 do not exhibit appreciable differences over the range of variables studied. The PC, CP, and CC lives do not differ by more than a factor of two from the PP life at any given strainrange. This feature should be considered as a virtue of the Rene' 80 alloy. The alloy, as most recent cast nickel-base superalloys, has been tailored to resist creep, principally by strengthening the grain boundaries so as to resist grain boundary sliding. Thus, not only is the alloy resistant to conventional/monotonic creep rupture, it is also resistant to creep introduced in cyclic straining tests such as those reported upon in this paper. This behavior is in sharp contrast to that exhibited by some other alloys that also see service at temperatures within their creep regime. For example, the austenitic stainless steels (which are susceptible to grain boundary sliding during creep) exhibit PP and CP lives that differ by a factor of 20 for the same inelastic strainrange (Ref. 3).

Although the inelastic strainrange versus life relationships for Rene' 80 at 1000°C do not show a strong dependency on creep, the relationship between total strainrange and cyclic life can be drastically influenced by creep. This is especially true at low strainranges. The reason for this is simple. The total strainrange consists of the sum of the elastic and inelastic strainranges. The introduction of creep strain is done at the expense of elastic strain, and hence, the greater the amount of creep, the lower the elastic strainrange and the greater the inelastic component of the total strainrange. The corresponding decrease in cyclic life which is evident in Fig. 3(e) for the PC, CP, and CC relationships thus is essentially a direct result of the greater inelastic strainrange.

Gatorized IN 100 - The least squares curve fit of the SRP data for Gatorized IN 100 at 760°C are presented in Figs. 4(a)-(e). The equations of the life relationships are given below:

Gatorized IN 100760°CLeast Squares Fit

$$\begin{aligned}
 \Delta \epsilon_{PP} &= 0.276(N_{PP})^{-0.80} \\
 \Delta \epsilon_{PC} &= 0.140(N_{PC})^{-0.87} \\
 \Delta \epsilon_{CP} &= 0.029(N_{CP})^{-0.43} \\
 \Delta \epsilon_{CC} &= 0.084(N_{CC})^{-0.62}
 \end{aligned}
 \quad \text{EQ(2)}$$

Because of the limited quantity of available material, few tests could be conducted with this alloy. Hence, the relationships are based upon limited information obtained over a limited cyclic life range. The least squares curve fit life relationships should not be extrapolated much beyond the cyclic life range of the existing data. Although the scatter in the PP, PC, and CC data appears to be very small, this may simply be due to the few data points, since the scatter in the CP points is substantial. For example, test specimen numbers 20 and 23 (Table IV of Appendix 1) are essentially duplicate tests, yet the observed cyclic lives were 12 and 41 respectively. This spread of nearly 4 to 1 in observed life limits the ability of SRP, and for that matter, any high-temperature fatigue approach, to accurately correlate the behavior of this group of specimens. A measure of how well SRP can correlate the baseline results is given in Fig. 4(f). Correlation within life factors of two is obtained except, of course, for the 12 cycle CP test which had a predicted life of 45 cycles. Caution should be exercised in extrapolating EQ(2) to longer times to failure at temperatures on the order of 760°C and higher. The creep-formed powder processed alloy may begin to exhibit greater creep deformation due to superplasticity at longer times and low stresses which could result in improvements in the alloy's resistance to CP and CC type strainranges.

The amount of improvement could be evaluated from a knowledge of creep-rupture ductility and an application of the DN-SRP life estimation equations of Ref. 6. Unfortunately, no ductility data were available for this alloy at the relatively high temperature of 760°C.

Cast IN 100 - A set of SRP life relationships for cast IN 100 tested at 925°C were included in Ref. (5). These were based upon the preliminary data available at that time. A few of the originally tested specimens had failed prematurely at thermocouple spot welds, so these data points have been eliminated from the data base. Some additional tests were conducted on specimens with the thermocouples located further from the critical test section to avoid premature failures. The currently available data for 925°C although somewhat meager, are displayed in Figs. 5(a)-(e) along with the least squares curve fit life relationships.

Cast IN 100925°CLeast Squares Fit

$$\begin{aligned}
 \Delta \epsilon_{PP} &= 0.053(N_{PP})^{-0.57} \\
 \Delta \epsilon_{PC} &= 0.053(N_{PC})^{-0.73} \\
 \Delta \epsilon_{CP} &= 0.040(N_{CP})^{-0.55} \\
 \Delta \epsilon_{CC} &= 0.033(N_{CC})^{-0.44}
 \end{aligned}
 \quad \text{EQ (3)}$$

The few data exhibit little scatter for PC, CP, and CC. However, this may again be misleading as was suggested previously for the Gatorized IN 100, since there is scatter of very nearly a factor of two in the PP data. Correlation of the results is within factors of two on cyclic life as demonstrated in Fig. 5(f).

Comparison With DN-SRP Equations

In a recently published paper (Ref.6) a set of equations was proposed which permits the estimation of the four SRP life relationships from a knowledge of a material's ductility. Referred to as the Ductility Normalized-Strainrange Partitioning (DN-SRP) equations, they were based upon a correlation of the SRP data available at the time of publication. All four inelastic strainrange components are related to life by power law equations with a constant exponent of -0.60. The coefficients in the equations are related to the ductility of the alloy at the temperature and in the environment of interest. Plastic ductility, D_p , as determined from percent reduction of area, R.A., obtained from conventional tensile tests, is used in the equations for PP and PC since these two types of strainranges have plasticity in the tensile half of the cycle. Similarly, creep-rupture ductility, D_c , is used in the expressions for CP and CC since creep strain is present in the tensile halves of these cycles. If creep-rupture ductility varies with time to failure, the DN-SRP equations imply that the CP and CC cyclic life relations are also a function of time. The DN-SRP life equations are as given below:

DN-SRPEQUATIONS

$$\begin{aligned}
 \Delta \epsilon_{PP} &= 0.50(D_p)(N_{PP})^{-0.60} \\
 \Delta \epsilon_{PC} &= 0.25(D_p)(N_{PC})^{-0.60} \\
 \Delta \epsilon_{CP} &= 0.20(D_c)^{0.60}(N_{CP})^{-0.60} \\
 \Delta \epsilon_{CC} &= 0.10(D_c)^{0.60}(N_{CC})^{-0.60}
 \end{aligned}
 \quad \text{EQ (4)}$$

There are two equations for CP. The first, with the 0.20 coefficient is for use when the creep-rupture cracking mode is transgranular. The latter is to be used when creep-rupture cracking is of the more detrimental intergranular mode.

Ductility data are available only for the uncoated Rene' 80 and the cast IN 100 alloys. However, implications of the DN-SRP equations with respect to the coated Rene' 80 will also be discussed.

Rene' 80 - Tensile ductility and creep-rupture ductility data for the uncoated Rene' 80 alloy are reported in Ref. (18) at several temperatures including 1000°C. For many alloys, the creep-rupture ductility decreases as rupture times become longer. This seems to be the case most frequently for alloys that crack in an intergranular mode. Rene' 80 is no exception in this regard. Creep-rupture cracking is intergranular. However, for the rupture times of interest (the same times as the failure times of the cyclic tests), the creep-rupture ductility, D_C , is essentially constant at a value of 0.17 over the time range from 2 to 150 hours to failure. The tensile plastic ductility is 0.40. Hence, the DN-SRP equations for uncoated Rene' 80 at 1000°C for a time span of up to 150 hours are:

$$\begin{array}{l} \text{RENE' 80,} \\ \text{UNCOATED} \\ \\ \text{1000°C} \\ \text{DN-SRP} \end{array} \quad \begin{array}{l} \Delta \epsilon_{PP} = 0.200(N_{PP})^{-0.60} \\ \Delta \epsilon_{PC} = 0.100(N_{PC})^{-0.60} \\ \Delta \epsilon_{CP} = 0.034(N_{CP})^{-0.60} \\ \Delta \epsilon_{CC} = 0.085(N_{CC})^{-0.60} \end{array} \quad \text{EQ (5)}$$

Equation (5) was used to predict the lives of the baseline tests for the uncoated Rene' 80. Fig.6(a) compares the predicted lives with the observed lives. All but two of the points are within factors of three in cyclic life.

It was shown earlier that little difference exists between the behavior of the coated and uncoated specimens. This condition is attributed to at least two factors, (a) the coating is compatible with the base alloy and does not adversely affect its fatigue resistance as evidenced by the 1000°C vacuum data of Refs. 8 and 9, and (b) the current testing times (less than 150 hours), are not long enough for the uncoated specimens to experience life degradation due to oxidation, i.e., the protective capabilities of the coating are not as yet required. However, for exposure times much greater than 150 hours, uncoated Rene' 80 may suffer from oxidation attack whereas coated Rene' 80 would not do so under the same circumstances. One way to anticipate whether the SRP life relations would be altered by long exposure times is to evaluate the DN-SRP equations using ductility data obtained from tensile tests on exposed material and long time creep-rupture tests. The creep-rupture ductility, $D_C = \ln [100/(100-\%R.A.)]$, of uncoated Rene' 80 in 1000°C air decreases from an average value of 0.17 in the 2 to 150 hour regime to 0.11 at 1000 hours to rupture.

We would thus expect the CP and CC SRP life relationships for uncoated Rene' 80 appropriate for 1000 hour lives to decrease in accordance with the decrease in D_C as indicated by the DN-SRP relations of Eq. (4). No plastic ductility data were available for uncoated material that had been exposed for long periods of time, nor were any ductility data available for the coated material. Hence, we can not presently evaluate whether the long time SRP life relations for the coated and uncoated material would be expected to differ or remain the same. The above discussion, however, does suggest how such an evaluation could be made without resorting to expensive long time cyclic tests.

Cast IN 100 - Ductility data for the cast IN 100 alloy were reported in Ref. 18. For the 925°C test temperature and failure times of less than 100 hours, the corresponding ductilities are: $D_P = D_C = 0.11$, with intergranular cracking being responsible for the creep-rupture failures. Hence, for these conditions, the DN-SRP equations for cast IN 100 at 1000°C are:

$$\begin{array}{l} \text{CAST IN 100} \\ \\ \text{925°C} \\ \text{DN-SRP} \end{array} \quad \begin{array}{l} \Delta \epsilon_{PP} = 0.055(N_{PP})^{-0.60} \\ \Delta \epsilon_{PC} = 0.028(N_{PC})^{-0.60} \\ \Delta \epsilon_{CP} = 0.025(N_{CP})^{-0.60} \\ \Delta \epsilon_{CC} = 0.063(N_{CC})^{-0.60} \end{array} \quad \text{EQ (6)}$$

Figure 6(b) compares the predicted lives of the cast IN 100 with the observed baseline lives. All of the data are contained within factors of three of the predicted lives, and nearly all within factors of two.

Verification Results

Verification tests designed to check the predictive capability of the SRP life equations were conducted only with specimens of cast IN 100, since sufficient specimens were simply unavailable for the other alloys. A primary requisite of a verification test is that it should contain some feature or complexity not present in the baseline test. For the present purposes, we selected an unusual strain-cycling test which contains periods of multiple stress relaxation as opposed to the baseline tests which contained periods of creep at constant stress. The process of determining the amounts of tensile and compressive creep and plasticity is straightforward. Referring to Fig. 2, the creep strain was determined from the amount of elastic strain converted to creep strain during each relaxation period. The plastic strain is the difference between the inelastic strain and the creep strain. For example, during the compressive portion of the multiple tensile relaxation cycle (MTRC) of Fig. 2(c), the compressive creep strain, ϵ_{C1} , is equal to the amount of relaxed stress ($\sigma_a - \sigma_b$) divided by the modulus of elasticity, E.

The compressive plastic strain is simply the difference between the inelastic strainrange $\Delta\epsilon_{IN}$ and ϵ_{C1} . In tension, there are three creep strain contributions, ϵ_{C2} , ϵ_{C3} , and ϵ_{C4} . Each is given by the amount of stress relaxation ($\sigma_c - \sigma_d$), ($\sigma_e - \sigma_f$), and ($\sigma_g - \sigma_h$) divided by the elastic modulus. The tensile plastic strain is given by $\Delta\epsilon_{IN} - (\epsilon_{C2} + \epsilon_{C3} + \epsilon_{C4})$. Procedures for determining the partitioned inelastic strainrange components are given in Ref. 5. For the MTRC example, three strainrange components are present, PP, CP, and CC. For a multiple compressive relaxation cycle (MCRC), PP, PC, and CC strainrange components are introduced.

For each verification test conducted, the inelastic strainrange was used to calculate the respective N_{PP} , N_{PC} , N_{CP} , and N_{CC} lives from the least squares curve fit life relations of EQ. (3). Knowing the partitioned inelastic strainrange components permitted calculation of the strainrange fractions, F_{PP} , F_{PC} , F_{CP} , and F_{CC} for use in the interaction damage rule so that the predicted cyclic lives N_{PRED} could be computed.

$$(F_{PP}/N_{PP}) + (F_{PC}/N_{PC}) + (F_{CP}/N_{CP}) + (F_{CC}/N_{CC}) = 1/N_{PRED} \quad \text{EQ (7)}$$

A series of three MTRC and three MCRC tests were conducted with the cast IN 100 at 925°C using the six minute cycle illustrated schematically in Fig. 2. Table IV of Appendix 1 lists the pertinent data for each verification test. Comparisons of the observed lives and predicted lives are presented in Fig. 8. It is seen that cyclic lives were predicted to within factors of two in every case.

SUMMARY AND CONCLUDING REMARKS

In keeping with the objectives of this Specialists Meeting, this paper focused on an evaluation of how well the Method of Strainrange Partitioning (SRP) can both correlate and predict the high-temperature, low-cycle fatigue lives of laboratory specimens of advanced gas turbine alloys.

Strainrange Partitioning characteristics were presented for two nickel-base superalloys: cast Rene' 80 with and without an aluminide (Codep B-1) coating, and IN 100 in both the Gatorized (creep-formed) and cast conditions. SRP life relationships were established for each of the four inelastic strainrange types (PP, PC, CP, and CC) for each alloy condition.

By comparing the observed lives of the baseline tests with the lives calculated from the established life relationships, it was shown that the method of Strainrange Partitioning successfully correlated the high-temperature, low-cycle fatigue lives of these alloys generally to within factors of two. It should, of course, be kept in mind that the SRP inelastic strainrange versus life relationships for the cast nickel-base superalloys studied in this program are not widely separated one from another. These circumstances are believed to result from the fact that these alloys were designed to resist creep deformation by the prevention of grain boundary sliding, a mechanism frequently associated with widely separated CP and PP SRP life relationships.

An evaluation was also made of how well the recently proposed Ductility Normalized-Strainrange Partitioning (DN-SRP) equations could predict the cyclic lives of the baseline tests. Values of tensile plastic ductility, D_p , and creep-rupture ductility, D_c , for use in the DN-SRP equations were determined at the temperature and failure times corresponding to the baseline data, and then used to determine the PP, PC, CP, and CC life relationships. These life relationships were then applied, in conjunction with the interaction damage rule to predict the cyclic lives of the baseline tests. Agreement between predicted and observed lives was generally within factors of 3. Only uncoated Rene' 80 and cast IN 100 were evaluated since ductility data were unavailable for the other conditions of these alloys.

A few verification type tests were conducted on specimens of cast IN 100 using a test cycle composed of hold periods at several different constant strain levels. Creep was thereby introduced into each cycle by the process of repeated stress relaxation. One series of tests was conducted which featured three hold periods in tension and a much shorter period at the peak compressive strain, thus producing partitioned inelastic strainrange components of CP, CC, and PP. Another series of tests reversed the holding pattern of strain and thus gave rise to PC, CC, and PP components. The lives of the verification tests were predicted on the basis of the life relationships established from the baseline tests which had introduced creep in a more direct manner by using hold periods at constant stress. The life of each verification test was predicted correctly to within factors of two, which is considered to be an acceptably high degree of predictability.

It is concluded that the method of Strainrange Partitioning can be used to accurately correlate and predict the high-temperature, low-cycle fatigue behavior of the nickel-base superalloys studied in this program.

REFERENCES

1. Manson, S.S.; Halford, G.R.; and Hirschberg, M.H.: Creep-Fatigue Analysis by Strain-Range Partitioning. Symposium on Design for Elevated Temperature Environment. ASME, 1971, pp. 12-28.
2. Manson, S.S.: A Review of the Development of Strainrange Partitioning. Proceedings, Characterization of Low Cycle High Temperature Fatigue by the Strainrange Partitioning Method, Sponsored by the AGARD Structures and Materials Panel, Aalborg, Denmark, April 1978.
3. Manson, S.S.: The Challenge to Unify Treatment of High Temperature Fatigue - A Partisan Proposal Based on Strainrange Partitioning. STP 520, ASTM, 1973, pp. 744-782.
4. Manson, S.S.: Observations and Correlations Emphasizing Wave Shape and Other Salient Features. Chapter 4, Time-Dependent Fatigue of Structural Alloys. A General Assessment(1975). ORNL-5073, Oak Ridge National Laboratory, January 1977, pp. 155-332.

5. Hirschberg, M.H.; and Halford, G.R.: Use of Strainrange Partitioning to Predict High-Temperature Low-Cycle Fatigue Life. NASA TN D-8072 1976.
6. Halford, G.R.; Saltsman, J.F.; and Hirschberg, M.H.: Ductility Normalized-Strainrange Partitioning Life Relations for Creep-Fatigue Life Prediction. Proceedings of the Conference on Environmental Degradation of Engineering Materials. Virginia Tech. Printing Dept., V.P.I. & State Univ., Blacksburg, VA 1977, pp. 599-612.
7. Hirschberg, M.H.: A Low-Cycle Fatigue Testing Facility. Manual on Low-Cycle Fatigue Testing. STP-465, ASTM, 1969, pp.67-86.
8. Kortovich, C.S.: Ultrahigh Vacuum, High Temperature, Low Cycle Fatigue of Coated and Uncoated Rene' 80. NASA CR-135003, April 1976. (TRW Inc., ER-7861).
9. Kortovich, C.S.; and Sheinker, A.A.: A Strainrange Partitioning Analysis of Low Cycle Fatigue of Coated and Uncoated Rene' 80. Proceedings, Characterization of Low Cycle, High Temperature Fatigue by the Strainrange Partitioning Method. Sponsored by the AGARD Structures and Materials Panel, Aalborg, Denmark, April 1978.
10. Wallace, R.M.; Annis, C.G.; and VanWanderham, M.C.: Low Cycle Fatigue Behavior of IN 100: Strainrange Partitioning Method. Proceedings, Characterization of Low Cycle High Temperature Fatigue by the Method of Strainrange Partitioning. Sponsored by the AGARD Structures and Materials Panel, Aalborg, Denmark, April 1978.
11. Coffin, L.F., Jr.: Observations and Correlations Emphasizing Frequency and Environmental Effects. Chapter 3, Time-Dependent Fatigue of Structural Alloys. A General Assessment(1975). ORNL-5073, Oak Ridge National Laboratory, January 1977, pp.37-153.
12. Ostergren, W.J.: Correlation of Hold Time Effects in Elevated Temperature Low Cycle Fatigue Using A Frequency Modified Damage Function. 1976 ASME-MPC Symposium on Creep-Fatigue Interaction, MPC-3, December 1976, pp. 179-202.
13. Ellis, J.R.; and Esztergar, E.P.: Consideration of Creep-Fatigue Interaction in Design Analysis. Symposium on Design for Elevated Temperature Environment, ASME, 1971, pp. 29-43.
14. Majumdar, S.; and Maiya, P.S.: A Damage Equation for Creep-Fatigue Interaction. 1976 ASME-MPC Symposium on Creep-Fatigue Interaction, MPC-3, December 1976, pp. 323-335.
15. Spera, D.A.: The Calculation of Elevated-Temperature Cyclic Life Considering Low-Cycle Fatigue and Creep. NASA TN D-5317, 1969.
16. Manson, S.S.; Halford, G.R.; and Spera, D.A.: The Role of Creep in High-Temperature Low-Cycle Fatigue. Ch. 12 in Advances in Creep Design. A.I.Smith and A.M.Nicolson, eds., Appl. Sci Publ.Ltd. London, 1971, pp. 229-249.
17. Section III, Boiler and Pressure Vessel Code, Code Case 1592, ASME, 1977.
18. Fritz, L.J.; and Koster, W.P.: Tensile and Creep Rupture Properties of 16 Uncoated and 2 Coated Engineering Alloys at Elevated Temperatures. NASA CR-135138, METCUT Research Associates, Inc.1977.

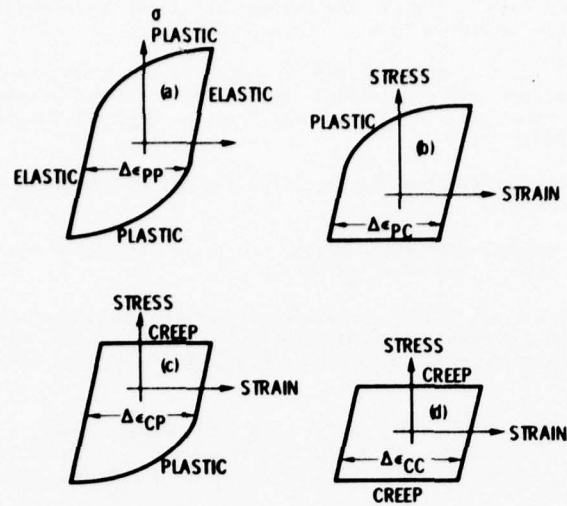


Figure 1. - Schematic illustration of hysteresis loops resulting from test cycles used to establish baseline strainrange partitioning life relationships for Rene[®] 80, Gatorized IN 100, and cast IN 100.

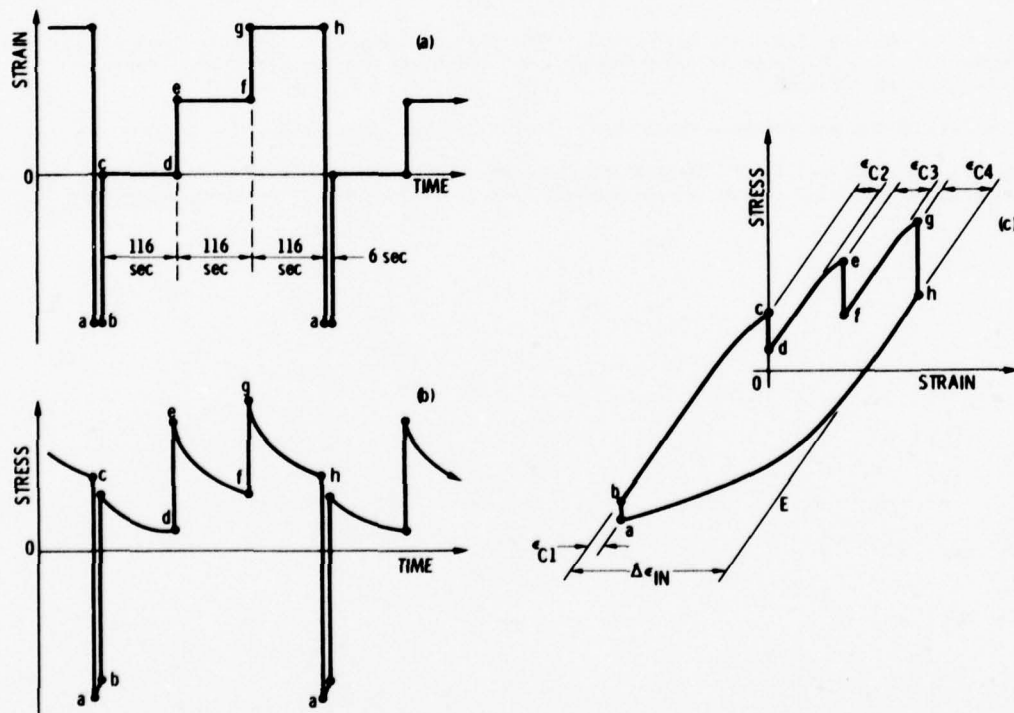


Figure 2. - Schematic representation of verification test cycle involving multiple strain hold periods. Multiple Tensile Relaxation Cycle (MTRC) shown. (a) Programmed strain-time waveform; (b) Stress-time response; and (c) Stress-strain hysteresis loop.

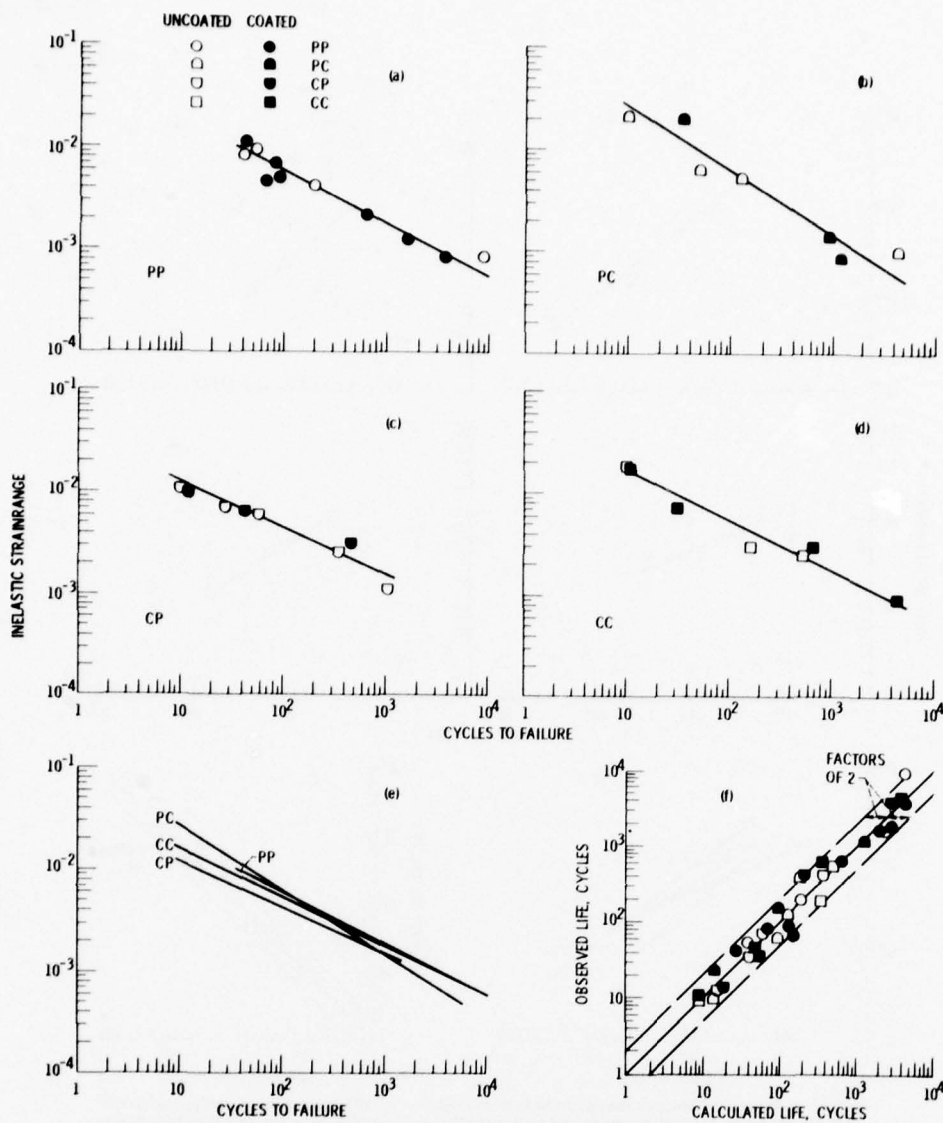


Figure 3. - Strainrange partitioning life relationships for cast Rene' 80 with and without Codep B-1 aluminide coating in air at 1000°C . Least squares curve fit of baseline data. Note little differences between coated and uncoated behavior. (a) PP life relationship; (b) PC life relationship; (c) CP life relationship; (d) CC life relationship; (e) Superposition of life relationships; and (f) Life relationships correlate baseline data to within factors of 2 in cyclic life.

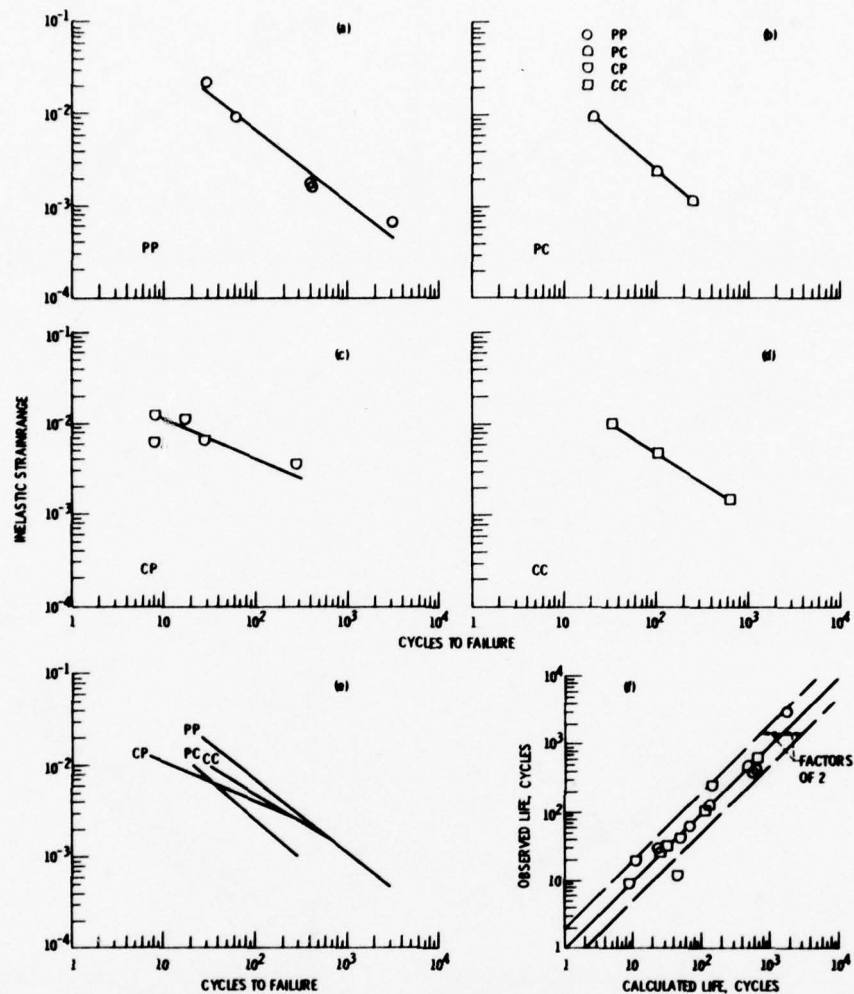


Figure 4. - Strainrange partitioning life relationships for Gatorized IN 100 in air at 760° C. Least squares curve fit of baseline data. (a) PP life relationship; (b) PC life relationship; (c) CP life relationship; (d) CC life relationship; (e) Superposition of life relationships; and (f) Life relationships correlate baseline data generally within factors of 2 in cyclic life.

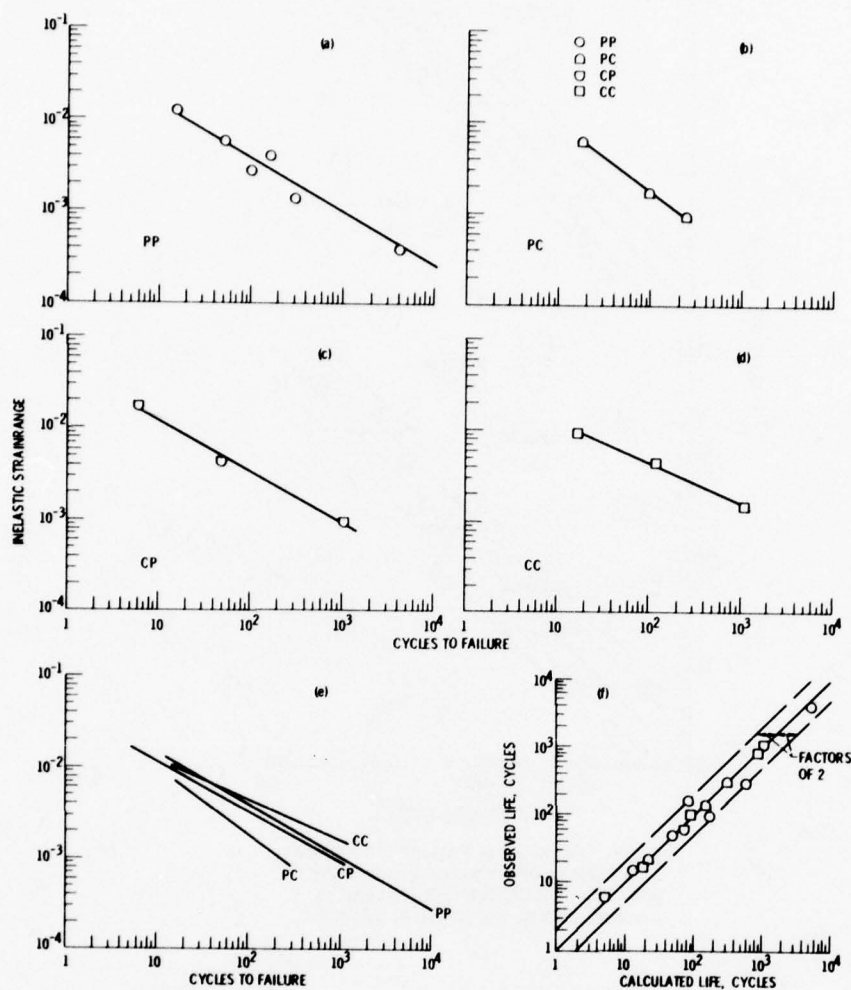


Figure 5. - Strainrange partitioning life relationships for cast IN 100 in air at 929° C. Least squares curve fit of baseline data. (a) PP life relationship; (b) PC life relationship; (c) CP life relationship; (d) CC life relationship; (e) Superposition of life relationships; and (f) Life relationships correlate baseline data to within factors of 2 in cyclic life.

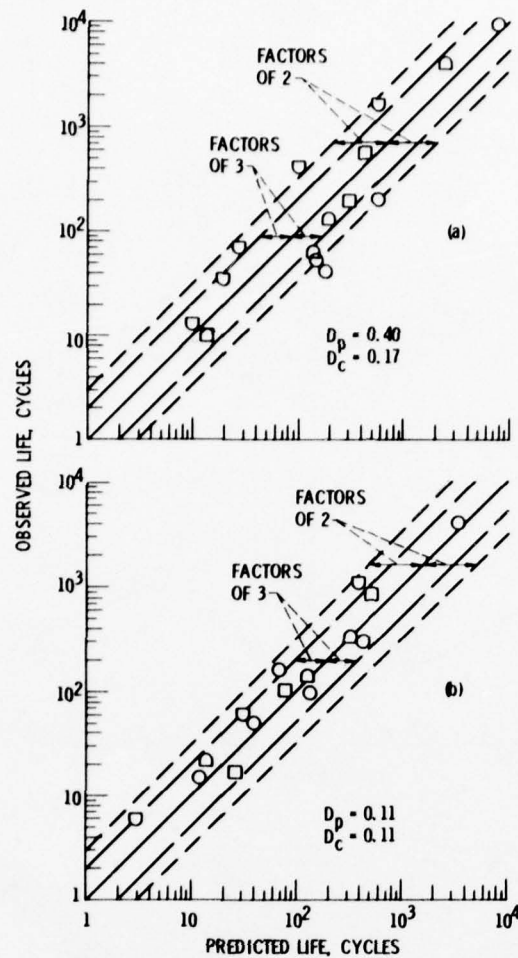


Figure 6. - Application of the ductility normalized-strainrange partitioning life equations to the prediction of the baseline data. (a) Rene' 80, uncoated, 1000°C ; and (b) Cast IN 100, 925°C .

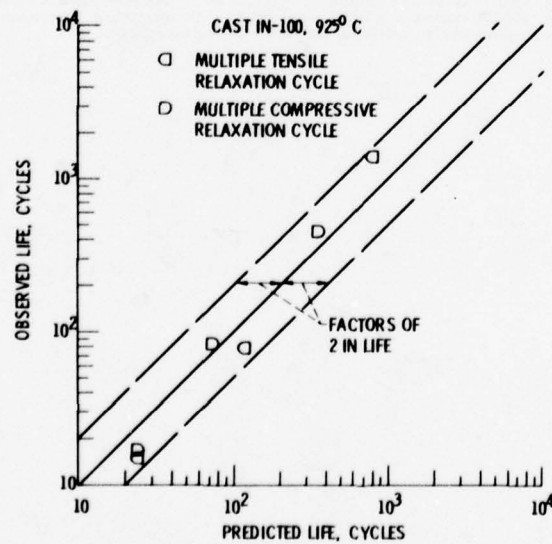


Figure 7. - Strainrange partitioning predicts lives of multiple strain hold time verification tests to within factors of two.

APPENDIX 1 - MATERIAL DATA SUMMARY

TABLE I: CHEMICAL COMPOSITION - WT %

MATERIAL	Al	Si	B	C	Co	Ti	V	W	Cr	Zr	Fe	Mo	Mn	Ni
RENE' 80	2.990	<0.050	0.015	0.170	9.730	4.870	-----	3.940	13.800	0.043	0.130	4.110	<0.020	BAL
IN 100 (GATORIZED)	4.980	-----	0.020	0.070	18.500	4.320	0.780	-----	12.400	0.060	-----	3.200	-----	BAL
IN 100 (CAST)	5.450	0.110	0.016	0.170	15.100	4.760	0.970	-----	10.300	0.084	-----	2.960	0.020	BAL

TABLE II: PROCESSING & HEAT TREATMENT

MATERIAL	PROCESSING	HEAT TREATMENT
Rene' 80	TRW master heat no. BL-5138, bare & coated with Codep B-1(aluminide). Individually cast bars (hole bored for tubular specimens). ASTM grain size = 3.	1220C-2hr. in vac., inert Q to RT; 1095C-4hr. in vac., inert Q to RT; 1050C-4hr. in vac., FC in 1 hr. to 650C, AC to RT (simulates coating cycle); 845C-16hr. in vac., FC to RT. Rough machine before heat treatment, finish grind after.
IN 100	Powder - GATORIZED(TM)	Solution 2050F, Stabilized 1600F and 1800F, precipitation 1200F and 1400F.
IN 100	CAST	None

TABLE III: MECHANICAL PROPERTIES
(1MPa = 0.145KSI)

MATERIAL	TENSILE PROPERTIES					CREEP-RUPTURE PROPERTIES					
	TEMP C	MODULUS MPa	0.2% YIELD MPa	ULTIMATE MPa	RA-%	10 HR		100 HR		1000 HR	
						MPa	RA-%	MPa	RA-%	MPa	RA-%
RENE' 80	20	198,600	821.0	996.0	6.2						
	1000	128,200	230.0	333.0	32.7	180.0	16.5	127.6	12.5	82.7	10.5
IN 100	20	205,500	866.0	1040.0	12.1						
(CAST)	925	155,100	467.0	622.0	10.2	430.0	10.3	262.0	10.3	158.6	10.3

TABLE IV - CREEP-FATIGUE DATA

Spec. No. REE-	Test Type	Freq. Hz	Stress at $N_f/2$, MPa			Strainrange at $N_f/2$, %						Cycles to Failure, N_f	Hours to Failure, t_f	
			Tens. Max.	Comp. Max.	Range	Total	Elastic	Inelastic	PP	PC	CP			CC
René 80, Uncoated, 1000°C														
205	PP	1.0E-00	420.9	420.9	841.8	1.525	0.656	0.869	0.869	0.000	0.000	42	0.01	
215		1.0E-00	370.9	370.9	741.8	1.557	0.578	0.979	0.979	0.000	0.000	55	0.01	
204		1.0E-00	358.2	358.2	716.4	0.989	0.558	0.431	0.431	0.000	0.000	202	0.06	
204		1.0E-00	206.2	206.2	412.4	0.410	0.321	0.089	0.089	0.000	0.000	9226	2.46	
200	PC	6.4E-05	467.1	179.3	646.4	2.612	0.504	2.108	0.222	1.866	0.000	10	40.75	
219		7.0E-04	355.0	136.0	491.0	1.007	0.383	0.624	0.268	0.356	0.000	63	23.53	
213		9.9E-04	321.7	179.5	501.2	0.916	0.391	0.525	0.258	0.267	0.000	132	36.64	
210		7.6E-03	183.3	119.7	303.0	0.339	0.237	0.102	0.031	0.071	0.000	3960	145.60	
223	CP	6.4E-05	127.7	405.7	533.4	1.472	0.416	1.056	0.299	0.000	0.757	13	56.00	
208		5.4E-04	172.6	341.4	514.0	1.098	0.400	0.698	0.218	0.000	0.880	35	17.97	
201		5.5E-04	172.0	276.7	448.7	0.927	0.350	0.577	0.195	0.000	0.382	70	35.63	
221		4.2E-03	110.4	250.2	360.6	0.534	0.281	0.253	0.089	0.000	0.164	616	27.26	
220		2.2E-02	89.0	225.6	314.6	0.354	0.245	0.109	0.055	0.000	0.054	1600	19.05	
211	CC	1.0E-03	244.1	244.1	488.3	2.214	0.381	1.833	0.276	0.000	0.000	1.557	10	1.56
212		6.2E-04	157.8	135.2	293.0	0.531	0.228	0.303	0.071	0.000	0.000	0.232	191	85.10
217		9.2E-03	156.3	112.7	269.0	0.461	0.211	0.250	0.067	0.000	0.000	0.183	548	16.60
René 80, Coated, 1000°C														
322	PP	1.0E-00	481.5	481.5	963.0	1.917	0.751	1.166	1.166	0.000	0.000	43	0.01	
317		1.0E-00	394.6	394.6	789.2	1.091	0.615	0.476	0.476	0.000	0.000	69	0.32	
310		1.0E-00	440.4	440.4	880.8	1.399	0.687	0.712	0.712	0.000	0.000	85	0.32	
304		1.0E-00	375.2	375.2	750.4	1.101	0.585	0.516	0.516	0.000	0.000	93	0.03	
306		1.0E-00	298.6	298.6	597.2	0.696	0.465	0.231	0.231	0.000	0.000	650	0.50	
300		1.0E-00	239.5	239.5	479.0	0.515	0.385	0.130	0.130	0.000	0.000	1664	0.64	
323		1.0E-00	198.2	198.2	396.4	0.397	0.309	0.088	0.088	0.000	0.000	3820	1.04	
311		1.0E-00	178.2	178.2	356.4	0.324	0.278	0.046	0.046	0.000	0.000	15000	0.28	
312	PC	5.0E-04	365.6	178.1	543.7	2.410	0.424	1.986	0.330	1.656	0.000	24	13.20	
301		2.2E-03	323.5	172.7	496.2	1.007	0.387	0.620	0.228	0.392	0.000	159	28.47	
303		1.9E-03	214.1	84.8	318.9	0.387	0.248	0.139	0.063	0.076	0.000	1200	97.25	
328		1.3E-01	210.1	77.3	287.4	0.312	0.224	0.088	0.044	0.044	0.000	1900	4.16	
315	CP	9.1E-04	169.1	353.2	522.3	1.369	0.407	0.962	0.238	0.000	0.724	14	4.25	
305		1.1E-03	152.9	349.9	502.8	1.022	0.392	0.630	0.134	0.000	0.886	49	11.68	
308		1.9E-03	100.0	284.7	384.7	0.631	0.311	0.320	0.088	0.000	0.232	432	63.47	
302		1.1E-03	90.3	210.6	300.9	0.337	0.235	0.102	0.058	0.000	0.044	3929	45.45	
309	CC	5.4E-04	203.1	236.9	440.0	2.133	0.343	1.790	0.342	0.000	0.000	1.444	11	5.62
316		4.9E-04	169.1	165.3	334.4	0.984	0.261	0.723	0.141	0.000	0.036	36	20.44	
313		2.6E-03	115.9	136.1	252.0	0.492	0.197	0.295	0.035	0.000	0.000	620	65.23	
314		4.8E-02	103.4	110.3	221.7	0.266	0.173	0.093	0.011	0.000	0.000	4457	25.92	
Galvanized IN 100, 760°C														
9	PP	6.0E-01	1305.0	1518.0	2823.0	3.924	1.637	2.287	2.287	0.000	0.000	0.000	29	0.01
17		6.0E-01	1178.0	1194.0	2364.0	2.305	1.373	0.933	0.933	0.000	0.000	0.000	63	0.02
18		6.0E-01	952.0	987.0	1939.0	1.256	1.077	0.179	0.179	0.000	0.000	0.000	401	0.14
12		6.0E-01	914.0	914.0	1828.0	1.222	1.057	0.165	0.165	0.000	0.000	0.000	413	0.15
8		6.0E-01	678.0	666.0	1366.0	0.845	0.776	0.069	0.069	0.000	0.000	0.000	3085	1.07
6	PC	2.5E-04	1117.0	433.0	1550.0	1.692	0.699	0.993	0.273	0.720	0.000	0.000	26	29.08
13		6.7E-03	804.0	215.0	1019.0	0.828	0.591	0.238	0.072	0.166	0.000	0.000	129	53.78
10		6.6E-03	628.0	434.0	1062.0	0.736	0.617	0.119	0.083	0.036	0.000	0.000	502	30.40
18	CP	1.4E-04	499.0	1279.0	1778.0	2.240	1.029	1.212	0.192	0.000	1.020	0.000	9	17.75
30		7.0E-04	568.0	1161.0	1721.0	1.633	0.999	0.634	0.204	0.000	0.430	0.000	12	4.74
15		7.1E-04	337.0	1163.0	1500.0	1.740	0.340	1.140	0.212	0.000	0.928	0.000	20	7.68
23		1.4E-03	662.0	1205.0	1867.0	1.718	1.082	0.636	0.276	0.000	0.360	0.000	81	7.08
4		5.0E-03	553.0	1050.0	1603.0	1.299	0.928	0.371	0.091	0.000	0.280	0.000	290	12.38
22	CC	7.1E-04	670.0	693.0	1363.0	1.754	0.791	0.973	0.193	0.000	0.044	0.736	33	12.98
3		3.0E-03	608.0	623.0	1231.0	1.192	0.715	0.477	0.181	0.000	0.048	0.240	112	0.26
19		1.2E-02	521.0	521.0	1042.0	0.755	0.604	0.151	0.022	0.000	0.002	0.127	652	16.40
Cast IN 100, 828°C														
2	PP	5.0E-01	736.0	774.0	1510.0	2.170	0.924	1.246	1.246	0.000	0.000	0.000	15	0.31
32		5.0E-01	573.6	619.2	1192.8	1.351	0.769	0.582	0.582	0.000	0.000	0.000	50	0.33
3		5.0E-01	403.0	520.0	1003.0	0.920	0.638	0.282	0.282	0.000	0.000	0.000	96	0.05
17		5.0E-01	548.7	544.1	1112.8	1.125	0.708	0.417	0.417	0.000	0.000	0.000	160	0.11
18		5.0E-01	385.3	400.7	786.0	0.640	0.500	0.140	0.140	0.000	0.000	0.000	300	0.17
16		5.0E-01	224.1	228.2	452.3	0.332	0.292	0.040	0.040	0.000	0.000	0.000	6815	2.23
20		5.0E-01	172.4	172.4	344.8	0.236	0.222	0.014	0.014	0.000	0.000	0.000	51261	28.36
74	PC	5.1E-04	584.7	241.3	746.0	1.324	0.481	0.843	0.207	0.436	0.000	0.000	22	12.82
13		6.4E-04	486.8	140.6	627.4	0.577	0.399	0.178	0.076	0.102	0.000	0.000	139	87.31
15		7.1E-04	412.3	141.3	553.6	0.450	0.352	0.098	0.034	0.064	0.000	0.000	332	129.11
99	CP	2.7E-04	322.7	674.3	997.0	2.300	0.443	1.657	0.169	0.000	1.288	0.000	6	6.09
11		1.0E-04	169.6	594.3	763.9	0.899	0.405	0.414	0.182	0.000	0.232	0.000	60	143.92
9		1.9E-03	142.0	360.6	502.6	0.414	0.320	0.094	0.047	0.000	0.047	0.000	1100	159.32
12	CC	1.6E-05	228.2	228.2	456.4	1.208	0.290	0.918	0.108	0.000	0.000	0.810	17	101.50
16		1.4E-04	171.0	171.0	342.0	0.650	0.218	0.432	0.039	0.019	0.000	0.374	102	203.17
89		3.0E-03	200.7	200.7	401.4	0.402	0.258	0.144	0.045	0.000	0.000	0.099	840	78.33
73	VERIF	2.8E-03	621.5	655.0	1276.5	1.625	0.823	0.802	0.677	0.107	0.000	0.018	17	1.73
72		2.8E-03	366.1	355.1	721.2	0.822	0.465	0.357	0.219	0.105	0.000	0.033	84	4.05
47		2.8E-03	345.4	259.2	604.6	0.517	0.390	0.127	0.054	0.043	0.000	0.030	454	47.11
75	VERIF	2.8E-03	436.4	582.4	1019.0	1.502	0.657	0.845	0.724	0.000	0.099	0.022	15	1.55
68		2.8E-03	375.1	462.6	837.7	0.866	0.540	0.326	0.181	0.000	0.132	0.013	79	7.97
66		2.8E-03	247.5	352.0	599.5	0.505	0.387	0.118	0.053	0.000	0.044	0.021	1400	140.00

LOW CYCLE FATIGUE BEHAVIOR OF IN-100: STRAINRANGE PARTITIONING METHOD

M.C. VanWanderham, R.M. Wallace, C.G. Annis, Jr.
 Mechanics of Materials and Structures
 Pratt & Whitney Aircraft
 Government Products Division
 West Palm Beach, Florida, U.S.A. 33402

SUMMARY

The elevated temperature, low cycle fatigue behavior of the gas turbine disk alloy IN-100 is evaluated using the Strainrange Partitioning method. Strainrange Partitioning, an advanced life prediction analysis procedure, assumes that any hysteresis loop can be represented by combinations of the four generic cycle definitions: PP, CP, PC, and CC. The first letter refers to the material response in tension, either Plastic (time independent) or Creep (time dependent), and the second letter refers to material response in compression.

There is considerable interest in the gas turbine industry in understanding and accurately predicting the effects of various types of possible dwells, e.g., pure creep or stress relaxation, on the LCF life of critical rotating components. In this investigation, PP and CP curves were developed for GATORIZED[®] IN-100 at 649°C, mean strain equal to half maximum strain. Tensile Hold Strain Cycle (THSC) and Tensile Creep Stress Dwell (TCSD) tests were used to determine CP-type response.

When cycled at the same inelastic strainrange (measured at half-life) THSC specimens survived approximately twice as long as TCSD tests. However, when Strainrange Partitioned, there is no significant difference between THSC and TCSD results and a single CP relation can be used to predict accurately the life of either type of tensile dwell test.

SYNOPSIS OF STRAINRANGE PARTITIONING METHOD

Strainrange Partitioning is a life prediction analysis procedure for high temperature, low cycle fatigue, involving creep-fatigue interactions, which addresses material behavior under cyclic deformation (hysteresis), paying particular attention to inelastic strain-time synergism.¹

The inelastic strains are divided into those which are time-dependent, and those which are not. For convenience, time-dependent inelastic strain is termed "creep," and time-independent inelastic strain "plastic." Since these strains can be experienced in both tension and compression, four combinations of inelastic strain are possible: (1) plastic in both tension and compression, PP, (2) plastic in tension, creep in compression, PC, (3) creep in tension, plastic in compression, CP, and (4) creep in both tension and compression, CC.

OBJECTIVE OF THIS RESEARCH

Gas turbine engine rotating components experience complex thermal-mechanical stresses caused by variations in flight operating conditions. The damage accrued during this cyclic loading can result in low cycle fatigue (LCF). At elevated temperatures, additional concerns are interactions of LCF with creep and environment.

The objective of this paper is to evaluate the low cycle fatigue behavior of the advanced gas turbine disk alloy IN-100 at 649°C with particular attention given to dwell effects. There is interest in understanding elevated temperature constitutive response of fracture critical locations of gas turbine disk components. For example, if a bolthole experiences sufficient elastic constraint to relax during dwell and a disk-blade attachment is kinematically free to creep, improved LCF prediction systems must be capable of accurately modeling the true material behavior. Experimental and analytical programs are currently addressing these questions at Pratt & Whitney Aircraft.

Strainrange Partitioning does not recognize differences in these types of dwells for equivalent, partitioned, inelastic strainranges. This investigation tests this tenet of SRP for IN-100.

MATERIAL CHARACTERIZATION

All evaluations were performed on GATORIZED IN-100, an advanced turbine disk alloy used in the F100 turbofan engine. The majority of the specimens used in this investigation were machined from heat BADU and found to be representative of typical IN-100. Heat treatment consists of solutionizing, stabilization, and precipitation hardening. When superplastically forged with the GATORIZING[™] forging process, IN-100 becomes a fine-grain (ASTM 12-14), isotropic material.

Typical tensile, stress rupture and creep rupture test results for IN-100 are given in Table I *(see Footnote on p.34).

EXPERIMENTAL METHODS

Axial-strain, low-cycle fatigue characteristics were determined at various strain rates and strain waveforms on servohydraulic, closed-loop, fatigue testing machines designed and built at Pratt & Whitney Aircraft.

The test specimen used in this program is shown in Fig. 1. This specimen was designed using photo-elastic and experimental elastic-plastic strain analyses.

A calibration procedure was established to relate the maximum strain to collar deflection during both the elastic and the plastic portions of the strain cycle. The plasticity correction accounts for the possible deviation of apparent (extensometer) strain, $\Delta l / l_0$, from the true strain.

Strain, of course, is defined as the ratio of increased length, Δl , to an original length, l_0 . In the elastic region, any increase in length occurs over the entire gage length but plastic deformation occurs locally. The plasticity correction changes the effective gage length with the onset of plasticity. The extensometer deflection accurately records Δl .

A finite element analysis of this specimen showed that the plasticity correction factor, C_1/C_2 , is uniquely related to material strain hardening exponent, n . Since the computation of n is straightforward, given the material cyclic stress-strain curve, the correction factor is also easily computed.

Specimen axial strain was measured and controlled by means of a proximity probe extensometer. Collar deflection was measured and controlled via proximity probes attached to the open ends of the extensometer tubes so that the extensometer rod ends move relative to the probes as the specimen collars deflect. Heating was accomplished using clamshell resistance furnaces.

RESULTS

Seven High Rate Strain Cycle (HRSC) tests were performed at 0.5 Hz to 0.05 Hz to determine PP-type behavior. Four Tensile Hold Strain Cycle (THSC) and six Tensile Creep Stress Dwell (TCS D) tests were used to determine CP-type response. The tests were performed at a mean strain equal to half maximum to simulate gas turbine disk operating conditions. Creep-fatigue data are summarized in Table II.

Figure 2 presents the resulting cyclic lives, N_f , as functions of total strainrange, $\Delta \epsilon_t$. It is interesting to note that differences between THSC and TCS D relationships (strain vs load dwell), compared at constant total strainrange, are obscured by the large elastic strain components.

Figures 3, 4, and 5 present N_f vs inelastic strainrange, $\Delta \epsilon_{in}$. Figure 6 is a composite of these figures. Notice that when cycled at the same inelastic strainrange, THSC specimens survived approximately twice as long as TCS D specimens.

It is assumed that the THSC and TCS D hysteresis loops are composites of pure CP and PP behavior. The PP component, represented by the High Rate Strain Cycle (HRSC) tests, must be subtracted from the THSC and TCS D loops to produce the desired pure CP relationship.

Any hysteresis loop can be described as some combination of these elements, each present in amounts represented by their constitutive fractions, $F_{a,b}$. The first literal subscript refers to the type of inelastic strain experienced in tension, the second subscript refers to that in compression. Only three of the four basic types of inelastic strainrange can be present in any real hysteresis loop. Both PP and CC can occur together in a cycle but only one PC or CP type can be present. This is because with PC or CP there is creep in only one-half of the cycle being reversed by plastic deformation. Since it is physically possible to have "more" creep in only one-half of any real hysteresis loop, only one, PC or CP type can be present.

When the constitutive fractions have been determined, the expected cyclic life can be calculated from The Interaction Damage Rule¹

$$1/N_f = F_{pp}/N_{pp} + F_{pc}/N_{pc} + F_{cp}/N_{cp} + F_{cc}/N_{cc}$$

where: N_f = cyclic life under some complex hysteresis loop

$F_{a,b}$ = constitutive fraction of type a,b inelastic strain contained in that hysteresis loop

and: $N_{a,b}$ = cyclic life expected assuming the entire inelastic strain to be of type a,b.

See the Appendix and Reference 2 for further discussion on Damage Rules.

Since only two generic components (PP and CP) comprise the THSC and TCS D relationships, The Interaction Damage Rule can be written as

$$1/N_f = F_{pp}/N_{pp} + F_{cp}/N_{cp}$$

where N_f is the observed cyclic life comprised of F_{pp} fraction PP and F_{cp} fraction CP

$$F_{pp} + F_{cp} = 1$$

F_{cp} and F_{pp} can be determined from a graphical analysis of the hysteresis loop.

The graphical method for obtaining $F_{a,b}$'s is as follows:

An elastic line is constructed through the tensile portion of the hysteresis loop. Through the peak stress point (at time of dwell initiation), a line is then constructed parallel to the elastic line. The fractions, F_{pp} and F_{cp} , are then established by measurements along the graphically intercepted ϵ -axis.

Solving for N_{cp} ,

$$N_{cp} = F_{cp} / (1/N_f - F_{pp}/N_{pp})$$

and N_f and N_{pp} are determined at the observed value of inelastic strainrange.

Calculating N_{cp} for each of the THSC and TCSD tests and plotting these vs $\Delta\epsilon_{cp} = F_{cp} \times (\Delta\epsilon_{in.})$ produces Figs. 7 and 8.

Figure 9 shows the "pure" (PP and CP) behaviors, CP as determined from both THSC and TCSD test types. Ideally, the resulting CP lines would be coincident; the small observed differences are attributable to random data scatter. A better representation of pure CP behavior should then result from regressing the data contained in Figs. 7 and 8 as an entity. The resulting regression is shown in Fig. 10. Finally, Fig. 11 presents the desired relationships of PP and CP cycles to failure vs their respective types of inelastic strains. An overall presentation of the effectiveness of SRP in describing IN-100 material response to HRSC, THSC, and TCSD cycling is found in Fig. 12, which provides actual vs calculated cyclic lives for the specimens tested.

CONCLUSIONS

For IN-100, tested at 649°C and mean strain equal half maximum, Strainrange Partitioning can be used to compute the cyclic lives for any loop shape from one extreme (strain dwell) to the other (load dwell) even though their respective behaviors vs total inelastic strainrange are different.

REFERENCES

1. Halford, G.R., H. M. Hirschberg, and S.S. Manson, "Temperature Effects on the Strainrange Partitioning Approach for Creep Fatigue Analysis," Fatigue at Elevated Temperatures, ASTM STP 520, American Society for Testing and Materials, 1973, pp. 658-669.
2. Annis, C.G., Jr., R.M. Wallace, M.C. Van Wanderham, "Strainrange Partitioning of an Automotive Gas Turbine Alloy," NASA CR-134974, February 1976.

APPENDIX INTERACTION DAMAGE RULES

Some type of damage rule is basic to the application of Strainrange Partitioning. In those cases where PP lives are found to be lower than the other three basic types (PC, CP, CC), the application of The Interaction Damage Rule to subtract any PP component in PC, CP, or CC would result in negative values of N_f . The following discussion compares The Interaction Damage Rule and a General Rule, of which The Rule is a special case.

1. The Interaction Damage Rule

The Interaction Damage Rule is given by:

$$1/N_f = F_{pp}/N_{pp} + F_{pc}/N_{pc} + F_{cp}/N_{cp} + F_{cc}/N_{cc}$$

where:

N_f = cyclic life under some complex hysteresis loop

$F_{a,b}$ = constitutive fraction of type a,b inelastic strainrange contained in that hysteresis loop

and:

$N_{a,b}$ = cyclic life expected were the entire inelastic strainrange of type a,b.

Since any real loop can contain, at most, three of these four constituents, so for simplicity The Rule may be written as:

$$1/N_f = \sum_{j=1}^3 F_j/N_j \quad \text{(Interaction Damage Rule)}$$

This Rule can be seen to be a special case of a more general cumulative damage rule:

$$N_f^n = \sum_{j=1}^3 F_j N_j^n, \quad -1 \leq n \leq +1 \quad \text{(General Rule)}$$

2. An Alternative Rule

To provide a basis for comparison, an alternative rule where $n = +1$, will be described. This rule can be written as:

$$N = \sum_{j=1}^3 F_j N_j \quad \text{(Alternative Rule)}$$

For illustrative purposes consider a hypothetical case where only two types of damage are present, and both in equal proportions, i.e., $F_1 = F_2 = 0.5$. Since it is not uncommon to observe an order of magnitude difference in life between the shortest and longest cycle definition, suppose also that $N_2 = 10N_1$.

Now compare the cyclic life computed using these two rules ($n = -1$) and ($n = +1$).

Using The Interaction Damage Rule

$$\begin{aligned} 1/N_f &= 0.5/N_1 + 0.5/N_2 \\ &= 0.5/N_1 + 0.5/10N_1 \\ &= (0.5 + 0.05)/N_1 \\ N_f &= (1/0.55)N_1 = 1.818N_1 \end{aligned}$$

Whereas an Alternative Rule would give:

$$\begin{aligned} N_f &= 0.5N_1 + 0.5N_2 \\ &= 0.5N_1 + 0.5(10N_1) \\ &= (0.5 + 5.0)N_1 \\ &= 5.5N_1 \end{aligned}$$

From this it can be seen that The Interaction Damage Rule favors the shorter life in this 50% type 1, 50% type 2 hypothetical case, and the Alternative Rule favors the longer life. Of course, the minimum value expected in either case is N_1 , and the maximum value, N_2 . Both results are bounded by these numbers.

Fig. A1 compares these two rules for cases where N_2 is some other multiple of N_1 . From this, an interesting conclusion can be drawn: The Interaction Damage Rule is asymptotic. That is, even if the other contributing lives were infinite, the maximum value possible for life computed using the Rule equals the shortest contributing life (PP, PC, CP or CC) times the inverse of its constitutive fraction.

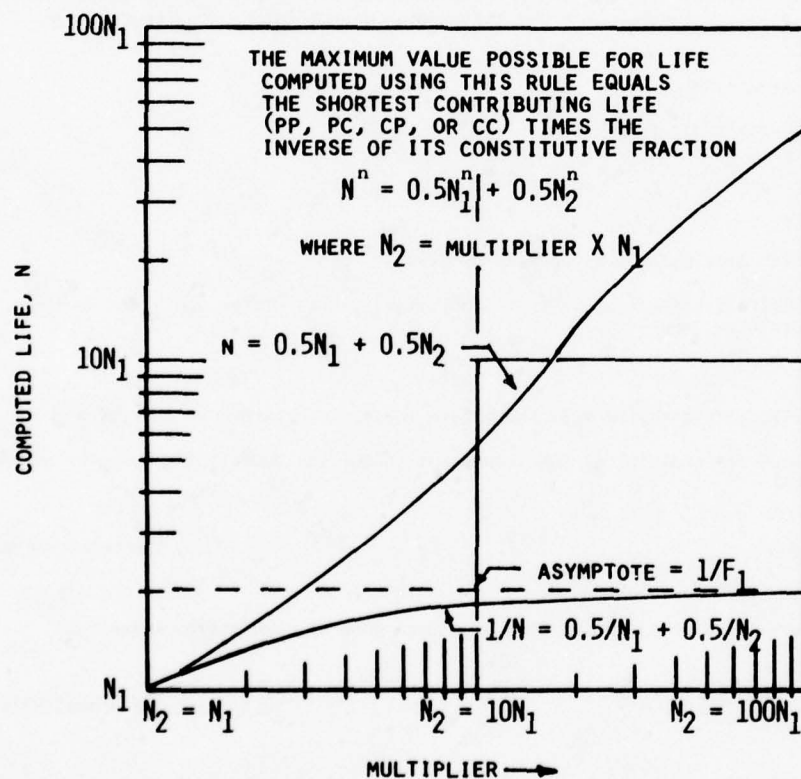


Fig. A1. The Interaction Damage Rule is Asymptotic.

* Chemical compositions, material processing, heat treatments and mechanical properties for each tested alloy, as well as the data generated in the programme, are given in Appendix A 1.

Table I
Typical Properties For IN-100 At 649°C

0.2% Yield Strength	Ultimate Tensile Strength	Elongation	RA
1100 MPa	1380 MPa	22%	25%
Stress Rupture Life			
100 hr	1000 hr		
1020 MPa	880 MPa		
Creep Rupture Life to 0.2%			
100 hr	1000 hr		
900 MPa	760 MPa		

Table II
Creep-Fatigue Data

LABORATORY PRATT&WHITNEY, FLORIDA, USA.
MATERIAL IN-100, GATORIZED

*** RATE DATA & STRESSES ***

SPEC NO	TEST TYPE	TEMP-C TEN/COMP	RATE DATA (HALF-LIFE VALUES)						STRESSES (HALF-LIFE VALUES) MPA					
			FREQ HZ	STRAIN-RATE TEN	/SEC COMP	MOLD TEN	TIME-SEC COMP	TEN MAX	COMP MAX	RANGE MAX	RELAXATION TEN	CYCLIC COMP	STRAIN HARDENING %	
PP-4	+MISC	650/650	5.0E-01	1.0E+00	1.0E+00	0.	0.	1137.	482.	1619.	0.	0.	0.0	
PP-3	+MISC	650/650	5.0E-01	1.3E+00	1.3E+00	0.	0.	1108.	793.	1901.	0.	0.	2.00	
00133	+MISC	650/650	5.0E-02	1.5E-01	1.5E-01	0.	0.	1106.	999.	2105.	0.	0.	6.00	
00134	+MISC	650/650	5.0E-02	1.5E-01	1.5E-01	0.	0.	1084.	944.	2028.	0.	0.	0.0	
00130A	+MISC	650/650	5.0E-02	1.0E-01	1.0E-01	0.	0.	1074.	421.	1495.	0.	0.	0.0	
00136	+MISC	650/650	1.0E-02	4.0E-02	4.0E-02	0.	0.	935.	694.	1629.	0.	0.	0.0	
00136B	+MISC	650/650	3.5E-02	1.4E-01	1.4E-01	0.	0.	1143.	1203.	2346.	0.	0.	-1.20	
00123	+MISC	650/650	5.0E-02	1.5E-01	1.5E-01	3600.	0.	977.	1016.	1995.	20.	0.	6.00	
00131	+MISC	650/650	5.0E-02	1.5E-01	1.5E-01	1800.	0.	1018.	1027.	2045.	9.	0.	6.00	
00132	+MISC	650/650	5.0E-02	1.5E-01	1.5E-01	300.	0.	981.	842.	1823.	70.	0.	2.50	
00244	+MISC	650/650	5.0E-02	1.0E-01	1.0E-01	120.	0.	911.	739.	1650.	86.	0.	-3.60	
00134A	+TCSU	650/650	5.0E-02	1.5E-01	1.5E-01	300.	0.	879.	1009.	1888.	0.	0.	3.70	
00120	+TCSU	650/650	5.0E-02	1.5E-01	1.5E-01	3600.	0.	963.	1097.	2060.	0.	0.	0.0	
00235	+TCSU	650/650	5.0E-02	1.5E-01	1.5E-01	120.	0.	886.	808.	1694.	0.	0.	-3.40	
00233	+TCSU	650/650	5.0E-02	1.0E-01	1.0E-01	120.	0.	798.	940.	1738.	0.	0.	4.00	
00137	+TCSU	650/650	5.0E-02	1.5E-01	1.5E-01	7200.	0.	935.	1111.	2046.	0.	0.	2.50	
00234	+TCSU	650/650	5.0E-02	8.5E-02	8.5E-02	120.	0.	985.	345.	1330.	0.	0.	0.0	

NOTE: * INDICATES ZERO TO TENSION STRAIN CYCLING.

*** STRAINS & FAILURE DATA ***

SPEC NO	TOTAL	STRAIN RANGES (HALF-LIFE VALUES) %						NO	FAILURE DATA-CYCLES			TF-MRS
		EL	IN	PP	PL	LP	LC		N1	N5	NF	
PP-4	0.990	0.962	0.028	0.028	0.0	0.0	0.0	0	2500	2600	2737	1.52
PP-3	1.260	1.206	0.054	0.054	0.0	0.0	0.0	0	1000	1060	1098	0.61
00133	1.400	1.257	0.142	0.142	0.0	0.0	0.0	670	0	0	737	4.09
00134	1.440	1.312	0.128	0.128	0.0	0.0	0.0	518	500	520	557	3.09
00130A	0.990	0.971	0.019	0.019	0.0	0.0	0.0	0	0	0	4697	26.09
00136	1.116	1.073	0.043	0.043	0.0	0.0	0.0	0	2300	2200	2412	40.20
00136B	1.750	1.440	0.308	0.308	0.0	0.0	0.0	0	0	0	212	1.68
00123	1.450	1.189	0.261	0.178	0.0	0.064	0.0	0	0	0	86	86.00
00131	1.430	1.211	0.219	0.143	0.0	0.076	0.0	0	0	0	236	118.00
00132	1.440	1.265	0.174	0.110	0.0	0.065	0.0	0	0	366	372	31.00
00244	0.990	0.954	0.036	0.008	0.0	0.012	0.0	3008	3008	3037	3109	103.60
00134A	1.346	1.237	0.109	0.046	0.0	0.057	0.0	0	279	279	301	25.10
00120	1.490	1.233	0.257	0.143	0.0	0.114	0.0	0	0	0	85	85.00
00235	1.030	0.996	0.034	0.013	0.0	0.019	0.0	0	2400	2400	2459	61.90
00233	1.120	1.080	0.040	0.024	0.0	0.016	0.0	0	1224	1255	1348	44.90
00137	1.520	1.178	0.342	0.226	0.0	0.113	0.0	0	0	0	67	134.00
00234	0.844	0.832	0.012	0.012	0.0	0.0	0.0	0	6288	0	6559	218.00

Fig. 1. Strain Control Specimen.

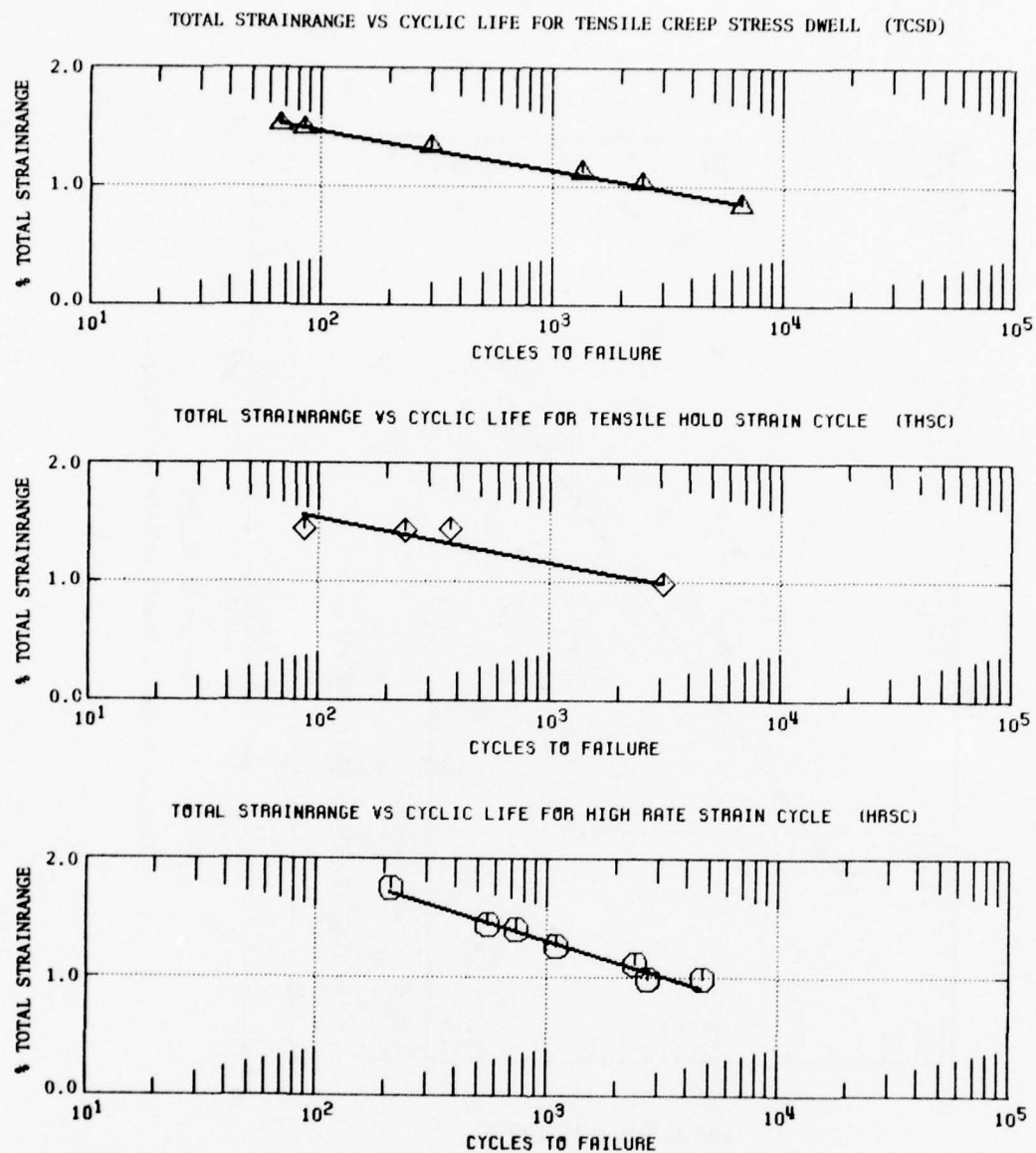


Fig. 2. Total Strainrange vs Cyclic Life.

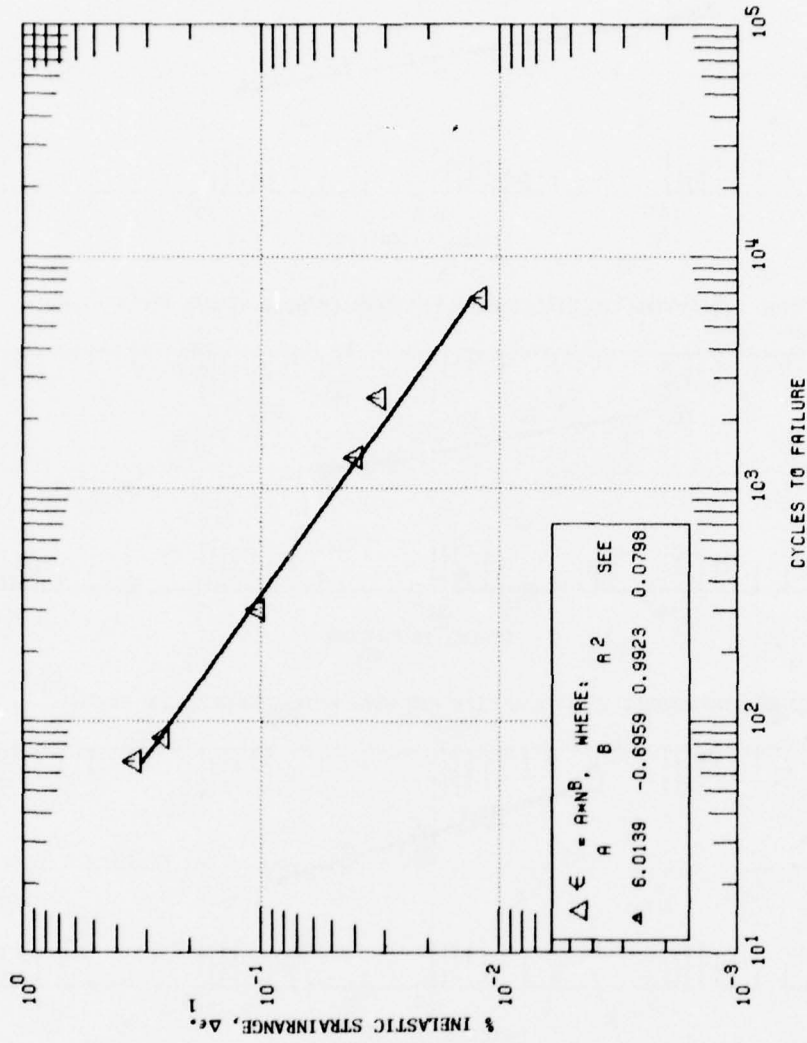


Fig. 3. Inelastic Strain vs Life for TCSD Cycle.

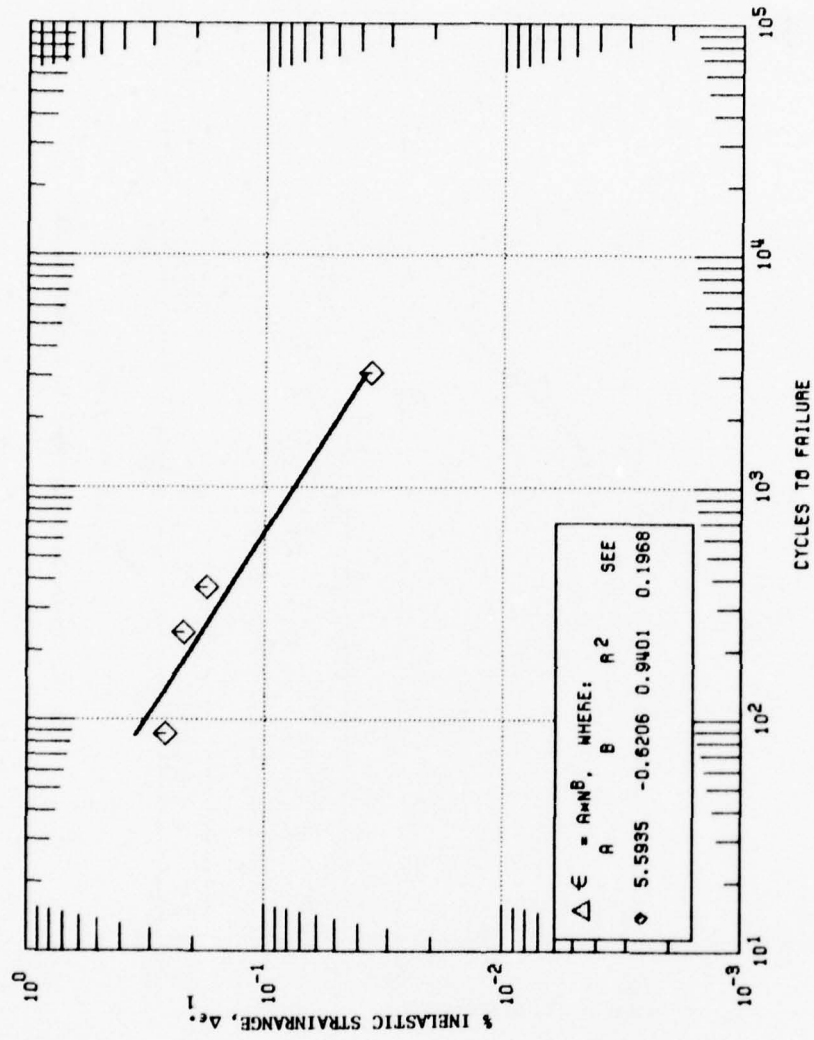


Fig. 4. Inelastic Strain vs Life for THSC Cycle.

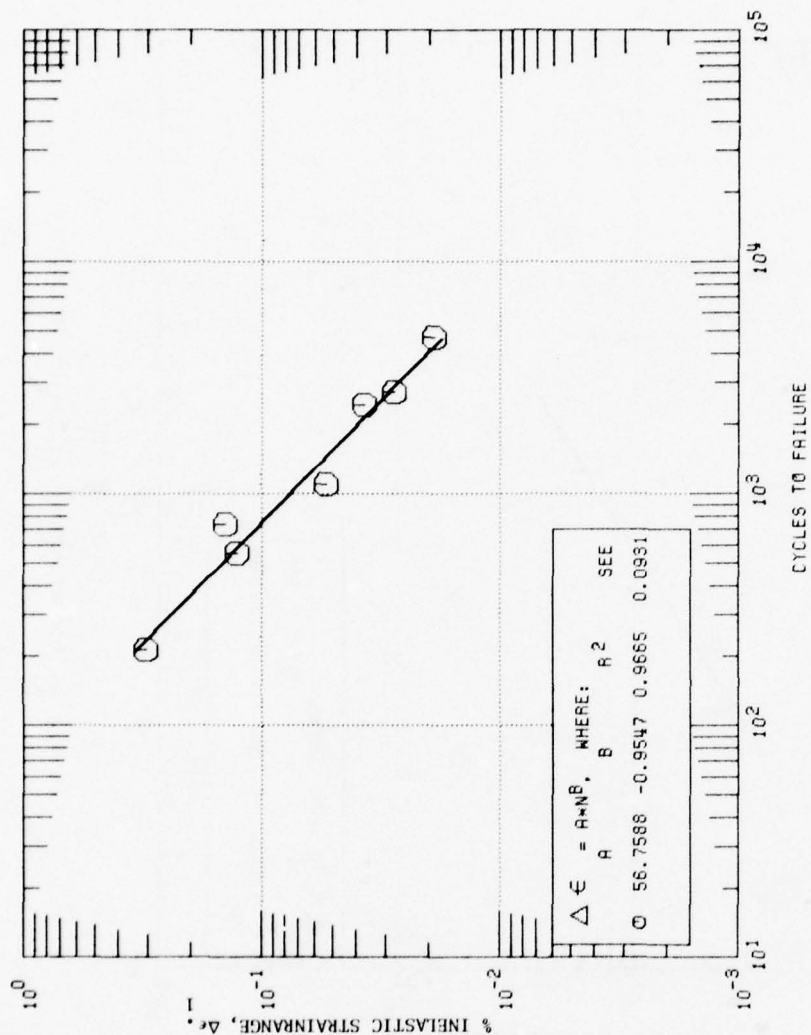


Fig. 5. Inelastic Strain vs Life for HRSC Cycle.

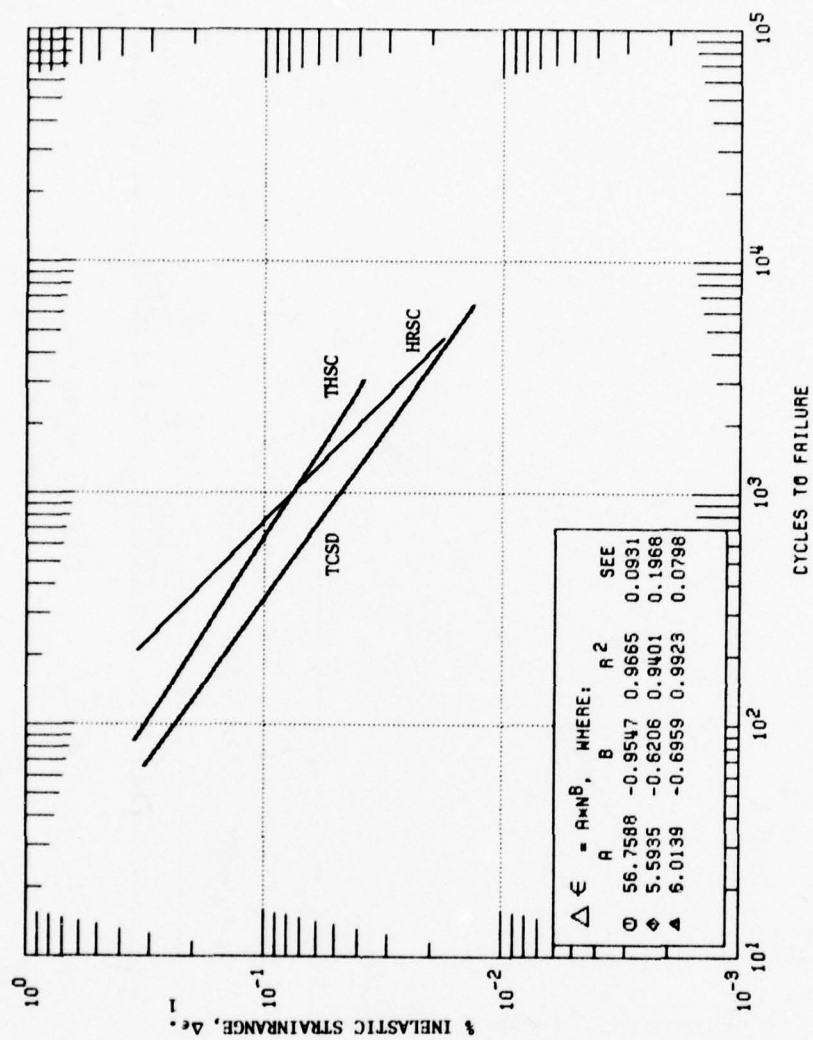


Fig. 6. Composite Plot for THSC, TCSD, and HRSC Tests.

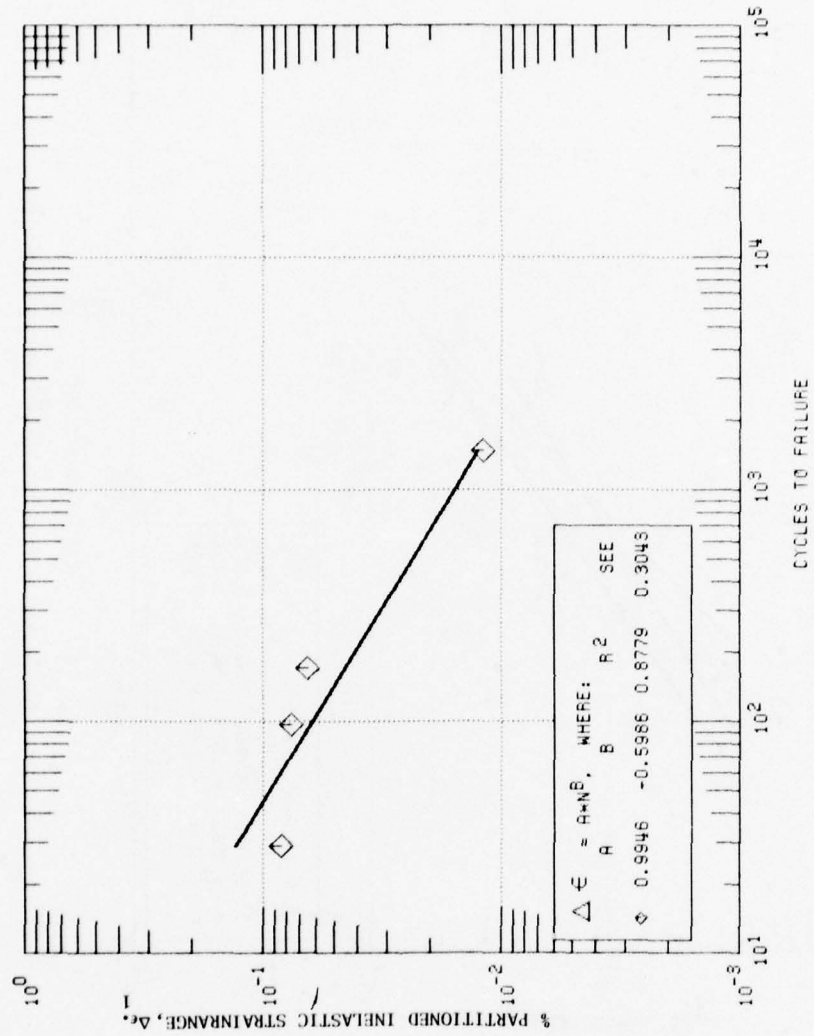


Fig. 7. Partitioned THSC Cycle.

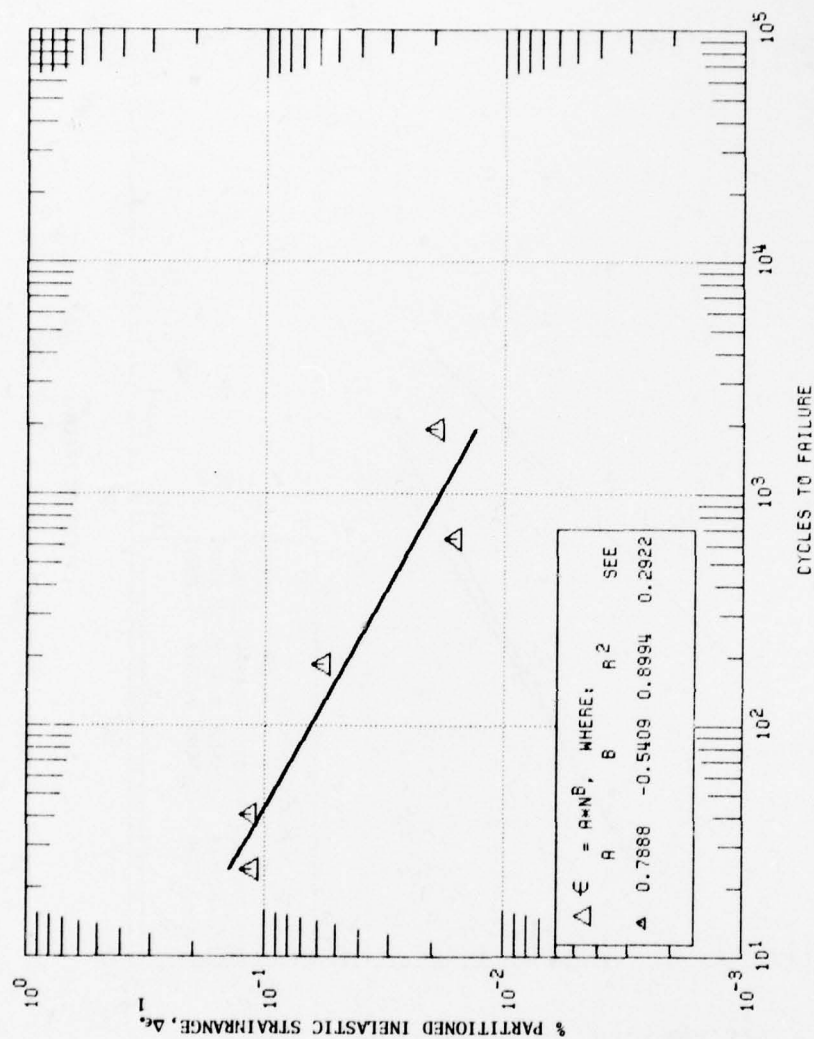


Fig. 8. Partitioned TCSD Cycle.

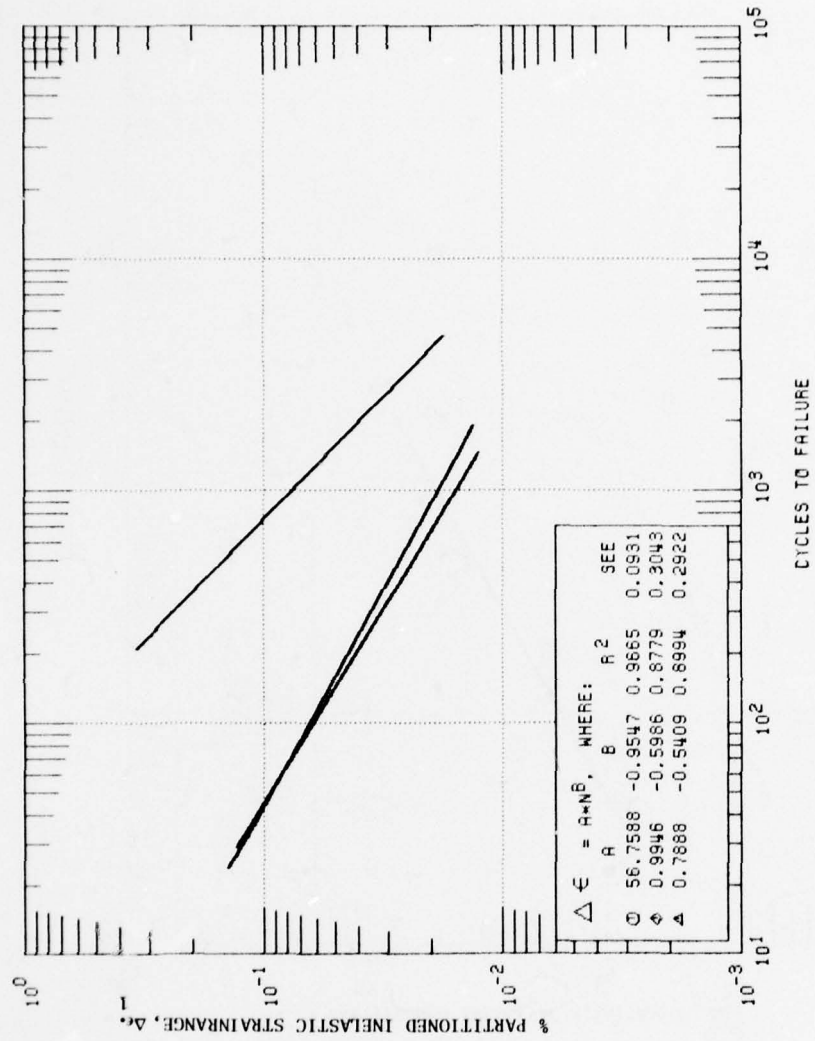


Fig. 9. Composite Plot for Partitioned THSC, TCSD, and HRSC Cycles.

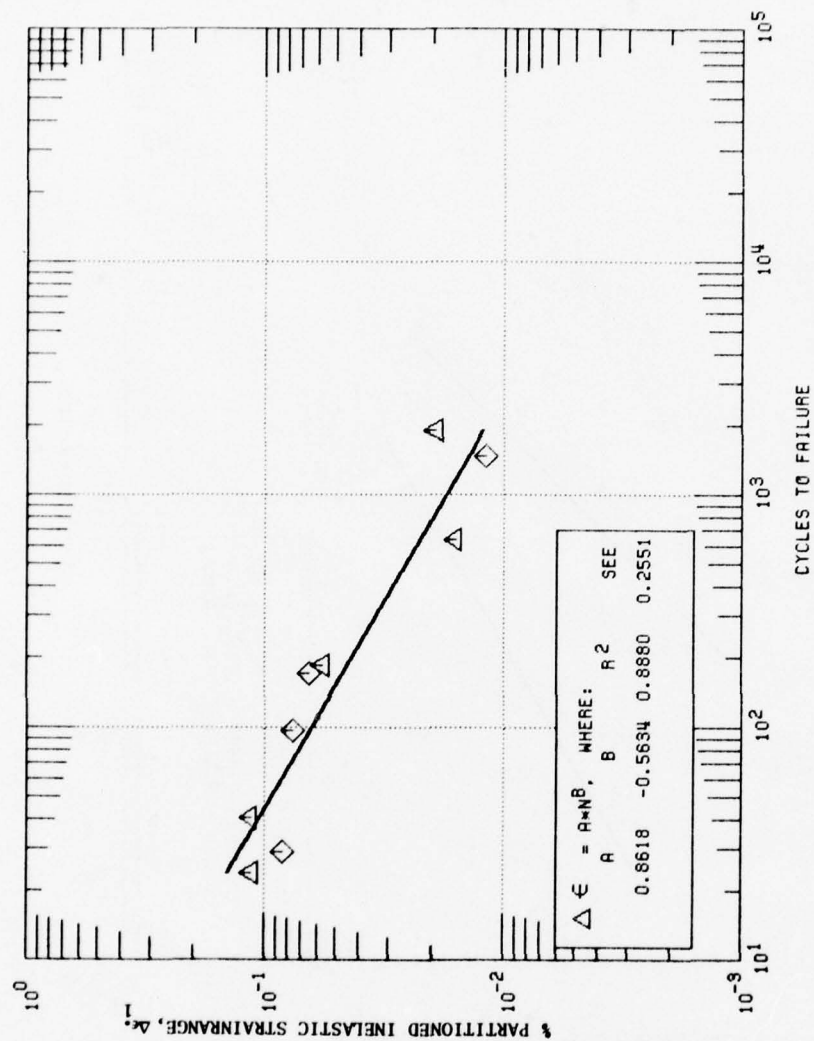


Fig. 10. Collective Regression of Partitioned TCSD and THSC Cycles.

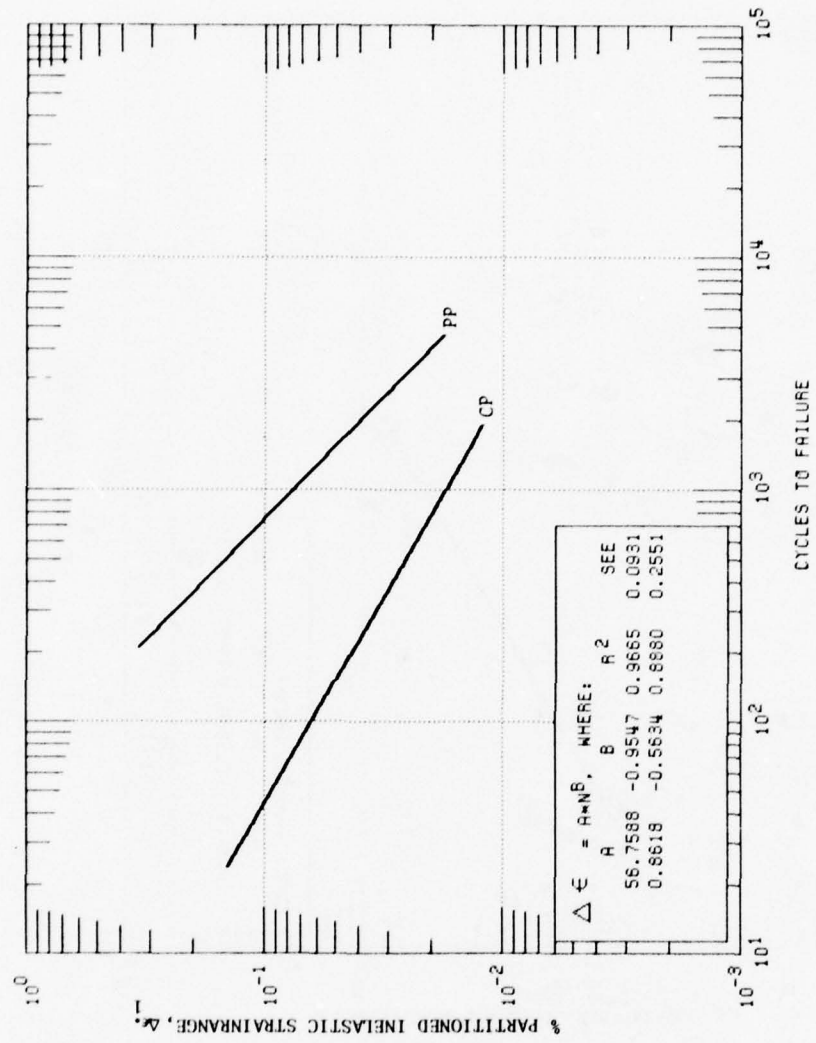


Fig. 11. PP and CP Inelastic Strain vs Cyclic Life.

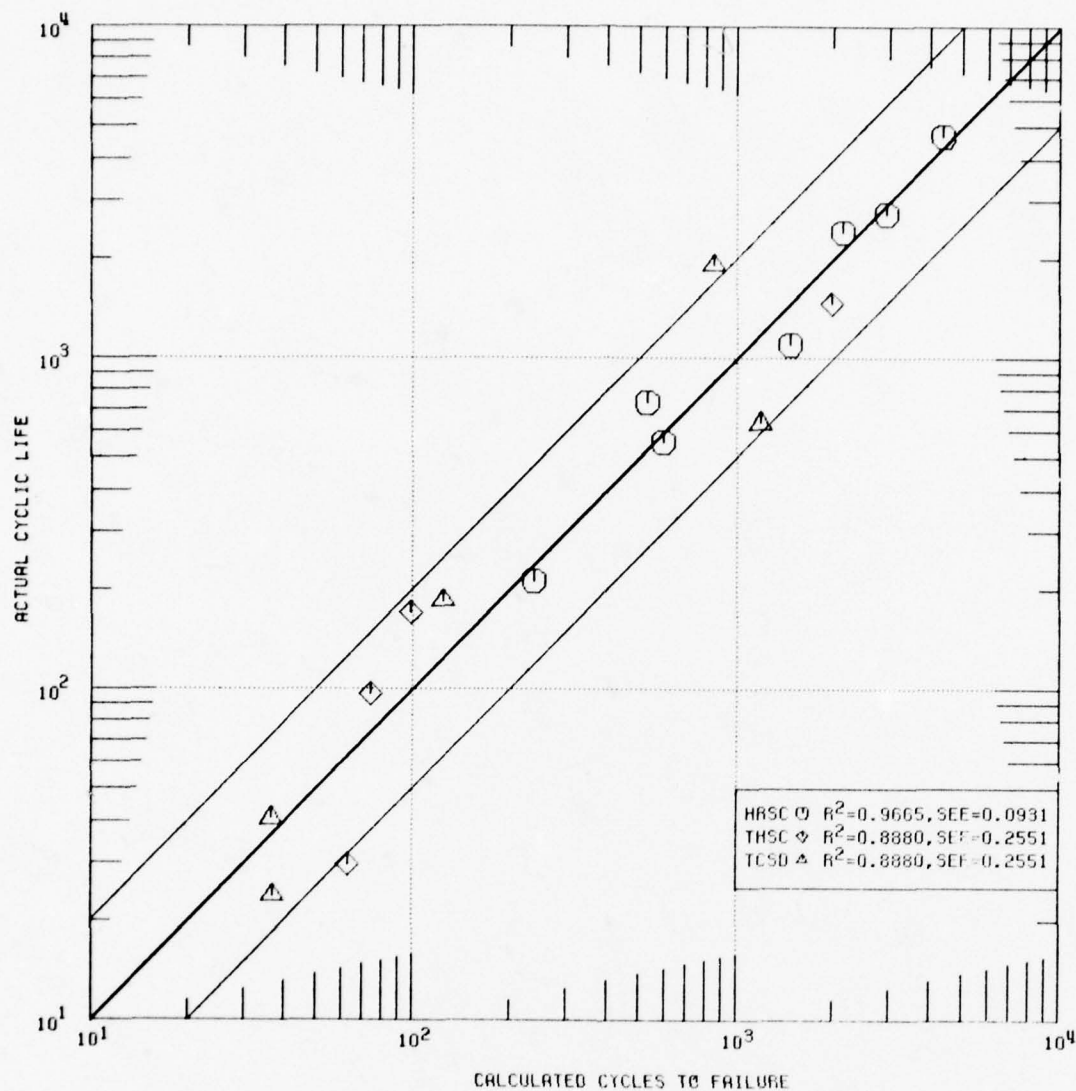


Fig. 12. Actual vs Calculated Cyclic Life for IN-100.

APPLICABILITY OF THE SRP METHOD AND CREEP-FATIGUE DAMAGE APPROACH TO THE LCHTF LIFE PREDICTION OF IN-100 ALLOY

by J.L. CHABOCHE, H. POLICELLA, H. KACZMAREK

*Office National d'Etudes et de Recherches Aéronautiques (ONERA)
92320 Châtillon (France)*



ABSTRACT

The main objective of the study is to compare the actual capabilities of two life prediction methods in the low cycle high temperature regime :

- the simplest one is the strain range partitioning which needs a number of special tests involving creep and fatigue interaction, but it is difficult to apply under complex situations where the inelastic strain components are small or when strain and temperature vary simultaneously ;
- the second one is the continuous damage approach, firstly proposed by the Russian, which can be applied to the prediction of the creep-fatigue interaction phenomenon by means of pure fatigue tests, pure creep tests and corresponding damage equations.

The two methods are evaluated for the IN-100 alloy at 900 and 1000°C. The comparative advantages are discussed under two complementary aspects :

- correlation of isothermal laboratory tests where stabilized cyclic loops are measured,
- prediction of isothermal or non isothermal conditions by using cyclic viscoplastic constitutive equations for mechanical behavior description of the material.



1 - INTRODUCTION

Owing to improvements in computer efficiency, calculation techniques and testing facilities during the past twenty years, we are now able to take into account the high temperature behaviour of materials in the design procedures of complex structures. The very strong requirements in various domains (safety, efficiency, economy, minimal cost . . .) lead to the use of lifetime prediction methods of continuously increasing sophistication, especially for gas turbine components [1, 2], nuclear plants and pressure vessels [3].

When a structure undergoes cyclic loading associated with high temperature conditions, its behaviour depends on several complex phenomena such as :

- the plastic and viscoplastic flows including hardening, creep, relaxation,
- the Bauschinger effects and the cyclic softening or hardening modifications under cyclic loading, which give rise or not to stabilized conditions,
- the high temperature-low cycle fatigue rupture process, induced by combination of creep and fatigue damage, which leads to macroscopic crack initiation in the most critical area of the structure.

From the engineer's point of view the size of this defect can be arbitrarily defined by reference to the need of taking it in account for the global equilibrium of the structures, with the Fracture Mechanics approach for example. Calculation of stress and strains in the structure with highly non linear behavior of the material and very complex situations including cyclic thermal stresses is a very difficult problem which solution can be reached either through sophisticated computer techniques [4, 5, 6] or simplified procedures as Neuber's rule [7, 8, 9] or Reference Stress methods [10, 11, 12].

The scope of the Agard Cooperative Program in the past three years was to contribute to the improvement of the lifetime prediction procedures based on these stress and strain calculations. In this area we examine two types of methods :

- The Strain Range Partitioning Approach [13, 14] which is defined by four basic rupture curves related to different components of the inelastic strain with separation of creep and plastic behaviors and of tensile and compressive effects. This method uses a number of special strain controlled tests with or without hold time, but modelizes only failure relations and not progressive damage : relatively simple to apply it must be considered as an efficient parametric interpretation of these

types of test. Other test correlations have been proposed in this high temperature regime, based on frequency [15] or strain rate [16, 17] dependence.

— On the other hand, the Continuous Damage Approach [18, 19, 20] give rise to the opportunity to describe the progressive deterioration processes taking place between initial undamaged state and final stage (failure of the specimen) which corresponds approximatively to initiation of the macroscopic crack in the structure [21]. This permits the modelization of several non linear cumulative effects [22] including the creep-fatigue interaction phenomenon [23, 24] : this last effect can be predicted by means of static creep and pure fatigue tests only, a few viscoplastic fatigue tests (cyclic tests with time effects) being used to check the predictions.

The main objective of the paper is to compare the accuracy of the two methods on the example of the turbine blade refractory alloy IN100 (coated), at 900 and 1000°C. The respective advantages can be discussed with reference to two complementary aspects : laboratory tensile-compressive test correlation and prediction, application to the lifetime prediction in actual complex structures.

2 — EXPERIMENTAL PROCEDURES AND TEST RESULTS

2.1. Description of test system

The cyclic tension-compression tests are realized with an electrohydraulic Schenck system, on high frequency induction heated cylindrical specimens. The working range of the machine is ± 2.5 tons, ± 10 mm displacement, with 100 Hz maximum frequency. The controlled parameter can be either the load or the measured elongation with wave form as desired.

The toroidal junction zones are designed in order to minimize stress concentration and buckling problems and to have a sufficient gauge length (fig. 1) [25].

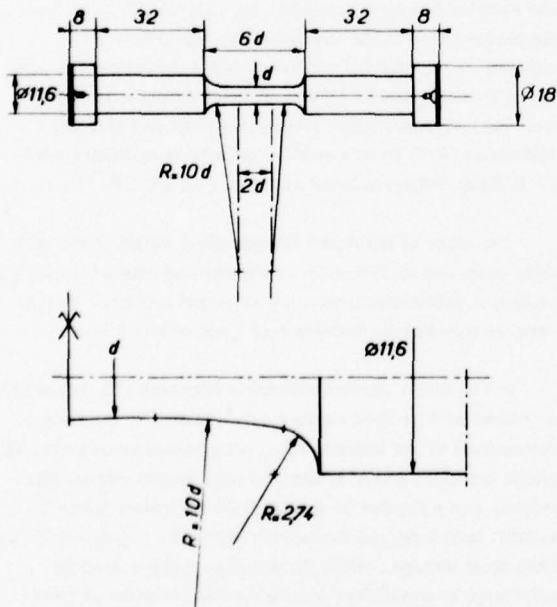


Fig. 1 — Cylindrical specimens.

The button head of the specimen are clamped with a special device (fig. 2) which gives a good stiffness and very good linearity in the considered loading range (axial preload of approximately 5 tons is applied by lock-nut screwing with a dynamometric spanner). Mounting and unmounting a specimen can be accomplished in a few minutes without difficulty [26].

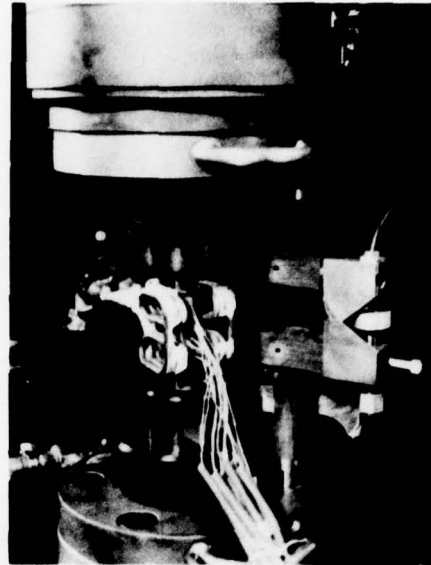


Fig. 2 — Gripping and heating systems.

The induction heating of the specimen is obtained by HF generator CELES GHF 2.5 AP, 2.5 kW with frequency between 100 and 500 kHz. The shape of the inductor spires are designed (fig. 2) in order to obtain the required temperature on the maximal length of specimen, including a large part of junction zones. The non classical transversal technique give rise to several advantages compared with helicoidal one [25] :

- heating is localized in the central part of the specimen, essentially in the junction zones, and sufficient degrees of freedom can be adjusted to have the best repartition,
- this type of inductor is more unsensitive to possible eccentricity : only the longitudinal position must be respected,
- the spires are setted up after mounting the specimen, which make easier mounting-unmounting operations.

Temperature calibration is first obtained on one or two specimens with a large number of thermo copples in the fatigue tests, thermocopples are spot-welded in junction zones and temperature control is accomplished by infrared technique (IRCON Modline 2000). Stability of the control is checked by a total radiation pyrometer (spectray-90-8885) in order to take into account possible variations of emittance induced by oxydation [26, 27]. Load, elongation and temperature measurements are recorded by means of X-Y recorders and a HP 2100S computer (magnetic tapes).

2.2. Strain measurements

The most difficult problem in this high temperature range is related to the axial strain measurement. Clipping of the extensometer by means of ridges has to be avoided owing to stress concentration and premature crack initiation risk [28]. The chosen method is to measure total displacement between the head of the specimen : either by optical extensometer (ZIMMER-OHG 203 X/50) sighting the head sides or by a displacement transducer (KAMAN KD 2300-25, ± 1.25 mm), fixed to the gripping system. In this way, an effective gauge length of the specimen must be defined in order to obtain inelastic strain in the central cylindrical part :

— the elastic part (linear) is analogically subtracted from the measured displacement u so as to give the inelastic elongation :

$$u_{in} = u - \frac{F}{R}$$

(R is the global stiffness of the specimen, F is the applied load),

— the inelastic strain is given by :

$$\epsilon_{in} = \frac{u_{in}}{L^*}$$

where L^* is defined by the relation between F (or ΔF) and u_{in} (or Δu_{in}) and the specimen geometry [25]. The correction due to junction zones are defined under the uniaxial approximation, neglecting the elastic limit and stress concentration [26]. For example, in the monotonic tensile test (neglect strain rate effect) the plastic behavior of the material is approximated by the power function :

$$\epsilon_{in} = \left(\frac{\sigma}{K} \right)^m$$

In that case one can show that the equivalent effective length is expressed as :

$$L^* = 2 \int_0^{L/2} \left[\frac{\phi(0)}{\phi(x)} \right]^{2m} dx$$

$\phi(x)$ being the diameter of cross section x .

Hence L^* depends only on geometry and strain hardening exponent m which can be determined before knowing

L^* (relation between u_{in} and F is identical to relation between ϵ_{in} and σ).

In the case of viscoplastic behavior or cyclic tests, other exponents can be defined giving rise to different values of L^* , but experience in this area [25] has shown that these different values are very close for a given material, given temperature, given geometry. The method has been checked at room temperature (with strain gauges) for monotonic and cyclic tests and by comparison with high temperature tests conducted in other laboratories.

2.3. Material and test results

The material is the high temperature refractory alloy IN100 which is used in gas turbine blades in the "as cast" conditions but with a protective coating. Under French specifications (AFNOR) this alloy is named NK15 CATu and was cast by SNECMA with chemical composition and coating procedure as follows :*

%	Mini	Maxi
C	0.15	0.20
Co	13	17
Cr	8	11
Al	5	6
Ti	4.3	4.8
Mo	2	4
V	0.7	1.2
Zr	0.03	0.06
B	0.010	0.014
Mn	—	0.2
Si	—	0.2
Ni	Balance	

Vapor phase aluminization coating head treatment :

- cleaning wet sandblasting with quartz "module 23",
- trichlorethylen vapor scouring,
- aluminization at 1150°C, 3 hours. Argon cooling.

Typical properties for the coated material are indicated at room temperature and 900, 1000°C :

Test temperature	Room	900°C	1000°C	
Elastic modulus (dynamic)	214 000	160 000	147 000	MPa
Yield strength (0.2 %)	770	550		MPa
Ultimate strength	890	715	470	MPa
Reduction of area	—	4	12	%
10 hour rupture stress	—	405	198	MPa
100 hour " "	—	280	128	MPa
1000 hour " "	—	187	82	MPa

Several type of tests were performed during two main periods : in 1973-74 [29, 25] and in 1977 [30] with two different casts : compatibility of the results was sufficiently checked by some high frequency fatigue tests and creep tests. Additional results have been obtained under repeated tension (5 Hz frequency) with small plate specimens [31]. (working part : 22 mm x 8 mm x 2 mm).

Table I summarizes the different types and numbers of tests at each temperature. Other creep tests made at SNECMA on uncoated specimens haven been used to define the stress rupture curves (reduction of rupture time by a factor 1.6 to 2 has been observed between uncoated and coated conditions if stress is defined with the total section area, after coating).

* Chemical compositions, material processing, heat treatments and mechanical properties for each tested alloy, as well as the data generated in the programme, are given in Appendix A 1.

Table I –
Review of the different types
of tests made in ONERA.

			Temperature (°C)						Total
Type			700	800	900	950	1000	1100	
Pure fatigue 5 Hz	push pull	x	4		13		6	5	28
	repeated	+				5			5
	two levels (push pull)	*			3		3		6
	two levels (repeated)	*				4			4
Creep				2	2	2	6	2	14
Creep after fatigue							5		5
Viscoplastic fatigue	2 cpm (Triangular)	□ ■ ○ ●		1	5		3		9
	with hold times	□ ■ ○ ●		2	12		12	2	28
	two temperature levels	◆			← 9 →				9
									108

The hold times in this work are relatively small (from 15 s to 870 s) because of the specific working domain of turbine blades [2].

2.4. Interpretation

The pure fatigue tests with zero mean stress can be used to define the pp basic curve of the strain range partitioning method (approximately zero mean strain is measured in the majority of these tests). Figure 3 gives the results for 700, 900, 1000°C ; at 1100°C creep effect seems not negligible even for this high frequency and number of cycle to failure is approximately reduced by a factor 3.

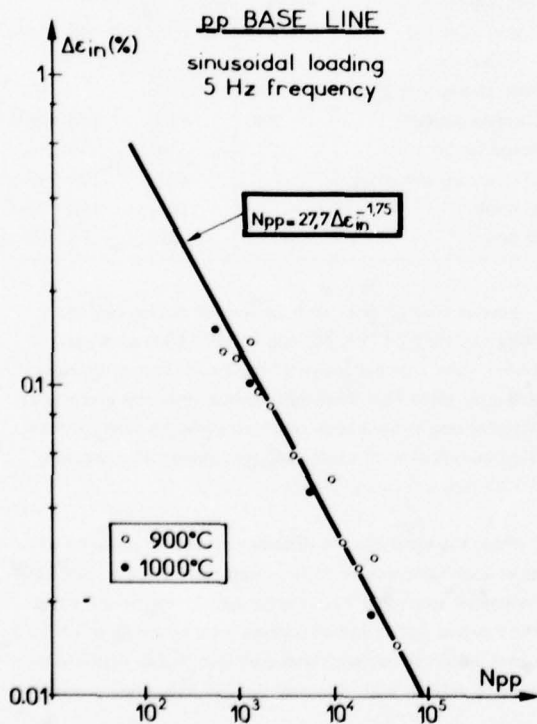


Fig. 3 – The pp basic curve as defined by 5 Hz frequency load controlled tests.

In the viscoplastic fatigue tests which have to be used in the cc, cp and pc curves, the transient periods are fixed to 15 s even in the hold time tests (this corresponds to 2 cpm for the triangular waves without hold time). As a consequence the creep contribution to the inelastic strain is never negligible in this transient period : obviously the zero hold time tests show a large reduction in life induced by creep mechanisms.

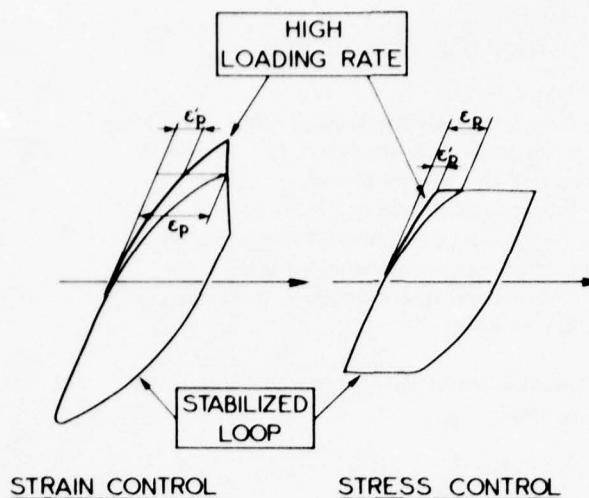
The problem is then to separate the creep and the plastic contribution in the transient periods : this can be made by the "Half Cycle Rapid Load-Unload Method" as indicated by the NASA Researchers [32]. In a few special tests, after the loop stabilization, the transient period is changed to 1.5 s for one cycle and one can measure the plastic component as the inelastic strain in this transient loading (corresponding to the stabilized maximum stress). Figure 4 illustrates schematically this method and Table II summarizes the obtained results. They can be used to check an empirical equation relating the stabilized transient inelastic strain ϵ_p' to the pp component (corresponding to higher strain rate). If the ratio of loading rate is approximately 10, we have :

$$(1) \quad \epsilon_p' = \alpha \epsilon_p^{1.7}$$

where α is equal to 53.3 for load control and 43.8 for strain control.

This empirical relation has been obtained by systematic application of a cyclic viscoplastic constitutive equation, which gives a very good modelization of the tensile-compressive high temperature cyclic behavior of IN100, including Bauschinger effects, strain rate influence and hold time effects [33]. These constitutive relationships are introduced and checked in the next paragraph.

Fig. 4 — The Half Cycle Rapid loading used to define the plastic contribution.



n ₀	Loading		Stabilized				High rate	
			σ _t	σ _c	Δε _{in}	ε _{pT}	N	ε' _{pT}
34	L	T + C 20	154	154	0.078	0.053	907	0.015
							1050	0.017
35	L	T + C 180	154	154	0.138	0.068	165	0.0195
							214	0.0245
36	E	T 300	185	248	0.180	0.132	206	0.082
37	E	T 300	135	212	0.096	0.061	208	0.017
38	E	C 300	261	100	0.098	0.088	256	0.020

Table II —
Results of special tests with the
half-cycle rapid loading, 1000°C.
Units : MPa, %, s.

3 — CYCLIC VISCOPLASTIC CONSTITUTIVE EQUATIONS

3.1. Phenomenological approach of internal variables

At high temperature under isothermal cyclic conditions, one can underline the following usually observed phenomena :

- monotonic hardening, primary creep, creep relaxation under tensile (or compressive) loading ; tensile curves are depending on the strain rate and of the control conditions (constant strain rate or constant stress rate),
- the Bauschinger effect which arises when compressive loading is applied after a tensile plastic prestrain : the compressive elastic limit is highly reduced but evanescence of this effect is observed as the compressive flow further progresses,
- under successive cycles the material can show either cyclic hardening or cyclic softening, until loop stabilisation is reached, which corresponds to an asymptotically stable cyclic behavior,
- other additional phenomena can be detected under longtime operation as secondary creep, accelerating or delay effects under varying the creep stress, strain recovery after unloading. . .

The internal variable approach [34, 35] is an interesting way to simulate most of these effects [36]. Under first approximation it is sufficient to define two specific hardening variables [37], :

- the isotropic variable which can describe the width of the actual elastic domain in stress space and is usually choosen as the accumulated plastic strain p :

$$(2) \quad \dot{p} = \sqrt{\dot{\epsilon}_{p,ij} \dot{\epsilon}_{p,ij}}$$

where $\dot{\epsilon}_{p,ij}$ are the components of the viscoplastic strain rate tensor (conventional summation is used) : this variable is physically related to the dislocation density variation from an arbitrarily initial state.

- the kinematic stress tensor (or internal stress, or additional stress [38] , or friction stress [39]) which represents the actual center of the elastic domain (also the center of all the viscoplastic equipotential surfaces or equidissipation surfaces). This variable, whose components are denoted χ_{ij} represents macroscopically the influence of the microscopic internal residual stresses induced in the polycrystal by the inelastic strain incompatibilities from one grain to another [40].

In the high temperature viscoplastic range the equipotentials can be written with Von Mises criterium and a power dependence. The classical normality condition leads to the following equation for the viscoplastic strain rate [41] :

$$(3) \quad \dot{\epsilon}_{p,ij} = \left\langle \frac{J(\sigma - \chi) - R(p)}{K} \right\rangle^{\frac{1}{n}} \frac{\sigma'_{ij} - \chi'_{ij}}{J(\sigma - \chi)}$$

where n and K are temperature dependent coefficients, σ'_{ij} and χ'_{ij} are the deviator components of stress and internal stress tensors. The notation $\langle u \rangle$ is defined by $\langle u \rangle = u$ if $u > 0$, 0 if $u \leq 0$. J denotes the Von Mises invariant of the active stress tensor :

$$J(\sigma - X) = \sqrt{(\sigma'_{ke} - X'_{ke})(\sigma'_{ke} - X'_{ke})}$$

$R(p)$ is a given function of the cumulated inelastic strain p which represents actual width of elastic domain. Schematically, an increasing function allows the description of monotonic hardening as well as cyclic hardening; on the other hand, a decreasing one, in conjunction with the kinematical effect can simultaneously modelize monotonic hardening and cyclic softening. An asymptotic value is reached as p increases, in order to give stabilization.

The kinematic internal variable evolution is given by the following equation:

$$(4) \quad \dot{X}_{ij} = C f(p) (a \dot{\epsilon}_{p,ij} - X_{ij} \dot{p}) - b X_{ij}^{m-1} X_{ij}$$

where C , a , b , m are temperature dependent coefficients and $f(p)$ is a given function, reaching an asymptotic value when p increases. The first term $a \dot{\epsilon}_{p,ij}$ corresponds to the linear kinematic hardening [42], the second one describing the evanescent strain memory effect as introduced by Armstrong and Frederick [43] in accordance to the "delay trace hypothesis" of Ilyushin [44]. These two terms give rise to a non linear kinematic hardening, where the dependence between the internal stress and the plastic strain is not unique: under tensile-compressive loading for example the internal stress-plastic strain relation accounts for hysteresis loops as seen on figure 5 for IN100 alloy. In particular this allows a good description of the Bauschinger effect and function $f(p)$ is sufficient to modelize the small cyclic softening observed on IN100.

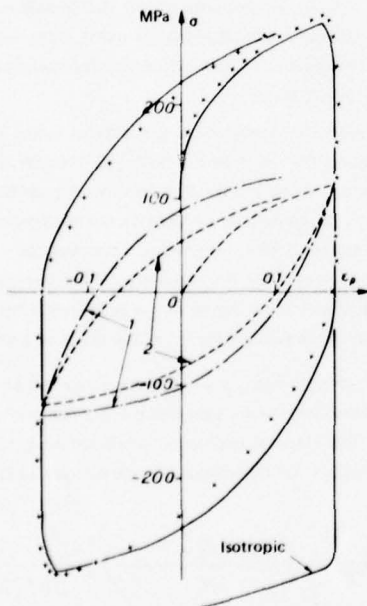


Fig. 5 — First cycle of a strain controlled test. Evolution of the internal stress (IN100 - 1000°C).

The last term in the equation (4) describes the time recovery phenomena, effectively observed under long time operation, with or without macroscopic plastic strain modifications: here the power dependency is in accordance with works of Bever [45], Malinin and Khadjinsky [38], and Lagneborg for an analogous dislocation density recovery model (isotropic hardening) [46].

Under one-dimensional tensile-compressive loading the constitutive equations can be written as:

$$\begin{aligned} \dot{\epsilon}_p &= \left\langle \frac{|\sigma - X| - R(\bar{\epsilon}_p)}{K} \right\rangle^n S_3(\sigma - X) \\ (5) \quad \dot{X} &= C f(\bar{\epsilon}_p) (a \dot{\epsilon}_p - X \dot{\bar{\epsilon}}_p) - b |X|^m S_3(X) \\ \dot{\bar{\epsilon}}_p &= |\dot{\epsilon}_p| \end{aligned}$$

Now, the values of K , C , a , b are easily deduced from the corresponding ones of the three-dimensional equations. Usually, it is sufficient to suppose functions $f(p)$ and $R(p)$ of exponential type:

$$\begin{aligned} f(\bar{\epsilon}_p) &= l + (1-l) e^{-\beta \bar{\epsilon}_p} \\ R(\bar{\epsilon}_p) &= k + h [1 - e^{-\gamma \bar{\epsilon}_p}] \end{aligned}$$

k and $k+h$ are respectively the initial and asymptotic values of the elastic domain width.

It must be underlined that these constitutive equations are thermodynamically acceptable as showed by the internal state variable approach which allows to formulate equations in accordance with the First and Second Laws: this is of great physical importance for justification of basic assumptions. In the low temperature regime, where time independent plasticity is a sufficiently good approximation, these equations can be easily extended [43, 47].

3.2. Application to IN100 alloy

For this alloy, high temperature elastic domain is sufficiently small to be neglected with $R(\bar{\epsilon}_p) = 0$, the other coefficients being determined by identification with monotonic and cyclic test results. At 1000°C, they are:

$$\begin{aligned} n &= 8, \quad K = 455, \quad a = 140, \quad C = 1150, \quad m = 8, \\ b &= 0.17 \cdot 10^{-11} \end{aligned}$$

The cyclic softening is sufficiently well described by the function:

$$f(\bar{\epsilon}_p) = 0.6 + 0.4 e^{-400 \bar{\epsilon}_p}$$

which allows stabilization after a few cycles only. Under cyclic loading (with hold times smaller than 1 h) the time softening term can be neglected so that five coefficients only are needed in order to describe the asymptotic state and two more for the description of monotonic tests and cyclic softening.

Validation has been made with primary creep tests and tensile relaxation as well as for the cyclic softening (see for example [33 or 36]). The figure 5 shows the first cycle of an elongation controlled test (triangular wave) in the stress-inelastic strain diagram, where comparison is very good with the choosen coefficients. Also several comparisons can be made on figure 6 for stress or elongation control (with or without hold times).

For the stabilized cyclic conditions ($\dot{\epsilon}_p \rightarrow \infty$) possibilities of the model are demonstrated in the stress range-inelastic strain range diagram 7 for several test controls, including hold time effects. Also the 5 Hz frequency tests are satisfactorily predicted, which underlines the adequacy of strain rate influence in the equations. Effect of the period in cyclic creep tests is shown on figure 8. Examples of initial or stabilized loops are showed on figure 9.

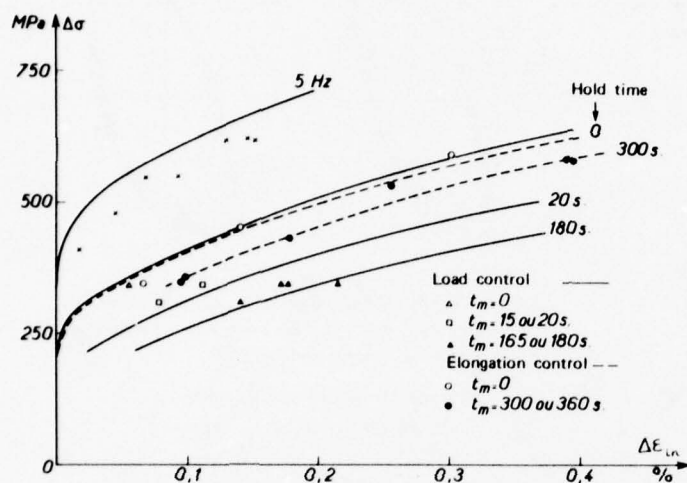


Fig. 7 — Effect of hold time and frequency on the relation between stress range and inelastic strain range.

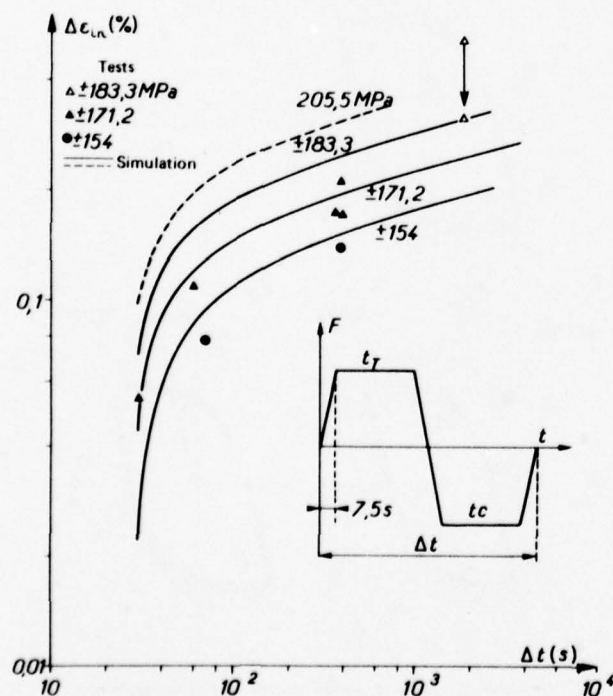


Fig. 8 — Effect of cycle period in the cyclic creep tests (the transient part of the cycle is 30 s).

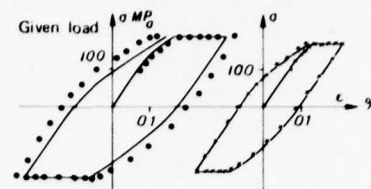


Fig. 6 —
Calculated and measured
first cycles of several
tests, IN100 - 1000°C.

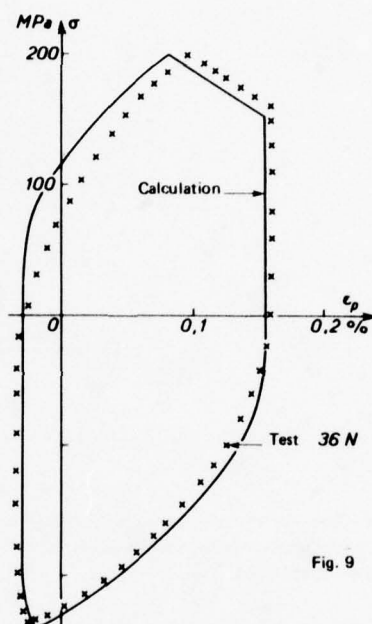
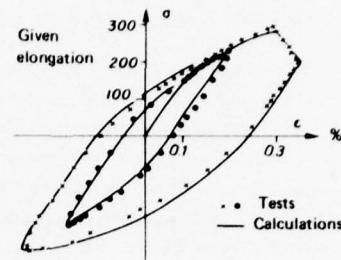


Fig. 9

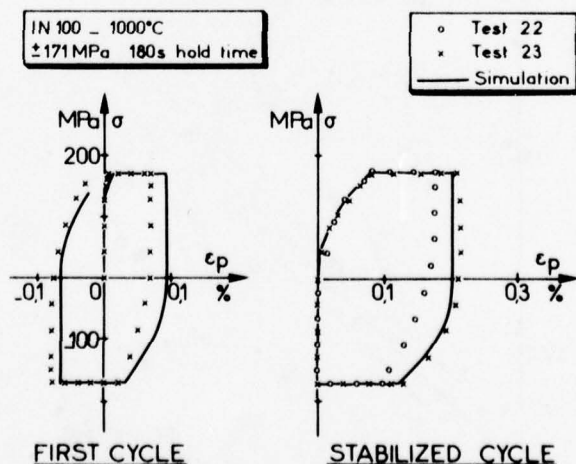


Fig. 9 — Examples of initial and stabilized loops.

All these comparisons, summarized in figure 10, demonstrate the efficiency of the proposed constitutive equations and the accuracy of coefficients. The comparison is also made for the higher strain rate results in the special tests (for this rapid loading the initial conditions are introduced as results from the stabilized calculated loop). Results of the systematic numerical study of this type of special tests, are indicated in figure 11 as interpreted by the empirical equation (1) with influence of the ratio of loading rates ($\alpha = 0.4$ and $a = 134$ or 110 for load or strain control).

Additional possibilities of the constitutive equations can be demonstrated by two simulations of typical cyclic tests : figure 12 shows an example of material with large cyclic hardening, figure 13 corresponding to the same tests with a pronounced cyclic softening. The stabilized loops are shown as saturated lines. Also two cases of stress control (cyclic hardening) are shown in figure 14, one of them giving rise to strain ratcheting (unsymmetrical loading).

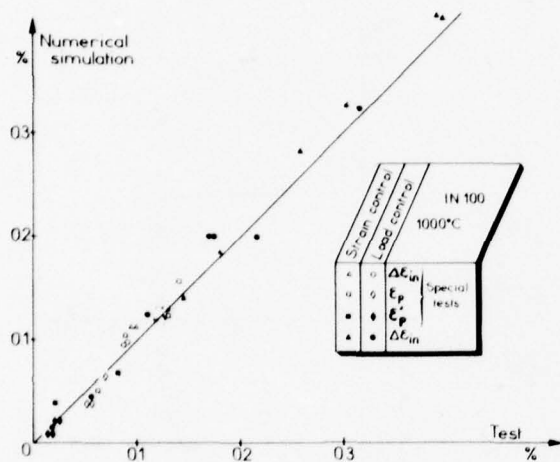


Fig. 10 — Measured and calculated values of the stabilized inelastic strain ranges, of the transient inelastic strains and of the plastic components as defined by rapid loading.

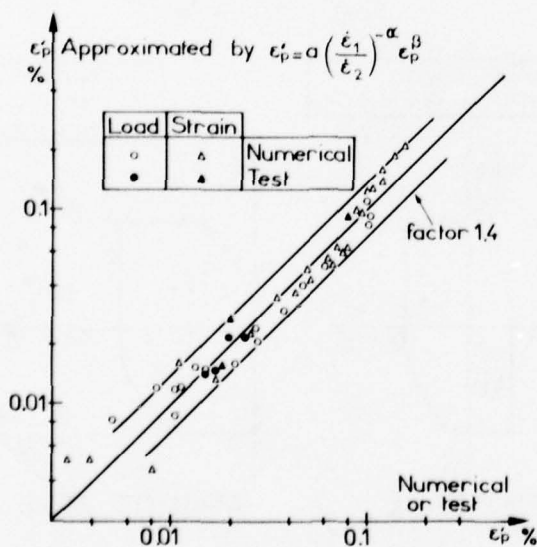


Fig. 11 — Values of plastic component obtained from empirical equation as a function of the calculated or measured ones.

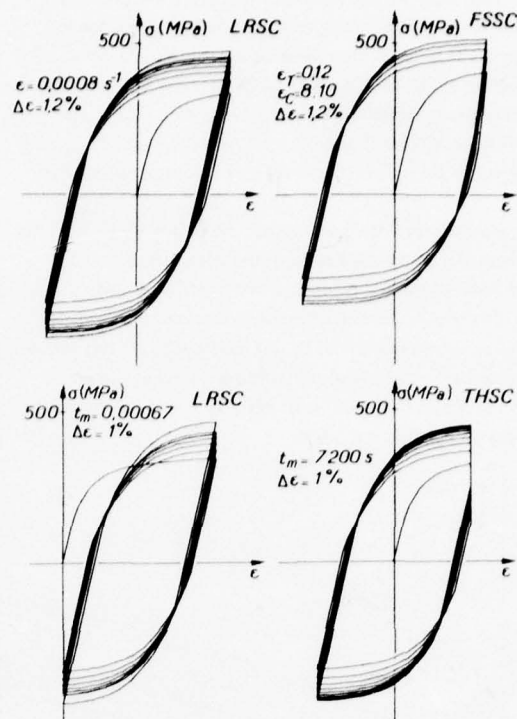


Fig. 12 — Examples of simulation with large cyclic hardening : (strain controlled tests : zero mean strain, zero minimum strain, high-low strain rates, tensile hold period).

$$n = 8 \quad k = 445 \quad a = 140 \quad C = 1150$$

$$\ell = 0.6 \quad \beta = 400 \quad k = 4 \quad h = 250 \quad \gamma = 5$$

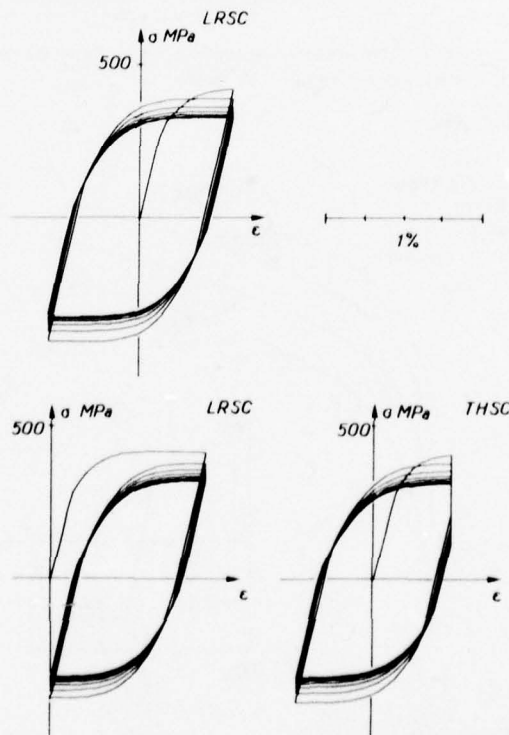
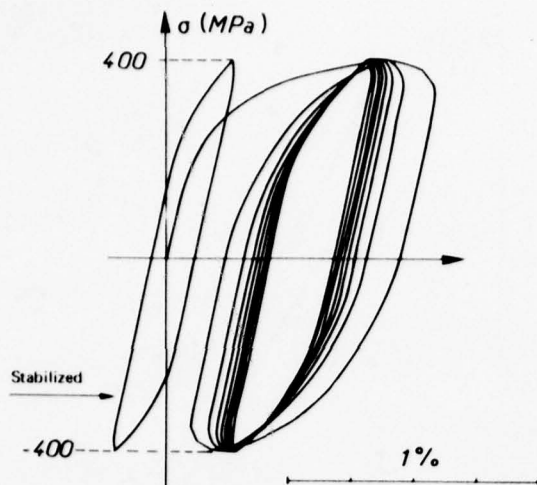


Fig. 13 — Examples of simulation with large cyclic softening.

$$n = 8 \quad k = 445 \quad a = 140 \quad C = 800$$

$$\ell = 1 \quad \beta = 0 \quad k = 120 \quad h = -115 \quad \gamma = 30$$



4 - STRAIN-RANGE PARTITIONING

4.1. Determination of the four basic lines

The problem is now to obtain the four SRP basic failure lines from the test results (parag. 2.4) in accordance with the preliminary study of the plastic part of transient inelastic strain.

Firstly the pp line is directly defined by the pure fatigue test results (5 Hz frequency) as shown on figure 3. In each of the low frequency tests the transient inelastic strain is measured on the stabilized loop (tensile and compressive).

The empirical equation (1), checked by some special test results (parag. 2.4) and by the numerical study based on constitutive equations (parag. 3.2), is used in order to define the plastic component in tension and in compression for each stabilized loop: values of \mathcal{E}'_{pe} (\mathcal{E}'_{pc}) are obtained from measured values of transient inelastic strains \mathcal{E}_t (\mathcal{E}_c). In relation (1) the ratio of usual transient period to the rapid load-unload period has been taken as 10, which leads in this rapid loading to strain rates of about $0.5 \cdot 10^{-2}$ to 10^{-2} s^{-1} .

Strain partitioning of the loop is now very easy by relations:

$$\begin{aligned} \Delta \mathcal{E}_{pp} &= M_{in}(\mathcal{E}'_{pe}, \mathcal{E}'_{pc}) \\ (6) \quad \Delta \mathcal{E}_{cc} &= \Delta \mathcal{E}_{in} - M_{ax}(\mathcal{E}'_{pe}, \mathcal{E}'_{pc}) \\ \Delta \mathcal{E}_{cp} &= (\Delta \mathcal{E}_{in} - \Delta \mathcal{E}_{pp} - \Delta \mathcal{E}_{cc}) \langle \mathcal{E}'_{pe} - \mathcal{E}'_{pc} \rangle \\ \Delta \mathcal{E}_{pc} &= (\Delta \mathcal{E}_{in} - \Delta \mathcal{E}_{pp} - \Delta \mathcal{E}_{cc}) \langle \mathcal{E}'_{pc} - \mathcal{E}'_{pe} \rangle \end{aligned}$$

where \mathcal{E}'_{pe} and \mathcal{E}'_{pc} denote the plastic tensile and compressive parts of the inelastic strain range $\Delta \mathcal{E}_m$; symbol $\langle \cdot \rangle$ is defined by:

$$\langle u \rangle = \begin{cases} u & \text{if } u > 0 \\ 0 & \text{if } u \leq 0 \end{cases}$$

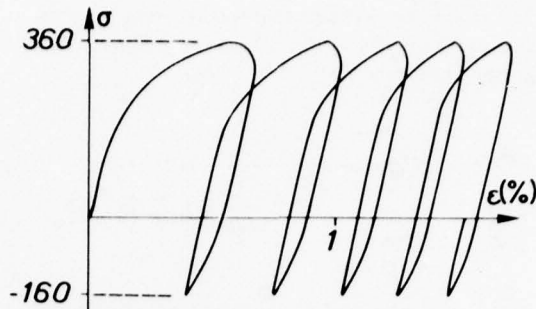


Fig. 14 - Cyclic hardening simulation for stress controlled tests.

The results have been indicated on the SRP summary record sheets. The corresponding strain ratios are obtained by equations of the type:

$$(7) \quad F_{ij} = \frac{\Delta \mathcal{E}_{ij}}{\Delta \mathcal{E}_{in}}$$

Now the cc basic failure is determined by the cyclic creep tests and some elongation controlled tests (without hold time), where $\Delta \mathcal{E}_{pc} = \Delta \mathcal{E}_{cp} = 0$:

$$(8) \quad N_{cc}(\Delta \mathcal{E}_{in}) = \frac{F_{cc}}{\frac{1}{N_R} - \frac{F_{pp}}{N_{pp}(\Delta \mathcal{E}_{in})}}$$

where N_R is the number of cycles to complete failure in the tests. Figure 15 shows this cc basic curve and quasi-independence on temperature is observed (900 and 1000°C).

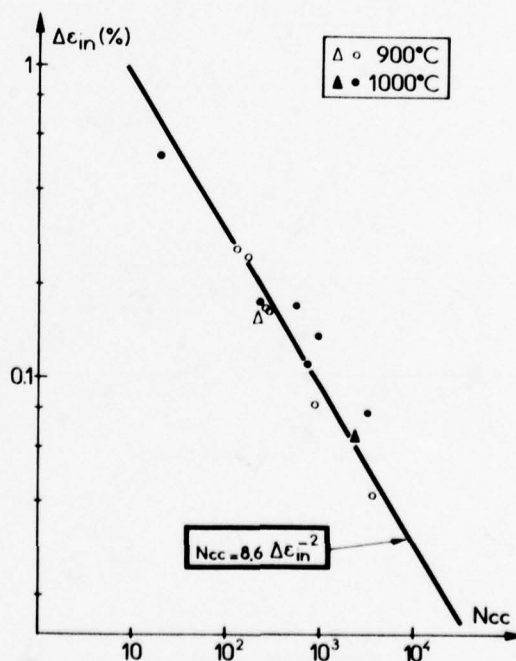


Fig. 15 - The cc basic curve as defined by cyclic creep tests and some strain controlled tests.

The cp baseline (or the pc one) is obtained by the other tests by taking into account the influence of $\Delta\epsilon_{pp}$ and $\Delta\epsilon_{cc}$ by equation of the type :

$$(9) \quad N_{cp}(\Delta\epsilon_{in}) = \frac{F_{cp}}{\frac{1}{N_R} - \frac{F_{pp}}{N_{pp}(\Delta\epsilon_{in})} - \frac{F_{cc}}{N_{cc}(\Delta\epsilon_{in})}}$$

N_R being the number of cycles to complete fracture in the cp (or pc) test. The figure 16 indicates the two curves : dispersion is more important, probably because of the relatively small values of F_{cp} or F_{pc} ratios in the tests. The four lines are plotted on figure 17 as interpreted by the following power expressions ($\Delta\epsilon_{in}$ is in % units) :

$$(10) \quad \begin{aligned} N_{pp} &= 27.7 \Delta\epsilon_{in}^{-1.75} \\ N_{cc} &= 8.6 \Delta\epsilon_{in}^{-2} \\ N_{cp} &= 4.3 \Delta\epsilon_{in}^{-2} \\ N_{pc} &= 33.3 \Delta\epsilon_{in}^{-1.5} \end{aligned}$$

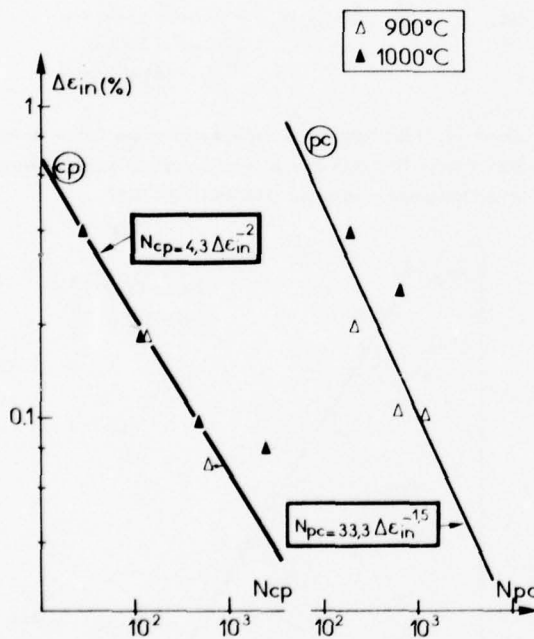


Fig. 16 – The cp and pc baselines.

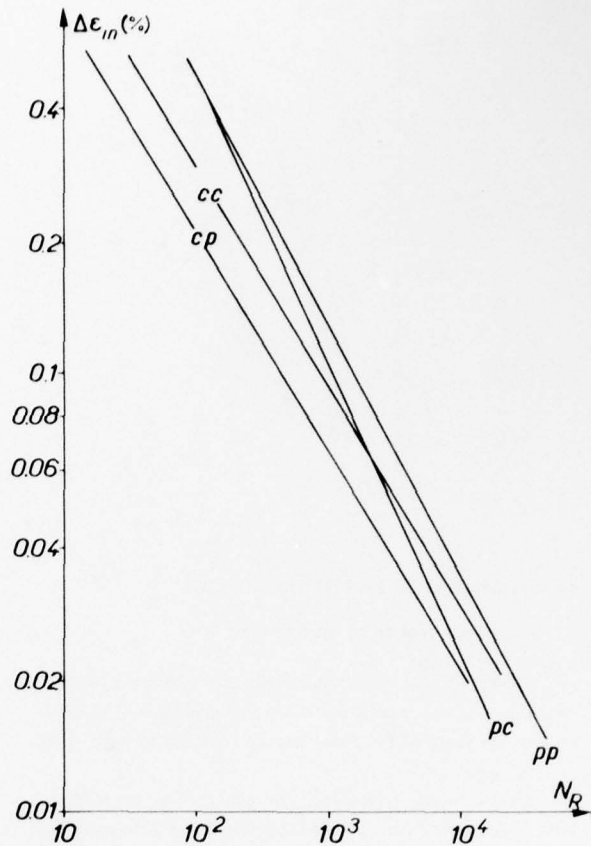
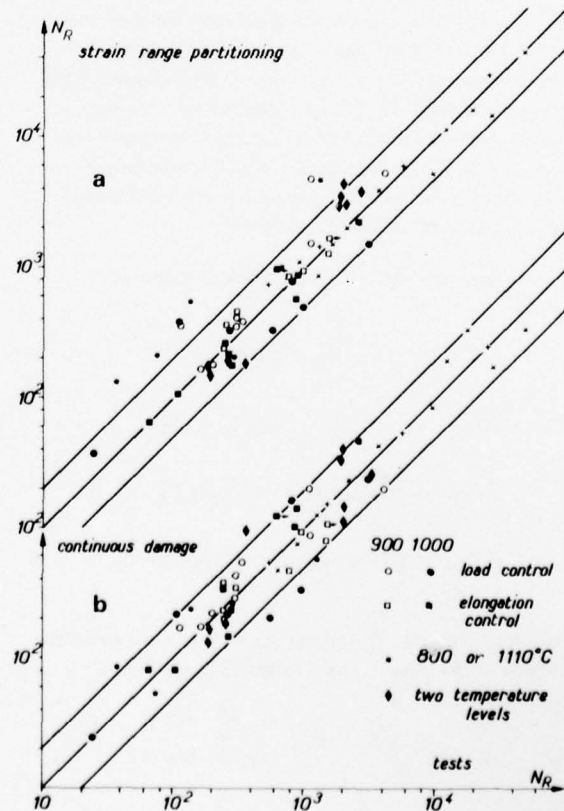


Fig. 17 – The four lines of the Strain Range Partitioning.

Fig. 18 – Predictability of the two methods (from measured stabilized loops)

- a) Strain Range partitioning.
b) Continuous Damage approach.



Differences between these relations are not very important for the IN100 alloy, as shown also by other laboratories [48].

All the results of this analysis are summarized in table III.

4.2. Predictability of the SRP Method

The same tests can be used in a reversed predictive analysis : test measurement of strain ratios F_{ij} allows to prediction of number of cycles to fracture N_R by the damage summation :

$$(11) \quad \frac{1}{N_R} = \frac{F_{pp}}{N_{pp}} + \frac{F_{cc}}{N_{cc}} + \frac{F_{cp}}{N_{cp}} + \frac{F_{pc}}{N_{pc}}$$

where the nominal N_{ij} are defined by relations (10) from the measured inelastic strain range. Results agree reasonably well (table VI and figure 18a), even for tests which were not included in the baseline determination. However, two special cyclic creep tests (n° 44 and 45), with reversed loading conditions but tensile hold time only, show ratchetting effect and considerably lower life as predicted by strain range partitioning. Next paragraph will show the better predictions in that case, when creep damage is explicitly included in the analysis.

Table III — Results of the partitioning analysis.

	n°	T	con- trol	$\Delta\epsilon_{in}$	F_{pp}	F_{cc}	$F_{cp/pc}$	N_R	N_{pp}	N_{cc}	$N_{cp/pc}$
cc	28	900	E	0.156	0.42	0.58		300	715	212	
	34	1000	E	0.065	0.192	0.808		2520	3310	2384	
	40	900	L	0.174	0.613	0.387		299	590	168	
	42	"	L	0.082	0.358	0.642		1130	2205	888	
	49	"	L	0.042	0.195	0.805		4014	7110	3630	
	51	1000	L	0.520	0.212	0.788		24	87	20	
	54	900	L	0.258	0.350	0.650		159	297	127	
	55	1000	L	0.175	0.250	0.750		263	585	222	
	56	900	L	0.164	0.324	0.676		338	655	274	
	57	1000	L	0.111	0.20	0.80		800	1300	730	
	N5	900	L	0.245	0.353	0.647		200	325	165	
	N6	"	L	0.165	0.193	0.807		294	650	260	
	N32	1000	L	0.172	0.210	0.790		568	603	559	
	N34	"	L	0.078	0.140	0.860		3108	2406	3262	
	N35	"	L	0.138	0.125	0.875		954	886	964	
cp	36	1000	E	0.392	0.540	0.255	0.205	64	143	56	28
	39	900	E	0.180	0.315	0.440	0.245	239	556	265	125
	N7	"	E	0.070	0.060	0.840	0.100	>1500	2910	1755	> 600
	N8	"	E	0.080	0.120	0.770	0.110	1493	2300	1350	2450
	N36	1000	E	0.180	0.300	0.492	0.208	243	556	265	121
	N37	"	E	0.096	0.125	0.735	0.140	870	1675	933	487
pc	37	1000	E	0.390	0.520	0.260	0.220	107	144	57	193
	N9	900	E	0.102	0.110	0.640	0.250	944	1505	827	1180
	N10	"	E	0.105	0.090	0.670	0.240	764	1430	780	620
	N12	"	E	0.196	0.280	0.210	0.510	250	480	224	206
	N13	1000	E	0.255	0.300	0.280	0.420	268	303	132	677

Table IV — Results of tests with changing temperature and stress after N_1 cycles. Predictions by the two methods.

n°	$t_T - t_c$	T_1	σ_1	N_1	$\Delta\epsilon_{in1}$	$\Delta\epsilon_{pp1}$	T_2	σ_2	$\Delta\epsilon_{in2}$	$\Delta\epsilon_{pp2}$	Failure : $N_1 + N_2$		
											Test	SRP	C D
15	0	900	411	200	0.125	0.058	1000	171	0.048	0.007	1948	3015	4133
16	20	900	411	100	0.320	0.137	1000	171	0.118	0.029	349	175	969
17	180	900	411	30	0.455	0.126	1000	171	0.180	0.0375	181	150	130
18	0	900	342	600	0.070	0.020	1000	171	0.047	0.0075	1889	3465	3444
19	0	900	342	850	0.069	0.020	1000	171	0.050	0.0105	1980	3012	1096
20	0	1000	171	2200	0.055	0.011	900	342	0.040	0.0082	2622	3815	2586
21	0	1000	171	875	0.055	0.011	900	342	0.043	0.085	1968	4420	1436
22	180	1000	171	160	0.172	0.029	900	342	0.032	0.0940	264	210	192
23	180	1000	171	160	0.215	0.032	900	411	0.485	0.1090	186	169	168

A few additional tests at 800 and 1110°C are also included in this analysis. Results are less accurate which indicate an effect of temperature, but no sufficient number of tests have been performed.

More significant is the verification by the special cyclic creep tests with varying temperature and stress in two blocks : a first level at temperature T_1 with stress σ_1 is applied for a given number of cycles; after unloading, temperature is changed to T_2 and cycling under stress σ_2 is continued until fracture with the same wave form. Results of the tests are reported on Table IV for the two blocks. Only pp and cc components are present and life prediction can be made by linear damage cumulation as follows :

$$(12) \quad \begin{aligned} \frac{1}{N_{R1}} &= \frac{F_{PP1}}{N_{PP1}} + \frac{F_{CC1}}{N_{CC1}} \\ \frac{1}{N_{R2}} &= \frac{F_{PP2}}{N_{PP2}} + \frac{F_{CC2}}{N_{CC2}} \\ \frac{N_1}{N_{R1}} + \frac{N_2}{N_{R2}} &= 1 \end{aligned}$$

The last equation allows to predict the total number of cycles to fracture by :

$$(13) \quad N_R = N_1 + N_2 = N_1 \left(1 - \frac{N_{R2}}{N_{R1}}\right) + N_{R2}$$

Predictions with this method, as indicated in Table IV, are in good accordance with experimental results : this can also be seen with comparisons made on figure 18a.

From the whole study the strain range partitioning approach seems sufficiently accurate to adequately describe the high temperature low cycle fatigue test results and to predict with simple equations the number of cycles to failure under complex wave forms and with step loading with varying temperature. The applicability of the linear cumulation rule is checked in the present case where inelastic strain components are of the same order, but seems more doubtful in hypothetical situations with large differences in strain components as in the case of isothermal two-step stress controlled tests (parag. 5.1). Another difficulty arises when inelastic strain ranges are too small (number of cycles to failure higher than 5000) : test results can be extrapolated by the power functions (10) but this approach seems not very useful for the structure life predictions because on the low degree of confidence on the small calculated plastic strains.

With the objective of life prediction methods for structures where plastic strain ranges are relatively small, or when ratcheting effects can occur, especially in the turbine blades, the damage approach gives another way to take into account the high temperature creep and fatigue effects. This approach is illustrated in the next paragraph.

5 - CONTINUOUS DAMAGE APPROACH

5.1. Development and determination of basic equations

Under high temperature conditions, the low cycle fatigue

crack initiation can be described from a macroscopic continuous damage concept : the damage internal variable (or damage structural parameter [49]) defines the actual strength of the material, taking in account the microscopic deteriorations induced by the cyclic loading. The relation between the density of microscopic cracks or voids and the value of damage is only phenomenological : for example the reduction in elastic modulus in the last part of the life or the reduction of apparent yield strength can be used to measure damage [21, 50].

This approach, initially introduced by Kachanov [18], and Rabotnov [19] for the creep rupture process, needs the definition and the determination of differential damage equations, that is constitutive equations which govern the evolution of damage. Usually damage D is taken as 0 in the initial undamaged state and 1 when specimen fails (which corresponds to a macroscopic crack initiation). This continuous damage approach has been extended recently to the fatigue process [22], the creep-fatigue interaction [23, 24], the monotonic tensile failure [20, 50, 51]. Also the three dimensional generalisation of the damage state variable and of the damage constitutive equations has been established [41], especially in the creep range [52], with particular reference to prediction of creep rupture in structures [53, 54]. It must be underlined that the present damage theory is very different from the classical time fraction rules as reviewed by Ellison and Smith [49] (especially with linear cumulation as in [55, 56, 57]) : based on residual strength of the material (in a strain sense), the present approach gives results similar as the *Remaining Life Concepts* [58].

Under high temperature loading we can schematically distinct two main deterioration processes : the time dependent creep deterioration (constant load or slowly varying load), which corresponds to microscopic intercrystalline cracks initiation and propagation [49, 59], the cycle dependent fatigue damage for which microscopic cracking is more transgranular [60, 61]. The last phenomenon can be identified by pure fatigue tests, running at frequency sufficiently high in order to give negligible creep effects.

When the two processes are simultaneously induced, which can be the case in low frequency high temperature fatigue tests, the two damage increases have to be added with possibility of non linear interaction. Then the general constitutive equation for damage growth is in the tension-compression case :

$$(14) \quad dD = f(\sigma, D, T) dt + g(\sigma_M, \bar{\sigma}, D, T) dN$$

Non linear interaction can arise, due to the presence of D in the two terms : creep damage increase (first term) induces acceleration of fatigue damage increase (second term) and so on. T is the temperature, σ_M and $\bar{\sigma}$ are respectively the maximum and the mean stress in the actual cycle.

The functions f and g can be chosen in order to describe some of the usually observed phenomena, and are respectively determined by creep test results and the pure fatigue test results. For the creep process it is generally sufficient to use the Rabotnov equation as :

$$(15) \quad dD = \left(\frac{\sigma}{A}\right)^r (1-D)^{-k} dt$$

where A , r , k are coefficients depending on temperature. The creep rupture time is now modeled by :

$$(16) \quad t_c = \frac{1}{k+1} \left(\frac{\sigma}{A}\right)^{-r}$$

The coefficients are determined by the creep rupture as well as by identification with the tertiary creep curves, which are well simulated by introducing damage in the viscoplastic constitutive equations [19, 53, 21, 36]. Let us note that equation (15) leads to a linear cumulation when step creep tests are considered [24].

The fatigue damage process is well described by the following equation [22] :

$$(17) \quad dD = [1 - (1-D)^{\beta+1}]^{\alpha(\sigma_H, \bar{\sigma})} \left[\frac{\sigma_H - \bar{\sigma}}{M(\bar{\sigma})(1-D)} \right]^{\beta} dN$$

which can easily be integrated under periodic loading to give the number of cycles to failure :

$$(18) \quad N_F = \frac{1}{(\beta+1)[1 - \alpha(\sigma_H, \bar{\sigma})]} \left[\frac{\sigma_H - \bar{\sigma}}{M(\bar{\sigma})} \right]^{-\beta}$$

The functions α and M can be chosen so as to accurately define the fatigue limit and the monotonic failure :

$$(19) \quad \begin{aligned} \alpha(\sigma_H, \bar{\sigma}) &= 1 - a \frac{\sigma_H - \sigma_L^*(\bar{\sigma})}{\sigma_u - \sigma_H} \\ \sigma_L^*(\bar{\sigma}) &= \sigma_L + (1 - b \frac{\sigma_L}{\sigma_u}) \bar{\sigma} \\ M(\bar{\sigma}) &= M_0 (1 - b \frac{\bar{\sigma}}{\sigma_u}) \end{aligned}$$

α , M_0 , β are temperature dependent coefficients. σ_u is the ultimate tensile strength (which corresponds here to $N_F = 0$), σ_L the fatigue limit under completely reversed loading (which gives $N_F = \infty$). Influence of mean stress is introduced by a linear dependence in accordance with a large number of room temperature test results [62, 63]; σ_L^* is the fatigue limit (expressed in maximum stress) for non zero mean stress. The coefficient b can be considered as temperature independent : value 0.78 is used for IN100.

The coefficients are determined by knowing the fatigue limit for different values of mean stress and the Wöhler curves. The coefficient a is obtained from damage measurements in some fatigue tests. All coefficients are indicated in table V.

An interesting property of the model is to give non linear cumulation effects [22] : in the two level test for example integration of (17) leads to :

Table V - Coefficients of the creep damage and fatigue damage models.

T	Creep damage			Fatigue damage				
	r	p	A	σ_u	σ_L	β	a	M
700				950	300	2.6	0.120	4750
800	10	15	1050	910	295	2.65	0.093	4260
900	6.3	15	870	715	240	3	0.072	2925
950				600	180	4.8	0.108	1485
1000	5.2	15	520	470	140	6	0.138	875
1100	3.58	15	345	250	70	4.7	0.162	635

$b = 0.78$

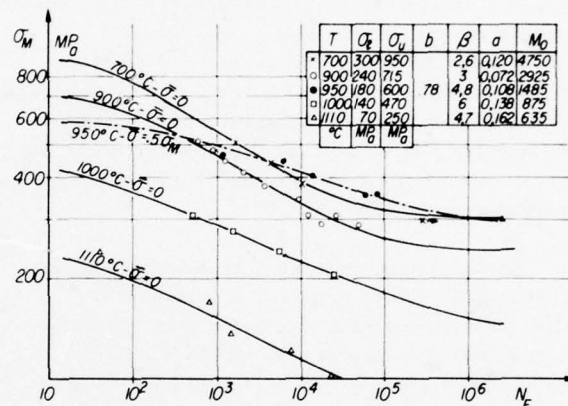


Fig. 19 - Wöhler curves of alloy IN100 as described from the fatigue damage equation (17).

$$(20) \quad \frac{N_2}{N_{F2}} = 1 - \left(\frac{N_1}{N_{F1}} \right)^P$$

$$\text{with } P = \frac{\sigma_{H1} - \sigma_L^*(\bar{\sigma}_1)}{\sigma_{H2} - \sigma_L^*(\bar{\sigma}_2)} \cdot \frac{\sigma_u - \sigma_{H2}}{\sigma_u - \sigma_{H1}}$$

where N_{Fi} is the number of cycles to failure corresponding to periodic cycling with σ_{Hi} , $\bar{\sigma}_i$, N_{F2} being the value corresponding to σ_{H2} , $\bar{\sigma}_2$. These equations give similar effects as the Double Linear Damage Rule [64].

Applicability of the model has been established for various materials at room or at high temperature [22, 41], especially for the alloy IN100 as shown on figure 19 for the Wöhler curves and on figure 20 for non linear cumulation in two level tests (frequencies are 5 or 10 Hz).

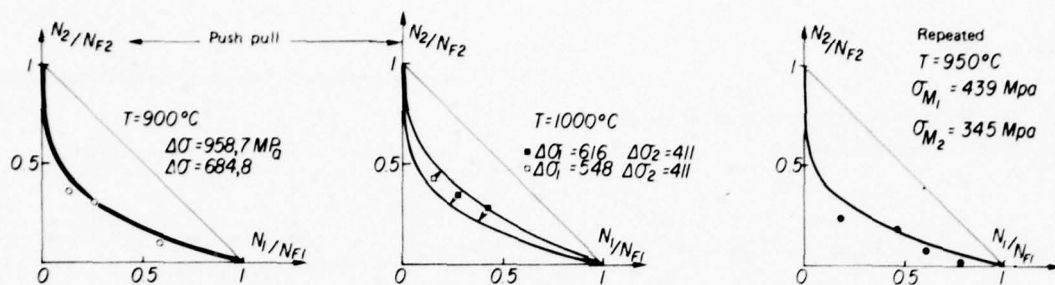


Fig. 20 — Prediction of two-stress-level tests.

5.2. Prediction of creep-fatigue interaction

At high temperature, under low frequency cycling (or holdtimes) the creep and fatigue damage processes can interact as predicted by damage equation (14) with the separately determined functions f and g . For the IN100 alloy creep damage under compressive loading is supposed to be identical to the tensile one, leading to a lower bound prediction. Different materials could be considered with zero compressive damage effect [65] or special cyclic creep tests could be used to determine the compressive influence [66] including possibility of an healing effect [49, 67].

Equation (14) is numerically integrated for a given stress cycle in order to obtain the number of cycles to failure N_R under creep-fatigue conditions. For strain controlled tests the measured stabilized stress response is used: this approximation is justified because of cyclic softening taking place in the first period and the stress decrease induced by damage increase in the last part of the test.

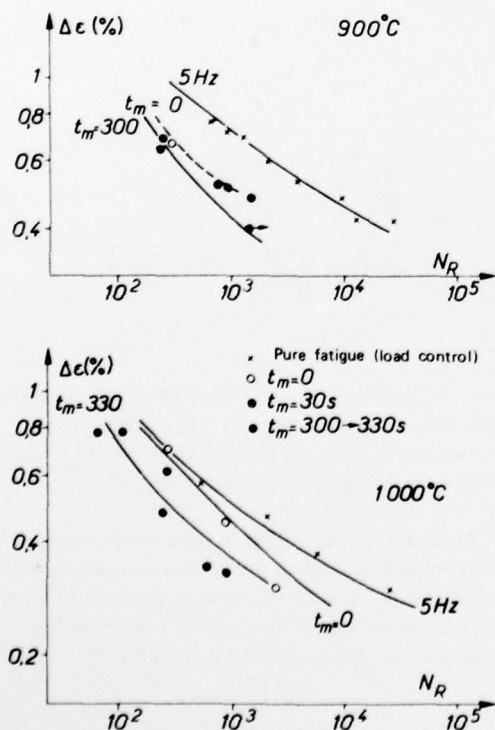


Table VI gives the predicted and experimental results for low frequency and holdtime tests and figures 21 and 22 show the comparisons as functions of stress or strain ranges and as a function of cycle period. N_c is the number of cycles to failure which could be predicted by neglecting pure fatigue damage:

$$(21) \quad \frac{1}{N_c} = (k+1) \int_0^{\Delta t} \left(\frac{|\sigma|}{A} \right)^r dt$$

Δt being the cycle period.

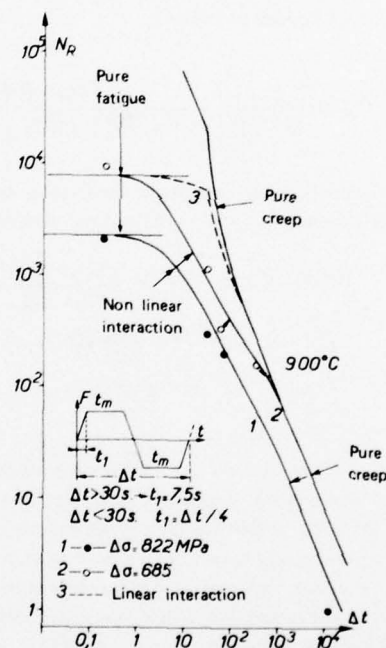


Fig. 22 — Continuous damage prediction of period influence in cyclic creep tests.

Fig. 21 — Continuous damage predictions of elongation controlled tests in the strain range diagram.

Table VI — Calculation of number of cycle to failure with the two methods from the measured stabilized loops

a

n°	T	Control	Hold time	$\Delta\sigma$	$\Delta\epsilon_{in}$	F_{pp}	F_{cc}	F_{cp}	F_{pc}	N_c	N_F	Calculated		Test
												CD	SRP	
28	900	E		845	0.156	0.42	0.58			4 186	1 744	358	449	300
39		E	T330	740	0.180	0.315	0.440	0.245		1 016	7 602	378	246	239
40		L		822	0.174	0.613	0.387			5 162	2 225	424	417	299
42		L		685	0.082	0.358	0.642			16 312	7 876	863	1 505	1 130
43		L		548	0.044	0.200	0.800			66 413	54 790	1 980	4 748	1 069
44		L	T330	685	0.150	0.230	0.575	0.195		239	7 876	167	354	116
49		L		548	0.042	0.195	0.805			66 413	54 790	1 980	5 193	4 014
54		L	T.C165	685	0.258	0.350	0.650			239	7 876	167	161	159
56		L	T.C15	685	0.164	0.324	0.676			2 348	7 876	539	383	338
N5		L	T.C20	832	0.245	0.353	0.647			575	2 228	223	178	200
N6		L	T.C180	624	0.165	0.193	0.807			427	17 704	282	350	294
N7		E	T300	524	0.070	0.060	0.840	0.100		12 750	72 200	1 086	1 630	> 1500
N8		E	T300	641	0.080	0.120	0.770	0.110		3 115	25 415	799	1 268	1 495
N9		E	C30	621	0.102	0.110	0.640		0.250	13 332	10 750	935	916	944
N10		E	C300	672	0.105	0.090	0.670		0.240	2 790	4 292	476	857	764
N12		E	C300	807	0.196	0.280	0.210		0.510	1 200	958	223	351	250

b

n°	T	control	hold time	$\Delta\epsilon$	$\Delta\epsilon_{in}$	F_{pp}	F_{cc}	F_{cp}	F_{pc}	N_c	N_F	Calculated		Test
												CD	SRP	
27	1000	E		451	0.140	0.490	0.510			3 074	8 682	1 050	578	850
33		E		590	0.300	0.750	0.250			790	795	228	171	275
34		E		343	0.066	0.192	0.808			13 415	128 400	4 750	2 198	2 520
36		E	T330	583	0.392	0.54	0.255	0.205		98	1 570	79	63	64
37		E	C330	581	0.390	0.52	0.260		0.220	142	401	81	101	107
45		L	T330	343	0.146	0.165	0.695	0.140		217	176 700	215	386	111
51		L	T.C870	376	0.520	0.212	0.788			25	60 780	25	36	24
55		L	T.C165	343	0.175	0.250	0.750			217	176 700	215	322	263
57		L	T.C15	343	0.111	0.200	0.800			2 082	176 700	1 655	769	800
N13		E	C300	531	0.255	0.300	0.280		0.420	308	594	140	211	268
N32		L	T.C180	343	0.172	0.210	0.790			200	176 700	194	326	568
N34		L	T.C20	308	0.078	0.140	0.860			2 809	786 000	2 374	1 500	3 108
N35		L	T.C180	308	0.138	0.125	0.875			345	786 000	336	480	954
N36		E	T300	433	0.180	0.300	0.492	0.208		430	25 230	368	252	243
N37		E	T300	347	0.096	0.125	0.735	0.140		1 719	337 000	1 480	860	870
N38		E	C300	355	0.098	0.100	0.702	0.198		2 475	20 055	1 278	972	> 600
29	800	E		1 024	0.045	0.232	0.768			116 780	1 505	552	4 592	1 280
41		E	T330	1 232	0.186	0.226	0.484	0.290		1 690	1 026	243	212	278
47		L	T.C165	1 024	0.133	0.225	0.775			892	1 482	231	545	135
38	1110	E	T330	261	0.233	0.24	0.43	0.33		90	5 950	84	132	36
48		L	T.C165	205	0.218	0.22	0.78			52	25 950	51	206	73

E : elongation L : load

The two temperature level tests are also correctly predicted by the method : results are indicated on table IV as well as in figure 23 which summarizes relation between predicted and measured lives. Pure fatigue tests including two level tests, pure creep tests and creep after fatigue tests [30, 41] (time to failure in minutes) are also plotted. Differences are generally less than a factor of two, which checks this continuous damage approach.

In that case the low frequency fatigue tests are correctly predicted from only creep and pure fatigue datas, which extends the range of applicability from static to high frequency tests as well as to non periodic loading (taking into account non linear cumulative effects).

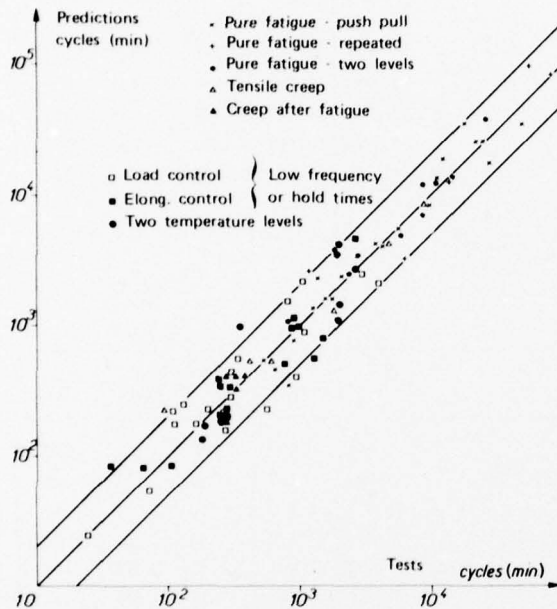


Fig. 23 - Correlation of measured and calculated lives from the continuous damage approach.

6 - APPLICABILITY OF THE TWO METHODS FOR THE PREDICTION OF CRACK INITIATION IN STRUCTURES

The prediction of crack initiation in structures working at high temperature is generally decomposed into successive steps [2] :

- definition of structure geometry, cyclic loading conditions and temperatures, including thermal gradients,
- elastic-viscoplastic analysis in order to obtain the stabilized stress-strain cycle in the most critical areas,
- application of the failure criteria to give the number of cycles to crack initiation.

The application of the two studied failure prediction methods present some specific difficulties :

- The SRP method needs plastic and creep separation of the inelastic strain : under cyclic variable temperature conditions this partitioning could be the result of a full plastic and viscoplastic structure analysis, but this type of analysis is less practicable than the viscoplastic one.

- The continuous damage approach demands to integrate the damage equations over the life : in actual structural situations where equilibrium equations have to be solved, this is unpracticable and one simplification is to consider only the stabilized cycle and to neglect the stress redistribution effect induced by damage increase (this effect is often beneficial to the life especially in structures where cyclic thermal loading is of particular importance).

In order to compare the two methods under conditions close to the problem of structural analysis, the tension-compression isothermal tests are reexamined with the following procedure :

- Inputs of the calculations are the control functions (stress or elongation),
- The cyclic viscoplastic constitutive equations are used in order to calculate the stress and the inelastic strain evolutions in the stabilized cycle,
- The rapid load-unload method is automatically used to separate the plastic component in the tensile and compressive transient periods (1.5 second for this rapid loading under stress control) ; application of the SRP relations (10) and (11) gives the number of cycles to failure as predicted by this first method.

- The calculated stress cycle is used in integration of damage equations (it is supposed to be periodic for the whole life of the specimen) which leads to the damage prediction of the number of cycles to failure

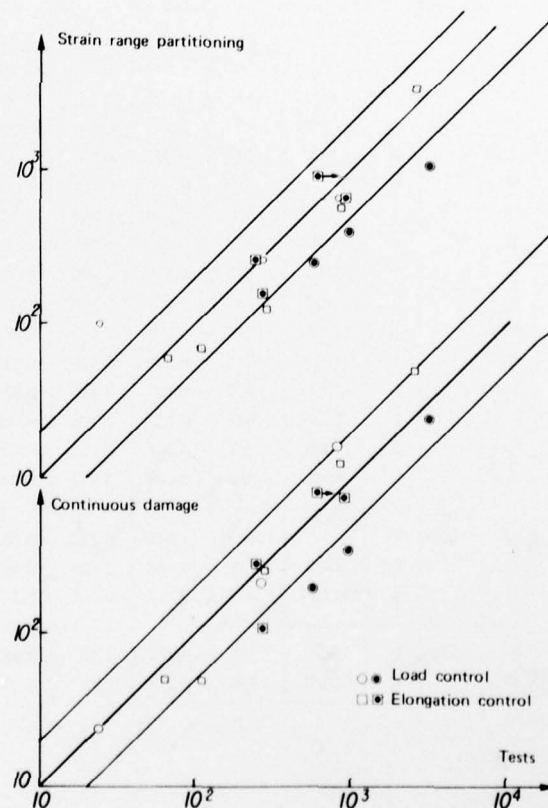


Fig. 24 - Comparison of predictions by the two methods with the measured lives (values of table VI).

Table VII — Failure predictions from stabilized calculated loops as obtained by viscoplastic constitutive equations.

n°	Loading	Stabilized loop				Strain partitioning				Continuous damage		
		σ_t	σ_c	$\Delta\epsilon$	$\Delta\epsilon_{in}$	$\Delta\epsilon_{pp}$	$\Delta\epsilon_{cc}$	$\Delta\epsilon_{cp/pc}$	N_R	N_c	N_F	N_R
27	E	221	222	0.439	0.137	0.057	0.080		562	3440	12 060	1 244
33	E	288	286	0.707	0.315	0.153	0.162		121	793	987	250
34	E	174	175	0.291	0.054	0.0095	0.0445		3134	12 177	142 200	4 956
36	E	T330	306	0.816	0.4155	0.152	0.236	0.0275	59	66	993	55
37	E	C330	306	0.816	0.4155	0.152	0.236	0.0275	67	66	644	52
51	L	T.C870	188.3	0.571	0.3145	0.0635	0.251		98	25	60 780	24
55	L	T.C165	171.2	0.428	0.195	0.037	0.158		252	217	176 700	211
57	L	T.C15	"	0.354	0.1215	0.0218	0.0997		636	2084	176 700	1 658
N13	E	C300	241.2	0.630	0.278	0.101	0.144	0.033	152	132	2 104	106
N32	L	T.C180	171.2	0.430	0.1975	0.037	0.1605		244	199	176 700	193
N34	L	T.C20	154	0.304	0.0945	0.0095	0.085		1006	2816	786 000	2 378
N35	L	T.C180	"	0.364	0.1540	0.020	0.134		387	345	786 000	338
N36	E	T300	200	0.482	0.1835	0.053	0.0995	0.031	250	318	17 935	275
N37	E	T300	164	0.359	0.1110	0.0165	0.074	0.0205	628	874	117 550	762
N38	E	C300	202	0.359	0.1110	0.0165	0.074	0.0205	872	949	76 547	801

Results of these numerical predictions are presented in table VII for the tests performed at 1000°C. Comparison of the calculated lives with the measured ones can be made on figure 24. The two life prediction methods give rise to the same order of difference (about a factor two), which check their applicability in cases where either the stress and the inelastic strain have to be calculated, especially in strain controlled tests : in that case test results and calculated lives are compared on figure 25 as a function of strain range. We can remark that the two rules of life prediction permit to bound the actual lives. It can be noted that Strain Range Partitioning gives smaller hold time influence in strain controlled tests as the continuous damage (figure 26) : this is because on the small increases in inelastic strain induced by increasing hold time [68]. Creep damage however is effectively increased as shown on several materials [49, 68] and C.D. gives more conservative predictions for large hold times. Figure 27 shows correlations between time to failure and cycle period (continuous cycling with triangular waves and tensile hold time tests) : predictions by the Strain Range partitioning allows to a linear relationship as observed on several alloys [49].

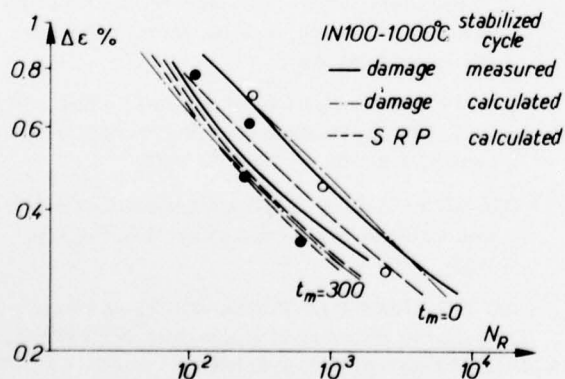


Fig. 25 — Strain range and life predictions by the two methods.

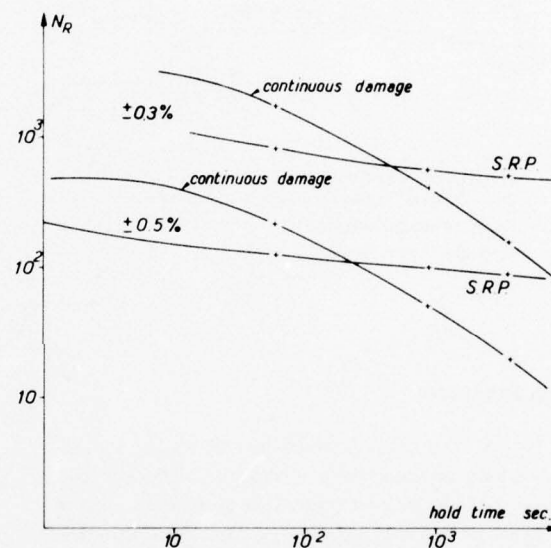


Fig. 26 — Prediction of tensile hold time influence in strain controlled tests.

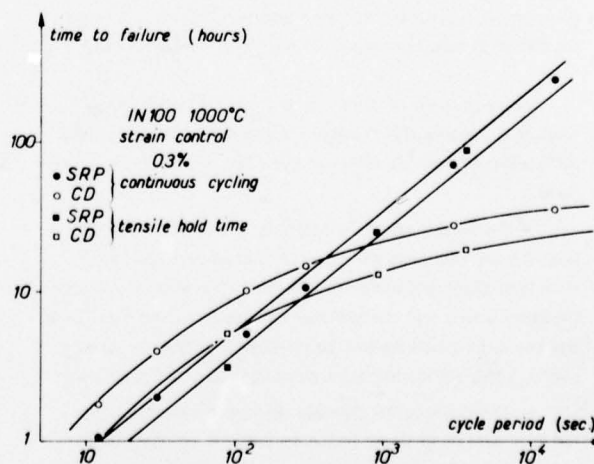


Fig. 27 — Predictions of time to failure under continuous cycling and hold time tests.

As a result of this comparative analysis we can conclude to assess the efficiency of the two life prediction procedures when associated to a well defined viscoplastic constitutive equation (in order to correctly solve the equilibrium of the structure). Moreover the two methods can bound the actual life, even if the viscoplastic behavior (or the structure calculations) are only approximate: as shown schematically in figure 28 for the strain controlled tests, an overestimate of the stress range corresponds to an underestimation of the inelastic strain range. This compensation effect allows us to underline the practical interest for life prediction in structures, of apply the two methods simultaneously in the high temperature structural design.

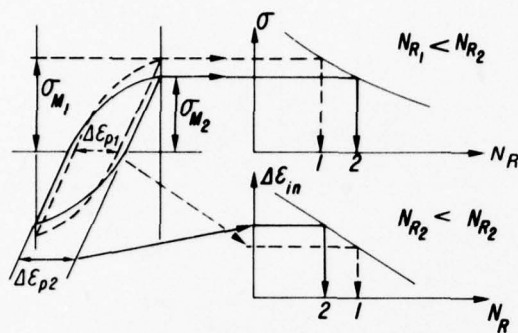


Fig. 28 — Schematic drawing of the compensation effect when applying the two life prediction methods from results of viscoplastic analysis.
(Example of strain controlled tests).

7 — CONCLUSION

For the alloy IN100 (alumine coating) the two studied methods are good enough to give laboratory life predictions which differ from the experimental life by a factor less than two. Moreover in addition to cyclic viscoplastic constitutive equations, these methods can predict number of cycles to failure from the control parameter only (stress or elongation waveform). It has been mentioned that Continuous Damage gives better simulation for large tensile hold times because on the small corresponding inelastic strain increases [68].

However each of them present some specific conveniences as regards their range of applicability as well as the difficulties of corresponding analysis for structure life predictions:

- the Strain Range Partitioning is very adequate to describe the intermediate range of frequency including effects of compressive flow on the tensile one and differences between tensile and compressive damage; but the non linear damage cumulation cannot be predicted (with non periodic cycling) and difficulties arise when inelastic strain are small.

- The Continuous Damage Approach covers a larger range of test conditions, including static creep tests, high cycle fatigue, mean stress or mean strain effects, non linear cumulative effects, but its application is presently limited to materials showing similar damaging influence for compressive loading than tensile one and where cyclic hardening is not

too important (which could lead to creep summation higher than 1 [69]). Further studies are needed in order to include these effects as well as some healing phenomena induced by the compressive part of the cycle [49].

- From the fundamental point of view the continuous damage is more justified, especially in its thermodynamical aspects [36], than the strain partitioning, which needs some arbitrary separation between plastic and viscoplastic flow. As a consequence, the damage approach can be more easily generalized to the three-dimensional case [41, 52], but its application to actual situations is also more complex and numerical calculations are always needed.

- For crack initiation prediction in structures, the SRP method seems applicable until the inelastic strain range is sufficiently large to overcome the uncertainties of calculations and if the ratchetting effect is small. Its application under non isothermal cyclic conditions (with thermal gradients) needs the use of plastic and viscoplastic flow rules which leads to some difficulties. The present study has shown the possibility to replace the plastic flow rule by the viscoplastic one and systematic computations by the rapid load-unload procedure (on the critical elements only).

- The damage integration is more easily included in the non isothermal viscoplastic analysis but only the stabilized stress cycle can be used, which gives a lower bound to the life, due to the neglect of damage induced stress redistribution effect. Possibility of simulation of this effect with simple structural models (like Reference Stress Method) is under study.

In view of actual design procedures we can conclude to the applicability of the two methods and to their complementarity as regards lifetime predictions. However, despite its more complex treatment of test results, the Continuous Damage Approach seems more promising in that concern creep-fatigue predictions from pure creep and pure fatigue, small inelastic strains, large hold times, temperature cycling.

REFERENCES

- 1 A. KAUFMAN — Steady-state stress relaxation analysis of turbine blade cooling designs, NASA TN D-5282, 1969.
- 2 J.L. CHABOCHE, C. STOLTZ — Détermination des durées de vie des aubes de turbine à gaz, Revue Française de Mécanique, No 52, 1974.
- 3 D.J. LEWIS — The application of computer methods to creep analysis, Recent Developments in High Temperature Design Methods, Proc. IME No C-271-77, 1977.
- 4 O.C. ZIENKIEWICZ — The finite element method in structural continuum mechanics, Mc Graw Hill, New York, 1967.
- 5 O.C. ZIENKIEWICZ, I.C. CORMEAU — Viscoplasticity solution by finite element process, Arch. of Mechanics, vol. 24, No 5-6, 1972, p. 873-889.
- 6 M. CHAUDONNET — Méthode des équations intégrales appliquées à la résolution de problèmes de viscoplasticité, J. de Mécanique Appliquée, vol. 1, No 2, 1977.

- 7 H. NEUBER — Theory of stress concentration for shear strained prismatical bodies with arbitrary non linear stress-strain law, *J. of Applied Mechanics*, Trans. ASME, 1961.
- 8 T.H. TOPPER, R.M. WETZEL, J.D. MORROW — Neuber's rule applied to fatigue of notched specimens, *J. of Materials*, vol. 4, No 1, 1969.
- 9 M. CHAUDONNET — Sur une méthode de calcul du coefficient de concentration de contrainte en viscoplasticité, *C.R. Ac. Sc.*, t. 283 B, 1976, p. 441-444.
- 10 D.L. MARIOTT, F.A. LECKIE — Some observations on the deflections of structures during creep, *Proc. Inst. Mech. Eng.*, vol. 178 (3L), 1963-64.
- 11 J.M. BILL, A.C. MACKENSIE — Reference stress for redistribution time in creep of structures, *J. Mech. Eng. Sci.* vol. 5, No 4, 1969.
- 12 F.A. LECKIE — Approximate procedure in high temperature design, *Recent Developments in High Temperature Design Method*, Proc. I.M.E., 1977.
- 13 S.S. MANSON, G.R. HALFORD, M.H. HIRSCHBERG — Creep-fatigue analysis by Strain Range Partitioning. Symp. on Design for elevated temperature environment, ASME, NASA TMX 67838, 1971.
- 14 M.H. HIRSCHBERG, G.R. HALFORD — Strain Range Partitioning. A tool for characterizing high temperature low cycle fatigue, NASA TMX 71691, 1975.
- 15 L.F. COFFIN Jr. — A generalized equation for predicting high temperature low cycle fatigue, including hold times, *Proc. Air Force Conf. on Fatigue and Fracture of Aircraft Structures and Materials*, AFFDL TR 70-144, Miami Beach, 1969, p. 301-309.
- 16 J.T. BERLING, J.B. CONWAY — A new approach to the prediction of low cycle fatigue data, *Met. Trans.*, vol. 1, 1970, p. 805-809.
- 17 W. SPERR — Eine Erweiterung der Manson-Coffin Formel, *Materialprüf.* 16, No 2, 1974, p. 41-45, No 4, 1974, p. 94-97.
- 18 L.M. KACHANOV — Time of the rupture process under creep conditions. *Izv. Akad. Nauk. SSR, Otd Tekh. Nauk*, No 8, 1958, p. 26-31.
- 19 Y.N. RABOTNOV — Creep problems in structural members, North Holland Publ. Comp., Amsterdam-London, 1969.
- 20 J. HULT — Creep in continua and structures. *Topics in Applied continuum Mechanics*, J.L. Zeman, F. Ziegler eds., Springer-Verlag, 1974, p. 137-155.
- 21 J. LEMAITRE, J.L. CHABOCHE — Aspect phénoménologique de la rupture par endommagement, à paraître *J. de Mécanique Appliquée*.
- 22 J.L. CHABOCHE — Une loi différentielle d'endommagement de fatigue avec cumulation non linéaire, *Revue Française de Mécanique* No 50-51 (1974).
- 23 M. CHRZANOWSKI — Use of the damage concept in describing creep-fatigue interaction under prescribed stress, *Int. J. Mech. Sci.*, vol. 18, 1976, p. 69-73.
- 24 J. LEMAITRE, J.L. CHABOCHE — A non linear model of creep-fatigue damage cumulation and interaction, *Symposium IUTAM*, Gothenburg Sweden (1974), Springer Verlag.
- 25 J.L. CHABOCHE, H. POLICELLA — Caractérisation expérimentale des matériaux sous chargement cyclique à haute température. *La Rech. Aérop.*, No 1977-5.
- 26 J.L. CHABOCHE, H. POLICELLA, H. KACZMAREK, Machine d'essais en fatigue oligocyclique à haute température, N.T. ONERA No 1977-10.
- 27 A.E. CARDEN, Thermal fatigue evaluation, *ASTM STP 465* (1969).
- 28 C.H. WELLS — Elevated temperature testing methods, *ASTM STP 465* (1969).
- 29 J.L. CHABOCHE, G. BAUDIN, S. SAVALLE — Etude phénoménologique du comportement et de la rupture de l'alliage IN100 à haute température, *Doc. Intérieur ONERA*, 1974.
- 30 J.L. CHABOCHE, H. KACZMAREK, H. POLICELLA, S. SAVALLE, J.P. CULIE, G. CAILLETAUD — Interaction fatigue-fluage sur l'alliage IN100 sous conditions de température variable par blocs. *Doc. Intérieur ONERA*, 1977.
- 31 J.L. CHABOCHE, H. POLICELLA, H. KACZMAREK, S. SAVALLE — Comportement et rupture des milieux troués en vue de la prévision de la durée de vie des aubes de turbine refroidies par film. *Doc. Intérieur ONERA*, 1976.
- 32 S.S. MANSON, G.R. HALFORD, A.J. NACHTIGALL, Separation of the strain components for use in Strain Range Partitioning, NASA TMX-71737, 1975.
- 33 J.L. CHABOCHE — Viscoplastic constitutive equations for the description of cyclic and anisotropic behavior of metals, 17e Conf. Polonaise de Mécanique des Solides, Szczyrk (1975), *Bull. de l'Acad. Polonaise des Sciences Série Sc. et Tech.*, vol. 25, No 1, 1977, p. 33-42.
- 34 F. SIDOROFF — On the formulation of plasticity and viscoplasticity with internal variables, *Arch. Mech.*, vol. 27, 5-6, 1975, p. 807-810.
- 35 J.R. RICE — Inelastic constitutive relations for solids : an internal variable theory and its application to metal plasticity, *J. Mech. Physics Solids*, vol. 19, 1971, p. 433-455.
- 36 J.L. CHABOCHE — Sur l'utilisation des variables d'état interne pour la description du comportement viscoplastique et de la rupture par endommagement, *Symp. Franco-Polonais de Rhéologie et Mécanique*, Cracovie, 1977.
- 37 J.R. RICE — On the structure of stress-strain relations for time-dependent plastic deformation in metals, *J. Applied Mech.*, Trans. ASME, 37, 1970, p. 728-737.
- 38 N.N. MALININ, G.M. KHADJINSKY — Theory of creep with anisotropic hardening. *Int. J. Mech. Sci.*, vol. 14, 1972, p. 235-246.
- 39 W.J. EVANS, G.F. HARRISON — The development of a universal equation for secondary creep rates in pure metals and engineering alloys, *Metal Science*, 1976, p. 307.

- 40 J. MANDEL — Plasticité classique et viscoplasticité. Cours du CISM, Udine (Italie), 1971.
- 41 J.L. CHABOCHE — Description thermodynamique et phénoménologique de la viscoplasticité cyclique avec endommagement. Publication ONERA No 1978-3.
- 42 W. PRAGER — Recent developments in the mathematical theory of plasticity, *J. Applied Phys.*, vol. 20, No 3, 1949, p. 235-241.
- 43 P.J. ARMSTRONG, C.O. FREDERICK — A mathematical representation of the multiaxial Bauschinger effect, CEBG report RD/B/N731, 1966.
- 44 A.A. ILYUSHIN — On the relation between stresses and small deformations in the Mechanics of Continuous Media, *Prikl. Mat. Mekh.*, vol. 18, No 6, 1954, p. 641-666.
- 45 M.B. BEVER — Creep and recovery, *A.S.M.*, 1957, p. 14.
- 46 R. LAGNEBORG — A modified recovery-creep model and its evaluation, *Met. Sci.*, J. vol. 6, 1972, p. 127-133.
- 47 D. MARQUIS — Thèse université Paris VI, à paraître.
- 48 H. HIRSCHBERG, G.R. HALFORD — Use of Strain Range Partitioning to predict high temperature low-cycle fatigue life, NASA TN D-8072, 1976.
- 49 E.G. ELLISON, E.M. SMITH — Predicting service life in a fatigue creep environment, *Fatigue at Elevated Temperatures*, ASTM STP 520, 1973, p. 575-612.
- 50 J. LEMAITRE, J. DUFAILLY — Modélisation et identification de l'endommagement plastique des métaux, 3e Congrès Français de Mécanique, Grenoble, 1977.
- 51 H. BROBERG — A new criterion for brittle creep rupture, *J. Appl. Mech.*, vol. 41, 1974, p. 809.
- 52 D.R. HAYHURST — Creep rupture under multi-axial state of stress, *J. Mech. Phys. Solids*, vol. 20, No 6, 1972, p. 381-390.
- 53 F.A. LECKIE, D.R. HAYHURST — Creep rupture of structures, *Proc. Royal Soc. of London*, vol. 340, No 1622, 1974, p. 323-347.
- 54 D.R. HAYHURST, P.R. DIMMER, M.W. CHERNUKA — Estimates of the creep rupture lifetime of structures using the finite element methods, *J. of Mechanics and Physics of Solids*, vol. 23, 1975, p. 335-355.
- 55 M.A. MINER — Cumulative damage in fatigue, *J. of Applied Mechanics*, *Trans. ASME*, vol. 67, 1945, p. 159-164.
- 56 S. TAIRA — Lifetime of structures subjected to varying load and temperature, *Creep in Structures*, N.J. Hoff, ed. Academic Press, 1962.
- 57 D.A. SPERA — The calculation of elevated temperature cyclic life considering low cycle fatigue and creep, NASA TN-5317, 1969.
- 58 D.A. WOODFORD — A critical assessment of the life fraction rule for creep rupture under nonsteady stress or temperature, *Int. Conf. on Creep and Fatigue in Elevated Temperature Applications*, Philadelphia (1973), Sheffield (1974).
- 59 S.S. MANSON — Interfaces between fatigue, creep and fracture, *Int. J. Fract. Mech.*, vol. 2, No 1, 1966, p. 327-363.
- 60 E.G. ELLISON, C.P. SULLIVAN — The effect of superimposed fatigue on the creep behavior of the nickel base alloy Udimet 700, *Trans. of ASME*, vol. 60, 1967, p. 88-98.
- 61 C.H. WELLS, C.P. SULLIVAN, M. GELL — Mechanisms of fatigue in the creep range, *Metal Fatigue Damage*, ASTM STP 495, 1971, p. 61-122.
- 62 G. SINES — Behavior of metals under complex static and alternating stresses, *Metal Fatigue*, G. Sines, J.L. Waisman eds. Mac Graw Hill Book Comp., 1959, p. 145-169.
- 63 K. DANG VAN — Sur la résistance à la fatigue des métaux, *Sciences et Techniques de l'Armement, Mémorial Artillerie Française*, vol. 47, No 3, 1973, p. 647-722.
- 64 S.S. MANSON, J.C. FRECHE, C.R. ENSIGN — Application of a double linear damage rule to cumulative fatigue, ASTM STP 415, 1967, p. 384-414.
- 65 D.A. SPERA — Calculation of thermal fatigue life based on accumulated creep damage, NASA TN D-5489, 1969.
- 66 G.R. HALFORD — Cyclic creep rupture behavior of three high temperature alloys, NASA TN D-6309, 1971.
- 67 E.G. ELLISON, A.J.F. PATERSON — Creep fatigue interactions in a 1 Cr Mo V steel, *Proc. Instn. Mech. Engrs.*, Vol. 190, No 12, 1976.
- 68 E. KREMPL, C.D. WALKER — Effect of creep-rupture ductility and hold time on the 1000F strain-fatigue behavior of a 1 Cr-1 Mo-0.25 V steel, ASTM STP 459 (1968).
- 69 C.E. JASKE, H. MINDLIN, J.S. PERRIN — Combined low cycle fatigue and stress relaxation of alloy 800 and type 304 stainless steel at elevated temperatures, ASTM STP 520, 1973, p. 365-376.

STRAINRANGE PARTITIONING OF MARMOO2 OVER THE TEMPERATURE
RANGE 750°C - 1040°C

by V.T.A. Antunes and P. Hancock

Department of Materials, Cranfield Institute of
Technology, Bedford MK43 0AL, U.K.

1. Summary

The fatigue behaviour of a cast nickel base superalloy Mar MOO2 has been studied in the temperature range 750° - 1040°C by the method of Strainrange Partitioning, (SrP).

The four basic strainrange vs life relationships $N_{ij} - \Delta \epsilon_{ij}$ ($i = P$ or C ; $j = P$ or C) were determined at 850° and 1040°C. A marked temperature sensitivity was observed and it was not possible to predict 1040° lives from 850 data.

However, satisfactory life prediction could be made by the SrP method over limited temperature ranges. Prediction within the range 750 to 850°C, or within the range 950 - 1040°C proved to be satisfactory, employing a unique set of $N_{ij} - \Delta \epsilon_{ij}$ strainrange vs life relationships for each temperature range.

Work is in hand to elucidate the mechanisms of failure in these two temperature regimes.

2. Introduction

The Strainrange Partitioning method, developed by Manson and co-workers (1), (2), (3), (4) is a general strain approach to predict lives under combined creep and fatigue loading. The method used, considers that any conceivable inelastic strain cycle can be separated into four possible types of strainrange, viz:

- PP - tensile plasticity reversed by compressive plasticity,
- CP - tensile creep reversed by compressive plasticity,
- PC - tensile plasticity reversed by compressive creep,
- CC - tensile creep reversed by compressive creep.

For predictions to be made it is first necessary to determine the individual failure-life relationships $N_{ij} - \Delta \epsilon_{ij}$ ($i = P$ or C , $j = P$ or C) for the above four basic types. Then, any particular hysteresis loop can be built from combinations of the above four basic types and the combined effects of these components estimated by using an interaction damage rule.

One important aspect of the Strainrange Partitioning approach is the influence of temperature. If the form of the partitioned strainrange vs life relationships is independent of testing temperature, this would greatly simplify the application of strainrange partitioning to thermal fatigue problems. As a first assessment of how strainrange partitioning can help in dealing with thermal fatigue of cast MAR MOO2 turbine buckets, the influence of temperature on the strainrange vs life relationships for this alloy was examined over the temperature range 750 - 1040°C.

3. Experimental

The material used in this series of experiments was an as cast nickel superalloy MAR MOO2, developed for strength and creep performance as a first stage cast turbine blade material. The chemical composition and tensile properties are shown in Table I.* Specimens were obtained in the as cast condition from the National Gas Turbine Establishment, were subsequently machined to shape as shown in Fig. (1), then heat treated for 16 hours at 870°C, furnace cooled and finally surface ground before testing.

The specimens were resistance heated in air through rods attached directly to the specimens. The specimens' temperature was measured by a Land optical pyrometer connected via a pyrometer amplifier to a Bristol Strip chart recorder. The recorder provided a control signal to a saturable reactor, proportional to the difference between the specimen temperature and the pre-set temperature. The saturable reactor was in series with the step-down transformer which provided the current through the specimen. An accuracy of ± 3 degrees centigrade was achieved with this set up for temperatures above 850°C.

The creep-fatigue tests were carried out on an electro hydraulic closed loop testing machine, the load supplied by a double acting hydraulic jack controlled by an electrically actuated precision spool valve. Specimen strain was measured by a variable reluctance transducer mounted on the water cooled end of a scissor type extensometer. The extensometer was located on the specimen by spring loaded ceramic contacts on V-ridges machined onto the specimen, Fig. 1. The testing machine and the wave generator for producing PC, CP and CC tests were designed specifically for strain-range partitioning and details are being prepared for separate publication.

The cycles involved in the strainrange partitioning tests of MAR MOO2 are shown in Fig. (2), which depicts schematically the corresponding stress-strain loops.

All PP tests were conducted at sufficiently high frequencies to exclude creep strains being introduced in these tests, respectively 0.6Hz at 850°C and 1 Hz at 1040°C. The tests were completely reversed strain controlled fatigue tests using a triangular strain-time wave form.

In the CP tests a tensile hold period of about 20 seconds was used. The tests were strain controlled fatigue tests using a trapezoidal stress vs time wave form with superimposed strain limits.

The PC tests were similar to the CP except that the load hold was introduced in the compression cycle.

The CC tests had load hold in both the tension and compression cycles.

4. Test Results

The test conditions and results of all the basic low cycle fatigue tests are presented in Table II.* Figs. (3) and (4) depict the four partitioned strainranges vs life relationships $N_{ij} - \Delta\epsilon_{ij}$ ($i = P$ or C , $j = P$ or C), for 850°C and 1040°C respectively. These partitioned strainrange vs life relationships were produced experimentally as follows:

a) PP type tests

In this type of test no creep strain is permitted. To preclude any significant introduction of creep, frequencies of 0.6Hz and 1Hz at 850°C and 1040°C were employed.

b) CP type tests

In these tests a constant tensile creep stress was reversed in the compressive part of the cycle by using a sufficiently high strain rate to prevent the occurrence of any creep. Before the $N_{CP} - \Delta\epsilon_{CP}$ relationships could be plotted, the damage due to the presence of any PP type strain was considered, using the interaction damage rule in a reverse manner.

$$\frac{F_{PP}}{N_{PP}} + \frac{F_{CP}}{N_{CP}} = \frac{1}{N_{OBS}}$$

where

$$F_{PP} = \frac{\Delta\epsilon_{PP}}{\Delta\epsilon_i} \quad \Delta\epsilon_{PP} - \text{inelastic strain of PP type}$$

$$F_{CP} = \frac{\Delta\epsilon_{CP}}{\Delta\epsilon_i} \quad \Delta\epsilon_{CP} - \text{inelastic strain of CP type}$$

$$\Delta\epsilon_i - \text{width loop}$$

Here the experimentally observed life N_{OBS} substitutes the predicted life N_{PRED} and the equation is solved for the unknown N_{CP} . Therefore, before the $\Delta\epsilon_{CP} - N_{CP}$ relationship can be plotted, it is first necessary to establish the $N_{PP} - \Delta\epsilon_{PP}$ relationship.

c) PC type tests

In these tests the creep portion of the cycle is in compression. The procedure is the same as for the CP tests but the tensile and compression notations are interchanged.

d) CC type tests

These cycles involved a cyclic creep rupture test where a constant tensile stress is servo controlled until a preset strain limit is reached. When this limit is reached the stress is rapidly reversed and a constant compressive stress applied until a preset strain limit is reached.

The $N_{CC} - \Delta\epsilon_{CC}$ relationship is the last to be determined because it needs the knowledge of the PP and PC or CP relationships.

The damage effect of a PP component and of a CP or PC component is achieved using the interaction damage rule in a reverse way

$$\frac{F_{PP}}{N_{PP}} + \frac{F_{PC}}{N_{PC}} \left(\frac{F_{CP}}{N_{CP}} \right) + \frac{F_{CC}}{N_{CC}} = \frac{1}{N_{OBS}}$$

where the unknown is here N_{CC} .

Using a linear regression analysis for each group of data, the following strain vs life relationships were obtained.

(i) - 850°C

$$\Delta\epsilon_{PP} = 0.26 N_{PP}^{-0.94}$$

$$\Delta\epsilon_{PC} = 0.24 N_{PC}^{-1.05}$$

$$\Delta\epsilon_{CP} = 0.01 N_{CP}^{-0.38}$$

$$\Delta\epsilon_{CC} = 0.04 N_{CC}^{-0.66}$$

(ii) - 1040°C

$$\Delta\epsilon_{PP} = 0.04 N_{PP}^{-0.55}$$

$$\Delta\epsilon_{PC} = 0.05 N_{PC}^{-0.58}$$

$$\Delta\epsilon_{CP} = 0.02 N_{CP}^{-0.46}$$

$$\Delta\epsilon_{CC} = 0.02 N_{CC}^{-0.34}$$

* Chemical compositions, material processing, heat treatments and mechanical properties for each tested alloy, as well as the data generated in the programme, are given in Appendix A 1.

where $\Delta\epsilon_{ij}$ is an inelastic strain of the type ij and N_{ij} the corresponding life.

Taking the results of Figs. (3) and (4) which presented the strainrange partitioning data grouped isothermally at 850°C and 1040°C, two salient features emerge

- (i) At 850°C the PC tests failed before any others for a given inelastic strain range whilst the CP test results were represented by a line of shallower slope and shifted to the right of the others (higher lives).
- (ii) In the 1040°C plots, all the tests could be considered as displaying a unique strainrange vs life relationship. The best fitting equation for the 1040°C data was found to be :-

$$\Delta\epsilon_{ij} = 0.03 N_{ij}^{-0.48} \quad \begin{pmatrix} i = P \text{ or } C \\ j = P \text{ or } C \end{pmatrix}$$

with a correlation factor of 0.84.

A microscopic analysis of longitudinal sections of specimens tested at both temperatures showed no evidence of intergranular fracture.

Using the basic strainrange vs life relationships for 850°C to predict the 1040°C results, ratios as large as ± 5 were found between the predicted and observed lives as shown in Fig. (5).

To find the temperature regions over which life predictions were possible, further sets of tests were made at 750 and 950°C as detailed in Table II. It was found that the 750 results could be predicted within a factor of ± 2 from the basic strainrange vs life relationship developed at 850°C and that the 950 results could be predicted with similar accuracy from the 1040°C behaviour as shown in Figure 6.

These results suggest that different deformation or fracture mechanisms apply over the two temperature ranges 750°C - 850°C and 950°C - 1040°C.

An obvious factor is that the fracture mechanisms may change from transcrystalline fracture at the lower temperatures to intergranular fracture in the higher ranges particularly for cycles involving a creep component in tension, i.e. the CP or CC cycles. This change from transcrystalline to intercrystalline fracture path has been suggested to be responsible for the shorter lives found for the CP or CC cycles in other systems (1), (5), (6). However, Wells and Sullivan (7) tested a nickel base alloy, Udimet 700, and Lord and Coffin (8), a cast nickel superalloy René 80, concluded that holding periods were more damaging in compression than in tension.

To check whether the change from intergranular to a transgranular fracture path was important over the particular conditions used in this study, detailed metallographic studies were made of the fracture surfaces. It was found that all failed predominantly by transgranular failure with no evidence of an increasing intergranular component at higher temperatures. It therefore appears that this is not the predominant reason for the difference in behaviour between the lower (750 - 850°C) and higher (950 - 1040°C) temperature regions and further work is in hand to determine the failure mechanisms occurring in the temperature range investigated. Current work is considering an assessment of the relative importance of hold periods on fracture initiation and propagation at both temperatures.

5. Conclusions

1. Strainrange partitioning measurements of MAR M002 over the temperature range 750 - 1040°C have been made and $N_{ij} - \Delta\epsilon_{ij}$ strainrange vs life relationships established.
2. The application of a unique set of strainrange vs life relationships to the whole temperature interval 750 - 1040°C resulted in unacceptable errors in lifetime prediction. Ratios as high as ± 5 were found for predicted/observed lives when using 850°C data to predict lives at 1040°C.
3. Satisfactory life prediction could be made over limited temperature ranges. Lives within a factor of ± 2 could be predicted over the separate temperature ranges 750 to 850°C and 950 to 1040°C.
4. The fracture path was found to be transgranular over the whole range of test conditions examined.
5. Current work indicates that crack propagation is the dominant factor in lifetime prediction at high temperatures whereas in the lower temperature region initiation is increasingly important, becoming dominant as lives increase.

6. References

1. MANSON S.S., HALFORD, G.R., HIRSCHBERG, M.H. - 'Creep-Fatigue Analysis by Strainrange Partitioning' NASA TMX-67838, May 1971.
2. HIRSCHBERG, M.H., HALFORD, G.R. - 'Strainrange Partitioning - A Tool for Characterizing High-Temperature Low Cycle Fatigue' - NASA TMX-71691, April, 1975.
3. MANSON, S.S., HALFORD, G.R. - 'Treatment of Multiaxial Creep Fatigue by Strainrange Partitioning' NASA TMX 73488, December 1976.
4. MANSON, S.S. - 'The Challenge to Unify Treatment of High Temperature Fatigue - A Partisan Proposal based on Strainrange Partitioning', ASTM S.T.P. 520, 1973, 744-775.
5. BERLING, J.T., CONNAY, J.B., 'Effect of Hold Time on the Low Cycle Fatigue Resistance of 307 Stainless Steel at 1200°F' - First Int. Conf. on Pressure Vessels Technology, Delt 1969.

6. CONWAY, J.B., BERLING, J.T., STENTZ, R.H. 'Strain Rate and Hold Time Saturation in Low Cycle Fatigue'. ASTM S.T.P. 520, 1973, 637 - 647.
 7. WELLS, C.H. and SULLIVAN, C.P. 'The Effect of Temperature on the Low Cycle Fatigue Behaviour of Udimet 700'. ASM, Trans. Quar. 60, 1967, 217-222.
 8. LORD, D.C. and COFFIN, L.F. 'Low Cycle Fatigue Hold Time Behaviour of Cast René 80.' Met. Trans. 4, 1973, 1647-54.
7. Acknowledgements

This work was sponsored by the Ministry of Defence Procurement Executive, to whom the authors would like to express their thanks. They also wish to thank Mr. T.E. Clifton for assistance with the experimental programme and for the design and construction of most of the equipment.

One of the authors, V. Antunes, wishes to acknowledge financial support received from Junta Nacional de Investigação Científica e Tecnológica, Lisbon and the leave of absence for research in Cranfield granted by Faculdade de Engenharia da Universidade do Porto, Portugal.

TABLE I - Chemical Composition and Mechanical Properties of MAR MOO2

A - Chemical Composition

C	Si	Cu	Fe	Mn	Cu	Ti	Al	Co	W	Mo	B	Zr	Ta	Hf	Ni
0.15	0.2	0.1	0.5	0.2	9	1.5	5.5	10	10	0.5	0.02	0.05	2.5	1.5	Bal.

B - Mechanical Properties

Temperature (°C)	Ultimate Tensile Stress (MN/m ²)	Reduction of Area (%)	Fracture Strain (%)	Young Modulus (MN/m ²) x 10 ³
20°C	1068	10	8	213
850°C	889	15	10	158
1040°C	482	23	10	138

Strainrate for all TESTS (0.2% s⁻¹)

(TABLE II follows on page 1E-5).

AD-A059 900

ADVISORY GROUP FOR AEROSPACE RESEARCH AND DEVELOPMENT--ETC F/G 11/6
CHARACTERIZATION OF LOW CYCLE HIGH TEMPERATURE FATIGUE BY THE S--ETC(U)
AUG 78

UNCLASSIFIED

AGARD-CP-243

NL

2 OF 4

AD
A059900



TABLE II - BASIC LOW CYCLE FATIGUE TESTS

Test No.	Specim. Identif.	Temp. (°C)	Cycle Definition	Total Strain $\Delta\epsilon_T$ (%)	Inelastic Strain $\Delta\epsilon_i$ (%)	$F_i = A\epsilon_i / A\epsilon_T$				Cycles to Failure N	N_{ij} (4)	Tensile Stress (MN/m ²)	Mean Stress (MN/m ²)	Stress Range $\Delta\sigma$ (MN/m ²)	Time to Failure (hr)
						F _{PP}	F _{PC}	F _{CP}	F _{CC}						
10	NJB2/1	850	PP-0.6Hz	0.685	0.039	1	-	-	-	825	825	447	-43	980	0.4
13	NJB2/2	850	PP-0.6Hz	1.065	0.170	1	-	-	-	220	220	754	+37	1432	0.1
14	NJB25/4	858	PP-0.6Hz	2.02	0.844	1	-	-	-	10	10	1102	+33	2146	0.005
18	NJB1/2	850	PP-0.6Hz	0.544	0.025	1	-	-	-	1790	1790	420	+4	831	0.8
19	NJB2/3	850	PP-0.6Hz	0.304	0.004	1	-	-	-	10960	10960	325	0	650	5
21	NJB1/3	1040	PP 1 Hz	0.705	0.180	1	-	-	-	370	370	320	-24	686	0.1
22	NJB15/1	1040	PP 1 Hz	0.502	0.067	1	-	-	-	1640	1640	292	0	584	0.5
24	NJB3/3	1040	PP 1 Hz	0.977	0.341	1	-	-	-	95	95	443	-14	914	0.03
25	NJB3/1	1040	PP 1 Hz	0.349	0.044	1	-	-	-	4600	4600	202	-10	423	1.3
37	NJB6/4	850	CP(1)	0.600	0.063	0.15	-	0.85	-	1896	3050	351	-187	1076	11.2
30	NJB5/2	850	CP	0.731	0.092	0.27	-	0.73	-	1076	2744	377	-169	1091	6.4
29	NJB5/1	850	CP	0.996	0.220	0.30	-	0.70	-	166	169	480	-189	1338	1
39	NJB4/1	850	CP	0.863	0.094	0.27	-	0.73	-	805	1306	430	-191	1243	4.9
40	NJB4/2	1040	CP	0.402	0.124	0.25	-	0.75	-	451	412	161	-93	507	2.6
26	NJB3/4	1040	CP	0.724	0.279	0.27	-	0.73	-	88	77	245	-94	677	0.5
27	NJB3/2	1040	CP	0.538	0.153	0.36	-	0.64	-	347	313	172	-79	502	2
32	NJB5/5	850	PC(2)	1.000	0.211	0.32	0.68	-	-	92	76	940	+142	1595	0.5
33	NJB5/4	850	PC	0.707	0.074	0.38	0.62	-	-	408	363	723	+143	1160	2.5
38	NJB6/1	850	PC	0.487	0.011	0.09	0.91	-	-	1261	1182	574	+156	842	7.6
31	NJB5/3	1040	PC	0.928	0.515	0.30	0.70	-	-	153	57	531	+123	816	0.3
34	NJB6/2	1040	PC	0.550	0.177	0.26	0.74	-	-	402	1135	414	+109	610	2.3
42	NJB4/5	1040	PC	0.315	0.066	0.39	0.61	-	-	1985	1965	311	+102	417	11.6
35	NJB6/3	850	CC(3)	0.796	0.211	0.30	-	0.16	0.54	180	188	678	+47	1262	2
44	NJB7/2	850	CC	0.489	0.052	0.05	-	0.05	0.90	1326	1304	467	+27	880	15
47	NJB7/5	850	CC	0.586	0.113	0.26	-	-	0.74	571	776	477	+14	925	6.6
36	NJB6/5	1040	CC	0.891	0.456	0.29	-	0.01	0.70	57	56	310	+11	597	0.6
41	NJB4/4	1040	CC	0.700	0.350	0.26	-	0.04	0.70	119	87	293	+5	575	1.4
45	NJB7/2	1040	CC	0.398	0.200	0.12	-	0.08	0.80	502	769	147	-6	308	5.8
46	NJB7/4	1040	CC	0.297	0.121	0.08	-	0.13	0.79	1237	1885	141	-8	295	14
6A	NJB14/4	750	PP	0.573	0.00(6)	1	-	-	-	9614	7395	520	+22	995	5.4
7A	NJB13/3	750	PP	0.771	0.036	1	-	-	-	1516	1099	656	+34	1244	0.8
8A	NJB14/2	750	PP	0.648	0.032	1	-	-	-	1977	1246	607	+41	1129	1
9A	NJB12/1	750	PP	0.872	0.104	1	-	-	-	327	356	753	-18	1543	0.2
10A	NJB12/3	750	PC	0.600	0.016	0.50	-	0.50	-	1674	1589	613	+76	1073	10
11A	NJB12/4	750	CP	0.670	0.040	0.45	0.55	-	-	2173	2010	429	-101	1060	11.3
12A	NJB13/4	750	CC	0.700	0.048	0.66	-	-	0.34	1377	1021	614	+24	1181	15.8
1B	NJB9/4	950	PP	0.664	0.155	1	-	-	-	511	403	461	+18	886	0.15
2B	NJB9/5	950	PC	0.423	0.072	0.57	0.43	-	-	1511	1594	415	+139	552	8.7
4B	NJB9/3	950	CC	0.360	0.086	0.16	-	0.07	0.77	1996	3290	217	0	434	21

The footnotes for this Table appear overleaf

- (1) Stress Dwells of approximately 20 seconds (Tension).
- (2) Stress Dwells of approximately 20 seconds (Compression)
- (3) Stress Dwells of approximately 20 seconds (Tension and Compression)
- (4) $-\frac{1}{N} = \sum \frac{F_{ij}}{N_{ij}}$

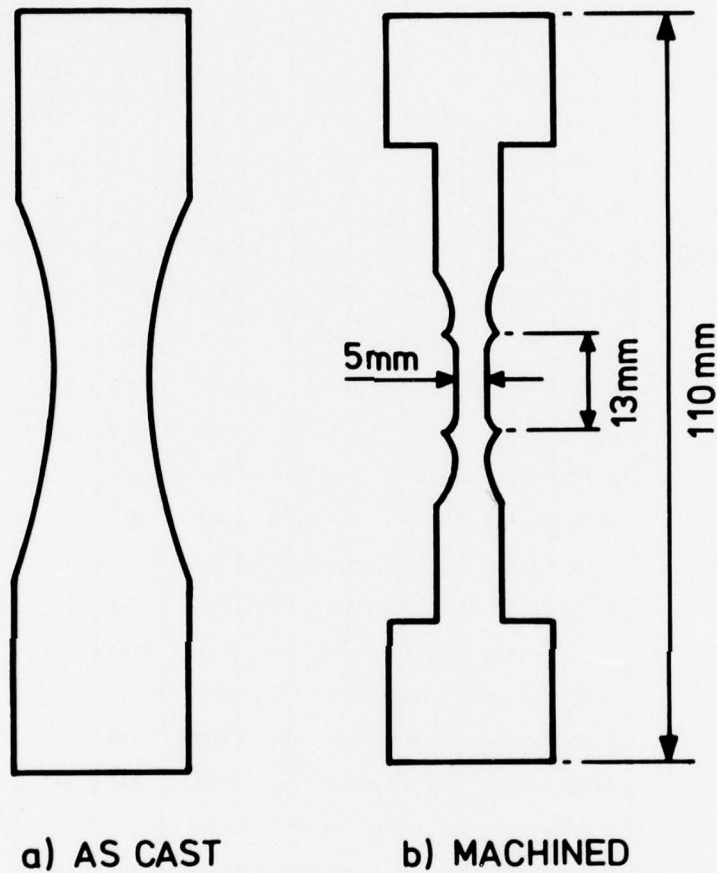


Fig.1 Mar M 002 specimens

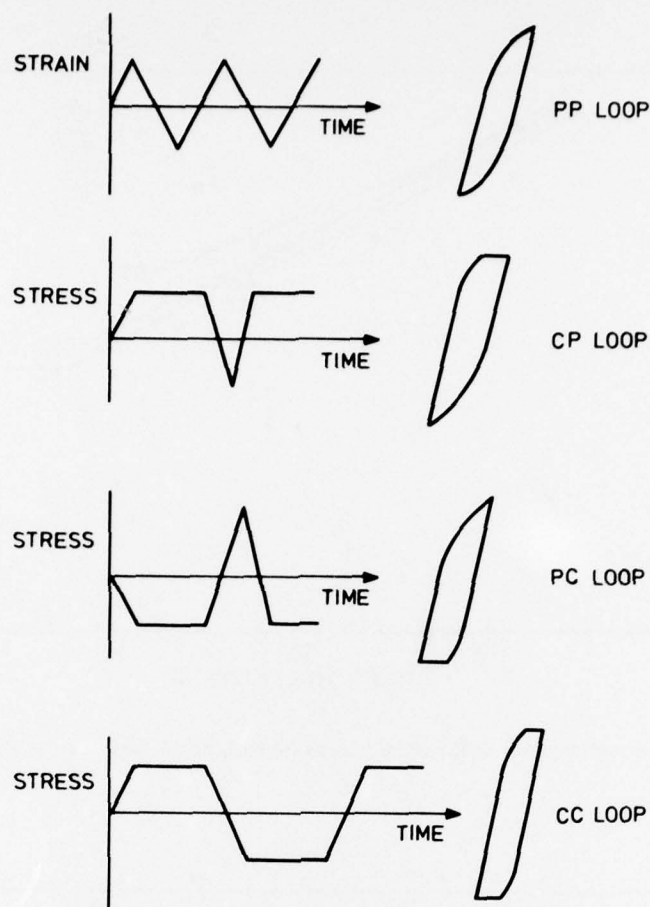


Fig.2 Axial strain and stress versus time wave forms for the isothermal low cycle fatigue tests

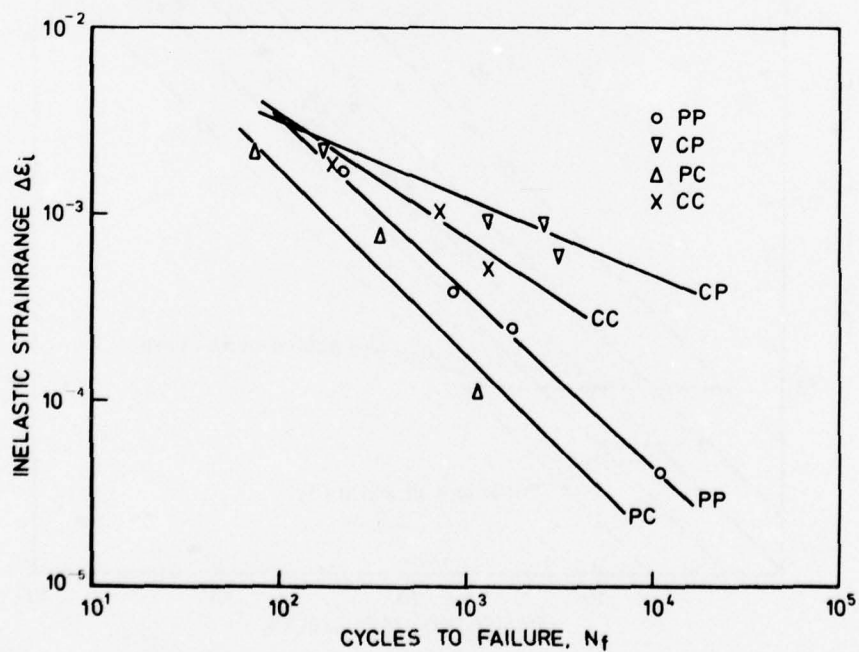


Fig.3 Strainrange versus life relationships for each of the basic tests at 850°C

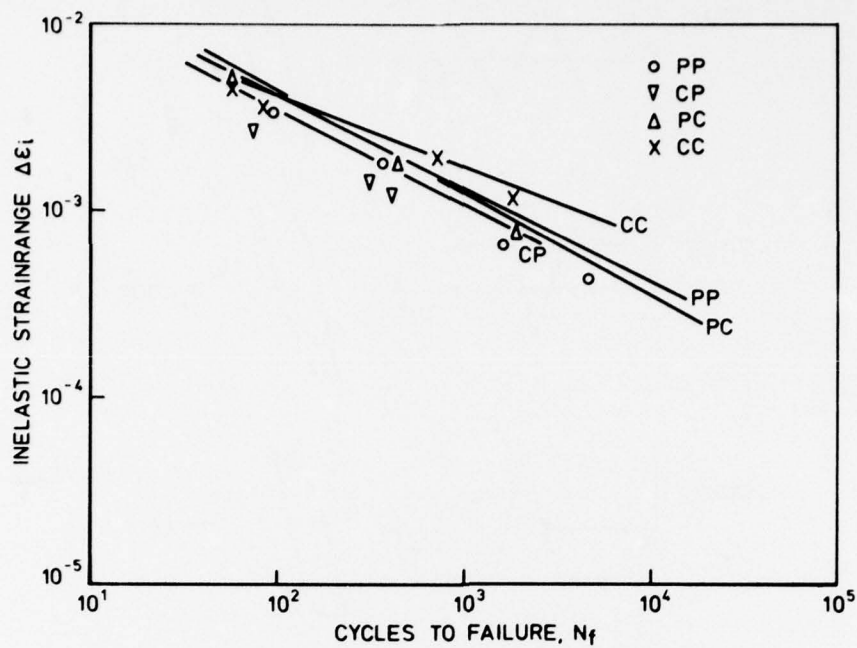


Fig.4 Strainrange versus life relationships for each of the basic tests at 1040°C

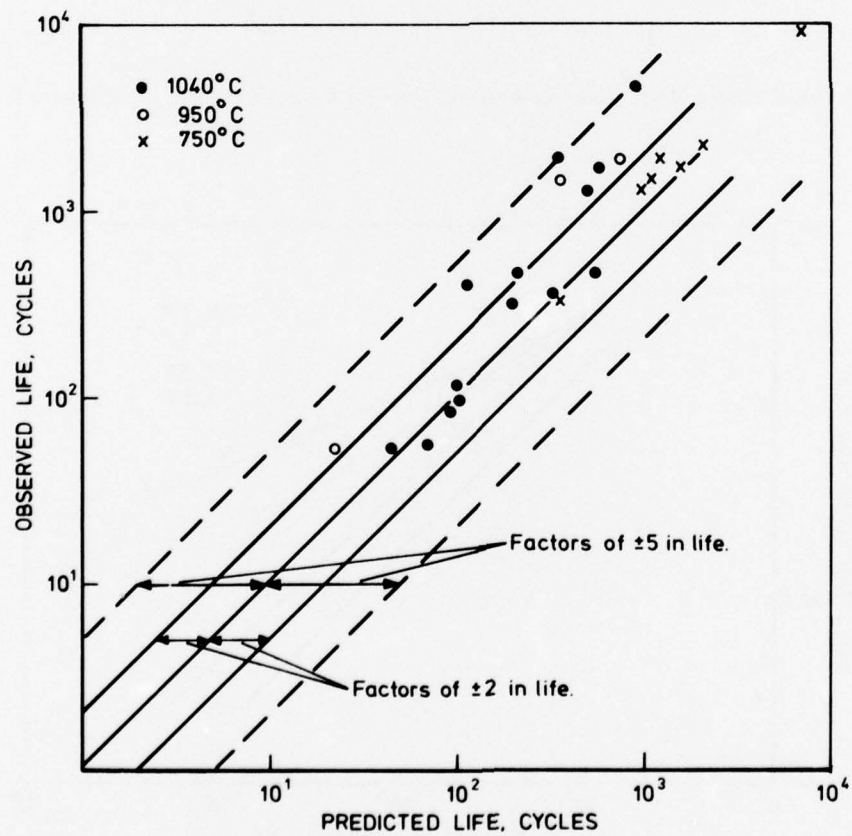


Fig.5 Comparison of observed and predicted lives using the 850°C basic $N_{ij} - \Delta\epsilon_{ij}$ relationships

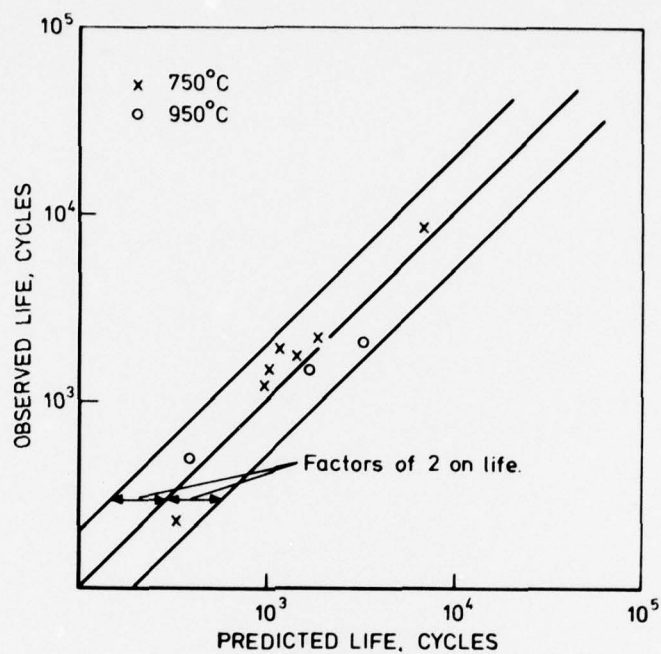


Fig.6 Comparison of observed and predicted lives using the 850°C basic relationships to predict the 750°C results and the 1040°C basic relationships to predict the 950°C results

DISCUSSION SUMMARY OF SESSION I

by

Hedley R. Tipler

Division of Materials Applications

National Physical Laboratory

Teddington

Middlesex

TW11 0LW

England

As the five papers presented in Session I contained results which had been obtained on similar alloys but by different organisations the Recorder opened the discussion period by comparing these results so that the extent of agreement in baseline SRP data between different laboratories could be assessed. These comparisons are reproduced in Table I, which also indicates other aspects of, and modifications or alternatives to, the SRP methods which had been investigated.

The discussion which followed centred mainly on the ability of the ductility-normalised SRP relationships to predict creep-fatigue interaction, and in particular it was questioned whether ductility, however defined, was a property which accurately reflected the various types of behaviour occurring during creep-fatigue interaction in a wide range of materials. A number of questions led to a restatement of the manner in which ductility-normalised relationships had been developed and their method of application. This information is available in the published literature and it will not be reported here. Other topics mentioned during the discussion concerned the micro-mechanisms associated with the various components of low cycle fatigue behaviour and the reasons for variations in the damaging potential of different combinations of straining cycle.

The main topic of discussion reflected the different approaches of the materials scientist and the engineer to the SRP method, differences which seemed to be more strongly emphasised in the field of low cycle fatigue than in others because of the complexity of the physical processes occurring and the testing variables applied. As the materials scientists pointed out, matrix deformation, grain boundary sliding, recovery processes, grain boundary cavitation, transgranular and intergranular cracking are proceeding to different degrees depending on stress, temperature, time and strain rate. It was, therefore, difficult to understand how a gross engineering property such as ductility was capable of describing accurately the behaviour of materials in which these, often highly localised, processes were going on together during the course of a test. There was considerable reluctance in applying ductility in a wide-ranging treatment to embrace phenomena which in some cases may be the antithesis of each other e.g. intergranular and transgranular failure modes, in other cases may cover widely different regimes in the fracture process, e.g. crack initiation and crack propagation, and in yet other cases may involve a greater or lesser degree of instability prior to failure.

Faced with these complexities, which the engineer recognised, he nevertheless had to make use of whatever mechanical property data were available, and maximise their application so as to refine his prediction procedures. Thus any property which reflected the behaviour of the material could be a tool towards his ultimate aim of predicting the performance of the components he was designing. When a variety of materials tested under identical conditions displayed differences in ductility the values obtained gave an indication of the capacity of the material to deform whether or not there was instability prior to fracture, i.e. ductility did indicate distinctions in material behaviour. Moreover, it had the advantage of being a readily available engineering property in contrast to others of a more complex nature which might be used. It was pointed out in this discussion that the use of ductility was not basic to the SRP method but had been developed to extend its application from situations where the basic relationships were available to those where they were not, e.g. when materials were tested in different environments, in different heat-treatment conditions or under complex stress, all of which might be expected to affect the ductility of a material. (An example was given where the damage relationships for a material in two environments converged as the ductilities became closely similar). Thus while the engineer did not claim that the application of the ductility criterion was exact or fully accounted for all the nuances of the response of a material to cyclic testing, this approach for predicting life expectancy was a positive alternative to no approach at all. In answer to other objections the proponents of the SRP method made clear that it was not intended for use under crack propagation conditions, for which a stress rather than a strain approach could be more suitable.

In discussing the low cycle fatigue behaviour of some materials in which cycles containing a tensile creep component were less damaging than those which contained a tensile plastic component, two possible reasons for this behaviour were suggested; (i) that the creep rupture ductility could be higher than that under tensile plastic strain and (ii) there was a mean tensile stress in the cycle (pc) having a tensile plastic component but a mean compressive stress in the cycle (cp) with a tensile creep component. From this and other standpoints there was a general interest in the influence of mean stress on low cycle fatigue behaviour, and some critical experiments would be valuable in this area. The results of micro-structural studies had not been altogether consistent in relating the different modes of damage to the type of cyclic test loop or to environmental effects, and it was clear from the discussion that further investigation of this aspect was required.

T A B L E 1
COMPARISON OF INTERLABORATORY TEST RESULTS ON SIMILAR MATERIALS

Authors	Material	Test Temperature °C	Order of decreasing damage		Range of cyclic lives	Slopes of partitioned life relationships				Correlation of cyclic lives
			Low life	High life		$\Delta t, cc$	$\Delta \epsilon, cp$	$\Delta \epsilon, pc$	$\Delta \epsilon, pp$	
KORTOVICH, SHEINKER	RENE 80 cc + coating	1000 and 871	pc, cp, cc, pp	pc, cp, cc, pp	at $\Delta \epsilon \sim 10^{-2}$	-	-	-	-	± 2
		Other observations:	No significant effect of temperature		3×10^3 to 4×10^4					± 2
		1000	cp, cc, pp, pc	pc, cp, pp, cc	18 to 50	$.51(N_{cc})^{-.49}$	$.034(N_{cp})^{-.45}$	$.116(N_{pc})^{-.64}$	$.062(N_{pp})^{-.51}$	± 2
HALFORD, NACHTIGALL	RENE 80 cc	Other observations:	Applied ductility normalised SRF equations and obtained correlation of ± 3		2×10^3 to 9×10^3					± 2
		760	cp, pc, cc, pp	pc, pp, cc, cp	13 to 70	$.084(N_{cc})^{-.62}$	$.029(N_{cp})^{-.43}$	$.14(N_{pc})^{-.87}$	$.276(N_{pp})^{-.80}$	± 2
		649	cp, pp	pp, cp	3×10^3 to 9×10^3	-	$.86(N_{cp})^{-.56}$	-	$.56.7(N_{pp})^{-.95}$	± 2
HALFORD, NACHTIGALL	1N100 gt 1N100 gt	Other observations:	Proposed General Damage Rule and discussed special cases of it.		3×10^2 to 4×10^3					± 2
		925	pc, cp, cc, pp	pc, cp, pp, cc	10 to 20	$.033(N_{cc})^{-.44}$	$.04(N_{cp})^{-.55}$	$.053(N_{pc})^{-.73}$	$.053(N_{pp})^{-.57}$	± 2
		Other observations:	Applied ductility normalised SRF equations and obtained correlation of ± 3 . Verified SRF method by using baseline data for complex cycling tests and obtained correlation of ± 2 .		5×10^2 to 2×10^3					± 2
CHABOCHÉ, FOLICELLA, KACZMAREK	1N100 cc + coating	900 and 1000	cp, cc, pp, pc	cp, pc, cc, pp	-	$.12(N_{cc})^{-.5}$	$.23(N_{cp})^{-.5}$	$.03(N_{pc})^{-.67}$	$.036(N_{pp})^{-.57}$	± 2
		Other observations:	No significant effect of temperature. Proposed use of continuous damage accumulation approach of Kachanov and Rabatnov.							± 2

cc = conventionally cast

gt = gatorised

THE LOW CYCLE FATIGUE BEHAVIOUR
OF NIMONIC 90 AT ELEVATED TEMPERATURE

by
G. F. Harrison and M. J. Weaver
Materials Science Department,
National Gas Turbine Establishment,
Pyestock, Farnborough, Hants GU14 0LS, England

SUMMARY

High temperature strain controlled fatigue data for the wrought nickel base alloy Nimonic 90* are presented together with their interpretation based on the concept of strain range partitioning. When this approach was used to predict data at 650 and 900°C using those generated at 810°C, the lives at 650°C were accurate to within a factor of two whereas at 900°C, actual test results were much less than the predicted values. Also discussed is the difficulty encountered when using the partitioning approach to predict low frequency test results, as answers are very sensitive to the ways in which cycles are partitioned into their creep and plastic components. Finally, the data are examined in terms of stress as opposed to strain and predictions using a stress/static-creep data approach are compared to those obtained using strain range partitioning.

1. INTRODUCTION

The biggest problem facing a designer when attempting to predict the life of a component, be it part of an automobile, airframe, building, bridge or gas turbine engine, is deciding what levels of stress, strain, temperature and time are likely to be imposed upon it. In reasonably static situations such as those encountered in civil engineering accurate predictions can often be made, but in more fluid situations, as experienced in nuclear reactors and gas turbine engines, the problem is far from simple as not only are imposed loads very variable in nature but also very high temperatures are encountered.

The classical approaches to summing damage accumulation - hence life prediction - under cyclic loading at low temperatures (that is, less than approximately 0.5 T_m where T_m = melting point in degrees absolute) involve the use of strain or stress controlled fatigue data, Goodman diagrams and Miner's Law. The basic assumption made is that damage is a function of the number of loading cycles but independent of time on load. Under conditions of strain range control, the effect of temperature is often ignored up to 0.5 T_m. If stress range is considered to be the controlling parameter, work at NGTE has shown that below 0.5 T_m, repeated tension low cycle fatigue data at various temperatures can be rationalised by considering the number of cycles to failure to be a function of the ratio of the imposed stress range to the ultimate strength of the material at the particular temperature in question⁽¹⁾.

Once temperature exceeds 0.5 T_m, it is unlikely that time on load effects can be ignored due to the introduction of a damage mechanism other than fatigue, namely creep. Advocates of the strain range approach have invoked either a 10 per cent rule,⁽²⁾ that is the life at high temperature may be only 10 per cent of that at low temperatures, or have introduced frequency terms into the equations describing low temperature data in order to fit those obtained at high temperatures⁽³⁾. Although partly successful, neither of these modifications is sufficiently biased towards the creep damage mechanism to ensure success at temperatures much above 0.5 T_m. A more realistic view of the influence of creep in high temperature cyclic loading has been incorporated in the most recent adaptation of the strain approach to high temperature low cycle fatigue, namely Strain Range Partitioning (SRP)⁽⁴⁾. A brief account of SRP is given in Section 2.

At NGTE on the other hand cyclic loading at high temperatures has been regarded as a form of cyclic-creep and not one of fatigue in the traditional meaning of the term. That is, damage accumulation is a function of time on load and not of the number of loading cycles. Load and not strain has been taken to be the controlling parameter and it has been shown for a variety of materials that when slow rates of change of loading are involved, rates in fact similar to those often seen in gas turbine engines (typically up to 10 cpm) isothermal cyclic load data can be predicted solely from a knowledge of the static creep properties⁽⁵⁾. Recently it has been shown that a similar approach also enables sensible life predictions to be made when both stress and temperature are continuously changing⁽⁶⁾.

Realistic life predictions of gas turbine components are likely to be possible only if a full appreciation of what is happening in terms of both stress and strain is known. In order to relate these two parameters a programme of work was set up at NGTE aimed at studying the high temperature cyclic strain behaviour of the wrought nickel base alloy Nimonic 90. As high temperature/strain controlled testing was a new test technique to NGTE, the decision was made to take part in the AGARD International Collaboration Exercise aimed at validating the concept of strain range partitioning, as this would enable NGTE to become involved quickly in the collection and exchange of strain controlled data, thereby allowing a more detailed comparison to be made between strain and stress parameters than would otherwise be possible.

After summarising the concept of strain range partitioning, this paper goes on to describe the technique of high temperature strain controlled testing developed at NGTE, the various results obtained for the alloy Nimonic 90 and the difficulties encountered in applying to these the concept of strain range partitioning. Finally life predictions made using SRP are compared to those made by the NGTE static creep approach.

*Trade Mark of Henry Wiggin Ltd, Hereford

2. STRAIN RANGE PARTITIONING

The basic premise behind strain range partitioning is that in any hysteresis loop there are combinations of just two directions of straining and two types of inelastic strain. The two directions are tension and compression while the two types of inelastic strain are either of a time dependent nature (creep) or of a time independent nature (plastic). It is therefore possible to represent any closed hysteresis loop by four possible kinds of strain ranges. These are:

1. tensile plasticity reversed by compressive plasticity, $\Delta\epsilon_{pp}$
2. tensile creep reversed by compressive creep, $\Delta\epsilon_{cc}$
3. tensile creep reversed by compressive plasticity, $\Delta\epsilon_{cp}$
- and 4. tensile plasticity reversed by compressive creep, $\Delta\epsilon_{pc}$

Each of these forms of inelastic strain range has its own relationship with the number of cycles to failure, and so can be represented in a form similar to the Manson-Coffin relationship. Once the hysteresis loop for the cycle being analysed is both known and partitioned into its inelastic components, life prediction is possible using an interaction damage rule specially designed to operate with a combination of strain ranges. The form of this damage rule is:

$$\frac{1}{N_{\text{predicted}}} = \frac{F_{pp}}{N_{pp}} + \frac{F_{cc}}{N_{cc}} + \frac{F_{cp}}{N_{cp}} + \frac{F_{pc}}{N_{pc}} \quad \dots(1)$$

where F_{pp} (etc) is the fraction of the total inelastic strain that is ϵ_{pp} and N_{pp} (etc) is the number of cycles to failure of an $\Delta\epsilon_{pp}$ test conducted at a strain range equal to the total inelastic strain range (this value being obtained from the basic set of SRP curves).

The original papers setting out the concept of strain range partitioning held out the promise that temperature was not an important parameter in determining life under conditions of totally reversed inelastic strain; that is, a series of SRP curves obtained at one temperature were equally valid at temperatures both above and below this level. This has since been shown not to be the case, a recent paper suggesting that temperature does affect the form of the SRP curves, but in many instances incorporating relevant values of either creep or tensile ductility into the equations helps to remedy the situation⁽⁷⁾.

3. TEST TECHNIQUES

The material used throughout the exercise was the wrought nickel base superalloy Nimonic 90⁽⁸⁾. Although no longer enjoying extensive useage in modern aero engines, it is a material that can be considered as being typical of its class, and is one that has previously been studied in depth. Details of the alloy used in this investigation are given in Table I *(see Footnote on p.6-9).

Testing was undertaken using a 20 KN closed loop servo-hydraulic machine. Continuously cycled triangular waveform fatigue testing was carried out under strain control using the waveform generator supplied with the machine. In order to conduct cyclic tests involving creep hold times either in tension or compression (or both) it was necessary to use a specialised external function generator. When using this generator it was possible to introduce a hold at any desired level of load, and maintain this load until a preset extension had been attained at which point the loading was reversed and the other half of the cycle completed.

Test specimens were heated to the appropriate test temperature using a conventional tube furnace, the temperature of which was controlled by a platinum resistance thermometer. Thermocouples were tied to the centre and each end of the parallel gauge length to ensure that the temperature gradient along the specimen did not exceed $\pm 1^\circ\text{C}$.

Specimen extension was measured using a single transducer extensometer and recorded using an X-time recorder and an X-Y plotter. Load was monitored continuously using either a DVM or X-time recorder and intermittently using an X-Y plotter.

When it was decided at NGTE to gather strain controlled fatigue in more detail than had been the practice in the past, the decision was made to measure axial strain. Previous work had shown that if strain was monitored during a fatigue test by measuring extension between ridges at the ends of a parallel gauge length, then in the majority of cases failure of the specimen occurred at the ridges due to the associated stress concentrations. In order to avoid the problem of ridge failure the design of specimen shown in Figure 1 was adopted; extension was monitored between the sharp corners high on the shoulders of the specimen, shown X-X' in the diagram. The large radius leading into the shoulder at either end of the 10 mm parallel gauge length was chosen to give a stress concentration at the shoulder/gauge-length interface of only 1.06. The disadvantage of this method of strain measurement is that elastic and plastic extensions can only be converted into strain in the parallel gauge length by use of computed effective gauge length factors. Details of the factors used and their means of derivation are given in Appendix A1.

4. PRESENTATION OF RESULTS

4.1 STATIC TENSILE AND CREEP DATA

Slow strain rate tensile data ($\approx 0.002/\text{min}$ to proof stress and $0.1/\text{min}$ thereafter) at temperatures of 650, 810 and 900°C are given in Table II, which also includes 810°C tensile data obtained at a high strain rate corresponding to a fully reversed triangular waveform frequency of 25 cpm. This high strain rate datum is shown in Figure 2. Actual creep rupture data obtained on the cast of Nimonic 90 used in these experiments are superimposed on a typical creep rupture map in Figure 3.

4.2 BASIC SRP DATA AT 810°C

The four basic partitioned strain range life relationships were determined by conducting isothermal (810°C) laboratory tests that featured the strain ranges of interest.

4.2.1 PP TESTS

These tests consist of plastic inelastic strain in both the tensile and compressive halves of the cycle. To achieve this condition at high temperatures, it is necessary to cycle the strain at a frequency sufficiently high to preclude the introduction of significant amounts of time dependent creep strain. Previous tests had shown that for Nimonic 90 at 810°C a frequency of 25 cpm (0.41 Hz) was sufficiently high to overcome the so called "frequency effect", and all PP tests were undertaken at this frequency using a triangular waveform. The results obtained are given in Table III and Figure 4. It is interesting to note that after work hardening for the first few cycles of a cyclic test, the Nimonic 90 work softened throughout the remainder of the test.

4.2.2 CP AND PC TESTS

Testing of this type was undertaken using the external function generator mentioned previously. This enabled either a tensile or compressive hold on load to be introduced into what otherwise would have been a PP cycle. The load hold was programmed to act for as long as was necessary to produce the predetermined amount of strain. When this limit was reached, the function generator reversed the loading and completed the other half of the cycle in true PP fashion. The loading rates during the fast cycling could be controlled and were set to be similar to those obtained in the basic PP tests (ie equivalent to approximately 25 cpm). This ensured that all the inelastic strain accumulated during the rapid part of the cycle was of the PP type.

As Nimonic 90 tends to work soften when cycled at 810°C it was found necessary, particularly at the beginning of a test, to make regular reductions to the creep stress level in order to maintain a constant balanced shape to the hysteresis loop. Even so, the duration of the creep portion of the cycle tended to decrease during the test. The results obtained are given in Table III; the CP and PC life/strain-range values calculated therefrom, after allowing for the PP contribution and utilising the prescribed damage fraction rule, are given in Figure 4.

4.2.3 CC TESTS

Testing of this type was identical to that for the CP/PC case except that creep hold times were introduced into both the tensile and compressive portion of what otherwise would have been a PP test. Test results are given in Table III and the corresponding CC life/strain-range curve is shown in Figure 4.

4.3 SUPPLEMENTARY TESTING

Additional testing was undertaken aimed at evaluating the predictive powers of SRP. The results of PP type tests undertaken at 650 and 900°C are given in Table IV and the data from low frequency tests undertaken at 810°C in Table V.

5. DISCUSSION

For the sake of clarity, the discussion will be subdivided into four major areas. In the first of these, the basic creep and tensile properties of the Nimonic 90 used in the programme will be discussed and compared to typical book data. The second and third sections will deal with the problems, both experimental and scientific, experienced in determining the basic SRP life lines and the accuracy of the predictions made using these life lines. Finally, mention will be made of the way the traditional NGTE stress-creep approach can be used to predict cyclic life.

5.1 BASIC TENSILE AND CREEP DATA

The slow strain rate tensile properties of the Nimonic 90 used in the test programme were similar to typical data reported in the literature, except that in all instances the actual measured values of reduction of area were a little lower than expected. It was interesting to note that whereas testing at a high strain rate produced the expected increases in proof stress and failure strength, there was little effect on the reduction of area value recorded.

The method adopted at NGTE for presenting static creep data is the one first proposed by Graham and Wallis⁽⁹⁾. This assumes that log stress/log time to failure data points fall on a continuous series of straight lines for each temperature, with slopes in the series -1/32, -1/16, -1/8, -1/4 etc. The positions of the slope changes and the distance between lines at different temperatures are dependent on a time-temperature relationship of the form:

$$t_f = A \sigma^{\frac{-B}{K}} (T' - T)^{-20} \quad \dots(2)$$

where t_f = rupture time, T = test temperature, A and T' are constants and $\frac{B}{K}$ has a value in the series 4, 8, 16 etc.

Typical Graham and Wallis curves for the alloy Nimonic 90 are given in Figure 2; also superimposed on this figure are actual data points obtained for the particular batch of Nimonic 90 used in the current programme. It can be seen that the slopes of the life lines are very dependent on stress and temperature. The relevance of the slopes of these lines to high temperature cyclic behaviour is discussed in Section 5.4. The 810°C creep ductility of the Nimonic 90 used in the test programme appeared to be independent of time to failure, typical values for reduction of area being in the range 8 to 12 per cent.

5.2. SRP LIFE LINE DETERMINATIONS

Whatever method is used to predict the life of an actual component, the accuracy obtained can only be as good as that of the basic data on which the prediction has been based. In strain range partitioning, therefore, the main factor affecting the accuracy of life prediction is the position and accuracy of the four basic life lines.

By far the biggest experimental difficulty when undertaking strain controlled fatigue testing is the measurement of strain itself. As mentioned previously, true longitudinal strain cannot be measured using ridged parallel gauge sections as failure invariably occurs at the ridges due to the stress concentration they induce; if in this type of specimen failure does not occur at the ridges in high temperature fatigue testing then in all probability stress redistribution is occurring as a result of creep processes and hence the result is no longer a valid fatigue failure. Diametral strain control using hour glass specimens can, if the radius of curvature is large, avoid damaging stress concentrations but still poses the problems of accounting for any anisotropic behaviour that may be present and converting diametral strain into the more useful longitudinal strain. In addition, diametral control often involves crack initiation at the extensometry position.

The advantage of using a design of specimen that enables longitudinal extension to be measured between points outside the parallel gauge length is that the measurement technique does not interfere with the failure process. The obvious disadvantage to the method is that strain within the gauge length can only be obtained by the use of equivalent gauge length factors that take into account the elastic and plastic extensions occurring outside the parallel portion. As shown in Appendix A1, the elastic factor is purely testpiece geometry dependent, whereas the plastic factor is dependent on the stress exponent of the appropriate stress-plastic strain curve. The elastic equivalent gauge length used throughout the programme was 24.1. Fortunately, values of the creep and fatigue stress exponents at 810°C were similar to one another (both being in the range 8 to 12) and so a constant value for the plastic equivalent gauge length of 14.5 was used throughout the analyses of 810°C data. (Similar values were also used in the analyses of data obtained at 900 and 650°C.)

The determination of the PP fatigue life-line involves testing at a frequency high enough to ensure that the number of cycles to failure is frequency independent. For Nimonic 90 at 810°C for example, this meant carrying out tests at a minimum frequency of 25 cpm. The need to test at such high frequencies can pose problems when it comes to recording hysteresis loops: PP life-lines were determined at what appeared to be the minimum acceptable value, ie 25 cpm, because this was the fastest speed that the mechanical carriage X-Y plotter, used to plot hysteresis loops, could accommodate. The hysteresis loops of the preliminary tests conducted at higher frequencies were analysed by photographing the trace as displayed on a large television screen, though this method was too time consuming to be adopted as a standard test technique.

Finally, while considering the experimental difficulties encountered in determining the basic life-lines, mention must be made that sensible creep component lines could only be obtained after the purchase of an additional function generator, capable of introducing hold times at constant load into the cycle whilst still maintaining overall control between fixed limits of extension. This need for additional specialised equipment over and above that normally associated with servohydraulic test machines could act as a deterrent to basic data collection.

The four basic life lines (derived from the data in Table III) for Nimonic 90 at 810°C are shown in Figure 4. The position of the PP line is very well defined, there being very little scatter amongst the data. The line can be described by an equation of the form:

$$N_{pp} = 0.057 (\Delta \epsilon_{pp})^{-1.67} \quad \dots(3)$$

Although there are fewer data for the CP and PC lifelines it would appear that over the range 10^1 to 10^5 cycles to failure, both sets can be represented by a single line which is parallel to the PP line but approximately an order of magnitude lower in the life attained for a given strain range. The equation takes the form:

$$N_{cp/pc} = 0.0054 (\Delta \epsilon)^{-1.67} \quad \dots(4)$$

The position of the CC line is less well defined. Because of the difficulties experienced in maintaining a fixed hysteresis loop profile, CC tests tended to revert to CP, PC or PP types if left unattended for long periods of time. Unfortunately the extent to which any change took place was not always known as automatic plotting facilities were not available. The CC lifeline could have a slope of between about -1.6 and -2.8, but the actual line chosen in Figure 4 is biased towards those data points (shown by an asterisk in Table III) for which stable loops were known to be maintained throughout the test. The equation of the chosen line is of the form:

$$N_{cc} = 0.000074 (\Delta \epsilon_{cc})^{-2.41} \quad \dots(5)$$

The CC life line is characterised by a strain exponent which is different from that of the other three life lines. One possible explanation for this difference may lie behind the proportions of life attributable to crack initiation and to crack growth. In the low cycle fatigue regime it is generally acknowledged⁽³⁾ that high strain crack growth dominates the fracture process and that initiation is less of a factor in determining life. In high cycle fatigue crack nucleation is thought to dominate the life to failure.

The two modes of behaviour, initiation and growth, have different strain exponents. Creep is also a process dominated by the nucleation of cracks, and so it could be argued that the slope of a CC life line should lie somewhere between the low and high cycle fatigue life lines.

Yet another explanation for the difference in slope between the CC lifeline and the other three may be linked to the phenomenon of anelasticity. If, during the course of a creep test the specimen is unloaded rapidly, the unloading is often followed by a period of reversed creep; one of the manifestations of anelasticity. Moreover, work at NGTE⁽¹⁰⁾ has shown that in load controlled square wave creep tests most of the creep strain monitored during each half cycle is strain that is being 'exchanged' between the tension and compression portions of the cycle and as a result is not contributing to the real strain accumulation. As anelasticity is not contributing to strain accumulation, it can be argued that it is not part of the damage mechanism. In strain controlled tests therefore, particularly those involving a creep component, there may be three not two types of inelastic strain, namely plastic, creep and anelastic.

To date there has been insufficient time to measure the amounts of anelasticity in the CC tests, but a preliminary assessment of that present in a small-strain-range/long life test indicated that up to half of the creep strain monitored may be anelastic. (Anelasticity in any particular test is difficult to estimate, but it increases with increasing stress range, reaching a limiting value such that the amount present in a high strain test will be proportionately less than that present in a low strain test.) For example, for Test 51 in Table III, $\Delta\epsilon_{pp}$ is given as 0.009 per cent and $\Delta\epsilon_{cc}$ as 0.041 per cent. Now if anelasticity accounts for 0.02 per cent of the creep strain, one is left with a 'damaging' inelastic strain of 0.030 per cent (0.009 PP + 0.021 CC). Applying the damage rule to these modified values gives a predicted life of 10,500 cycles for a $\Delta\epsilon_{cc}$ of 0.030, whereas the original analysis gave 13283 cycles for a $\Delta\epsilon_{cc}$ of 0.050. As anelasticity is only likely to affect low strain results, the slope of the anelasticity corrected CC life line will steepen and approach that of the other three life lines. It is hoped to pursue this line of investigation in future work programmes.

A recent publication on SRP suggests that first order approximations of the basic life-lines can be made using a set of universal ductility normalised life relations⁽⁷⁾. For example, the equation relating PP data is of the form:

$$N_{PP} = \left(\frac{2\Delta\epsilon_{PP}}{D_P} \right)^{-1.67} \quad \dots(6)$$

where D_P is a measure of the tensile plastic ductility and equal to the negative of the natural logarithm of (1-reduction of area). Values of reduction of area obtained with the present cast ranged from 16 to 20 per cent, though published data suggested values as high as 30 per cent. Substitution into Equation 5 gives equations:

$$N_f = 0.017 (\Delta\epsilon_{PP})^{-1.67} \quad \text{for RA} = 16\% \quad \dots(7)$$

$$N_f = 0.056 (\Delta\epsilon_{PP})^{-1.67} \quad \text{for RA} = 30\% \quad \dots(8)$$

The exponent of the predicted equations is exactly equal to the one found in practice and, although the constants in the equations calculated using the determined values of reduction of area are too low, the form of the predicted equation using published data (ie RA=30 per cent) is very similar to that obtained in practice - compare Equation 8 with Equation 3.

When a tensile RA value of 30 per cent (ie $D_P = 0.36$) is fed into the universal PC life relationship of:

$$N_{PC} = \left(\frac{4\Delta\epsilon_{PC}}{D_P} \right)^{-1.67} \quad \dots(9)$$

the predicted relationship is:

$$N_{PC} = 0.017 (\Delta\epsilon_{PC})^{-1.67} \quad \dots(10)$$

Although giving accurately the strain exponent of the experimentally determined line (Equation 4), the predicted life is nevertheless approximately three times that observed in practice.

As the mode of creep cracking in Nimonic 90 is intergranular, the universal CP lifeline is given by:

$$N_{CP} = D_C (10\Delta\epsilon_{CP})^{-1.67} \quad \dots(11)$$

Substituting a creep RA value of 10 per cent into the above equation gives:

$$N_{CP} = 0.002 (\Delta\epsilon_{CP})^{-1.67} \quad \dots(12)$$

that is the predicted life is less than half that obtained in practice (compare Equation 12 with Equation 4).

The creep/creep prediction (for a creep RA value of 10 per cent):

$$N_{cc} = D_c (4\Delta\epsilon_{cc})^{-1.67} = 0.10 (\Delta\epsilon_{cc})^{-1.67} \quad \dots(13)$$

falls down in giving a strain exponent of -1.67 whereas the experimentally determined value equalled -2.41 (see Equation 5). In this case unlike the other three there is an appreciable discrepancy between the anticipated and observed strain exponents. It may be that the 'universal' constants determined for one class of alloys (say steels) do not match exactly those of another (eg nickel base superalloys or titanium). It will be interesting to see the suggested form of the ductility normalised SRP life relationships after all the data being generated in the on-going AGARD collaborative exercise have been analysed.

5.3 SRP LIFE PREDICTION

To date only a limited amount of testing has been undertaken which has been aimed at assessing the prediction capabilities of SRP. In the first exercise 25 cpm PP data were determined at 650°C and 900°C, that is at temperatures both above and below that at which the majority of testing was undertaken. As can be seen from Figure 5, the results at 650°C resembled those at 810°C, the life line being parallel to that for 810°C but the actual lives being about 5 times greater for a given strain range. As the value for tensile reduction of area measured at 650°C was 30 per cent and that at 810°C may be as low as 16 per cent, the ductility normalised SRP prediction for PP data at 650°C could be, in terms of 810°C data.

$$N_{pp}(650) = N_{pp}(810) \times \left(\frac{D_{650}}{D_{810}} \right)^{1.67} = 3.5 N_{pp}(810) \quad \dots(14)$$

The predicted 650°C life line that is 3.5 times that at 810°C, is a little on the low side as the actual life was approximately 5 times that at 810°C. Nevertheless, the SRP approach has predicted the trend towards higher lives and the result obtained is correct to within a factor of 2.

Less successful was the prediction of the 900°C data. As shown in Figure 5, the slope of the 900°C lifeline obtained by actual testing is quite different from that of the 650 and 810°C lines. Strain range partitioning predicts that the line should be parallel to the other two and lie slightly to the right of the 650°C life line as the ductility of Nimonic 90 at 900°C is greater than that at 650°C - see Table II. A possible explanation for the observed behaviour is that at 900°C a test frequency of 25 cpm is too slow to avoid time dependent effects and so the inelastic strain measured includes both PP and CC fractions. It is hoped to pursue this observation by undertaking tests at frequencies greater than 25 cpm. Further evidence to support the suggestion that the 900°C data are in fact creep dominated is presented in Section 5.4.2.

The only other assessment of the predictive powers of SRP was an attempt to predict the frequency effect observed in Nimonic 90 at 810°C. To do this, continuously cycled triangular waveform tests have been carried out at frequencies much lower than the 25 cpm used in the determination of the basic life-lines. The main difficulty encountered was in the analysis of the hysteresis loops, as it was not easy to decide just how much of the measured inelastic strain was plastic and how much was creep. The method adopted was to assume that the amount of plasticity in a low frequency test having a stress range $\Delta\sigma$ was equal to the amount of inelastic strain observed in a 25 cpm PP test having the same stress range. The predicted values shown in Table V were obtained using this value of $\Delta\epsilon_{pp}$ in order to calculate the fractions F_{pp} and F_{cc} for use in the predictive equation. It can be seen that in only one instance - Test 7 - is the prediction within a factor of 2 of the actual value. Because of the large difference in life for a given strain range between the PP and CC life curves (for lives of 10^7 cycles to failure) the ratio F_{pp} to N_{pp} has only a small effect on the predicted life, the dominating factor being the ratio F_{cc} to N_{cc} . Small changes in F_{cc} therefore have a marked effect on predicted life, and as F_{cc} is derived from the estimated value of F_{pp} , it is this estimate which is dominating the final predicted value. There is a need obviously to improve the means by which time dependent inelastic strains are partitioned into their plastic and creep components.

5.4 THE STRESS-STATIC CREEP APPROACH

Earlier work at NGTE has shown that in many instances, particularly when rates of cycling are low, high temperature cyclic loading data can be predicted solely from a knowledge of static creep properties. Briefly, the approach is based on the Graham and Wallis concept of creep strain accumulation which states that strain is a function of stress, time and temperature such that

$$\epsilon = \Sigma A \sigma^B t^K (T' - T)^{-20K} \quad \dots(15)$$

This equation was originally developed for steady stress creep but it can be applied to the case of a test specimen which is subjected to varying cyclic stress. With a tension-tension triangular waveform, the time to failure, t_f , is given by:

$$t_f = (1 + \frac{B}{K}) t_c \quad \dots(16)$$

where t_c equals the time to rupture of a static creep test with a stress equal to the maximum stress of the triangular waveform and $\frac{B}{K}$ is the negative of the reciprocal of the slope of the Graham Wallis log stress/log time-to-failure plot at the particular maximum stress and temperature being considered. For push-pull loading the time to failure with a triangular waveform is given by:

$$t_f = 2^{\frac{1}{K}} \left(1 + \frac{B}{K}\right) t_c \quad \dots(17)$$

where, because of the low creep ductilities associated with Nimonic 90, $\frac{1}{K}$ is equal to $\frac{1}{3}$. When the simple static creep approach is used to predict the life in a triangular waveform test it can be seen that the time to failure is independent of the frequency of testing.

5.4.1 STRESS AND BASIC SRP DATA AT 810°C

Through the dynamic stress strain curve there is a linear relationship between log shakedown-stress and log inelastic-strain in the PP tests at 810°C. Hence an equally good correlation must exist between log stress and log N_f , the number of cycles to failure, a relationship shown in Figure 6. If it is assumed that the 25 cpm PP tests at 810°C were failing not by fatigue but by cyclic push-pull creep mechanisms then a reasonable estimate of the time to failure and hence N_f of these tests can be obtained by applying the appropriate shakedown stress and Equation 17. (This prediction will only give an approximate answer as the equation refers to constant stress conditions whereas in strain controlled tests, the stress range is varying throughout the test.) The predicted life line for creep dominated failures is also shown in Figure 6, whence it can be seen that for lives of less than 10^5 cycles to failure, the actual number of cycles to failure is less than the predicted creep failure line. This helps to confirm that the PP failures at 810°C were not creep dominated, but in fact were true fatigue failures.

There appears in most instances to be a link between peak shakedown stress versus actual number of cycles to failure in the CP and PC tests and the average shakedown stress versus cycles to failure in the PP tests. These data are also shown in Figure 6. The notable exceptions are the two CP/PC tests having very short lives - less than 10 cycles to failure in both cases. It is unlikely that one would get a correlation with so few cycles to failure because whereas the bulk of the PP data is based on Nimonic 90 work softening, in the case of only 10 or less cycles to failure the alloy would be in the work hardening regime. Less conclusive is the agreement between semi-stress range/total inelastic strain of the PC/CP tests and of the PP tests, data shown in Figure 7.

The above observations, coupled with the similarity in strain exponents (versus N_f) of the PP, PC and CP life lines suggests that the PP, PC and CP tests, are all 'fatigue' dominated; in other words the dominant factor is the number of cycles and not length of time. However, it is pointed out that if the CP/PC tests are assumed to consist of a $\frac{1}{2}$ cycle of square wave creep followed by a $\frac{1}{2}$ cycle of 50 cpm triangular waveform creep, for all but one of the tests lives are within a factor of two of those predicted by the creep approach.

The final comments in this section on the relationship between stress and basic life-lines at 810°C concern the CC data. The CC experiments are similar in nature to push-pull tests (except for the varying load as opposed to the constant level of load control tests); the NGTE creep based prediction for this type of test is:

$$t_f = 2^{\frac{1}{K}} t_c \quad \dots(18)$$

where t_f , t_c and $\frac{1}{K}$ are as described for Equation 17. The CC tests should therefore last slightly longer than their comparative static creep data. The actual 810°C static creep data for the alloy used in these experiments are replotted in Figure 8, which also includes the relevant data from the CC tests; there is very good agreement between the two sets of data. It is interesting to recall - see Section 5.2 - that when the CC data were plotted on a strain versus cycles to failure basis, the scatter was such that it was difficult to fix the position of the best fit line.

The results to date suggest that when "fatigue" is the major damaging mechanism data are best described in terms of inelastic strain and number of cycles to failure but when creep failure mechanisms are involved stress and time on load are the important life parameters.

5.4.2 STRESS AND LIFE PREDICTION

It was shown in Section 5.4.1 that at 810°C fatigue failures could be expected in 25 cpm triangular push-pull loading tests provided the number of cycles to failure did not exceed 10^5 . Similarly, creep summations show that fatigue must be the dominating failure mechanism in 25 cpm tests at 610°C. It is no surprise therefore to see the marked similarity between the PP life lines at these two temperatures. When the 900°C PP data were analysed using the stress - static creep approach it was clear that most of the tests were failing at around 3 times their predicted creep lives; data illustrating this point are given in Table VI. This may at first sight seem to be inconsistent but previous work at NGTE has shown that just as there is a frequency effect when one talks in terms of fatigue so there is a similar phenomenon connected with cyclic creep. In fatigue situations, life (in terms of the number of cycles to failure) is independent of frequency over a wide range of frequencies and only at the lower frequencies does life show a decrease. In cyclic creep, life (but this time in terms of time to failure) is independent of frequencies at low frequencies but increases as the rate of cycling is raised beyond a critical point. The frequency effect in cyclic creep therefore is seen as an increase in both the time and the number of cycles to failure. This life extension effect can be explained by the concept of effective stress and is described elsewhere¹¹. Briefly, it has been shown that alloys do not creep under the driving force of the full applied stress (σ_a) but under an effective stress (σ_e) equal to σ_a less an inherent stress termed the friction stress (σ_o) which is both structure and applied stress dependent. With low rates of cycling the instantaneous applied stress and the corresponding friction stress are in phase, with the instantaneous value of friction stress being equal to that observed in a static creep test at the same applied stress level as the instantaneous applied stress in the cyclic test. For low rates of cycling therefore the equilibrium balance between σ_a and σ_o is maintained and the prediction equations based on static creep data give an accurate forecast of life under cyclic loading.

However, whereas the rate of build-up of σ_a with increasing σ_a is almost instantaneous, its rate of decrease during the unloading part of the cycle is limited by normal metallurgical recovery processes and so for higher frequencies of loading, σ_a cannot fall sufficiently rapidly to maintain the equilibrium value corresponding to the applied stress. Under these conditions the effective stress operating ($\sigma_a - \sigma_o$) is lower than expected and hence less damage occurs than predicted from the simple creep approach. The overall effect of increasing frequency of testing is therefore to increase not only the time to failure but also the number of cycles to failure.

It may be recalled from Section 5.3 that the SRP approach was not very accurate when used to predict the lives of the cyclic tests conducted at 2 cycles per minute and 10 cycles per hour. The NGTE stress-static creep approach on the other hand should predict the lives of these tests accurately as it was for this type of testing that the method was devised; the stress/creep predictions for the low frequency tests are compared with the actual lives obtained and the lives predicted using SRP (from Table V) in Table VII. Predicted and observed lives for both the SRP and the creep predictions are also compared in Figure 9, which clearly shows that whereas all but one of the creep predictions are within a factor of 2 on life only one of the SRP predictions falls within the same bounds on life. This finding tends to support the comment made earlier that when time dependent mechanisms are involved stress and time are often better life parameters than strain and number of cycles to failure.

6. FINAL COMMENTS AND CONCLUSIONS

1. Strain range partitioning lifelines for Nimonic 90 at 810°C have been established and used to predict lives of tests carried out at low frequencies and at 650 and 900°C.
2. The number of cycles/strain approach to high temperature low cycle fatigue provides an excellent means of presenting data so long as the frequency of testing is sufficiently high to avoid time dependent damage mechanisms (creep). It is possible to predict PP fatigue data over a limited temperature range using a ductility normalised life relationship. For example, although 25 cpm PP data at 650°C could be predicted from those at 810°C, the prediction at 900°C greatly overestimated the actual life.
3. In practice, it may not be possible to attain the predicted fatigue life line at very high temperatures, even at high frequencies of testing, due to the introduction of creep damage. Earlier work at NGTE on the effect of frequency on the life of stress-controlled high temperature low cyclic fatigue suggested that at the upper end of the temperature scale a limiting time to failure was reached which was independent of frequency. The upper and lower bounds on life of the cyclic creep frequency effect can be predicted using the effective stress concept.
4. The CP/PC life lines at 810°C appeared to be fatigue dominated as strain exponents were similar to that of the PP data and a reasonable correlation was found between maximum stress/ N_f for the CP/PC tests and average shakedown stress/ N_f for the PP data. Lives predicted via the ductility normalised approach were rather inaccurate suggesting that the constants in the present 'universal' equations may need to be varied depending on the type of material under consideration.
5. The CC strain/ N_f data at 810°C showed a large amount of scatter, a fact not seen when the same data were plotted on a stress/time-to-failure basis. In fact, the results obtained in the CC tests were identical to the values predicted using the stress/static-creep data approach.
6. A point requiring further investigation is the possible effect of anelasticity on the partitioning of inelastic strains. Because of the likely magnitude of the anelastic strain component, its effect will be most marked at low levels of strain.
7. The SRP approach did not give accurate predictions of the lives of low frequency tests conducted at 810°C whereas the simple creep-stress/time-to-failure method was accurate to within a factor of about 2 on life.
8. There are indications that when true low cycle fatigue is the dominant failure mechanism strain and number of cycles are the best parameters on which to base life predictions but when creep damage is introduced greater accuracy may be obtained by using stress/time-to-failure relationships.

REFERENCES

1. Evans, W. J., "Low cycle fatigue behaviour of gas turbine alloys", Proc. Inst. Mech. Eng 188, 1974, pp 321-328
2. Manson, S. S. and Halford, G., "A method of estimating high temperature low cycle fatigue behaviour of materials", Int. Conf. on thermal and high strain fatigue, Metals and Metallurgy Trust, London 1967 pp 154-170
3. Coffin, L. F., "Fatigue at high temperature-prediction and interpretation", Proc. Inst. Mech. Eng 188, 1974, pp 109-127
4. Hirschberg, M. H. and Halford G. R., "Strain range partitioning - a tool for characterising high temperature low cycle fatigue", NASA TM X-71691, 1975
5. Harrison, G. F. and Tilly, G. P., "The static and cyclic creep properties of three forms of a cast nickel alloy", ASTM International Conference on creep and fatigue in elevated temperature applications. Philadelphia, September 1973 and Sheffield UK April 1974
6. Harrison, G. F., Goodwin, J. E. and Dennis, R. S., "Laboratory simulation of thermal fatigue" SEE Int. Conf. on creep and fatigue design Volume 1, London 1976

7. Halford, G. R., Saltsman, J. F. and Hirschberg, M. H., "Ductility normalised-strain range partitioning life relations for creep-fatigue life predictions" NASA TM 73737, 1977
8. Henry Wiggin and Co Ltd, "Nimonic alloy 90", Publication 3525, February 1971
9. Walles, K. F. A. and Graham, A., "On the extrapolation and scatter of creep data" October 1961, NGTE Report 247
10. Evans, W. J. and Harrison, G. F., "Anelastic deformation and stress reduction experiments during creep", Scripta Met. 9, 1975 pp 239-246
11. Harrison, G. F., "Simple predictions of temperature effects on low cycle fatigue lives of some gas turbine alloys", Jnl. Soc. Environmental Engineers, 16-4, December 1977, pp 13-21

ACKNOWLEDGEMENT

The authors wish to thank Mr. J. Hansen for his help in carrying out most of the tests and their subsequent analysis.

© Controller, Her Majesty's Stationery Office, London 1978

TABLE I*

Alloy details: Nimonic 90

Composition (wt %)	Al	B	C	Co	Ti	Cr	Zr	Ni
	1.46	0.035	0.09	16.20	2.43	19.45	0.06	Rem
Processing	Cold drawn bar. 14 mm diameter (STS 6409) ASTM Grain Size: 4							
Heat treatment	1080°C - 8 hours Air cool +700°C - 16 hours Air cool							

TABLE II

Tensile data

Temperature °C	0.2% Proof MN/m ²	UTS MN/m ²	Reduction of Area %	Rate of testing *
650	737	1087	30	slow
810	590	712	20	slow
	627	839	16	fast
900	348	383	40	slow

{ slow: $\dot{\epsilon}$ 0.002 strain per minute to proof stress and
 0.1 per minute thereafter
 * { fast: equivalent to 25 cpm triangular waveform testing

* Chemical compositions, material processing, heat treatments and mechanical properties for each tested alloy, as well as the data generated in the programme, are given in Appendix A 1.

TABLE III
Basic SRP life-line data at 810°C

Test	$\Delta\epsilon_{in}$ %	Partitioned strain %				Stress limits MN/m ²		N_f	t_f hours	N_{pred}
		$\Delta\epsilon_{pp}$	$\Delta\epsilon_{pc}$	$\Delta\epsilon_{cp}$	$\Delta\epsilon_{cc}$	σ_t	σ_c			
8	1.825	1.825				612	637	42	0.028	
31	0.862	0.862				605	628	120	0.08	
39	0.690	0.690				521	556	280	0.19	
32	0.472	0.472				476	507	370	0.25	
34	0.357	0.357				482	506	640	0.43	
35	0.229	0.229				430	481	2660	1.77	
30	0.127	0.127				378	545	3850	2.57	
33	0.029	0.029				251	528	32630	21.75	
41	0.007	0.007				295	353	343000	228.00	
45	1.336	0.234	1.102			849	578	9	0.23	8
46	0.297	0.116	0.181			586	409	126	1.28	82
47	0.041	0.011	0.030			486	271	3393	11.6	2590
42	1.265	0.251		1.014		528	808	10	0.15	9
43	0.284	0.108		0.176		376	594	91	0.95	59
44	0.053	0.014		0.039		318	501	1737	9.25	1314
53	0.026	0.014		0.012		281	412	14467	30.6	7871
48*	0.855	0.102			0.753	472	472	9	0.9	8
49*	0.293	0.062			0.231	388	381	129	6.65	105
54*	0.243	0.171			0.072	438	451	330	0.5	124
50	0.121	0.029			0.092	338	344	764	12.6	619
55	0.100	0.023			0.077	320	325	917	21.3	735
52	0.061	0.024			0.037	374	384	2116	5.2	1395
68	0.103	0.053			0.050	367	376	2247	5.9	1446
6	0.061	0.023			0.038	353	353	2933	10.3	1986
4	0.110	0.072			0.038	367	380	3515	6.8	2444
9*	0.067	0.010			0.057	280	264	5797	47.1	5440
51*	0.050	0.009			0.041	264	261	13563	110.5	13283

†: N_{pred} = Calculated life if ALL $\Delta\epsilon_{in}$ was CP, PC or CC

*: Well documented tests - see text

TABLE IV
PP data at 650 and 900°C

Test	Temperature °C	$\Delta\epsilon_{in}$ %	Stress limits MN/m ²		N_f	t_f hours
			σ_t	σ_c		
2	650	1.32	756	770	296	0.2
85		0.904	746	768	570	0.38
84		0.510	583	609	2021	1.35
3		0.390	554	572	2574	1.72
86		0.011	518	589	137000 UB	91.3 UB
82	900	0.876	366	386	200	0.13
79		0.351	348	372	640	0.43
80		0.050	320	348	4082	2.72
87		0.045	282	310	6181	4.12
83		0.023	270	270	15590	10.4
92		0.007	214	269	45730	30.5

TABLE V
Frequency effect at 810°C

Test	Frequency	$\Delta\epsilon_{in}$ %	$\Delta\epsilon_{pp}$ % *	$\Delta\epsilon_{cc}$ %	$\Delta\sigma$ MN/m ²	N_f		t_f hours
						Actual	SRP Prediction	
69	≈ 2 cpm (0.033 Hz)	0.138	0.138	0	892	1391	3350	11.6
7		0.176	0.115	0.061	900	1168	1372	9.6
10		0.825	0.570	0.255	1036	174	25	1.45
77	≈ 12 cph (0.003 Hz)	0.467	0.125	0.342	878	110	44	9.1
76		0.332	0.085	0.247	841	242	97	21.7
78		0.196	0.035	0.161	760	980	308	78.2

* Estimated from dynamic stress-strain curve

TABLE VI
Creep prediction of the 900°C PP data

Test	$\Delta\sigma/2$ MN/m ²	Time to Failure (hours)	
		Actual	Creep Prediction
82	376	0.13	0.2
79	360	0.43	0.4
80	334	2.72	0.6
87	296	4.12	1.7
83	270	10.4	3.6
92	242	30.5	9.0

TABLE VII
Comparison between SRP and Creep Predictions

Test	Frequency	N_f		
		Actual	SRP Prediction	Creep Prediction
69	≈ 2 cp minute (0.033 Hz)	1391	3350	1485
7		1168	1372	1369
10		174	25	405
76	≈ 12 cp hour (0.003 Hz)	242	97	226
77		110	44	163
78		980	308	592

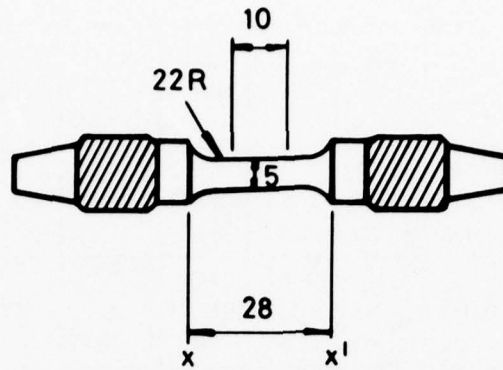


Fig. 1 Strain control test specimen

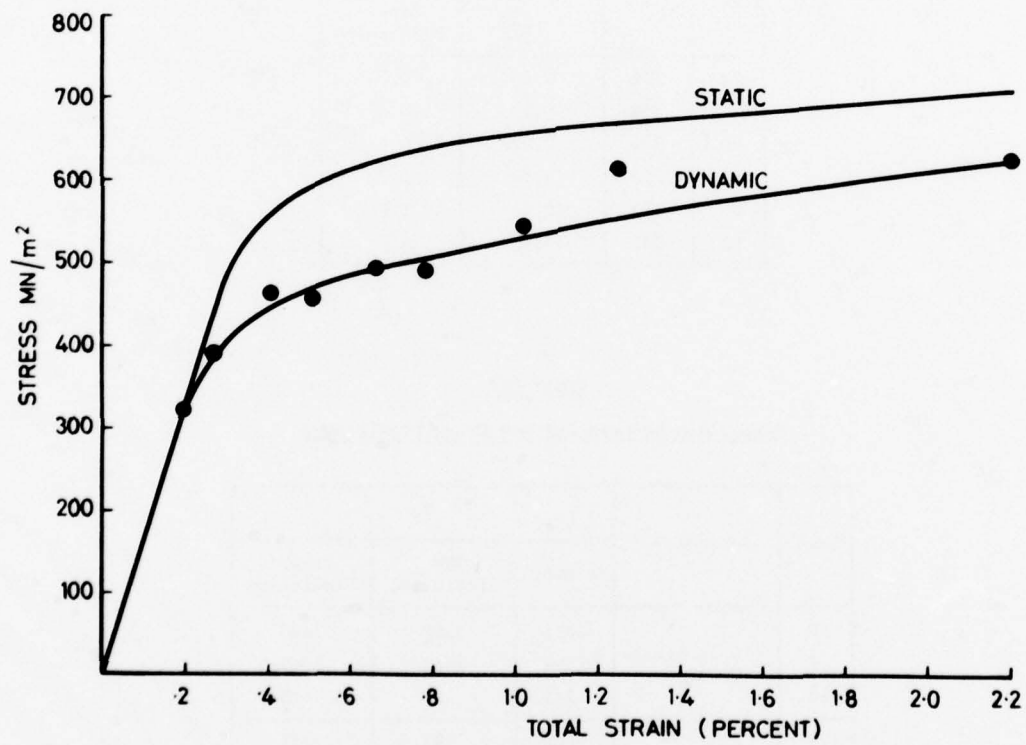


Fig. 2 Static and dynamic stress/strain curves for Nimonic 90 at 810°C

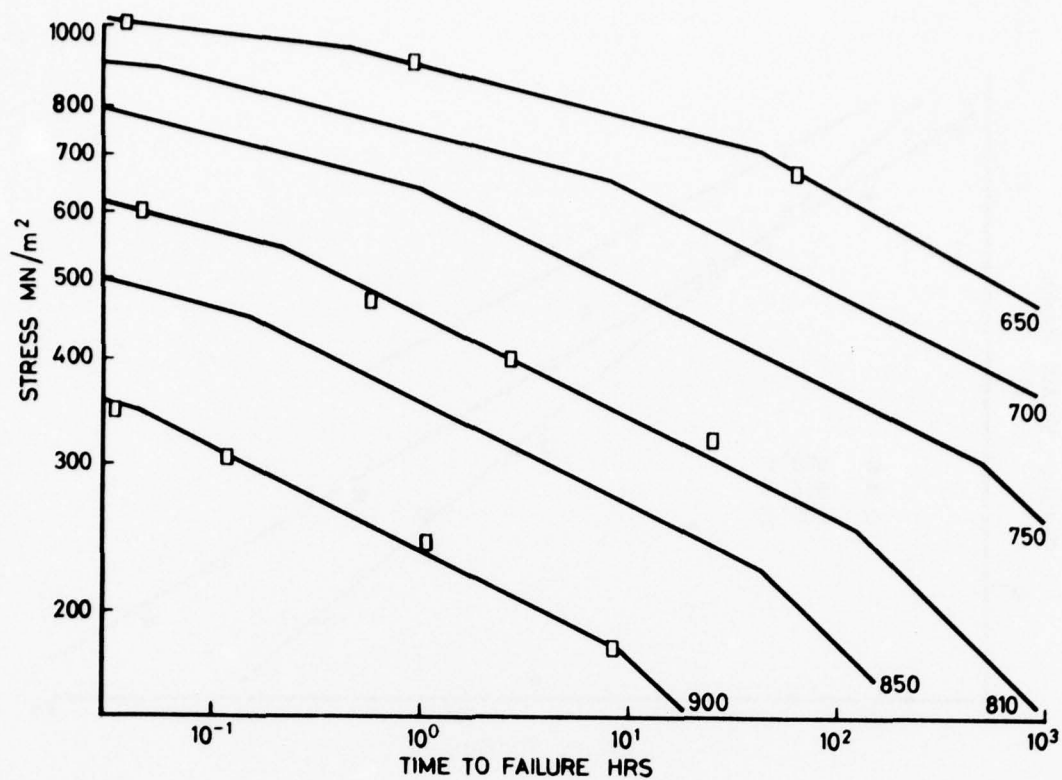


Fig. 3 Static creep rupture data for Nimonic 90

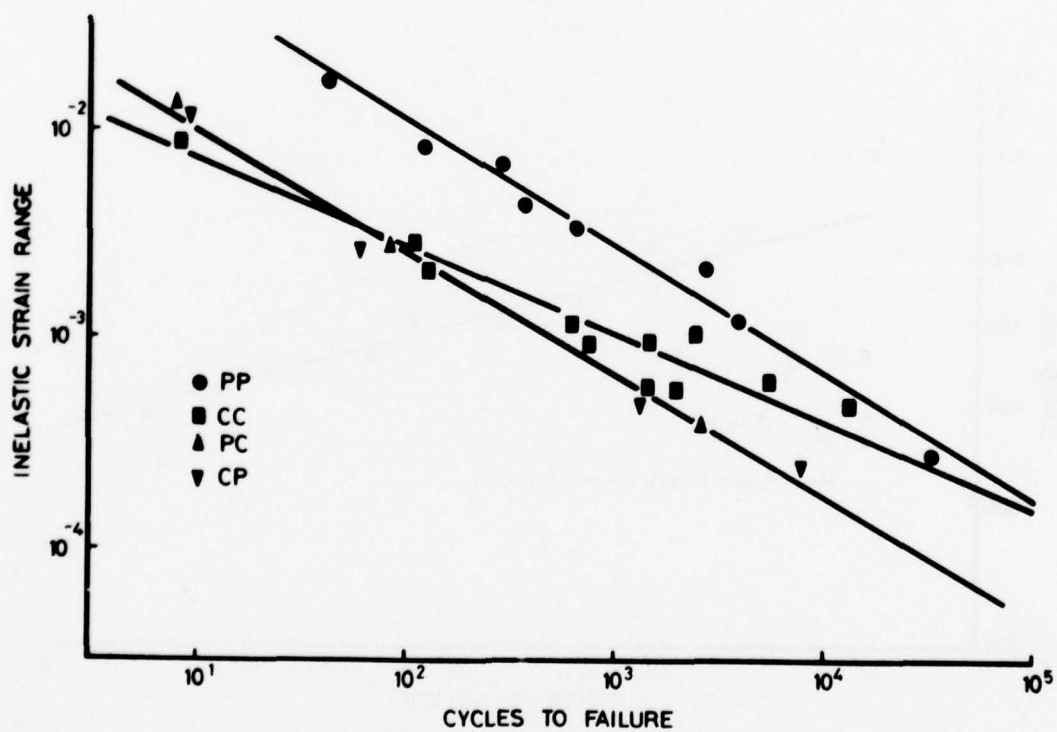


Fig. 4 SRP lifelines for Nimonic 90 at 810°C

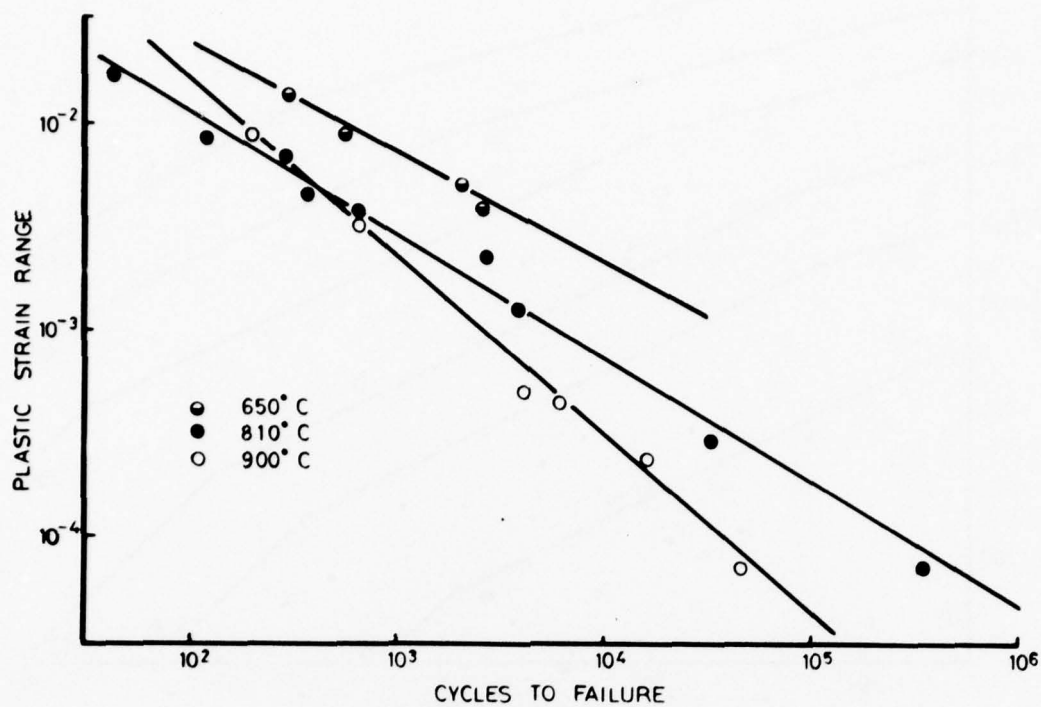


Fig 5 PP lifeline data for Nimonic 90 at 650, 810 and 900°C

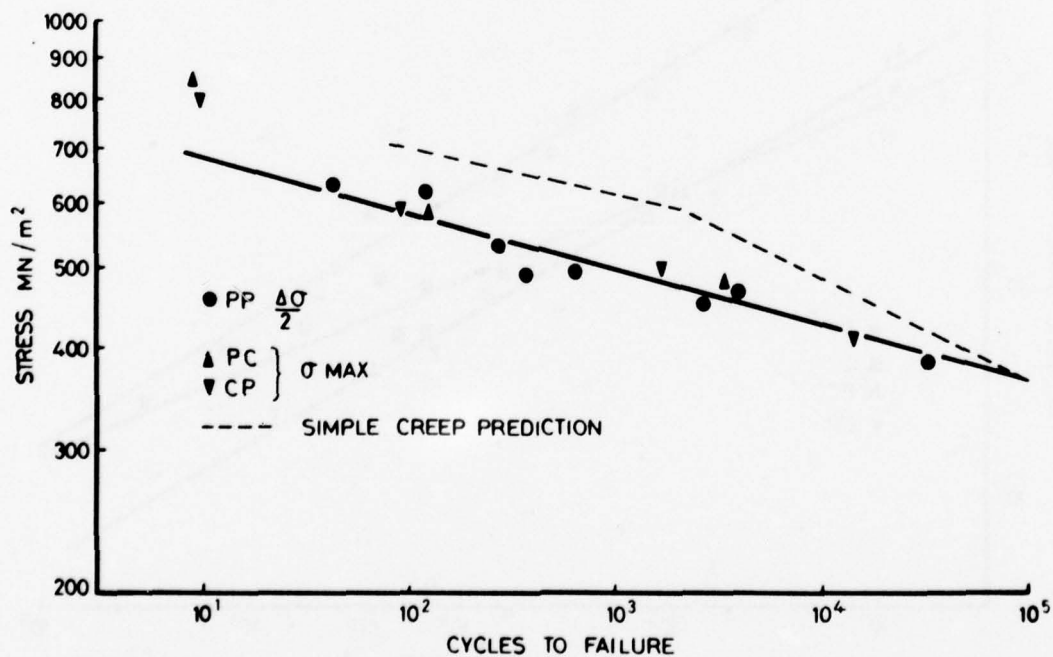


Fig 6 Stress/cycles to failure relationships for PP, PC and CP test data - Nimonic 90 at 810°C

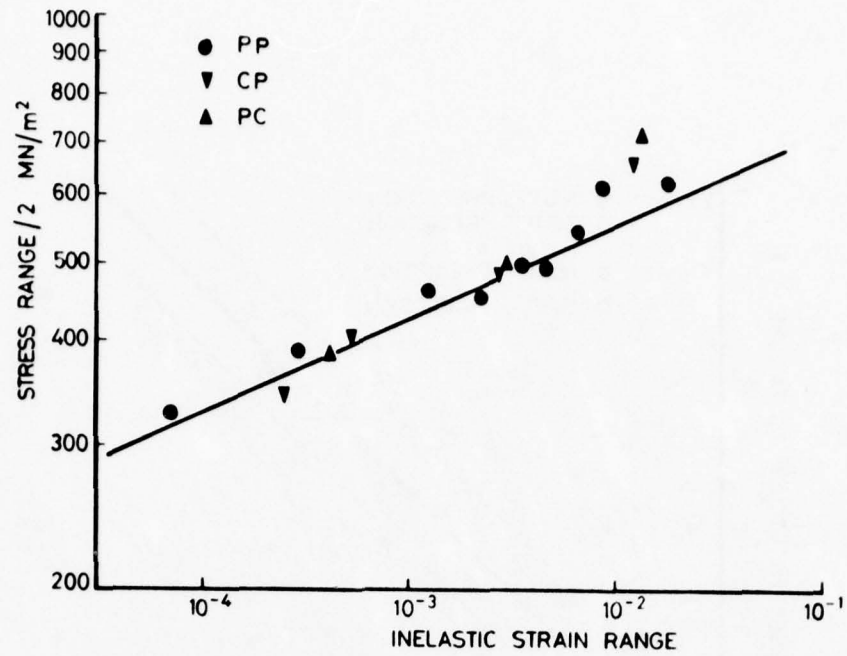


Fig 7 Semi stress range/inelastic strain range relationships for PP, PC and CP test data - Nimonic 90 at 810°C

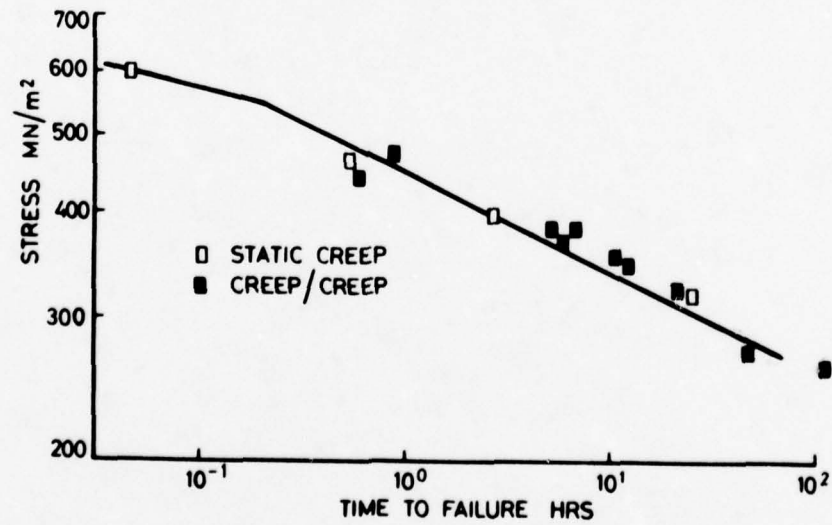


Fig 8 SRP creep-creep data superimposed onto static creep data - Nimonic 90 at 810°C

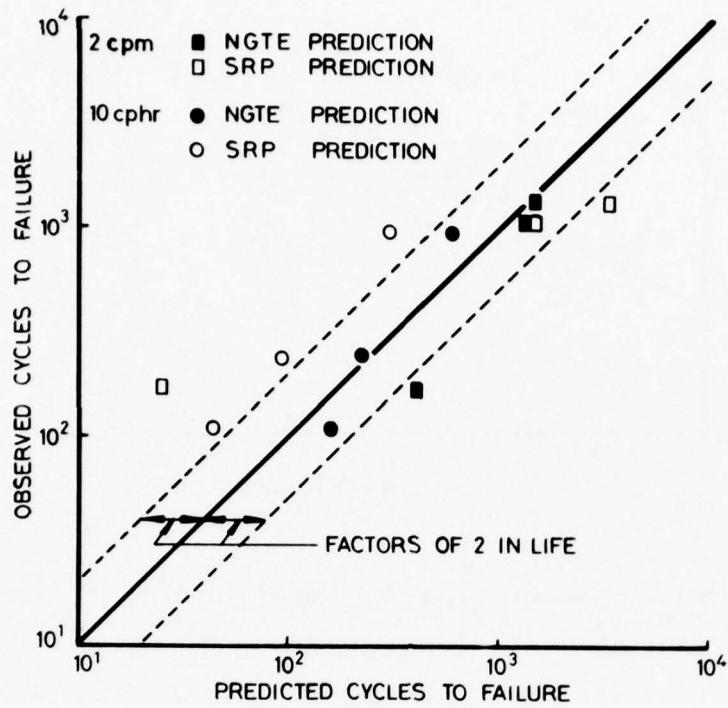


Fig. 9 Predictive capabilities of SRP and the creep data approach

APPENDIX A1

Calculation of equivalent gauge lengths for the
NGTE strain controlled testpiece

The form of the test specimen used at NGTE for strain controlled fatigue data acquisition is shown in Figure A1-1. The longitudinal extension actually measured is that occurring between the two extensometer shoulders, $X-X'$. In order to convert this extension into what is actually required, that is strain in the parallel gauge length, it is necessary to know the equivalent gauge lengths. These are the values which, when divided into the measured elastic and inelastic extensions, give the actual elastic and inelastic strains within the parallel sided section.

In order to calculate the equivalent gauge lengths, that portion of the specimen between the extensometer location points is assumed to be split up into a series of elements each of equal thickness and concentric to the specimen axis, Figure A1-1. It is further assumed that plane sections remain plane.

The plastic strain in any element can be related to the stress acting through an equation of the form:

$$\epsilon_p = B \sigma^m \quad \text{....A1-1}$$

Therefore, if the thickness of each element in the non parallel section is equal to H and the localised plastic strain equal to ϵ_{pi} , then the plastic extension of each element (X_{pi}) is given by

$$X_{pi} = H \epsilon_{pi} \quad \text{....A1-2}$$

The total plastic extension between the shoulders $X-X'$ ($X_{pxx'}$) is

$$X_{pxx'} = X_{pgl} + 2 \sum_{i=1}^n X_{pi} \quad \text{....A1-3}$$

where X_{pgl} is the plastic extension in the parallel gauge length.

By combining Equation A1-1, A1-2 and A1-3 it can be seen that

$$X_{pxx'} = X_{pgl} + 2HB \sum_{i=1}^n \sigma_i^m \quad \text{....A1-4}$$

If the stress and area in the parallel section are σ_o and A_o respectively, and those in element i equal to σ_i and A_i , then

$$\sigma_i = \sigma_o \left(\frac{A_o}{A_i} \right) \quad \text{....A1-5}$$

and, from Figure A1-1,

$$A_i = \pi \left[r + R - \sqrt{R^2 - y^2} \right]^2 \quad \text{....A1-6}$$

Equation A1-5 and Equation A1-4 can be combined to give

$$X_{pxx'} = X_{pgl} + 2HB \sigma_o^m A_o^m \sum_{i=1}^n \left(\frac{1}{A_i} \right)^m \quad \text{....A1-7}$$

Now if h_o is the length of the parallel section and F_p the plastic equivalent gauge length then

$$F_p = \left(\frac{X_{pxx'}}{X_{pgl}} \right) h_o \quad \text{....A1-8}$$

but X_{pgl} is equal to the length of parallel section (h_o) multiplied by the plastic strain (ϵ_{pgl}).

Therefore, from Equation A1-1

$$X_{pgl} = h_o B \sigma_o^m \quad \text{....A1-9}$$

Combining Equation A1-7, Equation A1-8 and Equation A1-9 gives

$$F_p = h_o + 2H A_o^m \sum_{i=1}^n \left(\frac{1}{A_i} \right)^m \quad \text{....A1-10}$$

The plastic equivalent gauge length is therefore material dependent and can only be obtained from a knowledge of the stress exponents governing plasticity. In static situations the monotonic stress exponent applies but in cyclic work the dynamic exponent is used. For the elastic situation, the stress exponent m is equal to unity and so the elastic equivalent gauge length is material independent and is given by

$$F_E = h_o + 2H A_o \sum_{i=1}^n \left(\frac{1}{A_i} \right) \quad \dots A1-11$$

The total strain in the parallel section in terms of the extension measured between points X-X' in Figure A1-1 is the sum of the elastic and plastic components,

$$\epsilon_{TOTAL} = \frac{X E_{XX'}}{F_E} + \frac{X P_{XX'}}{F_P} \quad \dots A1-12$$

Finally, for Nimonic 90 at 810°C static tensile plasticity, dynamic tensile plasticity and creep plasticity all have stress exponents in the range 8 to 12, and so for convenience, a single value of F_P equal to 14.5 mm was used throughout the strain range partitioning test programme.

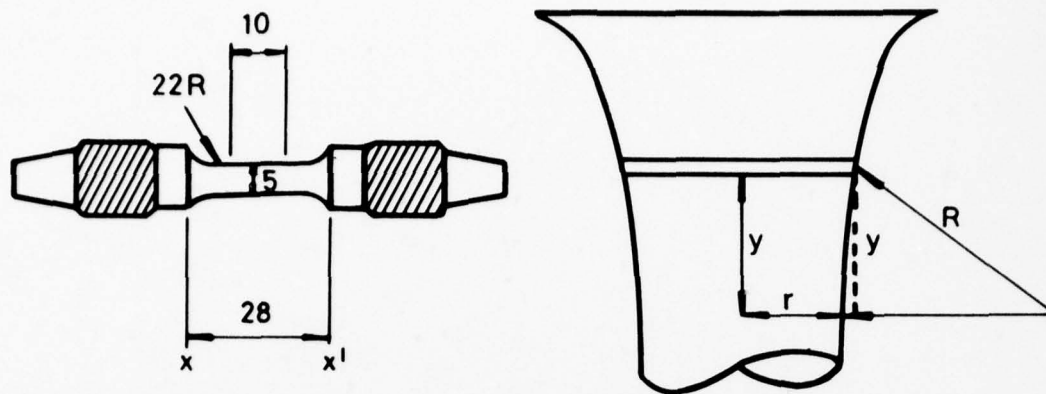


Figure A1-1 Strain control test specimen

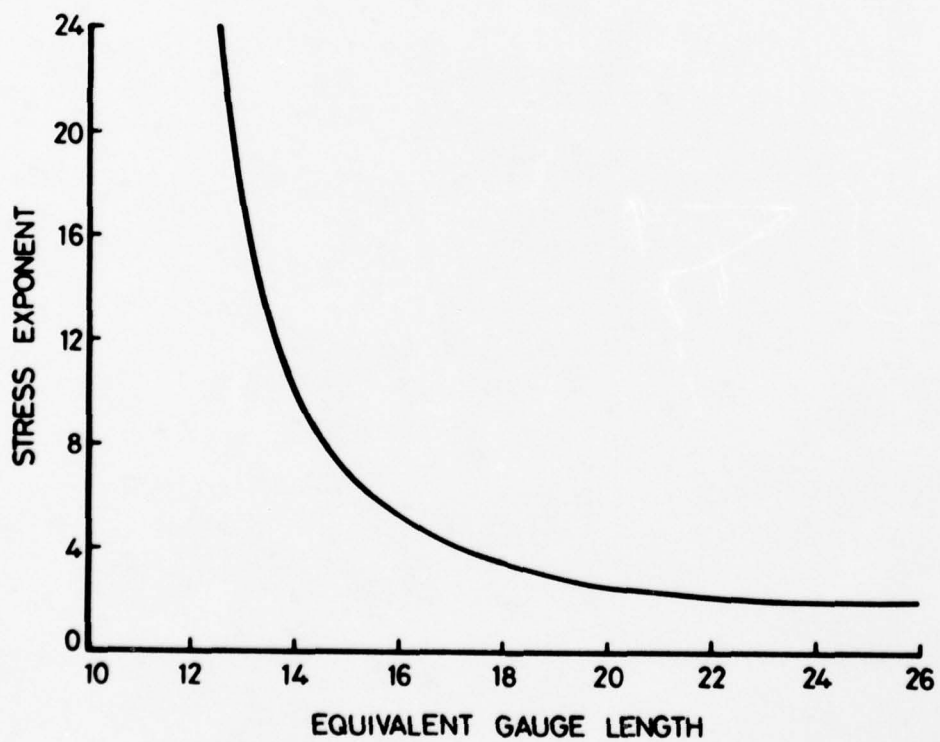


Figure A1-2 Relationship between stress exponent and equivalent gauge length for the NGTE strain control test specimen

AN APPLICATION OF STRAIN RANGE PARTITIONING
TO THE LOW CYCLE - HIGH TEMPERATURE
FATIGUE LIFE PREDICTION OF WASPALLOY

G ASQUITH AND S H SPRINTHALL
 ROLLS-ROYCE LIMITED - AERO DIVISION
 P O BOX 31 DERBY DE2 8BJ ENGLAND

SUMMARY

The ability of Strain Range Partitioning (SRP) to predict the low cycle fatigue life of the nickel base alloy WAPALLOY has been examined. From a limited series of fully reversed strain controlled low cycle fatigue and cyclic creep testing at 700°C the basic partitioned life relationships have been established. It is shown that from these basic relationships reasonable life to failure prediction is possible for more complex combined creep - fatigue interactions.

It is observed from the experimental test data that there are marked differences in the mean stress levels generated for each strain range component and level of inelastic strain range. It would appear from this preliminary examination of SRP that the analysis and life prediction of particular complex hysteresis behaviours is not limited by mean stress differences in the baseline data.

NOMENCLATURE

$\Delta \epsilon_{pp}$	-	Plastic/Plastic strain range
$\Delta \epsilon_{pc}$	-	Plastic/Creep strain range
$\Delta \epsilon_{cp}$	-	Creep/Plastic strain range
$\Delta \epsilon_{cc}$	-	Creep/Creep strain range
$\Delta \epsilon_{in}$	-	Total inelastic strain range
$\Delta \epsilon_{el}$	-	Elastic strain range
$\Delta \epsilon_t$	-	Total strain range
F_{pp}	-	PP inelastic strain fraction
F_{pc}	-	PC inelastic strain fraction
F_{cp}	-	CP inelastic strain fraction
F_{cc}	-	CC inelastic strain fraction
N_f	-	Cycles to failure
N_{fpp}	-	Derived PP cyclic life
N_{fpc}	-	Derived PC cyclic life
N_{fcp}	-	Derived CP cyclic life
N_{fcc}	-	Derived CC cyclic life
N_{fPRE}	-	Predicted cyclic life
σ_m	-	Mean Stress

INTRODUCTION

The Strain Range Partitioning approach to high temperature low cycle fatigue prediction has been the subject of extensive investigation by the NASA - Lewis Research Centre (Ref 1 and 2) to the stage where considerable confidence is being expressed in its capabilities. The concept of SRP is based on the recognition that any cyclic stress-strain history (hysteresis loop) is developed from two directions of straining ie tension and compression and two types of inelastic strain of either a time independent nature (plastic) or of a time dependant nature (creep). From the association of the two directions and the two types of strain there are the following four basic strain range combinations.

1. Tensile plasticity reversed by compressive plasticity, (PP)
2. Tensile creep reversed by compressive plasticity, (CP)
3. Tensile plasticity reversed by compressive creep (PC)
and
4. Tensile creep reversed by compressive creep (CC)

For each of the above basic strain ranges a life relationship can be established by laboratory testing and employed in an interaction damage rule to predict the life of the more complex stress-strain histories experienced in practice.

To establish greater confidence in the SRP concept a co-operative programme has been established by the Advisory Group for Aerospace Research and Development (AGARD) involving many participating organisations embracing different materials and testing techniques. This paper summarises the evaluation programme completed by the Rolls-Royce Limited Aero Division Laboratories.

The authors extend their apologies to AGARD and the participating organisations for not completing the evaluation programme in the agreed time scale, due solely to conflicting work pressures. As a result of this delay it was not possible to issue this paper in advance of the Specialist Meeting held at Aalborg Denmark in April 1978.

MATERIAL

The material employed in this evaluation is WASPALOY, a Ni Base Alloy used extensively for turbine discs in present day gas turbine engines. All specimens were machined from a single fully heat treated disc forging with the specimen axis in the radial direction. Basic materials data is given in Table I* (see Footnote on p.7-4).

A base temperature of 700°C was selected for this evaluation being somewhat higher than the normal application temperature for this material. The aim of selecting this relatively high temperature was to achieve a significant level of creep in the base tests.

EXPERIMENTAL METHOD

Axial strain controlled testing was conducted at various strain rates between 0.5 and 10%/sec. employing basically triangular waveform with and without tensile and/or compressive stress or strain hold periods. A fully reverse - zero mean strain cycle was used for all tests.

Testing was carried out on a "Mayes" 50 KN servo-hydraulic closed loop fatigue machine in association with an LVDT extensometer, resistance furnace and monitoring equipment (Fig.1).

The specimen design (Fig.2) was initially established from photoelastic analysis and has more recently been the subject of finite element plastic analysis. However, further analysis is in hand to establish the effective gauge length applicable and therefore for this preliminary paper all strains are based on a nominal gauge length.

THE SRP EVALUATION PROCEDURE

High temperature strain controlled low cycle fatigue tests were conducted as recommended by Hirschberg and Halford (Ref 2) to develop hysteresis loops of the type illustrated in Fig 3 in order to establish the four baseline SRP life relationships. Throughout the transient parts of each loop a high strain rate is maintained to minimise the time dependant or creep influence. On this basis it is assumed in the resulting loop analysis that creep is only present when tension and/or compression hold periods are introduced, either at constant stress or constant strain. Accepting this, hysteresis loops embracing PP only or PP and PC or PP and CP or PP and CC can be readily established.

By applying a fractional analysis of each half life (or stabilised) hysteresis loop relating the partitioned strain range to the total inelastic strain range and substituting the appropriate data in the following proposed interaction damage rule the four partitioned life relationships are derived.

Interaction Damage Rule

$$\frac{1}{N_f} = \frac{F_{PP}}{N_{PP}} + \frac{F_{PC}}{N_{PC}} + \frac{F_{CP}}{N_{CP}} + \frac{F_{CC}}{N_{CC}}$$

Having established the partitioned life relationships, the main objective of this programme is addressed, namely an examination of the predictive accuracy of the SRP method. This is examined by completing a number of complex tests and comparing the lives obtained with those predicted from the fractional strain range analysis of the particular test loop, the corresponding baseline data and the application of the interaction damage rule. The "complex" tests employed in this evaluation programme were limited to 3 unbalanced cyclic creep rupture tests embracing PP, CP and CC inelastic strain range components.

RESULTS AND DISCUSSION

A complete listing of baseline and "complex" test data is given in Table II.

At this point in time the baseline SRP lines have been established on a minimum of experimental data comprising of 4 PP tests, 2 CP and CC tests and a single PC test result (Fig 4). From this limited data the following SRP life to failure relationships are indicated:

$$\begin{aligned} \% \Delta \epsilon_{pp} &= 186 N_f^{-0.76} \\ \% \Delta \epsilon_{cp} &= 105 N_f^{-1.26} \\ \% \Delta \epsilon_{cc} &= 15.4 N_f^{-0.52} \end{aligned}$$

It will be noted (Fig 5) that marked differences in the partitioned inelastic strain range life relationships are indicated for Waspalloy at 700°C. In relation to the total inelastic strain range, CP and PC exhibit relatively high damage content and PP low damage. The CC relationship also suggest a higher damage content than PP, but somewhat more dependent on the applied inelastic strain range.

Initially some experimental difficulties were experienced particularly in developing a high fraction of the inelastic strain component being studied with strain hold testing. For this reason stress hold testing was adopted. A single THSC test result with a CP fraction of 0.26 (SF50) has however been used in the absence of any more meaningful data. The reliability of the CP curve may therefore be in some doubt.

Half life analysis of the base SRP tests show some notable behaviour patterns in relation to mean stress levels (Fig 6) and stress ranges (Fig 7) developed. Within the range of the tests covered, both PP and CP loops generate compressive mean stresses and PC tensile mean stress. The CC loops however generate tensile or compressive mean stresses depending on the level of the applied inelastic strain range. In both CC tests the specimen was subjected to tension in the first half cycle. Despite these differences in mean stress level close agreement is shown for the half life stress range - inelastic strain range relationship for PP, CP and PC loops. The stress range for the CC loops is somewhat lower. This observation of the linear relationship of half life stress range and inelastic strain range is possibly worthy of further study in-as-much it clearly indicates an equally good life relationship could be established in terms of stress range.

Whilst in general an understanding for the resulting stress levels can be obtained from a detailed examination of each hysteresis loop it is important for later discussion to recognise these behaviour patterns exist in the baseline data, both between partitioned strain ranges and within a particular partitioned strain range.

Having established the baseline relationships, albeit from a total of some 9 results, a preliminary examination of the prediction aspects of SRP have been made from the analysis of 3 "complex" experimental hysteresis loops. These tests were of an unbalanced cyclic creep rupture (UCCR) type embracing PP, CP and CC components. (Fig 8). Testing was arranged to provide an assessment of both variations in total inelastic strain range and component fraction. Care was also taken to ensure these tests were within or close to the experimental ranges of $\Delta \epsilon$ in, N_f and total time covered by the baseline curves, thus avoiding any serious extrapolation of this limited data.

For each "complex" test the total inelastic strain range was used to obtain the respective N_{fpp} , N_{fcp} and N_{fcc} lives (no PC component present) from the baseline relationships. Also, an analysis of each half life loop was made to establish the component inelastic strain range to total inelastic strain range fraction, thereby providing the data required for the proposed interaction damage rule, from which the predicted life to failure was obtained.

A comparison of the predicted and observed (experimental) lives for these three "complex" tests (Fig 9) shows some measure of agreement. Two tests are well within an acceptable life factor of 2 to 1, however a third test is less satisfactory, the predicted life being pessimistic (ie safe) by a factor of some 4 to 1 on life. Examination of the different parameters used in these three tests (Table II) offers no immediate explanation for this discrepancy except that the poor life agreement is associated with the longer life test. Accepting the limitation of the sparse baseline data this may be indicative of a problem with the SRP method.

Returning to the question of resulting stress levels, it is again observed that the mean stress level generated for the "complex" test loops is grossly different to the appropriate (ie same inelastic strain range) baseline data previously referred to and employed in the life prediction calculation. For example Specimen SF 19 the following applies:

$$\Delta \epsilon_{in} = 2.07\%$$

$$\sigma_m = +100.8 \text{ MPa}$$

Corresponding baseline data (See Fig 6 $\Delta \epsilon_{in} = 2.07\%$)

$$\sigma_{m_{pp}} = -40 \text{ MPa}$$

$$\sigma_{m_{cc}} = -100 \text{ MPa}$$

$$\sigma_{m_{cp}} = -175 \text{ MPa}$$

Thus, although the conditions of inelastic strain range are identical, the SRP method has employed baseline data with a compressive mean stress for the life prediction of a "complex" hysteresis loop with a tensile mean stress. At first sight this anomaly appears unacceptable since most methods of life prediction being applied to engineering components incorporate some allowance for mean stress or stress ratio, never-the-less the generally good life prediction obtained from this evaluation cannot be ignored. Further, the discrepancy in life prediction shown with the 3 "complex" tests is not readily explained by such stress effects.

Finally, it should also be mentioned that it has clearly not been possible from these results to obtain any indication of the overall scatter that may be expected to establishing the baseline data. This aspect is considered to be of utmost importance since it will ultimately reflect in the predictive accuracy of the SRP method.

CONCLUSION

From preliminary results on Waspaloy at 700°C and fully reversed strain cycling, promising life prediction is shown for the Strain Range Partitioning Method. Long life prediction may not be of acceptable accuracy.

REFERENCES

1. MANSON, S.S., HALFORD G.R. and HIRSCHBERG, M.H. Creep Fatigue Analysis by Strain range partitioning Symposium on Design for Elevated Temperature Environment. ASME 1971 PP 12.28 (NASA TM x 67838 1971).
2. HIRSCHBERG, M.H. and HALFORD, G.R. Strain range partitioning - a tool for characterising High-Temperature Low Cycle Fatigue. 40th Meeting of AGARD S and M Panel. (NASA TM x 71691) April, 1975.

ACKNOWLEDGEMENTS

The experimental work was carried out in the Rolls-Royce Material Services Laboratory, Derby, England and the authors register their appreciation for the co-operation and effort given. Particular thanks are addressed to Mr. Khan for the test work completed.

* Chemical compositions, material processing, heat treatments and mechanical properties for each tested alloy, as well as the data generated in the programme, are given in Appendix A 1.

DESCRIPTION : NICKEL BASE ALLOY : WASPALOY
VACUUM MELTED OR ELECTRO-FLUX REMELTED

FORM : DISCS AND OTHER ROTATING COMPONENTS

CHEMICAL COMPOSITION :

ELEMENT	NI	CR	CO	MO	TI	AL	C	ZR	B	FE	SI	MN	CU	P	S
MAX COMP	REM	21.000	15.000	5.000	3.300	1.600	0.100	0.080	0.010	2.000	0.150	0.100	0.100	0.015	0.008
MIN COMP		18.000	12.000	3.500	2.800	1.200	0.020	0.020	0.003	0.000	0.000	0.000	0.000	0.000	0.000

ROLLS-ROYCE DESIGNATION :- MSRR 7034 CODE QDY.

HEAT TREATMENT :- 4 HR 1018°C OQ + 4 HR 850 AC + 16 HR 760 AC.

SPECIMEN :- LCC 8007 CUT UP DWG :- RLH 4875

TYPICAL PROPERTIES S.I. UNITS

TEMP °C	UTS	0.1 PS	0.2 PS	EI %	RA %	CS.1% TPS 100 HRS	STRESS RUPTURE 100 HR 1000 HR
20	1308	896	927	23	25	-	-
600	1143	780	821	20	28	685	919 791
650	1127	769	809	21	30	560	780 664
700	1089	735	778	23	32	409	616 480
750	1019	681	713	28	38	240	471 346

TABLE 1 MATERIAL DATA

SPEC. No.	TEST TYPE	STRAIN RANGES (Nf/2 VALVES) %								S/R FRACTIONS (Nf/2)				STRESSES (Nf/2) MPa		FAILURE DATA - CYCLES			
		$\Delta \epsilon_t$	$\Delta \epsilon_{el}$	$\Delta \epsilon_{in}$	$\Delta \epsilon_{pp}$	$\Delta \epsilon_{PC}$	$\Delta \epsilon_{CP}$	$\Delta \epsilon_{CC}$	F_{PP}	F_{PC}	F_{CP}	F_{CC}	TENS	COMP.	RANGE	Nf	Nf _D	N _{PRE}	$\frac{N_{PRE}}{N_f}$
BASELINE SRP TESTS																			
SF34	HRSC	3.61	1.53	2.08	2.08	0	0	0	1.00	0	0	0	904.6	976.1	1880.7	318	318	-	-
SF35	HRSC	2.84	1.26	1.58	1.58	0	0	0	1.00	0	0	0	847.2	878.6	1725.8	645	645	-	-
SF33	HRSC	1.44	1.00	0.44	0.44	0	0	0	1.00	0	0	0	698.8	714.5	1413.3	3404	3404	-	-
SF6	HRSC	1.44	1.02	0.42	0.42	0	0	0	1.00	0	0	0	747.6	778.7	1526.3	2718	2718	-	-
SF50	THSC	4.51	1.25	2.76	2.03	0	0.73	0	0.74	0	0.26	0	991.4	1162.3	2153.7	57	18	-	-
SF24	TCCR	1.46	0.59	0.87	0.25	0	0.62	0	0.29	0	0.71	0	608.2	1016.6	1624.8	62	45	-	-
SF21	CCCR	2.89	1.21	1.68	0.62	1.06	0	0	0.37	0.63	0	0	1106.4	713.3	1819.7	96	62	-	-
SF17	BCCR	2.94	1.00	1.94	0.61	0	0	1.33	0.31	0	0	0.69	640.6	838.5	1479.1	76	55	-	-
SF43	BCCR	1.28	0.70	0.58	0.16	0	0	0.42	0.28	0	0	0.72	674.4	373.1	1047.5	710	570	-	-
"COMPLEX" TESTS																			
SF2	UCCR	1.53	0.93	0.60	0.20	0	0.22	0.18	0.33	0	0.37	0.30	652.7	717.6	1370.2	100	-	146	1.46
SF19	UCCR	3.12	1.05	2.07	0.60	0	0.21	1.26	0.29	0	0.10	0.61	901.3	699.6	1600.9	54	-	55	1.02
SF44	UCCR	1.38	0.86	0.52	0.19	0	0.05	0.28	0.36	0	0.10	0.54	596.0	631.4	1227.4	1840	-	418	0.23

$$* \quad \text{--- DERIVED } N_{fPC} = \frac{F_{PC}}{\frac{1}{N_f} - \frac{F_{PP}}{N_{fPP}}}$$

SIMILARLY FOR 'CP' AND 'CC'

$$** \quad \text{--- } N_f \text{ PREDICTED} = \frac{1}{\frac{F_{PP}}{N_{fPP}} + \frac{F_{PC}}{N_{fPC}} + \frac{F_{CP}}{N_{fCP}} + \frac{F_{CC}}{N_{fCC}}}$$

INTERACTION DAMAGE RULE

TABLE II SRP TEST DATA - WASPALOY 700°C

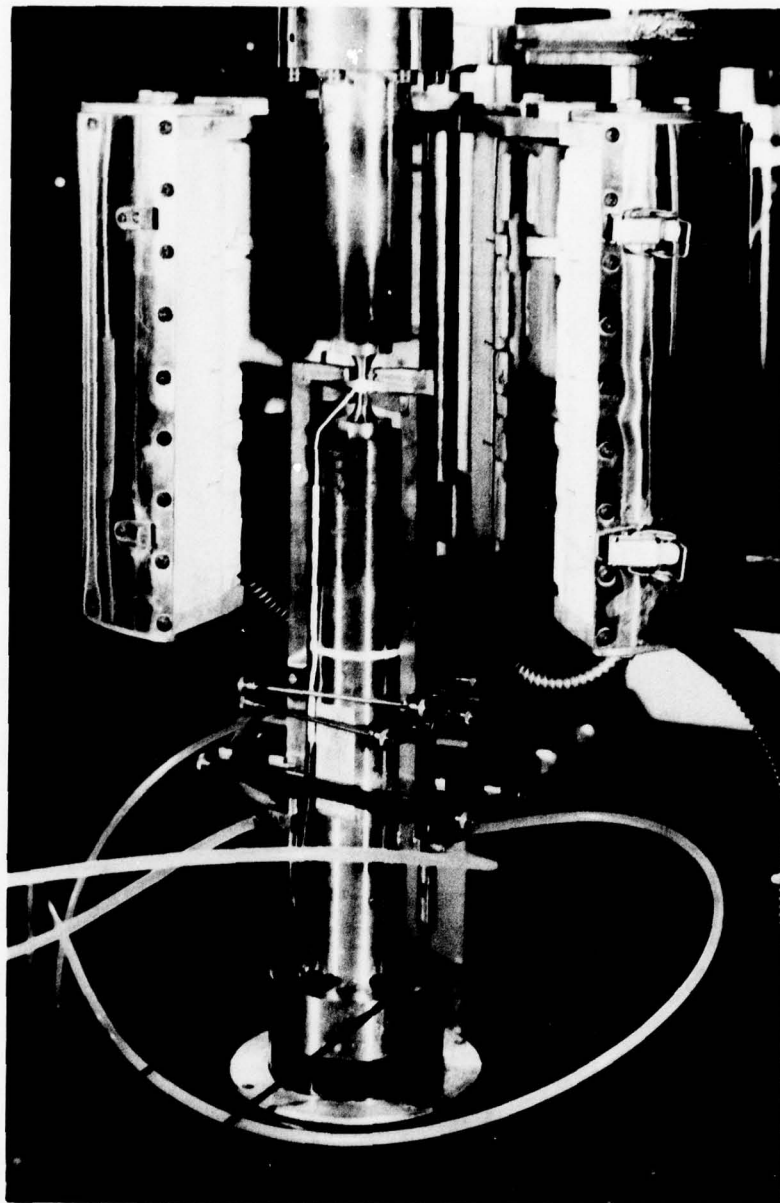


FIG 1. GENERAL VIEW OF TEST ASSEMBLY
SHOWING SPECIMEN, EXTENSOMETER AND FURNACE (OPEN)

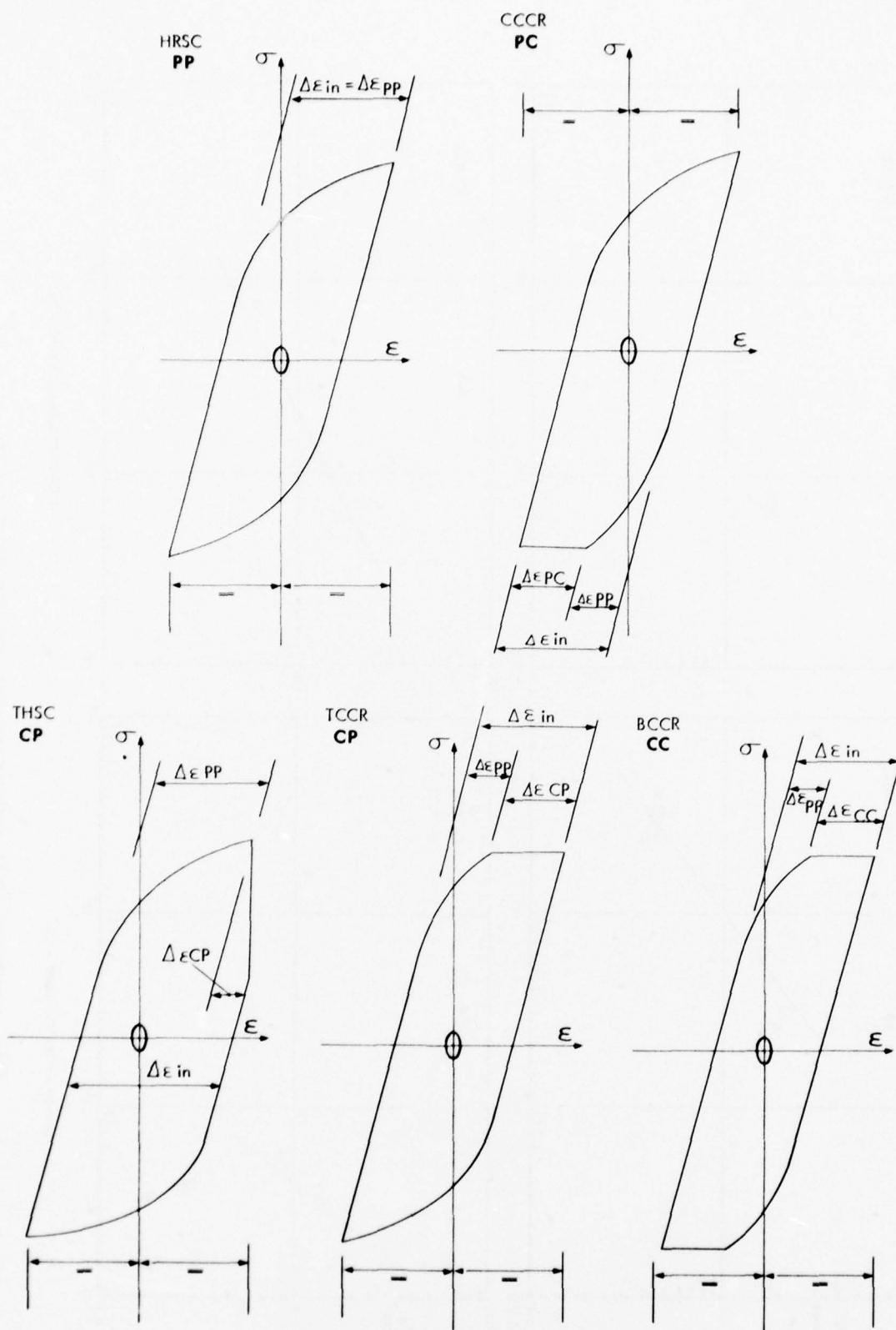


FIG 3. DIAGRAMATIC REPRESENTATION OF ACTUAL
TEST CYCLES USED FOR SRP BASELINE DATA

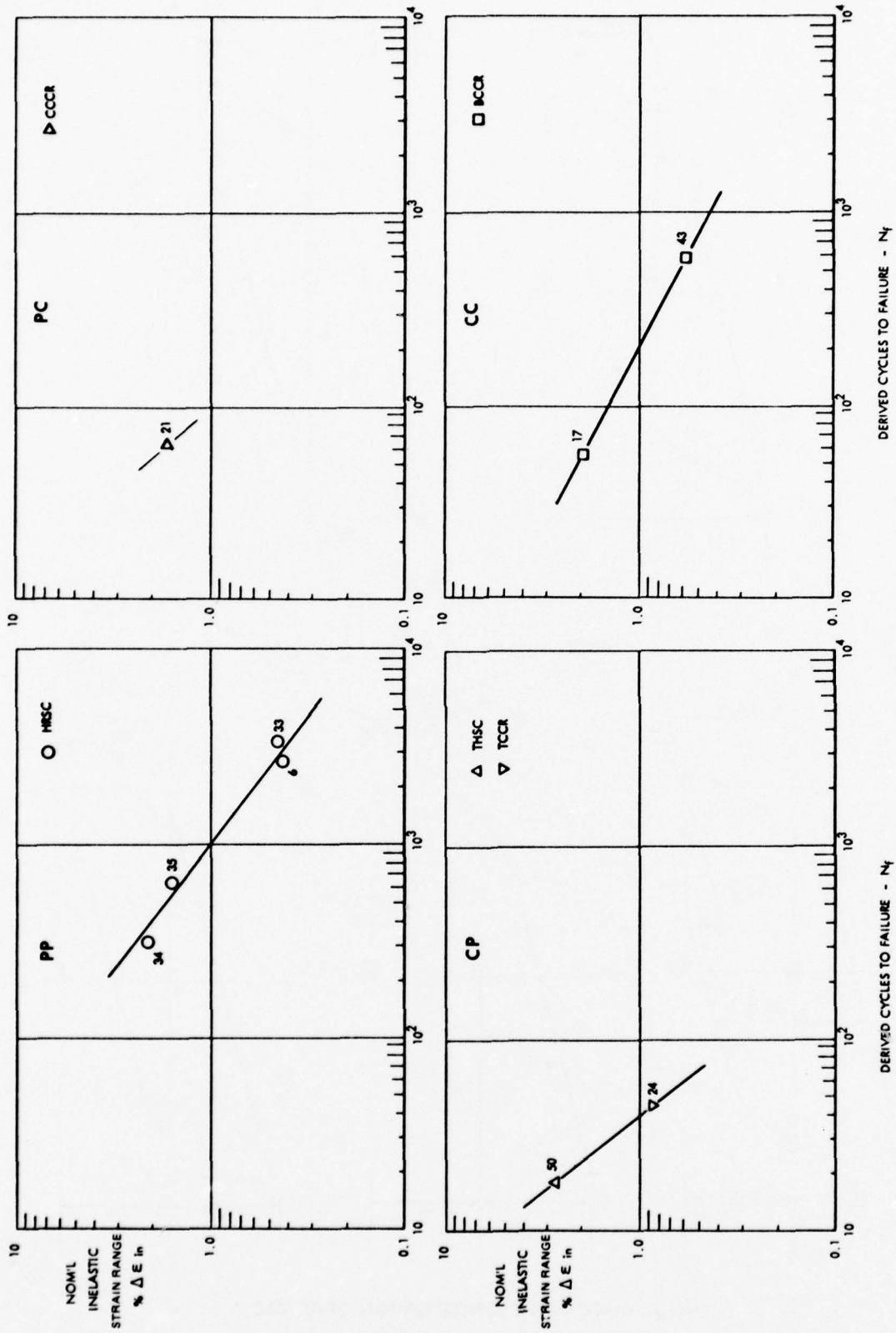


FIG 4. WASPALOY - 700°C BASELINE 'PP', 'PC', 'CP' AND 'CC' TEST DATA

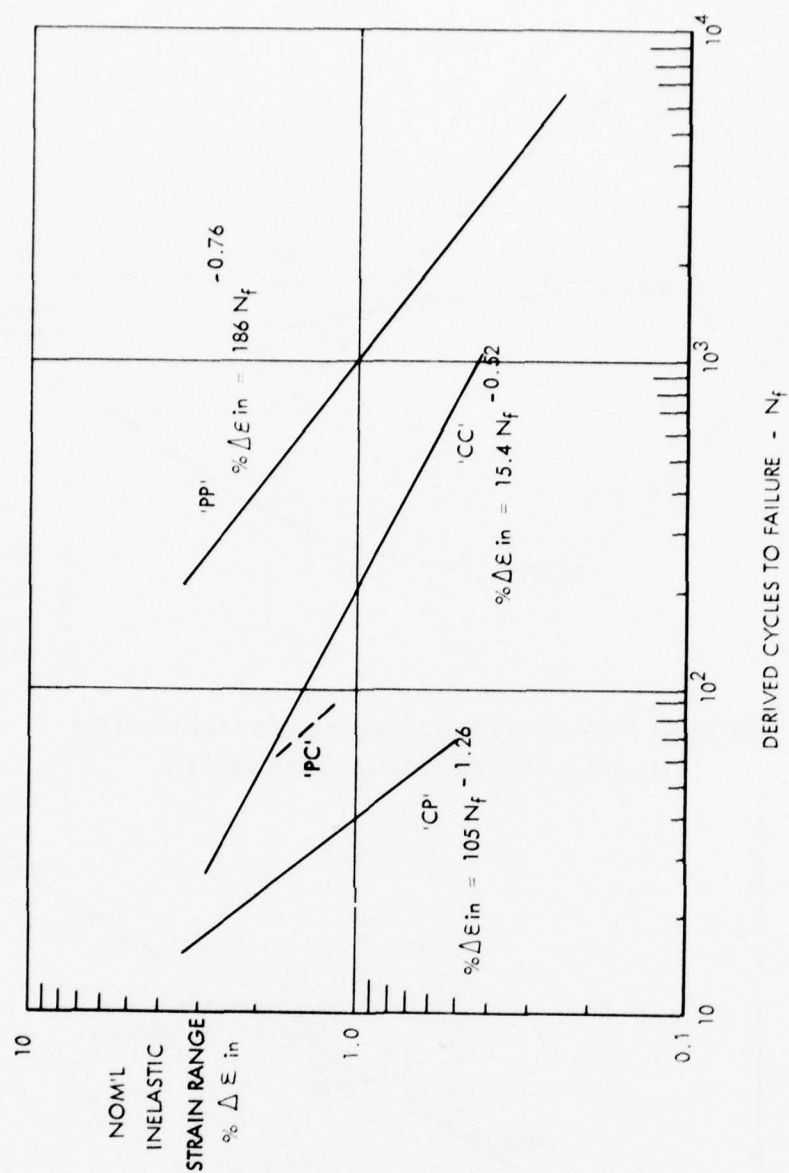


FIG 5. WASPALOY - 700°C. SRP LIFE RELATIONSHIPS (LIMITED DATA)

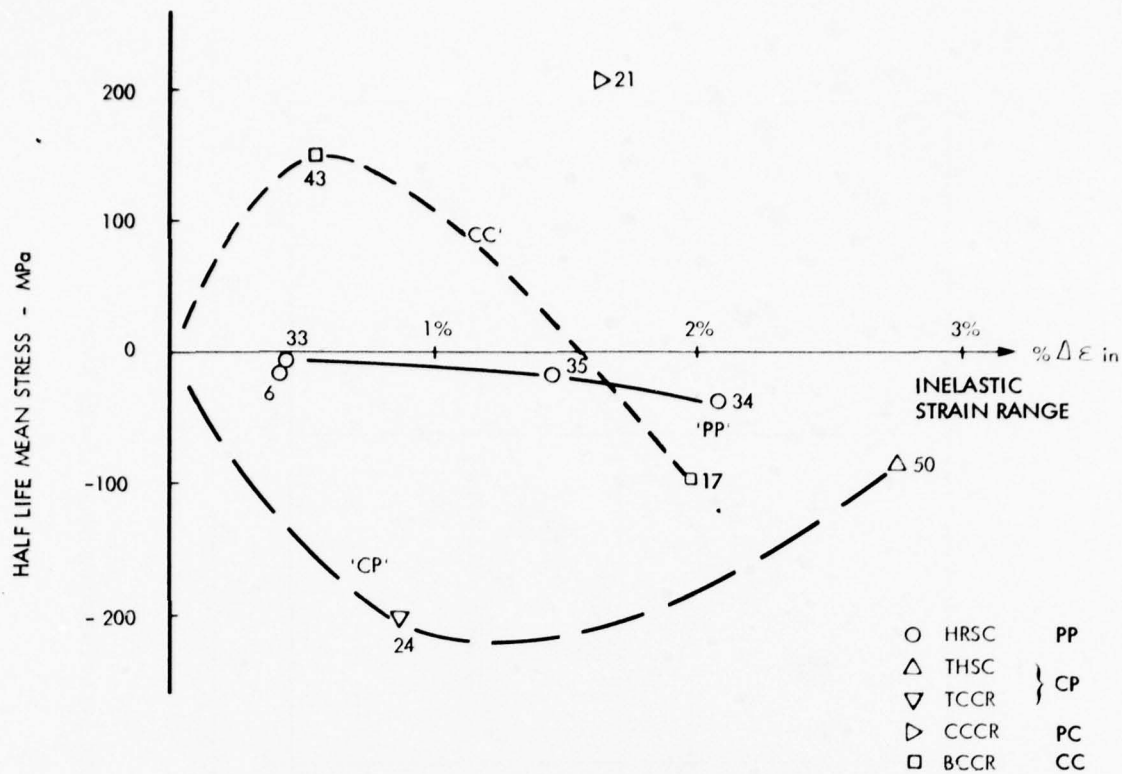


FIG 6. HALF LIFE MEAN STRESS/TOTAL INELASTIC STRAIN RANGE
RELATIONSHIPS OBSERVED IN BASELINE SRP TESTS

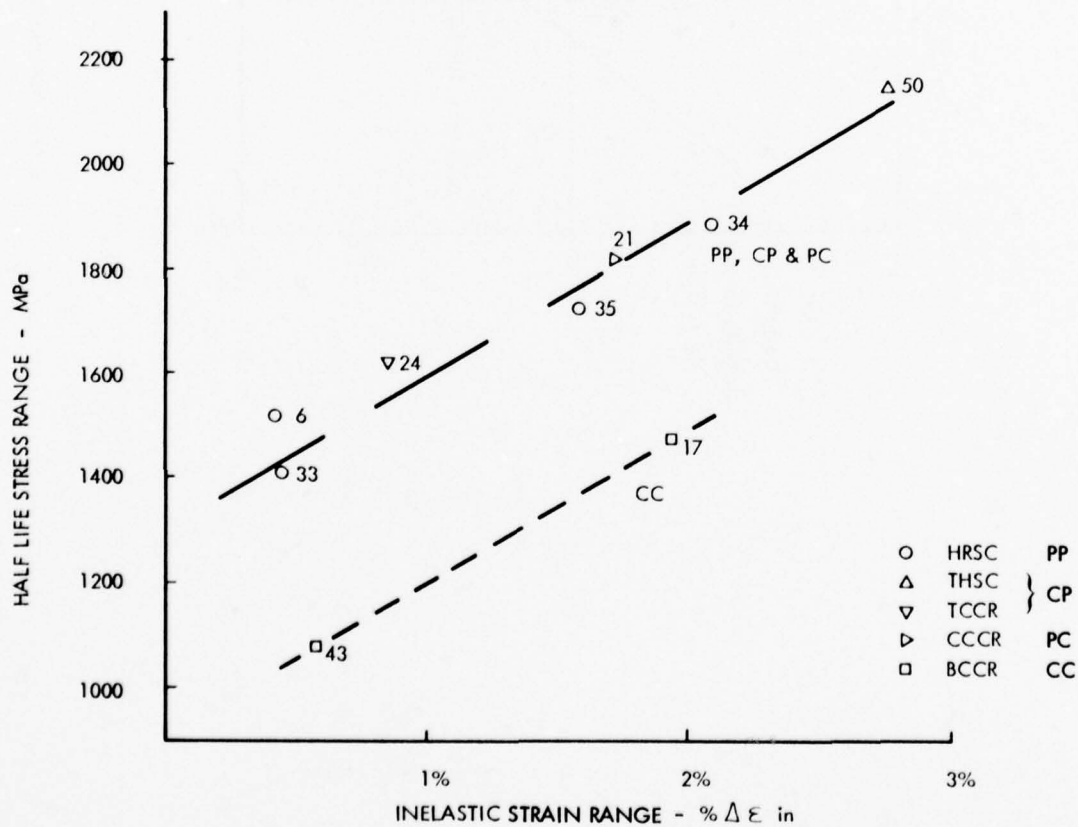


FIG 7. HALF LIFE STRESS RANGE/TOTAL INELASTIC STRAIN RANGE
RELATIONSHIPS OBSERVED IN BASELINE SRP TESTS

UCCR

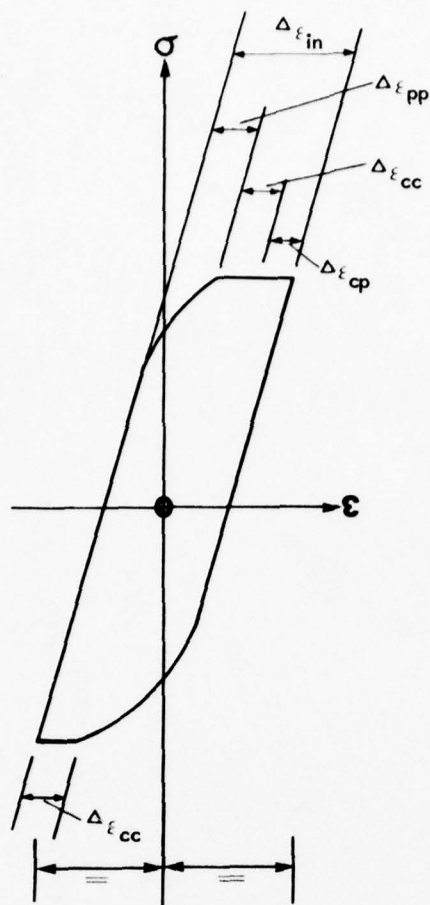


FIG 8. DIAGRAMATIC REPRESENTATION OF "COMPLEX" TEST CYCLE USED TO ASSESS THE SRP LIFE PREDICTION METHOD.

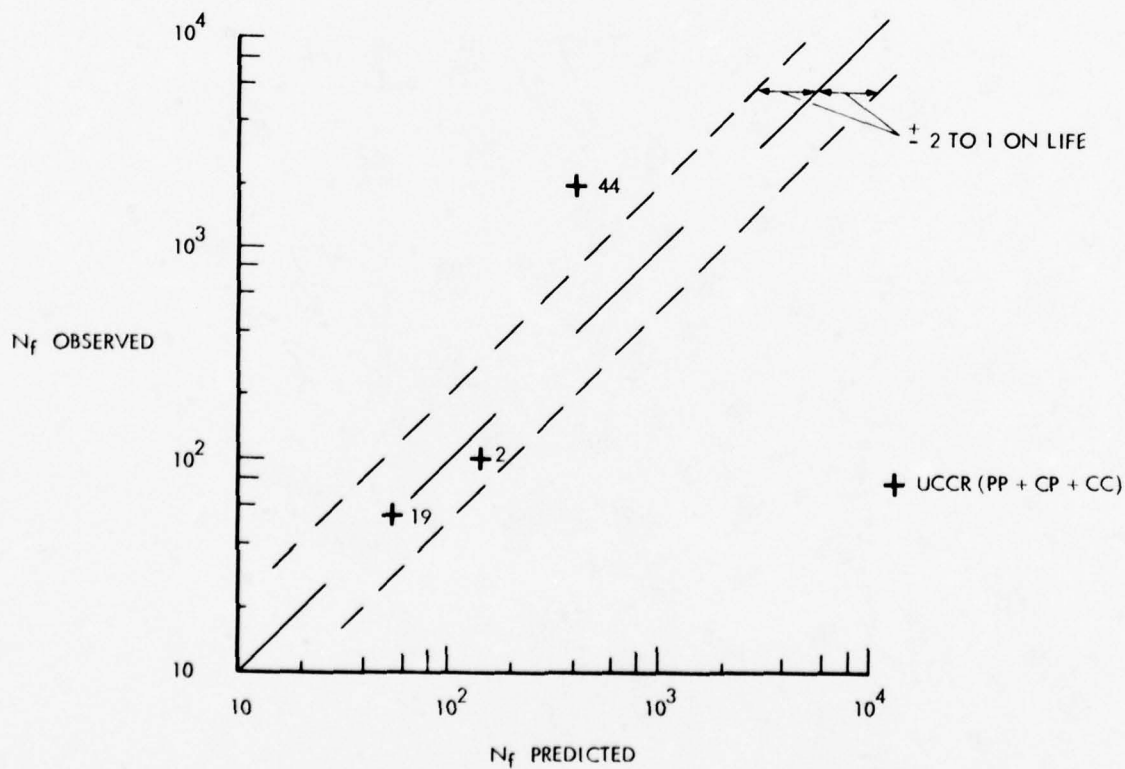


FIG 9. COMPARISON OF OBSERVED AND PREDICTED LIVES FOR "COMPLEX" TEST CYCLE - WASPALOY 700°C

HIGH TEMPERATURE LOW CYCLE FATIGUE BEHAVIOUR OF CAST IN738LC ALLOY

L. Massarelli

Laboratorio per la Tecnologia dei Materiali Metallici
non Tradizionali, CNR-LTM
Via Induno, 10 - 20092 Cinisello B. (Milano) Italy

SUMMARY

The high temperature low cycle fatigue behaviour of a nickel base alloy in the cast condition was investigated by carrying out tests under diametral strain controlled conditions.

The effect of anisotropy at diametral strain, which was especially marked in the cast alloys owing to the large grain size, was offset by mounting the diametral extensometer at a position along the minimum diameter section of the specimen where Poisson's ratio assumed its mean value. Cyclic and fatigue tests under conditions of constant amplitude diametral strain and at two different strain rates were carried out on IN738LC alloy at the temperature of 850°C. The results obtained confirm the repeatability of the tests carried out.

A start, therefore, was made into the study of the material's behaviour with a view to evaluating the applicability of the Strain Range Partitioning method also to this type of alloy.

1. INTRODUCTION

The study of high temperature low cycle fatigue (HTLCF) behaviour of metals is being carried out more and more with hourglass specimens and under diametral strain controlled conditions. The undeniable advantages resulting from the choice of these specimens which are, moreover, extensively described in the literature, offset by the uncertainties resulting from anisotropy at the diametral strain whose problems have not, on the other hand, been adequately investigated.

The hourglass specimen is considered to be a serious obstacle in the study of anisotropic materials owing to the difficulty of relating transverse and longitudinal strain, and it is thought that anisotropic materials generally require the use of cylindrical specimens (1).

For nickel base alloys, and more especially for materials used in the cast condition, it has been suggested, in order to overcome the effect of anisotropy accompanying diametral strain, that two diametral extensometers be positioned at right angles to one another on the specimen (2).

The degree of anisotropy at diametral strain seems to depend on the size and orientation of the crystal grains. Regarding this, it is undoubtedly useful, besides being appropriate, before making a study of the HTLCF behaviour under diametral strain controlled conditions, to evaluate effects of anisotropy on the results and this applies not only to materials with large grain size, but to any material.

The purpose of this work is to evaluate the degree of anisotropy at diametral strain for a cast nickel base alloy type IN738LC and to determine the experimental conditions which can be repeated at will to permit comparison of diametral strain controlled test data with longitudinal strain controlled test data. In order to provide experimental confirmation of the validity of the method adopted, HTLCF tests were carried out under diametral strain controlled conditions at two different diametral strain rates.

The results obtained from the fatigue tests at the higher diametral strain rates, more especially, form the starting in the study of the material using the strain range partitioning method in order to evaluate its applicability also to casting nickel alloys.

2. MATERIAL AND TEST PROCEDURE

The tests were carried out on Nimocast IN738LC alloy supplied by H. Wiggin Co. This alloy was precision cast into specimen blanks by Howmet Co. and casting was to specifications so as to obtain porosity levels lower than 5-7 pores per mm² with maximum pore size of 0.1-0.12 mm. The grain size was such as to give about 2 grains/mm when measured by linear intercept on a section of the specimen. This firm also carried out heat treatments in order to impart optimum tensile strength properties to the metal. The chemical composition of the alloy is as follows (wt. %):

Al	P	B	Si, Mn	C	S	Co	Ta	Nb	Cr	W	Zr	Cu	Fe	Mo	Al+Ti	Ti	Ni
3.4	0.001	0.012	<0.10	0.12	0.002	8.3	1.72	0.96	15.9	2.5	0.07	<0.10	0.22	1.6	7.7	3.3	Balance

The heat treatment consisted of 2 h at 1120°C in vacuum or hydrogen followed by cooling to room temperature, then 24 h at 845°C in argon or vacuum followed by cooling to room temperature. The specimens whose geometry is given in Fig. 1 were subsequently ground to remove casting stock.

The tests were carried out by means of a 25 ton M.T.S. closed loop electro-hydraulic testing system equipped with water cooled cast metal grips, diametral extensometer and module for converting the diametral signals into longitudinal signals for driving actuator.

The specimen was induction heated through a work coil fed by a R.F. generator. Four Chromel-Alumel thermocouples were spot welded on the specimen, with the two outer thermocouples at a distance of 10 mm and the two inner thermocouples at a distance of 5 mm from the narrowest section of the specimen. One of these thermocouples, was connected to a temperature controller, serving to hold the temperature, while the other three were used in controlling the temperature gradient and were recorded continuously. Variations in temperature with time around the section of minimum diameter were held between $\pm 1^\circ\text{C}$. Tests were strain controlled with a triangular wave form (where the value of mean strain is zero), and at two different strain rates: $\dot{\epsilon}_d = 1.82 \times 10^{-3}$ and $\dot{\epsilon}_d = 1.03 \times 10^{-5} \text{ s}^{-1}$. During the test, variations in load were recorded continuously with the hysteresis loop being recorded at intervals. The number of cycles to fracture was defined as the value at which, in curve $\Delta\sigma$ -n (number of cycles) a sudden variation in slope occurred (indicated by the arrow in Fig. 5).

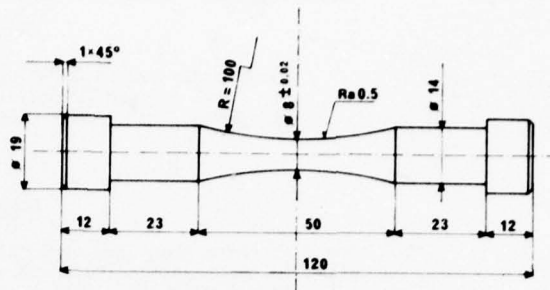


Fig. 1 - Test specimen.

The modulus of elasticity at a temperature of 850°C was measured on an 8 mm dia. cylindrical test specimen using an M.T.S. longitudinal extensometer fitted on the specimen by means of quartz rods (gauge length: 25 mm). The values were determined dynamically under conditions of controlled load and triangular cycling, with frequency approx. 0.05 Hz. The values of Poisson's ratio in relation to the position of the diametral extensometer were determined on an hourglass specimen under load control, with variation in diameter being read on a digital voltmeter.

The cyclic curves were obtained on the single test specimens by two methods: multiple step and incremental step. The curves represent the envelope of the tips of the stabilized hysteresis loops and were determined by stressing the specimen with increasing values of diametral strain (multiple step) or else with several blocks of increasing-decreasing diametral strain values (incremental step).

3. TEST RESULTS AND DISCUSSION

Fig. 2 shows the results obtained from the tests in which Poisson's ratio in relation to extensometer position was measured on two hourglass specimens one of which with a grain size conforming to casting specifications, and the other specimen with grain size considerably higher. Each point plotted on the curve

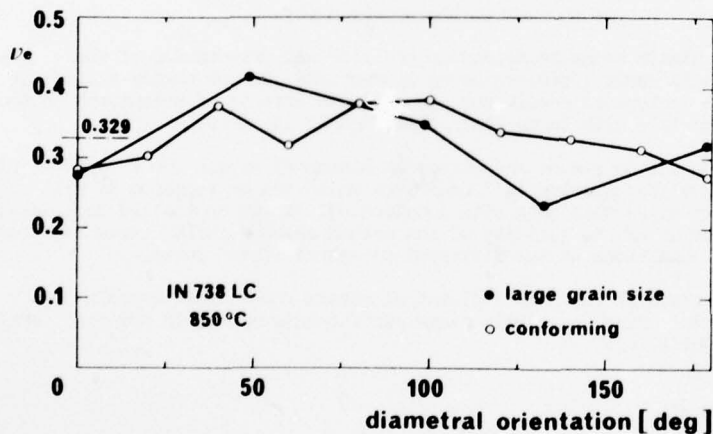


Fig. 2 - Value of Poisson's ratio vs. diametral orientation.

represents the mean value of at least ten measurements. It can be seen that there is a random relationship between ν_e against diametral orientation. The results confirm both the anisotropic behaviour at transverse strain for alloy IN738LC and, more especially, confirm that this anisotropy depends on crystal grain size seeing that the effect is magnified for the material with the larger grain size. The anisotropic effects are so marked, that they cannot be neglected when carrying out diametral strain controlled tests. The mean value of Poisson's ratio was then calculated ($\bar{\nu}_e = 0.33$) and, by positioning the diametral extensometer at a point along the narrowest section of the specimen where Poisson's ratio assumed the mean value, it was wished to show that the test results were reproducible.

The comparison of results was made in Fig. 3 by plotting the cyclic curves obtained from a specimen for each experimental condition, and the values of maximum stress determined in the constant amplitude diametral strain fatigue tests. From the figure it can be noticed first of all, that there is a high sensitivity of the alloy under test to the strain rate at 850°C . Furthermore, the cyclic curves obtained with the multiple step method give σ values greater than those determined with the incremental step method. The difference becomes more marked, the higher is the $\dot{\epsilon}_d$, more especially for values of diametral strain am-

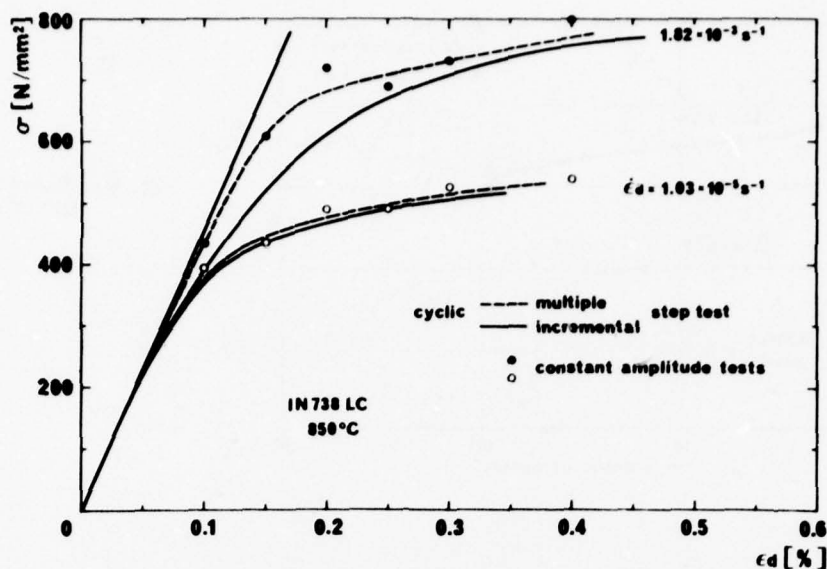


Fig. 3 - Comparison of cyclic stress-strain curves and constant amplitude tests results.

plitude up to $\epsilon_0 = 0.3\%$. Moreover, the figure shows that the σ values obtained from the fatigue tests lie around the cyclic curves obtained at the same strain rate, correlation being especially good with the curves obtained by means of the amplitude step method.

This result confirms that the experimental method adopted can give reliable results when the tests are carried out under diametral strain controlled conditions on a material which exhibits a marked degree of anisotropy at transverse strain.

The fatigue test results expressed as values of total longitudinal strain ranges corresponding to the values of imposed diametral strain ranges, are plotted against endurance in Fig. 4. It can be seen from the relationship given in Fig. 4 that the strain rate considerably affects the fatigue life of the material under test, for equal amplitude of controlled strain, with the longer endurances occurring at the higher strain rate.

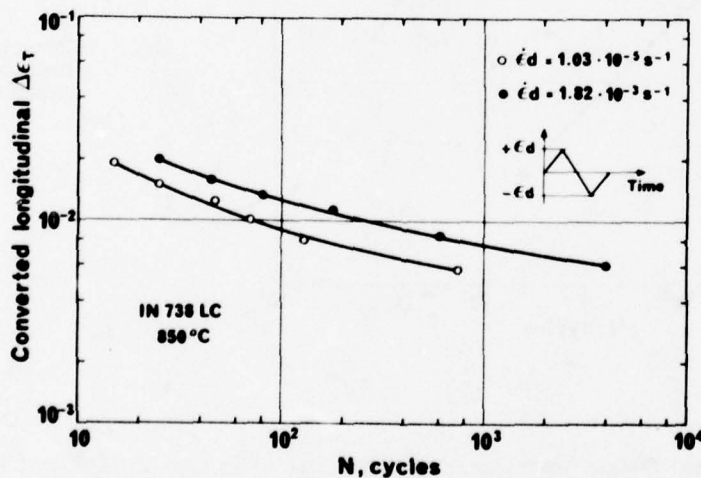


Fig. 4 - Total longitudinal strain ranges vs. endurances.

Fig. 5 shows the relationship between stress range and the number of cycles; the values were determined in two tests carried out with equal diametral strain range and at two different strain rates. The two

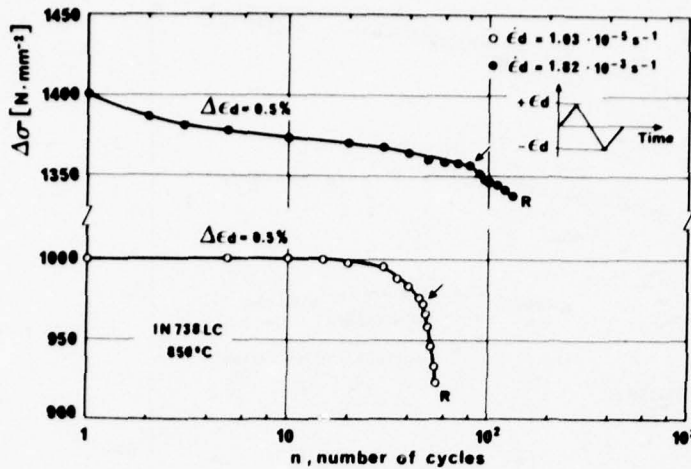


Fig. 5 - Stress ranges vs. number of cycles.

curves represent the typical behaviour at the two $\dot{\epsilon}_d$'s: at the high strain rate, there is a progressive drop in the curve with growing number of cycles, while at the lower strain rate, after an initial period of stabilization, there is a falling off of the curve until the final fracture. The arrows show the number of cycles we assume to fracture, while the point indicated by letter R gives the number of cycles withstood before the test piece broke into two halves. All number of cycles to fracture given in this paper, refer to the above mentioned method of determination using the $\Delta\sigma$ - n relationship because the tests were normally interrupted before the final fracture in order not to damage the diametral extensometer.

Fatigue test results obtained at the higher strain rate are plotted in the most convenient form for subsequent analysis and evaluation by the strain range partitioning method. Fig. 6 shows the relationship between the inelastic strain range values and endurance. The experimental points plotted lie about a straight line which represents the component obtained by the plastic-plastic hysteresis loops. Other tests will be performed in order to verify the applicability of the SRP method also to alloy IN738LC.

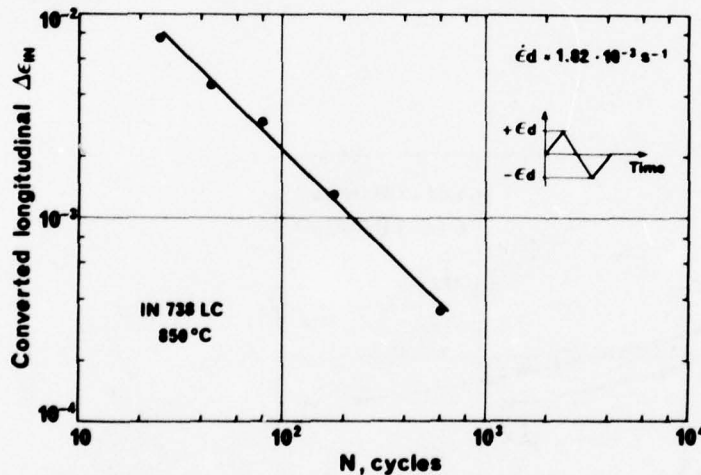


Fig. 6 - Converted longitudinal inelastic strains vs. endurance.

4. CONCLUSIONS

The high temperature low cycle fatigue behaviour of a nickel base alloy type IN738LC used in the cast condition was studied. More especially the study shows the marked anisotropy accompanying diametral strain, effect of which increases, the greater is the crystal grain size of the alloy.

The extent of the variation of Poisson's ratio in relation to the position of the extensometer on the hourglass specimen was too great to be neglected when investigating the high temperature low cycle fatigue behaviour under conditions of controlled diametral strain.

By placing the extensometer in a position where Poisson's ratio assumed its mean value as determined for

the material under test, it was possible to obtain reproducible results, which could therefore be used in a more general manner. Hence it is possible to determine the high temperature low cycle fatigue behaviour under conditions of controlled diametral strain also of highly anisotropic materials such as cast nickel base alloys making use of the advantages offered by the above method of approach.

If it is considered that most materials, and not only those used in the cast condition, exhibit a certain degree of anisotropy, it is most certainly useful, before carrying out diametral strain controlled tests, to evaluate whether the degree of anisotropy at diametral strain can be neglected or not. If not, then the technique of placing the extensometer at the point when Poisson's ratio assumes its mean value can be adopted.

The results obtained at the higher frequency, when evaluated by the strain range partitioning method, confirm that by analysis of the plastic-plastic curves, the points plotted in relationship $\Delta\epsilon_{\text{PP}}-N$ lie around a straight line. Other tests will be carried out to verify the SRP method.

REFERENCES

- 1) Slot, T., Stentz, R.H. and Berling, J.T. "Controlled-Strain Testing Procedures", Manual on Low Cycle Fatigue Testing, ASIM STP 465, 1969, p. 107.
- 2) Coffin, L.F. Jr. "Fatigue at High Temperature", Fatigue at Elevated Temperatures, ASIM STP 520, 1973, p. 10.

ACKNOWLEDGMENTS

The author wish to thank D. Ranucci and E. Picco for their assistance in conducting the experimental work.

This work has been carried out under the European Concerted Action on Materials for Gas Turbines (COAST 50).

CONTRIBUTION A L'EVALUATION
DE LA METHODE STRAINRANGE PARTITIONING
APPLICATION A L'ALLIAGE BASE NICKEL WASPALOY
par
C. PERRUCHET
Ingénieur des Etudes et Techniques d'Armement
Centre d'Essais Aéronautique de Toulouse
23, Avenue H. Guillaumet -31056-TOULOUSE CEDEX
France

SOMMAIRE

Dans une première phase, il a été effectué une étude des caractéristiques classiques de l'alliage :

- Analyse chimique
- Examens macrographiques et micrographiques
- Mesure du coefficient de dilatation linéaire
- Détermination des caractéristiques mécaniques jusqu'à 900° C
- Etude du comportement en traction cyclique

L'établissement des quatre courbes de base de la méthode SRP a ensuite été effectué à la seule température de 750° C suivant la méthodologie choisie par le CEAT :

- Mesure des déformations diamétrales totales et de l'effort sur une éprouvette à section évolutive,
- Asservissement de la machine d'essais par les déformations diamétrales totales,
- Chauffage de l'éprouvette par effet Joule.

La méthode de décomposition a ensuite été appliquée à un cycle complexe et pour deux niveaux de déformations diamétrales totales correspondant à des durées de vie faibles, quelques centaines de cycles.

Dans ce domaine, la validité de la méthode SRP est apparue comme excellente, l'écart moyen entre les durées de vie théoriques et expérimentales se situant aux environs de 12,5 %.

SUMMARY

Firstable, a Waspaloy's usual basic properties study has been completed :

- Chemical analysis
- Macrographic and micrographic investigations
- Linear thermal expansion coefficient measurement
- Monotonic tensile properties determination at room and elevated temperature (up to 900° C)
- Cyclic stress-strain properties evaluation

Then, establishment of the four basic life relationships of SRP has been completed at the only temperature of 750° C, and under experimental procedures chosen by CEAT :

- Load and total diametral strain measurement on an hourglass specimen
- Electrohydraulic servocontrolled testing machine command with a demand signal representative of total diametral strain
- Specimen heating by direct resistance (Joule effect)

Then, SRP Method has been applied to a complex strain cycle for two values of total diametral strain corresponding to very low cycle fatigue lives (a few hundreds of cycles). In this field, SRP Method validity has appeared as excellent, since average difference between predicted and tested values of fatigue life is about 12,5 percent.

1. INTRODUCTION

Les travaux initialement engagés portaient sur l'application de la méthode Strainrange Partitioning à l'alliage coulé base nickel INCO 713 C (appellation française NC13AD). Des difficultés de mise en oeuvre de la technique d'essais, liées à une forte hétérogénéité structurale du matériau, ont conduit à interrompre ce programme et à reprendre entièrement l'étude sur un matériau devant offrir à priori une structure beaucoup plus homogène.

L'alliage retenu est l'alliage base Nickel Waspaloy (appellation française NC20K14) sous forme de barres laminées de faible diamètre. Sous cette forme, il est utilisé par certains motoristes pour de petites pièces mécaniques très chaudes et très sollicitées. Il présente en effet des caractéristiques mécaniques encore largement acceptables ($R = 1091$ MPa) à sa température maximale admissible en utilisation prolongée (750° C). En courte durée, la température maximale d'utilisation peut être portée à 850° C.

La réduction importante du temps disponible pour la réalisation de l'étude, liée à l'abandon tardif du programme initial, a conduit à n'entreprendre que les deux thèmes principaux proposés dans le programme coopératif :

- Détermination des quatre relations fondamentales d'endurance
- Application de la méthode SRP à des essais effectués sous cycle complexe, avec comparaison des durées de vie calculées à celles relevées en essais.

Deux autres aspects de l'évaluation de la méthode SRP ont dû être écartés :

- Démonstration de la variation de la durée de vie entre les deux courbes limites lorsqu'on modifie systématiquement un des paramètres d'essais (vitesse de déformation, par exemple)
- Détermination de l'effet de la température sur les relations fondamentales d'endurance.

2. LA METHODE STRAINRANGE PARTITIONING

La méthode Strainrange Partitioning (Décomposition du domaine de variation des déformations) est une démarche particulière, tenant compte des interactions fatigue-fluage, pour la prévision des durées de vie en fatigue oligocyclique à haute température (Réf. 1). L'hypothèse de base de cette méthode est que, dans tout cycle d'hystérésis contraintes-déformations, il n'y a combinaison que de deux directions de déformation (traction et compression) et de deux types de déformations inélastiques (dépendant du temps : fluage, noté C, ou n'en dépendant pas : plasticité, noté P).

La combinaison des deux directions et des deux types de déformations conduit à quatre cas possibles qui constituent les quatre composantes fondamentales de tous les cycles d'hystérésis concevables. Chacun de ces cas est défini par la façon dont, au cours d'un cycle, une composante de traction (P ou C) est compensée par une composante de compression (P ou C). On obtient ainsi les quatre cycles de base : PP, PC, CP et CC.

Ainsi, la proposition du NASA Lewis Research Center (Réf. 2) est d'étendre la relation de Manson-Coffin, qui représente l'endurance en fonction du domaine de variation des déformations inélastiques de matériaux travaillant au dessous de la limite de fluage en lui substituant quatre relations séparées s'appliquant à des matériaux travaillant au dessus de la limite de fluage.

L'application de ces relations de base à un cycle complexe pour la prévision d'une durée de vie doit se faire en deux étapes :

- Connaissance du cycle d'hystérésis correspondant au cycle de fonctionnement à analyser et possibilité de décomposition de la déformation inélastique totale suivant trois au plus des quatre composantes fondamentales :

$$\Delta \epsilon_{in} = \Delta \epsilon_{PP} + \Delta \epsilon_{PC} \text{ (ou } \Delta \epsilon_{CP}) + \Delta \epsilon_{CC}$$

- Application d'une règle de dommage pour prévoir la durée de vie correspondant à la combinaison des composantes fondamentales : la part active de chacune de ces composantes dans la déformation inélastiques totale, $F_{ij} = \Delta \epsilon_{ij} / \Delta \epsilon_{in}$, entraîne un dommage par cycle F_{ij} / N_{ij} , N_{ij} étant la durée de vie que l'on obtiendrait si toute la déformation inélastique était de type ij , soit $\Delta \epsilon_{in} = \Delta \epsilon_{ij}$. Le dommage par cycle pour la déformation inélastique totale est obtenu par sommation des dommages élémentaires : $1/N_{pr} = \sum (F_{ij} / N_{ij})$ d'où la prévision de durée de vie N_{pr} pour le cycle de fonctionnement considéré.

3. PRESENTATION DE L'ALLIAGE ETUDIE

Il s'agit de l'alliage base Nickel Waspaloy (appellation française NC20K14) sous forme de barres de faible diamètre (25 mm) et dans une nuance particulière se distinguant des autres nuances du même alliage par un écrouissage contrôlé en cours de laminage à froid. Cette opération doit permettre d'obtenir un grain plus homogène sur pièces finies.

La matière d'origine a été élaborée par la Société Aubert et Duval (coulée HV 9454). Les barres ont été livrées à l'état hypereutecté.

3.1. Composition chimique

L'analyse chimique effectuée par le CEAT a donné les résultats suivants (valeurs moyennes obtenues pour les deux barres dans lesquelles ont été prélevées les éprouvettes)* (voir apostille en P.9-5):

Eléments	Teneur (%)	Spécification courante	Eléments	Teneur (%)	Spécification courante
Al	1,320	1,2 à 1,6	Cr	20,485	18 à 21
P	0,012	0,015 max	Zr	0,082	0,02 à 0,08
Si	0,060	0,15 max	Cu	0,006	0,10 max
B	0,009	0,003 à 0,010	Fe	0,165	2 max
S	0,003	0,008 max	Mo	3,940	3,5 à 5
C	0,037	0,03 à 0,10	Mn	0,003	0,10 max
Co	13,000	12 à 15	Pb	0,005	0,005 max
Ti	2,935	2,75 à 3,25	Ni	base	base

A noter que les résultats obtenus sont en accord avec la spécification courante à l'exception de celui concernant le Zirconium qui reste cependant voisin du maximum fixé.

3.2. Traitement thermique

Le traitement de livraison correspond au traitement AMS 5704 mais avec trempe à l'eau au lieu de refroidissement à l'air, soit :

- Mise en solution 1030° C. 4 H. trempe à l'eau

Le traitement effectué sur ébauches d'éprouvettes avant usinage finition correspond au traitement AMS 5707, soit :

- Stabilisation : 850° C. 4 H. Refroidissement à l'air
- Précipitation : 760° C. 16 H. Refroidissement à l'air

3.3. Structures métallographiques

3.3.1. Macrographie

Cet examen a été effectué sur chacune des deux barres à l'état de livraison et suivant les deux sens longitudinal et transversal.

Il a permis de mettre en évidence (Fig. 1) un fibrage peu marqué avec, entre les deux barres, une légère différence de granulométrie. Une des deux barres présente en outre, tout au moins au niveau de l'échantillon macrographique, une hétérogénéité de structure à proximité de sa surface. Aucun examen plus approfondi n'a été effectué, ce défaut n'affectant pas la partie utile des éprouvettes qui correspond au coeur de la barre.

3.3.2. Micrographie

Ces examens ont été effectués sur chacune des deux barres, suivant leur sens longitudinal et en deux zones différentes.

A l'état de livraison, hypere trempé, la structure est composée d'une matrice de solution solide γ avec des composés intermétalliques alignés par le laminage. La granulométrie varie d'une barre à l'autre et même suivant les différentes zones d'une même barre.

Dans un cas (Barre B1, Fig. 2 et 3) on observe des grains de grosseur IG = 4.5 ASTM avec des composés intermétalliques assez nombreux aux côtés de grains de grosseur IG = 2-3 ASTM avec des composés intermétalliques plus clairsemés.

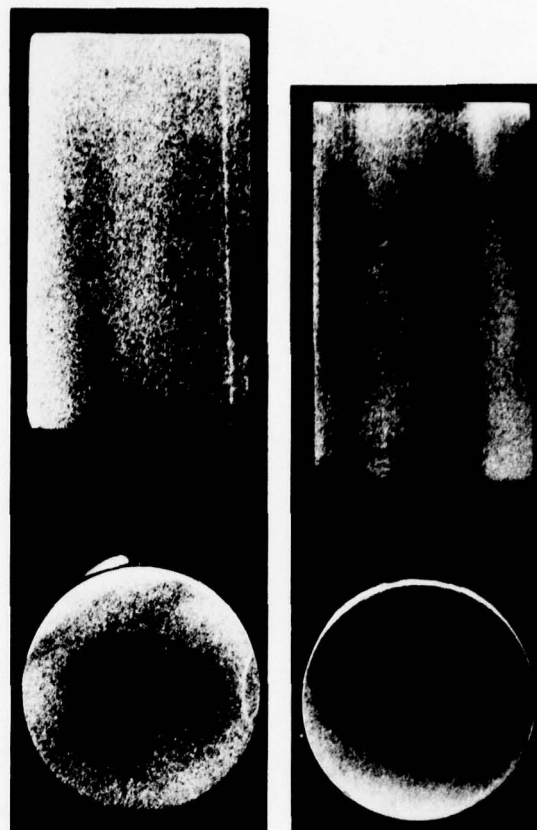


Fig. 1. Structures macrographiques

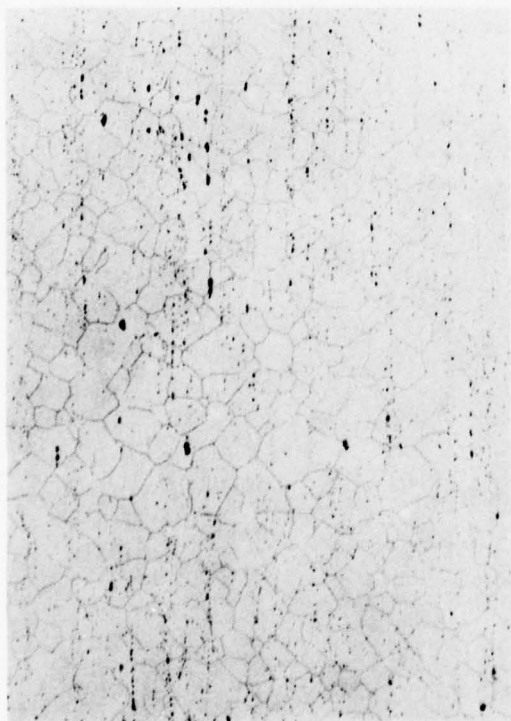


Fig. 2 Barre B1. IG = 4.5. ASTM

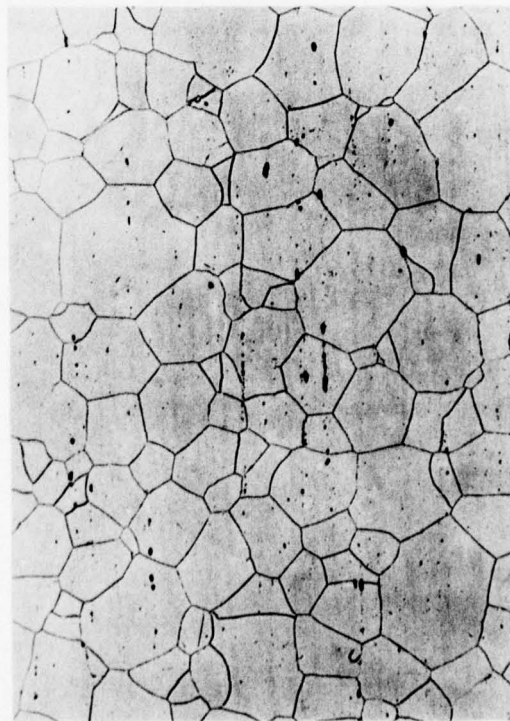


Fig. 3 Barre B1. IG = 2.3. ASTM

Dans l'autre cas (Barre B2. Fig. 4) on observe des grains de grosseur uniforme IG = 7.8 ASTM. Les composés intermétalliques rencontrés sont vraisemblablement des carbures du type $M_{23}C_6$ ou MC.

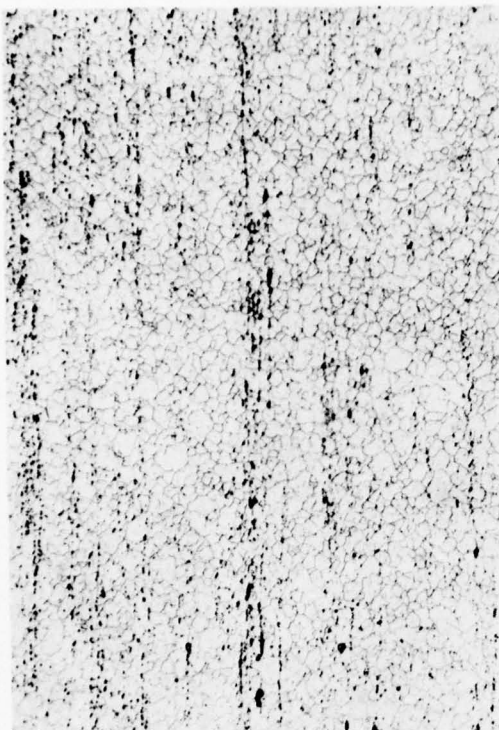


Fig. 4. Barre B2 . IG = 7.8 ASTM

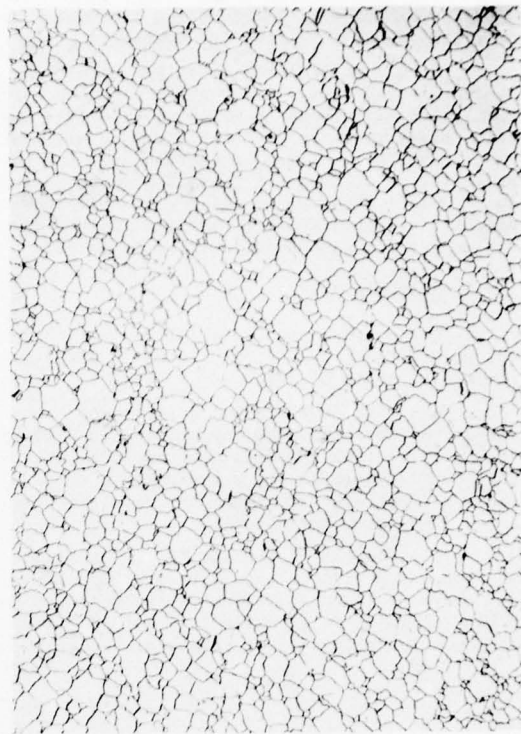


Fig. 5. Barre B1 . IG = 6.7 ASTM

A l'état entièrement traité, les différences observées entre les deux barres sont considérablement atténuées. La matrice de solution solide γ présente une granulométrie quasi uniforme IG = 6.8. ASTM (Fig. 5 et 6). Elle est, de plus, le siège d'une précipitation fine, abondante et régulière de phase γ' Ni_3 (Ti, Al). Les joints de grains sont marqués par un liseré quasi continu de carbures $M_{23}C_6$ formés lors du traitement de stabilisation à 850° C. La matrice de solution solide γ contient également quelques particules dispersées de carbures de type MC (Fig. 7 et 8).

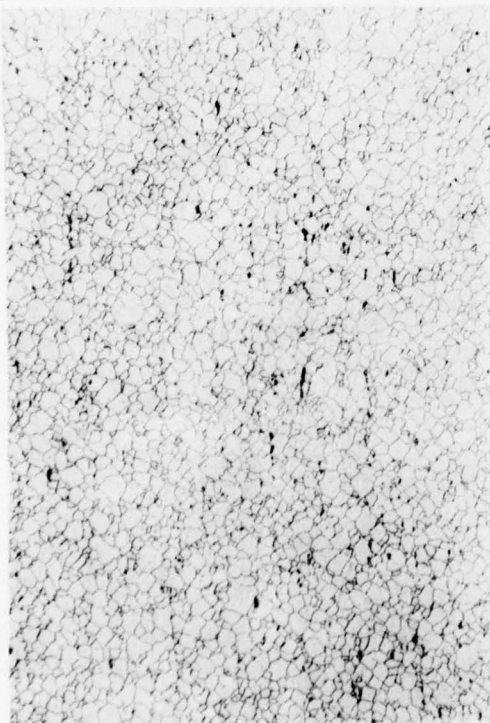


Fig. 6 Barre B2. IG = 7.8. ASTM



Fig. 7 Barre B1

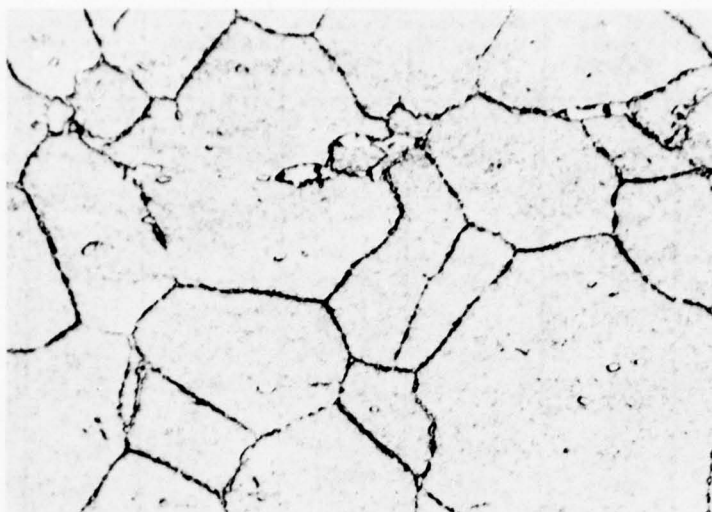


Fig. 8 Barre B2

3.4. Détermination du coefficient de dilatation linéaire

La méthode d'essais utilisée par le CEAT (Cf. paragraphe 4) impose la connaissance du diamètre initial des éprouvettes pour le calcul des déformations diamétrales totales, $\epsilon_t^d = \log(D/D_0)$. Or pendant la phase de chauffage jusqu'à la température d'essais (750° C), la dilatation de ce diamètre par rapport au diamètre initial à température ambiante correspond à des déformations diamétrales totales de l'ordre de 1 %, donc supérieures à la quasi totalité des déformations diamétrales totales recherchées en essais. Il a donc été jugé

nécessaire de procéder à la détermination du coefficient de dilatation linéaire de manière à disposer d'une valeur précise du diamètre initial des éprouvettes à la température d'essais.

Coefficient de dilatation moyen entre 20° C et	Sens long	Sens travers
300 ° C	$12,6 \cdot 10^{-6}$	$13,9 \cdot 10^{-6}$
600 ° C	$13,6 \cdot 10^{-6}$	$14,6 \cdot 10^{-6}$
700 ° C	$14,2 \cdot 10^{-6}$	$14,8 \cdot 10^{-6}$
750 ° C	$14,5 \cdot 10^{-6}$	$15,0 \cdot 10^{-6}$
800 ° C	$14,8 \cdot 10^{-6}$	$15,4 \cdot 10^{-6}$
900 ° C	$15,6 \cdot 10^{-6}$	$16,2 \cdot 10^{-6}$

Cette détermination a été effectuée sur des échantillons dilatométriques prélevés dans les sens long et travers des barres. Pour chacun des sens de prélèvement, aucune différence significative entre les deux barres n'a été mise en évidence. Par contre une légère différence a été observée entre les sens longitudinal et diamétral, comme le montre le tableau ci-contre donnant, pour chaque

sens, les résultats moyens obtenus pour les deux barres. La valeur retenue pour le dépouillement des essais de fatigue effectués à 750° C est celle correspondant à la direction de dilatation du diamètre des éprouvettes, donc le sens travers, soit $15 \cdot 10^{-6}$.

3.5. Caractéristiques mécaniques

3.5.1. Traction monotone

Les caractéristiques mécaniques classiques du matériau ont été déterminées entre la température ambiante et 900° C en effectuant simultanément une mesure des déformations longitudinales et une mesure des déformations diamétrales en tenant compte des variations initiales des grandeurs de référence avec la température. Cette méthode a permis de déterminer d'une part le coefficient de POISSON et d'autre part les valeurs vraies de la limite élastique conventionnelle ($\sigma_{0,2}$) à 0,2 % et de la contrainte à rupture (σ). Ces résultats, regroupés dans le tableau ci-dessous, sont représentés par les figures 9 et 10.

Les valeurs retenues pour le dépouillement des essais de fatigue effectués à 750° C sont les suivantes :

- Module d'élasticité : $E = 156100$ MPa
- Coefficient de POISSON : $\nu = 0,315$

Compte tenu de la dispersion importante observée entre 700 et 800° C, la valeur retenue pour le coefficient de POISSON est la moyenne des valeurs obtenues à 700, 750 et 800° C.

* La composition chimique, les procédés de fabrication, les traitements thermiques et les propriétés mécaniques de chaque alliage soumis à essai, ainsi que les données obtenues au cours du programme, figurent à l'Appendice A 1.

Rep. Epr.	Temp. d'essai (°C)	Limites élastiques		Contraintes à rupture		Allongement à rupture (%)	Striction (%)	Module d'Young (MPa)	Coef. de Poisson
		Convention RO,2 (MPa)	vraie $\sigma_{0,2}$ (MPa)	Convention R (MPa)	vraie σ (MPa)				
B1-4	20	1 095	-	1 306	-	29,3	43,4	204 400	0,309
B1-9	"	955	959	1 321	-	27,3	44,5	197 000	0,261
B2-11	"	993	996	1 369	1 646	-	-	216 800	0,318
B1-2	300	841	843	1 184	-	-	-	192 000	0,242
B1-8	"	880	883	1 211	1 446	27,3	41,8	189 200	0,267
B2-2	"	905	910	1 255	1 462	26,3	41,8	200 600	0,334
B1-3	600	871	875	1 136	1 329	23,3	40,5	174 600	0,314
B2-8	"	893	897	1 199	1 364	20,3	38,9	174 500	0,294
B1-6	700	844	848	1 169	1 354	24,3	36,3	159 700	0,306
B1-11	"	858	862	1 198	1 386	24,3	36,4	165 600	0,301
B2-4	"	862	866	1 218	1 398	21,3	40,4	161 400	0,292
B1-5	750	797	801	1 075	1 271	20	36,3	157 300	0,316
B2-3	"	844	849	1 112	1 296	23,3	36,3	156 500	0,342
B2-9	"	844	848	1 085	1 245	22,3	40,5	154 500	0,342
B2-1	800	796	801	976	1 129	25	44,5	149 700	0,319
B2-10	"	804	807	948	990	15	54,6	148 700	0,291
B1-10	900	525	528	645	714	30,6	65,7	116 600	0,297
B2-6	"	460	463	571	629	36,6	71,7	114 200	0,302

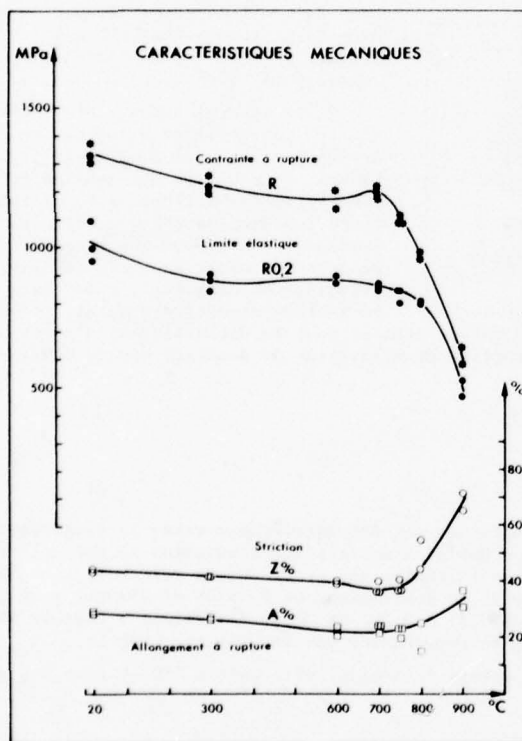


Fig. 9 Caractéristiques mécaniques

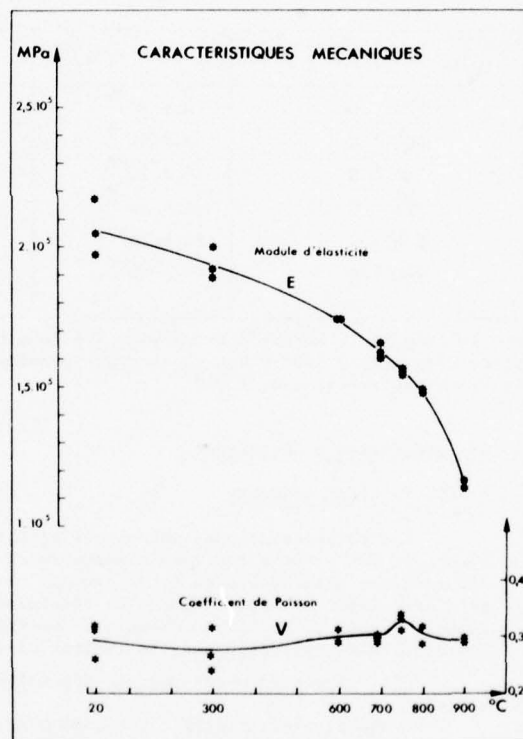


Fig. 10

3.5.2. Traction cyclique

Pour pouvoir comparer le comportement du matériau en traction cyclique à 750° C avec celui en traction monotone, il a d'abord été réalisé un essai de traction monotone dans les mêmes conditions que les essais de fatigue (cf. paragraphe 4) à savoir : même éprouvette, même capteur de déformations diamétrales, même machine d'essais. Les résultats obtenus : $RO,2 = 816$ MPa et $R = 1142$ MPa sont très voisins de ceux obtenus sur éprouvettes de traction classique ($RO,2 = 828$ MPa et $R = 1091$ MPa).

L'essai de traction cyclique a été effectué par la méthode de la variation incrémentale des niveaux de déformations. Une illustration de la commande en déformations et de la réponse du matériau en contraintes est donnée par la figure 11.

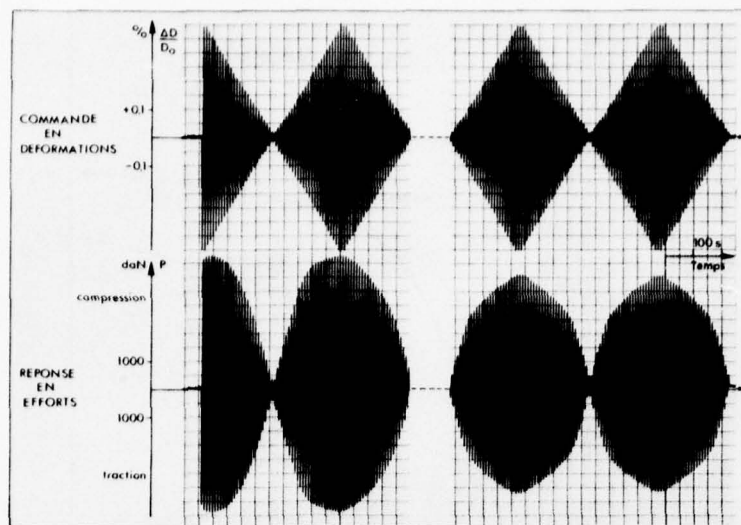


Fig. 11. Traction cyclique. Méthode à niveau incrémental

Au cours du premier bloc décroissant (Fig. 12), on observe un durcissement du matériau, puis un adoucissement au cours des blocs suivants, pour atteindre la stabilité au cours du dixième bloc (Fig. 13).

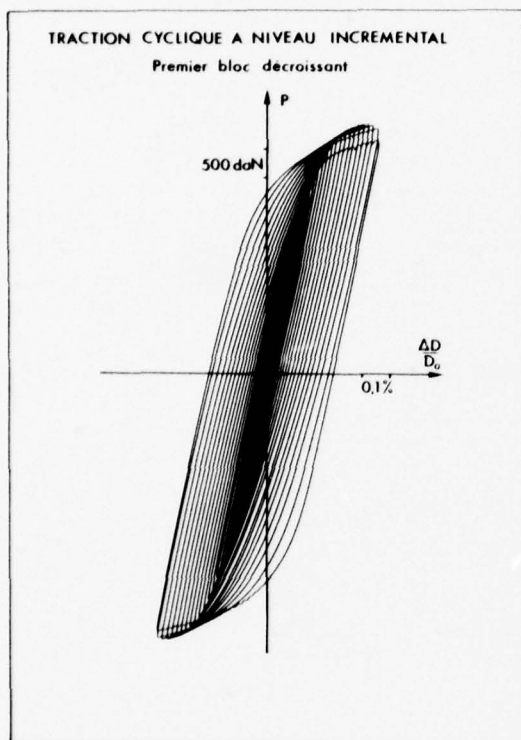


Fig. 12

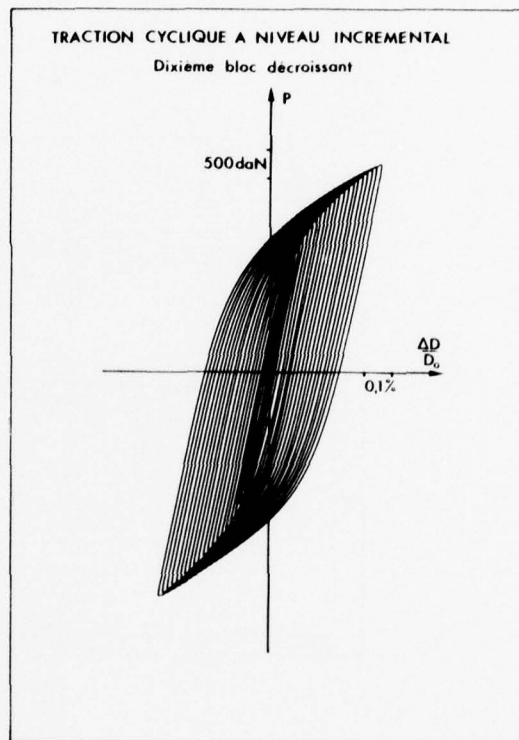


Fig. 13

La courbe de traction cyclique a ensuite été obtenue en effectuant une traction monotone sur la même éprouvette.

L'adoucissement du matériau est très net (Fig. 14) tant sur l'évolution des caractéristiques de traction ($R_{0,2} = 589 \text{ MPa}$, $R = 995 \text{ MPa}$) que sur celle de l'exposant de consolidation n de la loi $\sigma = K(\epsilon_p)^n$. En effet, de la valeur $n = 0,061$ correspondant à la traction monotone, cet exposant passe à la valeur $n = 0,147$ pour la traction cyclique (Fig. 15).

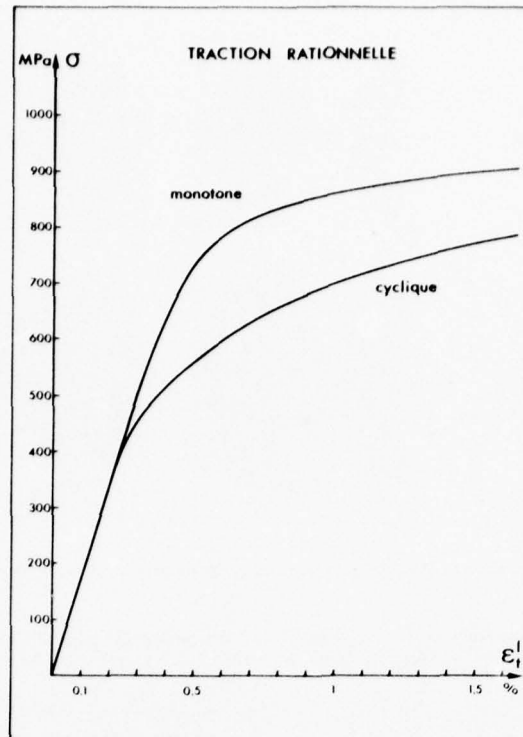


Fig. 14

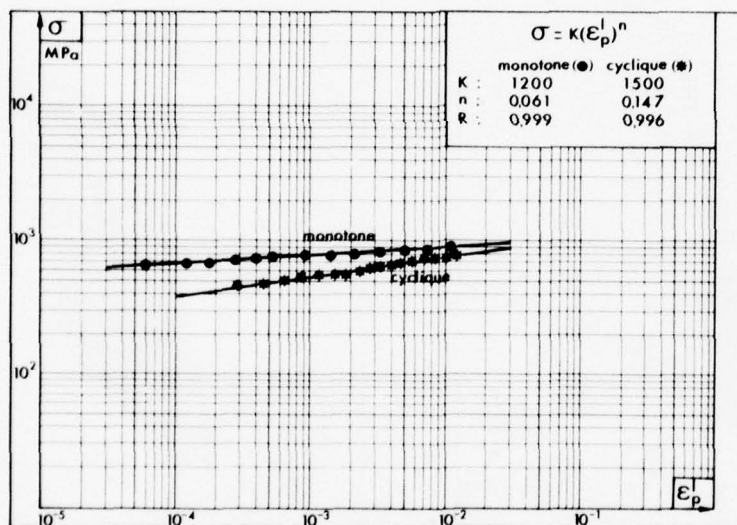


Fig. 15

4. MOYENS D'ESSAIS

4.1. Epreuve

L'éprouvette utilisée est montrée sur la figure 16. Notre choix s'est porté sur ce type d'éprouvettes (section évolutive) pour des raisons identiques à celles exposées par Slot, Stentz et Berling (Réf. 3), à savoir qu'il présente sur l'éprouvette cylindrique cinq avantages principaux :

1. Une concentration géométrique de contrainte ou de déformation relativement faible ($\alpha_K = 1,035$) permet de localiser la section de rupture. La déformation peut ainsi être mesurée et contrôlée dans la section même où se produit la rupture, ce qui permet éventuellement de contrôler la striction.
2. Une déformation en compression relativement importante peut être appliquée au matériau sans risque de flambage.
3. Les défauts internes ou de surface sont moins de nature à affecter le résultat de l'essai puisque seule une petite partie de l'éprouvette est soumise à la déformation maximale.

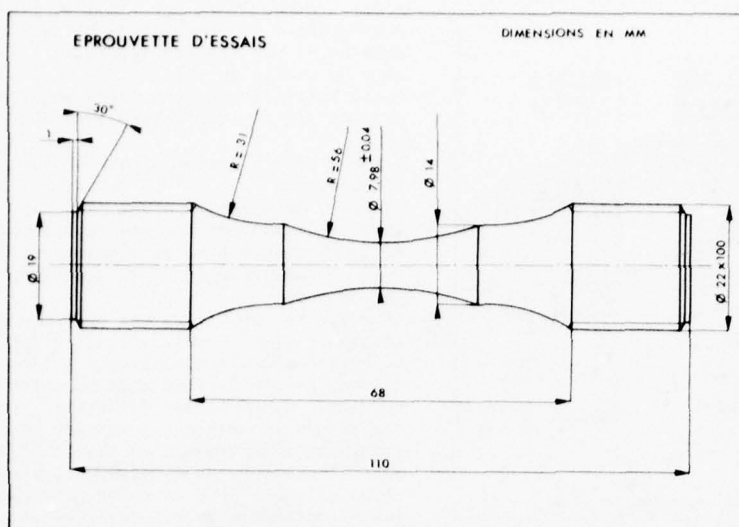


Fig. 16 Epreuve d'essai

fait que la contrainte moyenne de cisaillement sur une éprouvette torique est inférieure à la contrainte constante de cisaillement sur une éprouvette cylindrique.

4. Toute anisotropie éventuelle du matériau perturbera d'autant plus l'essai que le volume de matière concerné par la déformation maxima est faible.

4.2. Capteur de déformations

L'extensomètre utilisé est schématisé sur la figure 17. Il s'agit d'un extensomètre à capteur inductif dont l'étendue de mesure est de $\pm 0,5$ mm par rapport à la position zéro. La fréquence de travail de ce type de capteur est déterminée par le constructeur pour obtenir d'une part une linéarité optimale et d'autre part une dérive et une variation de sensibilité minima avec les variations de température. La caractéristique annoncée pour la dérive maxima de la position zéro avec la température ($0,00168$ mm/100° C) peut cependant entraîner une dérive importante lors d'essais réalisés à haute température si des précautions particulières ne sont pas prises pour éliminer les échanges thermiques entre l'éprouvette et le capteur. Dans ce but, les tiges des palpeurs et leurs supports sont construits en alliage INVAR, à très faible coefficient de dilatation, les palpeurs eux-mêmes étant en silice. On limite ainsi les échanges thermiques par

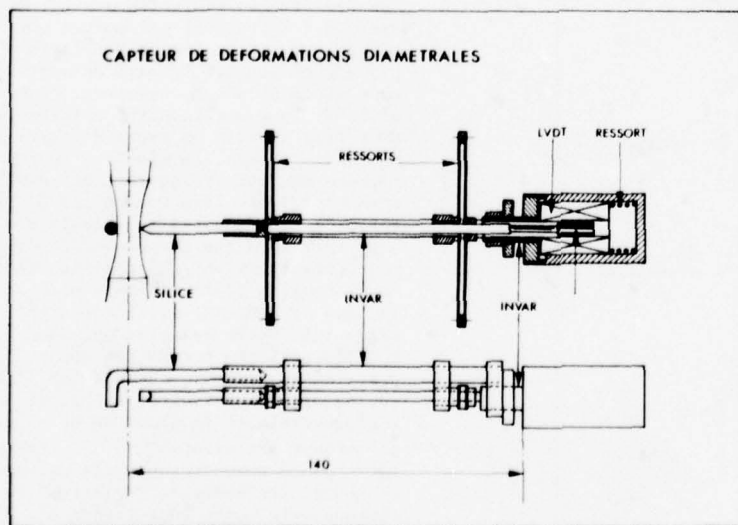


Fig. 17 Capteur de déformations

4. La déformation étant mesurée diamétralement dans la section minimale de l'éprouvette, il est possible de déterminer directement la contrainte vraie appliquée au cours de chaque cycle de sollicitation par détermination de la section instantanée.

5. Le chauffage local de l'éprouvette peut être réalisé aisément puisque le gradient de température ne doit être nul que sur une longueur relativement faible de part et d'autre de la section minima. Le choix de ce type d'éprouvettes présente cependant quatre inconvénients :

1. Les diamètres à mesurer ainsi que leurs variations sont nettement plus faibles que les longueurs de référence des éprouvettes cylindriques. La sensibilité des capteurs doit donc être d'autant plus grande.

2. Les déformations longitudinales ne sont accessibles qu'indirectement par calcul à partir des mesures de la charge et de la déformation diamétrale totale. Un asservissement de la machine d'essais directement en déformations longitudinales est donc plus difficile à mettre en oeuvre car nécessitant un intermédiaire de calcul (analogique ou numérique).

3. Il est possible que le comportement d'un même matériau diffère selon qu'il est sollicité en déformations imposées suivant le mode diamétral ou longitudinal. Certaines études (Réf. 4) semblent mettre en évidence de meilleurs résultats avec le mode diamétral, liés au

conduction. Les échanges thermiques par rayonnement sont limités par l'interposition d'un écran thermique ou d'un calorifugeage de l'éprouvette par un feutre réfractaire ou de la laine de silice. Les variations de diamètre à mesurer étant très faibles, tout frottement mécanique, même minime, peut nuire à la précision des mesures. Un montage particulier, visible sur la figure 17, a donc été réalisé pour éliminer ces frottements. Il consiste en deux ressorts bilame dont chacune des lames est solidaire d'une des tiges de palpeurs, évitant ainsi tout contact entre celles-ci. Avec ce montage et compte tenu des caractéristiques du capteur d'une part et des étalonnages effectués d'autre part, la résolution des mesures est de l'ordre de $0,5$ micron. La partie support de l'ensemble de l'extensomètre a été conçue pour être la plus légère possible de manière à pouvoir être montée sur une lame flexible. Ce montage permet aux palpeurs de suivre la section minima de l'éprouvette dans ses déplacements au cours du cycle de sollicitation.

4.3. Machine d'essais et asservissement

La machine d'essai utilisée est une machine servo-hydraulique de capacité 100 kN conçue et réalisée par le CEAT. Un schéma de principe en est donné par la figure 18.

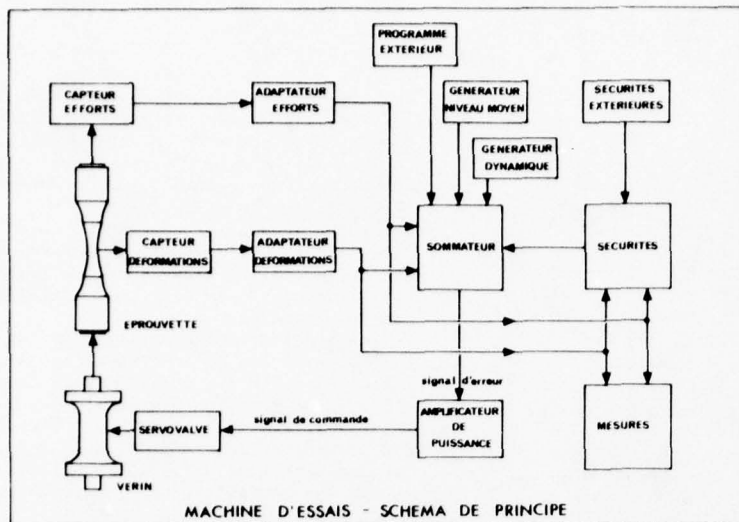


Fig. 18 Schéma de principe d'une machine de fatigue servo-hydraulique asservie

instant l'ordre fourni par le générateur de signal à la grandeur effective mesurée par le capteur de déformation équipé de son conditionneur.

Le servo amplificateur, lui-même surveillé par des modules de sécurité, émet alors un signal d'erreur qui est ensuite amplifié avant d'être envoyé sur le moteur d'entraînement du tiroir de la servovalve.

Les grandeurs effectives mesurées (variation de diamètre de la section minima de l'éprouvette et effort appliqué à cette éprouvette) sont également prélevées pour être enregistrées et éventuellement traitées par un calculateur.

4.4. Mesure de températures

La mesure directe de températures de surface élevées (jusqu'à 1000° C) est difficile à mettre en oeuvre. Les deux procédés les mieux adaptés sont la pyrométrie optique à radiations et le thermocouple.

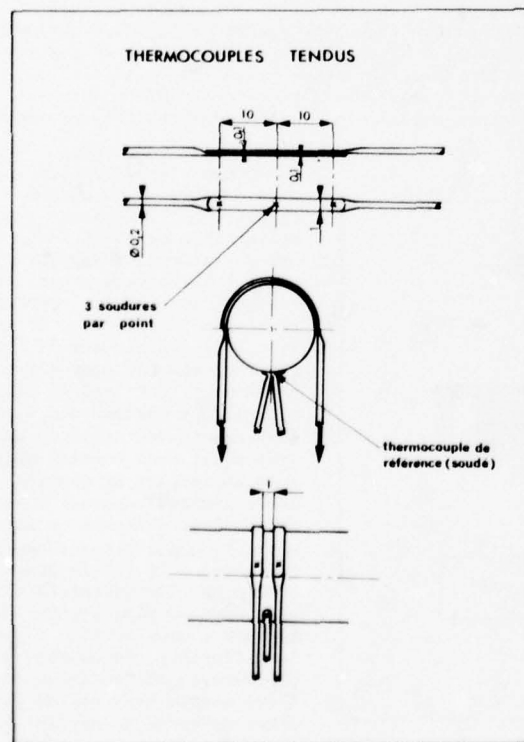


Fig. 19 Thermocouples

La sollicitation est générée par un vérin hydraulique et transmise à l'éprouvette, fixée par l'une de ses extrémités à la traverse du bâti de la machine et par l'autre extrémité à la tige du piston du vérin.

Cette sollicitation peut être pilotée suivant une loi quelconque appliquée soit :

- sur l'effort mesuré au niveau de l'éprouvette
- sur la déformation d'une base de référence constituée ici par le diamètre de la section minima de l'éprouvette
- sur le déplacement de la tige du piston du vérin.

Le mouvement du piston est commandé par le tiroir d'une servovalve qui détermine la section de passage offerte à l'huile et donc le débit admis dans la chambre du vérin. Ce débit est directement conditionné par la course, la vitesse et la fréquence du mouvement du piston. C'est donc l'ouverture du tiroir de la servovalve qui doit être asservie pour contrôler le paramètre de pilotage choisi (ici la déformation diamétrale de l'éprouvette).

Cet asservissement est effectué par un servo amplificateur qui compare à chaque

instant l'ordre fourni par le générateur de signal à la grandeur effective mesurée par le capteur de déformation équipé de son conditionneur.

Le servo amplificateur, lui-même surveillé par des modules de sécurité, émet alors un signal d'erreur qui est ensuite amplifié avant d'être envoyé sur le moteur d'entraînement du tiroir de la servovalve.

Les grandeurs effectives mesurées (variation de diamètre de la section minima de l'éprouvette et effort appliqué à cette éprouvette) sont également prélevées pour être enregistrées et éventuellement traitées par un calculateur.

Par rapport à un thermocouple de référence soudé, les écarts enregistrés avec un thermocouple tendu sont inférieurs à 1 % pour des températures allant de 400 à 1000° C.

4.5. Chauffage

Trois moyens de chauffage peuvent être utilisés pour réaliser des essais de fatigue à haute température : four, induction et effet Joule. Compte tenu de la dispersion couramment observée, aucun de ces trois moyens n'entraîne de différence significative sur les résultats d'essais de fatigue (Réf. 6).

Le choix de l'éprouvette d'essais (Cf. paragraphe 4.1), et notamment la possibilité de réaliser les essais avec une température homogène seulement sur une longueur faible de part et d'autre de la section minima, a conduit à éliminer deux des trois moyens de chauffage :

- le chauffage par four, car bien que l'existence courante de plusieurs zones de chauffe indépendantes permette d'obtenir une température homogène sur une longueur importante, l'accès à la partie utile de l'éprouvette est délicat pour la mesure de déformations diamétrales.
- le chauffage par induction car, bien que le gradient de température, très sensible à la forme et à la position de l'inducteur, puisse être nettement amélioré avec un enroulement à deux zones (Réf. 7), le capteur de déformations doit être de conception telle que l'élément actif soit le plus éloigné possible du champ induit à haute fréquence, ce qui ne garantit d'ailleurs pas l'absence de difficultés liées aux interactions possibles entre moyen de chauffage et capteur de déformations.

Le chauffage a donc été assuré par effet Joule. Dans ce cas, le gradient de température est uniquement fonction de la résistance de l'éprouvette, donc de sa géométrie, et présente ainsi les valeurs les plus faibles au voisinage de la section minima. Il peut être légèrement amélioré par un calorifugeage qui a également deux autres fonctions : limiter les échanges thermiques par rayonnement de l'éprouvette vers le capteur de déformations (cf. paragraphe 4.2.) et réduire les fluctuations de température autour de la valeur de consigne dues à des causes extérieures. L'allure du gradient de température obtenu, comparé à ceux obtenus avec les deux autres types de chauffage, est donnée par la figure 20.

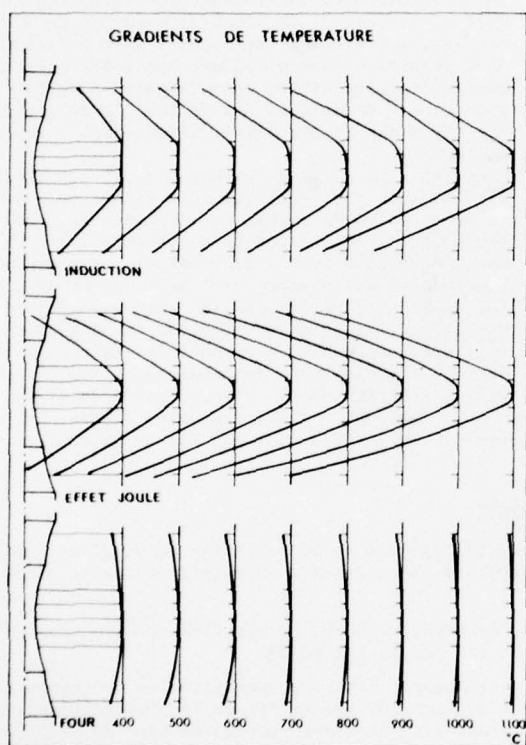


Fig. 20 Gradients de température

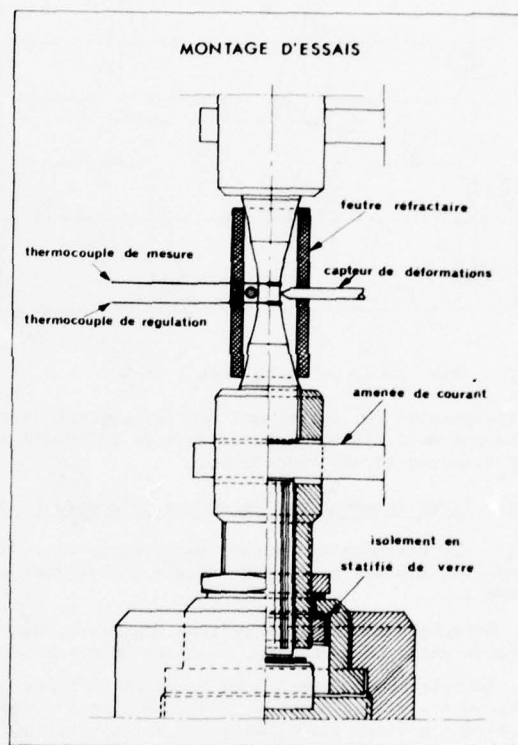


Fig. 21 Montage pour chauffage par effet Joule

La température étant fonction des dimensions de l'éprouvette, des variations de ces dimensions (entraînées par exemple par des variations de contraintes) provoquent des variations de température de même fréquence que la sollicitation mécanique. Toutefois, les moyens de régulation ayant une réponse suffisamment rapide, le phénomène se réduit à de faibles fluctuations autour de la valeur de consigne, généralement inférieures à 1%. L'ensemble du montage permettant le chauffage par effet Joule est montré sur la figure 21. Dans l'optique d'essais à température variable, ce moyen de chauffage est de plus le mieux adapté car étant capable de variations très rapides tant au chauffage qu'au refroidissement qu'il est possible d'accélérer par un jet d'air comprimé.

5. MISE EN ŒUVRE DE LA METHODE STRAINRANGE PARTITIONING

5.1. Forme des cycles de base :

La variation de diamètre de la section minimum de l'éprouvette est pilotée suivant les quatre cycles de base décrits sur la figure 22.

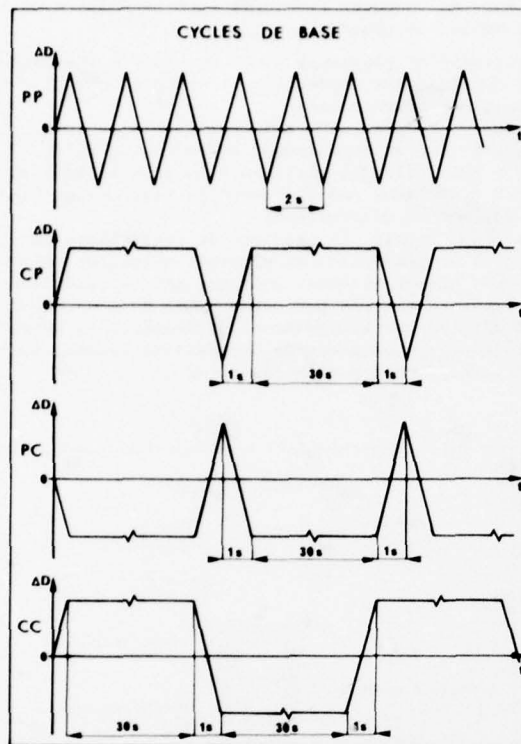


Fig. 22 Cycles de base

triangulaire PP, entraînant des relaxations de contrainte $\delta\sigma_t$ et $\delta\sigma_c$. La fréquence d'essais obtenue est de 0,016 Hz et la vitesse de déformation varie entre 0,2 et 1 %/sec. suivant les amplitudes de déformation totale recherchées.

5.2. Enregistrement des paramètres d'essais et dépouillement

Les paramètres d'essais enregistrés sont, d'une part, les valeurs de la variation de diamètre appliquée et, d'autre part, les valeurs de l'effort qui en résultent. Deux types d'enregistrement sont effectués :

1. Enregistrement, à intervalles réguliers, des boucles d'hystérésis effort - variation de diamètre. Pour chacun des cycles de base, l'allure de ces boucles est montrée par la figure 23.
2. Enregistrement continu en fonction du temps des deux paramètres : effort et variation de diamètre. Pour chacun des cycles de base, l'allure de ces enregistrements est montrée sur la figure 24. Les valeurs enregistrées n'étant pas directement celles utilisables pour l'établissement des courbes de base de la méthode SRP (contraintes ou déformations vraies appliquées au cours de chaque cycle, présentées sur la figure 25) il est nécessaire de procéder à un dépouillement à posteriori, à partir des valeurs relevées sur les boucles d'hystérésis (Fig. 26). Lorsque ces boucles ne correspondent pas exactement à la demi durée de vie des éprouvettes, les valeurs d'efforts et de variations de diamètre sont relevées sur les enregistrements en fonction du temps.

Deux remarques sont nécessaires concernant ce dépouillement :

1. Il suppose que la diminution des efforts, tant en traction qu'en compression et après relaxation s'il y a lieu, s'effectue suivant la droite élastique jusqu'à un effort nul.
2. Il est effectué en déformations diamétrales. En effet, le paramètre de pilotage étant la variation de diamètre de l'éprouvette, les paliers aux diamètres minimum et/ou maximum, s'ils entraînent effectivement un palier de la déformation diamétrale totale, n'entraînent pas un palier de la déformation longitudinale totale en raison de la relaxation des contraintes. Pour obtenir ce palier, il serait nécessaire, avec la méthodologie d'essais retenue, d'effectuer un calcul en temps réel pour piloter la machine d'essais par l'une quelconque des différentes composantes de la déformation longitudinale.

Cycle PP : Il est constitué par un signal triangulaire alterné de fréquence 0,5 Hz, suffisante pour ne pas laisser apparaître de phénomène de relaxation. La vitesse de déformation est constante au cours de chaque essai, identique pour chacune des phases de traction et de compression. La fréquence d'essais étant constante, cette vitesse varie évidemment en fonction de l'amplitude de déformation totale recherchée (variation entre 0,28 et 1,41 %/sec.).

Cycle CP : Un temps de maintien de 30 secondes est appliqué à la valeur maxima en traction du signal triangulaire précédent, entraînant une relaxation de contrainte $\delta\sigma_t$. La fréquence d'essais obtenue est de 0,031 Hz. Comme pour le cycle PP, la vitesse de déformation, constante au cours de chaque essai et identique pour chacune des phases de traction et de compression, varie en fonction de l'amplitude de déformation totale recherchée (variation entre 0,27 et 1 %/sec.). Le temps de maintien de 30 secondes a été choisi de façon à être suffisamment important pour entraîner une relaxation de contrainte appréciable et suffisamment faible pour ne pas conduire à des durées d'essais prohibitives devant les délais d'exécution à respecter.

Cycle PC : Le temps de maintien de 30 secondes est, dans ce cas, appliqué à la valeur maxima en compression du signal triangulaire PP, entraînant une relaxation de contrainte $\delta\sigma_c$ et une fréquence d'essais de 0,031 Hz. La vitesse de déformation varie entre 0,27 et 1 %/sec. suivant les amplitudes de déformation totale recherchées.

Cycle CC : Les temps de maintien de 30 secondes, appliqués séparément pour obtenir les cycles CP et PC, sont appliqués successivement aux valeurs maxima en traction et en compression du signal

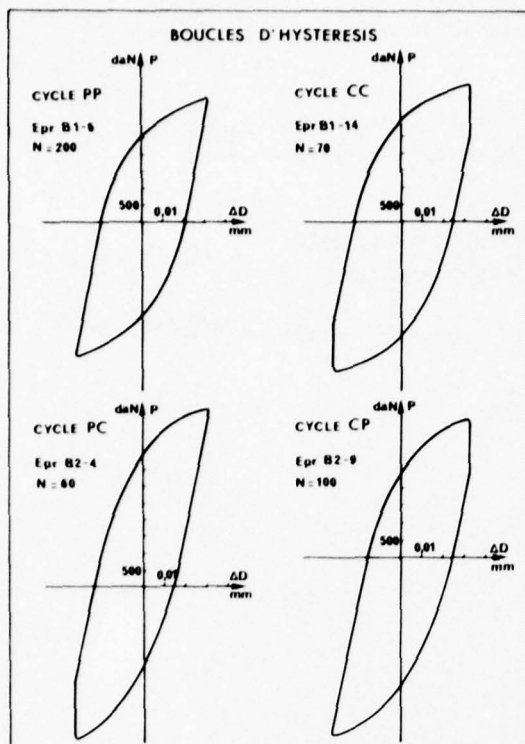


Fig. 23 Boucles d'hystérésis

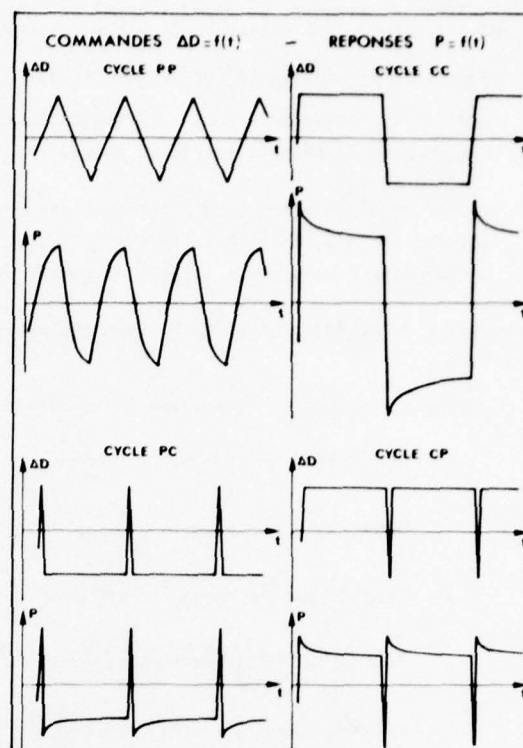


Fig. 24 Effort et variation de diamètre en fonction du temps

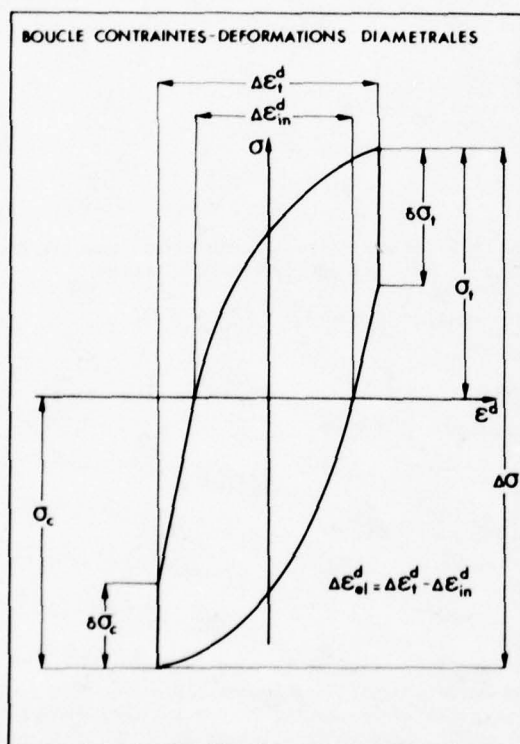


Fig. 25

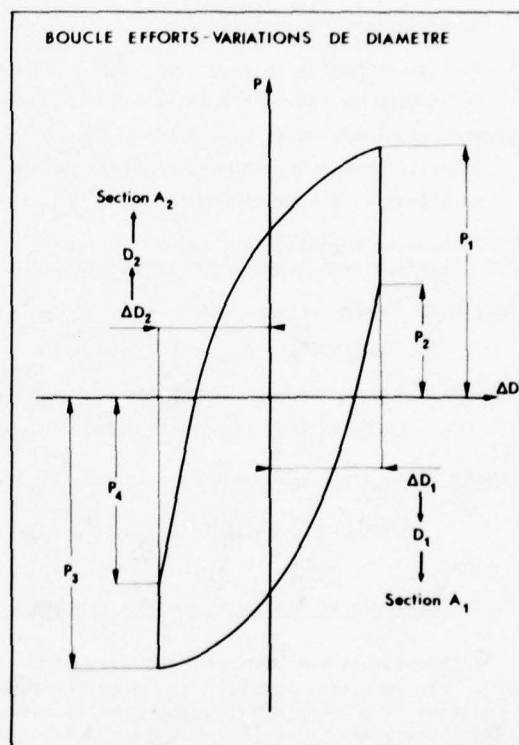


Fig. 26

Le schéma de principe du dépouillement des résultats d'essais en déformations diamétrales est donc le suivant (toutes les valeurs relevées sur les boucles sont considérées en valeur absolue) :

- Calcul de la déformation diamétrale totale $\Delta \epsilon_1^d$:

$$\begin{aligned} \text{déformation diamétrale totale en traction} &: (\epsilon_1^d)_1 = \left| \log(D_1/D_0) \right|, \text{ avec } D_1 = D_0 - \Delta D_1 \\ \text{déformation diamétrale totale en compression} &: (\epsilon_1^d)_2 = \left| \log(D_2/D_0) \right|, \text{ avec } D_2 = D_0 + \Delta D_2 \end{aligned} \quad \left. \vphantom{\begin{aligned} \text{déformation diamétrale totale en traction} \\ \text{déformation diamétrale totale en compression} \end{aligned}} \right\} \Delta \epsilon_1^d = (\epsilon_1^d)_1 + (\epsilon_1^d)_2$$

- Calcul de la déformation diamétrale élastique $\Delta \epsilon_{e1}^d$:

$$\begin{aligned} \text{déformation diamétrale élastique en traction} &: (\epsilon_e^d)_2 = \nu \sigma_2 / E, \text{ avec } \sigma_2 = P_2 / A_1 \\ \text{déformation diamétrale élastique en compression} &: (\epsilon_e^d)_4 = \nu \sigma_4 / E, \text{ avec } \sigma_4 = P_4 / A_2 \end{aligned} \quad \left. \vphantom{\begin{aligned} \text{déformation diamétrale élastique en traction} \\ \text{déformation diamétrale élastique en compression} \end{aligned}} \right\} \Delta \epsilon_{e1}^d = (\epsilon_e^d)_2 + (\epsilon_e^d)_4$$

- Calcul de la déformation diamétrale inélastique $\Delta \epsilon_{in}^d$: $\Delta \epsilon_{in}^d = \Delta \epsilon_1^d - \Delta \epsilon_{e1}^d$

- Décomposition de la déformation diamétrale inélastique :

$$\sigma_1 = P_1 / A_1 \longrightarrow (\epsilon_e^d)_1 = \nu \sigma_1 / E$$

$$\sigma_3 = P_3 / A_2 \longrightarrow (\epsilon_e^d)_3 = \nu \sigma_3 / E$$

$$\Delta \epsilon_{CC}^d = \inf \left\{ [(\epsilon_e^d)_1 - (\epsilon_e^d)_2], [(\epsilon_e^d)_3 - (\epsilon_e^d)_4] \right\}$$

$$\Delta \epsilon_{PP}^d = \Delta \epsilon_{in}^d - \sup \left\{ [(\epsilon_e^d)_1 - (\epsilon_e^d)_2], [(\epsilon_e^d)_3 - (\epsilon_e^d)_4] \right\}$$

$$\Delta \epsilon_{CP}^d = \left\{ [(\epsilon_e^d)_1 - (\epsilon_e^d)_2] - [(\epsilon_e^d)_3 - (\epsilon_e^d)_4] \right\} \text{ si } > 0$$

$$\Delta \epsilon_{PC}^d = \left\{ [(\epsilon_e^d)_3 - (\epsilon_e^d)_4] - [(\epsilon_e^d)_1 - (\epsilon_e^d)_2] \right\} \text{ si } > 0$$

- Détermination des contraintes :

Contrainte maxima en traction : $\sigma_1 = \sigma_1$

Relaxation de contrainte en traction : $\delta \sigma_1 = \sigma_1 - \sigma_2$

Contrainte maxima en compression : $\sigma_c = \sigma_3$

Relaxation de contrainte en compression : $\delta \sigma_c = \sigma_3 - \sigma_4$

Amplitude totale de contrainte : $\Delta \sigma = \sigma_1 + \sigma_c$

Ce schéma de dépouillement est valable pour les quatre types de sollicitation. En effet, pour le cycle CC, il s'applique intégralement tel que défini ci-dessus et pour les autres cycles il donne :

$$\begin{aligned} \text{Cycle PP} : P_1 = P_2 \text{ et } P_3 = P_4 &\longrightarrow \sigma_1 = \sigma_2 \text{ et } \sigma_3 = \sigma_4 \longrightarrow (\epsilon_e^d)_1 = (\epsilon_e^d)_2 \text{ et } (\epsilon_e^d)_3 = (\epsilon_e^d)_4 \\ \Delta \epsilon_{PP}^d &= \Delta \epsilon_{in}^d ; \Delta \epsilon_{CC}^d = \Delta \epsilon_{CP}^d = \Delta \epsilon_{PC}^d = 0 ; \delta \sigma_1 = \delta \sigma_c = 0 \end{aligned}$$

$$\begin{aligned} \text{Cycle CP} : P_3 = P_4 &\longrightarrow \sigma_3 = \sigma_4 \longrightarrow (\epsilon_e^d)_3 = (\epsilon_e^d)_4 \\ \Delta \epsilon_{CP}^d &= [(\epsilon_e^d)_1 - (\epsilon_e^d)_2] ; \Delta \epsilon_{PP}^d = \Delta \epsilon_{in}^d - \Delta \epsilon_{CP}^d ; \Delta \epsilon_{CC}^d = \Delta \epsilon_{PC}^d = 0 ; \delta \sigma_c = 0 \end{aligned}$$

$$\begin{aligned} \text{Cycle PC} : P_1 = P_2 &\longrightarrow \sigma_1 = \sigma_2 \longrightarrow (\epsilon_e^d)_1 = (\epsilon_e^d)_2 \\ \Delta \epsilon_{PC}^d &= [(\epsilon_e^d)_3 - (\epsilon_e^d)_4] ; \Delta \epsilon_{PP}^d = \Delta \epsilon_{in}^d - \Delta \epsilon_{PC}^d ; \Delta \epsilon_{CC}^d = \Delta \epsilon_{CP}^d = 0 ; \delta \sigma_1 = 0 \end{aligned}$$

5.3. Résultats et établissement des courbes de base

L'ensemble des résultats par éprouvette est donné par le tableau de la page suivante.

Les résultats obtenus avec le cycle PP permettent de déterminer directement les paramètres de la relation $(\Delta \epsilon_{in}^d)_{PP} = A(N_{PP})^B$ par la méthode des moindres carrés appliquée sur les coordonnées logarithmiques. On obtient ainsi $A = 0,332$ et $B = 0,689$ avec un coefficient de corrélation $R = 0,997$. Cette dernière valeur souligne la très faible dispersion des résultats d'essais obtenus avec ce cycle. La décomposition de la déformation inélastique ayant été réalisée pour l'ensemble des résultats obtenus avec les cycles PC, CP et CC, il est possible de déterminer les paramètres des relations $(\Delta \epsilon_{in}^d)_{ij} = A(N_{ij})^B$ correspondant à ces trois cycles. Il faut d'abord tenir compte, pour les cycles PC et CP, du dommage dû à la présence de la composante de type PP. Seules les composantes PP et PC (ou CP) étant présentes, les rapports f_{PP} et f_{PC} (ou f_{CP}) sont connus. La règle de dommage utilisée pour prévoir la durée de vie correspondant à la combinaison des composantes fondamentales, $1/N_{pr} = f_{PP}/N_{PP} + f_{PC}/N_{PC}$ (ou f_{CP}/N_{CP}), peut alors être utilisée par une procédure inverse.

Rep Epr	$\Delta \epsilon_t^d$ %	$\Delta \epsilon_{el}^d$ %	$\Delta \epsilon_{in}^d$ %	$\Delta \epsilon_{PP}^d$ %	$\Delta \epsilon_{PC}^d$ %	$\Delta \epsilon_{CP}^d$ %	$\Delta \epsilon_{CC}^d$ %	σ_t (MPa)	$\delta \sigma_t$ (MPa)	σ_c (MPa)	$\delta \sigma_c$ (MPa)	$\Delta \sigma$ (MPa)	N_f cycles
B1-19	0,571	0,261	0,310	0,310	-	-	-	628	-	667	-	1 295	1 109
B1-6	0,796	0,305	0,491	0,491	-	-	-	726	-	785	-	1 511	470
B1-9	0,981	0,350	0,631	0,631	-	-	-	835	-	899	-	1 734	303
B1-11	0,340	0,223	0,117	0,117	-	-	-	527	-	576	-	1 103	3 396
B1-10	1,410	0,390	1,020	1,020	-	-	-	930	-	1 004	-	1 934	142
B1-18	0,280	0,214	0,066	0,066	-	-	-	505	-	554	-	1 059	7 618
B1-2	0,607	0,290	0,317	0,279	0,038	-	-	887	-	739	187	1 626	305
B2-4	0,792	0,325	0,467	0,400	0,067	-	-	1 040	-	895	334	1 935	153
B1-16	1,006	0,332	0,674	0,594	0,080	-	-	1 072	-	973	397	2 045	135
B2-18	0,333	0,272	0,061	0,047	0,014	-	-	857	-	562	69	1 419	792
B2-6	0,270	0,259	0,011	0,005	0,006	-	-	806	-	509	29	1 315	1 076
B2-8	0,993	0,340	0,653	0,563	0,090	-	-	1 123	-	1 005	443	2 128	72
B1-12	0,601	0,241	0,360	0,318	-	0,042	-	609	206	795	-	1 404	384
B2-7	0,275	0,232	0,043	0,031	-	0,012	-	436	61	773	-	1 209	2 679
B2-1	0,994	0,322	0,672	0,588	-	0,084	-	909	415	1 102	-	2 011	160
B2-17	0,335	0,244	0,091	0,067	-	0,024	-	488	117	840	-	1 328	1 616
B2-9	0,801	0,307	0,494	0,427	-	0,067	-	824	334	1 030	-	1 854	210
B1-17	0,563	0,178	0,385	0,339	-	0,008	0,038	643	227	653	188	1 296	450
B1-20	0,999	0,224	0,775	0,695	-	0,005	0,075	914	395	963	371	1 877	136
B1-1	0,344	0,183	0,161	0,139	-	0,003	0,019	527	107	586	98	1 113	1 012
B1-14	0,796	0,220	0,576	0,517	-	0,004	0,055	804	294	854	275	1 658	192
B1-15	0,199	0,173	0,026	0,018	-	-	0,008	395	38	539	98	934	3 100

La valeur N_{Pr} est la durée de vie obtenue en essais, N_f , et il est donc possible de déduire la valeur N_{PC} (ou N_{CP}) de la relation précédente :

$$N_{PC} \text{ (ou } N_{CP}) = \frac{F_{PC} \text{ (ou } F_{CP})}{1/N_f - F_{PP}/N_{PP}}$$

Dans le cas du cycle CC, il faut également tenir compte du dommage dû à la présence de la composante PP mais aussi de celui dû à la présence d'une composante PC ou CP suivant qu'il existe une composante de fluage non compensée dans l'une ou l'autre des parties du cycles. On obtient ainsi :

$$N_{CC} = \frac{F_{CC}}{1/N_f - F_{PP}/N_{PP} - F_{PC}/N_{PC} \text{ (ou } F_{CP}/N_{CP})}$$

Les résultats obtenus sont regroupés dans le tableau ci-dessous :

Rep Epr	$\Delta \epsilon_{in}^d$ %	F_{PP}	F_{PC}	F_{CP}	F_{CC}	N_f	N_{PP}	N_{PC}	N_{CP}	N_{CC}
B1-2	0,317	0,881	0,119	-	-	305	853	53	-	-
B2-4	0,467	0,858	0,142	-	-	153	486	30	-	-
B1-16	0,674	0,881	0,119	-	-	135	285	28	-	-
B2-18	0,061	0,772	0,228	-	-	792	9 305	193	-	-
B2-6	0,011	0,454	0,546	-	-	1 076	114 423	590	-	-
B2-8	0,653	0,863	0,137	-	-	72	299	12	-	-
B1-12	0,360	0,884	-	0,116	-	384	711	-	85	-
B2-7	0,043	0,718	-	0,282	-	2 679	15 241	-	863	-
B2-1	0,672	0,875	-	0,125	-	160	287	-	39	-
B2-17	0,091	0,739	-	0,261	-	1 616	5 251	-	546	-
B2-9	0,494	0,864	-	0,136	-	210	448	-	48	-
B1-17	0,385	0,881	-	0,021	0,098	450	642	-	74	172
B1-20	0,775	0,897	-	0,006	0,097	136	233	-	31	29
B1-1	0,161	0,865	-	0,012	0,123	1 012	2 287	-	215	222
B1-14	0,576	0,897	-	0,007	0,096	192	358	-	45	38
B1-15	0,026	0,697	-	-	0,303	3 100	32 710	-	-	1 005

Ces résultats montrent qu'une des conditions de validité d'un résultat d'essai pour l'établissement d'une relation fondamentale d'endurance (Réf. 2-p 27), à savoir qu'il faut que la composante à laquelle on s'intéresse soit la composante dominante ($f_{ij} > 0,5$) n'est satisfaite que pour le cycle PP (f_{ij} toujours égal à 1). Dans les autres cas, et sauf pour une éprouvette (Epr. B2-6, cycle PC), les rapports f_{ij} varient entre 0,09 (Epr. B1-14, cycle CC) et 0,303 (Epr. B1-15, cycle CC). Par contre, si cette condition est appliquée sur les dommages (Réf. 2. p. 27), à savoir que la composante à laquelle on s'intéresse doit entraîner au moins la moitié du dommage total au cours d'un essai ($f_{ij} \times N_{ij} / N_{ij} > 0,5$), elle est alors vérifiée dans tous les cas, sauf pour trois éprouvettes essayées avec le cycle CC (Tableau ci-contre). Cependant une seule de ces trois éprouvettes a été éliminée pour la détermination de la relation $(\Delta \epsilon_{in}^d)_{CC} = A(N_{CC})^B$: il s'agit de l'éprouvette B1-17 ($f_{CC} \times N_{ij} / N_{CC} = 0,256$). Les deux autres éprouvettes ont été conservées, les valeurs obtenues ($f_{CC} \times N_{ij} / N_{CC} = 0,455$ et $0,485$) ayant été jugées acceptables. Les quatre relations fondamentales d'endurance de la méthode SRP ont ainsi pu être déterminées par la méthode des moindres carrés appliquée sur les coordonnées logarithmiques :

Rep. Epr.	$\frac{f_{PC}}{N_{PC}} N_{ij}$	Rep. Epr.	$\frac{f_{CP}}{N_{CP}} N_{ij}$	Rep. Epr.	$\frac{f_{CC}}{N_{CC}} N_{ij}$
B1-2	0,685	B1-12	0,524	B1-17	0,256
B2-4	0,724	B2-7	0,875	B1-20	0,455
B1-16	0,574	B2-1	0,513	B1-1	0,561
B2-18	0,936	B2-17	0,773	B1-14	0,485
B2-6	0,996	B2-9	0,595	B1-15	0,935
B2-8	0,822				

$$\text{Cycle PP : } (\Delta \epsilon_{in}^d)_{PP} = 0,332 (N_{PP})^{-0,689}$$

$$\text{Cycle PC : } (\Delta \epsilon_{in}^d)_{PC} = 0,195 (N_{PC})^{-1,123}$$

$$\text{Cycle CP : } (\Delta \epsilon_{in}^d)_{CP} = 0,131 (N_{CP})^{-0,819}$$

$$\text{Cycle CC : } (\Delta \epsilon_{in}^d)_{CC} = 0,184 (N_{CC})^{-0,929}$$

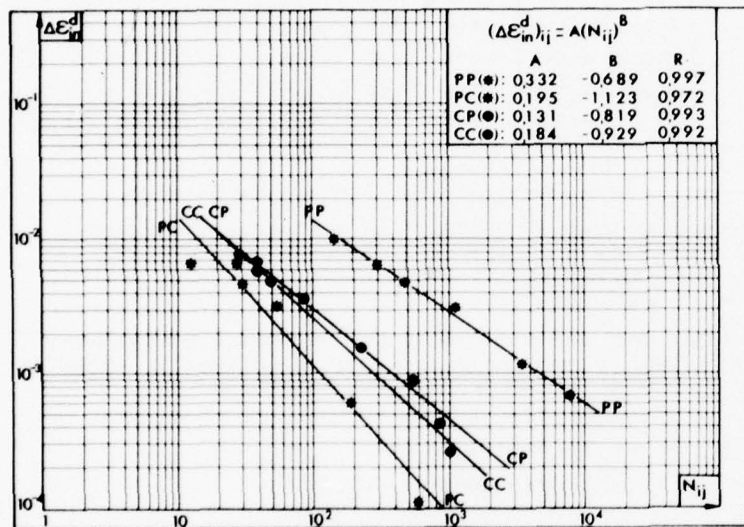


Fig. 27. Courbes de base

de déformations inélastiques, si le domaine de déformations inélastiques était entièrement de type PP la durée de vie maximum serait N_{PP} et si ce domaine était entièrement de type PC la durée de vie ne serait pas inférieure à N_{PC} . Pour des déformations diamétrales inélastiques supérieures à 2 %, les cycles PC, CP et CC conduisent à des durées de vie voisines, 3 à 5 fois inférieures à celles obtenues avec le cycle PP. Finalement, pour toute déformation inélastique, les limites inférieure et supérieure de la durée de vie peuvent être déterminées en faisant l'hypothèse que la durée de vie réelle doit être comprise entre la plus faible et la plus élevée des valeurs données par les relations liant l'endurance aux différents types de déformations.

5.4. Application à un cycle complexe

La démarche particulière préconisée par la méthode SRP pour la prévision des durées de vie en fatigue oligocyclique à haute température consiste, à partir d'une boucle d'hystérésis correspondant à un cycle de fonctionnement réel, à effectuer une décomposition du domaine de variation des déformations inélastiques en tenant compte des interactions fatigue-fluage.

Les coefficients de corrélation obtenus pour les différents cycles PP, PC, CP et CC, respectivement $R = 0,997 - 0,972 - 0,993$ et $0,992$ marquent la faible dispersion des résultats, et montrent qu'il est possible d'exprimer les relations fondamentales par des lois en puissance, autrement dit par des représentations linéaires de la déformation inélastique en fonction de l'endurance, en coordonnées logarithmiques. C'était là un des buts de l'évaluation de la méthode SRP, atteint ici dans le cas des déformations diamétrales. Les quatre droites obtenues sont tracées sur la figure 27. Dans le domaine de déformations diamétrales inélastiques allant de 0,01 à 1 %, la limite supérieure d'endurance est obtenue avec le cycle PP. La limite inférieure est obtenue avec le cycle PC. Les cycles CP et CC donnent, quant à eux, des durées de vie intermédiaires et voisines. En d'autres termes, considérant un point quelconque d'une structure ou d'une pièce, soumise à des sollicitations entraînant la présence

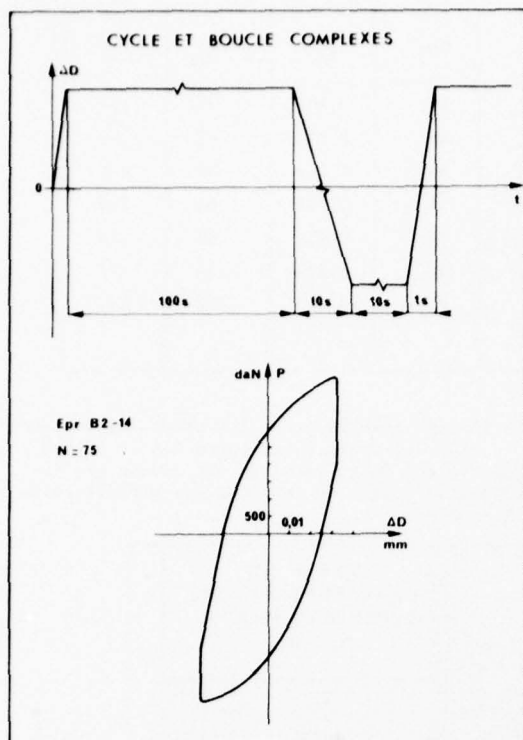
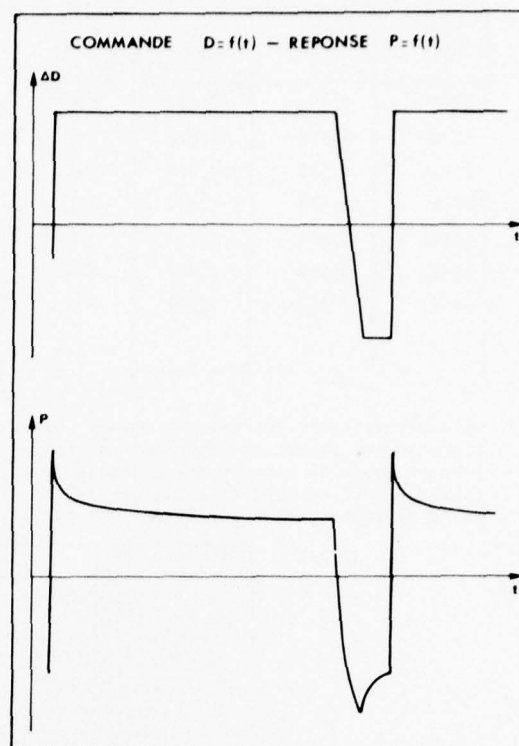


Fig. 28. Cycle et boucle complexes

Fig. 29. Commande $\Delta D=f(t)$ et réponse $P=f(t)$

Dans le but de pouvoir comparer aussi précisément que possible des résultats expérimentaux avec ceux résultant de prévisions de la méthode SRP, cette méthode a été appliquée à partir d'un cycle particulier de pilotage de la variation de diamètre des éprouvettes conduisant à une boucle d'hystérésis sur laquelle a été effectuée la décomposition (Fig. 28 et 29). Ce cycle est caractérisé par les différents éléments suivants :

- vitesses de déformation différentes en traction et en compression (rapport 10/1)
- temps de maintien différents aux valeurs maxima du cycle en traction et en compression (rapport 10/1).

Il conduit à une boucle comportant des composantes PP, CP et CC qui peuvent être déterminées par le schéma de dépouillement décrit au paragraphe 5.2.

Deux groupes d'essais ont été conduits, visant à des niveaux de déformations diamétrales totales de 0,6 et 0,8 %.

Ils donnent les résultats figurant dans le tableau ci-dessous.

Rep. Epr.	$\Delta \epsilon_t^d$ %	$\Delta \epsilon_{ol}^d$ %	$\Delta \epsilon_{in}^d$ %	$\Delta \epsilon_{PP}^d$ %	$\Delta \epsilon_{CP}^d$ %	$\Delta \epsilon_{CC}^d$ %	σ_t MPa	$\delta \sigma_t$ MPa	σ_c MPa	$\delta \sigma_c$ MPa	$\Delta \sigma$ MPa	N_t cycles
B2-3	0,788	0,214	0,574	0,469	0,045	0,060	912	392	965	298	1 877	140
B2-16	0,787	0,215	0,572	0,473	0,044	0,055	885	492	944	275	1 829	150
B2-14	0,791	0,219	0,572	0,473	0,040	0,059	903	490	965	294	1 868	152
B2-2	0,791	0,213	0,578	0,480	0,041	0,057	883	487	938	281	1 821	189
B2-11	0,597	0,214	0,383	0,306	0,033	0,044	785	383	874	216	1 659	210
B2-12	0,591	0,201	0,389	0,306	0,036	0,047	785	412	864	236	1 649	237
B1-21	0,596	0,194	0,402	0,342	0,025	0,035	671	298	762	173	1 433	351

Ces résultats permettent de déterminer d'une part, les différents rapports $F_{ij} = \Delta \epsilon_{ij}^d / \Delta \epsilon_{in}^d$ et d'autre part, les durées de vie $N_{ij} = [(\Delta \epsilon_{in}^d)_{ij} / A]^{1/B}$ qui sont déduites des relations fondamentales établies au paragraphe 5-3, pour aboutir aux prévisions de durée de vie $N_{pr} = 1 / [(F_{PP}/N_{PP}) + (F_{CP}/N_{CP}) + (F_{CC}/N_{CC})]$ (tableau ci-dessous).

Rep. Epr.	$\Delta \epsilon_{in}^d$	F_{PP}	N_{PP}	F_{CP}	N_{CP}	F_{CC}	N_{CC}	N_{pr}
B2-3	0,574	0,817	360	0,078	45	0,105	42	154
B2-16	0,572	0,827	362	0,077	46	0,096	42	160
B2-14	0,572	0,827	362	0,070	46	0,103	42	160
B2-2	0,578	0,830	357	0,071	45	0,099	41	158
B2-11	0,383	0,799	648	0,086	74	0,115	65	240
B2-12	0,389	0,787	634	0,093	73	0,121	64	227
B1-21	0,402	0,851	604	0,062	70	0,087	61	269

On constate alors, en calculant pour chaque éprouvette l'écart relatif entre les résultats des prévisions et les résultats expérimentaux : $|N_{pr} - N_f| / N_{pr}$, que cet écart varie entre 4,4 et 30,5 %, l'écart moyen se situant aux environs de 12,5 %. L'illustration de ce résultat est donnée par la figure 30, représentant les durées de vie réelles obtenues en essais en fonction des prévisions de durée de vie obtenues par la méthode Strainrange Partitioning.

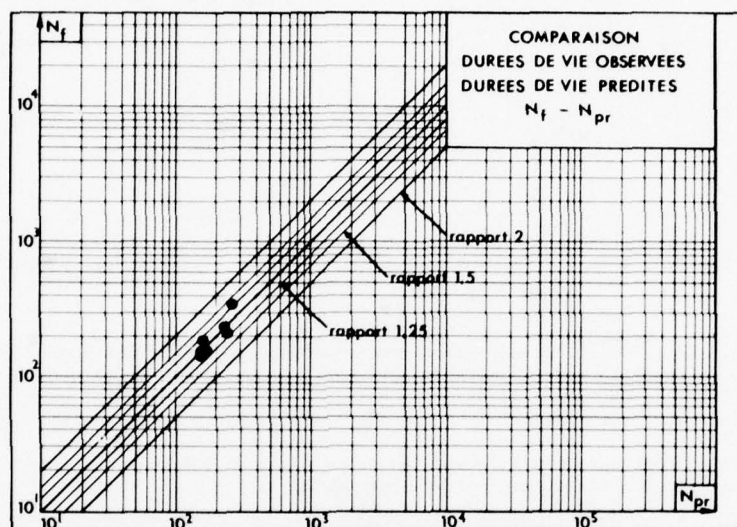


Fig. 30. Comparaison durées de vie réelles - durées de vie prévues

6. CONCLUSIONS

Après l'établissement des quatre relations fondamentales d'endurance relative à l'alliage base nickel Waspaloy, la méthode de décomposition a été appliquée à un cycle complexe, au sens où il entraîne la présence de trois des quatre composantes fondamentales, mais le plus simple possible dans sa définition, de manière à ne pas entraîner de difficultés particulières lors de sa mise en oeuvre.

Trois points essentiels sont à retenir de notre évaluation partielle de la méthode Strainrange Partitioning :

1. Elle a été effectuée sur les déformations diamétrales.
2. En ce qui concerne l'établissement des courbes de base et toujours à cause de la méthodologie d'essais utilisée (paliers de déformations, qu'elles soient diamétrales ou longitudinales), il semble difficile de retenir comme critère de validité d'un essai celui relatif à la composante dominante, qui n'est que rarement vérifié, contrairement à des essais conduits avec des paliers de contrainte entraînant des composantes importantes de type PC, CP ou CC. C'est donc le critère sur le dommage dominant qui a été retenu.
3. Dans le domaine relativement étroit où a été effectuée l'évaluation (deux niveaux de déformations diamétrales totales conduisant à des durées de vie faibles, de l'ordre de 150 à 250 cycles) la validité de la méthode Strainrange Partitioning est apparue comme excellente puisque les durées de vie réelles observées en essais et celles résultant des prévisions ne diffèrent que dans un rapport maximum de 1,30 (minimum 1,04) alors que la valeur couramment annoncée pour ce rapport, concernant cependant un domaine de durées de vie plus vaste, est de 2.

Deux remarques finales paraissent intéressantes à formuler. Elles concernent les deux aspects du programme coopératif qui n'ont pu être abordés par le C.E.A.T.

1. Les relations d'endurance définissent-elles réellement des limites à la durée de vie, notamment une limite supérieure avec un cycle type PP ?

Pour obtenir ce type de cycle à haute température, il est nécessaire que la fréquence d'essais soit suffisamment grande pour éviter l'apparition de déformations de fluage. Il est donc possible de définir une fréquence minima éliminant les effets de fluage, tous les essais de type PP étant conduits à une fréquence plus élevée. Mais n'y a-t-il pas également une borne supérieure à considérer sur la fréquence, puisque, généralement, une augmentation de la fréquence d'essais, pour une valeur donnée de déformation totale, augmente la déformation élastique et diminue la déformation plastique, ce qui peut entraîner une augmentation de la durée de vie (Réf. 8 et 9) ?

2. Les relations d'endurance sont-elles indépendantes de la température d'essais ?

Devant les différentes conclusions sur ce point, comme le montre les résultats obtenus au Cranfield Institute of Technology à l'occasion du présent programme coopératif, il semble indispensable de poursuivre ces études le plus loin possible.

Des essais classiques (effort ou déformations imposés), effectués au C.E.A.T. au cours d'autres études de caractérisation de matériaux à différentes températures, ont toujours montré, avec des cycles de type PP, une influence sensible de la température sur la durée de vie.

Cependant, certaines plages de températures, d'amplitude variables suivant les matériaux, peuvent peut-être être définies, dans lesquelles les relations d'endurance obtenues pour une température restent valables.

REFERENCES BIBLIOGRAPHIQUES

1. MANSON SS. HALFORD G.R. - HIRSCHBERG M.H. : Creep-Fatigue analysis by Strainrange Partitioning - Symposium on Design for Elevated Temperature Environment, ASME, 1971, pp 12-28 (NASA TM X - 67838, 1971).
2. HIRSCHBERG M.H. - HALFORD G.R. : Strainrange Partitioning . A tool for Characterizing High Temperature Low Cycle Fatigue - Fortieth Meeting of the AGARD Structures and Materials Panel, Brussels, Belgium, April 13-18, 1975 (NASA TM X - 71691, 1975).
3. SLOT T.- STENTZ R.H. - BERLING J.T. : Controlled Strain Testing Procedures - Manual on Low Cycle Fatigue Testing, ASTM STP 465, American Society for Testing and Materials, 1969, pp 100-128.
4. VIDAL G. - BERNARD J.L. : Fatigue oligocyclique et microfractographie de l'alliage de titane TA6V. Les mémoires scientifiques de la revue de métallurgie, N° 4 (1977) pp 249.260.
5. CARDEN A.E. : Thermal Fatigue evaluation - Manual on Low Cycle Fatigue Testing, ASTM STP 465, American Society for Testing and Materials, 1969, pp 163.188.
6. SAINT-SUPERY Y : Etude de l'influence du moyen de chauffage sur les résultats d'essais de fatigue à haute température. Rapport CEAT N° N4. 4619, 1978.
7. LORD D.C. - COFFIN L.F.Jr : High Temperature Materials Behavior. Manual on Low Cycle Fatigue Testing, ASTM STP 465, American Society for Testing and Materials, 1969, pp 129-148.
8. GUCER D.E - CAPA M. : Effect of loading frequency on the Strain behaviour and damage accumulation in low cycle fatigue. AGARD Report N° 572 (AGARD-R.572.70).
9. COFFIN L.F. Jr : The effect of frequency on the cyclic Strain and low cycle fatigue behaviour of Cast Udimet 500 at elevated temperature. Metallurgical Transactions, Vol 2, Nov 1971, pp 3105-3113.

CREEP-FATIGUE INTERACTION IN ALLOY IN738LC

by
M.F. Day and G.B. Thomas
Division of Materials Applications,
National Physical Laboratory,
Teddington, Middlesex, U.K.

SUMMARY

Low cycle fatigue test results on a cast Ni-Cr-base alloy IN738LC have shown that cycles containing tensile dwell periods have extended cyclic endurance. The results compared on total inelastic strain (hysteresis strain loop width) fall into two groups, HRSC and CCCR cycles, and BCCR and TCCR cycles. Strain range partitioning could not be successfully applied in its present form to the data produced.

Analysis of the data by the method proposed by Ostergren gave cyclic endurance predictions generally within a factor of ± 2 for all the types of test cycles employed at 750 and 850°C. Use of a simple fractional life approach using the pp and pc components to assess the fatigue contribution, and summed dwell times in tension to assess the creep contribution, has given predictions of similar accuracy.

Microstructural examination revealed typical fatigue failures in specimens tested with HRSC and CCCR cycles. In specimens tested with BCCR and TCCR cycles there was a tendency to intergranular creep damage which predominated at the higher strain ranges in TCCR tests.

1. INTRODUCTION

The results of a programme of Low Cycle Fatigue (LCF) testing on a cast Ni-Cr-base alloy IN738LC have been used to assess the Strain Range Partitioning approach (SRP) as a method for predicting LCF behaviour. The work has formed part of a cooperative AGARD project. Various types of testing wave forms, including some containing hold periods, have been employed in an attempt to determine the different strain components used in this analysis. The data have also been assessed by other predictive techniques.

2. MATERIAL

The alloy was supplied in the form of 76mm diameter cast stick which was subsequently cast into slightly oversize specimen blanks and plunge-ground to finished size* (see Footnote on p.10-4).

3. TEST EQUIPMENT AND TECHNIQUES

Furnaces, adaptors and extensometers were designed and manufactured for use in a 500kN MTS servo-hydraulic testing machine, and special function generators were obtained to produce the complex tension/compression wave forms required. Temperature control, including the gradient, was generally within $\pm 2^\circ\text{C}$ and was achieved with a 3-zone resistance furnace enclosing the specimen. Three thermocouples placed along the gauge length were used to measure the gradient, one of these being continuously monitored throughout the test duration. The principal test temperature was 850°C, but a few tests were carried out at 750°C.

Strain was measured axially by an extensometer similar in design to those used in creep tests. The extensometer was attached to the specimen (see Fig.1) on two machined ridges which defined the gauge length. MTS strain transducers on opposing sides of a specimen were attached to the lower end of the extensometer to enable the axiality to be checked. Creep properties required by one of the analyses employed were determined with the same type of specimen in the same equipment.

The four basic strain-controlled cycle wave forms identified by NASA as HRSC, CCCR, BCCR and TCCR are defined in Fig.2. All cycles with the exception of HRSC required load limitation in compression (CCCR), tension and compression (BCCR) or tension only (TCCR). Additionally, a few tests have been included involving either a tensile or compressive stress-relaxation hold for a fixed period of time at maximum tensile or compressive strain (cycle types THSC and CHSC also shown in Fig.2).

Cyclic frequencies were controlled by ramping rates which gave a strain rate of approximately 0.01s^{-1} . Thus, with the controlled strain ranges employed, the frequencies (ignoring hold periods) were 0.25 Hz or greater. Some preliminary checking of hysteresis loop behaviour for the cycles immediately following shake-down showed little detectable decrease in loop width at frequencies greater than this.

In the majority of the strain-controlled tests the period between crack initiation (detected from hysteresis loop behaviour) and failure occupied as much as 50% of total life. The rate of decay of the tensile load in this period was therefore very slow, and as a result failure was assumed to have occurred at the number of cycles at which the load had fallen to approximately 30% of the initial tensile level. Subsequent examination of these specimens showed that in the majority of cases a crack had proceeded across the section to an extent commensurate with the reduction in load.

A few tests with cycles either of sawtooth form or with fixed-time tension-hold periods are included in the analysis of the data by techniques other than SRP. These tests were cycled between equal tensile and compressive loads, but at a slower frequency (ignoring hold periods) of approximately 0.1 Hz.

4. RESULTS

Results for the four basic test cycles to determine the pp, pc, cc and cp hysteresis components used in strain range partitioning are given in Table 1. A graphical presentation of the total inelastic

strain (ϵ_{in}) against endurance is shown in Figs. 3a-d for the different cycles. Included on these diagrams are additional results of tests at 750°C or for other cycle forms.

5. METALLOGRAPHIC EXAMINATION

A longitudinal section from each specimen was polished mechanically and then etched at 1.5v in an aqueous solution comprising 10% nitric and 5% glacial acetic acids. The sections were examined by optical microscopy, and assessments of the damage in the specimen were made to establish the predominant mode of failure.

(a) General observations

The alloy exhibited a typical cast structure of relatively coarse grain size (average linear intercept 0.75mm). The highly irregular and convoluted grain boundaries reflected the dendritic nature of the grains. The spacing between the secondary dendrite arms was typically 0.1mm. Regions of the eutectic $\gamma - \gamma'$ were common, and in many cases features that were associated with them gave the appearance of sharp cracks at low magnification but, at sufficiently high magnification, these could be resolved as acicular particles. Carbide particles were well distributed and predominantly of an angular, chunky morphology. Porosity was generally uniformly distributed; on average 5-6 pores, typically 0.05mm diameter, were observed per mm² of polished section, although larger pores and clusters of pores were occasionally observed.

(b) Failure modes

(i) HRSC tests Failure resulted from the growth of transgranular fatigue cracks originating from the specimen surface as in Fig. 4. However, in the specimen tested at the highest total strain range (ϵ_t) of $\pm 1.0\%$ a significant amount of bulk damage in the interior of the specimen was also observed. The nature of this damage was similar to that observed in a specimen fractured in a tensile test at 850°C, see Fig. 5 for example, and included cracking from pores, short intergranular cracks and cracked carbides.

(ii) CCCR tests The introduction of compressive creep dwells did not markedly change the nature of the damage, apart from a tendency for the fatigue cracks to propagate along a mixed trans- and intergranular path. Again, the test at $\pm 1.0\% \epsilon_t$ showed bulk damage similar to that described above in addition to fatigue cracks.

(iii) BCCR tests At the two lower strain ranges, although creep dwell periods were introduced in both tension and compression the major cracks still originated at the specimen surface. The specimen tested at the lowest strain range, $\pm 0.35\% \epsilon_t$, exhibited transgranular fatigue cracks while in that tested at $\pm 0.5\% \epsilon_t$ the cracking was intergranular. However, at the higher strain range of $\pm 0.65\% \epsilon_t$ bulk damage of a creep or tensile nature became evident. At $\pm 1.0\% \epsilon_t$ some bulk damage was seen but premature failure could have resulted from a large cluster of pores observed at the fracture.

(iv) TCCR tests At the lower strain ranges the introduction of dwell periods in tension only did not change the predominance of typical fatigue damage, although some intergranular bulk damage was also evident. However, at the higher strain levels of $\pm 0.65\%$ and $\pm 1.0\% \epsilon_t$ (and also in the test with stress relaxation dwells at $\pm 0.5\% \epsilon_t$) the predominant form of damage in the specimens was intergranular, typical of that observed in specimens monotonically tested at comparable creep stresses (Fig. 6).

6. ANALYSIS OF DATA

(a) Strain range partitioning

In spite of the limited quantity of data at 750°C, it can be seen in Fig. 3a that endurance of tests with pp loops do not share a common relationship with those at 850°C. It would, therefore, be incorrect to assume that in this alloy there is no effect of temperature per se on endurance.

Attempts to derive partitioned strain relationships proved impossible using the expression

$$\frac{F_{pp}}{N_{pp}} + \left(\frac{F_{cp}}{N_{cp}} \text{ or } \frac{F_{pc}}{N_{pc}} \right) + \frac{F_{cc}}{N_{cc}} = \frac{1}{N_{obs}}$$

where F is the strain fraction corresponding to the appropriate loop component indicated by the suffix, N is the corresponding endurance and N_{obs} is the endurance for a cycle containing a mixture of strain components. This can be seen in Table 2, where negative values for the derived endurance were obtained in many cases. These negative values were in the main associated with tests where the partitioned strain required was less than 50% of the total strain range (ϵ_{in}), or where less than 50% of the damage was produced by the strain component of interest (i.e. damage $0 = F_{cp}/N_{cp} \times N_{obs} < 0.5$).

In order to meet these validity requirements in circumstances where the introduction of cp or cc components result in significantly increased endurance, the pp fraction has to be reduced to very low levels which are experimentally difficult to achieve. In some cases it would have been necessary to have $F_{pp} < 0.1$ to 0.2 to fulfil the latter criterion for the present alloy. As the creep resistance is so high, extremely long cycle times would have been required, or the temperature raised to a level considerably higher than that of the service conditions, particularly at lower ϵ_{in} levels. Another feature observed in the basic testing cycles TCCR, CCCR, and BCCR was the very rapid shortening of cycle times after the first 2 to 3 cycles, which necessitated a lowering of the stress levels to obtain hold periods of reasonable magnitude.

The ductility of the alloy was greater in creep than in tensile testing. Reduction of area was 4% in tensile tests, and ranged from 20 down to 8% in creep for times of 3 and 180 hours. An attempt was made, therefore, to employ the ductility - normalised SRP method, which gave some predictions of as little as 10% of the actual endurance.

A comparison of the total inelastic strain (ϵ_{in}) for the four basic types of test loops is shown in Fig.7. It can be seen that they fall into two groups. Those containing only pp and pc components having shorter cyclic endurance than those containing cp and cc components. For this material, therefore, it would appear that for equal inelastic strain ranges the introduction of a tension hold period extended the life. The principal controlling factor appeared to be the type of strain produced in the tensile part of the cycle which was associated with the tensile stress levels; these were considerably higher for those containing only pp or pc components.

(b) Ostergren's Analysis

Ostergren² has postulated that the basic Coffin-Manson equation will provide a correlation for various types of LCF data with different wave forms including hold periods, if account is taken of tensile stress levels. In the present work unbalanced stress loops containing cp and pc components resulted in cycles with higher stresses in the opposite direction to that containing the creep period. The stress levels of the tests which illustrate this are given in Table 3. Ostergren proposed a basic equation

$$\sigma_T \Delta \epsilon_p N_f^\beta = c$$

where σ_T is the tensile stress,

$\Delta \epsilon_p$ is the total inelastic strain

N_f is the number of cycles to failure, and

β and c are constants.

He found that for some materials a frequency term must be added but this was not found necessary for the present alloy. All the data generated in the present work are shown in Fig.8 using this expression. Included also are results of some load-controlled tests, some of which contained 5 min hold periods in tension. The results for these tests tend to lie toward the lower bound of the ± 2 scatter band, which may be explained by the fact that they were not closed loop cycles with a net tensile strain being produced. Nevertheless, the expression has produced a reasonable fit to many different types of test cycle results, with only 4 results out of 27 lying markedly outside the ± 2 scatter band.

(c) Fractional Life

The earliest attempts to predict the life when complex cycles contained creep and fatigue components assumed that failure would occur when the fractions of life which could be ascribed to each of these components added up to unity. This gives the expression

$$\frac{N}{N_f} + \frac{t}{t_r} = 1$$

where N_f is the number of cycles to failure for a constantly cycled stress or load range,

N is the number of cycles to failure for a specific combination of stress range and hold periods,

t_r is the rupture time of a normal creep test at the stress conditions prevailing during the hold period,

and t is the summed hold time.

This analysis requires creep data, whereas these are not needed in SRP analysis, but creep data are available for most high temperature materials.

In the present programme some modifying assumptions have been made to use this approach to the data produced by the cycles employed for SRP. These are:-

(i) pp loop tests These provide the data giving N_f , so that this is determined on a strain loop width basis and not on the stress range.

(ii) cp loop tests The ϵ_{pp} component provides the N/N_f term. The time at the tension hold stress compared with creep data provides the t/t_r term. Where hold periods are at constant strain resulting in stress-relaxation the effective stress has been taken as

$$\sigma_{eff} = \frac{\sigma_1 - \sigma_2}{3} + \sigma_2$$

where σ_1 is the stress at the beginning of the hold period

and σ_2 is the stress at the end of the hold period.

(iii) pc loop tests The whole hysteresis strain width is assumed to be ϵ_{pp} . This presupposes that compressive creep has very little effect, and is accounted for by the increased stress in tension resulting from it.

(iv) cc loop tests The ϵ_{pp} component is determined, giving N_f , and only the time in tension hold

period considered. Again it is assumed that there is no effect of compressive hold periods beyond the consequent longer tensile hold times.

All of these components have been determined at $N/2$ as in the SRP analysis. Also the tests which are included in this analysis, which were cycled with load control, were assessed for N_f by the ϵ_{pp} component.

A comparison of predicted and actual endurance using this approach is shown in Fig.9. Only 4 test points out of 20 lie markedly outside a ± 2 scatter band, and a factor of ± 3 would include all results.

For the pp, pc and cc tests, the metallographic evidence is broadly consistent with the above assumptions. However, the creep life fraction in the cp tests is generally much less than would be expected from the levels of creep damage seen in the fractured specimens.

7. CONCLUSIONS

(a) Application of the SRP analysis has not been possible for the test data produced for the IN738LC alloy. This material has exhibited unusual behaviour in that the introduction of tensile hold periods resulted in longer endurance for equal ϵ_{in} ranges. Consequently, it is very difficult to meet validity requirements for the generation of basic data for SRP analysis.

(b) Use of two alternative analyses, one proposed by Ostergren and the other a modified fractional life approach, both of which are suitable for the present data, have provided reasonable correlations for the various test cycle results.

(c) Metallographic examination of fractured specimens has shown that failure is dictated by fatigue for tests with sawtooth cycling, compressive hold periods, and for tests with tensile hold periods at the lower strain ranges. Grain boundary damage predominated in tests with tensile hold periods where controlled strains were $\pm 0.65\%$ or greater.

REFERENCES

1. HALFORD, G.R., SALTSMAN, J.F. and HIRSCHBERG, M.H. Ductility normalized-strain range partitioning life relations for creep-fatigue predictions. NASA Technical Memorandum NASA TM-73737.
2. OSTERGREN, W.J. A damage function and associated failure equations for predicting hold time and frequency effects in elevated temperature low cycle fatigue. Journal Testing and Evaluation, Vol.14, No.5., Sept.1976, pp 327-339.

* Chemical compositions, material processing, heat treatments and mechanical properties for each tested alloy, as well as the data generated in the programme, are given in Appendix A 1.

Table 1

Strain Range Components at Half Life ($N/2$)

Loop Type	Temp. °C	Control $\pm \epsilon_t$ (%)	Load Limits (N/mm ²)	Strain Range Components at $N/2$ (%)				Cycles to failure
				PP	CP	PC	CC	
HRGC	850	0.35	-	0.032	-	-	-	6178
HRSC	850	0.5	-	0.08	-	-	-	475 ⁺
HRSC	850	0.65	-	0.257	-	-	-	160
HRSC	850	1.0	-	0.845	-	-	-	19
HRSC	750	0.35	-	0.011	-	-	-	13100
HRSC	750	0.5	-	0.078	-	-	-	282
TCCR	850	0.35	+190	0.087	0.047	-	-	2099 ⁺
TCCR	850	0.5	+300	0.113	0.084	-	-	1056 ⁺
TCCR	850	0.65	+350	0.20	0.21	-	-	92 ⁺
TCCR	850	1.0	+450	0.285	0.875	-	-	25
THSC	850	0.5*	-	0.171	0.107	-	-	625
THSC	850	0.5*	-	0.170	0.10	-	-	610
CCCR	850	0.35	-300	0.036	-	0.021	-	1259 ⁺
CCCR	850	0.5	-400	0.17	-	0.10	-	228 ⁺
CCCR	850	0.65	-400	0.25	-	0.17	-	210 ⁺
CCCR	850	1.0	-500	0.43	-	0.80	-	15
CHSC	850	0.5 ^x	-	0.15	-	0.121	-	36
BCCR	850	0.35	± 350	0.032	-	-	0.136	2214
BCCR	850	0.5	± 400	0.12	-	-	0.29	147
BCCR	850	0.65	± 450	0.231	-	-	0.343	74
BCCR	850	1.0	± 550	0.20	-	-	1.145	3.5
BCCR	750	0.5	± 575	0.071	-	-	0.064	500

* - 5 min hold periods at max^m tensile strain.

x - 5 min hold periods at max^m compressive strain.

+ - Failure taken as cycles at which the maximum tensile stress <30% of initial level.

Table 2

Derived Values of N_{cp} , N_{pc} , and N_{cc}

For TCCR (pp + cp loop) test cycle wave forms:-

$$N_{cp} = \frac{F_{cp}}{\frac{1}{N_{obs}} - \frac{F_{pp}}{N_{pp}}}$$

Control ϵ (%)	ϵ_{in} (%)	F_{pp}	N_{pp} (cycles)	F_{cp}	N_{obs} (cycles)	Derived N_{cp} (cycles)
± 0.35	0.134	0.649	400	0.351	2099	-306.2
± 0.5	0.197	0.574	200	0.426	1056	-222
± 0.65	0.41	0.488	58	0.512	92	+218.9
± 1.0	1.16	0.246	9.5	0.754	25	+ 53.9

For CCCR (pp + pc loop) test cycle wave forms:-

$$N_{pc} = \frac{F_{pc}}{\frac{1}{N_{obs}} - \frac{F_{pp}}{N_{pp}}}$$

Control ϵ (%)	ϵ_{in} (%)	F_{pp}	N_{pp} (cycles)	F_{pc}	N_{obs} (cycles)	Derived N_{pc} (cycles)
± 0.35	0.057	0.632	1700	0.368	1259	+872
± 0.5	0.27	0.630	115	0.370	228	-34.0
± 0.65	0.42	0.595	54	0.405	210	- 64.6
± 1.0	1.23	0.350	8.5	0.650	15	+ 25.5

For BCCR (pp + cc loop) test cycle wave forms:-

$$N_{cc} = \frac{F_{cc}}{\frac{1}{N_{obs}} - \frac{F_{pp}}{N_{pp}}}$$

Control ϵ (%)	ϵ_{in} (%)	F_{pp}	N_{pp} (cycles)	F_{cc}	N_{obs} (cycles)	Derived N_{cc} (cycles)
± 0.35	0.168	0.19	260	0.810	2214	-2723
± 0.5	0.41	0.293	58	0.707	147	+ 449
± 0.65	0.574	0.402	32	0.598	74	+ 639
± 1.0	1.345	0.147	7.5	0.851	3.5	+ 3.2

Table 3

Cycle Stress Limits at Half Life ($N/2$)

Testing Wave forms	Temp. (°C)	Control ϵ (%)	$\Delta\sigma$ (N/mm ²)	σ_T (N/mm ²)
HRSC	850	± 0.35	885	343
HRSC	850	± 0.5	1075	427
HRSC	850	± 0.65	1577	751
HRSC	850	± 1.0	1808	892
HRSC	750	± 0.35	982	410
HRSC	750	± 0.5	1485	691
TCCR	850	± 0.35	830	190
TCCR	850	± 0.5	1010	300
TCCR	850	± 0.65	1196	350
TCCR	850	± 1.0	1408	450
THSC	850	± 0.5	1043	294
THSC	850	± 0.5	1013	279
CCCR	850	± 0.35	775	455
CCCR	850	± 0.5	1090	690
CCCR	850	± 0.65	1131	731
CCCR	850	± 1.0	1430	930
CHSC	850	± 0.5	1181	773
BCCR	850	± 0.35	700	350
BCCR	850	± 0.5	800	400
BCCR	850	± 0.65	900	450
BCCR	850	± 1.0	1100	550
BCCR	750	± 0.5	1154	533

 $\Delta\sigma$ = Total stress range. σ_T = Maximum tensile stress.

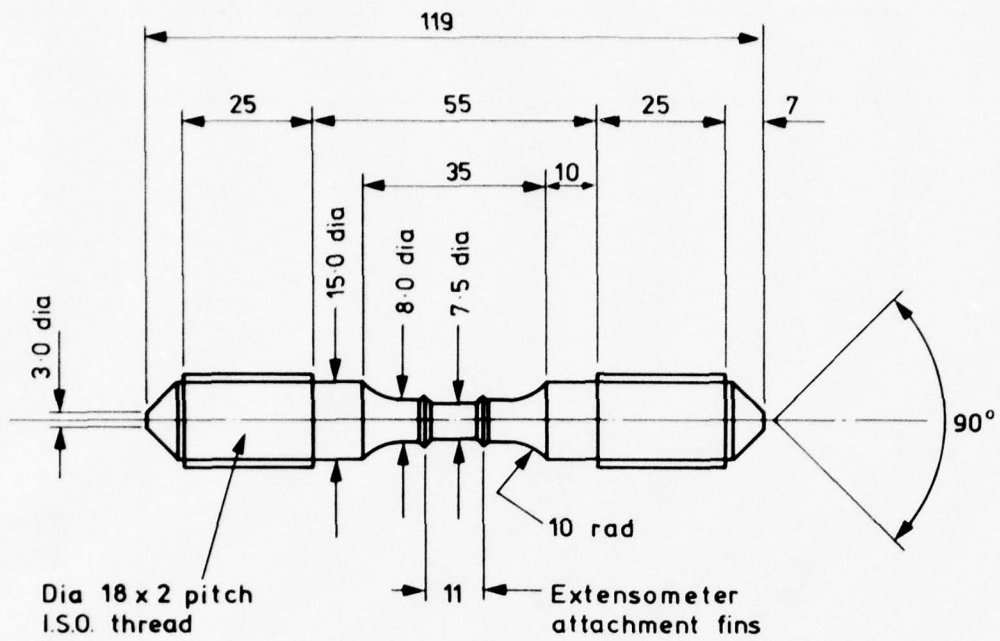


FIG.1 HIGH STRAIN FATIGUE TESTPIECE

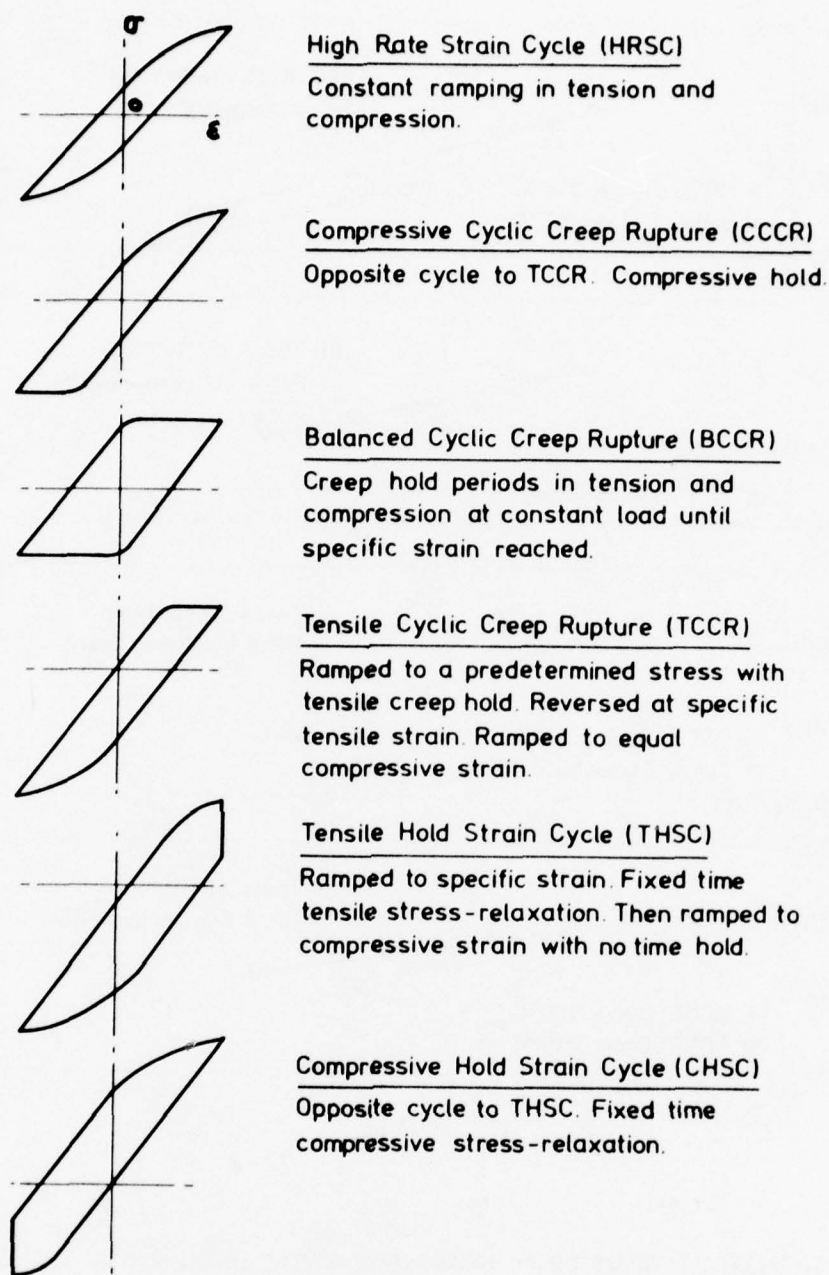


FIG. 2 CYCLIC WAVEFORMS

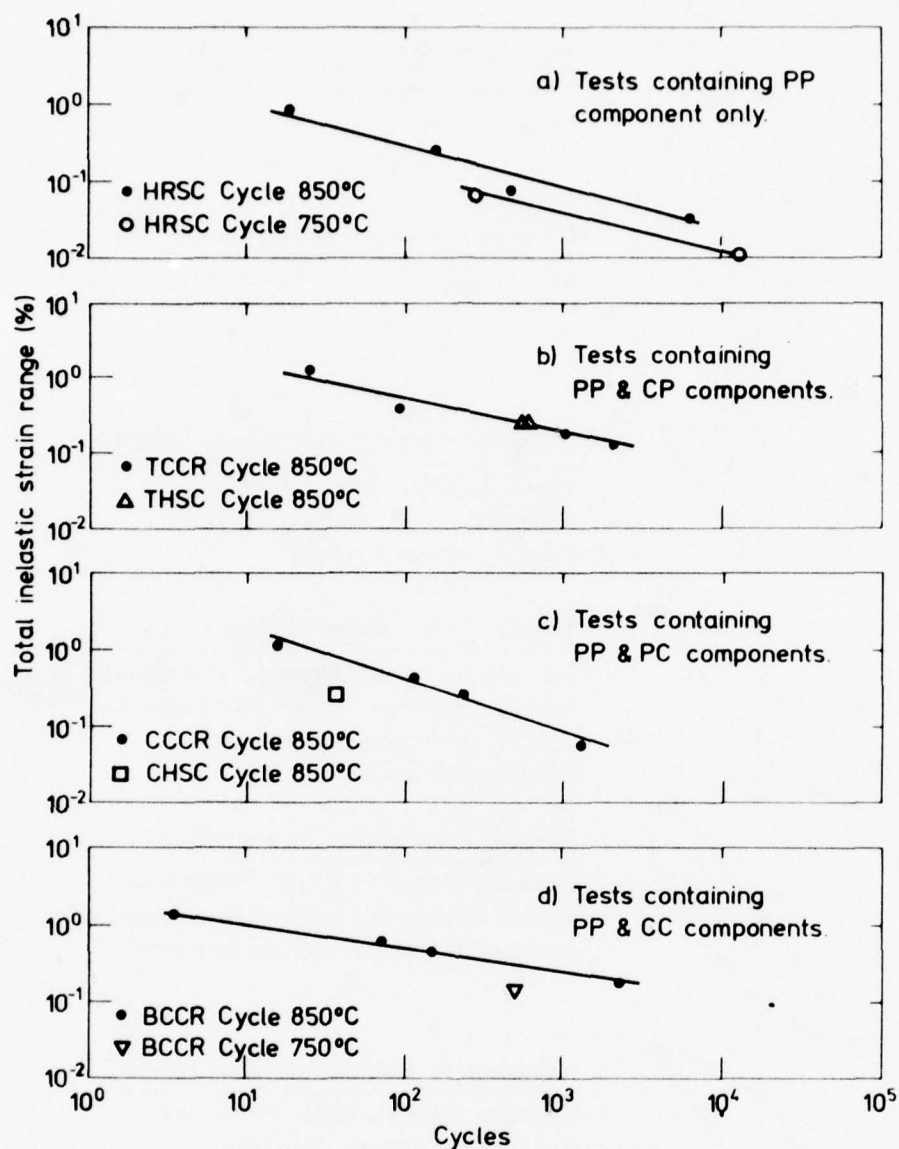


FIG. 3.

TOTAL HYSTERESIS LOOP WIDTHS FOR TESTS ON IN 738 LC ALLOY.

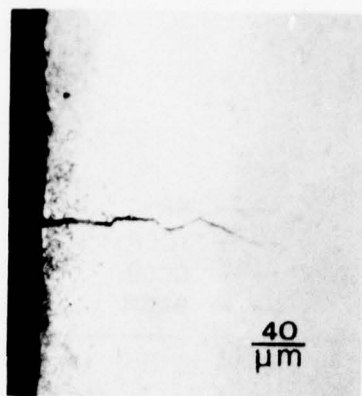


Fig.4
Transgranular fatigue crack in a specimen tested in HRSC at $\pm 0.65\% \epsilon_t$ at 850°C.

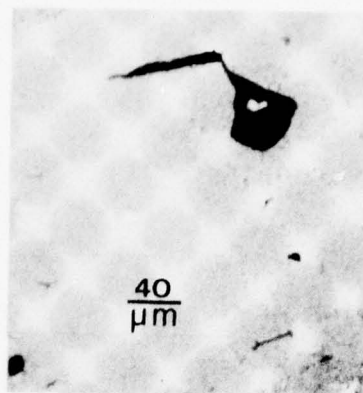


Fig.5
Cracking from pore and cracked carbides in a specimen fractured in a tensile test at 850°C.

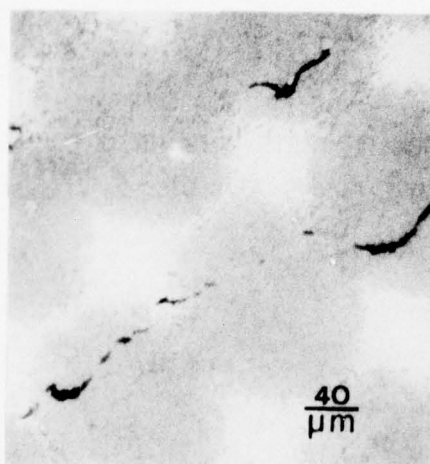


Fig.6
Intergranular damage in a specimen crept to fracture at 450 N/mm² and 850°C.

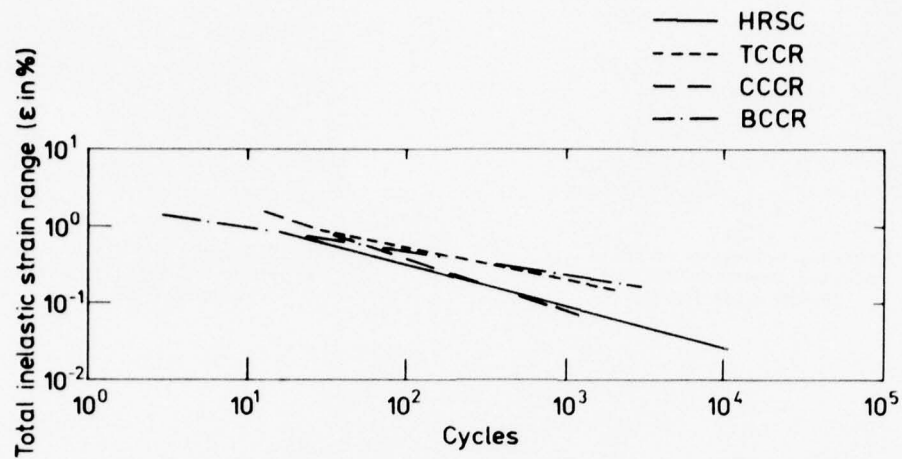


FIG. 7 COMPARISON OF TESTS WITH HRSC, TCCR, CCCR AND BCCR CYCLIC WAVE FORMS AT 850°C.

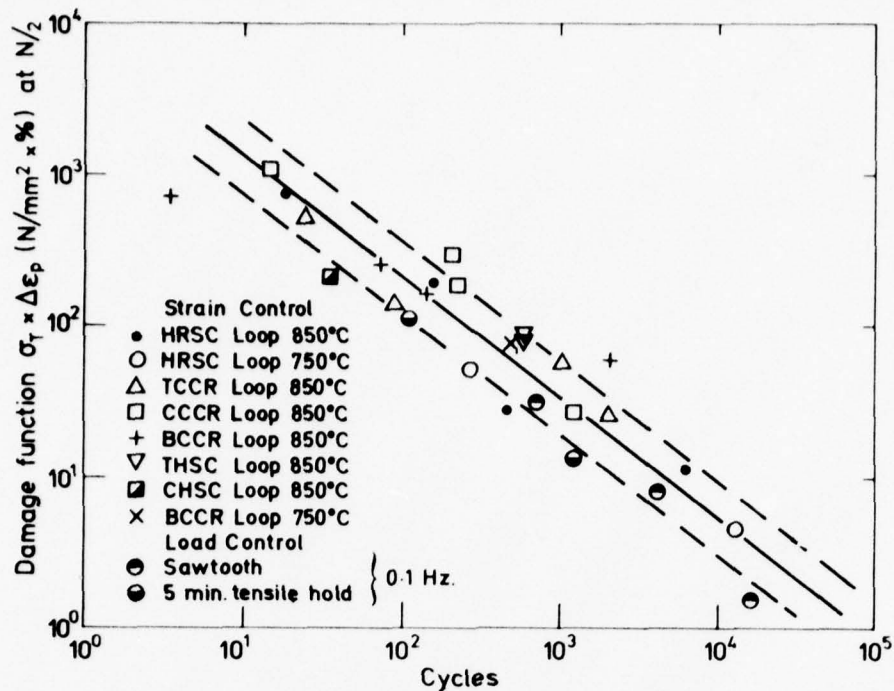


FIG. 8 OSTERGREN'S DAMAGE FUNCTION FOR VARIOUS CYCLE TYPES AGAINST ENDURANCE.

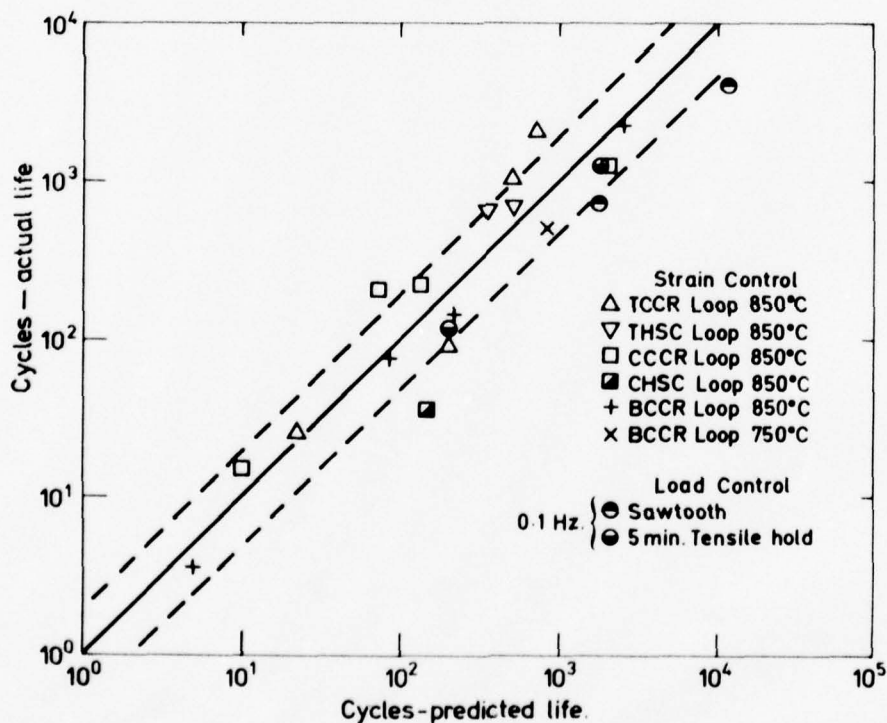


FIG. 9 LIFE PREDICTION BY MODIFIED FRACTIONAL EQUATION

AN ANALYSIS OF THE LOW CYCLE FATIGUE BEHAVIOR OF THE SUPERALLOY RENE 95 BY STRAINRANGE PARTITIONING

by

Capt Jack M. Hyzak
Metallurgist
Air Force Materials Laboratory (LLN)
Wright-Patterson Air Force Base
Dayton, Ohio 45433 U.S.A.

and

Henry L. Bernstein
Research Engineer
Systems Research Laboratories
Dayton, Ohio 45440 U.S.A.

SUMMARY

The applicability of Strainrange Partitioning (SRP) for predicting the low cycle fatigue (LCF) behavior of the superalloy Rene 95 at 922K (1200°F) is addressed. A three phase test plan is described which consists of baseline strain control testing, cyclic creep tests utilizing load control to strain limits, and validation testing comprised of less conventional waveforms. The data indicate that compressive strain hold cycles are more damaging than tensile strain hold cycles. It is also shown that the LCF behavior of this alloy depends largely on the time in tension per cycle and on the value of the maximum tensile stress which develops large biases during strain hold testing. SRP was not able to predict life within a factor of two for strain hold tests that generated the largest changes in the value of the maximum tensile stress compared to time independent behavior.

1.0 INTRODUCTION

A major area of concern in the development of recent military turbine engines has been life cycle management. A part of the technology needed to optimize the life of components, such as turbine disks, is the ability to accurately predict their crack initiation lives under typical cyclic conditions. With the increasing turbine temperatures that accompany performance gains, the turbine section operating conditions are becoming increasingly severe. Typical military flight missions include significant dwell periods at high power settings with the result that time dependent damage mechanisms operate. This has necessitated modification of existing life relationships previously relied upon at lower temperatures.¹ One such development has been the Strainrange Partitioning^{1,2,3} (SRP) method for predicting creep-fatigue interactions.

It has been shown in the literature that SRP can be a valuable tool in analyzing creep-fatigue interactions in many alloys.^{3,4,5} In one summary⁶, data for twelve different alloys were analyzed, and SRP was successful in correlating lives within a factor of two. The alloys that have been studied are, however, generally more ductile than the high strength nickel-base superalloys. Time dependent deformation constitutes a large fraction of the total inelastic strains in these more ductile alloys, and research has been concentrated in the cyclic life range where inelastic strains are also comparatively large. At these levels of inelasticity, the stress response of the alloys is generally more predictable than at lower strain ranges, in particular, significant mean stresses do not usually develop.

Menon⁷ has reported that, for the superalloy Rene 95, stress relaxation during strain hold cycles is rather limited at 922K (1200°F) and the fractions of time dependent strain are small. This behavior is particularly marked approaching the life range of interest for practical engineering design (5,000 - 50,000 cycles). Although the "creep" strains are small, the response of Rene 95 to strain hold cycles is rather pronounced. This paper will describe the reaction of Rene 95 to strain controlled fatigue at 922K and discuss the influence of various test parameters on the fatigue behavior. The high temperature LCF data will be analyzed using SRP and an evaluation will be made of how effective the model is in correlating the data base, as well as predicting crack initiation lives for different test conditions. This research was performed at the Air Force Materials Laboratory.

2.0 EXPERIMENTAL

2.1 Materials

Rene 95 is a high strength, nickel-base superalloy primarily used for turbine disks in recent turbine engines. The alloy composition is given in Table I (see also Appendix A1). In addition to the conventional strengthening mechanisms involving precipitation of a high volume fraction of gamma prime, and to a lesser degree solid solution hardening, Rene 95 derives part of its strength from the residual dislocation substructure introduced during a thermomechanical processing treatment (TMP). TMP is also responsible for the duplex structure of Rene 95, often called the "necklace structure", in which large warm worked grains (75µm) are surrounded by a necklace of fine recrystallized grains (4µm).

The result of TMP and conventional hardening treatments is an improvement in tensile and rupture strength at temperatures to about 922K.

The two pancakes of Rene 95 used in this program were taken from a vacuum induction melted and vacuum arc remelted ingot approximately 0.228m in diameter. The ingot was given a homogenization anneal in the range 1263K - 1436K for 3 hours and then furnace cooled. The pancakes were subsequently reheated to 1366K - 1410K and forged to bring the thickness to 40-50% above the final value. This was followed by a recrystallization anneal at 1436K for one hour. This results in a uniform grain diameter between .064 - .127mm. The forgings were cooled from the recrystallization temperatures at a rate greater than 93.3K per hour to 1172K and then air cooled and taken to final processing. The forgings were reheated to 1352K - 1380K and the final reduction was applied, resulting in a further 40-50% decrease in thickness. The pancakes were then partial solutioned at 1366K, oil quenched to a temperature below 755K, and aged at 1033K for 16 hours.

The Rene 95 forgings have been characterized in terms of microstructure⁸, tensile behavior⁹, and room temperature LCF crack initiation mechanisms.¹⁰ The tensile and creep properties of Rene 95 are summarized in Table III of the Appendix.

2.2 Test Procedures

The low cycle fatigue tests were performed using a servohydraulic closed loop system. The test specimens were of the standard hourglass design with a 6.35mm (.250 inch) minimum diameter. A diametral extensometer along with a strain computer was used to monitor and control the tests.¹¹ All tests were conducted at 922K (1200°F). Test cycles were completely reversed, zero mean strain. Specimens were heated using an induction system with control thermocouples attached in the radius section away from the minimum diameter.

The test plan consisted of three phases: baseline testing under strain control, cyclic creep tests utilizing load control to strain limits, and validation testing comprised of less conventional waveforms. The Phase I, baseline test procedures, will be discussed here. The cyclic creep tests and validation testing will be described in separate sections.

The baseline testing was designed to evaluate the LCF properties of Rene 95 at 922K and to provide sufficient data with which to establish the SRP life relations under PP, PC, CP, and CC loading. The test matrix was comprised of high rate strain cycles (HRSC), as well as tension, compression, and balanced strain hold tests (THSC, CHSC, BHSC).

The continuous cycling tests (HRSC) were diametrically monitored and the total axial strain was controlled. The specimens were tested at 20 cycles per minute (.333 Hz) using a triangular waveform. This frequency represents the upper limit of the test system and is at a high enough rate to preclude time dependent deformation in Rene 95 at 922K at the strain ranges tested.

The dwell cycles incorporated hold times in tension, compression, and both (balanced strain hold cycles). These tests were also strain controlled. The ramp rate was the same as for a 20 cycles per minute (cpm) test. The strain limit was maintained during the dwell and the load was allowed to relax. Both one and ten minute hold times were used. These tests will be denoted as (X/Y) tests where X is the number of minutes held in tension and Y is the time held in compression, i.e., a one minute tensile hold test is designated as (1/0).

2.3 Data Reduction

The SRP life relationships have been derived using the interaction damage rule⁶, which is expressed by the equation:

$$\frac{1}{N_f} = f_{PP}/N_{PP} + f_{PC}/N_{PC} + f_{CP}/N_{CP} + f_{CC}/N_{CC} \quad \text{Eq. (1)}$$

where: N_f = cyclic life under some complex hysteresis loop

f_{ij} = constitutive fraction of type i,j inelastic strain

N_{ij} = cyclic life expected where entire inelastic strain is of type ϵ_{ij}

The strain ranges were partitioned from the load and inelastic strain stripchart recordings. For the strain hold cycles, the creep strain was defined as the inelastic strain that developed during stress relaxation. The value was calculated by dividing the decrease in stress during the hold period by the elastic modulus.³

Because Rene 95 cyclically softens at 922K, there was generally a significant increase in the inelastic strain throughout a test. For the 20 cpm tests, the inelastic strain range increased between 13% and 130% of the original value. The amount of softening generally increased as the total strain range decreased. The reported values of load and strain are the values at half-life ($N_f/2$). These values were used in the SRP analysis.

All cyclic life values are cycles to failure (N_f). Several methods, however, were examined to establish a value of cycles to crack initiation (N_i). The most sensitive criterion was to visually determine the point at which the slope of the relationship of

the maximum tensile stress with time changed. This point was then designated the time of crack initiation. For the baseline strain controlled tests the earliest indication of initiation using this criterion was 85% of the cycles to failure. Most values, however, were greater than 90% N_f .

The data were also analyzed using the 5% and 10% load drop criteria. Initiation was defined as the point at which the maximum tensile load decreased the designated percentage from the cyclic softening load line. These values of N_i were necessarily even higher fractions of the total life than for the previously discussed criterion. In light of these results, it was concluded that no significant benefit would be realized by using some measure of N_i rather than N_f .

For the SRP analysis, the best fit life relationships of the form

$$\Delta \epsilon_{in} = C N_{ij}^B \quad \text{Eq. (2)}$$

C, B constants

have been determined. A least squares fit to the data was obtained in the sense that the sum of the squares of the error

$$\log N_{ij}^{\text{PRED}} - N_{ij}^{\text{OBS}} = \frac{1}{B} (\log(\Delta \epsilon_{in}) - \log C) - \log N_{ij}^{\text{OBS}} \quad \text{Eq. (3)}$$

was a minimum.

3.0 EXPERIMENTAL RESULTS

3.1 Baseline Tests - Cyclic Response

As has been mentioned, Rene 95 is a relatively creep resistant alloy at 922K. The reaction of the material to strain hold cycles, however, is significant. Results are presented in Fig. 1 for the various hold tests along with the high rate strain cycle tests performed at 20 cpm. Inelastic strainrange is plotted versus cycles to failure, and the best fit line is drawn through the 20 cpm test points. This is the Manson-Coffin relationship for time independent behavior. These data indicate that at the same inelastic strain compressive hold tests are the most damaging, while the tension strain hold tests produce longer lives than the creep free high rate strain tests. The latter result is particularly pronounced at the lower inelastic strain ranges. Fig. 1 further shows that the use of the Manson-Coffin relationship would result in a potential error of a factor of five in predicting the data.

3.2 Stress Behavior

The material response of Rene 95 is such that large shifts develop in the maximum tensile stress during some strain hold cycles as compared to the 20 cpm, time independent, behavior. These changes are in addition to the reductions in stressrange that accompany cyclic softening. A plot of the maximum tensile stress versus inelastic strainrange is shown in Fig. 2. These data are for the baseline strain controlled tests (THSC, CHSC, BHSC, HRSC). Compressive hold tests develop significantly higher peak tensile stresses at a given inelastic strainrange than do the 20 cpm tests, and the tensile and balanced strain hold tests have lower tensile stresses than the 20 cpm tests. The shift in peak tensile stress for these data increases as the strainrange is reduced and the hold time lengthened. This behavior is generally reflected in the value of the mean stress. Fig. 3 shows the mean stress as a function of inelastic strainrange for these same tests. Compressive hold tests develop a positive mean stress while the continuously cycling tests and tension and balanced hold cycles have negative mean stress values. As with the tensile stress data, Fig. 2, the largest biases develop in the tensile strain hold tests at the lower strainranges and longer hold times.

3.3 Strainrange Partitioning Analysis (Phase I)

The high rate strain cycle tests (HRSC) and the strain hold cycle tests (THSC, CHSC, BHSC) comprised the baseline testing program. These data were used to construct the four SRP life relations from which validation tests were predicted. All baseline test data are listed in Table IV of the Appendix.

3.3.1 PP Line

The high rate strain cycle tests (20 cpm) contained only plastic inelastic strains. They, therefore, formed the basis of the PP relationship. The data are shown in Fig. 4. The best fit power law equation for the PP line is:

$$\Delta \epsilon_{pp} = 0.736 (N_{pp})^{-0.896} \quad \text{Eq. (4)}$$

3.3.2 CC Line

Balanced strain hold tests were performed to generate CC data. These were both 1/1 hold (one minute hold in tension and one minute hold in compression) and 10/10 hold tests. Due to the differing stress relaxation response of the alloy in tension and compression, the tests in most cases contained small amounts of PC or CP strain. The partitioned strains, cycles to failure, and the calculated values of life and percent damage are listed in Table I. The percent damage attributed to a particular strain component is

calculated using the equation⁶:

$$\frac{f_{ij}}{N_{ij}} N_f(100) = \% \text{ damage} \quad \text{Eq. (5)}$$

The calculated CC data points are shown in Fig. 5. The equation of the CC line is:

$$\Delta \epsilon_{CC} = 0.198 (N_{CC})^{-0.852} \quad \text{Eq. (6)}$$

3.3.3 PC Line

The PC damage was partitioned from compressive strain hold tests. The hold periods were for one and ten minutes. The partitioned data are presented in Table II. The PC points and line are shown in Fig. 6. The equation of the PC line is:

$$\Delta \epsilon_{PC} = 0.135 (N_{PC})^{-0.914} \quad \text{Eq. (7)}$$

3.3.4 CP Line

The CP points were calculated from 1/0 and 10/0 tension hold strain data. These cycles have been previously shown to be less damaging than high rate strain cycles when compared at the same inelastic strain ranges (Fig. 1). Because tension hold cycles are significantly less damaging than PP cycles at lower strain levels, the values of N_{CP} calculated from the interaction damage rule are negative. These calculations suggest that not only is CP strain in this range less damaging than PP, but it can be considered "rejuvenating" when incorporated with PP damage. This is emphasized by considering that for those tests with a negative N_{CP} life, N_f was significantly greater than the life predicted for the partitioned $\Delta \epsilon_{PP}$ component alone.

The CP data are presented in Fig. 7 and Table III. The points with negative calculated N_{CP} lives are plotted at the appropriate strain levels. These data are also plotted on a less conventional semi-logarithmic plot (Fig. 8) in order to present the negative life values and to show the discontinuous nature of the function.

Because the present formulation of SRP does not provide a basis for describing negative life behavior, certain approximations will be made in order to continue the analysis. There seems to be no straightforward method for developing a single life relationship using both the positive and negative N_{CP} points. The graphical construction of a relationship representing all tests is unclear since it appears from Figs. 7 and 8 that the value of strain at which the N_{CP} lives change from positive to negative values depends on the hold time of the cycle. Therefore, a single CP life relationship has been established on the basis of only those data points with positive N_{CP} lives. This relationship will be conservative in predicting the negative N_{CP} lives.

The equation of the line through the positive N_{CP} points is:

$$\Delta \epsilon_{CP} = 2.20 (N_{CP})^{-1.217} \quad \text{Eq. (8)}$$

This relationship was used in the calculation of the CP damage in the balanced strain hold tests.

3.4 Data Acceptance Criteria

In order to establish a valid SRP life relationship, it is essential that a significant portion of the damage in a baseline test be due to the strain component of interest. A criterion has been proposed to determine if a test point meets this requirement.⁶ This standard requires that the percent damage, defined by Eq. (5), attributed to the strain component of interest be greater than 50%, and it further states that the fraction of creep strain (f_{CC} , f_{CP} , f_{PC}) in the test should be greater than one-half.

This validity criterion has not been applied to the data. Although the intent of the standard is appreciated, it appears that in this case it would unfairly bias the life relationships. In general, the CC and PC data points do have calculated values of percent damage greater than the required 50%. Several points that do not meet this criterion, however, have also been included. The reason for this is that points that last longer than predicted by the best fit lines have calculated values of percent damage less than points that scatter even farther from the line but into the lower life range. Also, for much of the data, the calculated values of percent damage did not change predictably with changes in the fraction of creep strain. A more consistent correlation would be expected if the percent damage was a good measure of the cyclic life expended due to creep. Therefore, omitting the points with less than 50% creep damage would in this case prejudicially bias the life lines toward the lower life range.

The CP points, in general, did not meet the percent damage criterion. However, because of the unusual results from applying the interaction damage rule to these data and because there was not a good correlation between percent damage and f_{CP} , the CP points were considered valid.

Although not strictly required by the criterion, the fractions of creep strain for the baseline tests were not greater than one-half. These small creep strains are a result

of the type of test cycle employed. Because there is stress relaxation in a strain hold cycle and due to the limited creep response of Rene 95 at 922K, the fractions of CC, CP, and PC damage in all baseline tests were small. The response of the material to these small creep strains, however, was significant with the result that most tests did meet the 50% damage criterion as required. The baseline test data were therefore considered valid points with which to establish the SRP life relationships.

3.5 Cyclic Creep Tests (Phase II)

In the strain hold cycle baseline testing previously reported, the strain component of interest (PC, CP, CC) comprised only 10-35% of the total inelastic strainrange. To corroborate the validity of these data, several cyclic creep tests were performed at the NASA-Lewis laboratory. In these tests, the load was ramped to a prescribed value and was then held constant. The specimen was then allowed to creep to a set liametral strain limit at which time the load was reversed. These tests were successful in generating approximately 50% of the total inelastic strain as creep strain.

Due to the cyclically softening behavior of Rene 95, cyclic creep tests need to be continually monitored. Adjustments must be made in the load level and strainrange in order to maintain the same proportions of each strain component while still limiting the tests to a reasonable cyclic period. The strain fractions, therefore, necessarily varied, and the reported values are the best estimate for each test.

It should also be noted that as a result of these tests being performed in a different laboratory, the specimen geometry and orientation were not the same as used for the baseline and validation testing. The purpose of presenting these data then is to see if incorporating larger percentages of creep damage in a test grossly alters the life relationship developed from the strain hold testing.

The results of the cyclic creep tests are presented in Table IV and Figs. 9-12. Two additional PP type tests were also performed and data points are plotted in Fig. 9. These points are consistent with the baseline PP data. Due to the limited number of data points, however, the original baseline PP relationship was used to partition the cyclic creep tests. The CC and PC points are shown in Figs. 10 and 11. They, too, are in good agreement with the strain hold data.

The relation of the cyclic creep CP points to the CP strain hold data is less obvious due to the large amount of scatter in the data (Fig. 12). Because of the potential error in characterizing the strain fractions of the cyclic creep tests and due to the limited strain range tested, these two points can be considered in the general scatter band of the strain hold points. However, in light of the overall uncertainty in defining the response of Rene 95 to CP damage and in an attempt to be thorough in this analysis, a second CP line has been constructed as a best fit through the two cyclic creep points and baseline tests #10 and #228. The choice of the two strain hold data points (#10, #228) is based on the fact that these two tests do contain the required 50% CP damage. This CP line is defined by the equation:

$$\Delta \epsilon_{CP} = .056 (CP)^{-0.689} \quad \text{Eq. (9)}$$

and will be referred to as the cyclic creep CP line. A summary of the SRP relationship for Rene 95 is presented in Fig. 13.

3.6 Data Correlation

Based on the four SRP life relationships developed from the Phase I baseline data, the expected lives for those same tests (HRSC, THSC, CHSC, BHSC) were predicted using the interaction damage rule. The predicted values (N_{pred}) are compared with the actual lives (N_f) in Table V and Fig. 14. The majority of data lie within a factor of two from the predicted lives. Five test points, however, lie outside this range. Three tensile hold tests are underpredicted while one compressive hold test and one 20 cpm test are non-conservatively predicted. The largest deviation is a factor of 5.5 for a low strain-range tensile hold test.

Similar results are presented in Fig. 15 for the lives predicted using the cyclic creep CP line. In this case, five tensile hold tests are underpredicted by more than a factor of two, and still the compressive hold test and the 20 cpm test are predicted non-conservatively.

3.7 Verification Tests - Phase III

In order to truly test the predictability of SRP, several additional tests were performed and their lives predicted on the basis of the SRP life relations previously presented. The waveforms for these tests were generally of a different character than utilized in the baseline testing. These include unbalanced strain hold tests, intermediate strain hold tests, 0.05 cpm slow rate strain cycles, and fast-slow and slow-fast strain cycles.

3.7.1 Waveforms and Partitioning

The unbalanced strain hold cycles consisted of strain hold times of differing durations in tension and compression. This cycle was an attempt to incorporate significant amounts of three types of strain in one test. Both 10/1 and 1/10 cycles were tested.

The creep strains were partitioned from the stress relaxation curves. Test conditions and partitioned strain values are presented in Table VI.

The intermediate strain hold cycle was conceived of as a means of altering the sequence of inducing time dependent and time independent strains. The strain hold was introduced at a total strain value less than the total strain limit (Fig. 16). Thus, the specimen was strained to a set value and maintained for a period at that strain level while the load relaxed. The specimen was then strained in the same loading direction to a final strain limit. Test conditions included one minute intermediate holds in either tension or compression (il/0, 0/il). The creep strains again were partitioned from the relaxation records. The data are presented in Table VII.

The third type of validation test was the 0.05 cpm low rate strain cycle (LRSC). Six tests were performed. Five of the tests were run under inelastic strain control; test 34 was tested under total strain control as were the baseline tests. Only three of the six tests were partitioned. The test conditions and the partitioned data for all 0.05 cpm tests are presented in Table VIII.

To partition the strains for the 0.05 cpm tests, the rapid load method was used on a companion specimen.¹² The companion test was first cycled at the appropriate strain level at 0.05 cpm under strain control. The test was then changed to load control and the load limits previously established in the 0.05 cpm testing were imposed. The specimen was then cycled under these conditions at 20 cpm. The difference in the inelastic strain ranges at the two frequencies (0.05 and 20 cpm) was then considered to be the creep component. The fractions of inelastic strain (f_{CC} , f_{PP}) were assumed to be the same for the actual 0.05 cpm test. As shown in Table VIII the fractions of creep strain in these tests approached zero.

The fourth type of verification test was the variable rate strain test involving fast-slow and slow-fast cycles. A fast-slow cycle consists of ramping from the minimum strain to the maximum strain in 1.5 seconds (20 cpm rate) and then ramping from the maximum strain back to the minimum strain in 600 seconds (0.05 cpm rate). A slow-fast cycle involves just the opposite sequence. Both test cycles are illustrated in Fig. 17. The rapid load method was used to partition the tests. The fraction of creep strain (f_{CC}) for both tests was 0.12. The results are presented in Table IX.

3.7.2 Life Prediction

The predicted fatigue lives for the verification tests were calculated from the partitioned data using the interaction damage rule and the SRP life relations previously established in Phase I. The expected values are compared with the observed lives in Fig. 18 and Table X.

SRP predicts both the unbalanced strain hold tests and the intermediate strain hold tests very accurately. The largest variation from the predicted life was a factor of 1.64. Both the 0.05 cpm tests and the variable rate tests, however, were not generally predicted within a factor of two. Two of the tests varied by a factor of 2.4 and the one slow-fast rate test was non-conservatively predicted by greater than an order of magnitude.

4.0 DISCUSSION

These data have shown that SRP can be used to predict crack initiation life for Rene 95 under certain test conditions. The majority of the baseline tests, particularly at the larger strain ranges, were effectively correlated using SRP, and all the strain hold verification tests were predicted within a factor of 2. Other test cycles, however, were not as accurately modeled. Several baseline tensile strain hold tests and one compressive hold test were not predicted by SRP within a factor of 2. The low rate continuously cycling tests were also poorly predicted. In addition, it has been noted that the results of the partitioned CP data do not appear consistent with the basis of SRP. In general then, the results of this research indicate that there are fundamental limitations in applying SRP in its present form to this type of alloy.

Of particular concern is the fact that a meaningful life relationship could not be established for CP damage in the longer life region. In the SRP analysis (Sect. 3.3), baseline tensile strain hold tests were partitioned and the N_{CP} lives were calculated using the interaction damage rule. As previously noted, the calculated values of N_{CP} for several of the low strain range tests were negative. This is a result of the fact that at low strain levels tensile strain hold cycles are considerably less damaging than high rate strain cycles. The interaction damage rule, as presently conceived, does not account for this behavior. This is because the rule can be considered asymptotic in nature.¹³ Thus, even for the hypothetical case where the other contributing lives were infinite, the maximum value possible for life computed using the rule equals the shortest contributing life (PP, PC, CP, or CC) times the inverse of its constitutive fraction.

There is, however, a more general inconsistency between the data and SRP. The results indicate that there is a direct and significant influence of the maximum tensile stress on fatigue life which is not accounted for by SRP. As has been described, stress shifts usually develop during strain hold testing. The value of the maximum tensile stress increases during a compressive hold test and decreases during tensile and balanced hold tests. For these data, the change in the value of the peak tensile stress compared to the 20 cpm continuously cycling behavior has been shown to increase as the inelastic

strainrange decreased and the hold time increased (Fig. 2). These results correlate with the trends observed in life (Fig. 1). Compressive hold tests consistently have shorter fatigue lives than tensile hold cycles for the same inelastic strainranges, and the differences in life are greatest at the lower strainranges and for longer hold times. Similar behavior has been reported for the high strength, low ductility alloy IN 738¹⁴, Rene 80¹⁵, and for the relatively ductile Cr-Mo-V steel when tested at lower strainranges.¹⁶

The strainhold baseline data have been plotted on semi-log axes to directly show the dependence of life on peak tensile stress, σ_{max} (Fig. 19). This type of analysis has been suggested by Conway^{17,18} for creep data. The data fall generally onto three straight lines. The fast rate strain data and the compressive strain hold data fall on one line, the 1/0 and 1/1 strain hold points fall on the second line, and finally the 10/0 and 10/10 data can be fit with a third line. Each line corresponds to a particular tensile hold time, t_t (0, 1, 10 minutes). Linearity on semi-log axes indicates an exponential relationship between maximum σ_{max} and N_f . The best fit lines are drawn through the appropriate data in each case. The values of N_f compare with the lives predicted from these lines within a factor of two except for one 0/1 test (#11). These relationships illustrate the influence of peak tensile stress and tension hold time on fatigue life. They are not, however, proposed as a predictive model.

In light of these findings, the results of the baseline data correlation (Sect. 3.6) can be more easily understood. Five baseline tests were not correlated by SRP within a factor of two (Fig. 14). The one PP test (#29) should be considered a statistical anomaly since it does not correlate well with the other data. The other four tests (#222, 233, 33, 237), however, are strain hold tests which display a consistent behavior. The three tensile hold tests developed the largest maximum tensile stress biases of the tensile hold baseline tests, while test #222 developed the largest tensile stress bias of the compressive hold tests (Fig. 2). The stress bias for this analysis is defined to be the difference between the value of the maximum tensile stress for the particular test and the value of the peak tensile stress for a PP test at the same inelastic strainrange. The PP data is defined by the best fit line through the 20 cpm tests (Fig. 2).

These results further highlight the influence of peak tensile stress on fatigue life, and they suggest that when the stress bias is greater than some critical value, SRP does not accurately predict life (within a factor of 2). Consistent with these results is the behavior of the balanced hold tests. These tests do not develop as severe a reduction in the peak tensile stress as do the tensile hold tests. The balanced strain hold tests would, therefore, not be expected to fall outside the range of predictability by SRP, as is observed.

The results of the verification tests, however, cannot be totally explained in terms of the stress bias. The maximum tensile stress for each of the verification tests is plotted versus inelastic strainrange in Fig. 20 along with the $\Delta\epsilon_{\text{in}}$ versus maximum σ_t relationship for the 20 cpm tests previously displayed in Fig. 2. The critical stress bias limits have also been constructed from Fig. 2. These limits represent the boundaries between satisfactorily correlated baseline tests and those not correlated within a factor of two. The maximum tensile stress values for the unbalanced and intermediate strain hold tests all lie within the stress bias limits. The actual fatigue lives for these tests were predicted by SRP within a factor of 2. The two 0.05 cpm tests that were not accurately predicted by SRP, however, do not have peak tensile stresses greater than the critical values, and the fast-slow test was predicted by SRP in spite of falling outside the critical stress units. These results suggest that for strain hold tests the peak tensile stress is a controlling parameter, but for low rate continuously cycling tests there is a more dominant factor.

The lives of the verification tests were also compared to the lives that would be expected on the basis of the peak tensile stress-tensile hold time correlation described by Fig. 20. For this analysis, the tension going time per cycle for the continuously cycling tests was used in place of the hold time in tension. Thus, the 0.05 cpm tests were compared to the 10 minute tensile hold data as was the slow-fast test, and the fast-slow test was compared to the zero hold time data. The intermediate tensile hold tests were also compared to the zero tensile hold time relationship since the tensile hold period for these tests was at a stress level less than the maximum stress. The data are presented in Fig. 21 and Table XI.

All the verification tests agreed with the tensile stress-time lines within a factor of 1.85 which further indicates that the high temperature, low cycle fatigue behavior of Rene 95 is dependent on the value of the maximum tensile stress and some measure of the cycle time in tension. It appears then from these results that SRP is unable to accurately predict certain tests because a totally strain based model, such as SRP, cannot in all cases account for changes in stress and waveshape which have been shown to significantly influence the life of Rene 95.

The fact that the 0.05 cpm verification tests were correlated using a factor for the tension going time may be the basis for explaining their behavior. The 0.05 cpm verification tests generally failed in one-half the cycles expected for 20 cpm tests at the same inelastic strainranges. As previously reported, however, the 0.05 cpm tests contained negligible partitioned creep strains. The results of the partitioning are supported by comparing the total stressranges and strainranges for the 0.05 cpm and 20 cpm tests (Fig. 22). Fig. 22 shows that both 0.05 cpm and 20 cpm cycles generated approximately equal stressranges when tested at the same total strainrange. A reduction in stressrange

would have been expected if time dependent creep deformation was present in the 0.05 cpm tests. These results indicate that although the time in tension per cycle is a controlling parameter, creep damage is not responsible for reducing the life of the 0.05 cpm tests. As previously stated, SRP in its present form cannot account for reductions in fatigue life not associated with a change in inelastic strains. This result also suggests that environmental factors may be governing crack initiation for low rate continuously cycling tests.

Other models^{19,20,21} have been suggested which directly account for the influence of time and peak tensile stress. Ostegren¹⁴, in particular, has proposed a model which includes terms for frequency and the product of the maximum tensile stress and inelastic strainrange. These models have not been critically examined with respect to these data and will not be treated in this analysis.

Only limited metallurgical studies have been performed on the fracture surfaces of the Rene 95 specimens to date. Additional electron microscopy and metallographic sectioning studies are required to identify initiation mechanisms, as well as crack propagation modes. Work also needs to be concentrated on examining the basic response of Rene 95 under different cyclic conditions. Strainrate effects, and cyclic softening and aging phenomena, need to be better understood. For example, the response of Rene 95 to the 0.05 cpm cycle and the variable rate verification cycles need to be more thoroughly studied in order to identify the failure controlling mechanisms.

It has been proposed²² that the advantage of SRP and the interaction damage rule is that data can be generated in the relatively low life region to develop functional life relations, and predictions can then be extrapolated into the longer life range. This research has shown that this is not the case for Rene 95. Predictions of long life compressive hold and low rate strain cycle tests could be dangerously nonconservative using this approach.

References have previously been made to alloys that behave similarly to Rene 95. On-going research at this laboratory indicates that the high strength nickel-base superalloy, AF2-1DA, also develops a large peak tensile stress shift during strain cycling. It is also possible that other more ductile alloys may develop similar stress biases when fatigued at very low inelastic strainranges.

As previously described, SRP was able to accurately predict crack initiation in Rene 95 for certain test conditions. For the strain hold tests, SRP was effective when the inelastic strainrange was relatively large and the hold time was short. In the range of more practical design interest, however, SRP did not consistently predict the data within a factor of two. This result has been related to the development of increasingly large biases in the value of the peak tensile stress produced at lower strainranges and with increasing hold times.

For the low rate continuously cycling tests, the applicability of SRP is not as clearly defined. SRP was not able to accurately predict lives even for high strainrange, low life tests. Additional testing and analysis is needed to further understand this behavior.

5.0 CONCLUSIONS

1) Strain hold tests on Rene 95 have shown that compressive hold cycles are more damaging than tensile hold cycles when the two are compared at the same inelastic strainranges. Compressive hold cycles also develop larger peak tensile stresses than do tensile hold cycles. For these data, the tensile stress bias increased with decreasing inelastic strainrange and increasing hold time.

2) Maximum tensile stress and time in tension have been shown to significantly influence crack initiation life for Rene 95.

3) Strainrange Partitioning was able to correlate the baseline data and predict validation tests for a limited range of conditions. SRP could not accurately predict crack initiation life for strain hold tests that developed large tensile stress biases, or for low rate continuously cycling tests.

4) For the type of alloy studied, it is suggested that SRP may be a useful prediction model for strain hold tests in the range where inelastic strains are relatively large and hold periods are short. At lower strainranges and for longer hold times where significant stress biases develop, however, SRP does not appear applicable in its present form.

6.0 REFERENCES

1. Greenstreet, W.L., et al, "Time-Dependent Fatigue of Structural Alloys", 1977, ORNL Report 5073.
2. Manson, S.S., Halford, G.R., and Hirschberg, M.H., "Creep-Fatigue Analysis by Strain-Range Partitioning", Symposium on Design for Elevated Temperature Environment, ASME, 1971, pp. 12-28. (NASA TM X-67838, 1971).

3. Saltsman, J.F. and Halford, G.R., "Application of Strainrange Partitioning to the Prediction of Creep Fatigue Lives of AISI Types 304 and 316 Stainless Steel", 1976, NASA TM X-71898.
4. Saltsman, J.F. and Halford, G.R., "Application of Strainrange Partitioning to the Prediction of MPC Creep-Fatigue Data for 2 1/4 Cr-1 Mo Steel", 1976, NASA TM X-73474.
5. Kortovich, C.S., "Strainrange Partitioning Behavior of Coated and Uncoated Rene 80 in Ultrahigh Vacuum", April 1976, NASA CR-135003.
6. Hirschberg, M.H. and Halford, G.R., "Strainrange Partitioning - A Tool for Characterizing High Temperature Low-Cycle Fatigue", 1975, NASA TM X-71691.
7. Menon, M.N., "Life Prediction Techniques for Analyzing Creep-Fatigue Interaction in Advanced Nickel-Base Superalloys", 1976, Air Force Materials Laboratory TR-76-172.
8. Menon, M.N., "Metallographic Characterization of Rene 95 Forgings", 1973, Air Force Materials Laboratory TR-73-180.
9. Menon, N.M. and Reimann, W.H., Met. Trans., 1975, Vol. 6A, pp. 1075-1085.
10. Menon, M.N. and Reimann, W.H., J. Matls. Science, 1975, Vol. 10, pp. 1571-1581.
11. Slot, T., Stentz, R.H., and Berling, J.T., "Controlled Strain Testing Procedures", Manual on Low Cycle Fatigue Testing, ASTM STP 465, 1969, pp. 100-128.
12. Manson, S.S., Halford, G.R., and Nachtigall, A.J., "Separation of the Strain Components for Use in Strainrange Partitioning", Symposium on Advances in Design for Elevated Temperature Environment, ASME, 1975, pp. 17-28. (NASA TM X-71737, 1975).
13. Annis, C.G., Van Wanderham, M.C., and Wallace, R.M., "Strainrange Partitioning Behavior of an Automotive Turbine Alloy", 1976, NASA CR-134974.
14. Ostergren, W.J., "Correlation of Hold Time Effects in Elevated Temperature Low Cycle Fatigue Using a Frequency Modified Damage Function", ASME-MPC Symposium on Creep-Fatigue Interaction, 1976, pp. 179-185.
15. Lord, D.C. and Coffin, L.F., Jr., Met. Trans., 1973, Vol. 4, No. 7, pp. 1643-1770.
16. Krempl, E. and Walker, C.D., "The Effect of Creep Rupture Ductility and Hold Time on the 1000°F Strain-Fatigue Behavior of a 1 Cr-1 Mo-.25V Steel", Fatigue at High Temperature, 1969, ASTM STP 459, p. 75.
17. Conway, J.B., "Development of a Standard Methodology for the Correlation and Extrapolation of Elevated Temperature Creep and Rupture Data: Volume I, A Summary of State of the Art Review and Workshop", to be published as Electric Power Research Institute Report (NTIS listing).
18. Conway, J.B., "Pre-Analysis Assessment of Creep and Rupture Data", to be published in the Proceedings of the ASME-CSME Pressure Vessel and Piping Conference, Montreal, Canada, June 1978.
19. Coffin, L.F., "The Concept of Frequency Separation in Life Prediction for Time-Dependent Fatigue", ASME-MPC Symposium on Creep-Fatigue Interaction, 1976, pp. 349-363.
20. Majumdar, S., Maiya, P.S., "A Damage Equation for Creep-Fatigue Interaction", ASME-MPC Symposium on Creep-Fatigue Interaction, 1976, pp. 323-336.
21. Tomkings, B., J. Engineering Mat. and Tech., 1975, Vol. 97, pp. 289-297.
22. Manson, S.S., et al, "Time Dependent Fatigue of Structural Alloys", ORNL Report 5073, 1977, pp. 245-307.

7.0 ACKNOWLEDGMENTS

The high temperature strain control testing was performed by Mar-Test Inc. under Air Force contract F33615-76-C-5245. The authors gratefully acknowledge the valuable discussions with Messrs. Stentz, Conway, and Berling of Mar-Test Inc. The authors also wish to thank Dr. G.R. Halford for his helpful discussions and for performing the cyclic creep tests in his laboratory. The results of the research of Dr. M.N. Menon while at the Air Force Materials Laboratory contributed to this work. The authors also wish to thank their colleagues, especially Dr. W.H. Reimann and Dr. T. Nicholas of the Air Force Materials Laboratory, and Dr. N. Ashbaugh of Systems Research Laboratories, for their assistance. Part of this research was performed under Air Force contract F33615-76-C-5191.

TABLE I
CC PARTITIONED DATA

SPEC	ϵ_{in}^1	ϵ_{pp}^1	ϵ_{CC}^1	ϵ_{PC}^1	ϵ_{CP}^1	f_{CC}	% DAMAGE	N_{CC}
1	.550	.437	.085	.000	.028	.15	42	57
2	.349	.276	.055	.000	.018	.16	46	81
32	.201	.163	.028	.000	.010	.14	54	92
9	.122	.087	.030	.005	.000	.25	23	1021
15	.078	.054	.020	.000	.004	.26	47	696
28	.701	.486	.188	.000	.027	.27	52	59
31	.497	.304	.170	.000	.023	.34	48	142
230	.175	.104	.060	.000	.011	.34	71	160

1) PERCENT STRAIN

TABLE II
PC PARTITIONED DATA

SPEC	ϵ_{in}^1	ϵ_{pp}^1	ϵ_{PC}^1	f_{PC}	% DAMAGE	N_{PC}
6	.429	.370	.059	.14	43	67
11	.468	.406	.062	.13	36	77
14	.324	.282	.042	.13	55	51
8	.192	.168	.024	.13	53	98
13	.098	.089	.009	.09	52	146
241	.049	.044	.006	.11	51	428
16	.010	*	----	---	--	---
238	.028	.023	.006	.20	43	2095
222	.136	.116	.020	.15	83	40
41	.185	.130	.055	.30	75	112

1 PERCENT STRAIN

* COULD NOT ACCURATELY PARTITION

TABLE III
CP PARTITIONED DATA

SPEC	ϵ_{in}^1	ϵ_{pp}^1	ϵ_{CP}^1	f_{CP}	% DAMAGE	N_{CP}
245	.657	.539	.118	.18	28	112
5	.522	.447	.075	.14	13	288
10	.297	.262	.035	.12	52	59
7	.206	.175	.031	.15	10	1125
12	.089	.083	.006	.07	33	274
39	.089	.070	.019	.21	22	1710
38	.049	.043	.006	.12	--	-2214
233	.061	.053	.008	.12	--	-762
33	.038	.036	.002	.05	--	-530
237	.046	.041	.005	.10	--	-578
228	.180	.150	.030	.17	51	156
40	.126	.102	.024	.19	--	-2510

1) PERCENT STRAIN

TABLE IV
CYCLIC CREEP TESTS - PARTITIONED DATA

SPEC	TYPE/ ϵ_{ij}	$\Delta \epsilon_{in}^1$	f_{PP}	f_{CC}	f_{CP}	f_{PC}	N_{ij}	N_f
RE-11	HRSC/PP	1.24	1.00	.000	.000	.000	72	72
RE-16	HRSC/PP	.308	1.00	.000	.000	.000	671	671
RE-20	TCCR/CP	.777	.529	.000	.471	.000	18	34
RE-14	TCCR/CP	.306	.530	.000	.470	.000	68	124
RE-4	CCCR/PC	.810	.498	.000	.000	.502	15	27
RE-15	CCCR/PC	.125	.610	.000	.000	.390	228	454
RE-7	BCCR/CC	.930	.342	.603	.055	.000	27	39
RE-13	BCCR/CC	.304	.345	.517	.138	.000	109	164
RE-10	BCCR/CC	.146	.611	.389	.000	.000	202	398

TABLE V
BASELINE DATA CORRELATION

SPEC	TYPE	N_f	N_{PRED}	N_f/N_{PRED}	N^*_{PRED}	N_f/N^*_{PRED}
21	20 cpm	203	158	1.28		
17	20 cpm	234	247	0.95		
18	20 cpm	307	330	0.93		
224	20 cpm	415	569	0.73		
22	20 cpm	461	446	1.03		
240	20 cpm	463	492	0.94		
26	20 cpm	784	667	1.18		
27	20 cpm	1629	1508	1.08		
29	20 cpm	5158	10792	0.48		
30	20 cpm	16215	17263	0.94		
234	20 cpm	19160	15209	1.26		
235	20 cpm	22364	24390	0.92		
239	20 cpm	28697	15209	1.89		
245	1/0	171	174	0.98	82	2.09
5	1/0	255	226	1.13	126	2.02
10	1/0	257	417	0.62	282	0.91
7	1/0	748	591	1.27	408	1.83
12	1/0	1289	1579	0.82	1450	0.89
39	1/0	1781	1274	1.40	1049	1.70
38	1/0	5013	2716	1.85	2668	1.88
233	1/0	6519	2158	3.02	2051	3.24
33	1/0	9609	4063	2.37	4173	2.30
16	1/0	3093	**	----	----	----
237	1/0	16418	2986	5.50	2977	5.51
228	10/0	481	668	0.72	467	1.03
40	10/0	1705	930	1.83	697	2.45
6	0/1	207	168	1.23		
11	0/1	209	155	1.35		
14	0/1	219	236	0.93		
8	0/1	413	427	0.97		
13	0/1	846	1022	0.83		
241	0/1	1940	2022	0.96		
238	0/1	4619	2842	1.63		

* PREDICTED LIFE VALUE CALCULATED USING CYCLIC CREEP CP LINE

** COULD NOT ACCURATELY PARTITION

TABLE V
BASELINE DATA CORRELATION (con't.)

SPEC	TYPE	N_f	N_{PRED}	N_f/N_{PRED}	N^*_{PRED}	N_f/N^*_{PRED}
222	0/10	224	581	0.39		
41	0/10	283	276	1.03		
1	1/1	156	165	0.95	154	1.01
2	1/1	238	273	0.87	259	0.92
32	1/1	358	522	0.69	495	0.72
9	1/1	959	699	1.37	727	1.32
15	1/1	1288	1259	1.02	1193	1.08
229	1/1					
28	10/10	115	105	1.10	116	0.99
31	10/10	199	144	1.38	155	1.28
230	10/10	331	450	0.74	451	0.73

* PREDICTED LIFE VALUE CALCULATED USING CYCLIC CREEP CP LINE

TABLE VI
UNBALANCED STRAIN HOLD TESTS - PARTITIONED DATA

TEST	TYPE	$\Delta\epsilon_{TOT}^1$	$\Delta\epsilon_{in}^1$	$\Delta\epsilon_{PP}^1$	$\Delta\epsilon_{CP}^1$	$\Delta\epsilon_{CC}^1$	σ_{TEN}^2	N_f
227	10/1	1.40	.292	.198	.042	.052	144.0	455
223	10/1	1.20	.158	.113	.025	.021	118.0	945
226	1/10	1.40	.221	.158	.009	.054	165.0	349
225	1/10	1.20	.162	.114	.006	.042	150.0	464

1) % TEST STRAIN

2) KSI

TABLE VII
INTERMEDIATE STRAIN HOLD TESTS - PARTITIONED DATA

TEST	TYPE	$\Delta\epsilon_{TOT}^1$	ϵ_{HOLD}^1	$\Delta\epsilon_{in}^1$	$\Delta\epsilon_{PP}^1$	$\Delta\epsilon_{CP}^1$	$\Delta\epsilon_{PC}^1$	σ_{TEN}^2	N_f
242	11/0	1.80	+0.80	.422	.371	.051	.000	163.0	472
244	11/0	1.60	+0.70	.266	.227	.039	.000	154.0	447
246	11/0	1.80	+0.70	.412	.347	.065	.000	170.0	253
247	0/11	1.80	-0.70	.356	.298	.000	.0579	172.0	263

1) % STRAIN

2) KSI

TABLE VIII
LOW RATE STRAIN CYCLE TESTS (.05 CPM) - PARTITIONED DATA

SPEC	$\Delta\epsilon_{TOT}^4$	$\Delta\epsilon_{in}^4$	f_{PP}	f_{CC}	σ_{TEN}^5	N_f
23 ¹	1.84	.450	0.96	.04	161.0	110
24	1.74	.350			168.0	159
20	1.59	.250			161.0	301
25	1.46	.180			145.0	282
34 ²	1.30	.120	1.00	0.00	137.0	526
19 ³	1.17	.100	1.00	0.00	117.0	1138

1) PARTITIONED FROM RESULTS OF SPEC. 249

2) PARTITIONED FROM RESULTS OF SPEC. 250

3) PARTITIONED FROM RESULTS OF SPEC. 248

TABLE VIII
LOW RATE STRAIN CYCLE TESTS (.05 CPM) - PARTITIONED DATA (con't.)

SPEC	0.05 cpm		20 cpm		f_{CC}
	$\Delta \epsilon_{in}^4$	$\Delta \sigma_{TOT}^5$	$\Delta \epsilon_{in}^4$	$\Delta \sigma_{TOT}^5$	
249	.450	375	.432	373	.04
250	.030	336	.035	335	.00
248	.103	346	.136	341	.00

4) % STRAIN

5) KSI

TABLE IX
VARIABLE RATE STRAIN CYCLE - PARTITIONED DATA

SPEC	TYPE	$\Delta \epsilon_{TOT}$	$\Delta \epsilon_{in}$	f_{PP}	f_{ij}	σ_{TEN}	N_f
251	FAST-SLOW	1.4	.098	.88	.12	161.0	636
252	SLOW-FAST	1.4	.066	.88	.12	166.0	194

TABLE X
VERIFICATION TESTS - SRP LIFE PREDICTION

SPEC	TYPE	N_{PRED}	N_f	N_f/N_{PRED}
227	10/1	302	455	1.51
223	10/1	616	945	1.53
226	1/10	400	349	0.87
225	1/10	557	464	0.83
242	i1/0	287	472	1.64
244	i1/0	455	447	0.98
246	i1/0	286	253	0.88
247	0/i1	191	263	1.38
23	.05 cpm	268	110	0.41
34	.05 cpm	1290	526	0.41
15	.05 cpm	1582	1138	0.72
251	FAST-SLOW	907	636	0.70
252	SLOW-FAST	1976	194	0.10

TABLE XI
LIFE PREDICTION - VALIDATION TESTS - STRESS/TIME EQUATIONS

SPEC	TYPE	N_{PRED}	N_f	N_f/N_{PRED}
227	10/1	354	455	.78
223	10/1	928	945	.98
226	1/10	342	349	.98
225	1/10	685	464	1.47
242	i1/0	481	472	1.02
244	i1/0	829	447	1.85
246	i1/0	315	253	1.24
247	0/i1	279	263	1.06

TABLE XI
LIFE PREDICTION - VALIDATION TESTS - STRESS/TIME EQUATIONS (con't.)

SPEC	TYPE	N_{PRED}	N_f	N_f/N_{PRED}
23	.05 cpm	188	110	.59
24	.05 cpm	145	159	1.10
20	.05 cpm	188	301	1.60
25	.05 cpm	341	282	.83
34	.05 cpm	459	526	1.15
19	.05 cpm	936	1138	1.22
251	FAST/SLOW	464	636	1.37
252	SLOW/FAST	156	194	.81

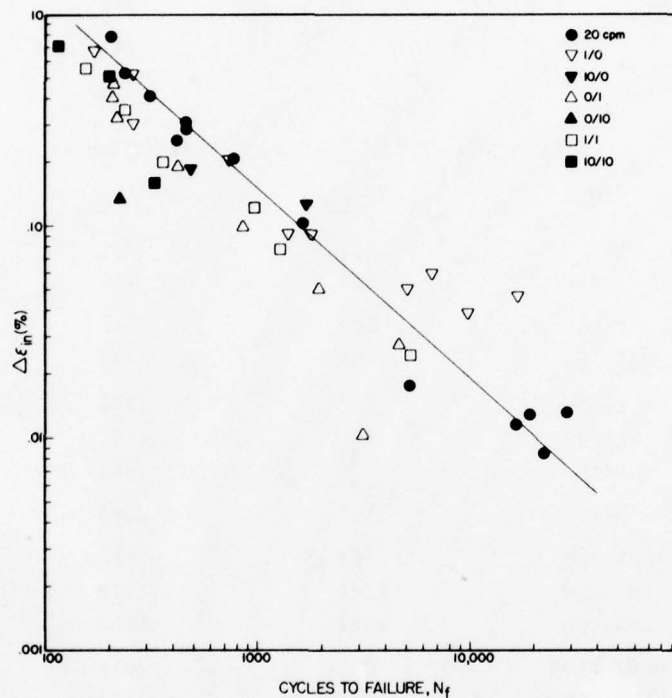


Fig. 1. Low cycle fatigue data for Rene 95 baseline strain controlled tests at 922K (1200°F). The line shown is the Manson-Coffin relationship for 20 cpm tests.

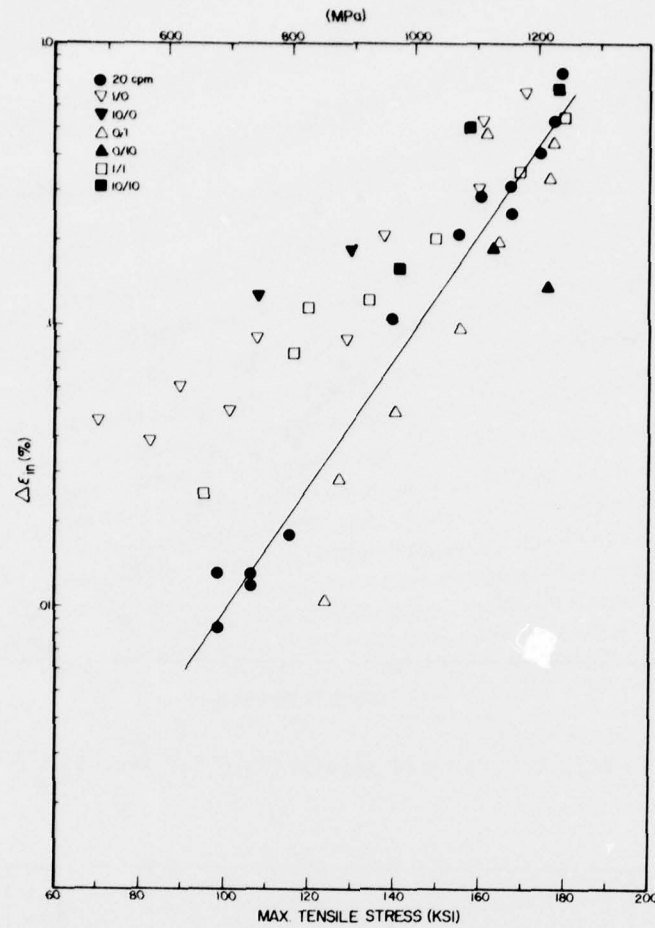


Fig. 2. Relationship of maximum tensile stress to inelastic strainrange for baseline tests. Best fit line constructed for 20 cpm data.

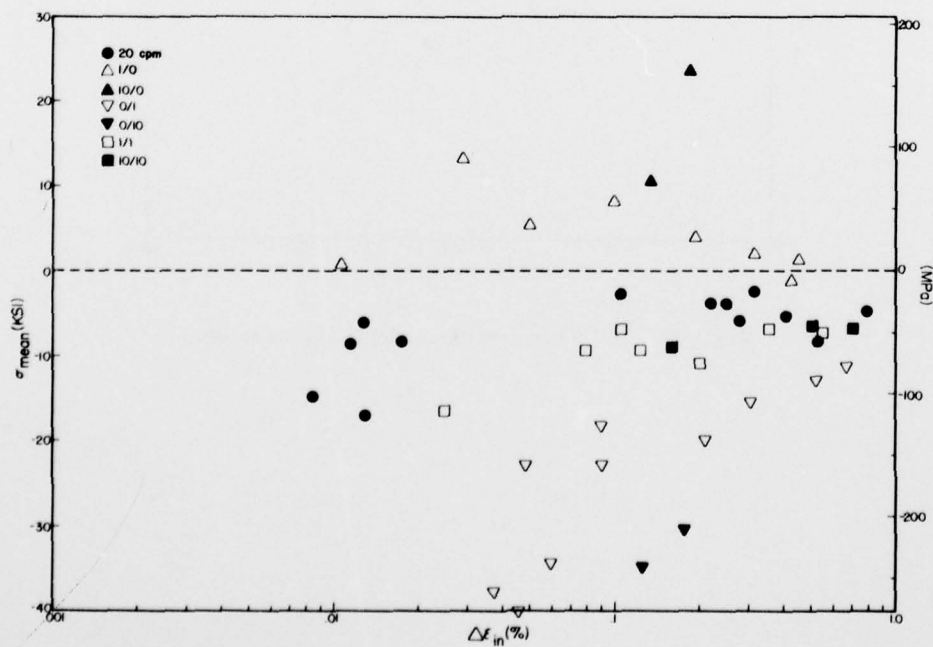


Fig. 3. Relationship of mean stress

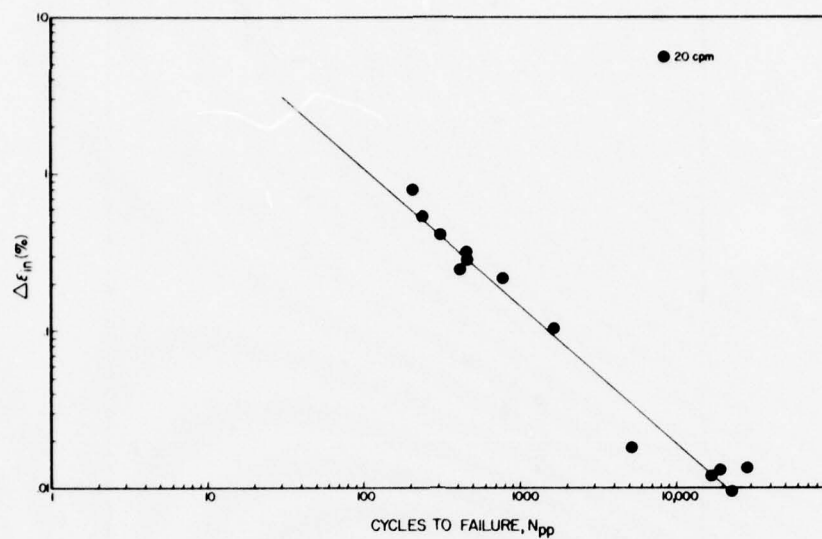


Fig. 4. PP life relationship for Rene 95.

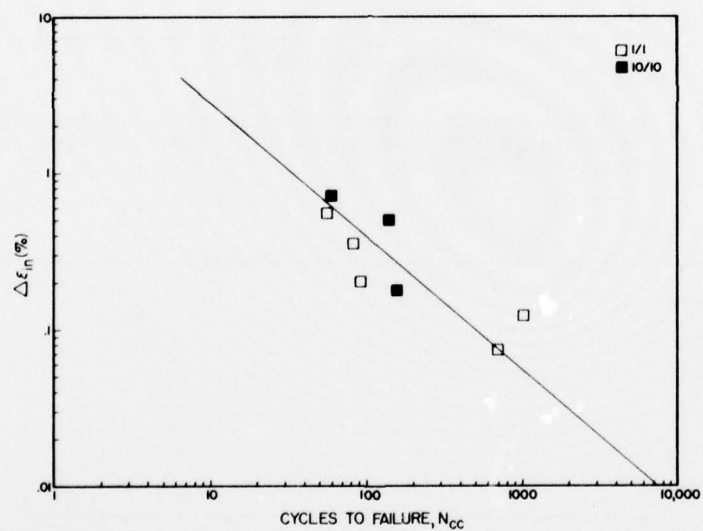


Fig. 5. CC life relationship for Rene 95.

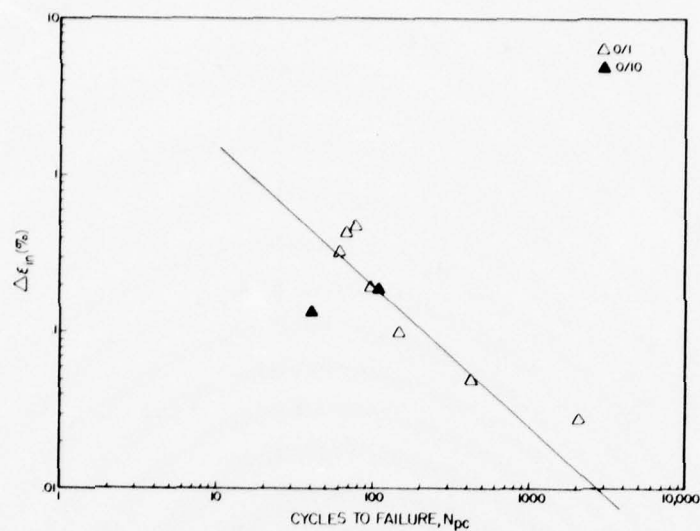


Fig. 6. PC life relationship for Rene 95.

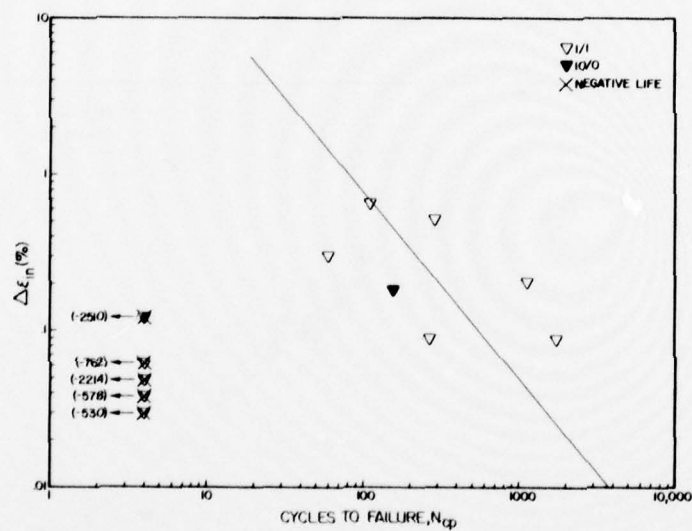


Fig. 7. CP life relationship for Rene 95 based on positive N_{cp} data only.

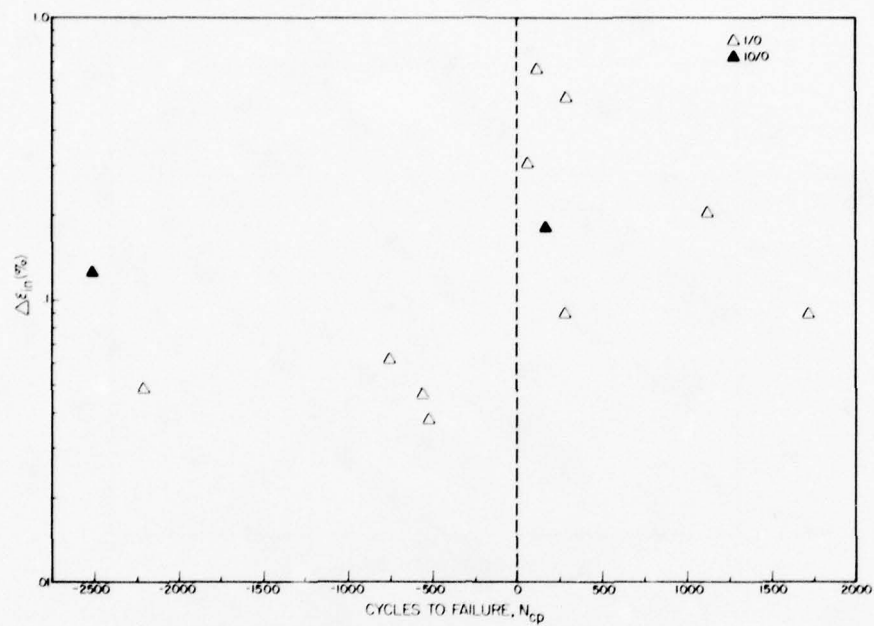


Fig. 8. Semi-logarithmic plot of N_{cp} data versus $\Delta \epsilon_{in}$ showing calculated negative N_{cp} lives.

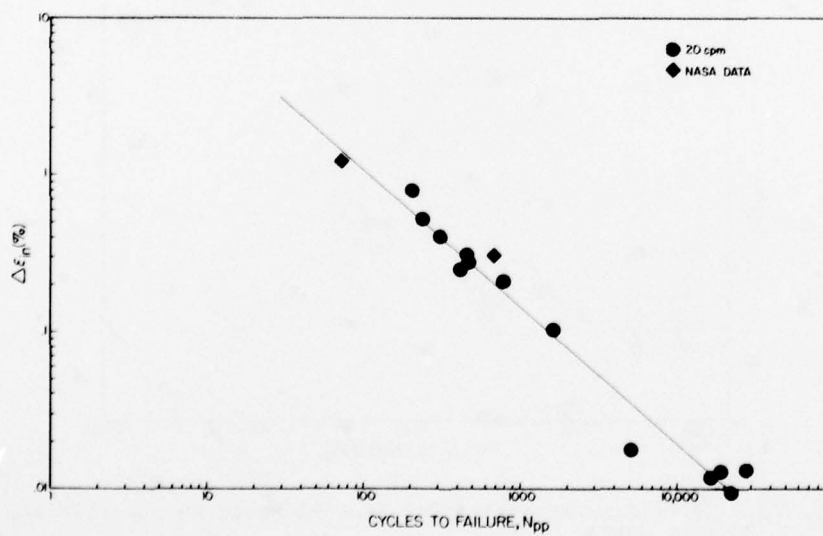


Fig. 9. Comparison of NASA PP data with baseline PP relationship.

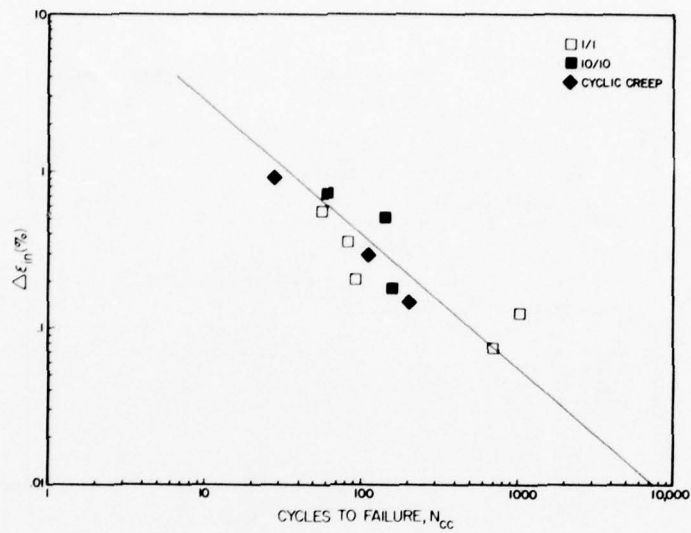


Fig. 10. Comparison of balanced cyclic creep data with the baseline CC relationship.

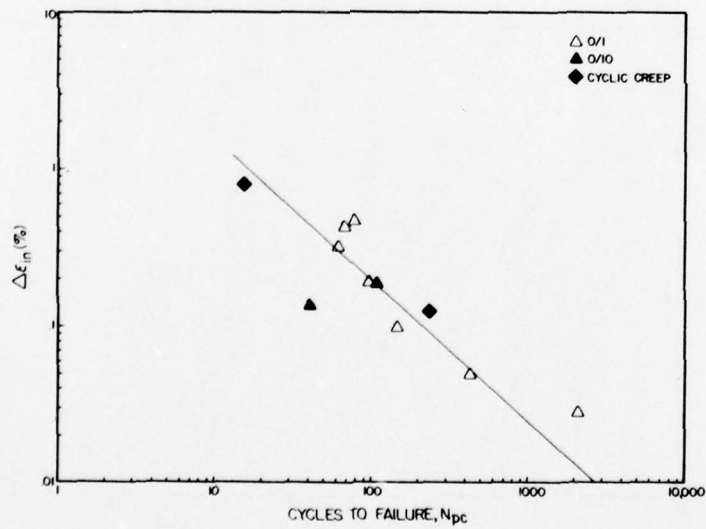


Fig. 11. Comparison of compressive cyclic creep data with the baseline PC relationship.

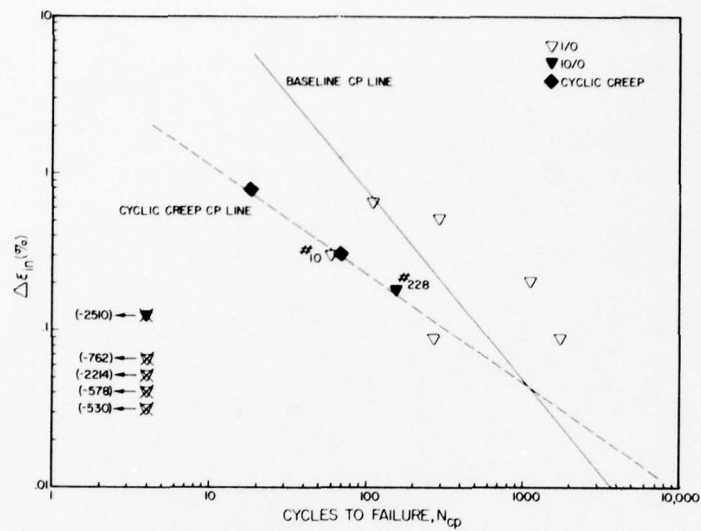


Fig. 12. Comparison of tensile cyclic creep data with the baseline CP relationship, and construction of the cyclic creep CP line.

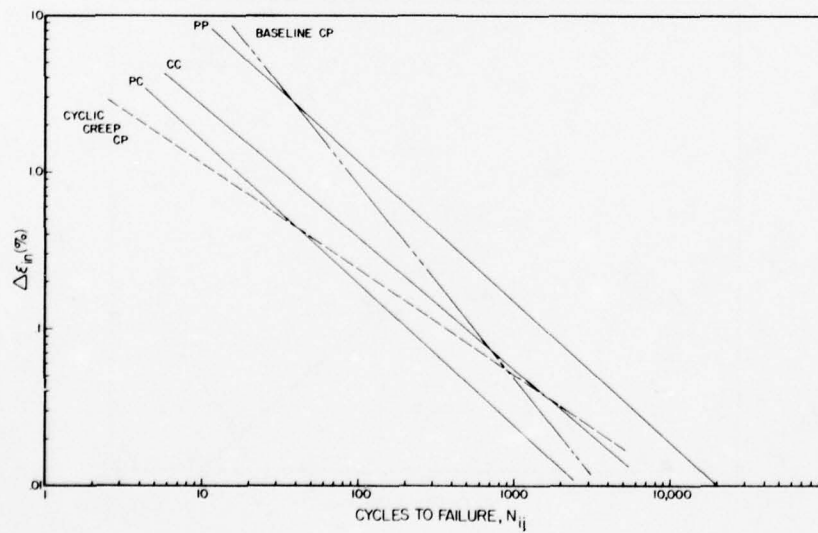


Fig. 13. Summary of partitioned strainrange-life relationships for Rene 95.

AD-A059 900

ADVISORY GROUP FOR AEROSPACE RESEARCH AND DEVELOPMENT--ETC F/G 11/6
CHARACTERIZATION OF LOW CYCLE HIGH TEMPERATURE FATIGUE BY THE S--ETC(U)
AUG 78

UNCLASSIFIED

AGARD-CP-243

NL

3 OF 4

AD
A059900



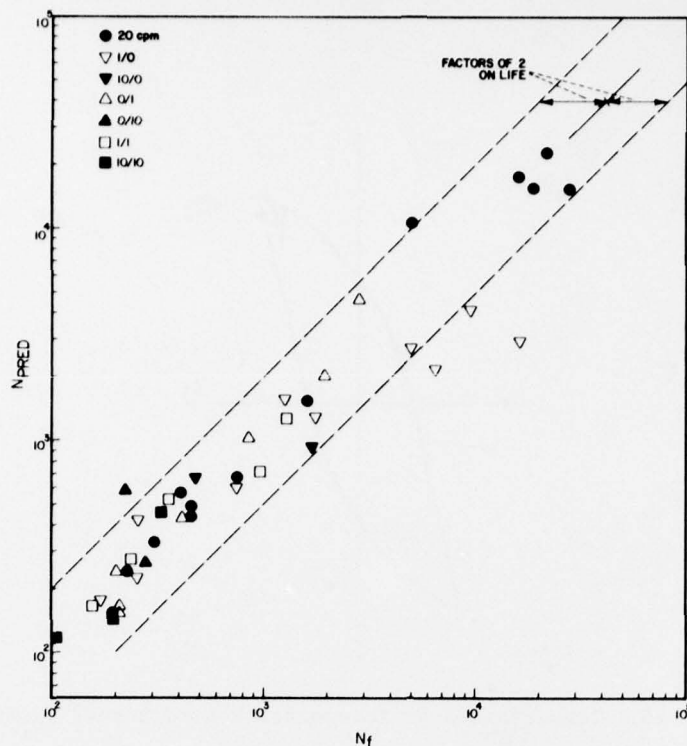


Fig. 14. Comparison of observed and predicted life for baseline tests.

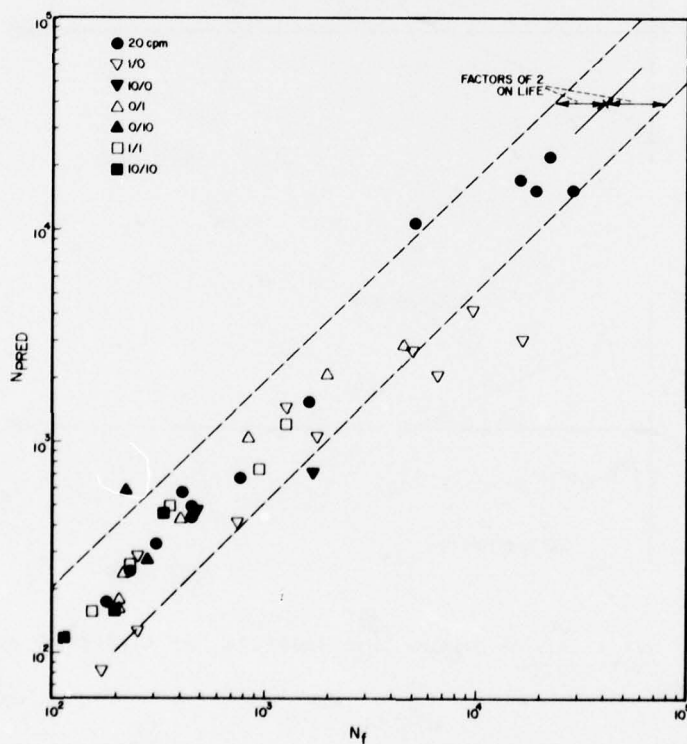


Fig. 15. Comparison of observed and predicted life for baseline tests based on cyclic creep CP line.

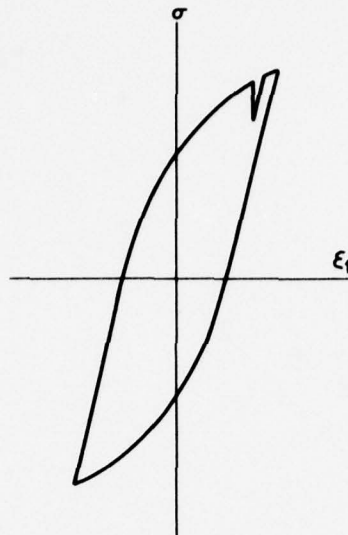


Fig. 16. Illustration of intermediate strain hold cycle.

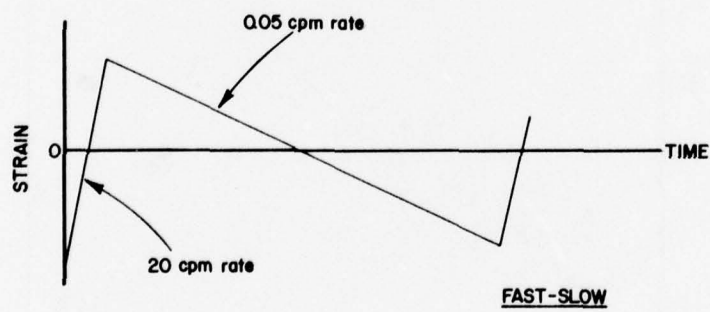
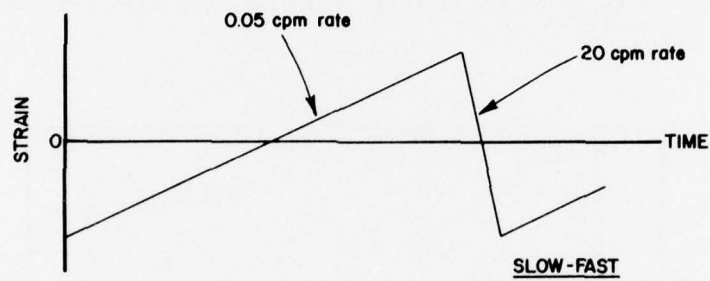


Fig. 17. Total strain versus time waveform for fast-slow and slow-fast tests.

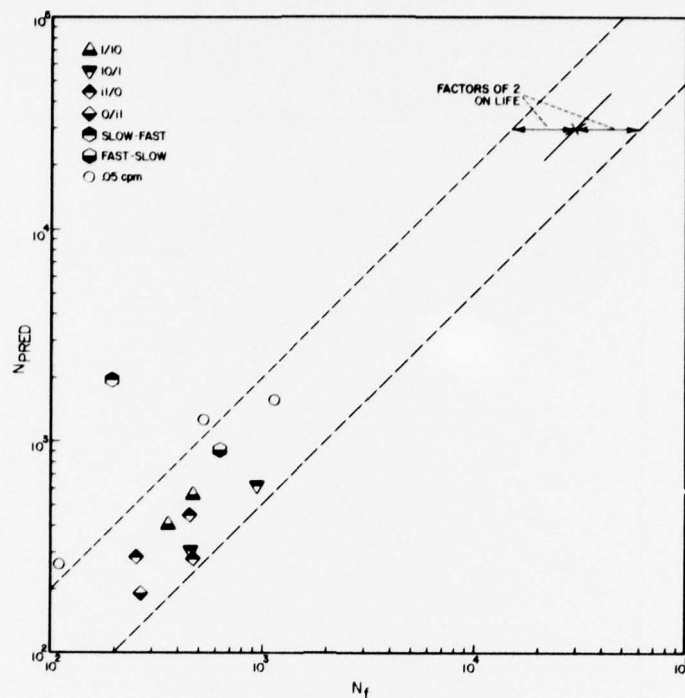


Fig. 18. Comparison of observed and predicted life for validation tests based on baseline SRP relationships.

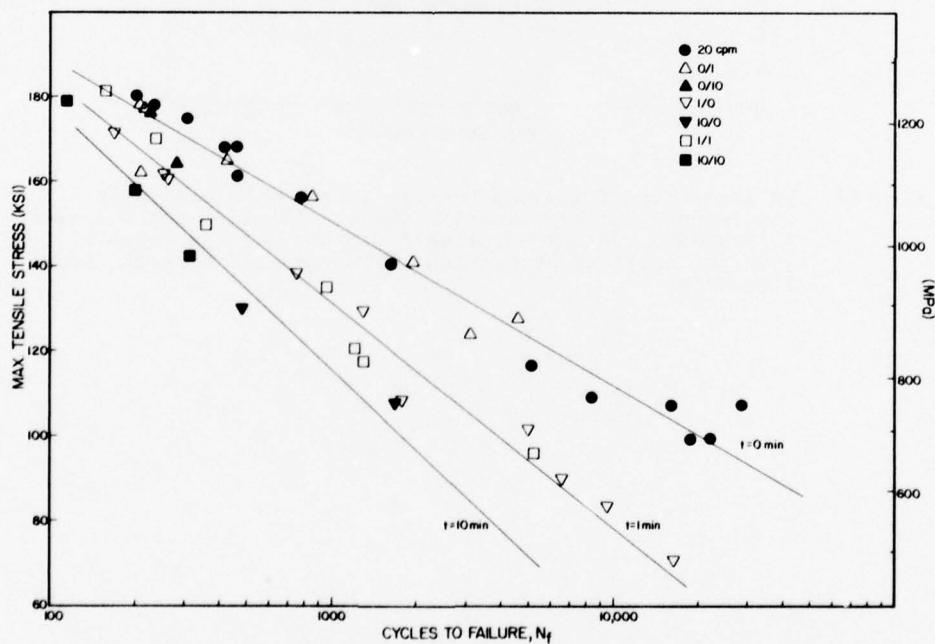


Fig. 19. Relationships of LCF life to maximum tensile stress for baseline tests with different hold times in tension.

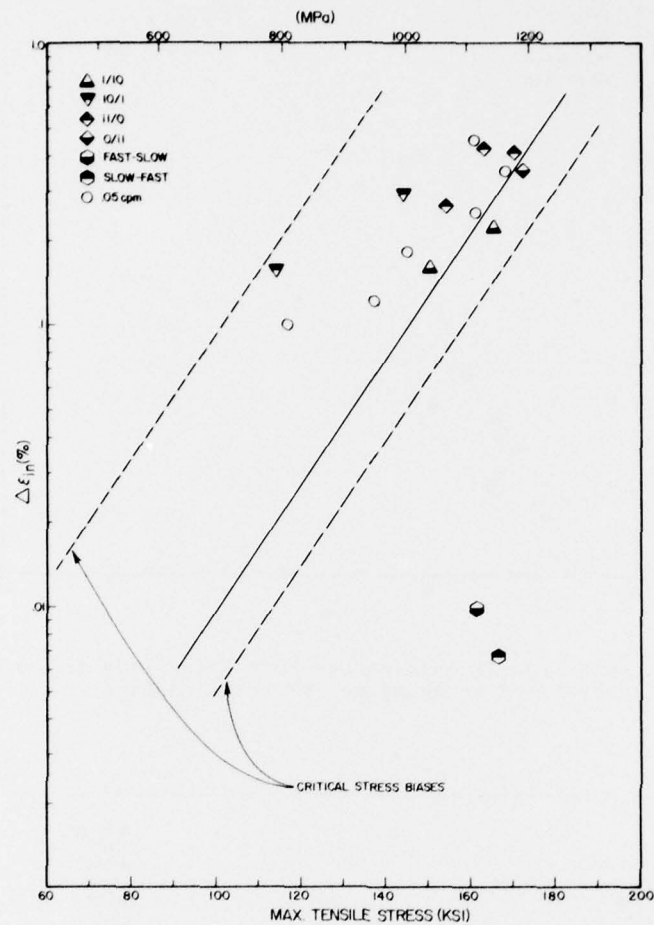


Fig. 20. Relationship of maximum tensile stress with inelastic strainrange for verification tests. The line for the time independent, 20 cpm baseline tests has been included along with the critical stress limits constructed from the base-line data.

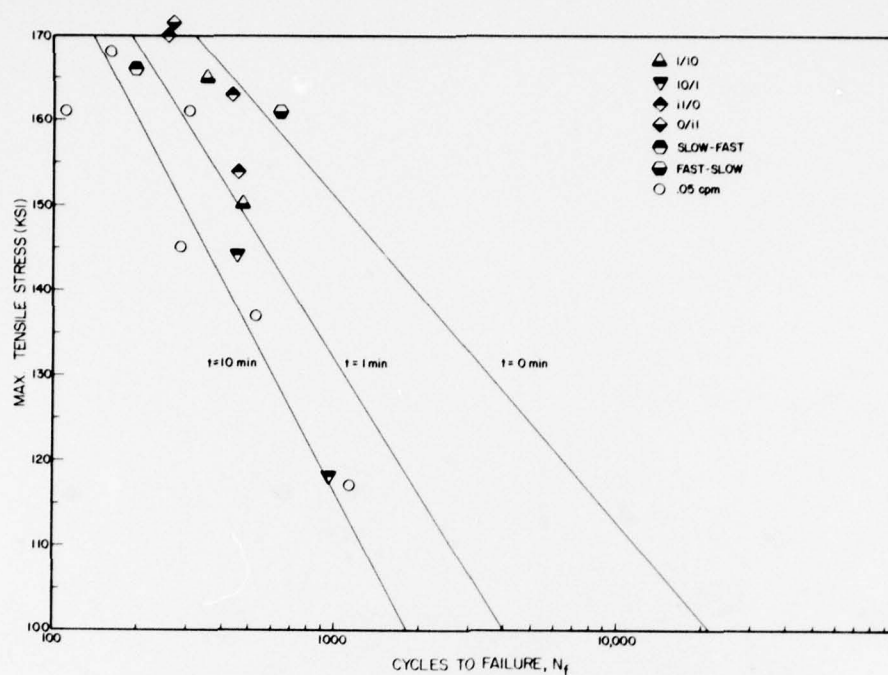


Fig. 21. Comparison of verification test data with the maximum tensile stress-tensile hold time correlation developed for the baseline tests.

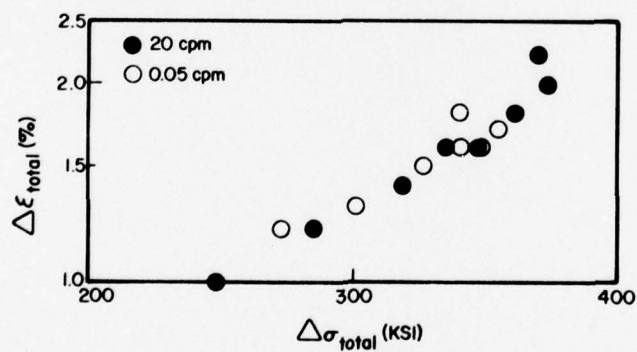


Fig. 22. Stressrange versus total strainrange for 20 cpm and 0.05 cpm continuously cycling tests.

DISCUSSION SUMMARY OF SESSION II

by

Dr.-Ing. Harald Zenner

Industrieanlagen-Betriebsgesellschaft mbH
Einsteinstraße, 8012 Ottobrunn, Germany

The seven papers read at the session presented new test results, i.e. strainrange vs. cyclic life relationship for numerous materials, experiences with test techniques, and interpretation of test results based on the concept of strainrange partitioning (SRP). Most of the discussion concerned the applicability of SRP to predicting high-temperature low-cycle behaviour. Especially the papers by M.F. Day and G.B. Thomas, and by J.M. Hyzak and H.L. Bernstein demonstrated that SRP, in its present form, cannot always be successfully applied. So, tension hold cycles were significantly less damaging than PP cycles. In this case the values of N_{cp} calculated from the interaction rule are negative. - Tests have shown that tensile strain hold cycles develop lower peak tensile stresses than do compressive hold cycles. Furthermore, the material response is such that larger shifts develop in the maximum stress during some strain hold cycles, than in cycles without hold periods. It is suggested that there is a direct influence of the maximum stress on fatigue life.

On this point, it was commented that cyclic peak tensile stress or mean stress show different effects for different materials. To separate these important effects from each other, a crucial type of test was proposed in which maximum tensile stress, or mean stress, could be controlled and other stress components - such as stress range - would be held constant. - Nor should it be supposed that crack propagation behaviour could explain the observed phenomenon. The low fracture toughness of the investigated alloy René 95 will not allow much cyclic crack propagation. Even a tiny flaw might result in a brittle fracture condition.

Other, more basic, remarks on SRP were related to the possible number of parameters. Trying to use SRP over a vast range of materials, over a vast range of temperatures, over regimes where the mechanism of failure changes, over the stage of crack initiation and propagation and different environmental conditions, it could not be expected that a single universal rule applies. The SRP, as currently formulated, is associated with eight independent material constants. However, with the introduction of further constants the method would be cumbersome to handle.

With regard to lifetime prediction, other questions were asked: What can be considered a good prediction, a prediction that is off by a factor of ± 4 , ± 2 , or ± 10 ? Do any experiences exist in applying SRP to component tests?

The originators of SRP emphasized that this particular conference was devoted to some of the preliminary investigations of SRP as the first necessary step to take. Any method should first correlate laboratory data. Only when this has been established, and further refinements have been made, the method should be checked as to whether it can be applied to components. To apply it too quickly could be disastrous.

According to S.S. Manson, the objective of the conference was to exchange experiences in the application of SRP in order to point out the range in which SRP is valid, to point out limitations and consider modifications that are needed to make it more valid. - For example, it would not seem very difficult to add, to SRP, a term covering the effect of mean stress. So, the ratio of maximum stress to stress range could be a suitable measure.

Another point of discussion concerned the problem of crack propagation. Crack propagation should be considered as important as crack initiation. It is necessary to know how much of life is initiation, and how much is propagation. According to S.S. Manson, a method for predicting crack propagation life, similar to SRP in involving four propagation laws, is already in the stage of proposal.

When looking for alternatives at this time, the question arises which framework would be the simplest for treating the different types of problems and which would be cumbersome. It is believed by the originators that SRP provides a sounder basis for potential modifications than other methods do.

An Application of Strainrange Partitioning to Copper-Base Alloys at 538°C

R.H. Stentz, Vice-President, Research and Development
 J.T. Berling, Vice-President, Engineering
 J.B. Conway, President

Mar-Test Inc.
 45 Novner Drive
 Cincinnati, Ohio 45215 - USA

Summary

Strain-controlled low-cycle fatigue tests on two copper alloys, NARloy Z and 1/2 Hard AMZIRC were performed in argon at 538°C. The tests employed symmetrical triangular strain-waveforms at strain rates from 4×10^{-5} to $1 \times 10^{-2} \text{ sec}^{-1}$ in addition to asymmetrical strain-waveforms of alternating fast and slow strain rates. Partitioned strainrange versus life relationships were established for both alloys with the $\Delta\epsilon_{cp}$ component of strain being identified as the most severely damaging in each case. The relationships for NARloy Z were then used effectively to predict fatigue life values for hold-time tests and for other tests involving asymmetrical waveforms.

LIST OF SYMBOLS

E	modulus of elasticity
$\Delta\epsilon_t$	total axial strain range
$\Delta\epsilon_e$	elastic strain range
$\Delta\epsilon_{inel.}$	inelastic strain range
$\dot{\epsilon}$	strain rate
N_f	cycles to failure
$\Delta\sigma$	stress range
σ_t	tensile portion of stress range
σ_c	compression portion of stress range
N_{pp}	PP cyclic life
N_{cc}	CC cyclic life
N_{cp}	CP cyclic life
N_{pc}	PC cyclic life
$\Delta\epsilon_{pp}$	PP component of inelastic strain range
$\Delta\epsilon_{cc}$	CC component of inelastic strain range
$\Delta\epsilon_{cp}$	CP component of inelastic strain range
$\Delta\epsilon_{pc}$	PC component of inelastic strain range
F_{pp}	PP inelastic strain fraction
F_{cc}	CC inelastic strain fraction
F_{cp}	CP inelastic strain fraction
F_{pc}	PC inelastic strain fraction

INTRODUCTION

Regeneratively-cooled, reusable-rocket nozzle liners such as found in the engines of the Space Shuttle, Orbit-to-Orbit Shuttle, Space Tug, etc., undergo a severe thermal strain cycle during each firing. To withstand the severe cycles, the liner material must have a proper combination of high thermal conductivity and high low-cycle fatigue resistance. Copper-base alloys possess these desirable qualities and for this reason a broad-based NASA-Lewis/Mar-Test program was initiated in 1972 to evaluate several candidate alloys by generating the material property data that are required for the design and life prediction of rocket nozzle liners.

This paper deals with a portion of the overall program that focused on the performance of a series of strain-controlled low-cycle fatigue tests to enable the partitioned strainrange versus life relationships to be determined for two copper-base alloys. All tests were performed in high-purity argon at 538°C and the results obtained at various strain rates were used in the identification of the strainrange relations for plasticity reversed by plasticity and creep reversed by creep. Then an asymmetrical strain-waveform was employed involving a low strain rate during the tension-going portion of each cycle. These tests results were used in conjunction with the PP and CC lines to determine the strainrange relationships for creep reversed by plasticity. Similar tests with fast-slow cycling enabled the strainrange relation for plasticity reversed by creep to be identified.

These partitioned strainrange versus life relationships were then used to estimate the fatigue life for other test conditions. Some additional slow-fast tests were performed along with some hold-time evaluations and the measured fatigue life values were then compared with the estimates obtained from the partitioned strainrange plots. Excellent agreement was noted and thus the strainrange partitioning concept was found to be an effective method in describing creep-fatigue interactions for the test conditions employed in this study.

MATERIAL

Specimen material for use in this portion of the program was supplied by NASA-Lewis Research Center, Cleveland, Ohio. A brief description of the two materials evaluated within this effort is given in Table 1. The specimen design shown in Figure 1 was employed in all tests.

After being machined, all specimens were wrapped in soft tissue paper and placed in individual hard plastic cylinders (about 9 cm in length and 2.2 cm inside diameter). The ends of these cylinders were then sealed with masking tape and the specimen code number was written on the external surface of the cylinder. These cylinders were used for storage before and after test.

In preparing for a test, each specimen was subjected to the following:

- 1) the specimen was washed with Freon to remove any surface oils which might have remained after machining;
- 2) a small quantity of dilute phosphoric acid was applied by hand to the complete surface of the specimen; this removed any surface oxides and any machining oil not removed by the cleaning with Freon; this operation was completed within 15 seconds;
- 3) the specimen was rinsed in warm water and dried using soft absorbent tissue;
- 4) the specimen was then subjected to a final cleaning with Freon.

TEST PROCEDURE

All tests were performed at 538°C using a servo-controlled, hydraulically actuated fatigue testing machine. Threaded, hourglass-shaped specimens were mounted in the holding fixtures of the test machine using special threaded adaptors. These tests were performed in high-purity argon gas with 3000 ppm of hydrogen added to provide a slightly reducing environment for additional protection of the specimens. In order to perform these tests in this argon environment (oxygen content less than 0.01 percent by volume) a cylindrical containment vessel, made of pyrex, was positioned between the holding fixtures of the fatigue machine and neoprene low-force bellows at either end provided the seal to enable the desired gas purity levels to be maintained throughout the test. Side outlets (with appropriate seals) on this containment vessel provided entrance ports to accommodate the extensometer arms and similar side outlets provided entrance ports for the copper tubing leads to the induction coil. In addition, special ports near the bottom of the containment vessel enabled the chromel-alumel thermocouples, used for specimen temperature measurement, to be routed out to the temperature control system. Specimen test temperatures were attained using induction heating and this was provided by positioning a specially designed induction coil around the test specimen (see Figure 2).

All force measurements were made using a load cell mounted within the loading train of the fatigue machine and specimen strains were measured by using a high temperature diametral extensometer. An analog strain computer was employed which allowed the diametral strain signal to be used in conjunction with the load signal so as to provide an instantaneous value for the axial strain which was then the controlled variable (1,2).

DISCUSSION OF RESULTS

NARloy Z Alloy

A series of low-cycle fatigue tests of this alloy was performed in argon at 538°C and at various strain rates to define the fatigue characteristics summarized in the Material Data Appendix. Originally, the intention was to use the higher strain rate data to generate the $\Delta\epsilon_{pp}$ - N_{pp} relationships directly. This, however, proved to be not feasible. The extremely low cyclic strain hardening exponent exhibited by the material at 538°C indicated that a substantial creep component was probably present even at the highest strain rate. Further evidence of this can be obtained from Figures 3 and 4 which contain $\Delta\epsilon_f$ vs N_f and $\Delta\epsilon_{inel}$ vs N_f relationships respectively. The results at various strain rates are shown to illustrate that time effects were present during all of the tests. Tests at even higher strain rates were considered but because of the limited response characteristics of the extensometer used in this program it was concluded that this approach could not be employed.

It was decided, therefore to employ an indirect determination of the PP and CC characteristics. This

was initiated by generating a plot of the cycles to failure, at a given strainrange, versus strain rate as shown in Figure 5. At each strainrange a tendency toward a saturation fatigue life in both the low and high strain-rate regimes is assumed similar to that reported previously (3,4) for other materials. Admittedly, without a great deal of justification at this point, the saturation values of N_{CC} and N_{PP} at the total strain ranges of 0.9% and 2.6% were assumed to be the values shown in Figure 5. Corresponding values of $\Delta\epsilon_{CC}$ and $\Delta\epsilon_{PP}$ were not directly obtainable since, for a given strainrange, the inelastic strain-range changed slightly as a function of strain rate. It was decided therefore to just use the value of the total strainrange for the values of $\Delta\epsilon_{CC}$ and $\Delta\epsilon_{PP}$ in preparing the strainrange partitioning plots. These results were then used to position the PP and CC lines for the NARloy Z alloy as shown in Figure 6.

Slow-fast and fast-slow strain cycling, in accordance with the strain profiles shown in Figure 7, was employed to establish the CP and PC partitioned strainrange versus life relationships. During the slow straining portion of the cycles a strain rate of $4 \times 10^{-4} \text{sec}^{-1}$ was employed while a strain rate of $1 \times 10^{-2} \text{sec}^{-1}$ was used during fast straining. A summary of the results obtained in these tests is presented in the Material Data Appendix (Specimens Numbers 107, 108, 109 and 110) to indicate that the slow-fast cycling is much more detrimental than the fast-slow cycling. In addition, it can be noted that a mean compressive stress develops during slow-fast cycling while a mean tensile stress is seen to exist in the fast-slow cycle.

In order to partition the strainranges involved in the slow-fast and fast-slow cycling, the creep and plastic strain components in each half cycle had to be determined. This was accomplished using Figure 5. For a given strainrange, the saturation values for N_f were noted and used for N_{PP} and N_{CC} in the Interaction Damage Rule (3):

$$\frac{F_{PP}}{N_{PP}} + \frac{F_{CC}}{N_{CC}} = \frac{1}{N_f} \quad (1)$$

$$\frac{F_{PP}}{N_{PP}} + \frac{(1-F_{PP})}{N_{CC}} = \frac{1}{N_f} \quad (2)$$

Then for each strain rate involved ($4 \times 10^{-4} \text{sec}^{-1}$ and $1 \times 10^{-2} \text{sec}^{-1}$) the N_f value was obtained from Figure 5 and used to solve equation (2) for the corresponding F_{PP} and F_{CC} fractions for the continuous cycling tests. These fractions, for the individual strain rates, were then assumed to apply within the appropriate half-cycle of the slow-fast and fast-slow tests. For example, at a strainrange of 2.6% and a strain rate of $1 \times 10^{-2} \text{sec}^{-1}$ the N_f value for continuous cycling from Figure 5 is 350. This together with $N_{PP}=800$ and $N_{CC}=33$ yields $F_{PP}=0.945$ and $F_{CC}=0.055$. Similar values for F_{PP} and F_{CC} at a strain rate of $4 \times 10^{-4} \text{sec}^{-1}$ are 0.82 and 0.18. These were assumed to apply at 2% strain range for the analysis of the slow-fast test ($4 \times 10^{-4} \text{sec}^{-1} / 1 \times 10^{-2} \text{sec}^{-1}$) at this strain range. Dealing in terms of total strainrange:

$$\Delta\epsilon = 2.0\%$$

For the slow strain rate portion of the cycle (tension-going):

$$F_P = 0.82 \\ F_C = 0.18$$

For the fast strain rate portion of the cycle (compression-going):

$$F_P = 0.945 \\ F_C = 0.055$$

Since the fully reversed plastic and creep strain fractions (F_{PP} and F_{CC}) must be equal to the lesser of those same fractions in tension and compression, it follows that:

$$F_{PP} = 0.82 \\ F_{CC} = 0.055 \\ \text{and } F_{CP} = 1 - 0.82 - 0.055 \\ \text{or } F_{CP} = 0.125$$

From the $\Delta\epsilon_{PP}$ and $\Delta\epsilon_{CC}$ lines in Figure 6 it can be determined that N_{PP} and N_{CC} at $\Delta\epsilon=2.0\%$ are 1450 and 55 cycles respectively. Therefore using:

$$\frac{F_{PP}}{N_{PP}} + \frac{F_{CC}}{N_{CC}} + \frac{F_{CP}}{N_{CP}} = \frac{1}{N_f}$$

and substituting the values above, in addition to $N_f=66$ cycles for this test, yields $N_{CP}=9$ cycles. Similar calculations for the other three tests led to the determination of the N_{CP} and N_{PC} versus partitioned strainrange relationships as shown in Figure 6.

In some additional slow-fast testing of the R-24 alloy, the strain rate of $1 \times 10^{-2} \text{sec}^{-1}$ was maintained for the fast portion of the cycle while rates of $4 \times 10^{-5} \text{sec}^{-1}$ and $7 \times 10^{-6} \text{sec}^{-1}$ were employed in the tension-going slow straining portion of the cycle. These evaluations led to the results summarized in the Material Data Appendix and presented graphically in Figures 8 and 9. These interesting comparisons highlight several important considerations. One is the fact that slow-fast cycling of this material at the conditions employed is much more detrimental than fast-slow cycling. Another is the fact that the fast-slow exposure leads to a fatigue life that is not significantly different from that observed in the continuous cycling tests at the fast ($1 \times 10^{-2} \text{sec}^{-1}$) strain rate. In other words, the introduction of a strain rate of $4 \times 10^{-4} \text{sec}^{-1}$ into the compression-going portion of the cycle led to a small but not significant reduction in the fatigue life. The third observation made in connection with Figures 8 and 9 relates to the continual reduction in fatigue life as the tension-going strain rate is decreased. Based on a strain range of 0.50%, the introduction of a tension-going strain rate of $7 \times 10^{-6} \text{sec}^{-1}$ leads to a fatigue life reduction of more than two orders of magnitude based on the use of a strain rate of $1 \times 10^{-2} \text{sec}^{-1}$ throughout the cycle.

Prediction of Results

In addition to those tests used to determine the partitioned strainrange versus life relationships quite a few additional low-cycle fatigue tests of various types were performed for the NARloy Z material. These tests employed constant strain rates in some evaluations and slow-fast and fast-slow strain rates in other evaluations; some other evaluations employed hold-period type waveforms. Strain ranges varied from 0.5% to 3.5%, strain rates from $1 \times 10^{-2} \text{ sec}^{-1}$ to $7 \times 10^{-6} \text{ sec}^{-1}$, and in the hold-period tests a dwell of 300 seconds was employed in each cycle. The total life regime studied was from 16 cycles to about 14,000 cycles. It was obviously desirable to be able to predict these results by using the partitioned strain-range life relationships of Figure 6.

One problem encountered in these predictions was the partitioning of the strains in tests at strain ranges (and waveforms) other than those used to generate the fatigue life versus strain rate curves of Figure 5. To overcome this difficulty the 0.9% and 2.6% data were used to produce the F_{pp} versus cycle period curves shown in Figure 10. The suggestion is, therefore, that the cyclic period, at least for the continuous cycling tests on this material, can be used to estimate the F_{pp} fraction of strain, and that this relationship is essentially insensitive to strain range over a fairly large regime. This figure, along with Figure 6 was, therefore, used to estimate the lives of all of the tests on this material except those used in the generation of these two figures. The procedure used can best be explained with the aid of sample calculations made for each type of test conducted.

Continuous Cycling Tests

Specimen 102; $\Delta\epsilon = 2.0\%$, $\dot{\epsilon} = 2 \times 10^{-3} \text{ sec}^{-1}$, $N_f = 535$ cycles, cycle period = 20 seconds;
So, from Figure 10, $F_{pp} = 0.895$ and therefore $F_{cc} = 0.105$;
From Figure 6 at $\Delta\epsilon = 2.0\%$

$N_{pp} = 1450$ cycles and $N_{cc} = 55$ cycles
Therefore:

$$\frac{0.895}{1450} + \frac{0.105}{55} = \frac{1}{N_f}$$

or:

$$N_f \text{ (predicted)} = 396 \text{ cycles}$$

Slow-fast Tests

Specimen 111; $\Delta\epsilon = 3.0\%$, $\dot{\epsilon}_{ten.} = 4 \times 10^{-4} \text{ sec}^{-1}$
 $\dot{\epsilon}_{comp.} = 1 \times 10^{-2} \text{ sec}^{-1}$
 $N_f = 35$ cycles

From Figure 10 the plastic strain fraction associated with the tension-going strain rate of $4 \times 10^{-4} \text{ sec}^{-1}$ (period) = 150 sec. when based on a complete cycle at that rate) is 0.81 and the creep strain fraction is 0.19. These are defined as:

$$\begin{aligned} \text{Tension-going} \\ F_p &= 0.81 \\ \text{and } F_c &= 0.19 \end{aligned}$$

Similarly, for the compression-going strain rate of $1 \times 10^{-2} \text{ sec}^{-1}$,

$$\begin{aligned} \text{Compression-going} \\ F_p &= 0.936 \\ F_c &= 0.064 \end{aligned}$$

Therefore:

$$\begin{aligned} F_{pp} &= 0.81 \\ F_{cc} &= 0.064 \\ \text{and } F_{cp} &= 0.126 \end{aligned}$$

From Figure 6 the corresponding life values at $\Delta\epsilon = 3.0\%$ are:

$$\begin{aligned} N_{pp} &= 600 \text{ cycles} \\ N_{cc} &= 25 \text{ cycles} \\ N_{cp} &= 5 \text{ cycles} \end{aligned}$$

$$\text{and } \frac{0.81}{600} + \frac{0.064}{25} + \frac{0.126}{5} = \frac{1}{N_f}$$

or:

$$N_f \text{ (predicted)} = 34 \text{ cycles}$$

Fast-slow tests are predicted in a similar manner.

Hold-Period Tests

Specimen 40; 300 sec. hold in tension

no-hold $\dot{\epsilon} = 2 \times 10^{-3} \text{ sec}^{-1}$

$$\begin{aligned} \Delta\epsilon &= 2.6\% \\ N_f &= 75 \text{ cycles} \end{aligned}$$

Assuming a cycle period exclusive of the hold-period of 26 seconds, F_{pp} from Figure 12 is 0.885. A known component of $\Delta\epsilon_{cp}$ exists, however, which is equal to $\delta\sigma_t$ divided by E or for this test 0.077%. The strain components are then computed using the assumption that the total strain range is inelastic.

$$\begin{aligned} \Delta\epsilon_{pp} &= (0.885) (2.6\% - 0.077\%) = 2.233\% \\ \Delta\epsilon_{cp} &= 0.077\% \\ \Delta\epsilon_{cc} &= 2.6\% - 2.233\% - 0.077\% = 0.290\% \end{aligned}$$

and

$$F_{pp} = \frac{2.233}{2.6} = 0.859$$

$$F_{cc} = \frac{0.290}{2.6} = 0.111$$

$$F_{cp} = \frac{0.077}{2.6} = 0.030$$

From Figure 6 the life values for the various strain components at 2.6% are:

$$N_{pp} = 800 \text{ cycles, } N_{cc} = 33 \text{ cycles and } N_{cp} = 6.2 \text{ cycles.}$$

Therefore:

$$\frac{0.859}{800} + \frac{0.111}{33} + \frac{0.030}{6.2} = \frac{1}{N_f}$$

or:

$$N_f (\text{predicted}) = 108 \text{ cycles}$$

A comparison between the predicted and observed lives is shown in Figure 11. The agreement is within a factor of 2 in all cases.

At this point it might be fitting to comment on the validity of the original assumptions for saturation values of N_{cc} and N_{pp} of Figure 6 upon which the partitioned strainrange-life relationships were based. It might be asked whether the excellent agreement between predicted and observed lives justifies the assumptions or whether other reasonable assumptions would produce equally good results. The latter is probably more correct. Companion calculations have indicated that when completely different saturation values for N_{cc} and N_{pp} are chosen outside the range of the existing data, the partitioned strainrange-life relations are different as are the F_{pp} vs cycle period curves. The new relationships and curves are still effective, however, and lead to predictions that are just as accurate as those based on the original assumptions.

1/2 Hard Amzirc Copper Alloy

Test results for this alloy are summarized in the Material Data Appendix and encompass the same types of evaluation performed for NARloy Z. The Amzirc material presented much the same type of problem encountered with the first alloy tested in this program in that extensive amounts of creep component were present in all the continuous cycling tests. As a result the same indirect approach used in evaluating the PP and CC components was employed. This plot of N_f versus strain rate is shown in Figure 12 and this led to the PP and CC lines positioned in Figure 13.

In an attempt to obtain more information on the effect of the CC type of inelastic strain the special cycle shown in Figure 14 was employed. These tests involved inelastic strain limits of 1% in tension and compression, 1.5%/1.5% and 2.0%/2.0% with a ramp stress rate of about 100 MN/m² per second but the fatigue life values were essentially the same as those noted for continuously cycling strain-controlled tests at similar strain ranges. These observations supported the conclusion reached earlier that the inelastic strains encountered in the continuous cycling tests contained a large portion of creep component.

Fast-slow and slow-fast cycling (1×10^{-2} and $4 \times 10^{-4} \text{ sec}^{-1}$) of the type shown in Figure 7 was employed to generate PC and CP components in accordance with the approach described for NARloy Z tests. These tests led to the PC and CP lines shown in Figure 13 and as noted for NARloy 2 the slow-fast cycling was more detrimental than any other type of cycling. A unique problem emerged in the tests of the Amzirc alloy in that a dimensional instability (barrelling) was noted that was particularly pronounced in fast-slow cycling tests and also in tests with a hold period in compression. For this reason the PC line in Figure 13 could not be accurately established.

CONCLUSIONS

Strain-controlled low-cycle fatigue tests of NARloy Z and 1/2-Hard Amzirc were performed in argon 538°C and led to the definition of the partitioned strainrange versus life for these materials. For both alloys a substantial creep component was always present for the cyclic conditions employed and limitations on extensometer response characteristics precluded the use of strain rates high enough to eliminate the creep component. As a result the PP and CC strainrange versus life relationships could not be identified directly. An indirect approach was employed based on an assessment of saturation limits on N_f in the very low and very high frequency regimes. Fast-slow and slow-fast cycling was then employed to identify the PC and CP relationships. The effectiveness of the partitioned strainrange versus life relationships for NARloy Z was evaluated by using this plot to predict the fatigue life for tests not included in the establishment of the lines for the partitioned strainranges. These comparisons were very impressive and demonstrate that the strainrange partitioning concept is a valuable tool for estimating the low-cycle fatigue behavior of the alloys studied for the test conditions imposed.

Slow-fast cycling proved to be much more detrimental than fast-slow cycling for the materials involved. For NARloy Z at a strainrange of 0.50%, slow-fast cycling at $7 \times 10^{-6} / 1 \times 10^{-2}$ leads to a fatigue life reduction of more than 2 orders of magnitude compared to continuous cycling results at $1 \times 10^{-2} \text{ sec}^{-1}$.

REFERENCES

1. T. Slot, R.H. Stentz, and J.T. Berling, Controlled-Strain Testing Procedures, ASTM STP-465, 1969, p.100.
2. J.B. Conway, R.H. Stentz and J.T. Berling, High Temperature, Low-Cycle Fatigue of Advanced Copper-Base Alloys for Rocket Nozzles; Part I - NARloy Z, NASA CR- 134627, May, 1974.
3. S.S. Manson, The Challenge to Unify Treatment of High Temperature Fatigue - A Partisan Proposal Based on Strainrange Partitioning. STP 520, ASTM, 1973. pp. 744-755.
4. J.B. Conway, J.T. Berling and R.H. Stentz, Strain Rate and Holdtime Saturation in Low-Cycle Fatigue: Design Parameter Plots. STP 520, ASTM, 1973. pp. 637-647.
5. Hirschberg, M.H. and Halford, G.R.: Use of Strainrange Partitioning to Predict High-Temperature Low Cycle Fatigue Life. NASA TN D-8072, 1976.

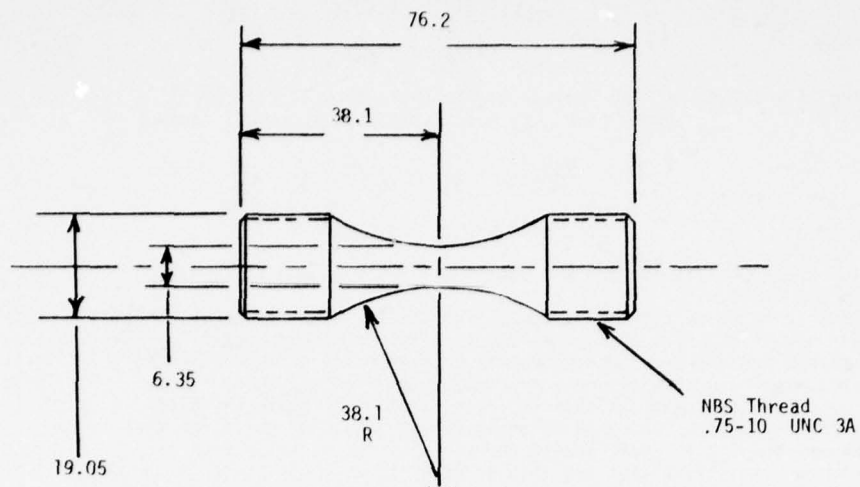


Figure 1 - Hourglass-Shaped Specimen
used in Low-Cycle Fatigue Tests.
(all dimensions in mm)

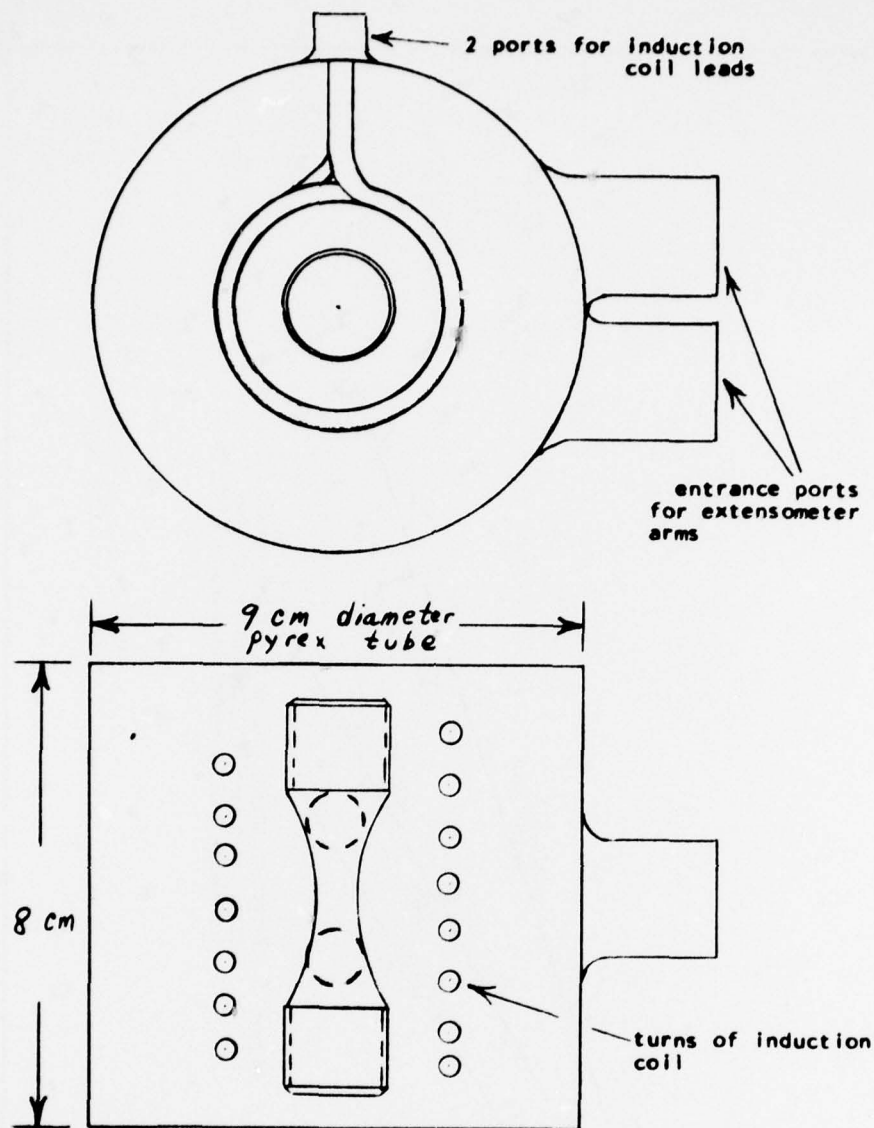


Figure 2 — Schematic of Pyrex Environmental Chamber

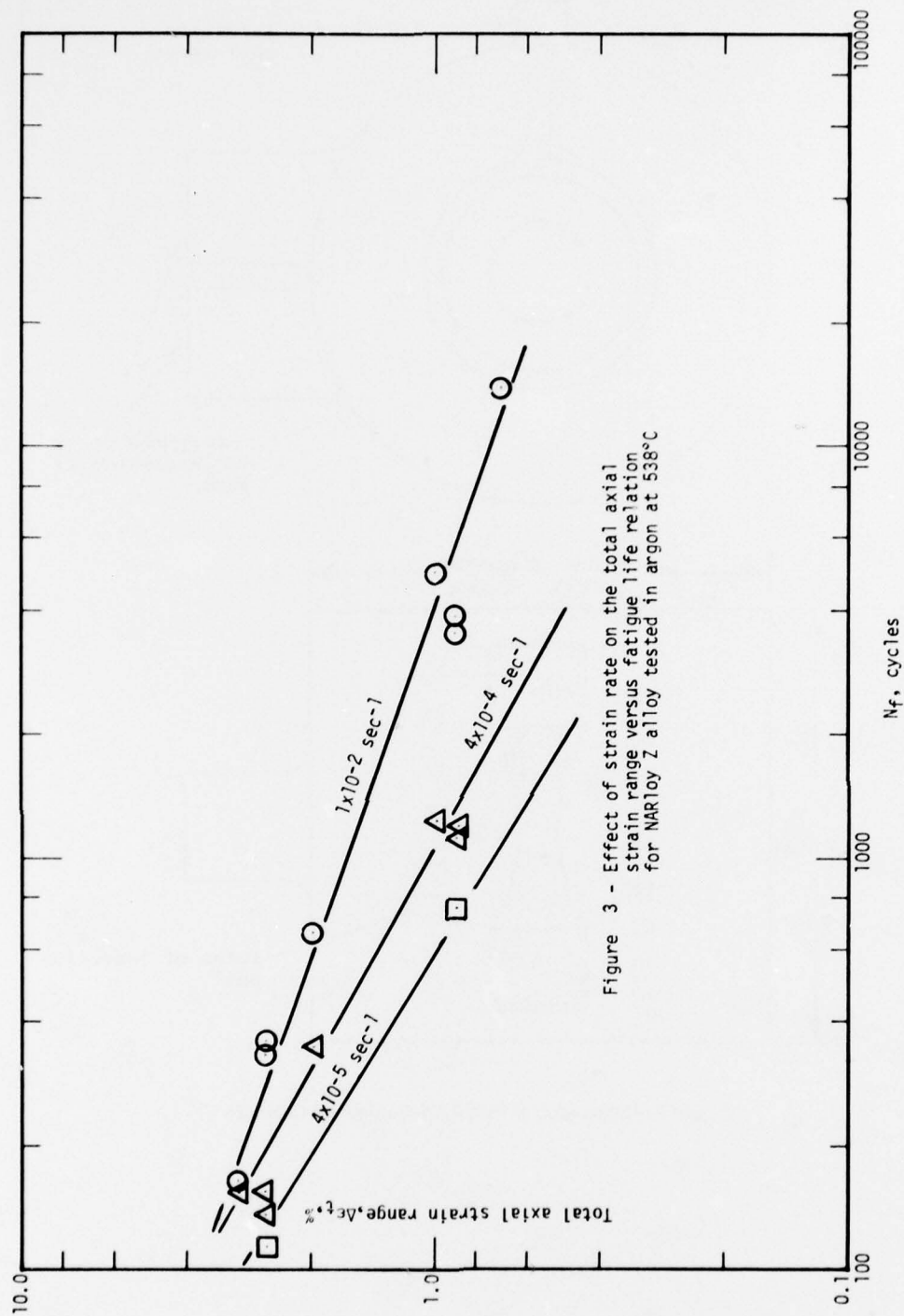
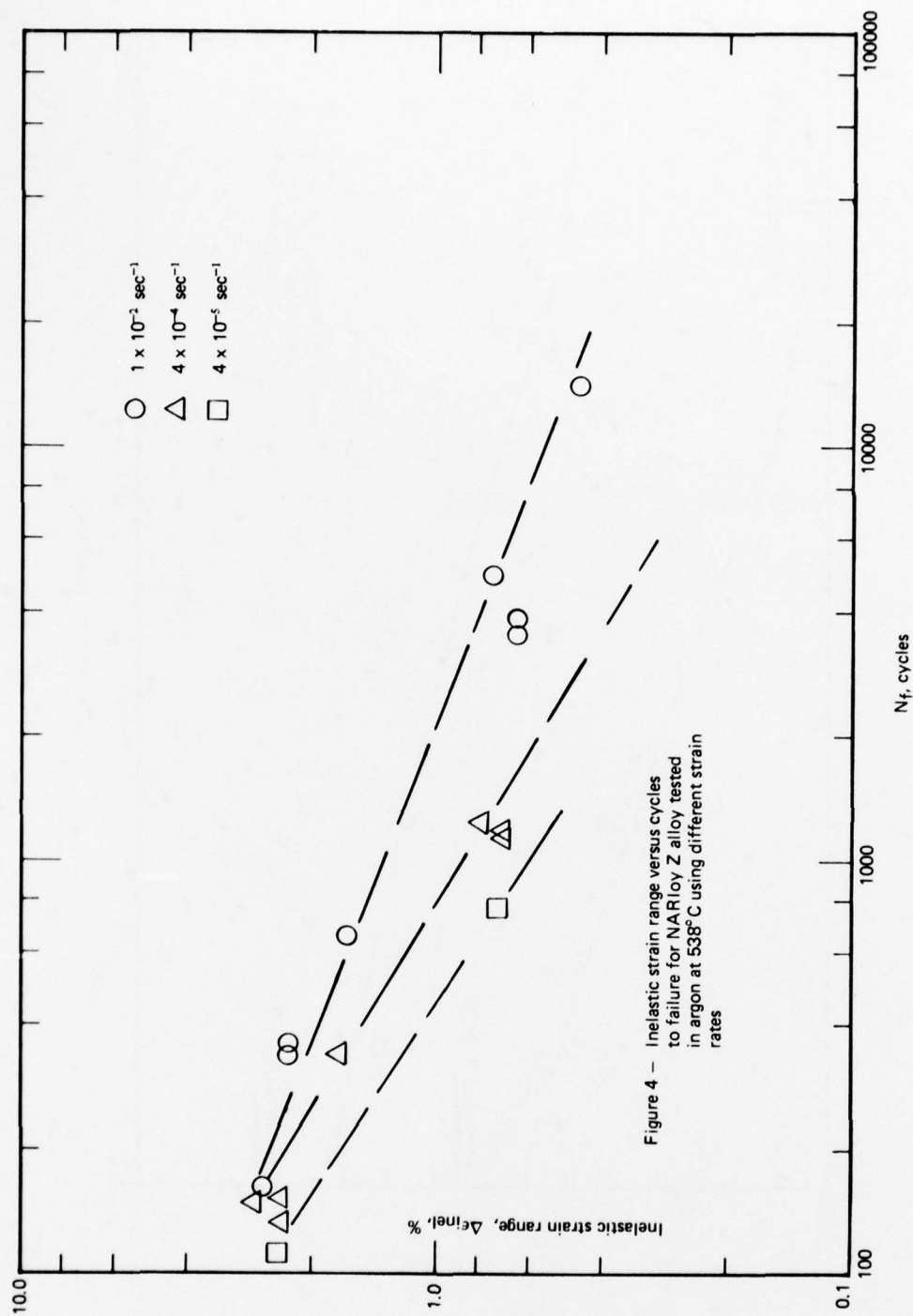
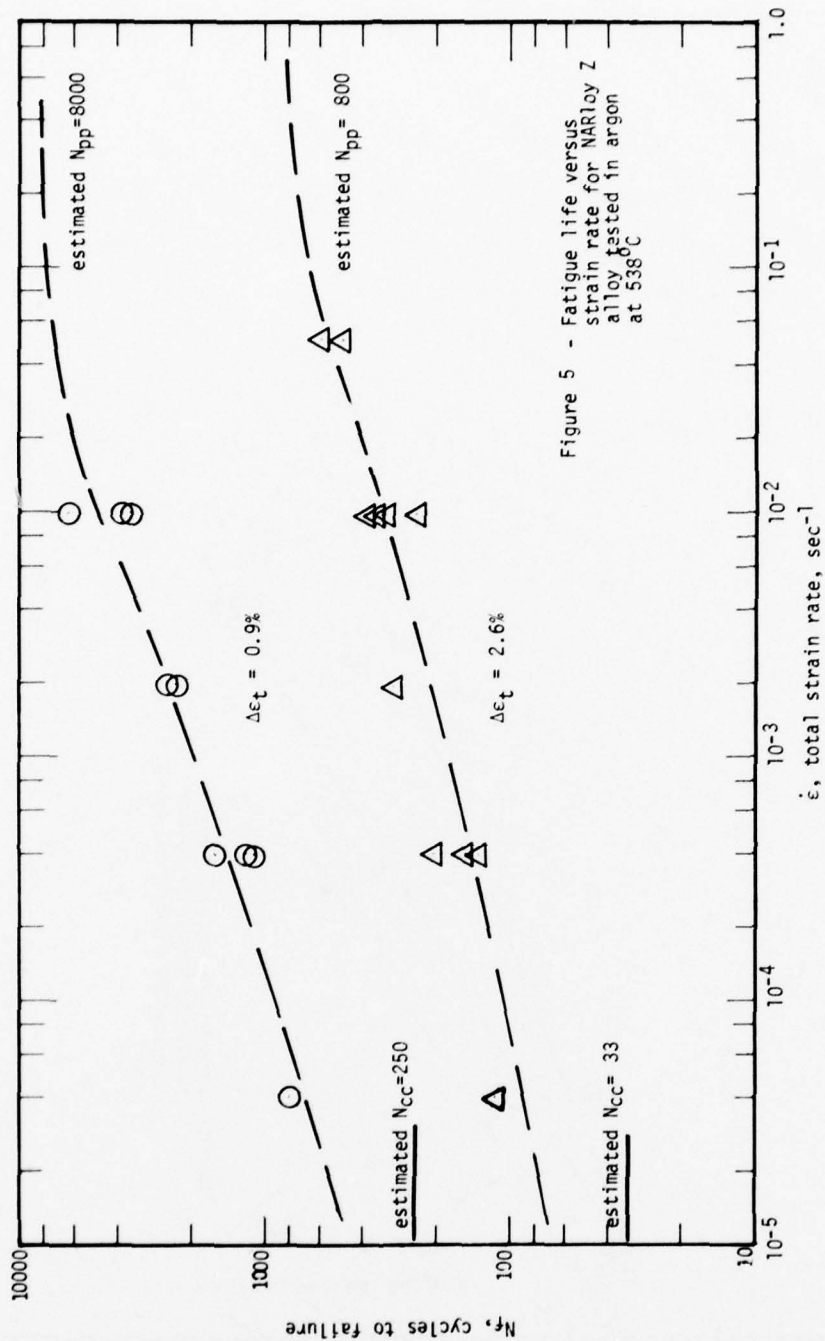
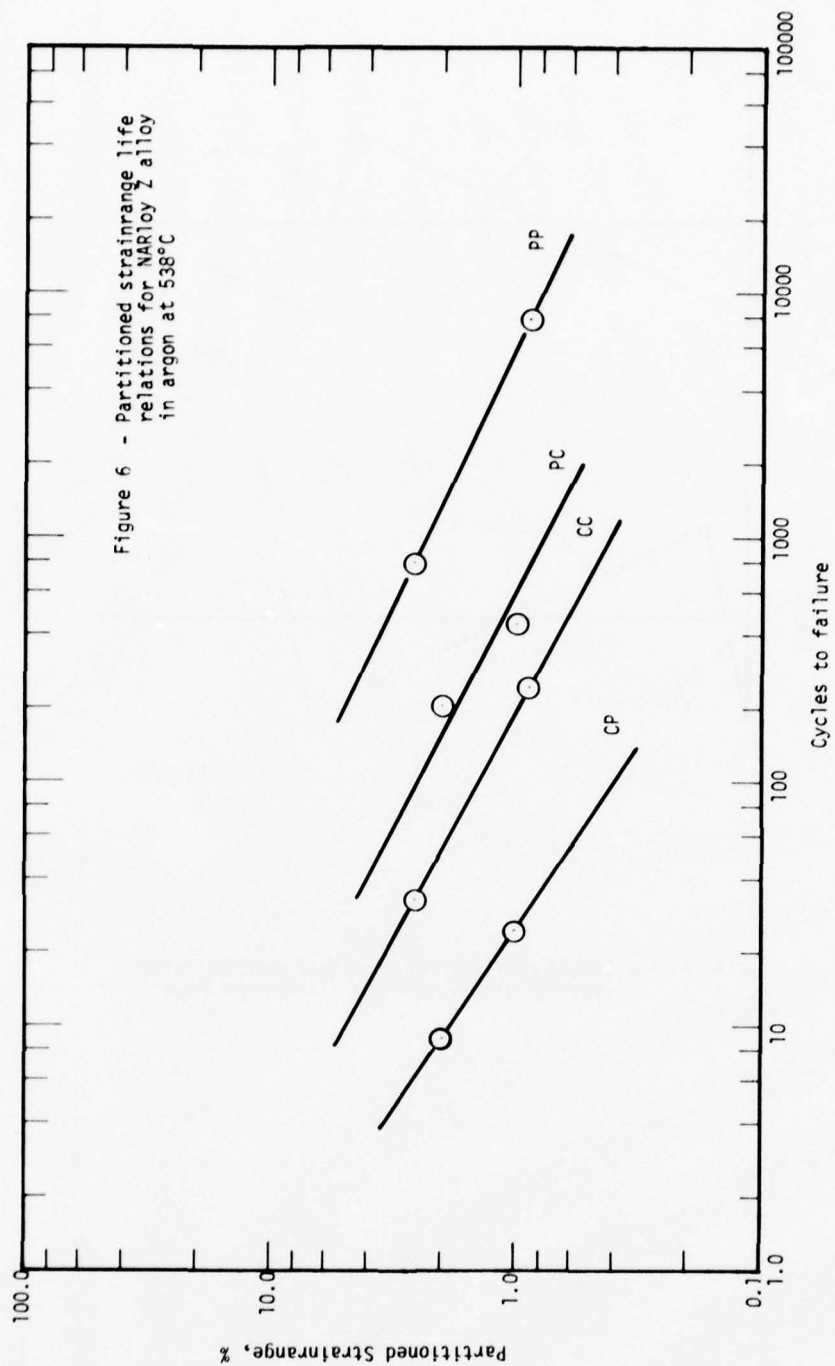


Figure 3 - Effect of strain rate on the total axial strain range versus fatigue life relation for NARloy Z alloy tested in argon at 538°C







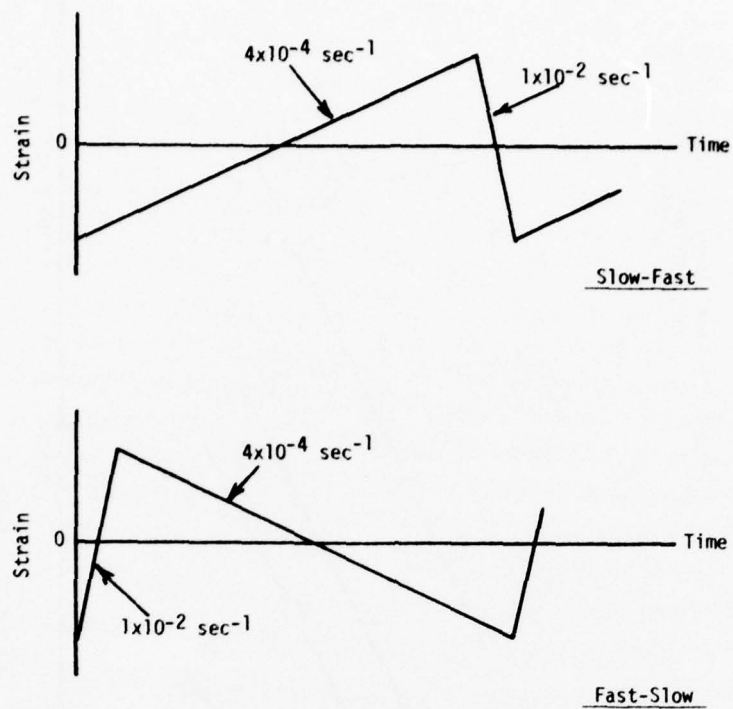
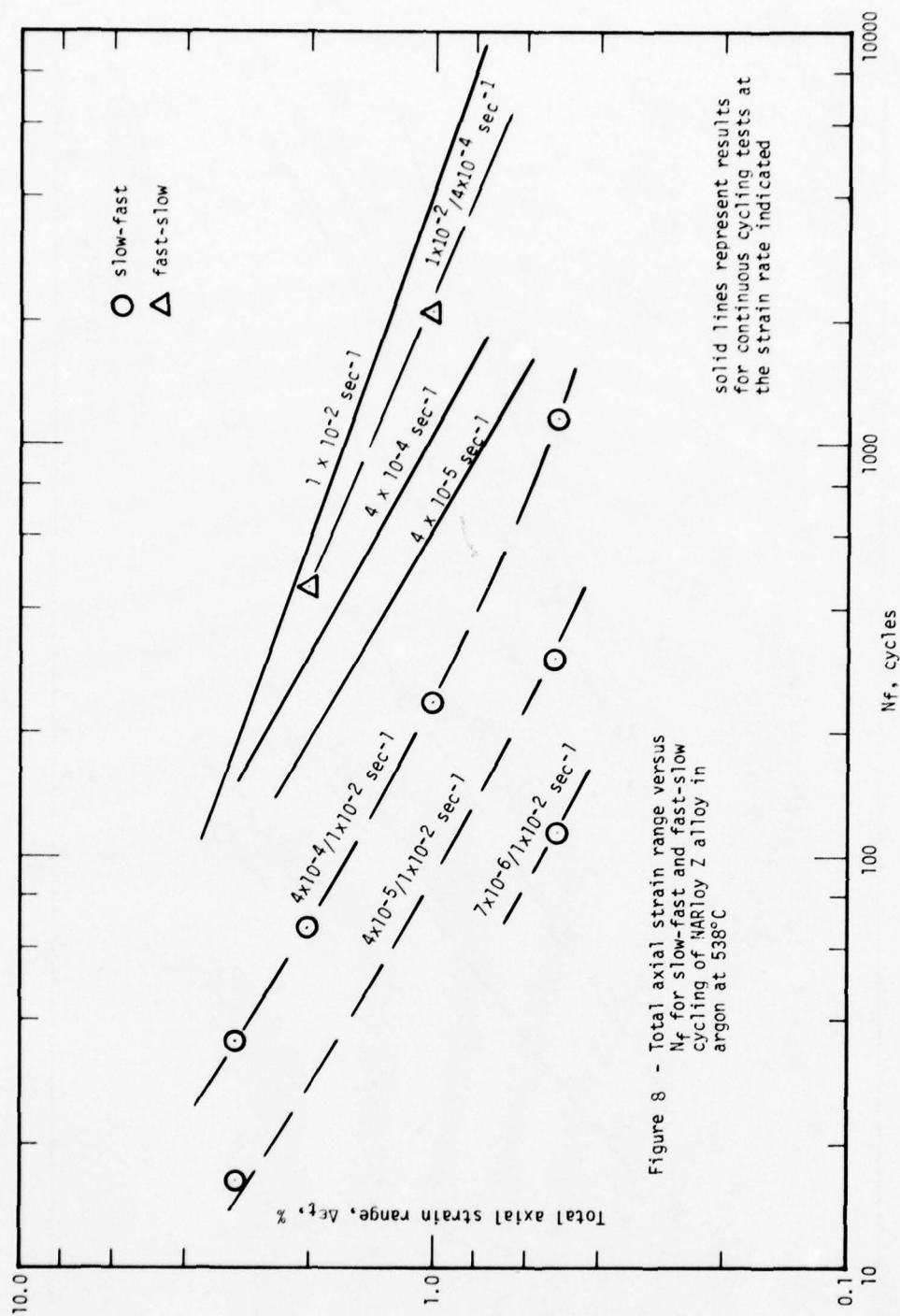
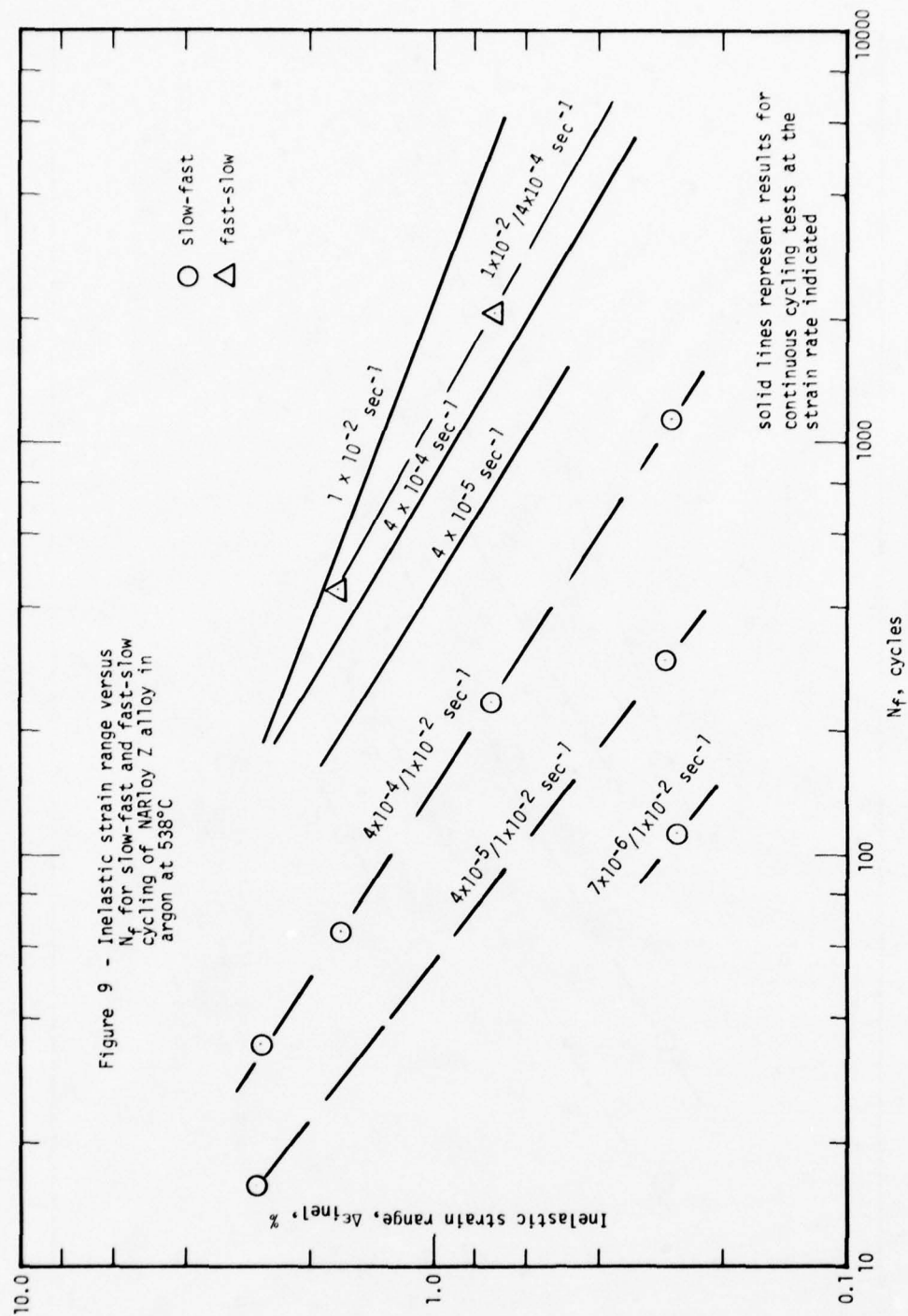
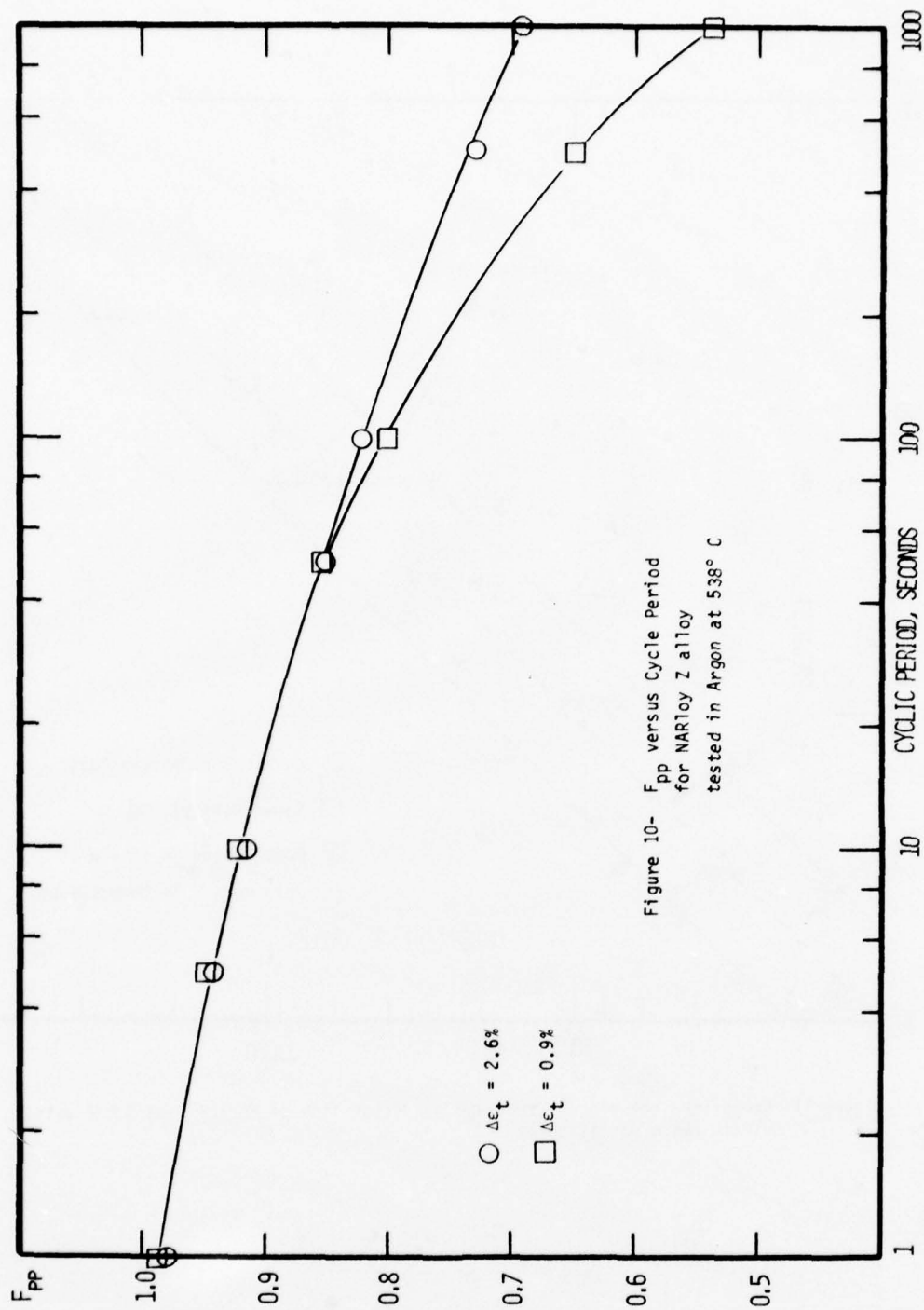


Figure 7 - Strain profiles for slow-fast and fast-slow cycling using $4 \times 10^{-4} \text{ sec}^{-1}$ and $1 \times 10^{-2} \text{ sec}^{-1}$







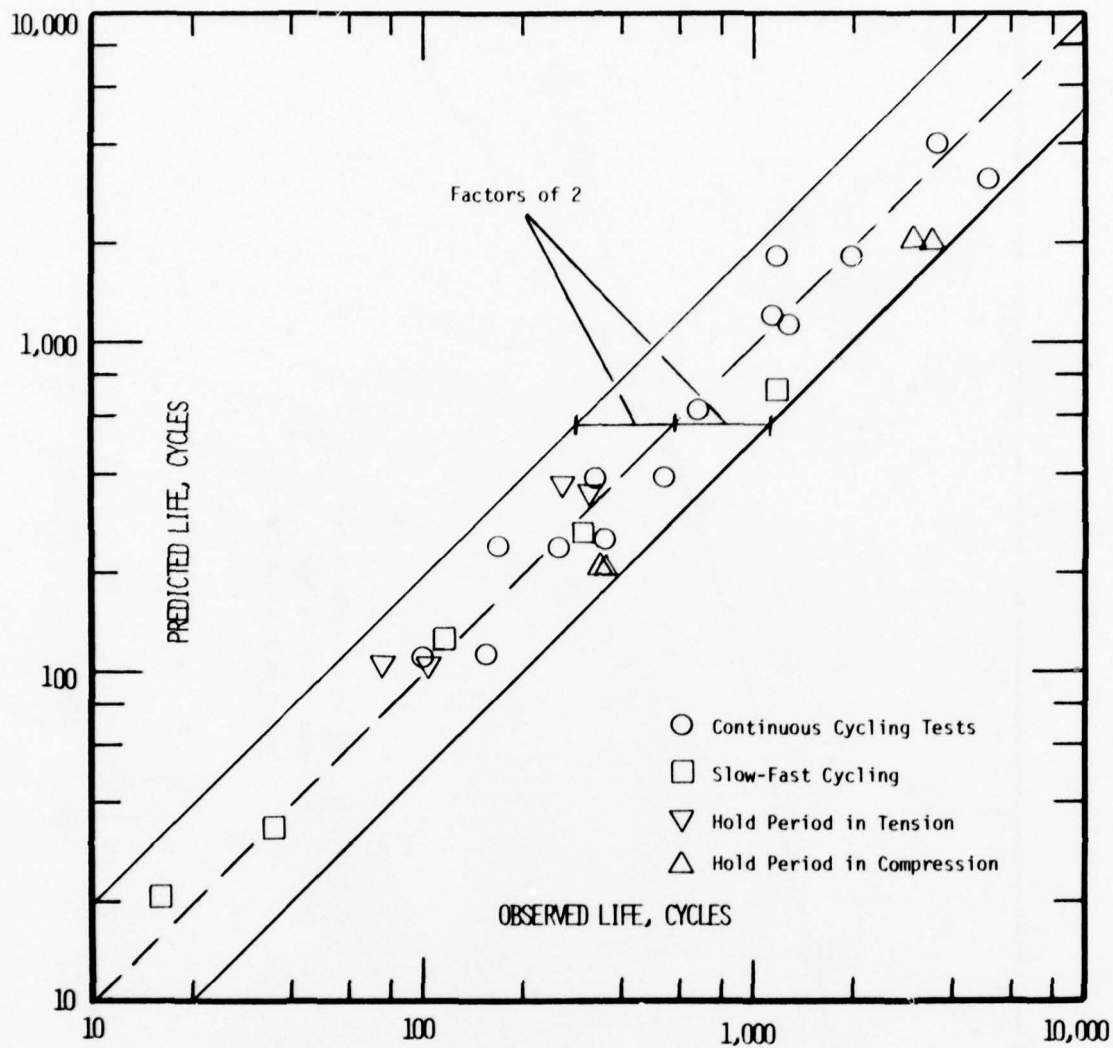
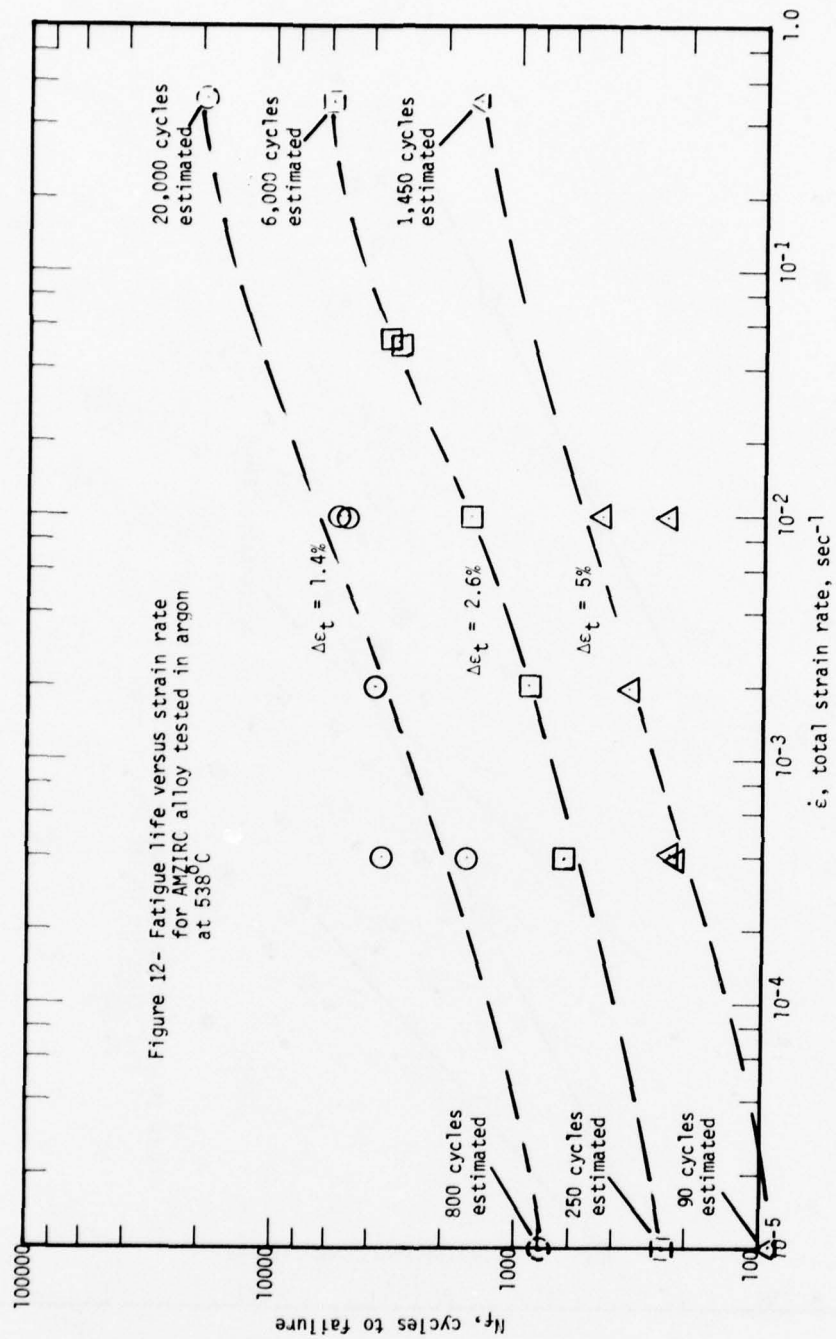


Figure 11 Comparison between observed and predicted life of NARloy Z at 538°C using strain range partitioning.



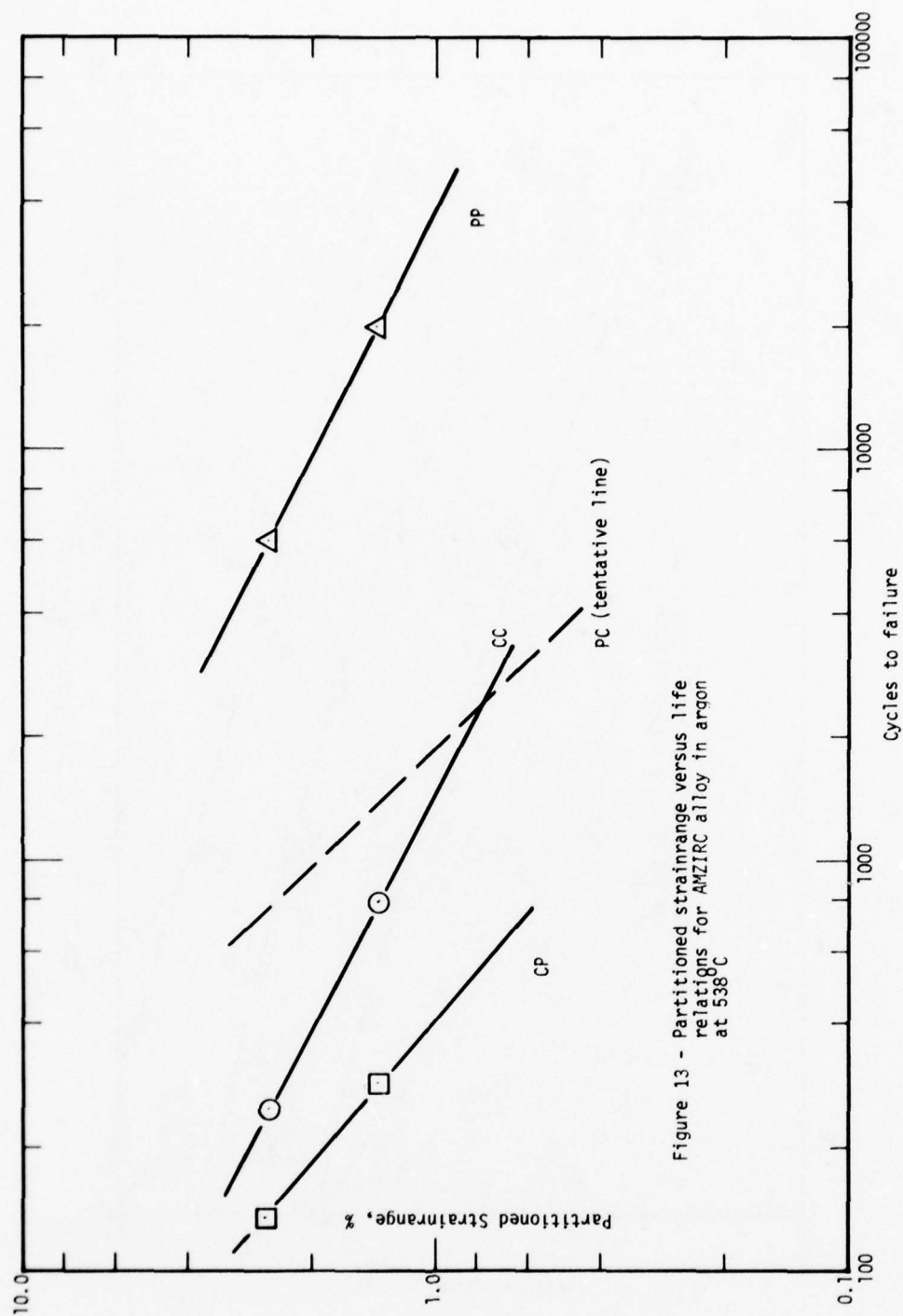


Figure 13 - Partitioned strainrange versus life relations for AMZIRC alloy in argon at 538°C

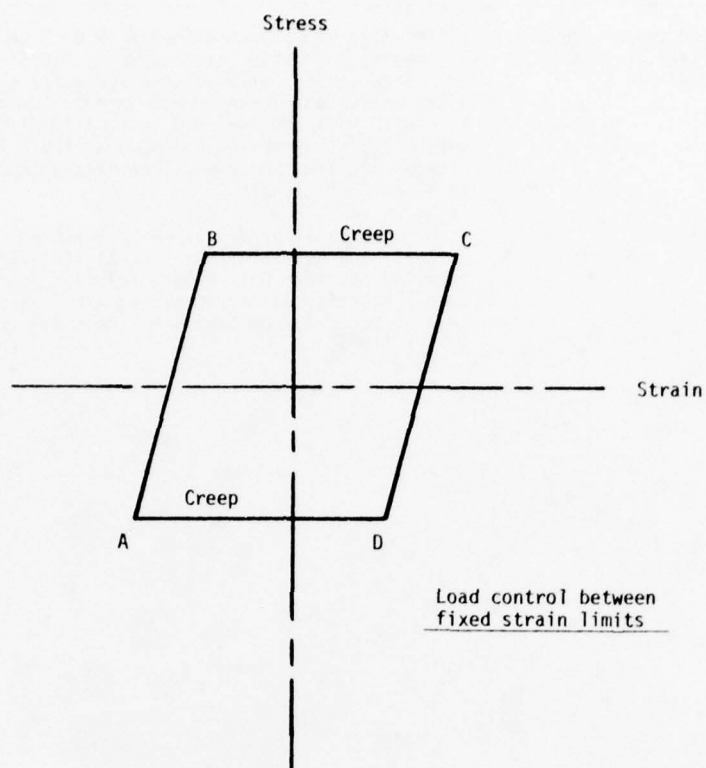


Figure 14 - Idealized CC Type Cycle (Ref. 5)

Table 1 - Description of the Materials Evaluated in this Study

Material	Description
AMZIRC Copper, 1/2 Hard (0.2% Zr, 0.002% Ni, 0.002% Fe)	Billet size of 20.3 cm diameter by 63.5 cm (8" x 25") in length; extrusion temperature of 960°C; extruded to 2.7 cm (1.06") diameter rod and water quenched after extrusion; drawn to 50% hard in two passes to 2.2 cm (0.87") and then 1.9 cm (0.75") diameter; stress relief by springing; aged at 420°C in cracked natural gas atmosphere and then straightened and cut to 91 cm (36") lengths.
NARloy Z (3% Au, 0.5%Cr)	A copper-base alloy developed by North American Rockwell and was furnished in centrifugally cast form and had been hot-rolled, solution annealed and aged. Material was furnished in the form of a rectangular bar, 23.2 cm long x 5.1 cm x 4.1 cm (9.12" x 2" x 1.6").

STRAINRANGE PARTITIONING APPLIED TO Ti-6Al-4V

by

Dr. H. Nowack
Department Head
andDipl.-Ing. J. Vreke
Research AssistantDFVLR (German Aerospace Research Establishment)
- Institute for Materials Research -
Linder Höhe, 5000 Köln 90, Germany

SUMMARY

In the present study, the SRP-method is applied at Ti-6Al-4V in a temperature range where significant creep occurs (450 °C). From the tests with HRSC, TCCR and BCCR cycle types it has been determined that the TCCR and CCCR cycles lead to alterations in the mean stress level and that the CCCR type reduces the crack initiation life significantly. The predictions of the SRP method for complex cycles coincided well with the corresponding test results, when the test durations for the HRSC, TCCR, CCCR and for the complex cycles remained of the same order of magnitude. When the testing time with complex cycles significantly increased a deviation was observed. Some possible explanations for the observed behaviour are given.

1. INTRODUCTION

High strength Titanium alloys attain an increasing importance as construction materials for gas-turbine compressors. Because there is still a considerable lack of knowledge about the damage accumulation under loading conditions where an interaction of fatigue and creep occurs, the Titanium alloys are usually used today at stresses and temperatures which lay far below the actual capabilities of the materials in order to avoid any risk of failures in service. The Strainrange Partitioning (SRP)-method as originally proposed by Manson, Hirschberg, Halford et al. [1] offers a basis for crack initiation life predictions under arbitrary loading conditions. In the present paper the SRP-method is applied at the Titanium alloy Ti-6Al-4V.

In order to investigate the range in application of the SRP-method under severe conditions the test temperature was chosen high above 350 °C. (The latter temperature is usually not exceeded for engineering applications of the Ti-6Al-4V alloy at present.) Because high temperatures and mechanical treatments can lead to considerable changes in the microstructural condition of a material and, with that, to significant differences in the mechanical properties, the microstructure was carefully observed with a light- and with a scanning electron-microscope.

The test program included the test series to generate the basic partitioned strain-range life relations, and to determine the tensile and creep properties of the material as well as tests, where comparisons between the predictions by the SRP-method and the actual fatigue life behaviour could be performed. Unfortunately, the long duration of the tests and the time available for the present test program put some severe limitations on the extent of the program. That was the reason, why the number of tests with complex creep-fatigue cycles could not be further increased and that additional tests for the determination of the scatter in the high temperature low cycle fatigue properties were not always possible.

2. MATERIAL, TENSILE AND CREEP PROPERTIES

For the test program the Ti6-4 alloy was used in the as received condition. The chemical composition of the material is given in Table 1. Fig. 1a shows the microstructure of the Ti6-4 alloy. It is of the $\alpha+\beta$ type and exhibits an equiaxed β -phase. For a continuous check of the microstructure small cylindrical plates were taken from the bars between every two specimens. These checks revealed some variations. An example of an extreme deviation from the normally observed microstructure shows Fig. 1b.

In the present study no additional thermomechanical treatments were performed on the Ti6-4 alloy.

The tensile properties of the material are summarized in Table 2* for room temperature as well as for the test temperature (450 °C). In Fig. 2 the magnitude of the Young's modulus, E , of the monotonic yield strength, σ_{ys} , and of the fracture ductility, D_p , at three different temperatures (room temperature, 350 °C, 450 °C) are shown. Fig. 3 shows the experimentally determined monotonic stress-strain curve and the cyclic stress-strain curve at 450 °C.

For the characterization of the creep behaviour of the Ti6-4 alloy at 450 °C, creep rupture tests were performed. The test temperature was measured using PtRh-Pt thermocouples and remained constant within 1 % during the tests. The results of the creep tests are shown in Fig. 4a and 4b.

* see also Appendix A.

To get a further insight in the scatter of the creep behaviour 5 tests were performed with the same loading conditions. The results of the test series are shown in Fig. 5. It can be seen that there is a considerable scatter in the rupture times. Fig. 6 shows the creep rupture life data as derived from the creep test results in Fig. 4 and Fig. 5. Because of the observed scatter in the creep behaviour extrapolations to higher creep rupture lives are highly inaccurate.

For a further characterization of the creep behaviour Fig. 7 shows the observed creep ductility, D_c , and also the engineering (longitudinal) strain, e , at fracture.

In addition to the creep tests the microstructure of the Ti6-4 alloy was observed. Of special interest was, if changes in the microstructure occurred as a function of the duration of the creep tests and if there were any correlations between the microstructural appearance and the scatter observed in the creep tests. Fig. 8a shows scanning electron microscope photographs of the β -phase at the beginning of the creep tests and Fig. 8b after a test duration of 200 hours. It can be seen that the appearance of the β -phase changed: the microstructure behaved unstable at the test temperature of 450 °C. In Fig. 9 light microscope photographs of the undeformed material at the beginning of the creep tests and of the deformed material in the vicinity of the crack after final failure in the creep test are shown. The β -phase in the fracture area elongated during the test by a factor of about 4. The magnitude of the elongation depended on the creep rupture time (comp. Fig. 4) and increased as the test duration increased.

A correlation between the scatter in the creep tests (comp. Fig. 5) and specific microstructural phenomena could not be observed.

3. SPECIMEN AND TESTING EQUIPMENT

In Fig. 10 the specimen for the low cycle fatigue tests is shown. It exhibits ridges for the mounting of the strain extensometer. In order to achieve a uniform microcrack initiation in the tests, the gage length of the specimen has a slightly curved shape and was carefully polished before each test.

The fatigue tests were performed in a 100 kN servohydraulic testing machine (Type Schenck Hydropuls). The tests without any hold times were performed in the strain control mode. In the tests with hold times the machine was operated in the load control mode, whereby the strain limits were adjusted and controlled by a specially developed electronic device which triggered a function generator (Type DANA Model 336). The strains were measured with the extensometer shown in Fig. 11.

A three-zone resistance furnace was used for the heating of the specimens. For the temperature control a CrNi-Ni thermocouple was mounted on the specimen by spot-welding. The temperature variations during the test remained within 1 %.

During the tests the following data were registered on-line:

- load and strain as a function of the testing time with a two-channel X-t plotter
- the load vs. strain hysteresis behaviour with a X-Y plotter. In order to achieve clearly visible plots of the hysteresis behaviour each loop was electronically shifted by a fixed amount.
- temperature as a function of time with a second X-t plotter.

4. GENERATION OF THE BASIC DATA FOR THE SRP-METHOD

For the generation of the basic data for the application of the SRP-method test series were performed with the following types of strain cycles [2]:

- high rate strain cycles with merely plastic deformations (HRSC-cycles)
- strain limited cycles with creep period in tension (TCCR-cycles)
- strain limited cycles with a creep period in compression (CCCR-cycle)
- strain limited cycles with equal portions of creep in tension as well as in compression (BCCR-cycle).

Three failure criteria were considered:

- N_0 : that cycle number where the first decrease in the stress range after stabilization was observed in the strain controlled cycles
- N_5 : the cycle number, where a decrease in the stress range of 5 % compared to the stable hysteresis loops in the tests occurred
- N_f : the cycle number at final failure.

In Fig. 12 the hysteresis behaviour in the tests with the different types of strain cycles is shown. The following phenomenon shall be specially pointed out: in the course of the tests with TCCR- and CCCR-cycles a mean stress builds up, whereas in the tests with the HRSC- and the BCCR-cycles the mean stress remains close to zero. In the tests

with the TCCR-cycles the mean stress is compressive and in tests with the CCCR-cycles it builds up in the tension direction. Further on it was observed that in the tests where lower total strain ranges were applied, the decrease or the increase in the mean stress were more pronounced. The observed mean stress variations are shown in Fig. 13.

Fig. 14 shows the experimentally determined crack initiation life behaviour as a function of the total inelastic strain applied in the tests.

For the SRP-method the N_0 , N_5 and N_f (life) values have to be evaluated from the test results following the procedure as described in detail in [2] and to be plotted as a function of the inelastic strain ranges for the pp- as well as for the cp- and the pc- and the cc-components of the inelastic strain ranges. Fig. 15 shows the partitioned strain range-life relations for the Ti6-4 alloy. (In Table 3 further details of the tests are given.) When the four curves are compared it can be seen that there are only small differences between the curves for the pp-, cp-, and cc-components of the inelastic strain ranges. In the case of the pc-component, however, a significant decrease in life takes place. A reasoning for this behaviour can be seen in the development of the tensile mean stress during the tests, as already mentioned before (comp. Fig. 13).

The durations of the tests for the determination of the basic data for the SRP-method as described in this section were between 0.5 and 200 hours.

5. APPLICATION OF THE SRP-METHOD AND DISCUSSION OF THE RESULTS

Because of the reasons mentioned in section 1 and some delays in the performance of the test series due to various technical difficulties, the remaining testing time for the tests with complex cycles and variations in temperature, where the prediction capability of the SRP-method could be examined, was limited. That was the reason why the test program had to be carefully designed. The intention was to cover a range in test durations from the testing times as they were required for the tests for the generation of the basic SRP data as well as much longer testing times. The test program with 5 different types of complex cycles is shown in Table 4. During the tests mean stresses built up analogous to the behaviour as it was already observed in the tests with the CCCR- and TCCR-cycles. (Larger creep strains in the tension direction than in the compression direction caused a compressive mean stress and vice versa.) The N_5 -value observed in the tests are given in Table 4.

For the fatigue life prediction of the SRP-method the following equation is used [2]:

$$\frac{1}{N_{\text{pred}}} = \frac{F_{\text{pp}}}{N_{\text{pp}}} + \frac{F_{\text{pc}}}{N_{\text{pc}}} + \frac{F_{\text{cp}}}{N_{\text{cp}}} + \frac{F_{\text{cc}}}{N_{\text{cc}}}$$

Fig. 16 shows a comparison of the predicted and of the actual life data as observed in the tests with the complex cycles. It can be seen that the data agree well within a factor of about 2 except for one test. The testing time for this test was about 1100 hours and considerably exceeded the duration of the tests for the generation of the basic data for the SRP-method. A further test with the same loading conditions could not be performed within the time available for the present program. However, because repeated re-examinations of the testing conditions and of the specimen gave no indications for any errors or other disturbances, the low crack initiation life (compared to the prediction of the SRP-method) must be accepted as a correct value.

Upon various considerations the following possible causes for the observed behaviour were found:

- a change in the microstructure of the Ti6-4 alloy due to the extremely long testing time. The changes can include modifications of the β -phase similar to those as they were observed in the creep tests (Fig. 8) and which may be accelerated due to the cyclic loading. Because of the long hold times per cycle precipitation-, diffusion-, and recovery-processes may also take place.
- the influence of the environment on the processes at the specimen surface, especially, the influence of oxygen, which is stronger the longer the hold time per cycle in a test is and the longer the test lasts. The oxygen layers built up at the specimen surface usually show a brittle behaviour which favours the formation and also the extension of microcracks. Besides that a more intensive penetration of the oxygen into the material regions below the specimen surface can occur in a long running test. To get a more qualified insight in the environmental effects an artificial oxygen layer was generated at the surface of a specimen by annealing it at 800 °C in air. The same heat treatment was performed on another specimen in vacuum to maintain a similar microstructure of the bulk material. The test results, where the same HRSC-cycles were applied in the tests showed that the specimen with the artificial oxygen layer failed at a lower cycle number. In order to avoid possible additional influences of variations of the hydrogen content during the heat treatment on the test results, further tests are planned to be performed with an artificial oxygen layer generated at 450 °C.
- the different mechanical environment due to the longer action of the force at the specimen during the tests. Tension stresses in connection with a corrosive environment initiate and favour stress corrosion cracking processes in the Ti6-4 alloy.

For a quantitative evaluation of these influencing factors further systematic investigations are necessary.

Besides the afore mentioned prediction capability of the SRP-concept was considered for two further cases.

- Table 4 and Fig. 16 show the test results and the SRP-method predictions, when the test temperature is increased to 550 °C. Both, the test results and the predictions based on the data shown in Fig. 15 agree well.
- Additional strain controlled tests without any hold times were run at 300 °C. It came out that the ductility normalized life relationship given in [3, 4]:

$$N_{pp} = (C \Delta \epsilon_{pp} / D_p)^k$$

(C, k constant and exponent, respectively) could be applied to represent the experimentally determined crack initiation life data at both temperatures.

6. CONCLUSIONS

The present study was designed to get more insight in the possibilities to characterize the crack initiation life behaviour of Ti6-4 at temperatures higher than they are tolerated today for practical design purposes. The investigations showed that the creep behaviour of the technical Ti6-4 alloy exhibited an extremely large scatter at 450 °C. When the SRP-method was applied to predict the crack initiation life behaviour in tests with various complex cycles, a good correlation between the experimentally determined and the predicted data was observed, except in one case. Further investigations to find a satisfactory explanation for this discrepancy could not be performed because of limitations in the time available for the present program. Additional investigations will be performed at DFVLR.

7. REFERENCES

- [1] Manson, S.S., Halford, G.R. and Hirschberg, M.H.: Creep-Fatigue Analysis by Strain-Range Partitioning. Symposium on Design for Elevated Temperature Environment, ASME, 1971, pp. 12-28. (NASA TM X-67838, 1971).
- [2] Hirschberg, M.H. and Halford, G.R.: Strainrange Partitioning - a Tool for Characterizing High-Temperature Low-Cycle Fatigue. 14th Meeting AGARD-SM Panel, Brussel April 13-18, 1975. (NASA TM X-71691).
- [3] Manson, S.S.: The Challenge to Unify Treatment of High-Temperature Fatigue - A Partisan Proposal Based on Strainrange Partitioning. STP 520, ASTM, 1972, pp. 744 - 782.
- [4] Halford, G.R., Saltsman, J.F. and Hirschberg, M.H.: Ductility Normalized-Strainrange Partitioning Life Relations for Creep-Fatigue Life Predictions. Conf. on Environm. Effects and Degradation of Eng. Mats., Blacksburg Va., October 10-12, 1977.

8. ACKNOWLEDGEMENT

The authors wish to thank W. Bunk for the initiation of the present investigation and M. Majdic and A. Gysler for the fruitful discussions of the test results.

Al	V	Fe	C	O	N	H	Ti
6.4	4.1	.08	.026	.127	.01	.0083	Balance

Table 1: Chemical composition of the material

Test temperature, °C	20	450
Modulus of elasticity, MPa	106 x 10 ³	89.1 x 10 ³
Yield strength, MPa	1046	637
Ultimate strength, MPa	1069	729
Reduction of area, %	42	49.1

Table 2: Tensile properties

RATE DATA & STRESSES

SPEC NO	TEST TYPE	TEMP-°C TEN/COMP	RATE DATA (HALF-LIFE VALUES)				STRESSES (HALF-LIFE VALUES) MPA						
			FREQ HZ	STRAIN-RATE-%/SEC TEN	HOLD TIME-SEC COMP	TEN	COMP	TEN MAX	COMP MAX	RANGE MAX	RELAXATION TEN	CYCLIC STRAIN COMP	HARDENING %
194/06	UCCR	350/450	1.0E-01	5.6E-01	5.6E-01	6.0	9.0	540.0	519.1	1059.1	0.0	0.0	-8.27
190/14	UCCR	450/450	1.0E-01	9.6E-01	8.4E-01	2.0	8.4	594.9	565.2	1160.1	0.0	0.0	-8.32
190/05	UCCR	450/450	1.0E-01	6.3E-01	5.1E-01	15.0	510.0	650.6	545.6	1196.2	0.0	0.0	-5.14
190/01	UCCR	450/450	5.0E-02	7.0E-01	7.0E-01	4.5	19.2	624.6	645.4	1270.0	0.0	0.0	-10.29
194/07	TCCR	450/450	1.0E-01	5.9E-01	5.5E-01	420.0	0	379.8	849.7	1229.5	0.0	0.0	1.03
069/16	TCCR	450/450	1.0E-01	8.2E-01	8.4E-01	990.0	0	567.6	1031.6	1599.2	0.0	0.0	10.29
069/25	TCCR	450/450	1.0E-01	1.6E 00	2.1E 00	59.0	0	672.5	840.7	1513.2	0.0	0.0	-6.54
069/14	TCCR	450/450	1.0E-01	1.6E 00	2.1E 00	122.0	0	674.3	861.0	1535.0	0.0	0.0	-4.52
190/15	CCCR	445/445	1.0E-01	5.9E-01	5.7E-01	0	3.6	557.0	493.0	1050.0	0.0	0.0	-7.77
190/19	CCCR	450/450	1.0E-01	7.0E-01	6.5E-01	0	117.0	633.1	484.0	1117.1	0.0	0.0	-9.59
190/02	CCCR	450/450	1.0E-01	7.5E-01	6.5E-01	0	687.0	671.5	495.9	1167.4	0.0	0.0	-7.38
069/15	CCCR	452/452	1.0E-01	1.3E 00	1.2E 00	0	3000.0	846.3	608.9	1455.2	0.0	0.0	-2.23
069/18	HRSC	458/458	3.0E-01	6.3E-01	6.3E-01	0	0	522.1	532.3	1054.4	0.0	0.0	-6.36
069/12	HRSC	450/450	3.0E-01	8.2E-01	8.2E-01	0	0	586.1	586.1	1172.2	0.0	0.0	-5.83
190/09	HRSC	453/453	3.0E-01	1.1E 00	1.1E 00	0	0	625.3	639.8	1265.1	0.0	0.0	-5.90
069/23	HRSC	459/459	3.0E-01	2.2E 00	2.2E 00	0	0	674.2	728.2	1402.4	0.0	0.0	-2.99
190/08	HRSC	452/452	3.0E-01	5.6E-01	5.6E-01	0	0	502.9	412.6	915.5	0.0	0.0	--
194/01	HRSC	455/455	3.0E-01	5.4E-01	5.4E-01	0	0	476.2	494.5	970.7	0.0	0.0	-2.56
194/05	HRSC	450/450	3.0E-01	6.8E-01	6.9E-01	0	0	557.3	554.7	1112.0	0.0	0.0	-9.80
194/09	HRSC	452/452	3.0E-01	6.1E-01	6.3E-01	0	0	503.6	549.9	1053.5	0.0	0.0	-5.53
190/17	TCCR	454/454	1.0E-01	5.9E-01	6.7E-01	168.0	0	384.2	658.3	1042.5	0.0	0.0	-6.17
194/04	TCCR	452/452	1.0E-01	6.1E-01	4.9E-01	300.0	0	305.8	835.0	1140.8	0.0	0.0	-3.80
190/18	BCCR	450/450	1.0E-01	5.7E-01	5.7E-01	6.0	10.2	503.6	470.1	973.7	0.0	0.0	-4.56

Table 3a: Creep fatigue test rate data and stresses

STRAINS & FAILURE DATA

SPEC NO	STRAINRANGES (HALF-LIFE VALUES) %							FAILURE DATA-CYCLES				
	TOTAL	EL	IN	PP	PC	CP	CC	NO	N1	N5	NF	TF-HRS
194/06	1.103	0.874	0.229	0.149	0.000	0.009	0.071	1410	--	1539	1639	83.70
190/14	1.627	1.009	0.618	0.478	0.013	0.000	0.127	500	--	583	645	14.83
190/05	1.638	0.998	0.640	0.389	0.013	0.000	0.238	290	--	334	401	66.68
190/01	2.680	1.088	1.585	1.178	0.000	0.090	0.317	168	--	203	213	2.45
194/07	1.208	0.945	0.263	0.147	0.000	0.116	0.000	1120	1209	1214	1889	165.65
069/16	2.215	1.304	0.911	0.445	0.000	0.453	0.000	223	252	241	272	51.82
069/25	4.244	1.323	2.921	1.523	0.000	1.398	0.000	74	103	90	106	2.78
069/14	4.205	1.286	2.919	1.558	0.000	1.361	0.000	53	--	74	81	3.58
190/15	1.087	0.882	0.205	0.154	0.051	0.000	0.000	1300	--	1552	1665	19.13
190/19	1.304	0.944	0.360	0.231	0.129	0.000	0.000	520	--	619	698	95.60
190/02	1.505	1.025	0.480	0.324	0.156	0.000	0.000	327	--	345	420	108.90
069/15	2.291	1.206	1.085	0.617	0.470	0.000	0.000	124	--	133	142	78.68
069/18	0.920	0.863	0.073	0.073	0.000	0.000	0.000	3500	3700	3650	5393	4.98
069/12	1.190	1.091	0.100	0.180	0.000	0.000	0.000	1725	2000	1900	2765	2.57
190/09	1.450	1.016	0.434	0.434	0.000	0.000	0.000	550	664	610	765	0.78
069/23	2.438	1.256	1.182	1.182	0.000	0.000	0.000	306	335	315	357	0.33
190/08	0.903	0.850	0.053	0.053	0.000	0.000	0.000	14600	--	15216	18140	16.80
194/01	0.864	0.825	0.039	0.039	0.000	0.000	0.000	8732	--	9354	13700	12.68
194/05	0.952	0.720	0.232	0.232	0.000	0.000	0.000	1500	--	1600	2750	2.63
194/09	0.937	0.839	0.098	0.098	0.000	0.000	0.000	3500	--	3786	6005	5.55
190/17	1.067	0.896	0.179	0.105	0.000	0.074	0.000	2250	--	2668	4225	59.00
194/04	1.100	0.908	0.192	0.085	0.000	0.107	0.000	1760	--	1915	3388	242.78
190/18	1.105	0.893	0.212	0.109	0.000	0.000	0.103	2400	--	2750	2994	40.50

Table 3b: Creep fatigue test failure data and strains

RATE DATA & STRESSES

SPEC NO	TEST TYPE	TEMP-°C TEN/COMP	FREQ HZ	RATE DATA (HALF-LIFE VALUES)				STRESSES (HALF-LIFE VALUES) MPA					
				STRAIN-RATE-%/SEC		HOLD TIME-SEC		TEN	COMP	RANGE	RELAXATION	CYCLIC STRAIN	
				TEN	COMP	TEN	COMP	MAX	MAX	MAX	TEN	COMP	HARDENING %
195/06	UHSC	449/449	1.0E-01	9.0E-01	9.6E-01	1356.0	0.8	532.5	864.9	1397.4	0.0	0.0	2.96
195/17	UHSC	447/447	1.0E-01	9.6E-01	9.8E-01	1080.0	0.5	573.7	867.2	1440.9	0.0	0.0	1.94
195/07	UHSC	450/450	1.0E-01	7.9E-01	7.8E-01	1800.0	0.6	465.2	856.2	1321.4	0.0	0.0	2.57
195/13	UHSC	452/452	1.0E-01	6.9E-01	6.8E-01	0.5	7344.0	714.3	412.7	1127.1	0.0	0.0	-0.37
194/14	UHSC	450/450	1.0E-01	6.2E-01	5.9E-01	0.5	13680.0	740.3	275.3	1015.3	0.0	0.0	-1.02
194/18	UHSC	551/551	1.0E-01	7.6E-01	7.3E-01	2.0	4.0	473.5	437.5	911.0	0.0	0.0	-2.75
195/18	UHSC	547/547	1.0E-01	6.2E-01	6.1E-01	1.8	12.0	502.9	340.4	843.3	0.0	0.0	--

STRAINS & FAILURE DATA

SPEC NO	TOTAL	STRAINRANGES (HALF-LIFE VALUES) %						FAILURE DATA-CYCLES				
		EL	IN	PP	PC	CP	CC	NO	NI	N5	NF	TF-HRS
195/06	2.434	1.325	1.109	0.477	0.000	0.426	0.206	85	--	137	137	55.33
195/17	2.418	1.198	1.220	0.549	0.000	0.437	0.234	89	--	150	150	26.48
195/07	1.976	1.177	0.799	0.287	0.000	0.351	0.161	195	--	215	215	95.32
195/13	1.465	1.051	0.414	0.175	0.123	0.000	0.116	210	--	255	284	448.95
194/14	1.229	0.989	0.241	0.073	0.091	0.000	0.078	270	--	292	384	1127.90
194/18	1.252	0.915	0.337	0.213	0.033	0.000	0.091	720	--	964	1153	3.32
195/18	1.052	0.767	0.286	0.114	0.057	0.000	0.114	806	--	903	1020	6.03

Table 4: Creep fatigue test data of complex cycles

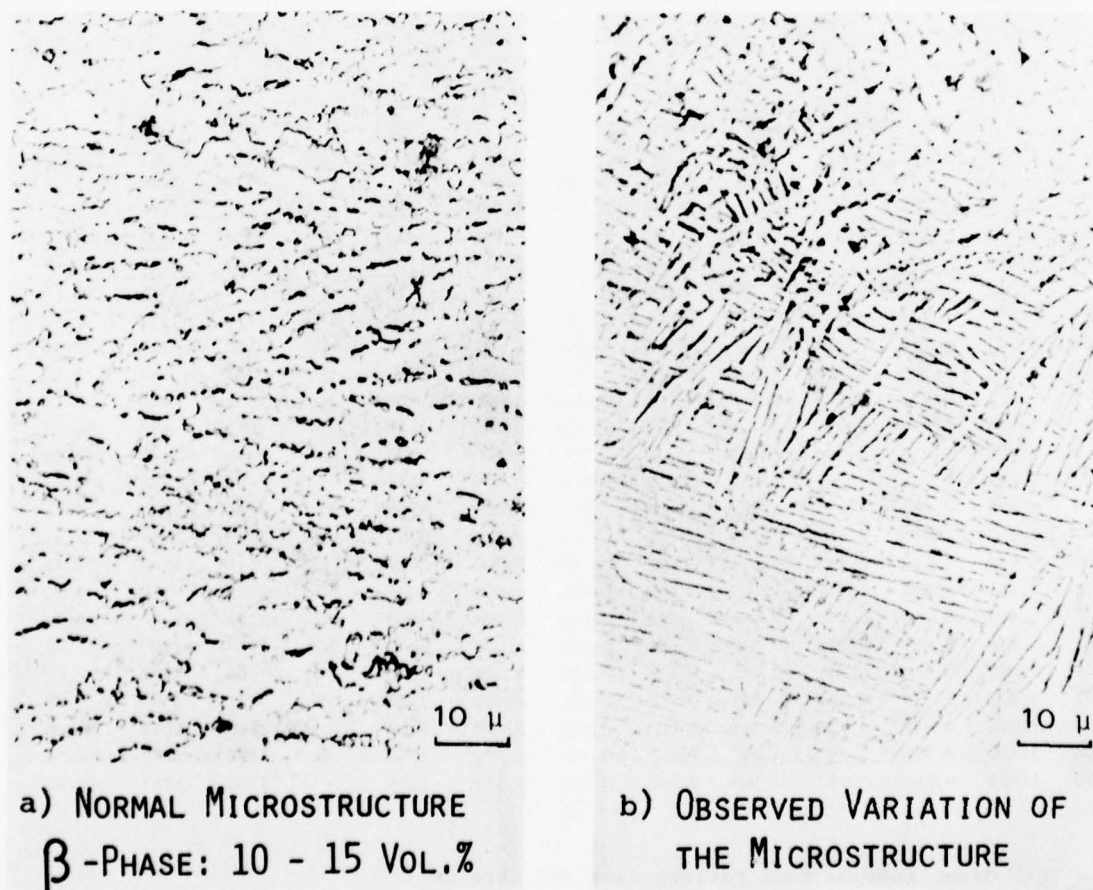


Fig. 1: Microstructure of the Ti6-4 alloy in the as received condition

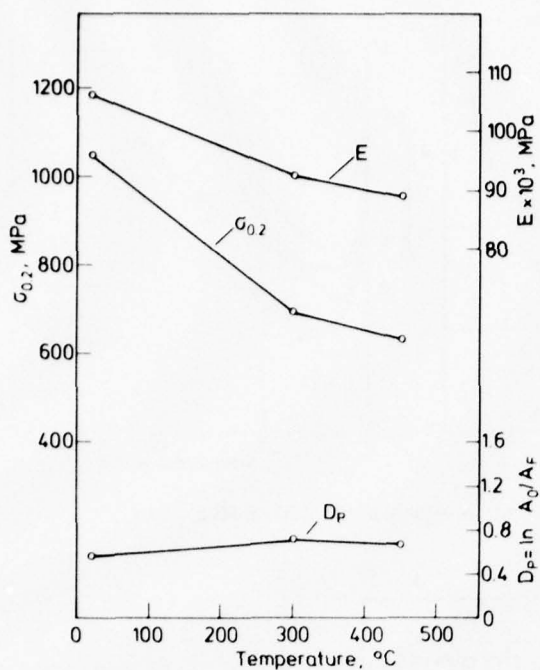


Fig. 2: Young's modulus, monotonic yield strength and fracture ductility as a function of the temperature

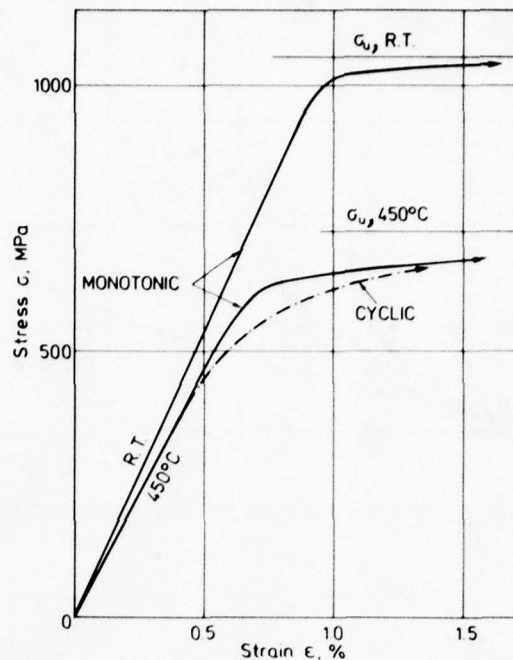


Fig. 3: Stress strain behaviour of the Ti6-4 alloy at R.T. and at 450 °C

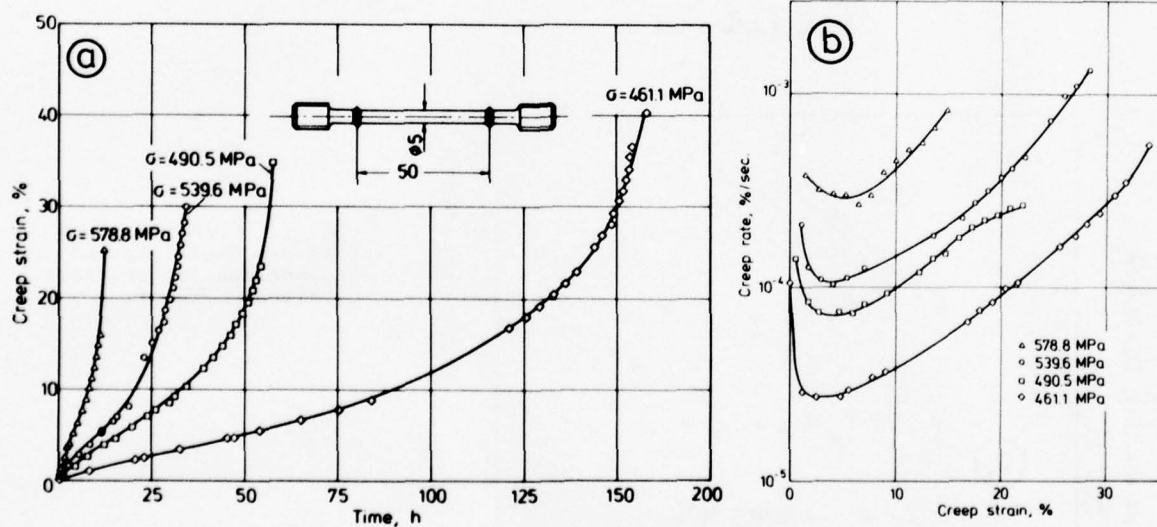


Fig. 4: Creep behaviour of the Ti6-4 alloy at 450 °C

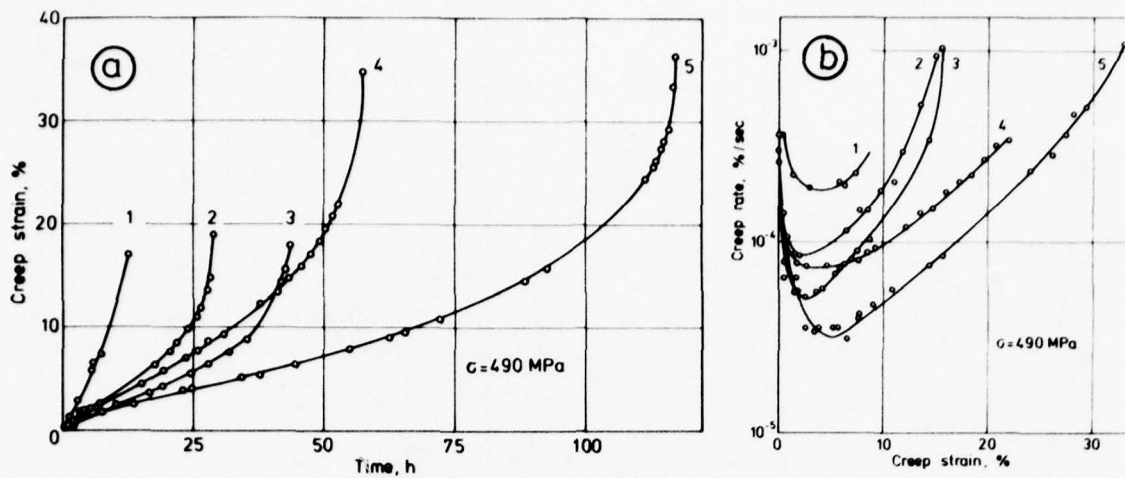


Fig. 5: Observed scatter of the creep behaviour at a stress of 490.5 MPa

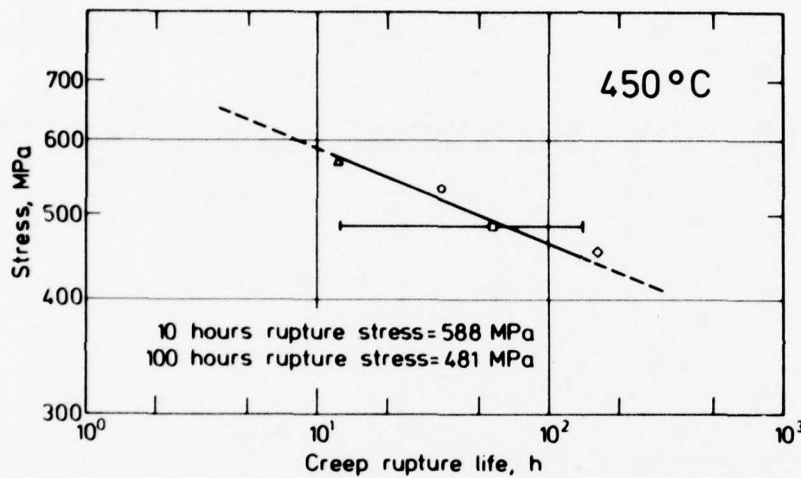


Fig. 6: Creep rupture life behaviour of the Ti6-4 alloy as derived from Figs. 4 and 5

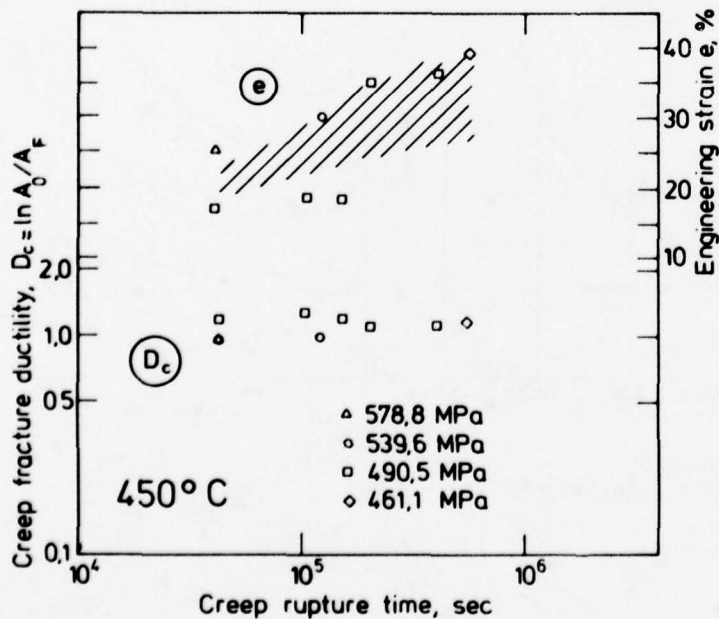


Fig. 7: Observed creep fracture ductility and engineering longitudinal strain at fracture

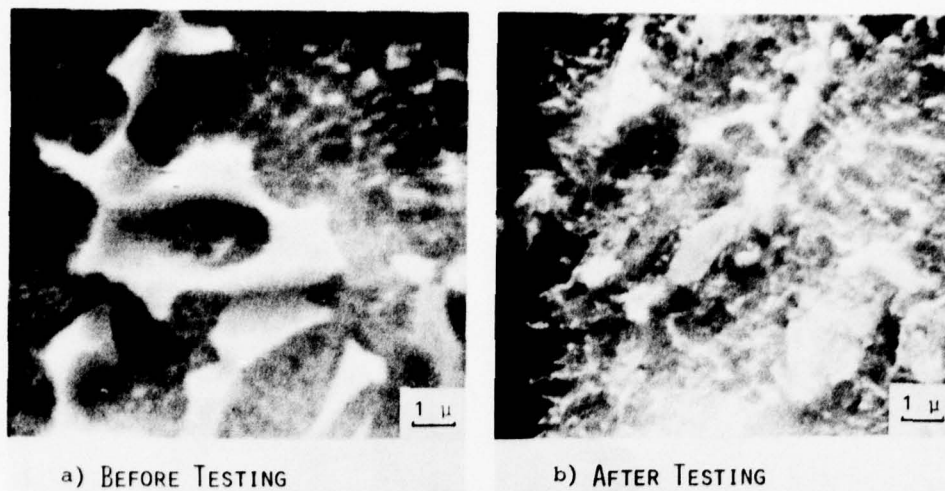


Fig. 8: Changes of the β -phase during a creep test at 450 °C

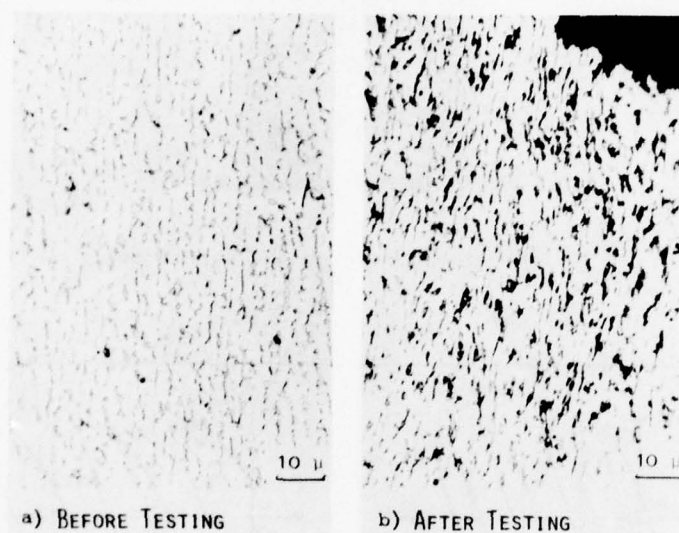


Fig. 9: Elongation of the β -phase in a creep test at 450 °C.

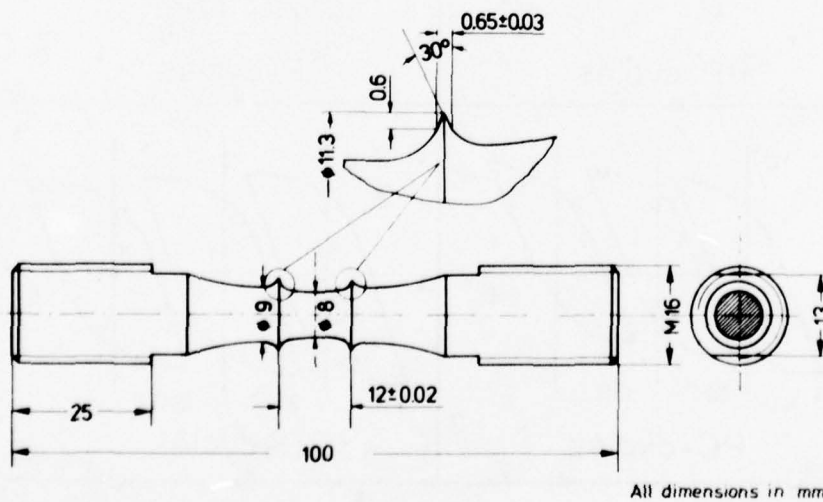


Fig. 10: Specimen for the creep fatigue tests at 450 °C

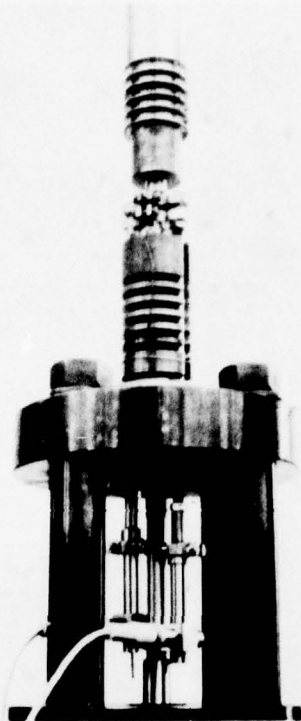


Fig. 11: Specimen mounting and extensometer

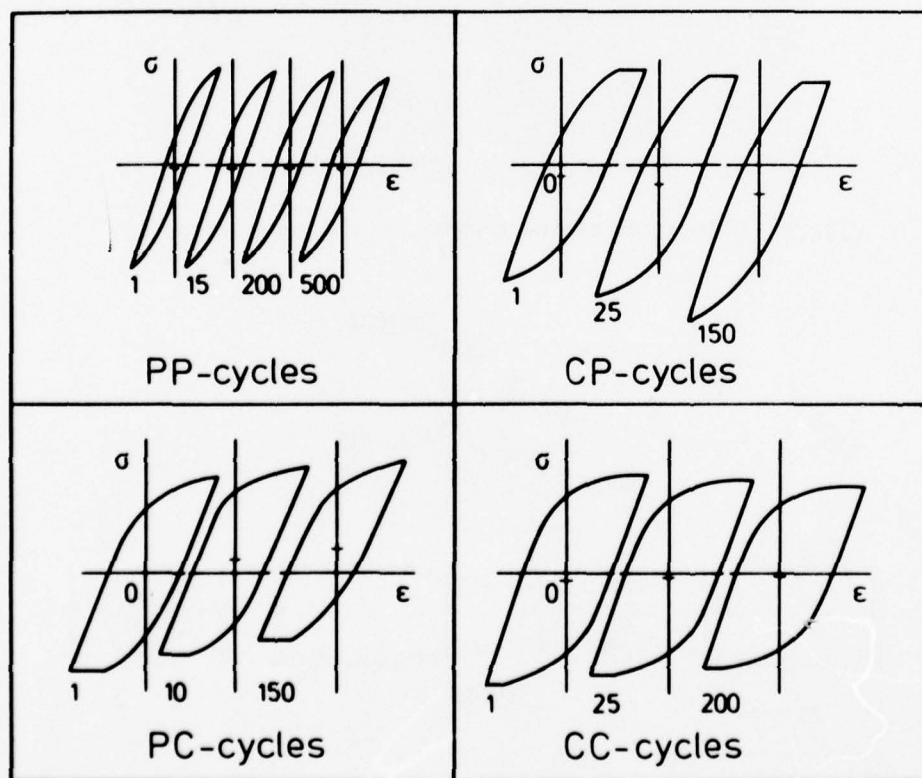


Fig. 12: Observed stress-strain behaviour in the creep fatigue tests with different cycle types

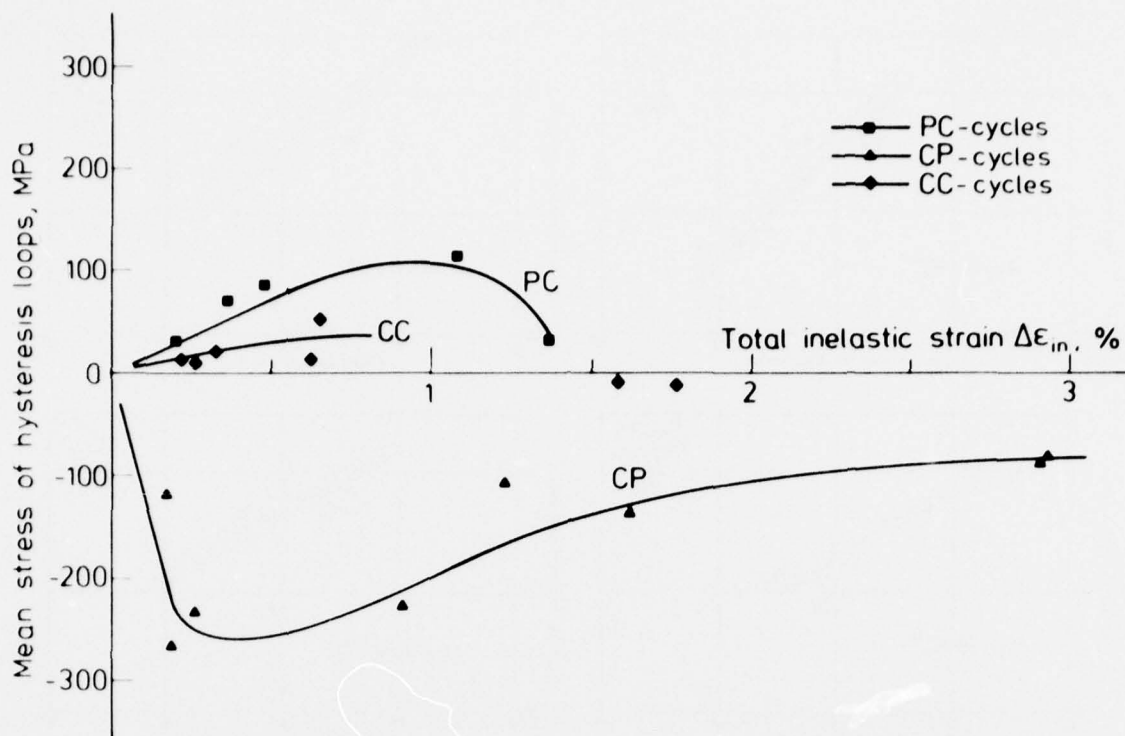


Fig. 13: Observed half-life values of the mean stress in the creep fatigue tests at 450 °C with different cycle types

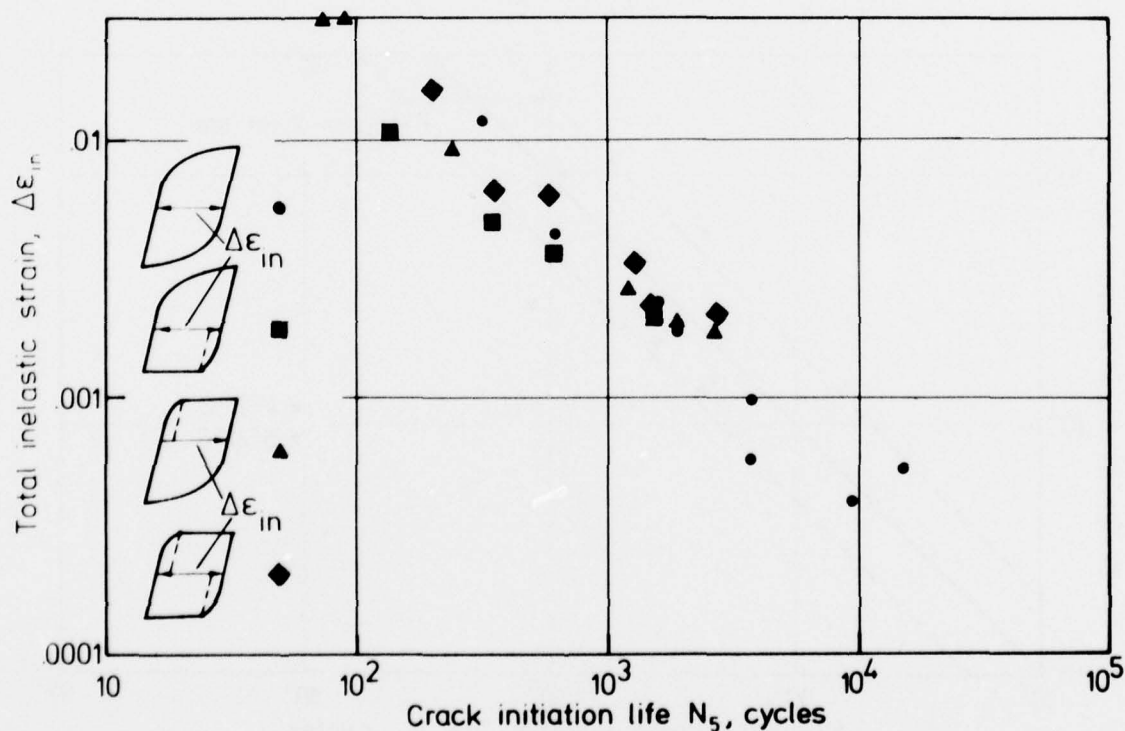


Fig. 14: Observed crack initiation life behaviour in the creep fatigue tests at 450 °C

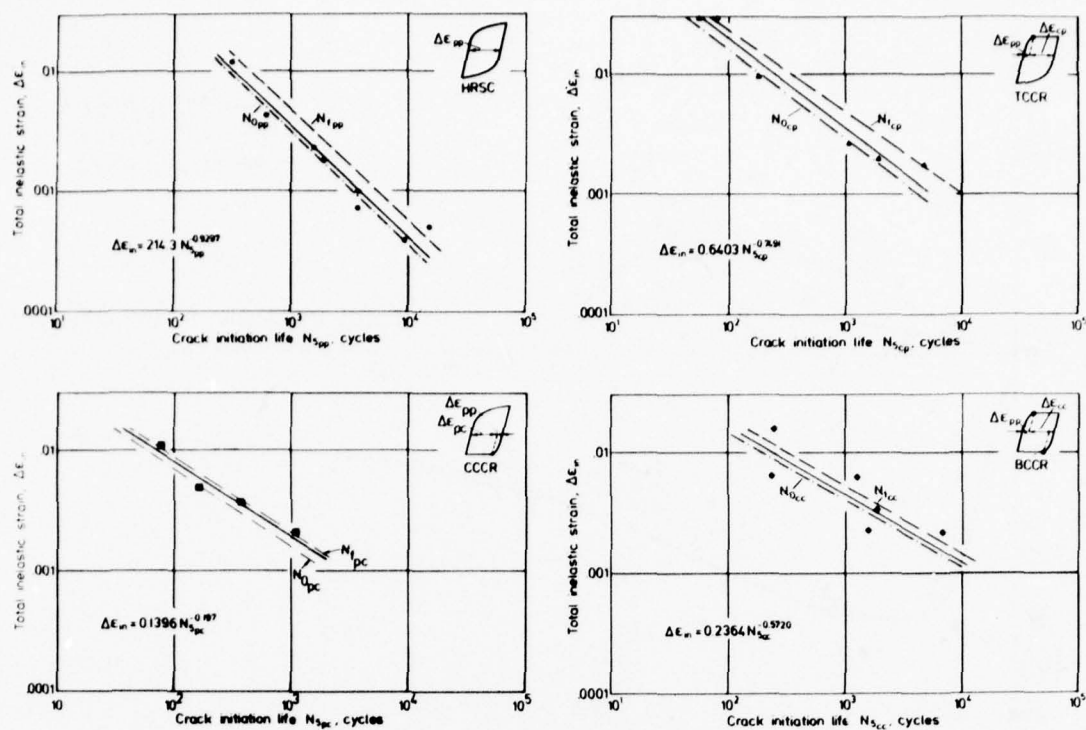


Fig. 15: Partitioned strainrange-life relationships for the Ti6-4 alloy at 450 °C

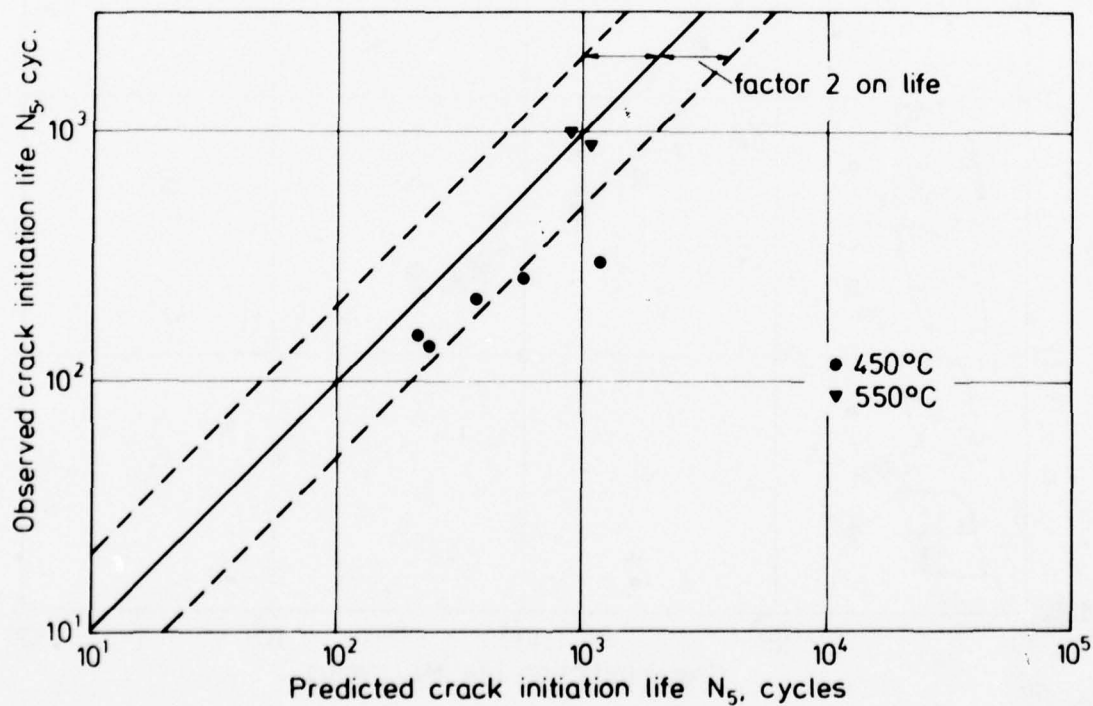


Fig. 16: Comparison of the observed and predicted lives for the Ti6-4 alloy

STRAIN RANGE PARTITIONING IN CYCLIC CREEP OF A 1 Cr Mo V STEEL

E. G. Ellison, PhD, BSc, CEng, MIMechE
 Reader, Mechanical Engineering Department, University of Bristol,
 Queen's Building, University Walk, Bristol, BS8 1TR

SUMMARY

A 1 Cr Mo V ferritic steel has been subjected to fatigue/creep conditions at 565 °C. Most of the data obtained were from strain controlled tests with and without hold periods. Some load controlled results were also obtained. The strain range partitioning (SRP) method for predicting lives at long hold periods, and under complex load cycles, was applied. With this material, good correlation of data using the Ductility Normalized SRP was obtained, although even better correlation resulted when the SRP method was modified to take account of the length of the hold period.

NOMENCLATURE

PP,CC,PC,CP	Denotes features associated with strains partitioned according to the SRP rules, Ref. (4)
CP _b	CP feature related to brittle creep
CP _d	CP feature related to ductile creep
$\epsilon_{pp,---\epsilon_{**}}$	Inelastic strain related to the subscripts
ϵ_{ntd}	Non-time dependent strain
ϵ_{td}	Time dependent strain
N _{pp,---N_{**}}	Cycles to failure for a cyclic test whose inelastic strain range is described by the subscripts
N _f	Number of cycles to failure
F _{pp,---F_{**}}	Fraction of a total inelastic strain range that relates to inelastic strain described by the subscripts
D _c	Creep ductility
D _p	Plastic flow ductility
tr _{eq}	Time to rupture for a static creep test equivalent to a complex cyclic creep test
30T/3C	Description of hold times in a strain controlled cycle, e.g. 30 min tensile hold plus 3 min compressive dwell

1. INTRODUCTION

In modern power plant such as gas turbines, nuclear reactors, and conventional steam generation plant, the presence of complex load/temperature conditions, often in an adverse environment, makes for design difficulties. The consequences of failure in critical components can be catastrophic. The high temperature transients can cause large thermal strains with consequent cyclic plasticity. At the elevated temperatures involved, creep processes are also present in the material.

Clearly, this complex situation poses problems for the designer who has to design for a specific life. The simple question is how do we "add" all these processes; fatigue, creep, plus environment, together to form a total damage. At this time, our difficulty lies in the fact that we do not understand precisely the possible interactions which may arise between them and there is a definite need for more suitable material behaviour data to elucidate the situation. It must also be borne in mind that under these high cyclic strain/creep conditions it is probable that cracks initiate early in the life and that the propagation of this type of damage is the matter to be considered. In other words, we simply do not know the constitutive equations which describe the material behaviour under these simulated complex service load/temperature conditions. Since we do not understand the interactive processes, it is not possible to propose constitutive equations based on fundamental parameters, and we have to rely therefore on continuum type predictive methods. In recent years, several such methods of life prediction have been attempted with various degrees of success, for example, straightforward fatigue plus creep cumulative damage, frequency modified life, and now strain range partitioning.

This paper presents data for a single batch 1 Cr Mo V ferritic steel which has been subject to various combinations of fatigue and creep at elevated temperature as part of a larger programme of work at Bristol. In particular, the material behaviour for long hold

periods under strain control is predicted by means of a method which is based on strain range partitioning.

2. EXPERIMENTAL

All cyclic tests¹ were carried out in a servo-hydraulic axial push/pull machine capable of either load or strain control in the cycle. Specimens had a parallel sided gauge length with thin ridges at the ends of the gauge length for attachment of extensometry (Fig. 1). Measurement and control of strain was by means of a pair of LVDT's in the extensometry; since the LVDT's were arranged to record strains on diametrically opposite sides of the specimen, it was possible also to check for any bending present. Loading alignment of better than 0.02 mm TIR between the loading columns reduced bending to negligible proportions and eliminated the possibility of buckling during compression.

The specimen was heated by a non-inductively wound three-zone furnace, control being achieved by a proportional controller and a Pt/Pt 13% Rh thermocouple clamped to the specimen. Temperature was monitored, on a data-logger, by Cr/Al thermocouples spot welded to the specimen and was controlled to within $\pm 1^\circ\text{C}$ of the nominal 565°C .

A summary of the test results considered with regard to the strain range partitioning method are given as follows:

Control	Hold Time - Minutes		SRP Element in Cycle	
	Tension	Compression		
Strain	0	0	PP	†
Strain	0	0	CC	*
Strain	30 180 960	0 0 0	PP, CP	
Strain	0 0	3 30	PP, PC	
Strain	30	30	PP, CC	
Strain	30 960	3 0.2	PP, CC, CP	
Load	30-45	0	PP, CP	

The strain rate used in the dynamic sections of all cycles was 0.4%/sec with the following exceptions:

† One test was carried out at 4.5%/sec to confirm that there was no significant creep strain present at strain rates of 0.4%/sec.

* All these tests were carried out at a strain rate low enough to eliminate any PP element. The cycle frequency was 2 cy/hr and the stress never exceeded the cyclic yield point.

3. MATERIAL

3.1 Composition

The material used in this work is a low alloy, 1 Cr Mo V steel taken from a single batch. The composition is shown as follows (see Footnote on next page):

Element	C	Si	Mn	Ni	Cr	Mo	V	S	P
%	0.24	0.29	0.64	0.21	1.02	0.57	0.29	0.01	0.016

3.2 Heat treatment

Austenitise at 1000°C .
Furnace cool to 690°C at 50°C/hr .
Hold for 70 hrs and air cool.
Re-austenitise at 975°C .
Quench into salt bath at 450°C .
Hold for 5 hrs and air cool.
Rough machine.
Anneal in salt bath at 700°C for 20 hrs.
Finish machine.

It was in order to achieve maximum homogeneity that the isothermal treatment was incor-

porated to produce a mid-bainite structure. Following the correct heat treatment cycle the hardness was in the range 240-253 VHN.

Further details concerning the material and its metallography are to be found in Ref. (2).

3.3 Monotonic test results

	Room Temp.	565 °C	
	$\dot{\epsilon}=0.4\%/sec$	$\dot{\epsilon}=0.1\%/min$	$\dot{\epsilon}=0.4\%/sec$
0.02% proof stress MN/m ²	635	300	400
Ultimate tensile stress MN/m ²	805	420	500
Elongation %	36	40	
Reduction in area %	64	80	
Modulus of Elasticity GN/m ²	203	153	

3.4 Principle fatigue/creep characteristics

The 1 Cr Mo V steel has three important features when considering its behaviour under cyclic plasticity and/or creep conditions.^{1,3}

- (i) Under cyclic strain the material exhibits rapid cyclic softening followed by a more stable period so that at half-life there is a reduction of approximately 25% in the stress range (Fig. 2). This amount of cyclic softening was present at both room temperature and 565 °C.
- (ii) The second important characteristic of this material is that, under isothermal creep conditions, it has a very sharply defined ductile/brittle transition (Fig. 3). Above a transition stress of 240-250 MN/m² all failures are said to be ductile and are characterized by a reduction in area of about 50%. In this ductile régime little or no cracking occurs before failure. In contrast, below the transition stress the failures exhibit a reduction in area of approximately 10%, which then decreases with lower values of creep stress. There is clear intergranular cracking at prior austenitic grain boundaries and the fracture may loosely be termed a brittle failure. An important point is that the transition stress does not appear to be affected by cyclic softening either before or during a creep test. This feature is shown in Fig. 4 which summarises previously reported data³ for the same batch of material including: (a) static load creep; (b) repeated tension creep; (c) creep after prior cyclic strain. The same ductile/brittle transition applies to all this data.
- (iii) The third feature occurred in the strain controlled tests at 565 °C with hold periods at maximum strain. It was observed that the peak stress at the beginning of the hold period, whether in tension or compression, relaxed very rapidly in the first few seconds. As a typical example, the stress may decrease by one-third of its total stress relaxation in the first 10 seconds and by nearly two-thirds after 1 minute even for hold periods measured in hours. Careful experimental checks ensured that this behaviour was a definite material effect and it was hypothesized that the initial rapid stress decrease was not solely due to creep processes; the possibility of some anelastic process was put forward. Whether the process is anelastic or creep, it seems likely that it is caused by a rapid dislocation mechanism.

4. PREDICTIVE METHODS AND RESULTS

The strain range partitioning (SRP) method of predicting lives for a high strain, complex fatigue/creep cycle is described in detail by Hirschberg and Halford.⁴ This gives the interaction damage rule as

$$\frac{1}{N_f} = \frac{F_{pp}}{N_{pp}} + \frac{F_{cc}}{N_{cc}} + \frac{F_{cp}}{N_{cp}} + \frac{F_{pc}}{N_{pc}} \quad (1)$$

This section details the straightforward application of SRP, without modification, to a 1 Cr Mo V steel at 565 °C and then two developments of this technique.

4.1 Direct application of SRP

Strain range partitioning calls for the generation of Manson-Coffin type lines for ϵ_{pp} , ϵ_{cc} , ϵ_{cp} , and ϵ_{pc} against life. These lines should then characterize a material for any cycle according to Eq.(1). At Bristol, data has been obtained from strain controlled tests, with and without hold periods at maximum strain in the cycle. It is a feature of this type of test that the inelastic strain is usually predominantly ϵ_{pp} .

* Chemical compositions, material processing, heat treatments and mechanical properties for each tested alloy, as well as the data generated in the programme, are given in Appendix A1.

The SRP points are shown in Fig. 5 and it can be seen that the ϵ_{pp} and ϵ_{cc} results are good, yielding straight lines as expected. The ϵ_{cp} data produces a wide scatter band which would not inspire confidence in the use of Eq.(1) since a single CP line does not appear reasonable.

Following the results obtained for ϵ_{cp} using strain controlled data, a further series of tests using load controlled tensile creep was carried out. This enabled a much higher proportion of the inelastic strain range to be of the ϵ_{cp} form and so reduce errors. The constant stress in the tensile hold was always greater than 250 MN/m² to cause a failure in a reasonable time; i.e. the stresses were above the transition stress and therefore always in the ductile régime.

It was found that the CP results from these tests did not agree with the previous strain controlled CP data (see Section 4.2); in fact, they were not as damaging as the latter. It was an experimental fact that, in the strain controlled tests, the stresses in the hold period always relaxed down to values below the transition stress into the brittle régime for the majority of the hold period. Hence a possible reason for the discrepancy might be in the considerable difference in creep ductilities above and below the transition stress; the load controlled CP tests were carried out exclusively in the ductile régime and the strain controlled CP tests predominantly in the brittle régime. An analytical procedure based on creep ductility will be considered in Section 4.2.

An alternative explanation may be associated with the fact that the CP data from the strain controlled tests with longer hold periods lay further to the left in Fig. 5, i.e. were more damaging. An analytical method based on the length of the hold time will be proposed in Section 4.3.

4.2 ϵ_{cp} lines based on ductility normalized SRP

Halford, Saltsman and Hirschberg⁵ have proposed a modification to the SRP method based on creep ductility. Generalised SRP equations may be written to include a ductility term.

$$N_{pp} = (2\Delta\epsilon_{pp}/D_p)^{-1.67} \quad (2)$$

$$N_{cc} = D_c (4\Delta\epsilon_{cc})^{-1.67} \quad (3)$$

$$N_{pc} = (4\Delta\epsilon_{pc}/D_p)^{-1.67} \quad (4)$$

$$N_{cp} = D_c (5\Delta\epsilon_{cp})^{-1.67} \quad (5)$$

$$N_{cp} = D_c (10\Delta\epsilon_{cp})^{-1.67} \quad (6)$$

For the 1 Cr Mo V steel results presented in this paper, Eq.(2-6) do not hold true either in the slope or constants. Experimental lines for ϵ_{pp} and ϵ_{cc} have been obtained from the strain controlled tests. Accepting that above the transition stress the ϵ_{cp} is ductile and below it is brittle, the ϵ_{cp} may be partitioned into ϵ_{cpd} and ϵ_{cpb} in the normal SRP manner. The CP_d line was obtained from the load controlled CP tests. A true CP_b line would have to be produced by load controlled CP tests with creep stresses below the transition stress; such tests would be very long. However, strain controlled tests with 960 min tension holds have been carried out and, since the stresses relax to low values in this long hold period, the vast majority of this hold is in the brittle régime. Hence, let us assume that this cycle produces a reasonable CP_b line.

Eq.(1) should now be written:

$$\frac{1}{N_f} = \frac{F_{pp}}{N_{pp}} + \frac{F_{cc}}{N_{cc}} + \frac{F_{cpd}}{N_{cpd}} + \frac{F_{cpb}}{N_{cpb}} \quad (7)$$

where F_{cpd} and F_{cpb} are the fractions spent in the ductile and brittle régimes respectively. A CP_b line may now be produced using Eq.(7), see Fig. 6.

Figure 3 shows creep ductility against stress. In the case of a 960 min hold the stress is sensibly constant after a small percentage of the hold time, so a ductility may be read off Fig. 3. Thus the equation of the CP_b line in Fig. 6 is

$$N_{cpb} = D_c (2.79 \times \Delta\epsilon_{cpb})^{-1.412} \quad (8)$$

Using SRP lines for N_{pp} , N_{cc} , N_{cpd} with Eq.(8) predictions can now be made with Eq.(7).

4.3 ϵ_{cp} lines based on hold time modified SRP

For strain controlled tension only hold time tests,¹ the stress in the hold period decreases from a high peak value very rapidly to a level well below the transition stress (Fig. 7). The initial stress relaxation is so rapid that some doubt is expressed as to whether this is solely due to creep relaxation processes. In fact, the CP strain due to this initial stress relaxation forms a considerable fraction of the whole ϵ_{cp} recorded. Ellison and Paterson¹ proposed a model for ratchetting grain boundary damage to explain the low lives obtained for tension only hold cycles and the longer lives obtained in a balanced cycle with equal tension and compression hold periods; in the latter cycle the

time dependent grain boundary "damage" balanced out in each cycle. In many respects this model agrees with the SRP philosophy except that there is an allowance in the former for time independent deformation during a creep hold period, Fig. 8.

When considering the stress relaxation curve for a strain hold period (Fig. 7) let us assume for this material that during the period of relaxation down to the transition stress, the inelastic strain is wholly time independent, and that time spent below the transition stress gives rise to wholly time dependent inelastic strain. Metallographic examination of failed specimens certainly suggest that different mechanisms operate either side of the transition. Thus, as the load controlled CP data was all taken for creep stresses above the transition stress, in the ductile régime, let us assume that the CP line generated will apply to the non-time dependent part of any ϵ_{cp} in a cycle, i.e. a CP_d line.

In the case of a strain controlled tensile hold test, the majority of the hold is spent in the time dependent (brittle) régime giving rise to brittle creep strain, ϵ_{cpb} . Hence, again, we have for a tension only dwell cycle, Eq.(7)

$$\frac{1}{N_f} = \frac{F_{pp}}{N_{pp}} + \frac{F_{cc}}{N_{cc}} + \frac{F_{cpd}}{N_{cpd}} + \frac{F_{cpb}}{N_{cpb}}$$

To produce a line relating to time dependent CP_b , time dependent data should be used. Let us assume the usual damage approach applied to the time dependent part of the loop:

$$\text{Creep Damage/cycle} = \frac{t}{t_{req}} \quad (9)$$

where t = time of hold below the transition stress and t_{req} is the time to rupture for a static creep test equivalent to the sum of the creep that occurs in the hold periods below the transition stress. Eq.(9) is equivalent to F_{cpb}/N_{cpb} in Eq.(7).

$$\text{Thus } \frac{F_{cpb}}{N_{cpb}} = \frac{t}{t_{req}} \quad (10)$$

When calculating creep rupture times, parameters based on strain are less susceptible to errors than those based on stress. This is because the relationship between stress and time to rupture depends on a power function of higher order than that relating strain and time to rupture. Minimum creep rate plotted against time to rupture on a log/log basis yields a straight line. For this material, this is true irrespective of the type of creep, be it static load, cyclic load, reversed cyclic load; with or without prior fatigue, Fig. 9. This forms the basis of obtaining t_{req} for Eq.(10). For a constant strain hold the minimum creep rate is that at the end of the hold time, so t_{req} may be found from Fig. 9. Using Eq.(10) and experimental data, CP_b points were t_{req} plotted. This yielded a series of CP_b lines related to the tensile dwell time. These lines now complete the SRP data to enable life predictions to be made with Eq.(7). Figure 10 shows the completed SRP lines.

Sample calculations for N_{cpb} are shown in Appendix I(a).

5. DISCUSSION

Using SRP as originally envisaged, Fig. 5 shows that PP and CC provide good results but PC and CP data has some shortcomings for strain controlled hold tests. The PP line can be drawn through pure fatigue data with good correlation. This data includes one point with a strain rate ten times that of the remainder, demonstrating that there was negligible creep present in the fatigue tests. The CC line, drawn through data derived from slow cycle tests, is near parallel to the PP line and is slightly more damaging. This result is as expected.

Only a small amount of PC data is available and this shows no obvious trend. The strain controlled tests yielded $F_{pc} \approx 0.1$ with $F_{pp} \approx 0.9$ for inelastic strains in the range $\pm 0.25\%$ to $\pm 0.75\%$. For this type of test it was noted that $N_{pp} \approx N_{obs}$ so that in the equation

$$N_{pc} = \frac{F_{pc}}{\frac{1}{N_{obs}} - \frac{F_{pp}}{N_{pp}}} \quad (11)$$

the denominator is a small difference of small numbers. This makes N_{pc} particularly sensitive to small errors. Load controlled PC data may produce better correlation as the difference in the terms in the denominator increases. This data is now being generated in the Bristol Laboratories.

The CP data exhibits a large scatter for a given inelastic strain range, lifetimes varying by up to four times. However, a closer analysis reveals a consistent trend for the longer hold tests, at similar inelastic strain ranges, to yield shorter lives.

When considering the Ductility Normalised SRP results, as indicated in Section 4.2, the CP component of the inelastic strain range was split into a CP_b and a CP_d part. The

lines so produced, along with the PP and CC lines, are shown in Fig. 6. Correlation of these lines with Eq.(2) to (6) is poor, however, and to use ductility normalized SRP to predict lives the experimentally derived CP_b line was used to evaluate the slope and constants to be used in Eq.(6). Life predictions based on experimentally derived PP, CC and CP_b lines and the corrected Eq.(6) were made. Figure 11 shows the predicted lives against those observed. Correlation is good. With the exception of one point, all predictions were within times 2 of life. The original data for the anomalous point indicated that this test result possessed a longer life than expected though there was no apparent reason for this.

Using hold time modified SRP, a series of CP_b lines have been plotted dependent on the length of the hold periods and can be seen to be near parallel to PP and CC, Fig. 10. These lines show that CP_b is far more damaging than other types of inelasticity and a longer hold time increases the damage.

Figure 12 shows a graph of predicted against observed lives for various complex cycles including constant strain holds. Correlation is extremely good. With the exception of the one point, all predictions are better than $1\frac{1}{2}$ times of life. The exception discussed previously is still within 2 times of life. The predicted results include examples for long, 960 min, hold periods under strain control, and complex cycles in which unequal hold periods in both tension and compression are present.

In contrast to the PC case, the CP test shows a much greater difference between N_{pp} and N_{obs} . Thus, in Eq.(11) (for the CP case), the denominator would now be a larger difference and so is less sensitive to errors. To obtain some feel for the effect of errors in the damaging CP line, it is instructive to consider the following example. Generally, for life predictions using Eq.(7), if a 50% change in the value of N_{cpb} is made, the resultant shift in the predicted lives is approximately 30%.

The two methods of modifying the basic SRP method discussed above, based on ductility and on time dependent data, have much in common. They both approach the phenomenon of time dependent damage using material characteristics. The 1 Cr Mo V steel is a particularly good vehicle to examine the validity of the ductility modified model as it can be idealised as having a step change in ductility (Fig. 3). However, examination of Figs 3 and 4 shows that while the ductility exhibits a sharp, well defined discontinuity for this material, the creep properties do not. Creep data describes more precisely the time dependent damage and so is inherently more accurate. The limitation in the approach made here lies in the assumption that the non-time-dependent inelastic deformation contains no time dependent inelasticity and vice versa. In reality, each régime will contain a small proportion of the other, the degree depends on the material under consideration.

A limitation that applies to both methods of analysis is that there is little or no compressive ductility or creep data available for this material at present. This inhibits the application of either model to PC deformation.

6. CONCLUSIONS

For the 1 Cr Mo V steel considered in this report the following conclusions may be drawn.

- (1) PP and CC data produced linear plots when unmodified SRP techniques were used for analysis.
- (2) Tests involving tension only holds were the most damaging whether under load or strain control. The longer the hold time in tension, the more damaging the cycle.
- (3) The SRP approach for the prediction of lifetimes of specimens experiencing tensile hold periods is promising, provided certain modifications are made.
- (4) Ductility Normalized SRP results generally predicted lifetimes to within a factor of 2 times the observed lifetimes for a variety of tests involving tension and tension plus compression holds.
- (5) An alternative modification to the SRP approach based on the time of the hold period yielded even better correlation of predicted with observed lifetimes for the range of tests considered. Predicted lifetimes were generally within a factor of 1.5 of the observed lifetimes.
- (6) Tests involving compression only holds were less damaging than any containing tensile hold. Specimen lifetimes approached those expected from pure fatigue tests at the same strain range.

REFERENCES

1. Ellison, E. G. and Paterson, A. J. F., "Behaviour of a 1 Cr Mo V steel subject to combinations of fatigue and creep under strain control", Proc. I.Mech.E., Vol. 190, 12/76, p. 333, 1976.
2. Plumbridge, W. J. and Bartlett, R. A., "The metallography of 1 Cr Mo V steels", University of Bristol report No. 77/9, 1977.

3. Ellison, E. G. and Paterson, A. J. F., "Creep fatigue interactions in a 1 Cr Mo V steel", Proc. I.Mech.E., Vol. 190, 12/76, p. 321, 1976.
4. Hirschberg, M. H. and Halford, G. R., "Strain range partitioning - a tool for characterizing high-temperature low-cycle fatigue", NASA TMX-71691, April 1975.
5. Halford, G. R., Saltsman, J. F. and Hirschberg, M. H., "Ductility normalized strain range partitioning life relations for creep-fatigue life predictions", NASA TM 73737, Oct. 1977.
6. Paterson, A. J. P. and Ellison, E. G., "Predictions of deformation and life under fatigue/creep conditions", Proc.I.Mech.E., Vol. 190, 12/76, p. 341, 1976.

ACKNOWLEDGMENT

The assistance of the C.E.G.B. Berkeley Nuclear Laboratories in providing facilities to carry out the 960T/OC and the 960T/O.2C tests is gratefully acknowledged.

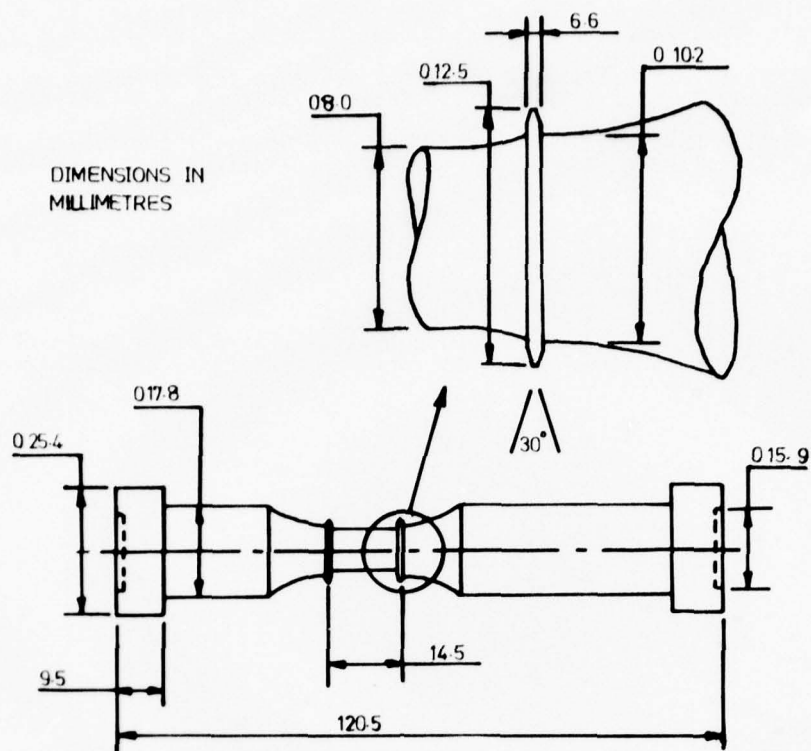


Fig.1 High strain fatigue/creep specimen

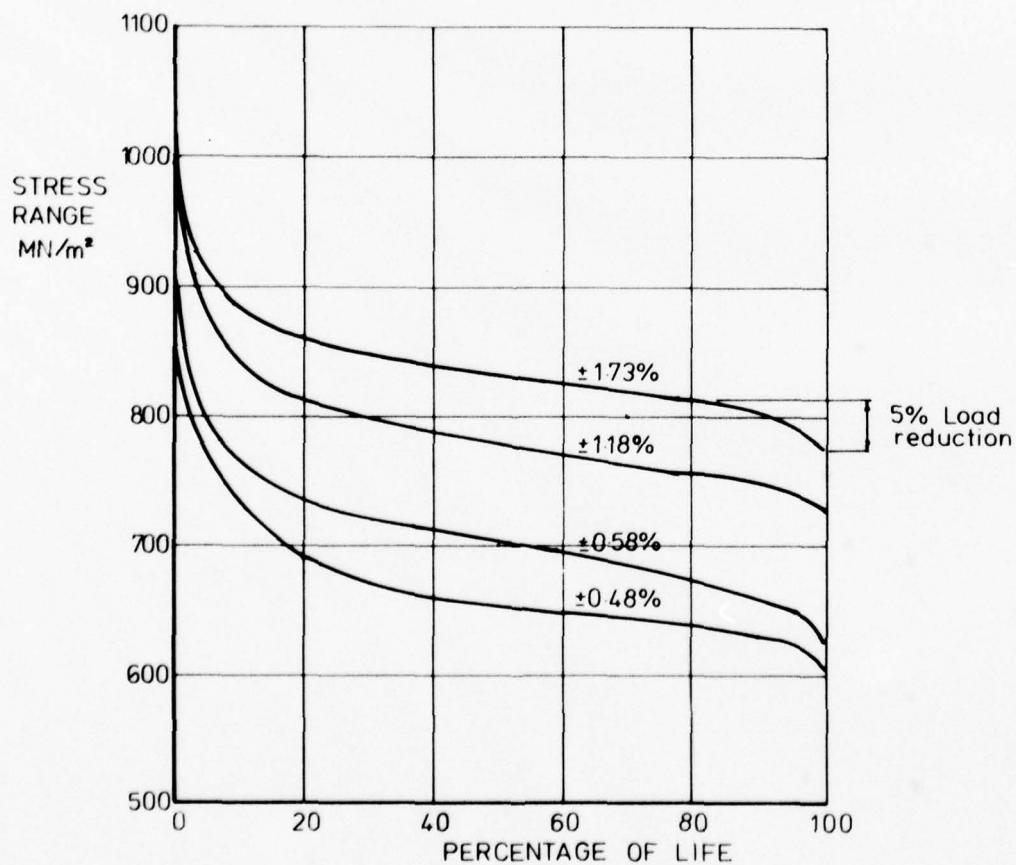


Fig.2 Cyclic softening curves for various total strains at 565°C

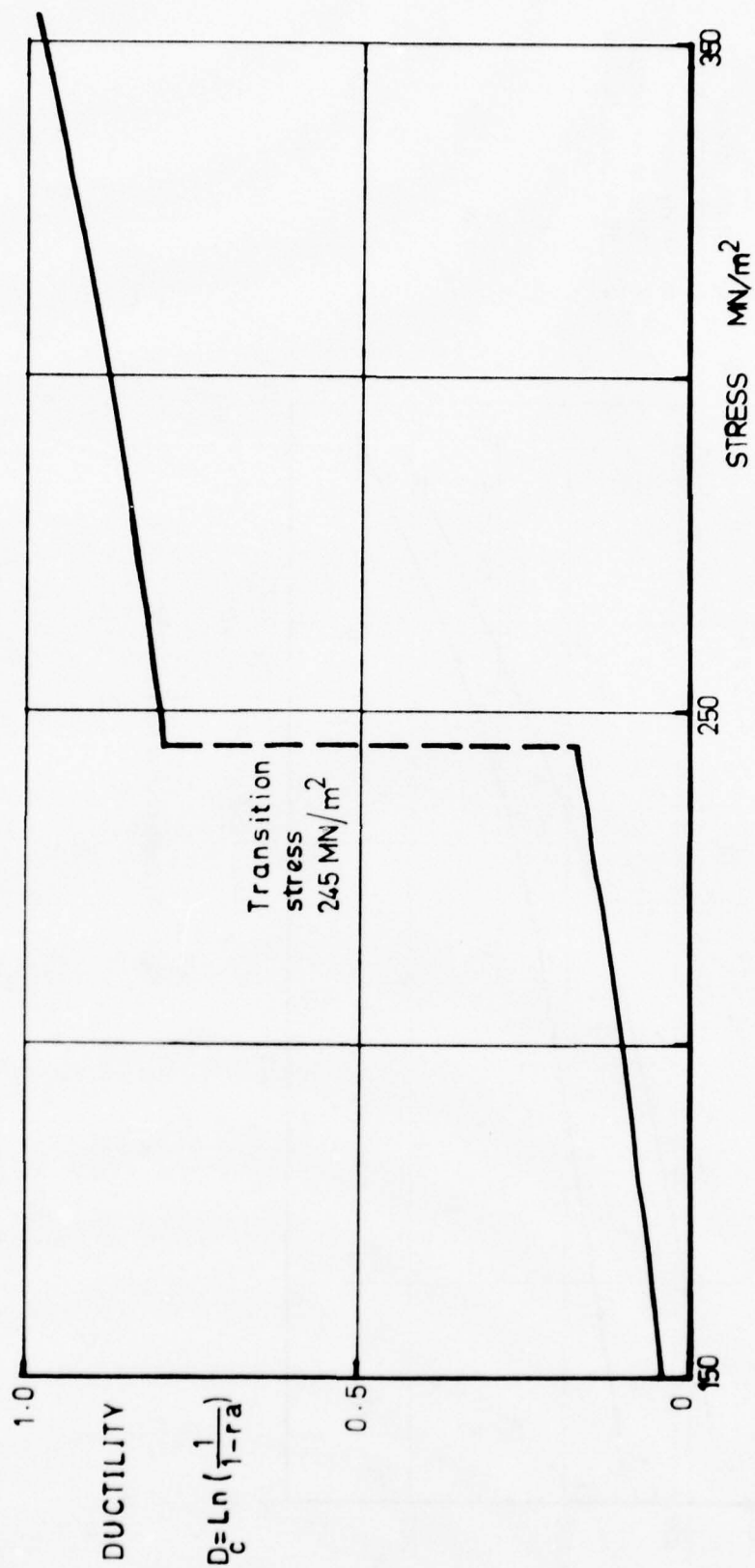


Fig.3 Creep ductility at 565°C

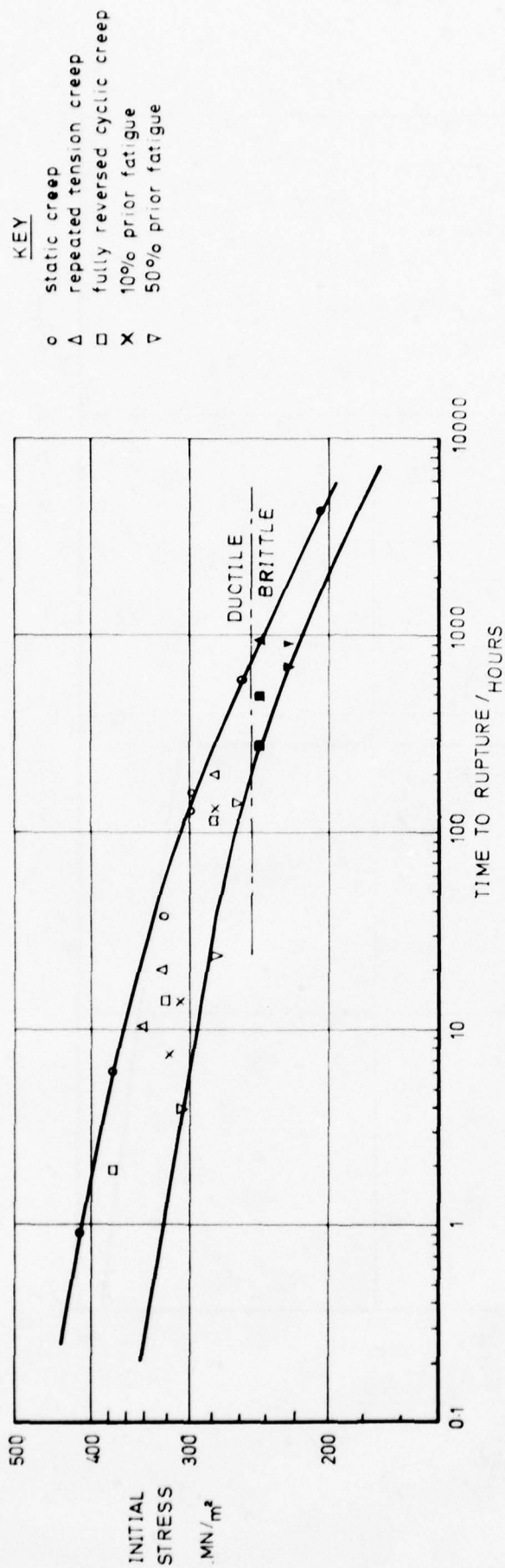


Fig.4 Summary of creep tests at 565°C

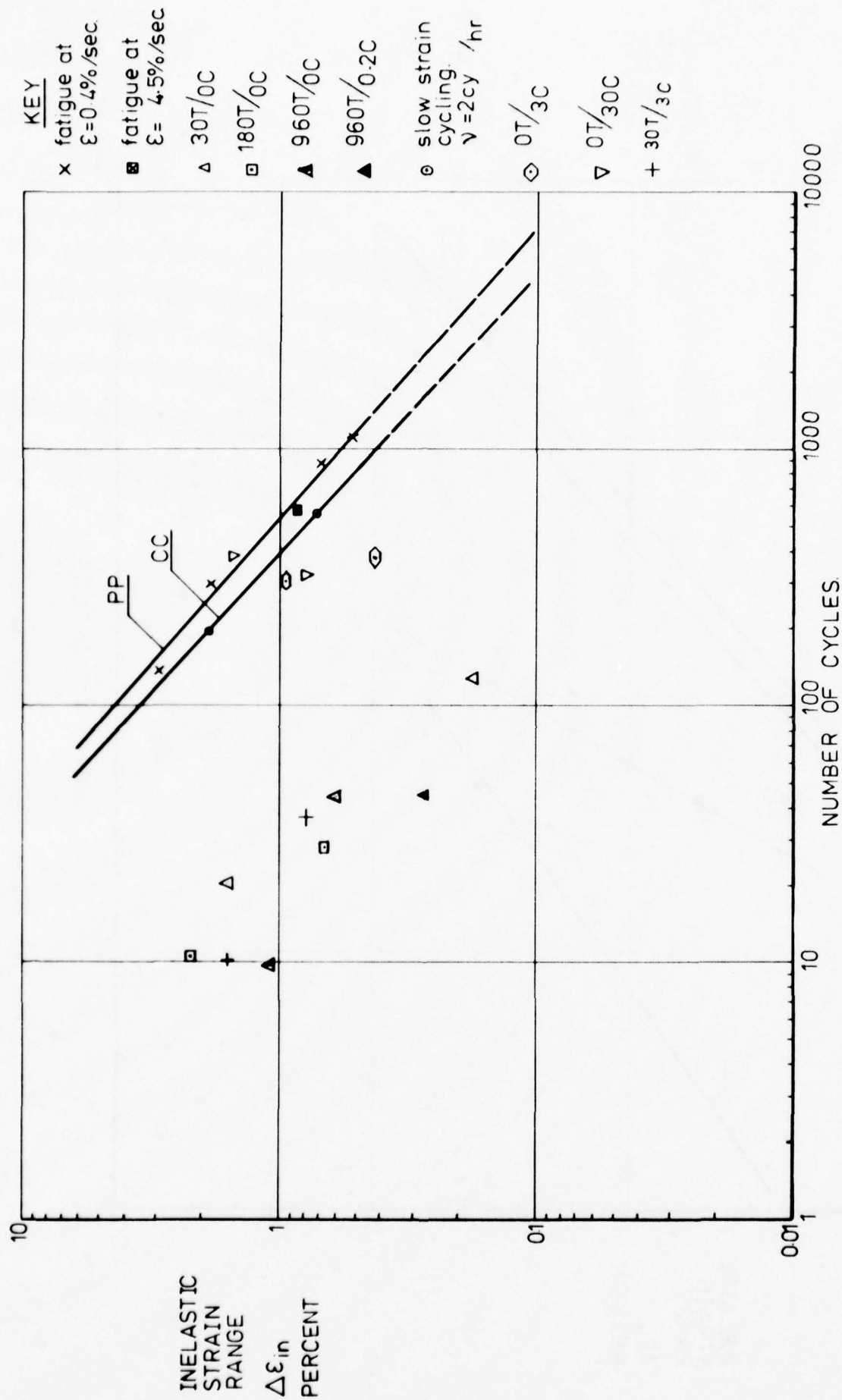


Fig.5 Summary of strain range partitioned tests

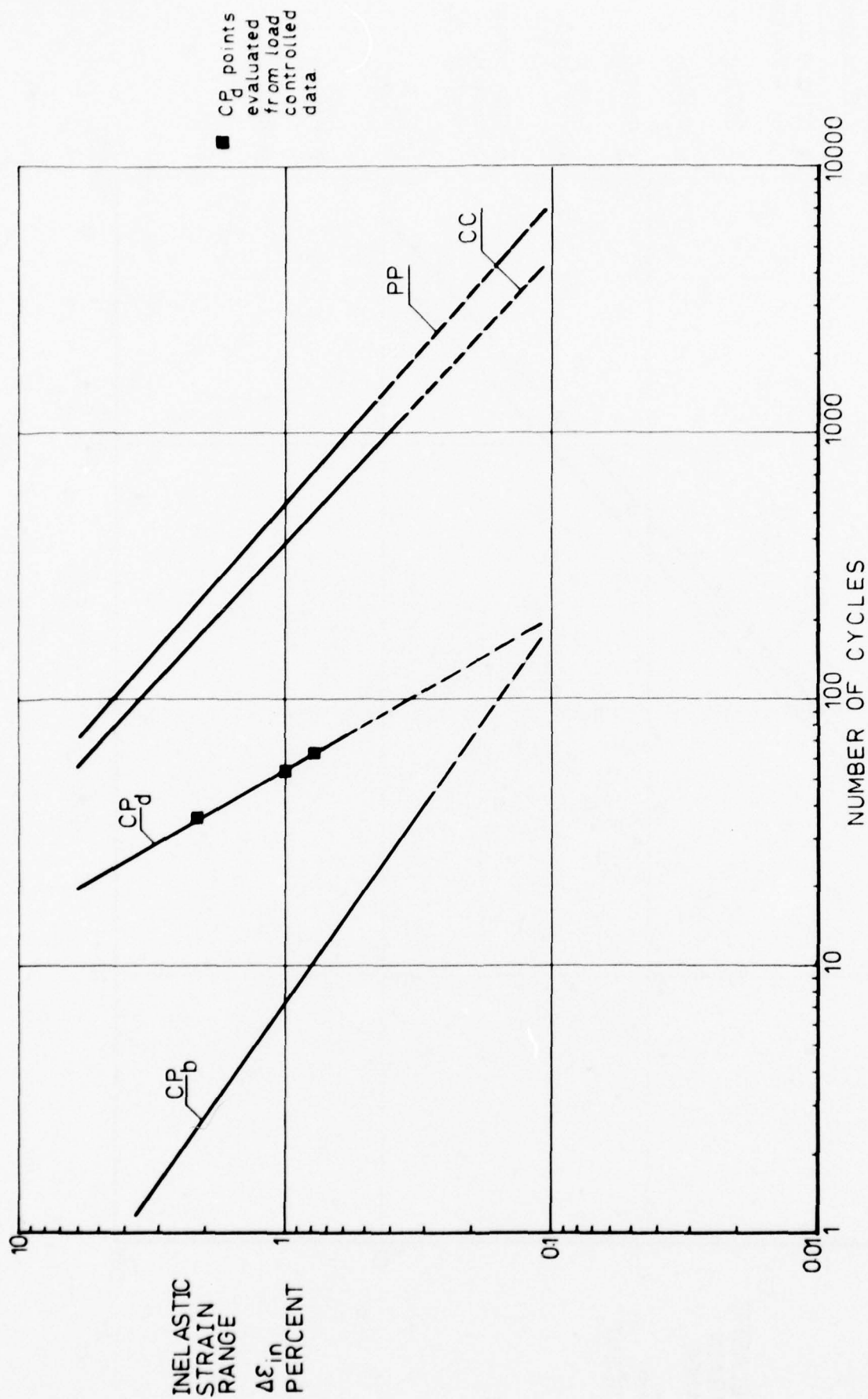


Fig. 6 Strain range partitioning life relationships, CP_b evaluated from 960T/OC data

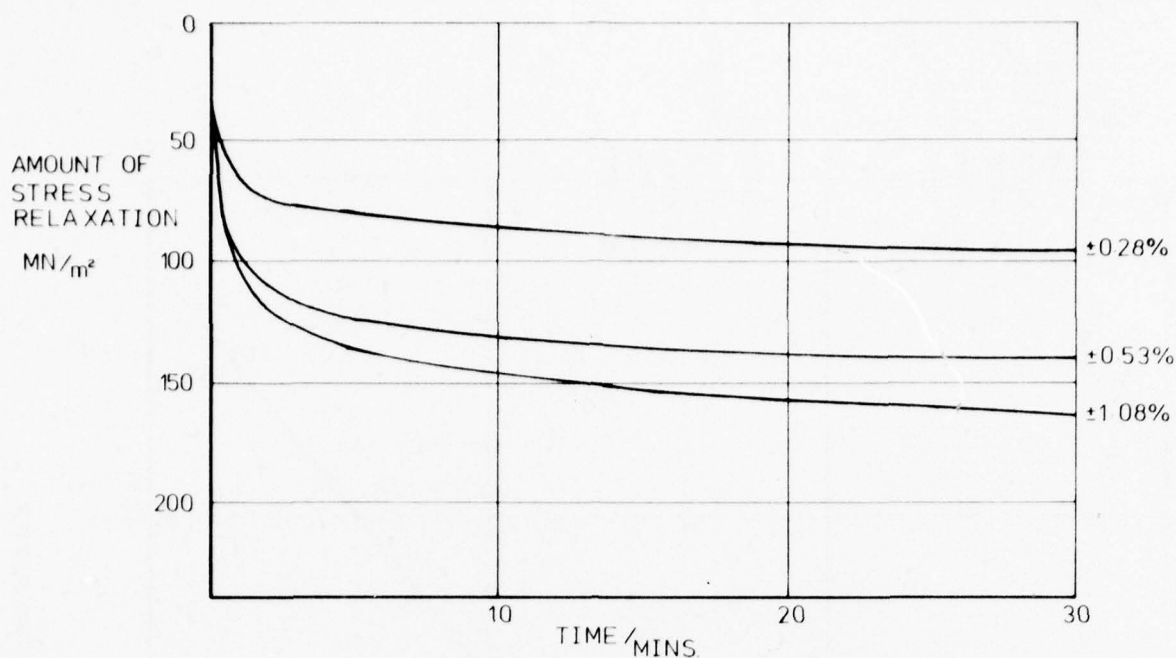


Fig.7 Creep stress relaxation curves for 30T/OC at 565°C at various total strains

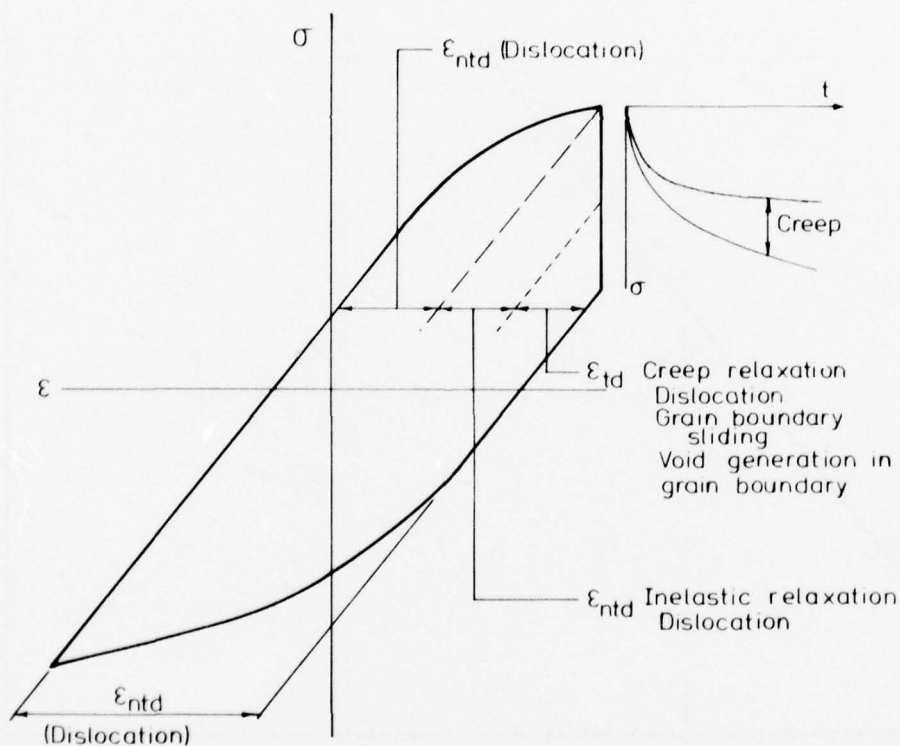


Fig.8 Schematic model for ratchetting grain boundary damage

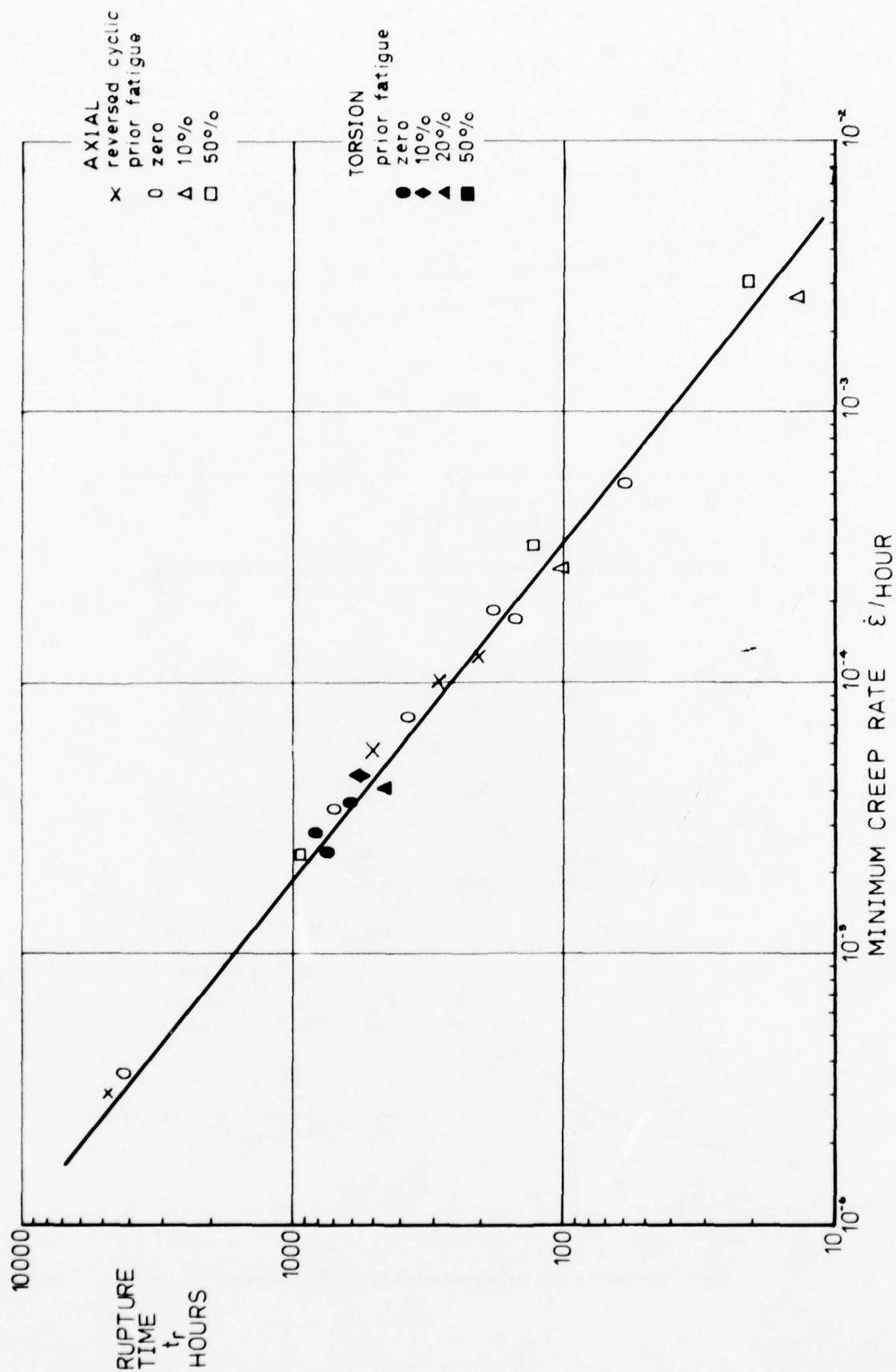


Fig.9 Relationship between creep rupture time and minimum creep rate

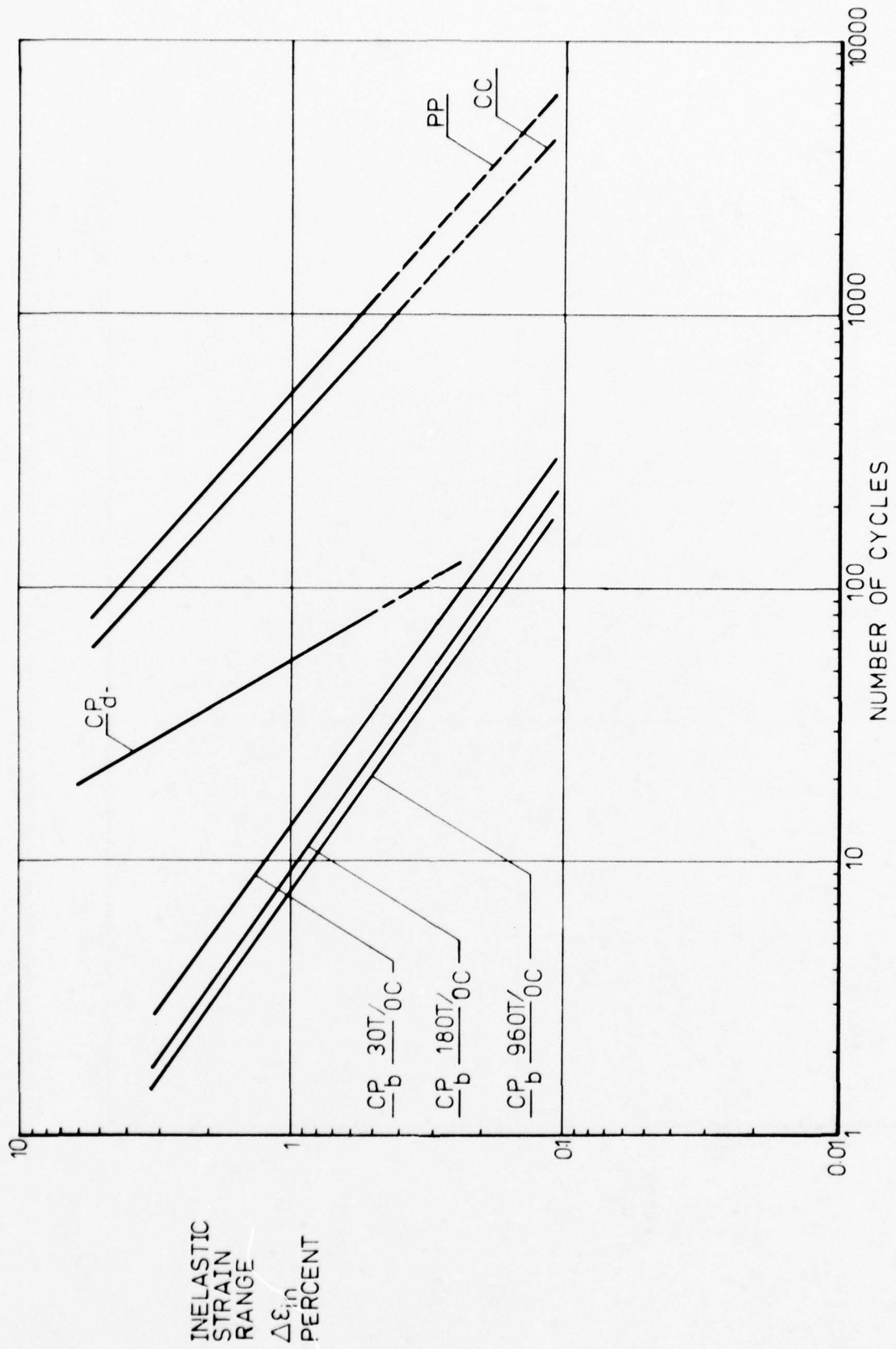


Fig. 10 Strain range partitioning life relationships. CP_b derived from equivalent creep data giving hold time modified life relationships

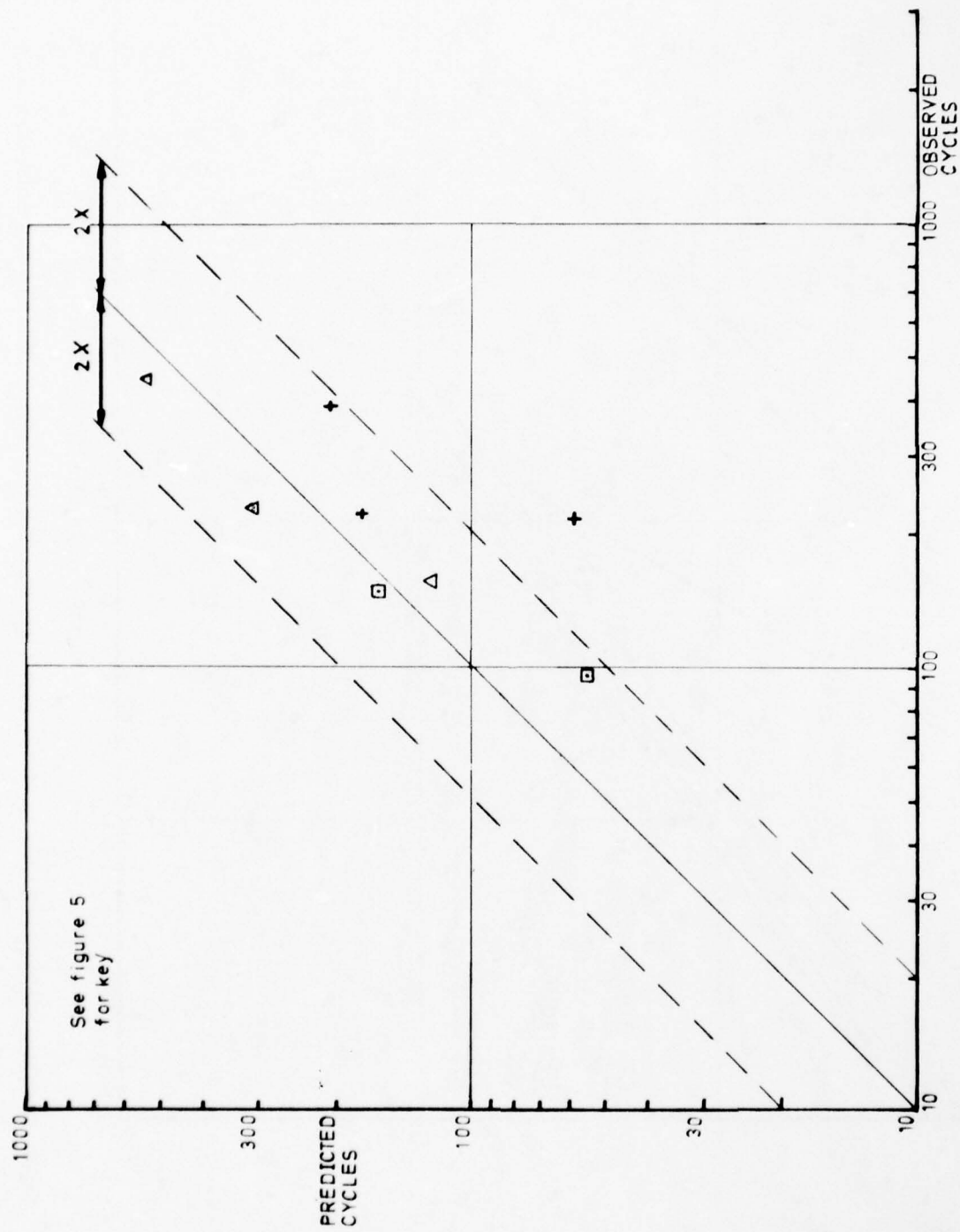


Fig.11 Comparison of observed and predicted cyclic lives. Predictions based on ductility normalized SRP life relationships

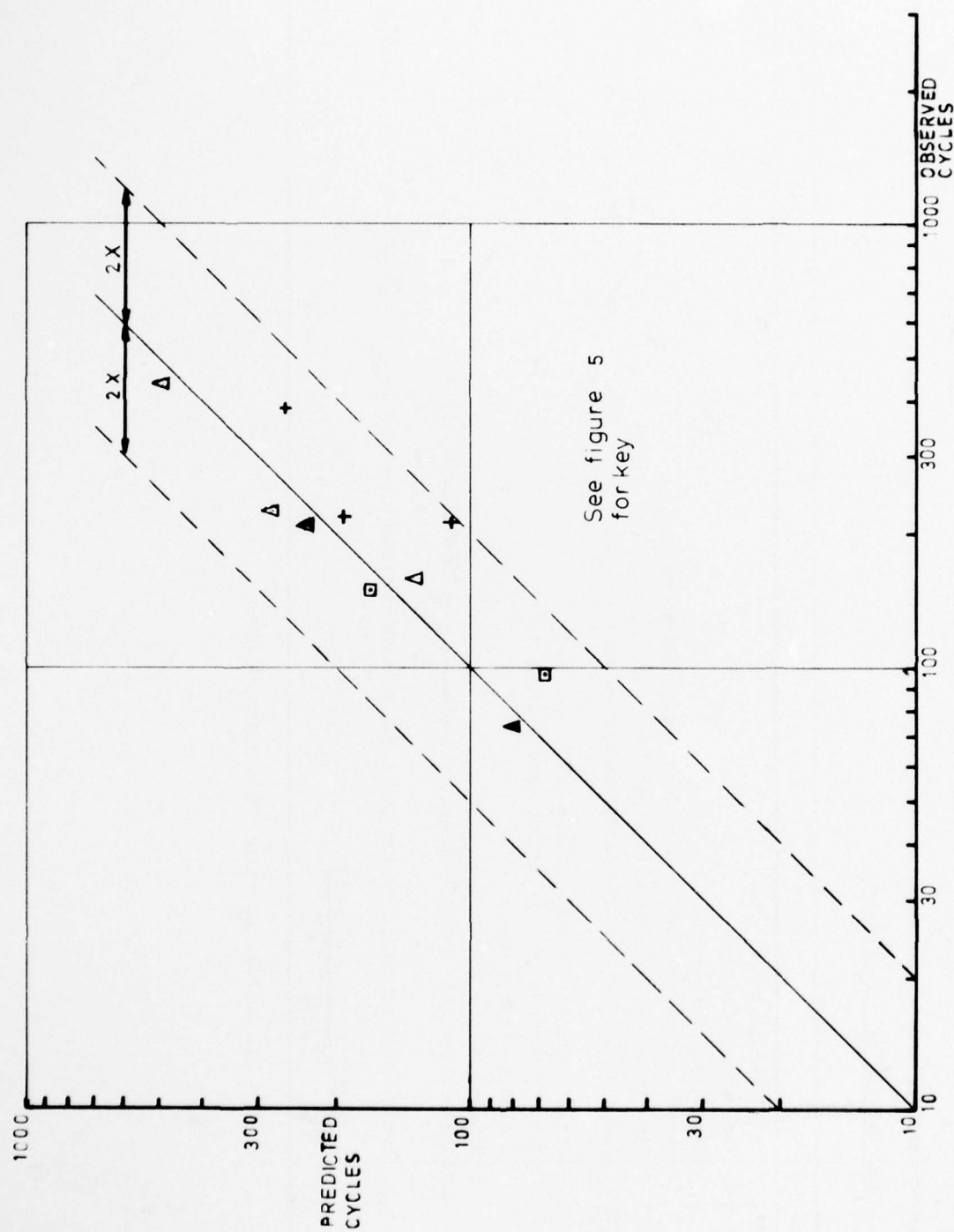


Fig.12 Comparison of observed and predicted lives. Predictions based on hold time modified SRP life relationships

APPENDIX I - Worked examples showing the application of equivalent creep data to SPP predictions

(a) Calculation of N_{cp} values

	Source		960T/OC	30T/OC	
1	Raw data	Total strain range	1.4	2.02	%
2	Raw data	Peak tensile stress	315	355	MN/m ²
3	1 and 2	Transition stress	245	245	MN/m ²
4	Ref. 6 Fig. 3	Stress relaxed in time independent regime (line 1-line 2)	70	110	MN/m ²
5	Fig. 7 or raw data for 960T/OC	Time to relax to transition stress	1.72×10^{-2}	11.66×10^{-3}	hr
6	5	Slope of unified stress relaxation curves at $t = t_{hold}$	2.55×10^{-2}	5×10^{-1}	MN/m ² min
7	Fig. 9	Strain rate at $t = t_{hold}$ (line 5/E)	1.18×10^{-5}	1.96×10^{-4}	hr ⁻¹
8	Raw data	Time to rupture for equivalent static creep test	1450	150	hr
9	Raw data	Inelastic strain range	1.008	1.62	%
10	2 and 9	Relaxed stress when $t = t_{hold}$	148	185	MN/m ²
11	10 and 8	Inelastic strain in time dependent regime $\left[\epsilon_{cp} = \left(\frac{\text{line 2} - \text{line 9}}{E} \right) \right]$	0.0746	0.0392	%
		Fraction of inelastic strain range due to time dependent process $\left(F_{cp} = \frac{\text{line 10}}{\text{line 9}} \right)$	0.074	0.0242	%
12	Eq ⁿ 10	$N_{cp} = \frac{(\text{line 11} \times \text{line 7})}{t_{hold} - \text{line 4}}$	6.71	7.44	cycles

For use on Fig. 10 - Hold Time Modified SPP.

APPENDIX I -

(b) Prediction of lives with complex cycle using N_{cpb} values based on hold time data

	Source		30T/3C	960T/0.2C	
		Total strain range ϵ_{tot}	1.84	0.62	%
13	Raw data	Inelastic strain range ϵ_{IN}	1.589	0.275	%
14	Raw data	ϵ_{pp}	1.47	0.182	%
15	Raw data	ϵ_{cc}	0.095	0.0375	%
16	Raw data	$\epsilon_{cp} + \epsilon_{cc}$	0.119	0.0925	%
17	Raw data	Peak tensile stress	355	280	MN/m ²
18	Raw data	Relaxed tensile stress	175	162	MN/m ²
19	2,15,17	$\epsilon_{cpd} = \frac{\text{line 17-line 2}}{E} - \text{line 15}$	<0	<0	%
20	15,17,18	$\epsilon_{cpb} = \left(\frac{\text{line 17-line 18}}{E} \right) - (\text{line 15})$	0.0226	0.055	%
21	13,14	$F_{pp} = \epsilon_{pp} / \epsilon_{IN}$	0.925	0.664	-
22	13,15	$F_{cc} = \epsilon_{cc} / \epsilon_{IN}$	0.0598	0.136	-
23	13,19	$F_{cpd} = \epsilon_{cpd} / \epsilon_{IN}$	<0	<0	-
24	13,20	$F_{cpb} = \epsilon_{cpb} / \epsilon_{IN}$	0.0142	0.200	-
25	Fig. 10	N_{pp}	315	2450	cycles
26	"	N_{cc}	230	1640	cycles
27	"	N_{cpd}	41	115	cycles
28	"	N_{cpb}	7.2	50	cycles
29	Eq ⁿ 7, 21+28	N_{pred}	193.5	230	cycles
30	Raw data	N_f	220	208	cycles

EXPERIENCES IN THE USE OF STRAINRANGE PARTITIONING
FOR PREDICTING TIME DEPENDENT STRAIN-CONTROLLED
CYCLIC LIFETIMES OF UNIAXIAL SPECIMENS
OF 2 1/4 Cr-1 Mo STEEL, TYPE 316
STAINLESS STEEL, AND HASTELLOY X*

C. R. Brinkman, J. P. Strizak, and M. K. Booker
Metals and Ceramics Division
Oak Ridge National Laboratory
Oak Ridge, Tennessee 37830

ABSTRACT

The concept of strainrange partitioning was used to estimate the cyclic life of uniaxial specimens subjected to strain controlled fully reversed cycling at constant temperatures within the creep range. Strain-time waveforms consisted of ramp loading with tension, or compression, or both tension and compression hold periods at peak strain. Materials examined included 2 1/4 Cr-1 Mo steel in the annealed condition, solution annealed Hastelloy X, and solution annealed, thermally aged, or irradiated type 316 stainless steel. Inelastic strain life relationships were either developed directly from appropriate experimental data or obtained via the ductility normalization concept and used with the interaction damage rule. Generally good agreement between experimental and predicted cyclic lifetimes was found, although a number of uncertainties were identified and discussed. In the case of 2 1/4 Cr-1 Mo, extrapolations were performed to indicate the influence of hold periods of up to 100 hr at various strainranges.

INTRODUCTION

Operational cycles of advanced nuclear reactor power generating systems include power adjustments, response to emergency or hypothetical accident situations, and refueling. This mode of operation will subject structural material components to cyclic strain-controlled loading conditions at elevated temperatures such that the possibility of time-dependent fatigue and creep damage must be considered in their design. Typically, these cycles produce strain ranges that are small, normally being less than about 0.5% with hold periods that are projected to range from as low as perhaps 10 to as high as 1000 hr and with design lifetimes of 30 or 40 years. Accordingly, appropriate elevated temperature strain-controlled fatigue data must be generated in the laboratory and methods developed which will allow extrapolation to conditions anticipated in actual service.

It was the objective of this paper to apply concepts of strainrange partitioning to predicting the strain-controlled time-dependent fatigue behavior of several structural materials projected for use in the High Temperature Gas-Cooled Reactor (HTGR), Fast Breeder Reactor (FBR), and the Brayton Isotope Power System (BIPS). Comparisons were made between predictions and data generated under isothermal and uniaxial loading conditions for annealed 2 1/4 Cr-1 Mo steel (482-538°C), type 316 stainless steel (593°C) in both the irradiated and unirradiated conditions, and solution annealed Hastelloy X (871 and 704°C). In the case of 2 1/4 Cr-1 Mo steel, extrapolation of cyclic peak and relaxed stress ranges was performed by several different methods in order to predict the shape of hysteresis loops resulting from both high and low strain range loading conditions such that the inelastic strain ranges necessary for use in the method of strainrange partitioning could be estimated. These values were then employed to develop fatigue life reduction factors as a function of hold time for several different iso-strain range loading conditions.

The effort reported herein represents an interim report of ongoing test activity and evaluation of several different methods for extrapolating and correlating uniaxial time-dependent fatigue data.

EXPERIMENTAL MATERIALS AND PROCEDURE

Annealed 2 1/4 Cr-1 Mo Steel

Material used in generating much of the data reported herein was taken from commercial heats of 2 1/4 Cr-1 Mo steel. This consisted of 25-mm-thick (1-in.) plate obtained from Babcock and Wilcox Company, heats 20017 and 3P5601. Chemical analyses of representative material from the plates are compared in Table I; other data are in Table II* (see Footnote on next page).

* Research sponsored by the Department of Energy under contract with the Union Carbide Corporation.

Table I. Chemical Composition of Alloys

Alloy	Heat	Analysis	Content, Wt %											
			Fe	C	Mn	Si	Cr	Mo	Ni	S	P	N	Co	B
2 1/4 Cr-1 Mo	20017	Vendor	Bal	0.11	0.55	0.29	2.13	0.90		0.014	0.012	0.012		
		ORNL	Bal	0.135	0.57	0.37	2.2	0.92	0.16	0.016	0.012			
	3P5601	Vendor	Bal	0.12	0.35	0.27	2.3	0.96	0.20	0.022	0.009	0.013		
Hastelloy X ^a	2600-3-4936	Vendor	19.09	0.07	0.58	0.44	21.82	9.42	Bal	<0.005	0.016		1.68	<0.002
Type 316 SS ^b	B65808	Vendor	Bal	0.06	1.72	0.40	17.30	2.33	13.30	0.007	0.012		0.030	0.0005

^aAlso 0.63 W.^bAlso 0.065 Cu, 0.003 Ti, 0.0014 Pb, 0.013 Sn, 0.012 Al.

Table II. Product Form and Grain Size of Alloys

Alloy	Heat	Product Form	Specification	Grain Size	
				ASTM	(mm)
2 1/4 Cr-1 Mo	20017	Plate	ASME SA-387 Grade D	4-5	55-80
	3P5601	Plate	ASME SA-387 Grade D	5	55
Hastelloy X		13-mm (1/2-in.)	ASME SB-435	4	78
		Plate	(NO 6002)		
Type 316 SS		Rod		4	80

Sections of the plates were heat-treated according to the following schedule, which is referred to as an isothermal anneal:

Austenitize at $927 \pm 14^\circ\text{C}$ for 1 hr, cool to $704 \pm 14^\circ\text{C}$ at a maximum cooling rate of 83°C/hr , hold at $704 \pm 14^\circ\text{C}$ for 2 hr, and cool to room temperature at a rate not to exceed 6°C/min .

Examination of the microstructure of the plate material indicated that the steel contained proeutectoid ferrite, fine pearlite and some bainite.

Hastelloy X

Specific details concerning the product form, heat number, grain size, and chemical composition of the Hastelloy X are given in Tables I and II.

Type 316 Stainless Steel

Type 316 stainless steel referred to in this investigation came from Heat B65808. Specific details are given in Tables I and II.

Specimen Preparation

Following heat treatment, as given above, specimen blanks of either 2 1/4 Cr-1 Mo steel or Hastelloy X were cut from the plate material. Blanks were generally prepared such that their longitudinal axis was parallel to the plate rolling direction. Fatigue specimens had an hourglass-shaped gage section configuration with a radius-to-diameter ratio (R/D) of 6. The minimum diameter of the fatigue specimens was either 6.35 mm (0.25 in.) or 5.08 mm (0.2 in.).

In the case of type 316 stainless, all the data were taken from the open literature¹⁻³ and no new tests were performed. Data were available from tests that had been conducted on type 316 stainless steel in three conditions:

Condition	Treatment
Solution annealed	Solution annealed 1/2 hr at 1075°C followed by a helium quench
Aged	Aged 3096 or 5040 hr at 593°C in helium filled capsules or aged 1000 hr at 565°C
Irradiated	Irradiated in helium filled capsules in Experimental Breeder Reactor II to a fluence of $1-2.63 \times 10^{26} \text{ n/m}^2$ ($E > 0.1 \text{ MeV}$). The irradiation temperature was 580 to 610°C .

* Chemical compositions, material processing, heat treatments and mechanical properties for each tested alloy, as well as the data generated in the programme, are given in Appendix A 1.

Test Procedure

Fully reversed axial push-pull testing was accomplished in closed-loop electro-hydraulic fatigue test machines. Axial strain control was maintained by employing a diametral extensometer and a simple diametral-to-axial strain computer. Total strain range, $\Delta\epsilon_t$, was thus determined by the relation

$$\Delta\epsilon_t = (\Delta\sigma/E)(1 - 2\nu) - 2\Delta\epsilon_d, \quad (1)$$

where E is Young's modulus, ν is Poisson's ratio, $\Delta\epsilon_d$ is the diametral strain range, and $\Delta\sigma$ is the peak-to-peak stress range from the hysteresis loops. Heating of the specimens was accomplished by induction and all testing was accomplished in air. Additional details of test procedure can be found elsewhere.⁴

In addition to the continuous cycling and strain hold time tests which were generally conducted at a ramp strain rate of $4 \times 10^{-3}/s$, a number of cyclic creep tests were conducted to verify some of the basic strain range life relationships for annealed 2 1/4 Cr-Mo steel.⁵ These tests were conducted in air at 538°C and used a bumpless transfer computer system, which kept the test in strain control for a given cycle except during the hold period, when the test was in load control. Switching from strain control to load control occurred at the onset of the hold period, when a predetermined load was achieved, while switching from load control to strain control occurred at the end of the cycle hold period when a predetermined strain level was obtained. Creep deformation thus occurred each cycle and showed a general acceleration in creep rate as the cycles were continued toward specimen failure.

RESULTS

Annealed 2 1/4 Cr-1 Mo Steel

Results of the cyclic creep tests on annealed 2 1/4 Cr-1 Mo steel are given in Table III. A visual comparison of the cyclic creep curves generated for heat 3P5601 at the same stress level for two specimens tested with either tension or compressive creep hold periods, indicated similar creep rates in tension and compression. However, for heat 20017 generally higher creep rates in tension than in compression were observed. Compressive cyclic creep rates of heats 3P5601 and 20017 were similar for equivalent stress holds.

Table III. Summary of Cyclic Creep Data for 2 1/4 Cr-1 Mo Steel Generated at 538°C

Specimen	Heat	Total Strain Range (%)	Stress Hold, MPa		Inelastic Strain Components, %					Observed Cycles to Failure, N_{obs}	Time to Failure, t_f (hr)	Stress Amplitude, MPa		ϕ^b
			Tensile	Compressive	$\Delta\epsilon_{in}^a$	$\Delta\epsilon_{pc}$	$\Delta\epsilon_{cp}$	$\Delta\epsilon_{cc}$	$\Delta\epsilon_{pp}$			Tensile	Compressive	
ITL-62	3P5601	2.98		248	2.66	2.33			0.33	293	274	319	248	0.93
I606T	20017	2.97		248	2.65	2.25			0.40	320	133	312	248	0.90
ITL-11	3P5601	2.00		243	1.69	1.18			0.51	496	227	288	243	0.83
I6009	20017	2.00		243	1.69	1.42			0.27	509	202	305	243	0.91
ITL-16	3P5601	1.00		243	0.72	0.31			0.41	1,386	15.4	252	243	0.68
I6006	20017	1.00		243	0.72	0.37			0.35	1,252	29.3	248	243	0.75
ITL-12	3P5601	0.71		226	0.44	0.16			0.28	2,758	47.7	233	226	0.61
I6016	20017	0.71		226	0.43	0.24			0.19	2,345	58.3	250	226	0.78
ITL-17	3P5601	0.56		207	0.32	0.13			0.19	2,593	59.0	221	207	0.86
I607T	20017	0.56		209	0.31	0.14			0.17	3,248		231	209	0.85
ITL-20	3P5601	2.98	253		2.63		2.11		0.53	147	136	253	346	0.94
I602T	20017	2.97	250		2.62		2.48		0.14	158	231	230	364	0.98
ITL-61	3P5601	2.00	241		1.69		1.30		0.39	532	172	241	303	0.86
I604T	20017	2.00	241		1.69		1.34		0.35	460	50.2	241	300	0.89
I608T	20017	2.00	246		1.68		1.42		0.26	313	64.6	246	309	0.94
ITL-100	3P5601	1.02	241		0.73		0.28		0.45	1,480	7.6	241	271	0.62
I603T	20017	1.02	241		0.71		0.44		0.28	1,264	38.3	241	286	0.81
ITL-19	3P5601	0.72	217		0.46		0.14		0.32	4,376		217	240	0.29
I6018	20017	0.72	222		0.43		0.31		0.12	2,473		222	276	0.86
ITL-22	3P5601	2.96	245		2.68	0.16		1.72	0.80	315	240	252	245	0.67
I609T	20017	2.99	209		1.77	0.05		1.08	0.64	534	120	209	210	0.69
ITL-79	3P5601	1.01	234		0.74	0.06		0.28	0.40	1,527	36.6	234	228	0.44
I6007	20017	1.00	224		0.75	0.04		0.32	0.39	1,508	79.2	224	224	0.52
ITL-68	3P5601	0.70	214		0.46		0.01	0.13	0.32	2,974	50.6	214	207	0.47

^aCalculated using a Young's Modulus value of 174 GPa. The ramp strain rate was $4 \times 10^{-3}/s$.

^bDamage factor, $F_{pc} \times N_{obs}/N_{pc}$, $F_{cp} \times N_{obs}/N_{cp}$, or $F_{cc} \times N_{obs}/N_{cc}$. Values should be greater than 0.5 in order to establish life relationship.

Results of the cyclic creep tests given in Table III and strain controlled relaxation tests^{6,7} were combined with the results of Manson et al.⁵ to form the life relationship lines via the Interaction damage rule given by:

$$\frac{1}{N_{pred}} = \frac{F_{pp}}{N_{pp}} + \frac{F_{pc}}{N_{pc}} + \frac{F_{cp}}{N_{cp}} + \frac{F_{cc}}{N_{cc}}, \quad (2)$$

where

N_{pred} = the predicted cyclic life,

$F_{cp} = \Delta\epsilon_{cp} / \Delta\epsilon_{in}$,

$F_{pp} = \Delta\epsilon_{pp} / \Delta\epsilon_{in}$,

$F_{pc} = \Delta\epsilon_{pc} / \Delta\epsilon_{in}$,

$F_{cc} = \Delta\epsilon_{cc} / \Delta\epsilon_{in}$,

$\Delta\epsilon_{in}$ is the total inelastic strain range while the inelastic strain components are defined as follows:

$\Delta\epsilon_{pp}$ = tensile plastic strain reversed by compressive plastic strain,

$\Delta\epsilon_{pc}$ = tensile plastic strain reversed by compressive creep strain,

$\Delta\epsilon_{cp}$ = tensile creep strain reversed by compressive plastic strain, and

$\Delta\epsilon_{cc}$ = tensile creep strain reversed by compressive creep strain.

Here "plastic" strain is defined as time-independent inelastic strain, while "creep" strain is defined as time-dependent inelastic strain. Equations for the life relationship lines thus obtained were as follows:

$$N_{cp} = 255\Delta\epsilon_{in}^{-1.777}, \quad (3)$$

$$N_{cc} = 450\Delta\epsilon_{in}^{-1.24}, \quad (4)$$

$$N_{pc} = 386\Delta\epsilon_{in}^{-1.07}, \quad (5)$$

$$N_{pp} = 521\Delta\epsilon_{in}^{-2.67}, \quad \Delta\epsilon_{in} \leq 0.45\%, \quad (6)$$

$$N_{pp} = 1648\Delta\epsilon_{in}^{-1.24}, \quad \Delta\epsilon_{in} > 0.45\%, \quad (7)$$

where $\Delta\epsilon_{in}$ values are measured in percent. It should be noted that in formulating the best fit life relationship lines expressed by Eqs. (4-7), all cyclic creep and relaxation data were employed even though the particular damage strain fraction⁸ for a given test, e.g., $\emptyset = (F_{cc})(N_{obs}/N_{cc}) > 0.5$ for a "cc" cycle, was not obeyed. In the case of the strain controlled relaxation tests, particularly those conducted at low total strain ranges, which was our particular interest, the most dominant inelastic strain range was always $\Delta\epsilon_{pp}$. However, it was thought appropriate to include the strain controlled data in these formulations, since our purpose was to generate guideline relationships appropriate for design conditions referred to in the introductory section of this paper.

Equations (6) and (7) indicate that in the case of the $N_{pp} = f(\Delta\epsilon_{in})$ relationship, expressed in log-log coordinates, a bilinear relationship was most appropriate. Reasons for the break in the otherwise linear relationship on log-log coordinates have been discussed elsewhere.⁷ A comparison of the formulations given in Eqs. (3) through (7) with the appropriate formulations for this material as originally proposed by Manson et al.⁵ generally showed good agreement. An example of such a comparison and including actual data is shown for the $N_{cc} - \Delta\epsilon_{in}$ relationship in Fig. 1.

Unlike comparisons between cyclic relaxation and cyclic creep data made with the other life relationship lines, omitted for brevity, Fig. 1 also shows that the results of the strain controlled or cyclic relaxation tests fell somewhat below those of the cyclic creep tests. Therefore, as of this writing, it remains an open question as to whether or not the results obtained to date represent normal scatter or, indeed, that an additional formulation is required to best characterize the strain controlled "cc" type of loading.

With the life relationships thus established, the objective was to develop, for fully reversed loading, estimates of the reduction in cyclic lifetimes due to increasing hold periods (times) in strain controlled situations over the temperature range of 482 to 538°C. This estimation can be accomplished via the method of strainrange partitioning if satisfactory approximations of the hysteresis loops appropriate for a given strain range and hold time can be made. Figure 2 shows an example of the changes in hysteresis loops that normally occur for a given strain range and with increasing tensile only hold times at elevated temperatures. If one can estimate or measure the appropriate steady state or stabilized stress ranges $\Delta\sigma_1, \Delta\sigma_2, \dots, \Delta\sigma_i$ and associated

total amount of stress relaxation, i.e., $\Delta\sigma_{r1}, \Delta\sigma_{r2}, \dots, \Delta\sigma_{ri}$ for increasing hold periods t_1, t_2, \dots, t_i then the key features of the proposed hysteresis loops and associated inelastic strain ranges can be calculated.

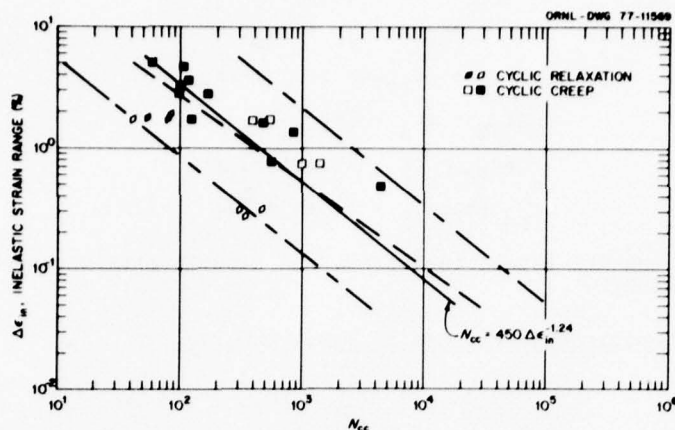


Fig. 1. Strain Range Life Relationship Lines for "cc" Strain for 2 1/4 Cr-1 Mo Steel. Solid line indicates best fit of the data, while the dashed line is the original line proposed by Manson et al. The ± 2 Standard Error of the Estimate lines are also shown.

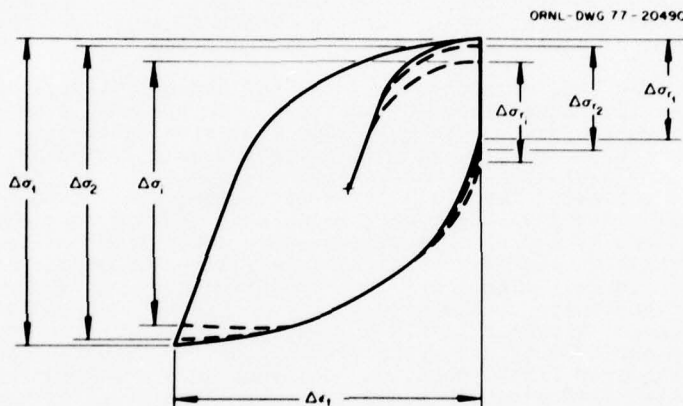


Fig. 2. Schematic Diagram of a Typical Strain-Controlled Hysteresis Loop Showing Changes in Stabilized Stress Ranges that Occur at a Constant Strain Range with Increasing Hold Time.

The first step taken was to estimate total stress ranges ($\Delta\sigma$) associated with particular hold periods, strain ranges, and temperatures. This was accomplished using the available data base and extrapolating graphically on semi-logarithmic coordinates (stress range versus time). It was also found that log-log coordinates could be used. Estimates of the relaxed stress amplitude (σ) from the peak stress amplitude ($\sigma_0 = \Delta\sigma/2$) can be made in a number of ways as follows:

1. employing the Gittus Relaxation Equation

$$\ln(\sigma_0/\sigma) = Ct^m, \quad (8)$$

where C and m are constants for a given strain range and temperature and are determined experimentally, and t is the required time for relaxation from σ_0 to σ ,

2. using an appropriate creep-equation to predict relaxation behavior,⁹
3. using isochronous cyclic stress relaxation curves for the material involved, and
4. graphical extrapolation from known values of σ_0 .

In the case of estimating the time dependent fatigue behavior of 2 1/4 Cr-1 Mo steel only the first two methods were employed.

Hypothetical hysteresis loop inelastic time dependent and independent strain range values were then calculated using the following equations (assuming zero mean stress):

1. Compressive or Tensile only Hold Periods

$$\Delta \epsilon_t = \Delta \epsilon_{in} + \Delta \epsilon_e, \quad (9)$$

$$\Delta \epsilon_{in} = \Delta \epsilon_{pc} \text{ or } \Delta \epsilon_{cp} + \Delta \epsilon_{pp}, \quad (10)$$

$$\Delta \epsilon_{in} = \Delta \epsilon_t - (\Delta \sigma - \Delta \sigma_p)/E, \quad (11)$$

$$\Delta \epsilon_{in} = \Delta \epsilon_t - (\sigma_0 + \sigma)/E, \quad (12)$$

$$\Delta \epsilon_{pc} \text{ or } \Delta \epsilon_{cp} = \Delta \sigma_p/E = (\sigma_0 - \sigma)/E, \quad (13)$$

where $\Delta \epsilon_t$, $\Delta \epsilon_{in}$, $\Delta \epsilon_e$ are the total, inelastic, and elastic strain ranges, respectively, and E is Young's Modulus.

2. Compressive and Tensile Hold Periods of Equal Duration

$$\Delta \epsilon_{in} = \Delta \epsilon_{pp} + \Delta \epsilon_{cc}, \quad (14)$$

$$\Delta \epsilon_{in} = \Delta \epsilon_t - (\Delta \sigma - 2\Delta \sigma_p)/E = \Delta \epsilon_t - 2\sigma/E, \quad (15)$$

$$\Delta \epsilon_{cc} = \Delta \sigma_p/E = (\sigma_0 - \sigma)/E. \quad (16)$$

Estimating the relaxed stress range, $\Delta \sigma_p$, and hence the inelastic strain components in the above manner obviously introduces some uncertainty. Accordingly, estimated $\Delta \sigma_p$ values were multiplied by an arbitrary factor of 1.2 as a first approximation to the possible uncertainty and in an effort to see the impact of this variation at various strain ranges and modes of damage, e.g., "pc," "cp," and "cc."

Figures 3 and 4 then show predictions of the influence of increasing the duration of compressive hold times to 100 hr, imposed each cycle, on the hold time reduction factor, N_f^0/N_h , at a temperature of 482°C. The hold time reduction factor is simply defined for a given strain range as the cycle life, N_f^0 , of a continuously cycled specimen for which the strain rate was $4 \times 10^{-3}/s$ divided by the estimated cycle life, N_h , for the indicated hold time. Figure 3 shows estimates for a single strain range, i.e., 0.4%, and for the two heats of 2 1/4 Cr-1 Mo steel under investigation. Two bands, shown by the slashed lines, the width of which is defined by 1.2 or 1.0 $\Delta \sigma_p$, are shown since these heats, i.e., 3P5601 and 20017, characteristically show different high cycle fatigue endurance levels at this temperature and strain range. Also shown for comparison purposes are results of actual strain controlled fatigue tests conducted with the indicated compressive hold periods. Estimates of the amount of stress relaxation, $\Delta \sigma_p$, projected for the stabilized hypothetical hysteresis loops were achieved by using the Gittus equation to establish the relaxed stress amplitude (σ). The required Gittus equation constants were obtained from an analysis of some of the experimental data shown in these figures. Also shown by the dashed line is an estimate of the approximate duration of hold period required to cause failure in 250,000 hr at that strain range, e.g., (35 hr hold per cycle)(289,868 cycles or continuous cycle life)/(40 hold time reduction factor for 35 hr hold) = 253,634 hr.

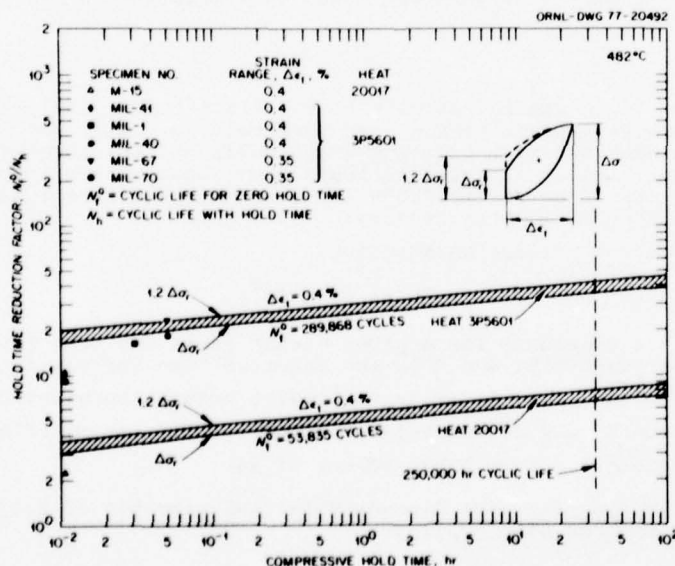


Fig. 3. Comparison of Measured and Predicted Hold Time Reduction Factors for 2 1/4 Cr-1 Mo Steel Subjected to Compressive Hold Times at 482°C.

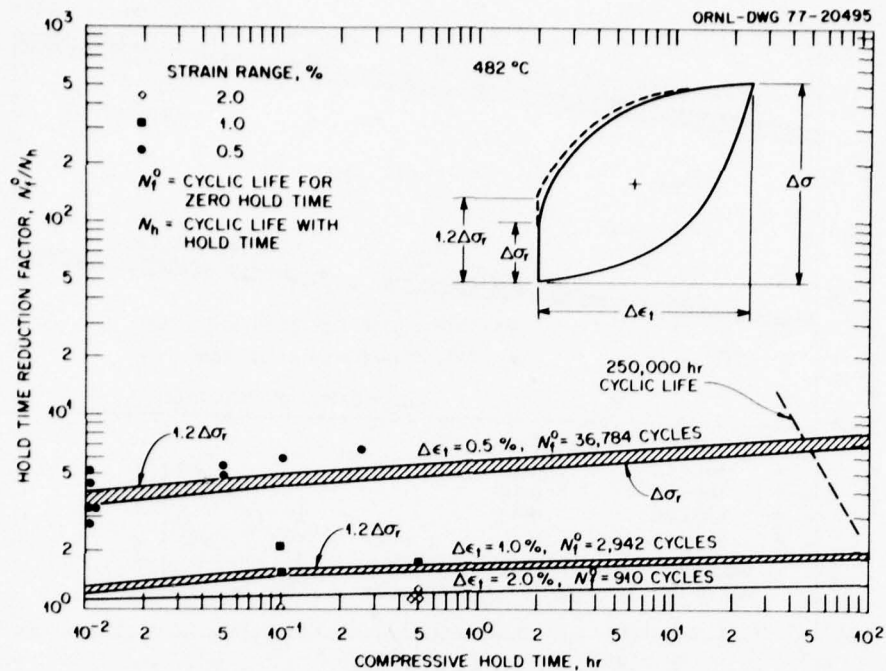


Fig. 4. Comparison of Measured and Predicted Hold Time Reduction Factors for 2 1/4 Cr-1 Mo Steel Subjected to Compressive Hold Times at 482°C.

Figure 4 shows additional comparisons between experimental results from both heats of 2 1/4 Cr-1 Mo steel for compressive hold times and predicted estimates for total strain ranges of 2, 1.0, and 0.5%. No distinction between heats is made in Fig. 4 since similar behavior was indicated at these strain ranges. Characteristically, the width of the estimated predictive band increases with decreasing strain range. Both Fig. 3 and 4 show good agreement between estimated and actual hold time reduction factors.

Figures 5 and 6 show similar results for behavior at 482°C for various strain ranges involving tensile and both tensile and compressive hold times respectively. In Fig. 6 the arrows associated with several of the data points indicate points where failure would be predicted to occur from a knowledge of the stabilized hysteresis loop for that particular test.

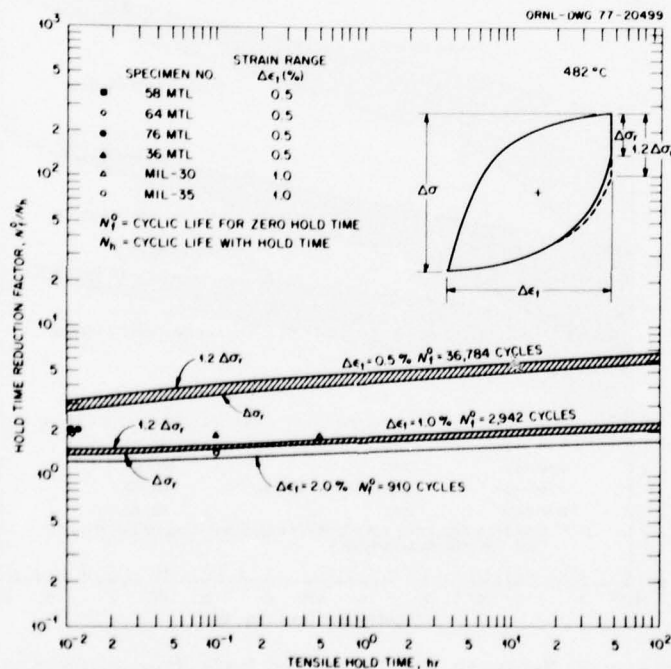


Fig. 5. Comparison of Measured and Predicted Hold Time Reduction Factors for 2 1/4 Cr-1 Mo Steel Subjected to Hold Tensile Times at 482°C.

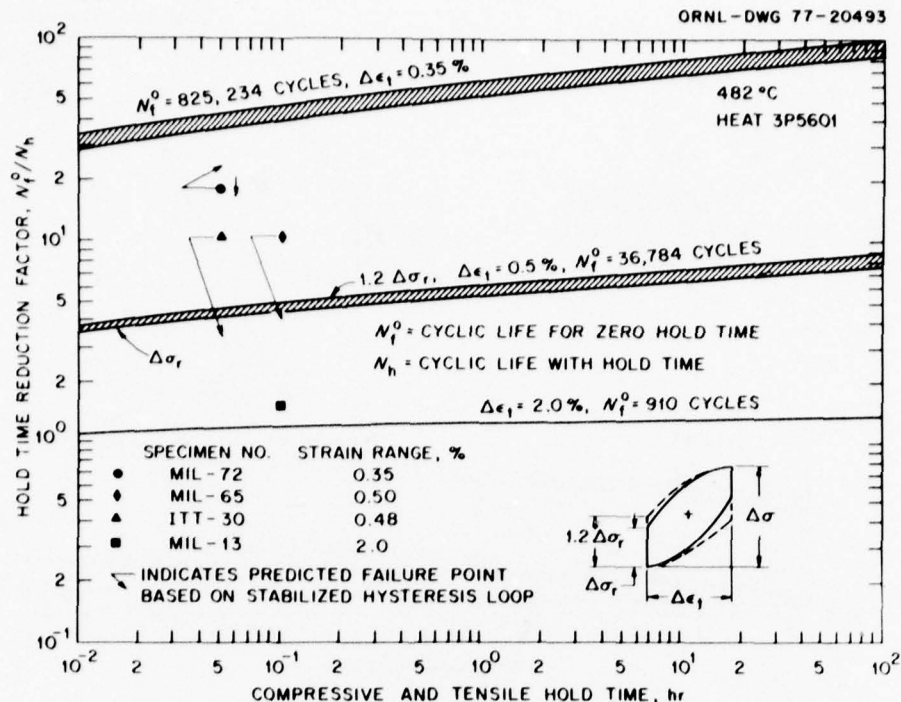


Fig. 6. Comparison of Measured and Predicted Hold Time Reduction Factors for 2 1/4 Cr-1 Mo Steel Subjected to Both a Tensile and Compressive Hold Time of Equal Duration at 482°C.

Figures 7 and 8 taken as representative examples, show similar comparisons between experimentally generated strain controlled fatigue data obtained at 538°C and predictions based on estimates of stress values from hypothetical hysteresis loops. At this temperature, however, estimates of the relaxed stress amplitude, σ_r , and hence the relaxed stress range, $\Delta\sigma_r$, were made by two different methods. The first method employed

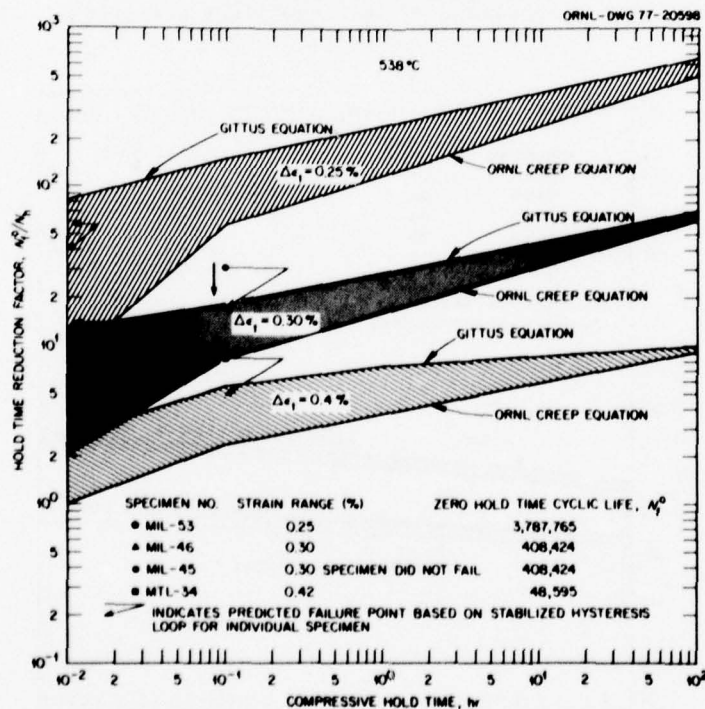


Fig. 7. Comparison of Measured and Predicted Hold Time Reduction Factors for 2 1/4 Cr-1 Mo Steel Subjected to Compressive Hold Times at 538 °C. Relaxation behavior predicted by both the ORNL creep and Gittus equations.

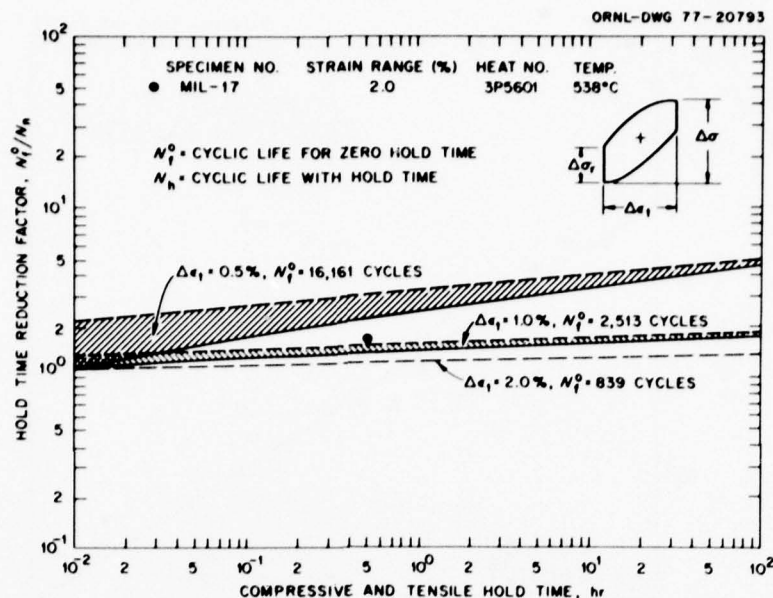


Fig. 8. Comparison of Measured and Predicted Hold Time Reduction Factors for 2 1/4 Cr-1 Mo Steel Subjected to Both a Tensile and Compressive Hold Time of Equal Duration at 538°C.

the Gittus equation with appropriate constants and was identical in format as previously explained for the 482°C estimates. The second method involved use of the ORNL creep equation for this material as recently developed by Booker.³ In the latter method of estimating relaxed stress amplitudes, the resultant predictions are independent of the test data used for comparison purposes except for estimation of the peak stress range values, $\Delta\sigma$, which were obtained as explained previously.

Characteristically, the Booker creep equation tends to underpredict the amount of relaxation that occurs in the first portion of a relaxation test while the Gittus equation may actually predict more relaxation than occurs for long hold periods. Hence, estimates obtained by these two methods in this case were used to serve as arbitrary upper and lower bounds to the resultant predictive estimates of hold time reduction factors. Figures 7 and 8 show a tendency towards convergence for the two methods as the hold times approach 100 hr.

Hastelloy X

Results⁴ of continuous cycling strain controlled fatigue test conducted over the temperature range of 649 to 871°C showed that the low cycle (80 to about 3×10^3 cycles) fatigue life of this material was essentially independent of temperature. However, from about 3×10^3 to 10^5 cycles this same set of data indicated a temperature dependence of fatigue life with the 871°C data falling somewhat below that of the 649°C data. These findings suggest that a single temperature independent relationship between cycle life of N_{pp} and plastic strain range or time independent inelastic strain range, $\Delta\epsilon_{in}$, is appropriate particularly in the low cycle region over this temperature interval. Indeed, when a plot of plastic strain range versus cycle life was prepared as shown in Fig. 9, this was found to be the case. Data are plotted from tests conducted at two strain rates which indicate that cycle life is independent of strain rate for strain rates equal to or in excess of 4×10^{-3} /s. Figure 9 also shows that characteristically the scatter in the data increases with decreasing inelastic strain range.

Currently, results are available from both continuous cycling fatigue tests as shown in Fig. 9 and from strain controlled hold time tests.⁴ However, the required cyclic creep tests have not been conducted to date such that the other three required life relationships could be formulated directly from applicable experimental data. However, recently Halford et al.¹⁰ have proposed a set of ductility normalized equations ("Universal"). These equations can be used in the absence of experimental data in conjunction with the interaction damage rule to obtain an estimate of time-dependent fatigue life of a new material for which the required life relationships were not or only partially available. Using the N_{pp} relationship given in Fig. 9 and the other three general Halford equations the four required life relationship equations are as follows:

$$N_{pp} = 416.2 (\Delta\epsilon_{in})^{-1.55}, \quad (17)$$

$$N_{pc} = 216.1 (\Delta\epsilon_{pc}/D_p)^{-1.67}, \quad (18)$$

$$N_{cc} = 216.1 D_c (\Delta\epsilon_{cc})^{-1.67}, \quad (19)$$

$$N_{cp} = 148.8 D_c (\Delta\epsilon_{cp})^{-1.67} \quad (20)$$

ORNL-DWG 77-21232

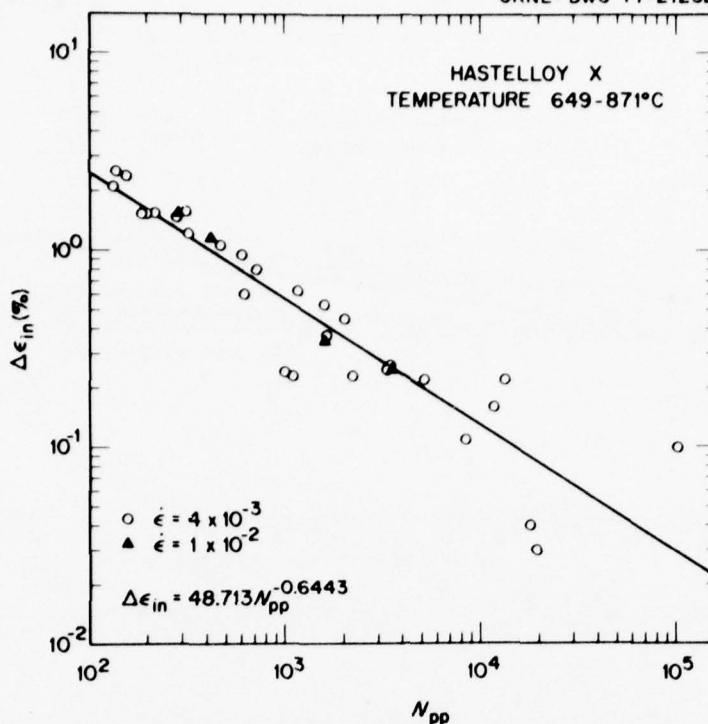


Fig. 9. Plastic Strain Range ($\Delta\epsilon_{in}$) Versus Cyclic Life (N_{pp}) for a Single Heat of Hastelloy X. Indicated strain rates ($\dot{\epsilon}$) are in units of s^{-1} .

where the time independent and dependent inelastic strain ranges, i.e., $\Delta\epsilon_{in}$ or $\Delta\epsilon_{pp}$, $\Delta\epsilon_{pc}$, $\Delta\epsilon_{cc}$, and $\Delta\epsilon_{cp}$ are in percent. D_p and D_c are true fracture tensile and creep-rupture ductilities respectively, i.e., $D = -\ln(1 - R.A./100)$ where R.A. is the reduction of area given in percent.

Tensile ductility as a function of temperature is shown for Hastelloy X along with several other alloys in Fig. 10. Interim results of ongoing creep-rupture tests now in progress are given in Fig. 11 and show available creep-rupture ductilities. Results presented in Figs. 10 and 11 show a ductility minimum in the temperature regime of about 500 to 700°C, which is also strain rate dependent.

ORNL-DWG 76-20907

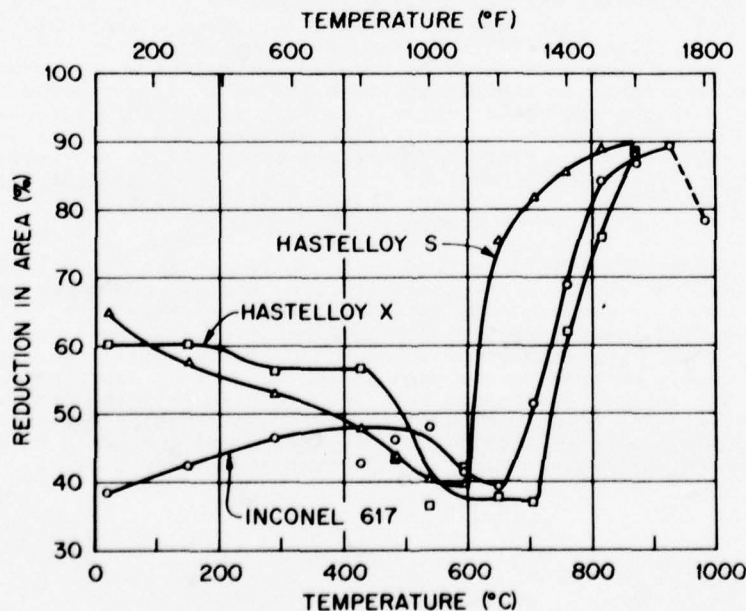


Fig. 10. Tensile Ductility of Several Superalloys. Tensile strain rates were 0.4%/min.

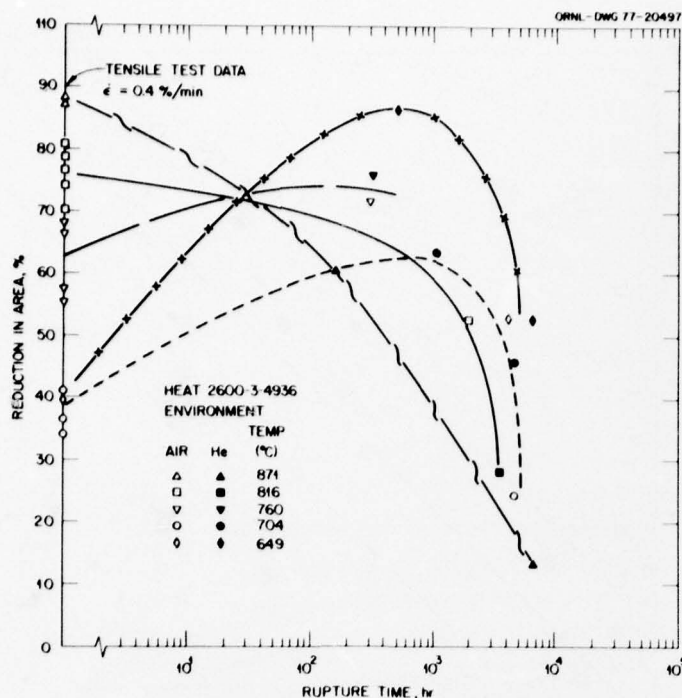


Fig. 11. Creep-Rupture Ductility as a Function of Time for Hastelloy X Tested at Several Temperatures.

Limited data from strain controlled fully reversed fatigue tests conducted with various hold periods are available from tests conducted at 704 and 871°C.⁴ The total test time for each of these tests did not exceed several hundred hours, however, and most of the data were generated at fairly high strain ranges, i.e., 2.0 and 0.6%. Appropriate ductilities then used for estimating the cycle lives of these tests were as follows:

Temperature, °C	Tensile Ductility, R.A., %	Creep Ductility, R.A., %
704	37	50
871	88	60

Comparisons of actual versus predicted fatigue life for the available test data are given in Fig. 12. While test times as indicated above were short, the fatigue life reduction factors due to hold periods fairly small, and the data presently available limited, good agreement between actual and predicted fatigue life is apparent.

Type 316 Stainless Steel

Time independent inelastic strain range, $\Delta \epsilon_{in}$ or $\Delta \epsilon_{pp}$, versus associated cyclic life, N_{pp} , values are plotted in Fig. 13 for three conditions of a single heat of type 316 stainless steel. Specific treatments given this material prior to testing were cited earlier in this paper. All of the data^{2,3} shown in Fig. 13 were generated from continuous cycling strain controlled tests conducted at 593°C at a strain rate of 4×10^{-3} /s. The effect of a pre-aging thermal treatment (3096 or 5040 hr at 593°C) was to displace the high cycle portion of the solution annealed curve upward, thereby also changing the slope of the aged relationship in comparison to the solution annealed line. Identical tests recently conducted at 593°C on other heats of type 316 stainless steel in the solution annealed and aged condition have also verified this aging effect.^{12,13} A comparison of the equation given in Fig. 13 for solution annealed material was also made with test results generated on heat B65808 in the solution annealed condition by two other laboratories.¹³ These data, however, were generated at 565°C and showed excellent agreement indicating little temperature dependence or inter-laboratory variation over this range.

Since the other three required life relationship expressions for this heat of material have not been generated to date, it was necessary to again use the ductility scaling concept. Saltsman and Halford¹⁴ have established the required relationships for another heat of type 316 stainless steel at 704°C. Accordingly, the required relationships for test waveforms involving either tensile or compressive holds expressed in terms of appropriate ductility scaling factors are as follows:

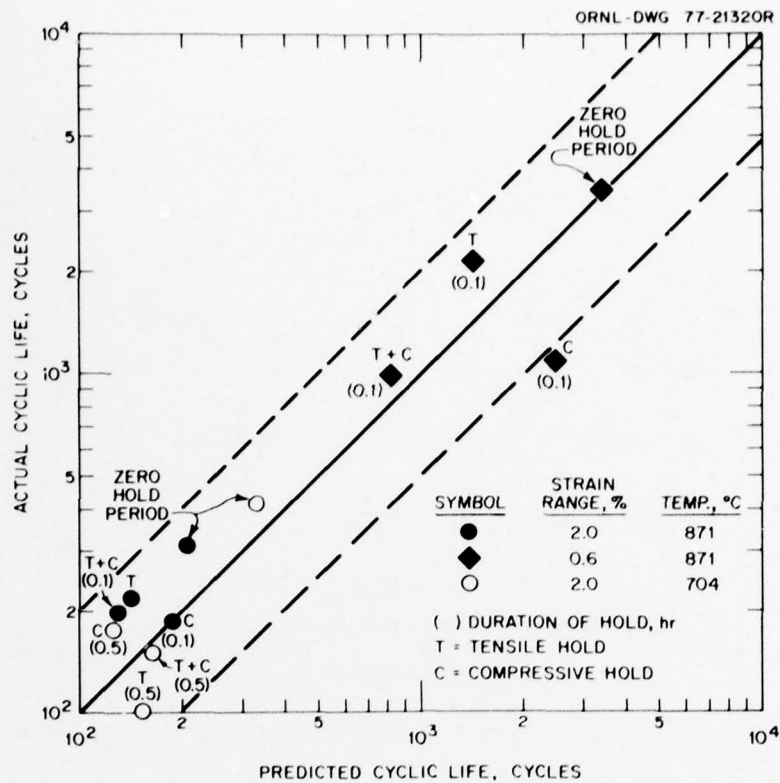


Fig. 12. Comparison of Actual and Predicted Fatigue Life for Hastelloy X Tested in Strain Control with a 0.1 or 0.5 hr Hold Period.

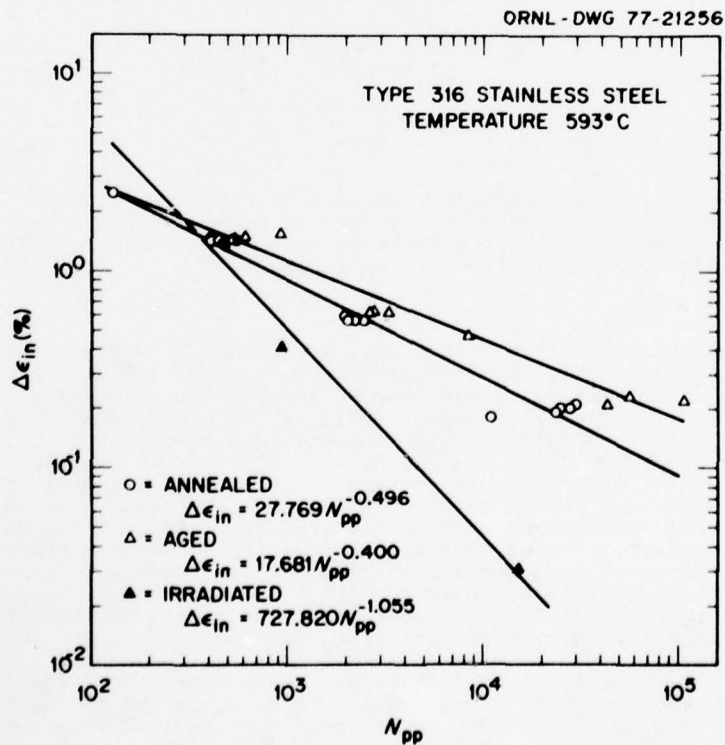


Fig. 13. Plastic Strain Range ($\Delta\epsilon_{in}$) Versus Cycle Life (N_{pp}) for a Single Heat (B65808) of Type 316 Stainless Steel in Three Different Conditions.

$$N_{cp} = (D_e^{593^\circ\text{C}}/D_e^{704^\circ\text{C}})65.88\Delta\epsilon_{cp}^{-1.721}, \quad (21)$$

$$N_{pc} = 395.1(\Delta\epsilon_{pc}/D_p^{593^\circ\text{C}}/D_p^{704^\circ\text{C}})^{-1.183}, \quad (22)$$

where $\Delta\epsilon_{cp}$ and $\Delta\epsilon_{pc}$ are expressed in percent and D_p and D_c are the appropriate tensile and creep ductilities, respectively.

Appropriate ductilities for use in Eqs. (21) and (22) as obtained from the literature are given in Table IV. Tensile ductility of another heat (65805) of type 316 stainless steel was included in Table IV. It showed similar behavior with respect to thermal aging in comparison to heat B65808 i.e., a decrease in tensile ductility upon aging.

Table IV. Tensile and Creep Ductilities of Several Heats of Type 316 Stainless Steel at 593 and 704°C

Heat	Temperature (°C)	Condition	Reduction of Area, %	
			Tensile	Creep
NASA	704		64(10)	77(10)
B65808	593	Irradiated	29(2)	3(15)
B65808	593	Annealed	62(3)	19(15)
B65808	593	Aged ^a	47(2)	19 ^b
65805	593	Annealed	72	
65805	593	Aged ^c	61	

^a5040 hr at 593°C in helium.

^bAssumed to be the same as annealed.

^c5000 hr at 593°C vacuum.

Isothermal tensile and creep ductilities for heat 65808 are plotted as a function of strain rate in Fig. 14. Ductilities for heat 8092297 are given for comparison purposes only. Tensile and creep ductilities are particularly strain rate sensitive over the temperature range of 538 to 649°C as shown by the comparisons for these two heats of type 316 stainless steel.

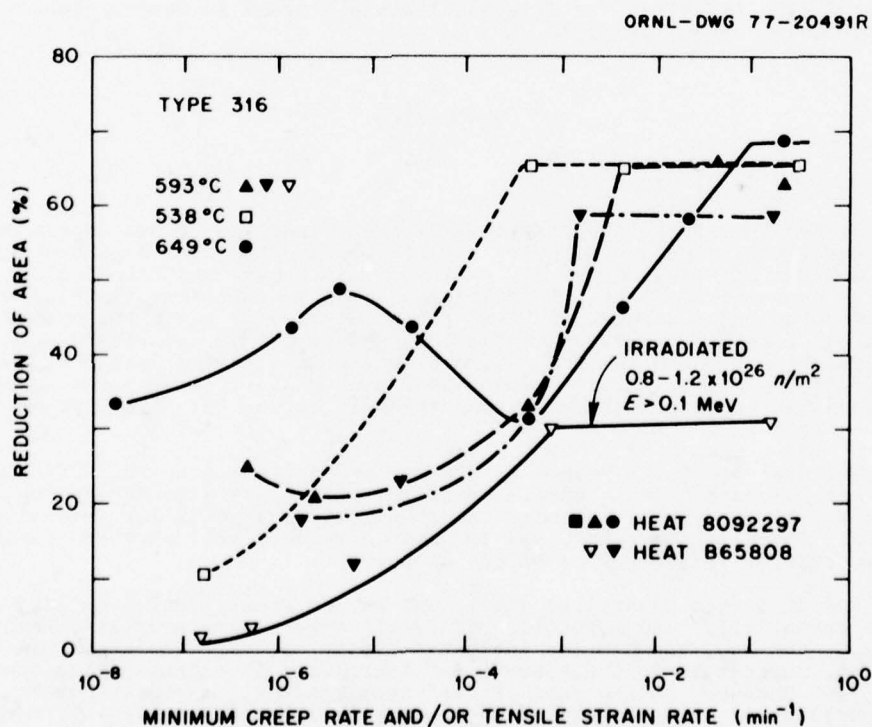


Fig. 14. Ductility of several Heats of Type 316 Stainless Steel as a Function of Temperature and Strain Rate for Irradiated and Unirradiated Type 316 Stainless Steel.

Using the ductilities given in Table IV, the expressions for N_{pp} given in Fig. 13, Eqs. (21) and (22), and the Interaction damage rule, estimates were performed of the fatigue life of test data given in the literature.¹⁻³ Comparisons between actual and predicted cyclic lifetimes for test data available on heat B65808 involving either tensile or compressive only hold times are shown in Fig. 15. Particularly good agreement between actual and predicted cyclic lives, considering the many assumptions, is apparent for the irradiated material data.

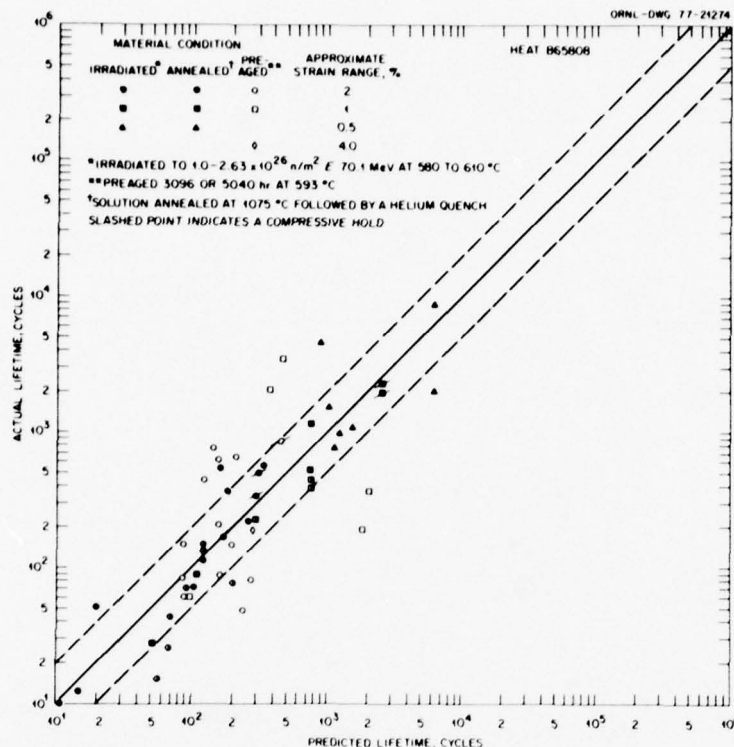


Fig. 15. Comparison of Predicted Cyclic Lifetimes Based on Strain Range Partitioning Versus Actual Cyclic Lifetimes for Type 316 Stainless Steel in Several Conditions. All tests were conducted at 565 or 593°C.

DISCUSSION

Annealed 2 1/4 Cr-1 Mo Steel

As was stated initially, the objective of this paper was to evaluate the method of strainrange partitioning as a predictive tool for estimating time dependent fatigue behavior of several materials primarily at low strain ranges and for long hold periods. In the case of annealed 2 1/4 Cr-1 Mo steel, this was accomplished via hold time reduction factor versus duration of strain hold time plots (Figs. 3-8) since the method not only permits a direct comparison between predictions and available laboratory data, but also allows extrapolation to hold periods that are appropriate to the design of nuclear reactor systems. Further, plots of this type have been used historically by the formulators of ASME Code Case 1592 in establishing elastic analysis curves for time dependent fatigue behavior.

In the authors' view, the method of strainrange partitioning was effective in predicting the general data trends, particularly for the compressive strain hold data (Figs. 3, 4, and 7) apparently the most damaging mode of loading for this material at low strain ranges. Overall, the method was found to work very well when the various life relationships [Eqs. (3-7)] were accurately known.

Evaluation of strain controlled situations at low strain ranges usually requires extrapolating the essentially load controlled or cyclic creep formulated life relationships, i.e., N_{cp} , N_{pc} , and N_{cc} , down to low inelastic strain values. The available strain controlled data suggest that little error was introduced in extrapolating the N_{pc} relationship [Eq. (5)]. However, in the case of "cc" type loading, extrapolating Eq. (4) may introduce considerable error resulting in predicting excessive fatigue life as shown by the fact that all of the available strain controlled data lie to the left of the "cc" life relationship line given in Fig. 1. This suggests that either two relationships may be

appropriate, i.e., one for strain and the other for load controlled situations, or that the data scatter is particularly large and additional data are required to modify the existing life relationship [Eq. (4)]. In the case of "pp" damage, it was shown that two equations [Eqs. (6-7)] were required. In an effort to further substantiate this finding, continuous cycling fatigue tests were conducted on an additional heat (heat 50557) of 2 1/4 Cr-1 Mo steel. This heat contained a fairly low carbon content ($C = 0.026$), but the results verified the bilinear "pp" relationship as plotted on log-log coordinates. Data from this heat generally scattered throughout the existing N_{pp} life relationship data indicating that Eqs. (6 and 7) were appropriate for the low-carbon heat as well.

Another problem area associated with the method, and for that matter any method, is that of defining the appropriate stress ranges, i.e., peak and relaxed, after long hold periods at low strain ranges. Indeed, the material may not even exhibit a stabilized hysteresis loop that is repeated from one cycle to the next after an initial period of cyclic hardening or softening. This was found to be the case for heat 20017 which exhibited cyclic softening during much of the cyclic life at low strain ranges.⁷

Defining the minimum strain range below which essentially no stress relaxation occurs after prolonged hold periods, and hence no time dependent fatigue damage accrues, is another problem area. Figure 16 shows an experimental stress relaxation curve obtained after an initial period of cyclic hardening on heat 3P5601 at 538°C. The strain range was 0.2%. Predictions of relaxation behavior by several different methods are also given for comparison. When this same heat of material was cycled at 482°C and at a strain range of 0.30% with a compressive hold period of 0.01 hr, no relaxation occurred. Instead, the stress required to maintain the strain a constant increased as the data in Table V indicate.

Table V. Compressive Stresses Required to Maintain a Constant Strain Range of 0.30% with a 0.01-hr Compressive Hold In Heat 3P5601 at 482°C.

Ramp Strain Rate (s ⁻¹)	Compressive Stress Amplitude, MPa		Inelastic Strain Range (%)	Cycle
	Beginning of Hold Period	End of Hold Period		
4×10^{-3}	193.1	204.8	0.08	405,000
4×10^{-4}	210.3	220.6	0.07	420,000
4×10^{-3}	196.5	205.5	0.08	438,000

This phenomenon which is ramp rate dependent, as shown above, is thought to be due to dynamic strain aging.

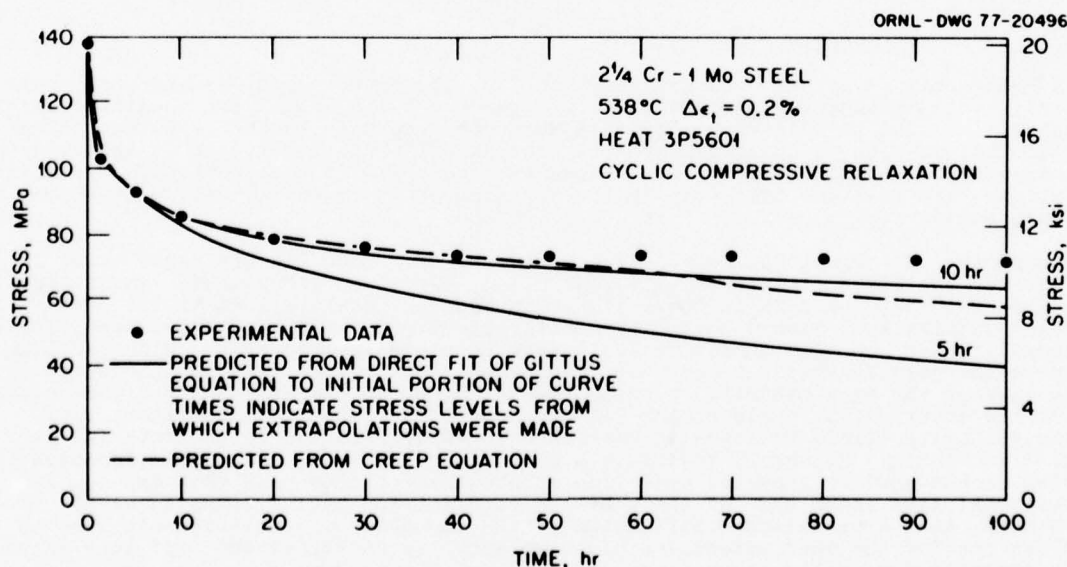


Fig. 16. Cyclic Relaxation Behavior of 2 1/4 Cr-1 Mo Steel Held at a Constant Strain Range of 0.2%. Comparisons of predicted behavior are also shown.

In making estimates of long term time dependent fatigue behavior of this material, no attempt was made to ductility normalize the life relationships to account for a time dependent decrease in creep-rupture ductility. Creep-rupture ductility data available (Fig. 17) for heat 20017 suggest that this may not be necessary for temperatures in the range of 454-510°C. However, heat-to-heat variations are apparent and for temperatures much above

510°C long term estimates, e.g., lifetimes in excess of 10,000 hr, may require a modification factor to account for a ductility loss. Long term cyclic and monotonic tests are underway to determine specific requirements.

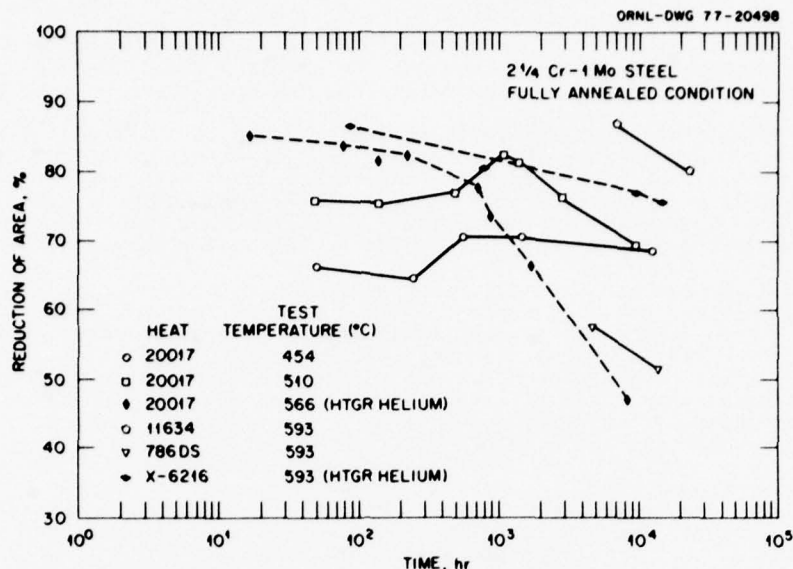


Fig. 17. Creep-Rupture Ductilities for Several Heats of 2 1/4 Cr-1 Mo Steel Tested in Air Except as Indicated.

Hastelloy X

Comparisons between expected cyclic life and actual cyclic life from tests run to date have shown excellent agreement (Fig. 12). However, test times to date have been fairly short such that reductions in continuous cycle fatigue life due to hold periods have not exceeded factors of about four. Further, additional verification tests at lower strain ranges are required, since the data have shown increased scatter at lower total and inelastic strain range levels (Figs. 9 and 12). Further, available creep-rupture data (Fig. 11) indicate a precipitous drop in creep-rupture ductility for test times in excess of about 2000 hr. Long term tests are required to determine if a simple time dependent ductility modification will indeed compensate for the low creep ductility.

Type 316 Stainless Steel

As was previously mentioned and shown in Fig. 15, rather good results were achieved in nearly every instance when comparisons were made between actual and predicted lifetimes for material in the irradiated condition. This occurred despite the fact that all of the material had not been irradiated to exactly the same fluence level. It is believed that for this material the irradiation conditions were such that the reduction in ductility and fatigue life were due primarily to the presence of agglomerated helium (bubbles) at the grain boundaries.

Comparing the relationships for $\Delta \epsilon_{in}$ versus N_{pp} for type 316 stainless steel in Fig. 13, for the three conditions, i.e., annealed, aged, and irradiated, considered herein it is apparent that the data indicate different slopes. Scaling then in the case of the N_{pp} relationships by a simple ductility modification from say the annealed condition to the irradiated or the aged condition would have resulted in some error, since scaling displaces the relationship but does not change the slope of the life relationship line. In the case of the aged material, a prior thermal aging treatment increased the fatigue life in the intermediate cycle regime (10^3 to 3×10^4 cycles) while the short term tensile ductility (Table V) actually decreased somewhat relative to the material in the annealed condition. Figure 13 indicates a cross-over between the N_{pp} relationships for material in the aged or annealed condition at about 10^2 cycles such that the N_{pp} line for aged material lies above that of the annealed material for cyclic lives in excess of 10^2 . Accordingly, then a ductility modification of the annealed life relationship line to establish one for the aged material would have actually displaced the "pp" line in the wrong direction for cyclic lives in excess of about 10^2 cycles.

Figure 15 indicates that agreement between actual and predicted lifetimes for material in the aged and to a lesser extent in the annealed condition for tensile hold times was generally not as good as that for the corresponding comparisons for material in the irradiated condition. The reasons for this increase in scatter are not known, but of course may be due to heat-to-heat variations and the scaling assumptions necessary to obtain the required life relationship line, i.e., "cp", given as Eq. (21). Accordingly, cyclic creep tests will be initiated on this heat of material at 593°C to verify Eq. (21).

A question that one might logically ask in conjunction with the use of the ductility scaling concept is how sensitive are the predicted cycles to failure to changes in or significant errors in the estimation of appropriate ductilities. To at least partially answer this question, calculations of the predicted cyclic lives were compared for the irradiated stainless steel using the actual creep-rupture ductility, i.e., $R.A. = 3\%$ from Table IV, and a significantly higher value, i.e., $R.A. = 29\%$. Thus the creep-rupture ductility was arbitrarily assumed equal to the tensile ductility as given in Table V. Actual cyclic life and predicted values using the above creep-rupture ductilities are compared in Table VI. These results from calculations using the " N_{pp} " relationship for irradiated material given in Fig. 13, Eq. (21), and the Interaction damage rule indicated that predictions were sensitive to the input ductilities.

Table VI. Comparisons Between Predicted Cycles to Failure Using Different Creep-Rupture Ductilities ($R.A.$) for Irradiated Type 316 Stainless Steel^a

Specimen	Total Strain Range (%)	Duration of Tensile Hold, hr	Predicted Cycles to Failure		Actual Cycles to Failure
			$R.A. = 3\%$	$R.A. = 29\%$	
D-104	1.0	5.0	48	386	27
D-108	2.0	5.0	10	98	10
D-109	1.0	0.5	100	570	60
D-113	2.0	0.5	15	120	12
D-106	0.5	0.1	1,125	4,409	757
D-114	1.0	0.1	112	649	88

^aTest temperature was 593°C.

CONCLUSIONS

The method of strainrange partitioning was employed to predict strain controlled time dependent cyclic life of a number of structural materials including annealed 2 1/4 Cr-1 Mo steel, Hastelloy X, and irradiated and unirradiated type 316 stainless steel. The following are specific conclusions:

1. Iso-strain-range hold time reduction factor versus duration of hold time plots were established for two heats of annealed 2 1/4 Cr-1 Mo steel at 482 and 538 C. This influence of either tension, compression, or both tension and compression strain holds was estimated for dwell periods of up to 100 hr on the continuous cycle fatigue life. A comparison between actual and estimated cyclic lifetimes (cycles) generally showed good agreement, particularly in the case of the compression only strain hold situation.

2. Whereas only one of the four required life relationships equations was directly available for predicting cyclic life times (cycles) for Hastelloy X, ductility scaling or normalization provided the required relationships for interim use. Comparisons between predicted and actual lifetimes (cycles) for relatively short-term experimental data generated at fairly high strain ranges at both 704 and 871°C showed good agreement.

3. Good agreement between predicted and actual cyclic lifetimes (cycles) was generally found for irradiated type 316 stainless steel. Agreement between actual and predicted cycles to failure was not as good for material in the pre-aged, i.e., up to about 5000 hr at 593°C, condition. The increased scatter for aged material may have been due to some uncertainty in use of the available " ep " life relationship.

4. Specific problem areas or uncertainties in the authors' view identified, but which are not necessarily unique to strainrange partitioning, which contribute to the uncertainty in making predictions for low-strain-range long hold time situations were discussed and are as follows:

- extrapolation of life relationship equations to low inelastic strain ranges that were generated primarily from load controlled short term cyclic creep tests,
- heat-to-heat variations which cause differences in constitutive behavior,
- metallurgical and strain rate induced changes or instabilities such as thermal aging response, strain aging, and creep-rupture ductility changes, and
- endurance limits or strain ranges below which time dependent effects are expected to be non-existent.

Other important factors such as cumulative damage and environmental (atmosphere) effects were not discussed in this paper but will be addressed in subsequent reports.

ACKNOWLEDGMENTS

The authors gratefully acknowledge the assistance of L. K. Egner in conducting the experimental tests, R. W. Swindeman and R. K. Nanstad for reviewing the paper, and Linda Croff for typing the manuscript.

REFERENCES

1. D. L. Keller, *Progress on LMFBR Cladding, Structural and Component Materials Studies During July 1971 Through June 1972, Final Report, Task 32*, BMI-1928, Battelle Columbus Laboratories.
2. C. R. Brinkman and G. E. Korth, "Low Cycle Fatigue and Hold Time Comparisons of Irradiated and Unirradiated Type 316 Stainless Steel," *Metall. Trans.*, 5, (March 1974) 792-94.
3. C. R. Brinkman, G. E. Korth, and R. R. Hobbins, "Estimates of Creep-Fatigue Interaction in Irradiated and Unirradiated Austenitic Stainless Steels," *Nucl. Technol.*, 16 (October 1972), 297-307.
4. C. R. Brinkman et al., *Application of Hastelloy X in Gas-Cooled Reactor Systems*, ORNL/TM-5405, Oak Ridge National Laboratory, October 1976.
5. S. S. Manson, G. R. Halford, and M. H. Hirschberg, *Creep-Fatigue Analysis by Strain-Range Partitioning*, NASA TMX-67838, NASA-Lewis Research Center, 1971.
6. C. R. Brinkman et al., "Time-Dependent Strain-Controlled Fatigue Behavior of Annealed 2 1/4 Cr-1 Mo Steel for Use in Nuclear Steam Generator Design," *J. Nucl. Mater.*, 62(2,3) (November 1976) 181-204.
7. C. R. Brinkman et al., *Interim Report on the Continuous Cycling Elevated Temperature Fatigue and Subcritical Crack Growth Behavior of 2 1/4 Cr-1 Mo Steel*, ORNL/TM-4993, Oak Ridge National Laboratory, December 1975.
8. M. H. Hirschberg and G. R. Halford, *Use of Strainrange Partitioning to Predict High-Temperature Low-Cycle Fatigue Life*, NASA TN D-8072, NASA-Lewis Research Laboratories, January 1976.
9. M. K. Booker, *Interim Analysis of the Creep Strain-Time Characteristics of Annealed and Isothermally Annealed 2 1/4 Cr-1 Mo Steel*, ORNL/TM-5831, Oak Ridge National Laboratory, June 1977.
10. G. R. Halford, J. F. Saltsman, and M. H. Hirschberg, *Ductility Normalized Strainrange Partitioning Life Relations for Creep-Fatigue Life Predictions*, NASA TM-73737, NASA-Lewis Research Laboratories, October 1977.
11. K. Natesan et al., "Effect of Sodium Environment on the Creep-Rupture and Low-Cycle Fatigue Behavior of Austenitic Stainless Steel," presented at the IAEA/IWGFR Specialists Meeting on Properties of Primary Circuit Structural Materials, October 17-21, 1977, Bensburg, Federal Republic of Germany.
12. P. N. Flagella, "Effects of High Temperature Sodium Exposure on the Microstructural and Time-Dependent Mechanical Behavior of Type 316 Stainless Steel," presented at the IAEA/IWGFR Specialists Meeting on Properties of Primary Circuit Structural Materials, October 17-21, 1977, Bensburg, Federal Republic of Germany.
13. D. R. Diercks, *A Compilation of Elevated-Temperature Strain-Controlled Fatigue Data on Type 316 Stainless Steel*, Argonne National Laboratory, to be published.
14. J. F. Saltsman and G. R. Halford, "Applications of Strainrange Partitioning to the Prediction of Creep-Fatigue Lives of Types 304 and 316 Stainless Steel," presented at the ASME Joint Pressure Vessel and Piping and Petroleum Mechanical Engineering Conference, September 19-23, 1976, Mexico City, Mexico.
15. A. Ward, private communication, Westinghouse Hanford, November 1977.

THE APPLICATION OF "STRAINRANGE PARTITIONING METHOD" TO MULTIAXIAL CREEP-FATIGUE INTERACTION

S. Y. Zamrik, Professor
 Department of Engineering Science and Mechanics
 The Pennsylvania State University
 University Park, PA 16802
 U.S.A.

ABSTRACT

The method of strain range partitioning was applied to a series of torsional fatigue tests conducted on tubular 304 stainless steel specimens at 1200°F (649°C). Creep strain was superimposed on cycling strain, and the resulting strain range was partitioned into four components; completely reversed plastic shear strain, plastic shear strain followed by creep strain, creep strain followed by plastic strain and completely reversed creep strain. Each strain component was related to the cyclic life of the material. The paper describes the experimental procedure used to achieve strain partitioning and the torsional test results are compared to those obtained from axial tests. The damaging effects of the individual strain components were expressed by a linear life fraction rule.

NOMENCLATURE

$\Delta\gamma$	=	total torsional inelastic shear strain range
$\Delta\gamma_{pp}$	=	completely reversed plastic shear strain
$\Delta\gamma_{cc}$	=	completely reversed creep shear strain
$\Delta\gamma_{pc}$	=	plastic shear strain reversed by creep shear strain
$\Delta\gamma_{cp}$	=	creep shear strain reversed by plastic shear strain
N_f	=	observed no. of cycles to failure
N_{cp}	=	cyclic life associated with a given $\Delta\gamma_{cp}$ strain range
N_{cc}	=	cyclic life associated with a given $\Delta\gamma_{cc}$ strain range
N_{pp}	=	cyclic life associated with a given $\Delta\gamma_{pp}$ strain range
τ_{xy}	=	torsional inelastic shear stress
γ_{xy}	=	torsional inelastic shear strain
σ_x	=	axial inelastic stress
ϵ_x	=	axial inelastic strain
$\bar{\sigma}_e$	=	effective inelastic stress
$\bar{\epsilon}_e$	=	effective inelastic strain
$\bar{\Delta\epsilon}_{pp}$	=	effective plastic strain in tension and compression
$\bar{\Delta\epsilon}_{cp}$	=	effective creep strain in tension and plastic strain in compression
$\bar{\Delta\epsilon}_{inel}$	=	$\bar{\Delta\epsilon}_{pp} + \bar{\Delta\epsilon}_{cp}$
F_{pp}	=	$\bar{\Delta\epsilon}_{pp} / \bar{\Delta\epsilon}_{inel}$
F_{cp}	=	$\bar{\Delta\epsilon}_{cp} / \bar{\Delta\epsilon}_{inel}$
R	=	$\Delta\gamma_{xy} / \Delta\epsilon_x$
α, c	=	material constants

I. INTRODUCTION

The strainrange partitioning method has attracted considerable attention in the past few years in dealing with the problem of creep-fatigue analysis. The method considers mechanisms of deformation that a material may undergo as a result of imposing loads at elevated temperatures. The type of deformation consists mainly of two essential elements: plastic deformation, and creep deformation. These two basic components may be mixed to give two additional components. Thus, the life of the material is affected by each of these components.

A considerable amount of data has been presented on the applicability of the method to specimens subjected to uniaxial loading. In this paper, the method is examined from the biaxiality point of view, since structural components, in most cases, are subjected to a biaxial state of stress.

The method of strainrange partitioning was applied to two cases of stress biaxiality; one case consisted of pure torsion loading under stress controlled loading, and the other case consisted of a combined axial and torsional loading under a strain controlled loading.

The torsional stress controlled tests were conducted at 1200°F and the biaxial strain controlled tests at 1000°F.

II. PARTITIONING INELASTIC SHEAR STRAINRANGE

The strainrange partitioning concept implies that four distinct inelastic strains exist. Therefore, it is essential that a cycle be partitioned into a completely reversed plastic strain, $\Delta\epsilon_{pp}$, a completely reversed creep strain, $\Delta\epsilon_{cc}$, a tensile plastic strain followed by a compressive creep strain, $\Delta\epsilon_{pc}$, or tensile creep strain followed by compressive plastic strain, $\Delta\epsilon_{cp}$.

Each type of strain bears a relation to the cyclic life of the material, once the strain life relations are related through a linear damage summation rule.

In treating torsional creep-fatigue, it is assumed that the total inelastic shear strain in a one cycle can also be partitioned into four similar strain components with corresponding cyclic lives. The simplest measurable component is the plastic shear strain $\Delta\gamma_{pp}$ which can be obtained from a completely reversible torsional strain cycling at a rapid loading that will eliminate any induced creep strain. This type of test will result in a hysteresis loop as shown in Figure (1), where cycling is carried between the strain limits A and C. The width of the loop DB represents $\Delta\gamma_{pp}$ which can be related to the cyclic life through Manson-Coffin type equation [5] in the form of:

$$\Delta\gamma_{pp} N_{pp}^a = C \quad (1)$$

The other three shear strain components have to be determined from tests specifically designed to produce a hysteresis loop which includes creep strain.

III. EXPERIMENTAL PROCEDURE

The material used in this study was 304 stainless steel supplied in the form of one inch (25.4mm) round bars. Tubular specimens were machined to a gage length of 1" (1.5mm) with a wall thickness of 0.060" (1.55mm) and an outside diameter of 0.456" (11.4mm). Two keyways on each end of the specimen were cut to provide the torsional loading. After machining, specimens were annealed at 2000°F (1092°C) for 30 minutes in an argon atmosphere. The chemical composition and mechanical properties of the material are given in Tables (1) and (2), respectively * (see Footnote on next page).

A temperature of 1200°F (649°C) was imposed on specimen through glo-bar heating elements manufactured by the Carborundum Corporation. The element, 6-3/4 inches (171.5mm) long and 1/4 inch (6.4mm) diameter, is silicon carbide with a central heating section or "hot zone" that varies from 1-1/2 inches (38.1mm) to 2 inches (50.8mm) long. The element was inserted in the tubular specimen and left free to expand or contract. Electrical connections were made through aluminum metallized terminals. Because of high temperature environment, torsional shear strain was controlled through a rotary variable differential transformer (RVDT) extensometer which was calibrated with strain gages at room temperature. The torsional load was measured through a torque cell. Detail of the experimental procedure and equipment can be found in reference [6]. Briefly, in a strain partitioned test, a load overshoot can be encountered. This effect has been experienced by the authors who first interpreted it as a load relaxation that could influence the test; however, since a constant load is essential to produce creep, it was found that the overshoot can be eliminated experimentally by throttling the oil flow to the load actuator. It should be pointed out that a constant cycling frequency cannot be programmed but has to be dictated by the amount of creep the material exhibits. For example, to maintain a constant creep at each cycle, the load has to be applied at a different rate for each cycle.

IV. TEST RESULTS AND DISCUSSION

The concept of strainrange partitioning shows a distinction between $\Delta\epsilon_{cp}$ and $\Delta\epsilon_{pc}$ components. This is due to an effective difference that exists between tensile or compressive strain. In the pure torsion strain cycling case, these two components are equal since the loading direction is applied in either a clockwise or counterclockwise direction; therefore, the tensile strain is the same as the compressive strain. Assuming the load directionality does not influence any added creep strain, one finds that only three strain components exist rather than four. In view of this observation, the test procedure was designed to produce three shear strain components, namely, $\Delta\gamma_{pp}$, $\Delta\gamma_{cc}$ and $\Delta\gamma_{cp} = \Delta\gamma_{pc}$. The tests were stress controlled at 1200°F.

A total of 14 tests were conducted: four (4) tests under a completely reversed torsion that produced $\Delta\gamma_{pp}$, six (6) tests under clockwise creep reversed by plastic shear strain, and four (4) tests under completely reversed creep cycling. The basic data from all tests is found in Reference [9].

Figure (2) shows the recorded hysteresis loops obtained under cp. Under cp-type test, the loop width represents the total inelastic shear strain which was partitioned into $\Delta\gamma_{cp}$ (BF) and $\Delta\gamma_{pp}$ (DF), and the total life for this test was recorded. The life that corresponds to the partitioned plastic shear strain $\Delta\gamma_{pp}$ was calculated from Equation (1), while the remaining life which is attributed to the effect of creep was calculated from an assumed linear damage summation in the form of:

$$\frac{N}{N_{pp}} + \frac{N}{N_{cp}} = 1 \quad (2)$$

where N is the recorded total experimental life. Equation (2) was later modified.

In the cc-type test, a pure creep-creep strain cannot be obtained experimentally without imposing a plastic component. Therefore, the hysteresis loop shown in Figure (3) has to be analyzed under the proposed strain range concept technique. This is performed by partitioning the total inelastic shear strain \overline{EB} into three components, $\Delta\gamma_{pp} = \overline{HB}$, $\Delta\gamma_{cc} = \overline{FB}$ and $\Delta\gamma_{cp} = \Delta\gamma - (\Delta\gamma_{cc} + \Delta\gamma_{pp})$ or $\Delta\gamma_{cp} = \overline{EB} - \overline{FB} - \overline{HB}$. The individual life that corresponded to each shear strain component was computed from:

$$\frac{N}{N_{pp}} + \frac{N}{N_{cp}} + \frac{N}{N_{cc}} = 1 \quad (3)$$

Where N is the recorded total life while N_{pp} was recorded from the pure $\Delta\gamma_{pp}$ test and N_{cp} calculated from Equation (2). Thus, it was possible to construct a $\Delta\gamma$ - N diagram that encompasses the three strain components with their associated lives as shown in Figure (4). Caution must be exercised in determining N_{pp} experimentally, otherwise error will result in the entire life calculation procedure.

The experimental data obtained under each strain component showed a power law relationship. In the first case under $\Delta\gamma_{pp}$, this relationship is:

$$\Delta\gamma_{pp} = 2.25 (N_{pp})^{-0.65} \quad (4)$$

If Equation (4) is compared to Manson's tentative universalized life relationship [6] of

$$\frac{\Delta\epsilon_{pp}}{D_p} = 0.75 (N_{pp})^{-0.6} \quad (5)$$

one finds that a similarity exists between these two relations with respect to their slope characteristics. The difficulty lies in evaluating the intercept of the line since the ductility factor D_p is not easily measured under torsion.

In the case of $\Delta\gamma_{cp}$ - N_{cp} relation, one has to compare the form:

$$\Delta\gamma_{cp} = 2.40 (N_{cp})^{-1.22} \quad (6)$$

with the assumption that

$$\Delta\gamma_{cp} = \Delta\gamma_{pc} \quad (7)$$

to the axial relation of:

$$\frac{\Delta\epsilon_{cp}}{D_c} = 0.25 N_{cp}^{-0.8} \quad (8)$$

and

$$\frac{\Delta\epsilon_{pc}}{D_p} = 1.25 N_{pc}^{-0.8} \quad (9)$$

The $\Delta\epsilon_{pc}$ component does not have an equivalent value in shear, therefore, the results from the second component $\Delta\epsilon_{cp}$ can be compared to the torsional results of $\Delta\gamma_{cp}$. In both cases, the cp-component has exhibited the most detrimental creep effect on life; however, deviation exists between the slope characteristics. A comparison can be best seen when the third shear creep strain component is evaluated. The resulting relation of

$$\Delta\gamma_{cc} = 1.45 (N_{cc})^{-0.96} \quad (10)$$

can be compared to

$$\frac{\Delta\epsilon_{cc}}{D_c} = 0.75 (N_{cc})^{-0.8} \quad (11)$$

On the basis of these torsional tests, several observations can be made. In the axial case, three partitioned strain components exhibited a common hardening effect as reflected by the exponent of 0.8; however, in the torsional case, the material showed a different degree of hardening depending on the difference between the slope characteristics of each type of shear strain. A possible explanation of this difference may lie in the measure of the ductility, which, as stated, was difficult to determine. It should be pointed out that hardening was assumed since this material exhibits this characteristic. In either case, the $\Delta\gamma_{pp}$ showed the least detrimental effect on life while the $\Delta\gamma_{cp}$ component showed the most detrimental effect. For the material tested at 1200°F (649°C) a large reduction in life was recorded between these two components. For example, at 1% level a factor of 50 was observed.

* Chemical compositions, material processing, heat treatments and mechanical properties for each tested alloy, as well as the data generated in the programme, are given in Appendix A I.

V. PARTITIONING INELASTIC EFFECTIVE STRAINRANGE

On the basis of the pure torsional data that was generated under 1200°F, the multiaxial investigation was extended into a broader range, whereby axial, torsional and a combination of axial and torsional tests were obtained. The data under these three loading conditions were generated under 1000°F. The loading system is shown in Figure (5). The ratio of shear loading to axial loading is designated by R . Therefore, $R = 0$, $R = 2$, and $R = \infty$, represents uniaxial, biaxial and torsional strain loading respectively.

Creep was imposed through hold-time procedure that varied in length. The data was analyzed on the basis of "equivalent multiaxial stress-strainrange".

The equivalent multiaxial stress-strainrange is defined as the Mises-Hencky type. It will be used as a parameter to compare axial, biaxial and torsional data. An important element in this procedure is that one has to know at each instant of time within the cycle, an equivalent stress $\bar{\sigma}_e$ and an equivalent strain $\bar{\epsilon}_e$. These values can be calculated from:

$$\begin{aligned}\bar{\sigma}_e &= \frac{1}{\sqrt{2}} \sqrt{(\sigma_1 - \sigma_2)^2 + (\sigma_2 - \sigma_3)^2 + (\sigma_3 - \sigma_1)^2} \\ \bar{\epsilon}_e &= \frac{\sqrt{2}}{3} \sqrt{(\epsilon_1 - \epsilon_2)^2 + (\epsilon_2 - \epsilon_3)^2 + (\epsilon_3 - \epsilon_1)^2}\end{aligned}\quad (12)$$

where $\sigma_1, \sigma_2, \sigma_3$ are the principal stresses, and ϵ_1, ϵ_2 and ϵ_3 are the principal strains.

For the case of $R = 2$, equations (12) reduce to:

$$\begin{aligned}\bar{\sigma}_e &= (\sigma_x^2 + 3\tau_{xy}^2)^{1/2} \\ \bar{\epsilon}_e &= \frac{1}{\sqrt{3}} (3\epsilon_x^2 + \gamma_{xy}^2)^{1/2}\end{aligned}\quad (13)$$

and for the torsional case where $R = \infty$,

$$\begin{aligned}\bar{\sigma}_e &= \sqrt{3} \tau_{xy} \\ \bar{\epsilon}_e &= \frac{1}{\sqrt{3}} \gamma_{xy}\end{aligned}\quad (14)$$

To achieve a relation between $\bar{\sigma}_e$ to $\bar{\epsilon}_e$, an equivalent hysteresis loop was constructed from axial and torsional hysteresis loops that were recorded during the test at a given cycle. A schematic diagram shown in Figure (6) illustrates the procedure used in generating an equivalent loop. Since the triangular wave form loading provided a linear movement on the strain scale, respective strain range of each loop was divided into ten equal strain increments. Thus, these intervals are equal in time where the principal stresses are known at each instant of time throughout the cycle. Therefore, each divided point on the axial loop does correspond in time with a point on the torsional loop, resulting in an equivalent multiaxial loop as shown in Figure (7).

Once the equivalent loop is obtained, the SRP lines were determined. This is also shown in Figure (8).

The multiaxial effective plastic strainrange, $\Delta\bar{\epsilon}_{pp}$, component was obtained from the continuous cycling data. The data is shown in Figure (9) as $\Delta\bar{\epsilon}_{pp}$ vs N_{pp} for $R = 0, 2$, and ∞ .

The $\Delta\bar{\epsilon}_{cp}$ component was determined from the equivalent hysteresis loops shown for $R = 0, 2$, and ∞ . The corresponding life was calculated from the modified relation:

$$\frac{f_{pp}}{N_{pp}} + \frac{f_{cp}}{N_{cp}} = \frac{1}{N_f}$$

where

$$f_{pp} = \frac{\Delta\bar{\epsilon}_{pp}}{\Delta\bar{\epsilon}_{inel.}} \quad \text{and} \quad f_{cp} = \frac{\Delta\bar{\epsilon}_{cp}}{\Delta\bar{\epsilon}_{e.inel.}}\quad (15)$$

The data of $\Delta\bar{\epsilon}_{cp}$ is then plotted vs the calculated N_{cp} as shown in Figure (10). Data for Figures (9, 10) is listed in Table (3).

For the case of $R = \infty$, both $\Delta\bar{\epsilon}_{pp}$ and $\Delta\bar{\epsilon}_{cp}$ data lines have shown an upper bound when compared to axial and biaxial case. This observation was reported by the author in previous investigations. As a result of this observation, the idea of triaxiality factors was proposed. Manson and Halford have shown the application of this factor in unifying the three cases of $R = 0, 2$, and ∞ , (8).

Since the intent of this report is the application of SRP to multiaxial case, the data is reported in detail. Power law relations can be fitted to the data, such as for the pp-component:

$$\begin{aligned}\Delta \bar{\epsilon}_{pp} &= 0.587 (N_{pp})^{-0.51} & R &= \infty \\ \Delta \bar{\epsilon}_{pp} &= 0.208 (N_{pp})^{-0.56} & R &= 0, 2\end{aligned}\quad (16)$$

and for the cp-component:

$$\begin{aligned}\Delta \bar{\epsilon}_{cp} &= 0.0036 (N_{cp})^{-0.37} & R &= \infty \\ \Delta \bar{\epsilon}_{cp} &= 0.0012 (N_{cp})^{-0.40} & R &= 0, 2\end{aligned}\quad (17)$$

The important part of these relations is the slope characteristics that varied from 0.5 to 0.4. The variation is a considerable improvement on the data that was reported in Figure (4).

A better comparison can be made when both types of data for $R = \infty$, Figures (4), (9) and (10), were superimposed as shown in Figures (11, 12); for the case of pp-data, the slope of the lives are similar to those proposed by the SRP method. The slight difference that is shown is mainly a temperature effect. The great and the most dramatic difference appears in Figure (12). The effective multiaxial strain approach is more favorable to the SRP method than the $\Delta \gamma_{cp}$ approach. The resulting slope of $\Delta \bar{\epsilon}_{cp}$ approach is in line with the proposed SRP exponents for the uniaxial case and perhaps more realistic in nature. This can be attributed to the effective stress-strain hysteresis loop that was obtained where the principal stresses when their signs were considered with respect to time. This factor was not introduced in the $\Delta \gamma_{cp}$ data.

Figure (10) shows a comparison between $R = \infty$ and $R = 0$, and 2 in terms of $\Delta \bar{\epsilon}_{cp}$ component. The triaxiality factor is also applicable to this case, since both slopes are similar in nature reflecting the ductility factor as in the case of pp-component.

SUMMARY AND CONCLUSIONS

The objective of the NASA research program is the evaluation and application of the method of strain-range partition to biaxial creep-fatigue interaction. Data was obtained by subjecting 304 SS specimens to axial, biaxial and torsional loading. Torsional data was presented in terms of shear strains vs corresponding number of cycles to failure. The results showed a considerable deviation from the proposed values that may be used in applying the SRP method. However, when the data was analyzed on the basis of an effective multiaxial strainrange through the use of an effective hysteresis loop, the SRP method established lines that are more consistent with the uniaxial SRP data for the material tested.

ACKNOWLEDGEMENTS

The author wishes to express his gratitude to NASA, Lewis Research Center for financial support under Grant No. NGR-39-009-034, and to C. Lange, Laboratory Assistant, for conducting the tests and preparing the data.

REFERENCES

- [1] Manson, S. S. "Interfaces Between Fatigue, Creep and Fracture," International Journal of Fracture Mechanics, Vol. 2, No. 1, March 1966, pp. 327-363.
- [2] Coffin, L. F., Jr. "Fatigue at High Temperature," Fatigue at Elevated Temperatures, ASTM STP 520, American Society for Testing and Material, 1973, pp. 5-34.
- [3] Berling, J. T. and Conway, J. B. "A New Approach to the Prediction of Low-Cycle Fatigue Data," Metallurgical Transactions, Vol. 1, No. 4, April 1970, pp. 805-809.
- [4] Manson, S. S., Halford, G. R., and Hirschberg, M. H. "Creep Fatigue Analysis by Strain-Range Partitioning," Design for Elevated Temperature Environment; American Society of Mechanical Engineers, New York, 1971, pp. 12-28.
- [5] Manson, S. S., "Behavior of Metals under Conditions of Thermal Stress," NASA TN 2933, 1953.
- [6] Zamrik, S. Y. "The Effect of Biaxiality in Creep-Fatigue at Elevated Temperatures," ORNL-Sub-2649-3, March 1975.
- [7] Manson, S. S. "The Challenge to Unify Treatment of High Temperature Fatigue - A Partisan Proposal Based on Strain Range Partitioning," Fatigue at Elevated Temperatures, ASTM STP 520, American Society for Testing and Materials, 1973, pp. 744-782.
- [8] Manson, S. S. and Halford, G. R. "Multiaxial Creep-Fatigue Life Analysis using Strainrange Partitioning", ASME-MPC3 Symposium on Creep-Fatigue Interaction, New York, 1976, pp. 299-322.
- [9] Zamrik, S. Y. "The application of 'Strain Range Partitioning Method' to Torsional Creep-Fatigue Interaction", Journal of Engineering Materials and Technology, Vol. 98, July 1976, pp. 244-248.

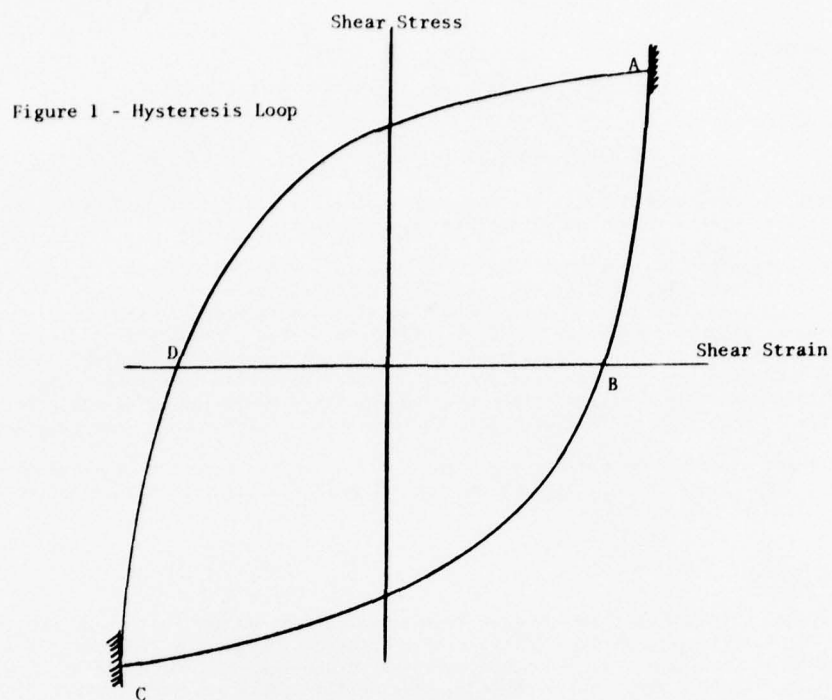


Figure 1 - Hysteresis Loop for a Completely Reversible Plastic Shear Strain Under Torsional Cycling

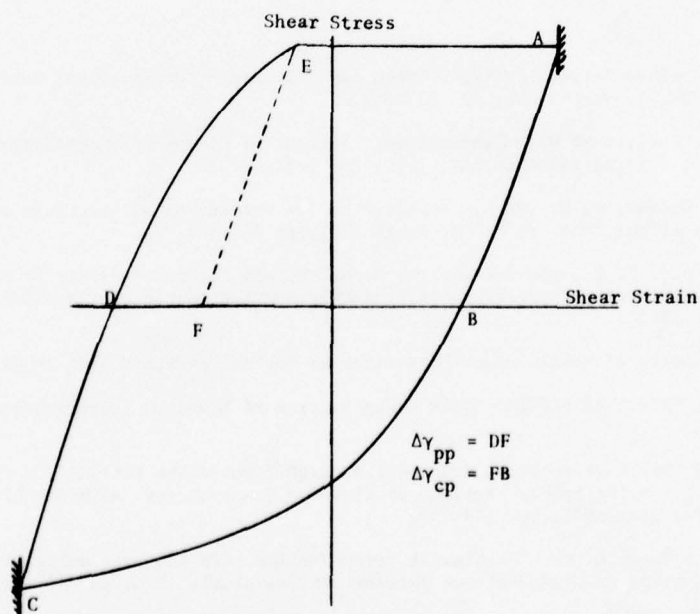


Figure 2 - Hysteresis Loop for a $\Delta\gamma_{CP}$ Type Shear Strain Test

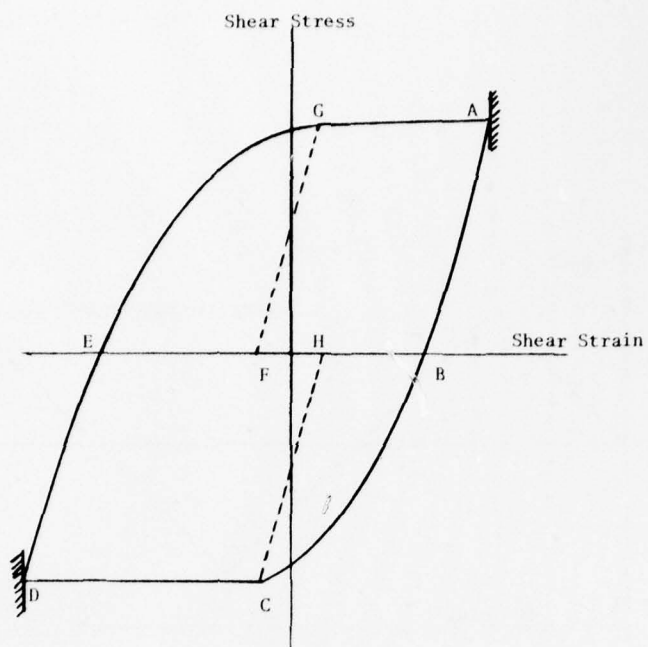


Figure 3 - Hysteresis Loop for a $\Delta\gamma_{cc}$ Type Creep Shear Strain Test

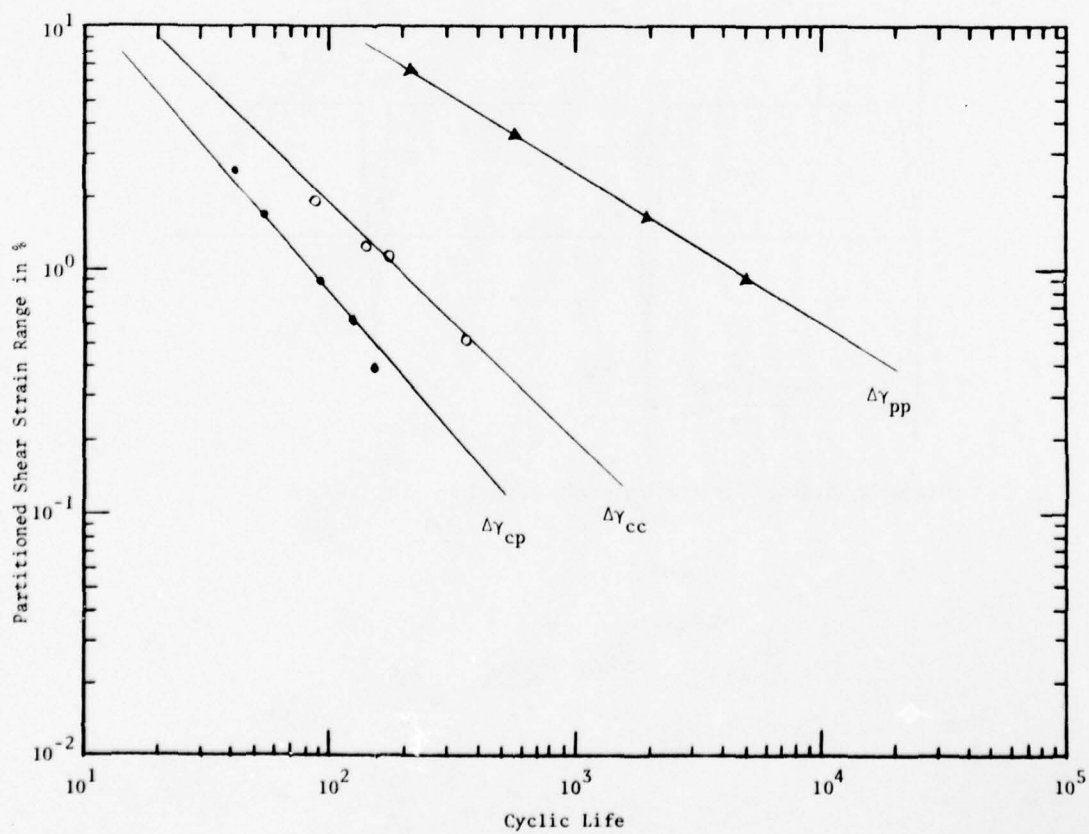
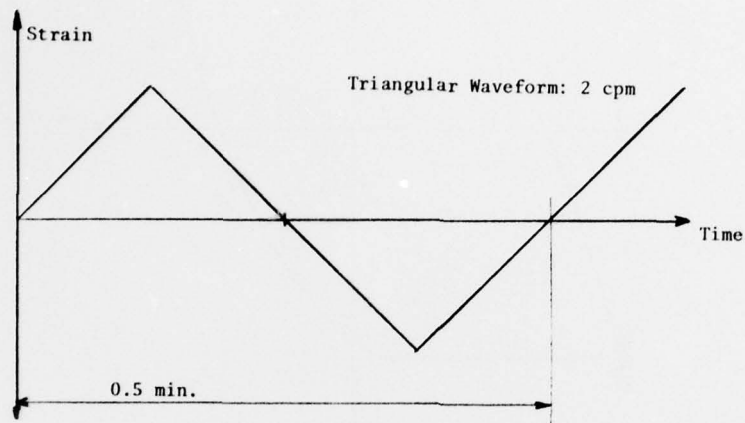
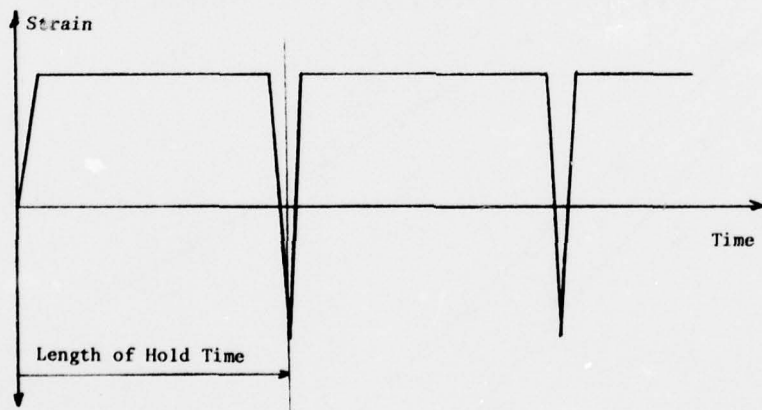


Figure (4) - Partitioned Plastic Shear Strain Range Components Under Torsional Loading

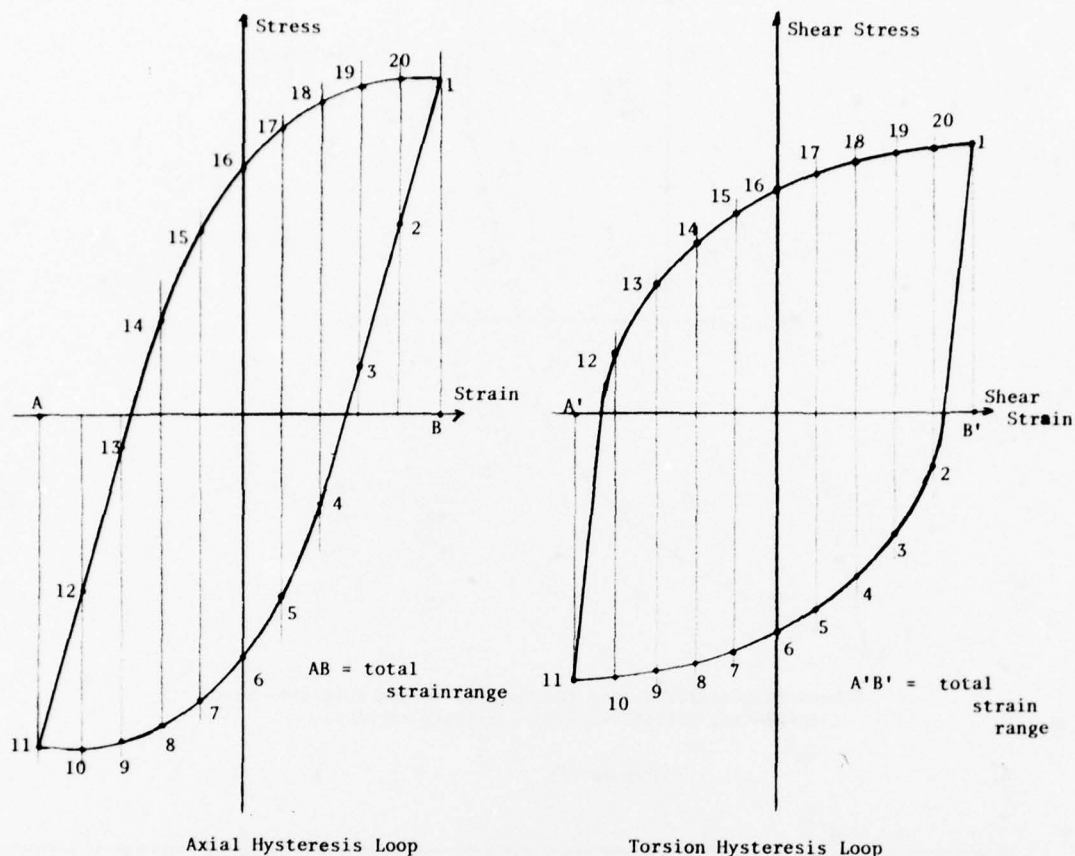


Schematic diagram illustrating triangular waveform used in continuous cycling tests.



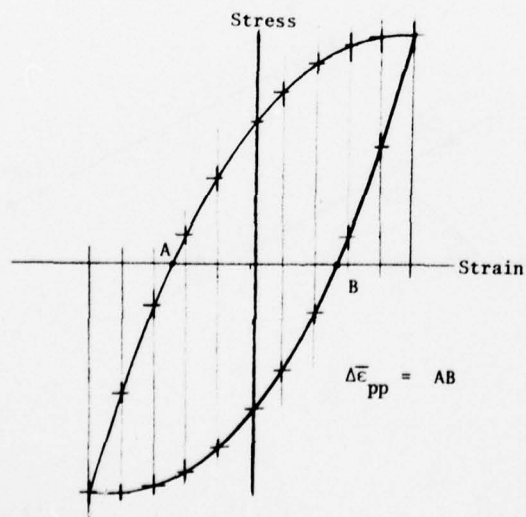
Schematic diagram illustrating waveform used in hold time tests

Figure 5



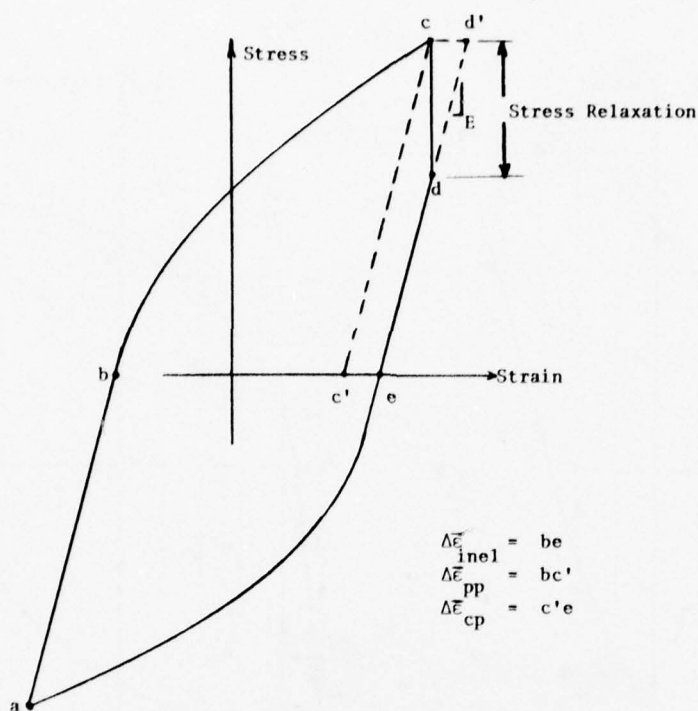
Schematic Hysteresis Loops showing the subdividing of the total strainrange into ten equal divisions.

Figure (6)



Typical effective hysteresis loop illustrating the completely reversed plastic strain range for a continuous cycling test.

Figure (7)



Schematic hysteresis loop for tensile strain hold-time test illustrating partitioning of inelastic strains.

Figure (8)

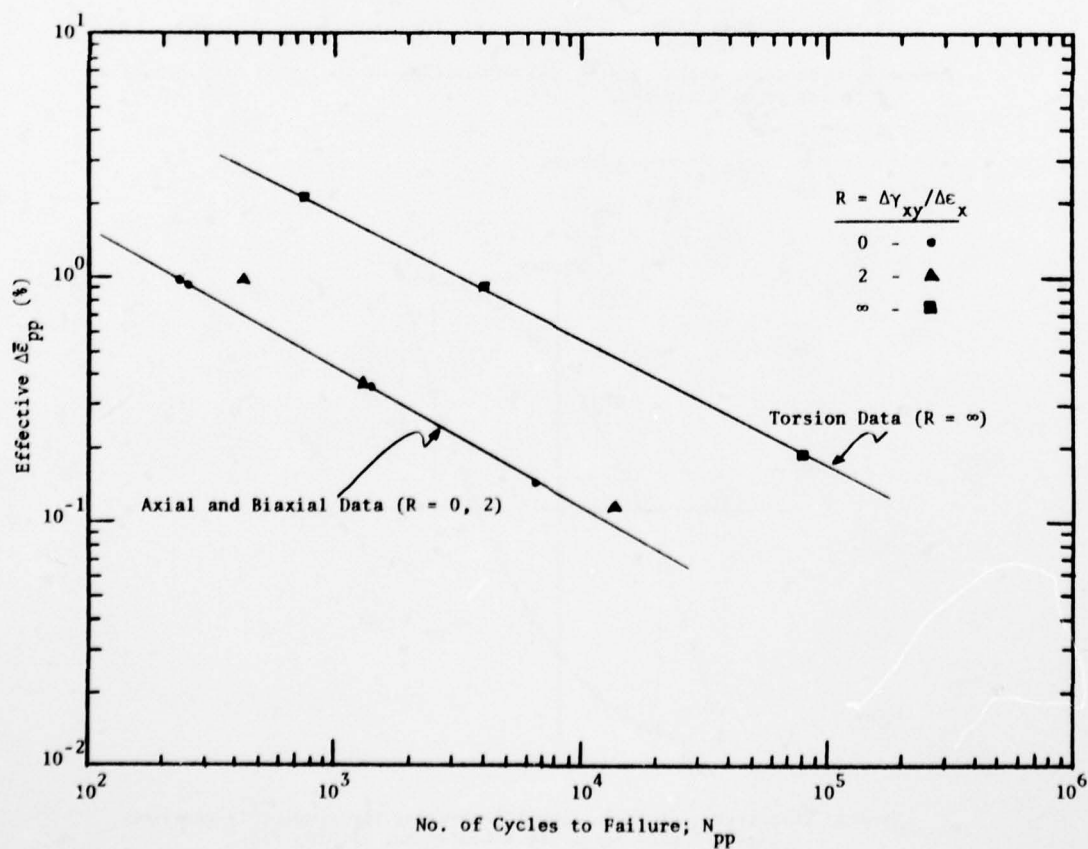


Figure (9)

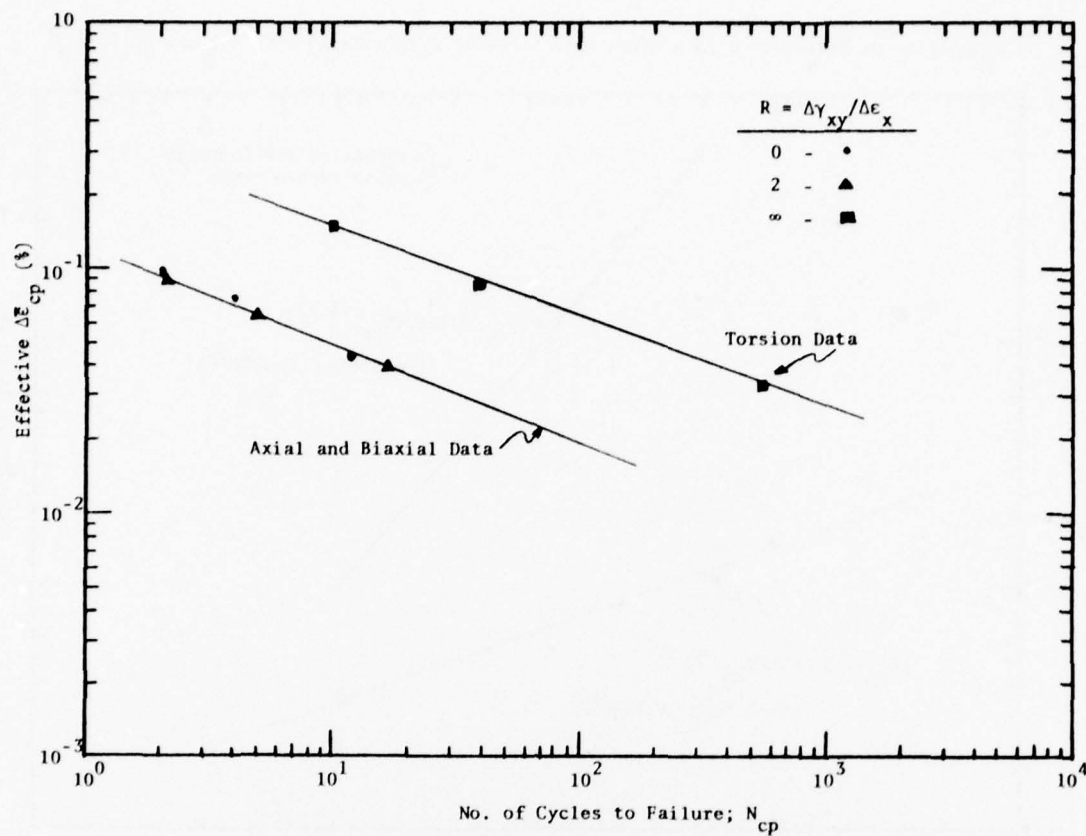


Figure (10)

Comparison of Effective Strain Range Data to Shear Strain Range Data for pp type

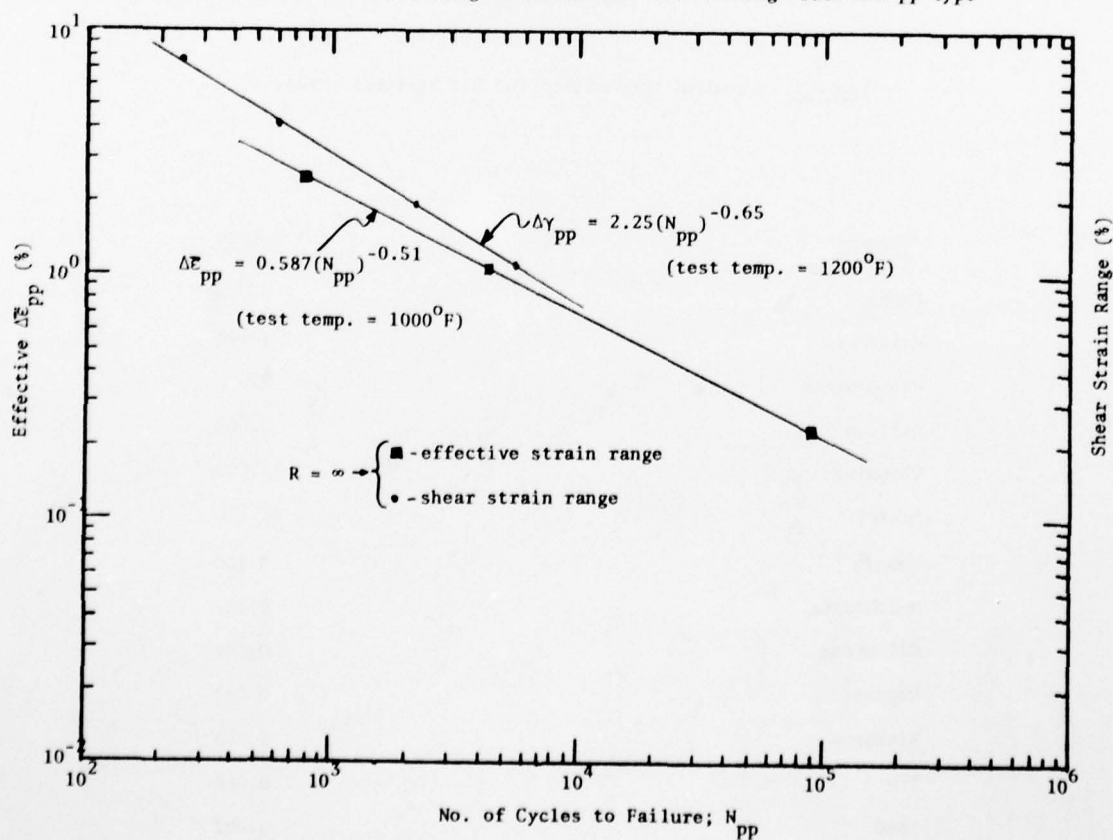


Figure (11)

Comparison of Effective Strain Range Data to Shear Strain Range Data for the cp Type

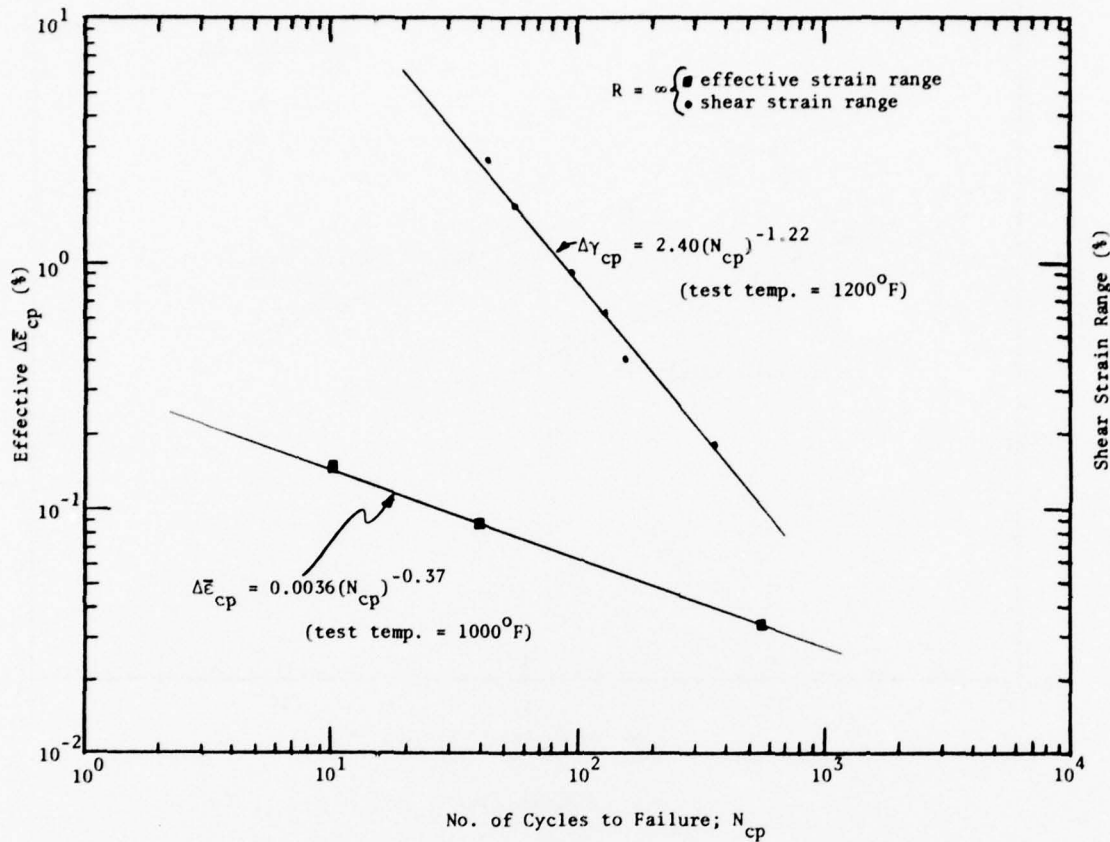


Figure (12)

Table 1 - Chemical Composition for 304 Stainless Steel

Element	% Weight
Carbon	0.048
Manganese	1.340
Phosphorous	0.039
Silicon	0.500
Chromium	18.600
Nickel	10.100
Cobalt	0.100
Molybdenum	0.300
Columbium	0.002
Copper	0.200
Nitrogen	0.030
Tin	0.018
Lead	0.002
Tantalum	0.002

Table 2 - Mechanical Properties of 304 Stainless Steel

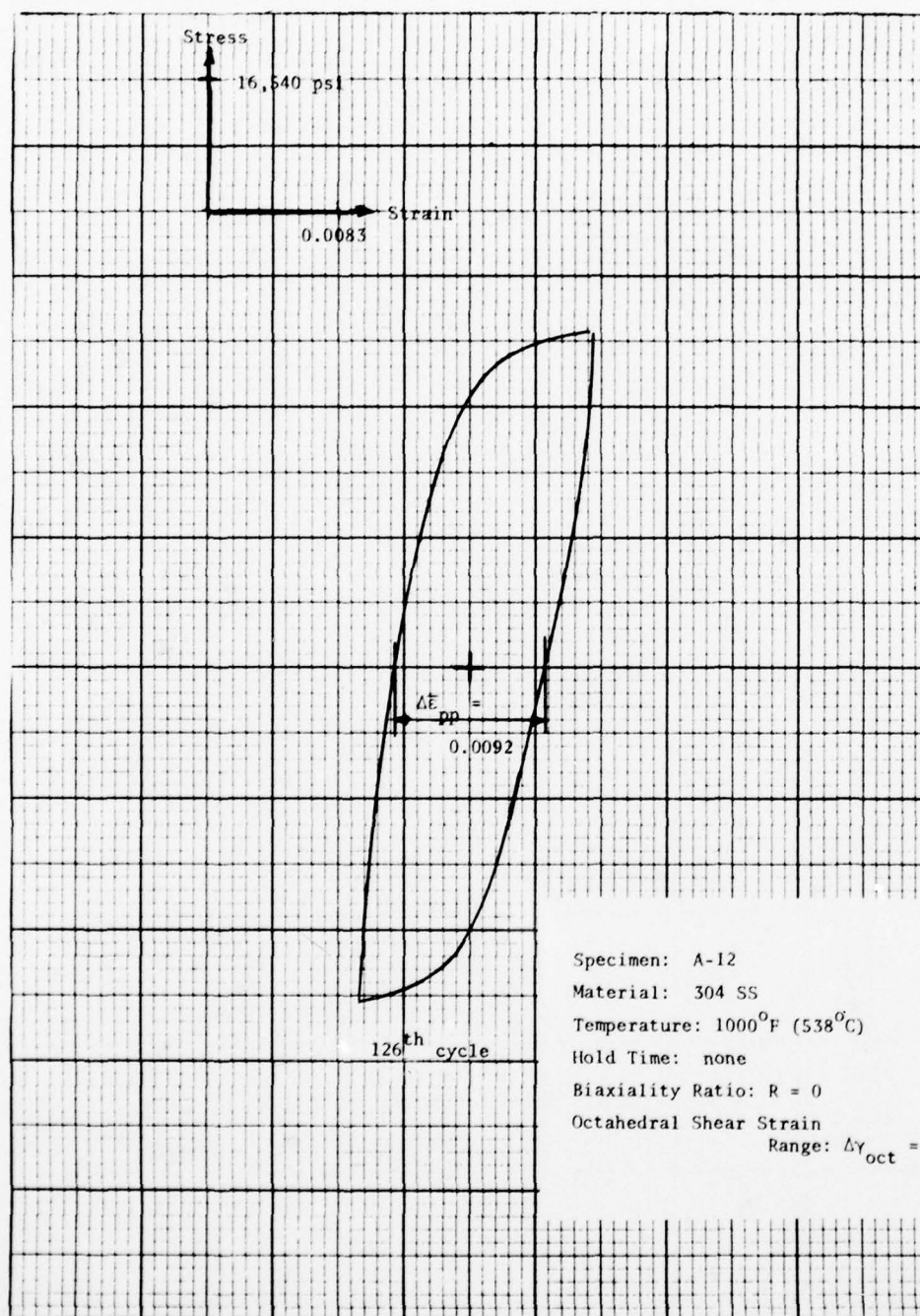
Test Temp. [°F (°C)]	Strain Rate min ⁻¹	0.2 % Yield Stress [ksi (MPa)]	Ultimate Strength [ksi (MPa)]	Elongation in 2.375 in (60.3 mm) %	Reduction (a) in Area %	Fracture (b) Ductility %
Room	0.0421	27.4 (189)	78.2 (539)	42.11	75.61	141.10
1000 (538)	0.0421	11.7 (81)	50.5 (348)	21.33	49.50	68.50
1200 (649)	0.0421	10.7 (74)	36.8 (254)	16.30	35.68	44.47

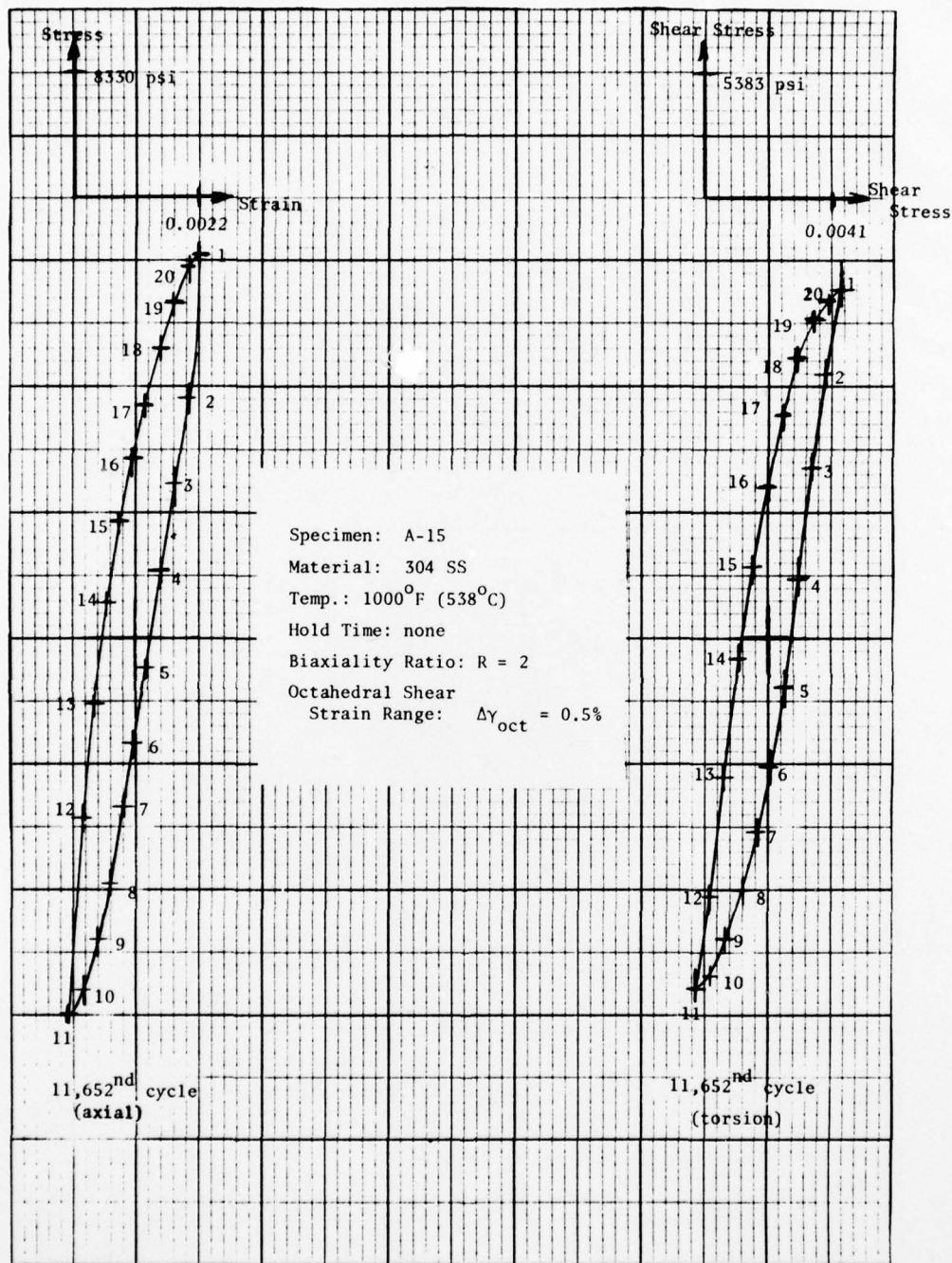
(a) Reduction in area: $RA = (A_i - A_f)/A_i$, where A_i is initial area A_f is final area.

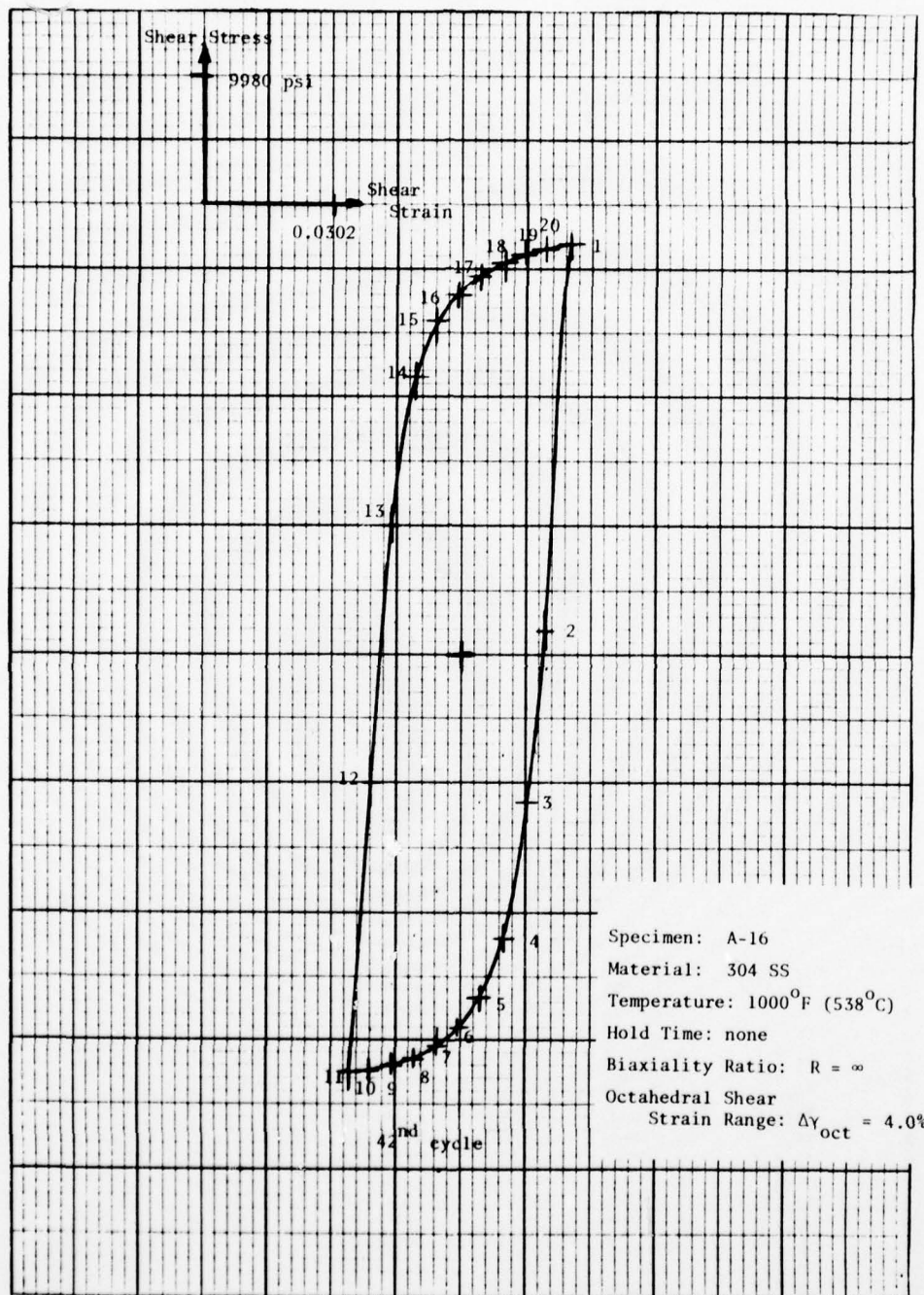
(b) Fracture ductility: $FD = \ln 1/(1-RA)$.

Table 3

Specimen	Hold Time hrs.	Octahedral Total				$\Delta\bar{\epsilon}_{\%pp}$	F_{pp}	N_{pp}	$\Delta\bar{\epsilon}_{\%cp}$	F_{cp}	calculated cycles
		Biaxiality Ratio	Shear Strain Range %	Inelastic Strain Range %	N_f						
A-7	none	0	2.0	0.950	240	0.950		240			
A-8	none	0	1.0	0.350	1400	0.350		1400			
A-9	none	0	0.5	0.140	6944	0.140		6944			
A-12	none	0	2.0	0.920	258	0.920		258			
A-13	none	2	1.0	0.352	1392	0.352		1392			
A-14	none	2	2.0	0.960	428	0.960		428			
A-15	none	2	0.5	0.113	14184	0.113		14184			
A-5	none	∞	2.0	0.896	4092	0.896		4092			
A-6	none	∞	0.67	0.187	85088	0.187		85088			
A-16	none	∞	4.0	2.050	754	2.050		754			
N-1	1.0	0	2.0	0.935	38	0.858	0.918	300	0.0765	0.082	4
N-5	1.0	0	1.0	0.377	96	0.333	0.884	1600	0.0435	0.116	12
N-9	10.0	0	2.0	1.051	17	0.956	0.910	230	0.0945	0.090	2
N-2	1.0	2	2.0	0.740	47	0.676	0.914	420	0.0640	0.086	5
N-6	1.0	2	1.0	0.316	134	0.277	0.877	2200	0.0390	0.123	17
N-10	10.0	2	2.0	0.942	23	0.851	0.903	300	0.0913	0.097	2
N-3	1.0	∞	2.0	0.900	396	0.815	0.905	4800	0.0850	0.094	40
N-4	1.0	∞	4.0	2.383	130	2.238	0.939	680	0.1450	0.061	10
N-8	0.1	∞	1.0	0.360	5060	0.327	0.908	52000	0.0330	0.092	544







Calculations for Effective Hysteresis Loop
Specimen: A-15 (R = 2)

Pt. No.	τ_{xy}	γ_{xy}	σ_x	ϵ_x	$\bar{\sigma}_e$	$\bar{\epsilon}_e$
1	14,908	0.002315	25,410	0.001155	36,230	0.001764
2	11,302	0.001852	16,080	0.000924	25,332	0.001411
3	7,270	0.001389	10,330	0.000693	16,282	0.001059
4	2,583	0.000926	4,415	0.000462	6,285	0.000706
5	-2,153	0.000463	-2,000	0.000231	-4,231	0.000353
6	-5,651	0.000000	-7,080	0.000000	-12,080	0.000000
7	-8,342	-0.000463	-11,330	-0.000231	-18,362	-0.000353
8	-10,980	-0.000926	-16,329	-0.000462	-25,066	-0.000706
9	-12,917	-0.001389	-20,078	-0.000693	-30,060	-0.001059
10	-14,478	-0.001852	-23,577	-0.000924	-34,420	-0.001411
11	-15,000	-0.002315	-25,400	-0.001155	-36,333	-0.001764
12	-11,033	-0.001852	-11,997	-0.000924	-22,564	-0.001411
13	-5,920	-0.001389	-4,500	-0.000693	-11,197	-0.001059
14	-969	-0.000926	2,249	-0.000462	-2,806	-0.000706
15	2,906	-0.000463	7,665	-0.000231	9,170	-0.000353
16	6,351	0.000000	11,830	0.000000	16,154	0.000000
17	9,526	0.000463	15,329	0.000231	22,521	0.000353
18	11,948	0.000926	19,245	0.000462	28,261	0.000706
19	13,670	0.001389	22,410	0.000693	32,600	0.001059
20	14,424	0.001852	24,576	0.000924	35,046	0.001411

$$\text{Equations: } \bar{\sigma}_e = (\sigma_x^2 + 3\tau_{xy}^2)^{0.5}$$

$$\bar{\epsilon}_e = (\epsilon_x^2 + \gamma_{xy}^2/3)^{0.5}$$

Calculations for Effective Hysteresis Loops
Specimen: A-16 (R = ∞)

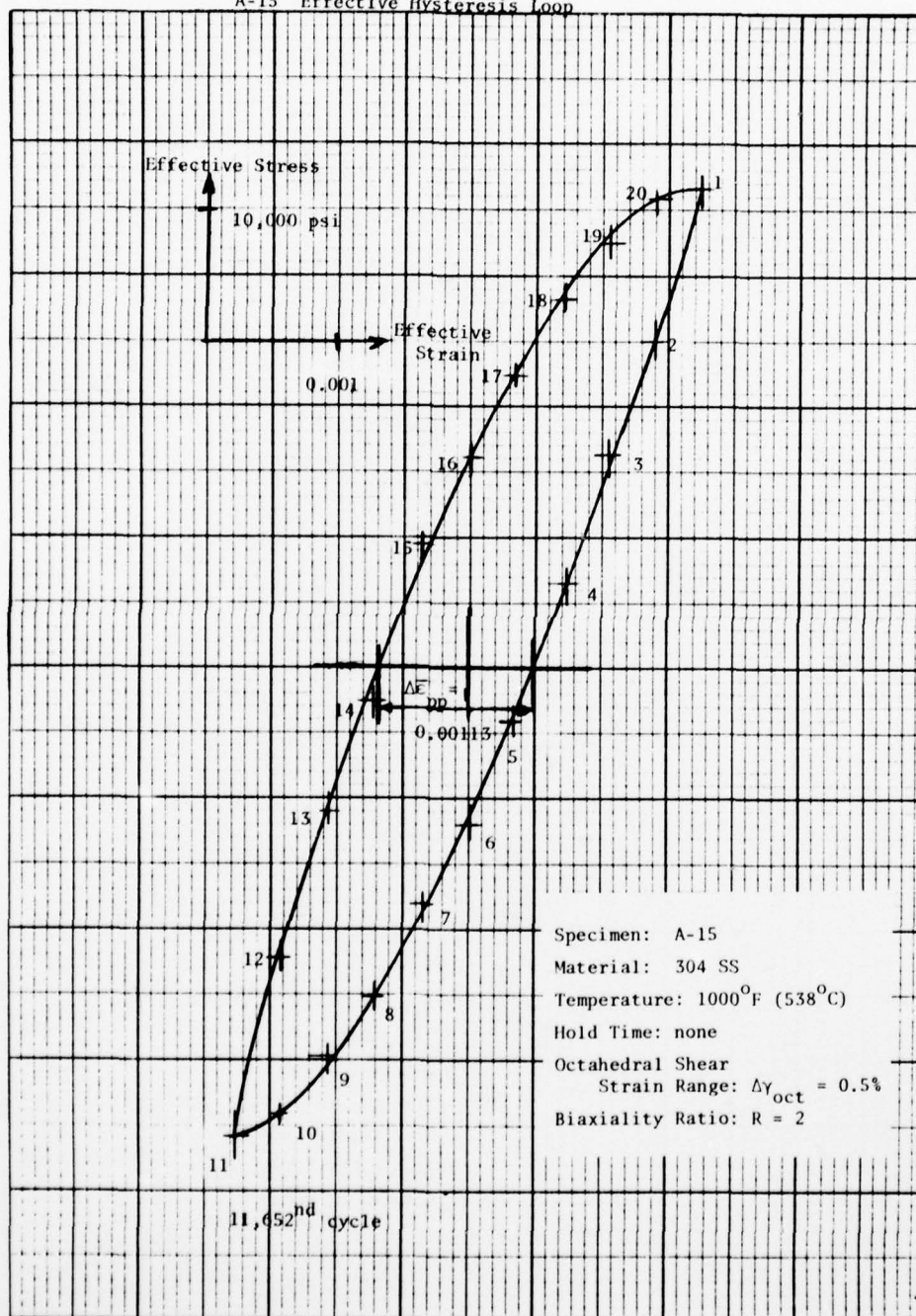
Pt. No.	τ_{xy}	γ_{xy}	$\bar{\sigma}_e$	$\bar{\epsilon}_e$
1	31,933	0.024495	55,310	0.01414
2	1,996	0.019596	3,457	0.01131
3	-11,477	0.014697	-19,879	0.00848
4	-21,954	0.009798	-38,025	0.00566
5	-26,444	0.004899	-45,802	0.00283
6	-28,938	0.000000	-50,122	0.00000
7	-30,435	-0.004899	-52,715	-0.00283
8	-31,435	-0.009798	-54,447	-0.00566
9	-31,933	-0.014697	-55,309	-0.00848
10	-31,947	-0.019596	-55,334	-0.01131
11	-32,431	-0.024495	-56,172	-0.01414
12	-9,979	-0.019596	-17,284	-0.01131
13	9,979	-0.014697	17,284	-0.00848
14	21,467	-0.009798	37,182	-0.00566
15	25,945	-0.004899	44,938	-0.00283
16	27,941	0.000000	48,395	0.00000
17	29,439	0.004899	50,989	0.00283
18	30,435	0.009798	52,715	0.00566
19	30,936	0.014697	53,583	0.00848
20	31,438	0.019596	54,452	0.01131

Equations:

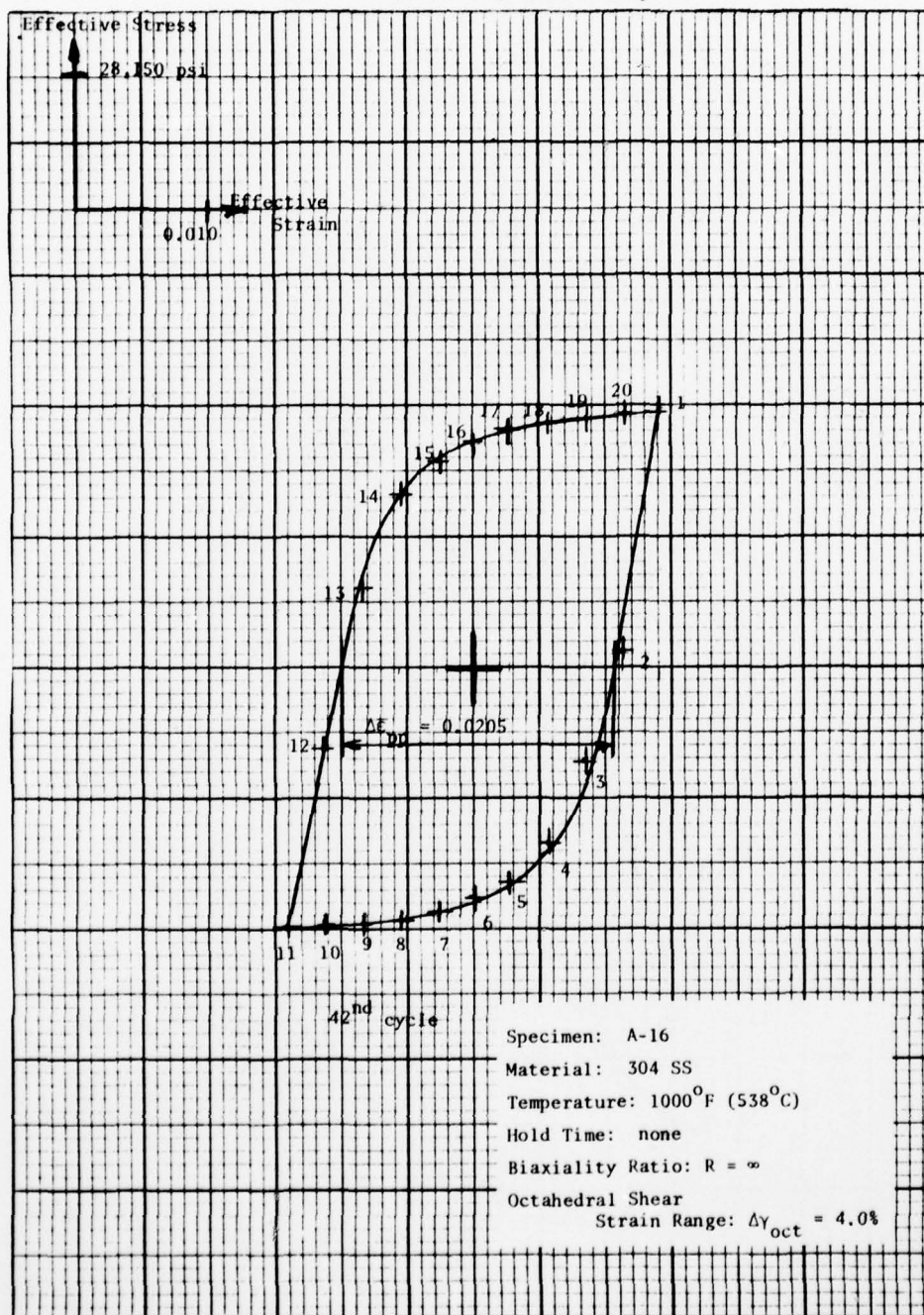
$$\bar{\sigma}_e = \sqrt{3}\tau_{xy}$$

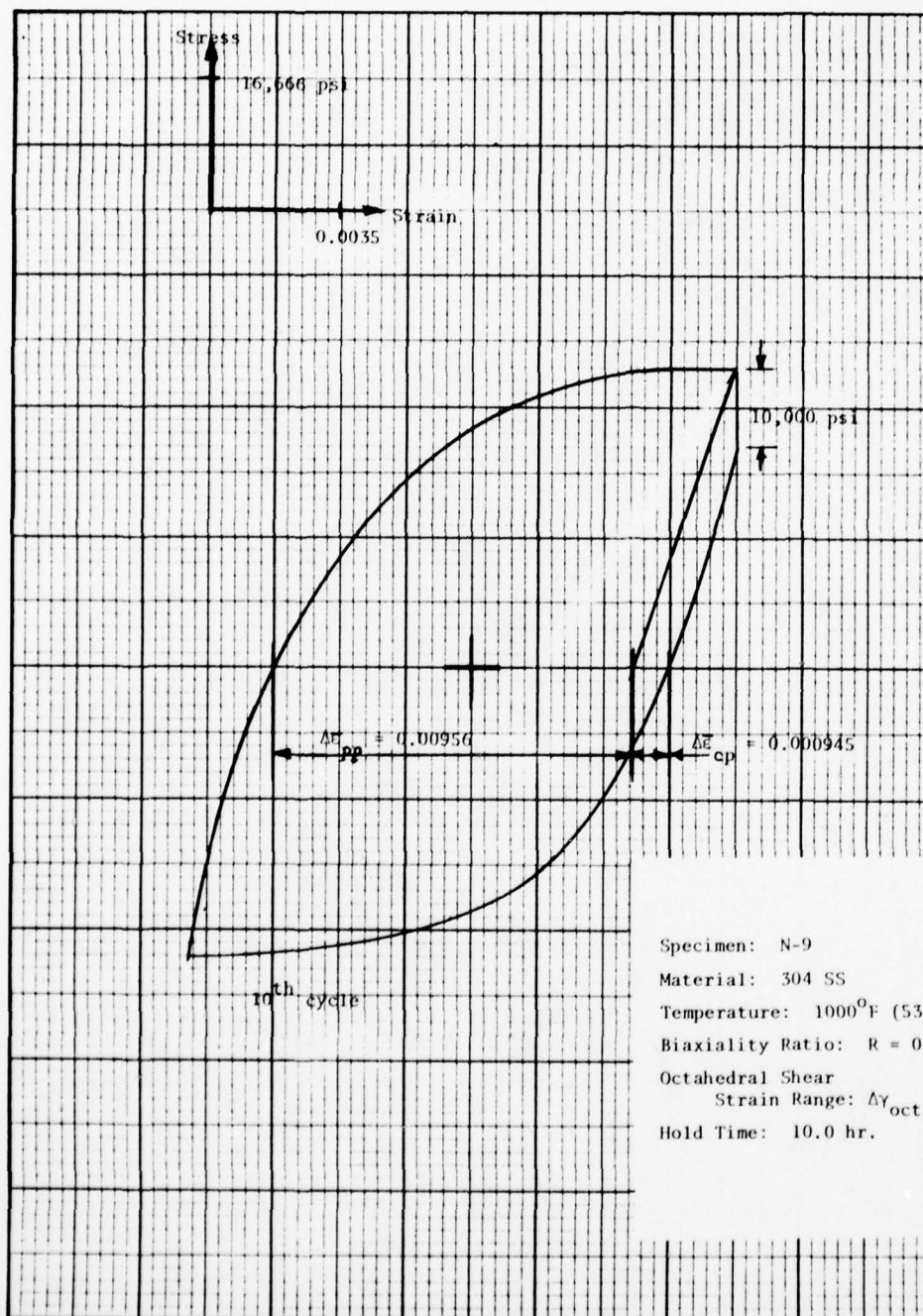
$$\bar{\epsilon}_e = \gamma_{xy}/\sqrt{3}$$

A-15 Effective Hysteresis Loop



A-16 Effective Hysteresis Loop





AD-A059 900

ADVISORY GROUP FOR AEROSPACE RESEARCH AND DEVELOPMENT--ETC F/G 11/6
CHARACTERIZATION OF LOW CYCLE HIGH TEMPERATURE FATIGUE BY THE S--ETC(U)
AUG 78

UNCLASSIFIED

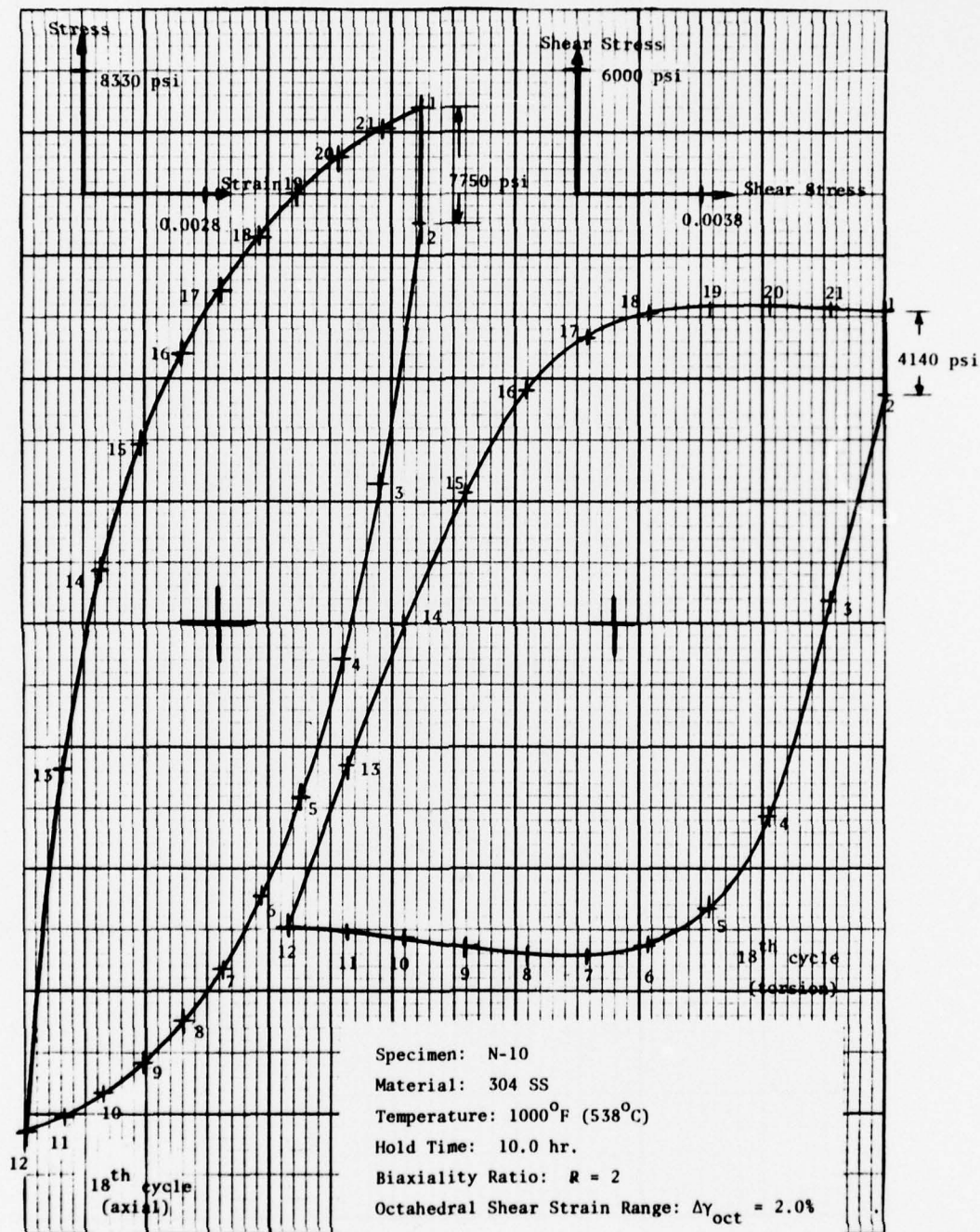
AGARD-CP-243

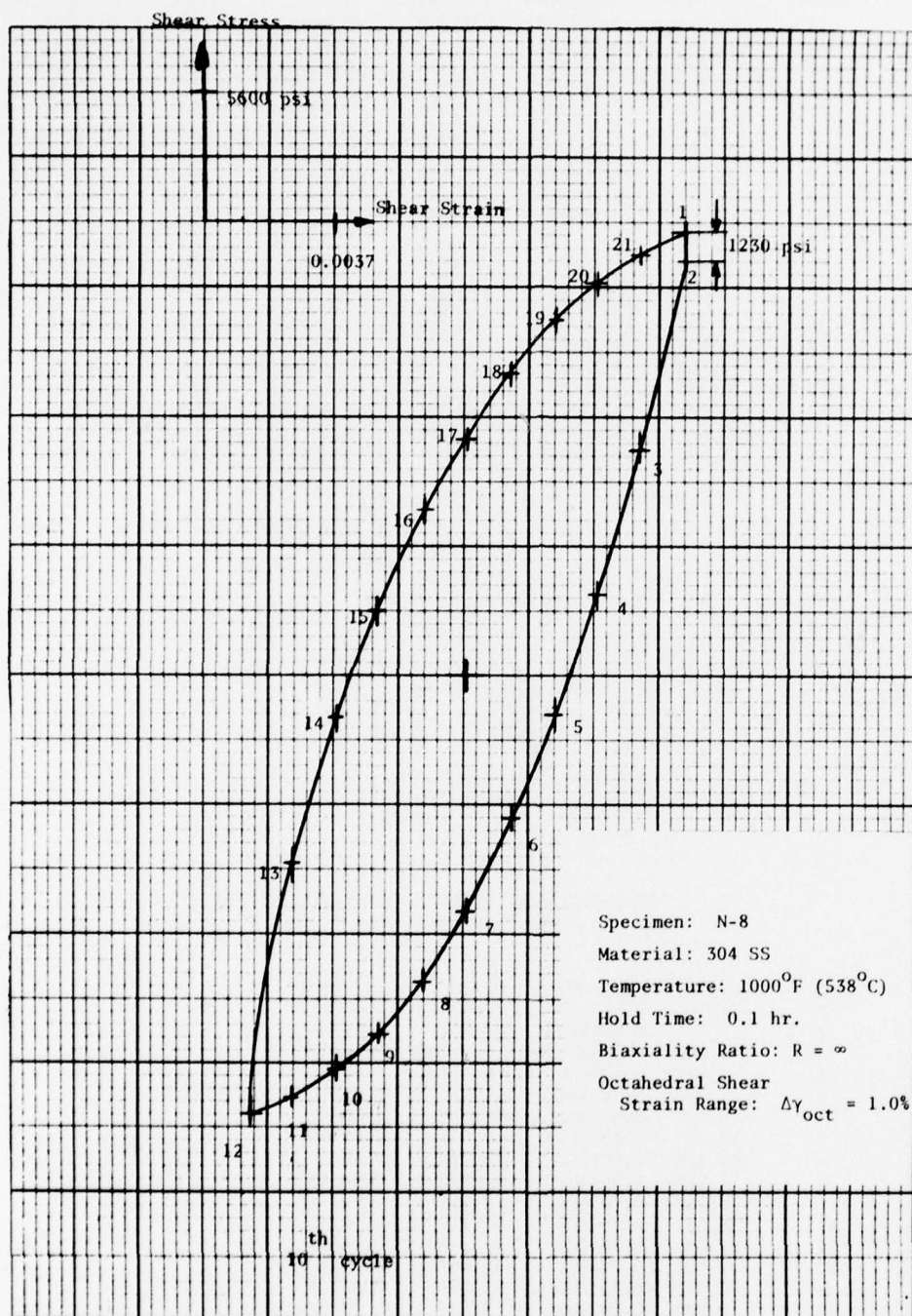
NL

4 OF 4
AD
A059900



END
DATE
FILMED
12-78
DDC





Calculations for Effective Hysteresis Loop

Specimen: N-10 (R = 2)

Pt. No.	τ_{xy}	γ_{xy}	σ_x	ϵ_x	$\bar{\sigma}_c$	$\bar{\epsilon}_c$
1	15,600	0.009272	35,000	0.004508	44,220	0.00700
2	11,280	0.009272	27,100	0.004508	33,410	0.00700
3	1,080	0.007418	9,330	0.003606	9,520	0.00560
4	-9,360	0.005563	-2,500	0.002705	-16,400	0.00420
5	-13,680	0.003709	-11,830	0.001803	-26,500	0.00280
6	-15,600	0.001854	-18,660	0.000902	-32,840	0.00140
7	-16,200	0.000000	-23,490	0.000000	-36,600	0.00000
8	-16,080	-0.001854	-27,160	-0.000902	-38,900	-0.00140
9	-15,720	-0.003709	-30,000	-0.001803	-40,510	-0.00280
10	-15,360	-0.005563	-32,070	-0.002705	-41,670	-0.00420
11	-15,000	-0.007418	-33,700	-0.003606	-42,550	-0.00560
12	-14,760	-0.009272	-34,800	-0.004508	-43,181	-0.00700
13	-7,080	-0.007418	-10,160	-0.003606	-15,900	-0.00560
14	0	-0.005563	3,500	-0.002705	3,500	-0.00420
15	6,300	-0.003709	12,100	-0.001803	16,300	-0.00280
16	11,580	-0.001854	18,330	-0.000902	27,200	-0.00140
17	14,160	0.000000	22,660	0.000000	33,400	0.00000
18	15,360	0.001854	26,320	0.000902	37,400	0.00140
19	15,600	0.003709	29,000	0.001803	39,600	0.00280
20	15,600	0.005563	31,500	0.002705	41,500	0.00420
21	15,600	0.007418	33,650	0.003606	43,200	0.00560

Equations:

$$\bar{\sigma}_c = (\sigma_x^2 + 3\tau_{xy}^2)^{0.5}$$

$$\bar{\epsilon}_c = (\epsilon_x^2 + \gamma_{xy}^2/3)^{0.5}$$

Calculations for Effective Hysteresis Loop

Specimen: N-8 (R = ∞)

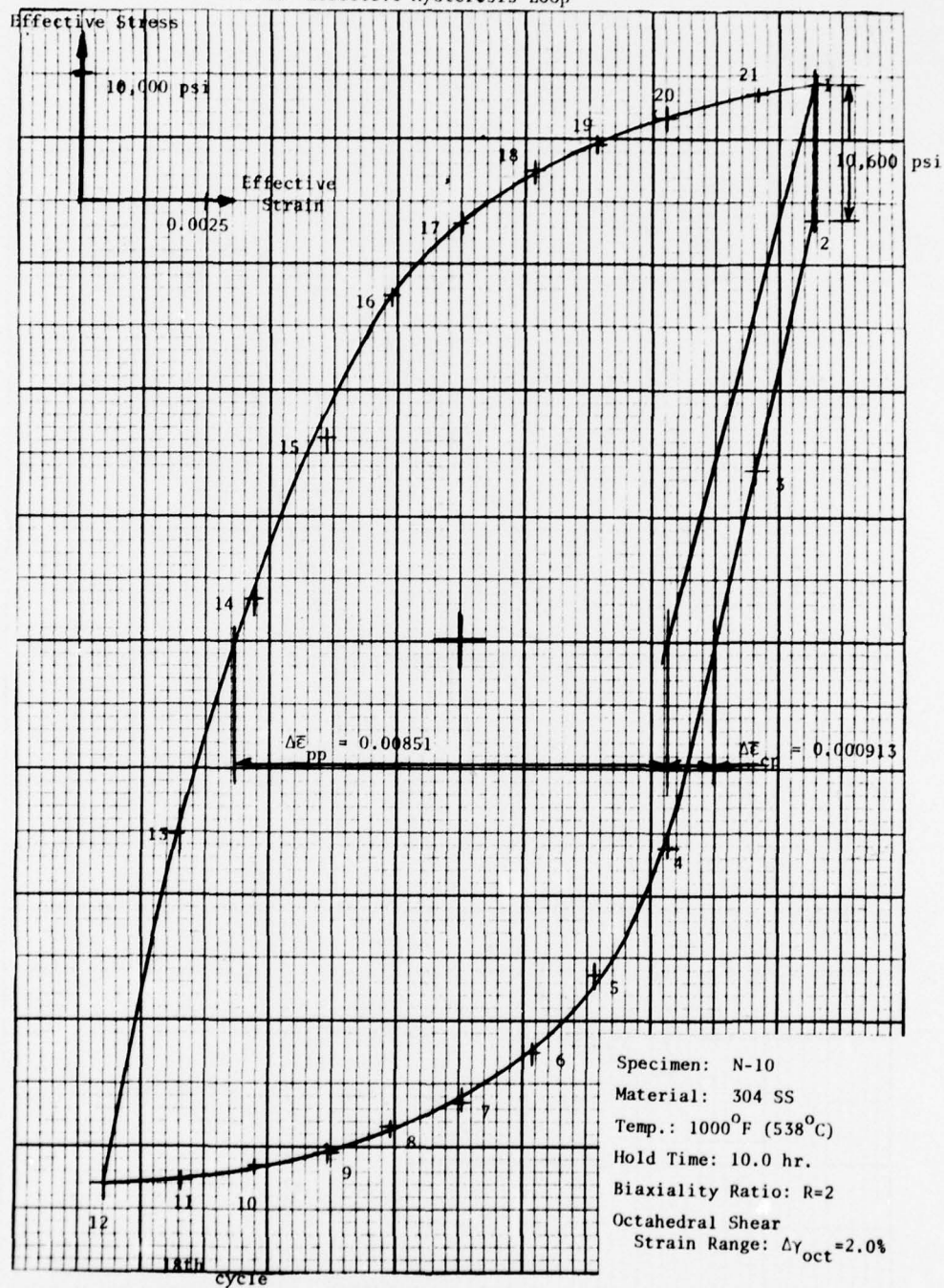
Pt. No.	τ_{xy}	γ_{xy}	$\bar{\sigma}_c$	$\bar{\epsilon}_c$
1	19,040	0.006160	32,980	0.00356
2	17,920	0.006160	31,039	0.00356
3	9,800	0.004928	16,974	0.00285
4	3,472	0.003696	6,014	0.00213
5	-1,680	0.002464	-2,910	0.00142
6	-6,160	0.001232	-10,670	0.00071
7	-10,192	0.000000	-17,653	0.00000
8	-13,328	-0.001232	-23,085	-0.00071
9	-15,568	-0.002464	-26,965	-0.00142
10	-17,080	-0.003696	-29,583	-0.00213
11	-18,368	-0.004928	-31,814	-0.00285
12	-19,040	-0.006160	-32,978	-0.00356
13	-8,120	-0.004928	-14,064	-0.00285
14	-1,792	-0.003696	-3,104	-0.00213
15	2,800	-0.002464	4,850	-0.00142
16	7,280	-0.001232	12,609	-0.00071
17	10,192	0.000000	17,653	0.00000
18	12,993	0.001232	22,503	0.00071
19	15,400	0.002464	26,674	0.00142
20	16,912	0.003696	29,292	0.00213
21	18,032	0.004928	31,232	0.00285

Equations:

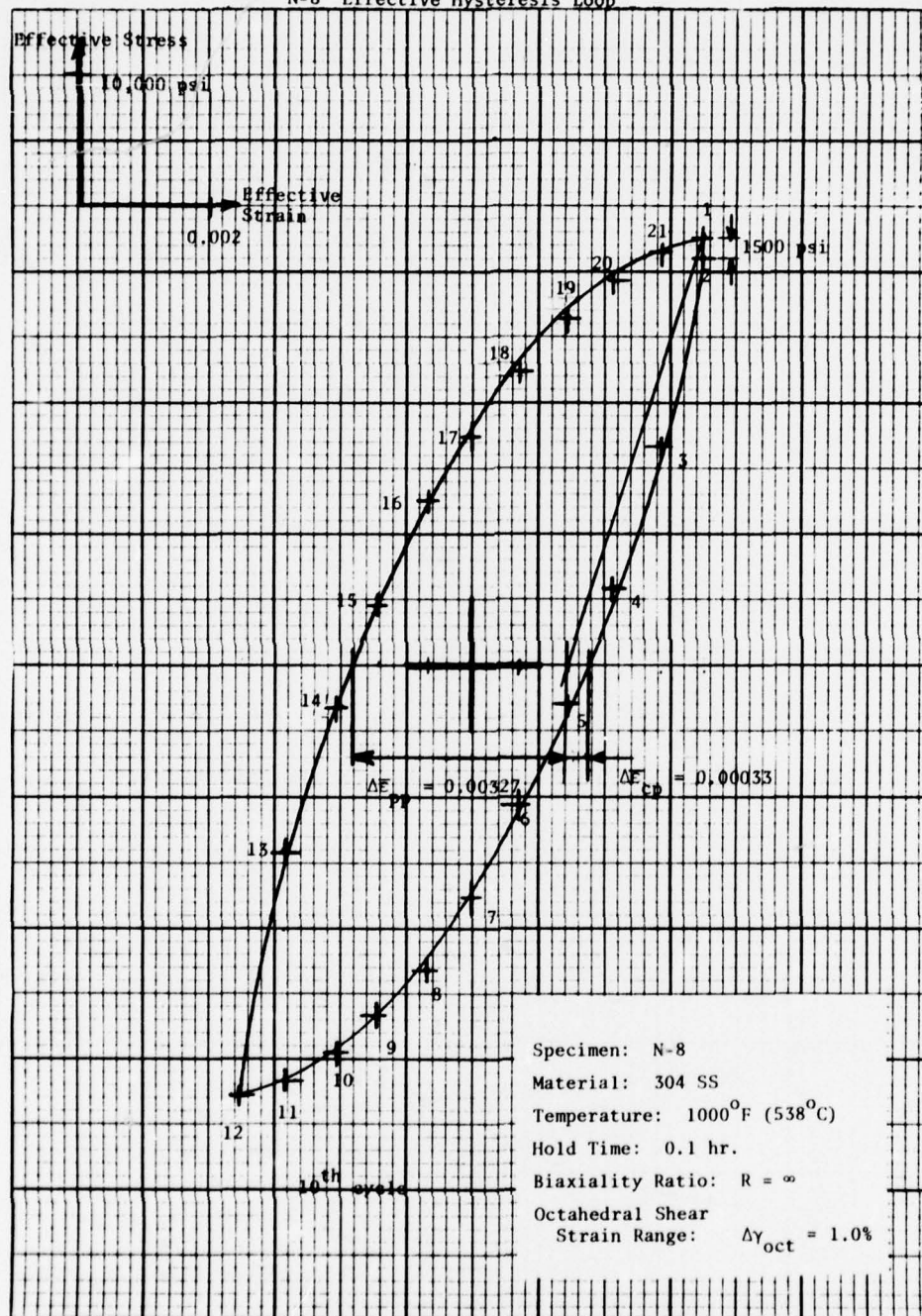
$$\bar{\sigma}_c = \sqrt{3}\tau_{xy}$$

$$\bar{\epsilon}_c = \gamma/\sqrt{3}$$

N-10 Effective Hysteresis Loop



N-8 Effective Hysteresis Loop



DISCUSSION SUMMARY OF SESSION III

By

Gary R. Halford
 NASA-Lewis Research Center
 Cleveland, Ohio USA

If one were to identify the unifying characteristics of the papers presented in Session III, two features would stand out----the diversity of the properties of the materials studied and most importantly the authors' perseverance in dealing with complicating factors. Because of the individual nature of each material or the loading system (multi-axial) involved, it was necessary in each instance for the investigators to be motivated to find ways around complications as they arose.

In the opening paper, Mr. Stentz demonstrated his resourcefulness in the determination of the SRP life relationships for two copper-base alloys. The alloys possess extremely high thermal conductivity, high ductility, and reasonably high strength, making them ideally suitable for liners in reusable, regeneratively cooled rocket nozzles. In that capacity, the alloys would undergo severe thermal fatigue strain cycles with strain-ranges on the order of 2%. At this straining level, strain hold time tests could not impart enough creep strain for the tests to be considered valid as characterization tests, and because of the alloys cyclic strain softening behavior, conventional stress hold tests were not practical. Creep was thus introduced by means of slow straining rates. An indirect technique for partitioning the creep and plastic strains was established which then permitted the SRP life relationships to be determined by a trial and error process. The success of this innovative procedure was demonstrated by the fact that the lives of constant strain hold time tests could be predicted quite accurately from the established life relationships. Accurate life predictions were also made for tests with intermediate straining rates. The CP type deformation was shown to be extremely damaging for these materials.

Dr. Nowack representing DFVLR elected to determine the SRP behavior of titanium 6Al-4V, an alloy well suited for gas turbine engine compressor blades because of its low density, high strength, and moderate stiffness. At its normal use temperature, this alloy experiences only minute amounts of creep for the use times of concern. Hence, to study the alloy's creep-fatigue behavior, it was necessary to conduct tests at temperatures above the conventional use temperature. Determination of the four SRP life relationships was thus possible without having to resort to extremely long (and thus prohibitive) test times. Hastening of the tests by conducting them at higher temperatures could be justified by the fact that the tensile ductility was not a function of the elevated temperature of testing. However, at the longest test time considered, (1100 hours) there was evidence of a detrimental change in the microstructure which corresponded to a detrimental effect on cyclic life that would not have been anticipated on the basis of shorter time test results. Whether the DN-SRP life relations could have been used to anticipate this behavior was not determined because of the lack of creep-rupture ductility information at the longer test times. Overall, the SRP method was capable of characterizing and predicting the high-temperature creep-fatigue behavior of titanium 6Al-4V to within approximately factors of two in cyclic life. However, the effect on cyclic life of type of cycle was not a very large one. In fact, the PC type cycle gave the lowest life (lower than PP by factor of 2 to 5 in cyclic life). Since the PC cycle had a higher tensile mean stress than the other cycles involving creep, Dr. Nowack emphasized this as a possible cause for the shortest lives. Certainly, a systematic study is called for which can separate the effects of strain type and mean stress.

Perhaps it was Dr. Ellison of the University of Bristol who demonstrated the greatest degree of ingenuity in the use of SRP to characterize the behavior of a 1 Cr-Mo-V steel. This heat of material exhibited a sharply defined ductile-brittle transition in its creep-rupture ductility at a creep rupture stress of 245 MN/m². Curiously, the transition seemed to occur independently of prior history of deformation. Creep-rupture ductility dropped from about 0.8 to 0.2, then continued to decrease slowly with decreasing stress and increasing time to rupture. In effect, Dr. Ellison was working with a material whose properties were constantly changing within a certain regime. This changing behavior seemed to affect only the CP strainrange versus life relationship. To make the problem tractable, two CP life relationships were defined; one called the ductile CP life relation and the other the brittle CP life relation. Recognizing that the brittle CP life relation was a function of the hold time, the author devised a procedure for factoring this time effect into account. Once the SRP life relations had been determined, they were used quite successfully to predict the cyclic lives of specimens subjected to complex strain cycles.

Note was made of the modes of cracking: PP and PC tests gave rise to transgranular cracking only, whereas CP cracking was almost entirely intergranular and CC cracking was partially intergranular and transgranular.

An item of concern was the interpretation of the inelastic strain accompanying the very rapid initial drop in stress during the strain hold time tests. From the standpoint of damage, Dr. Ellison suggested that the initial rapidly obtained strain should probably not be considered as creep strain. This item was the only one to come up in the open discussion reserved for Session III. Professor Manson pointed out that he and his colleagues had puzzled over the problem a few years ago and had made two recommendations as to how to deal with this behavior. There were brought out in Professor Manson's

opening paper. Of the two approaches, Dr. Ellison strongly urged that the simplest one be adopted.

In the final paper, Professor Zamrik reminded us that nearly every piece of hardware in service has some degree of biaxiality of stress and strain that creates a need for rules on how to deal with this complicating aspect of low cycle fatigue. The central issue is how to use uniaxial behavior to predict multiaxial lives. Using a combined tension-torsion testing machine, Professor Zamrik and his students at the Pennsylvania State University have generated creep-fatigue data in an attempt to uncover problems and point to solutions to those problems which might be peculiar to the application of SRP to biaxial loading. In this respect, the program was highly successful. Useful rules have been proposed for generalizing uniaxial SRP properties to cover any degree of multiaxial cyclic loading, provided the loading is of a proportional nature. Zamrik's SRP results on type 304 austenitic stainless steel tested under torsional loading have been used to verify the applicability of the proposed rules.

Discussion of the papers in Session III was exceptionally brief (being limited to the complimentary dialogue between Professors Manson and Ellison as noted above) owing to the press of the time schedule and the fact that the meeting attendees were anxious to begin the more general discussion of the entire Conference which was scheduled to follow immediately thereafter.

FINAL DISCUSSION SUMMARY

by

J. M. Drapier

FN. Formetal

Division of FN Herstal

B-4400 Herstal

Belgium

Dr. N. M. TALLAN, Chairman (AFML, USA)

In contrast to the discussions of the previous sessions, which we have tried to limit to questions of clarification or questions which were primarily addressed to the content of the immediate papers presented, we will now discuss somewhat more general questions, looking at all of the papers that have been presented as a whole. What are the particular advantages of applying strainrange partitioning, taking into account the results obtained on a variety of different materials under a variety of different test techniques? At the same time, what are the general difficulties that have been encountered? What might we anticipate as the general difficulties that remain to be overcome? Are there classes of materials and applications where perhaps we would anticipate difficulties in using the strainrange partitioning method? Generalizing upon what we have seen, are there factors, such as states of stress or dynamic environmental interactions and so on that have not adequately been taken into account?

Also, in the original scope of this study, which I believe has been one of the best that this Panel has undertaken in a cooperative testing programme, each participant has been asked to compare the strainrange partitioning technique to the techniques that he has used in the past and that he is familiar with. We may therefore ask:

- How does the strain range partitioning technique compare to other techniques?
- What are its specific advantages or disadvantages?
- Are there important gaps at this point in our understanding of this approach that might be addressed in future activities of this panel?

Mr. R. H. STENTZ (MAR-TEST, U.S.A.)

I would like to comment on the use of SRP for nickel-base superalloys, in relation to several impressions that I have received.

First, there seems to be some scatter in the data, one of the reasons for this scatter obviously being the inability to measure or to account for the small inelastic strains.

Also, the strainrange partitioning lines seem to lie very close together. In fact, in some cases, they could be collapsed into one line and in other cases, various investigators have had different orderings of these lines.

In addition, the calculations can cause difficulties; investigators encounter negative numbers and they don't know what to do with them.

It just seems to me, that in talking about a modified strainrange partitioning technique to accommodate these problems, we have to take into account the fact that other techniques or other correlations actually seem to be simpler and work a little better. One of these is the simple stress correlation.

Prof. S. S. MANSON (Case Western Reserve University, USA)

I think one of the points that has not been brought out at this conference, and which relates to the questions that Dr. STENTZ raised, is the usefulness of SRP in establishing bounds rather than accurate quantitative information.

Attempting to push the application of SRP in all cases to a quantitative level is, first, not justified and, second, not even desirable because the real merit of SRP, I think, is to give you a bound of lower life and a bound of upper life for a particular type of application.

It tells you the kind of test that you likely need in order to get lower and upper bounds. If you attempt to run tests PP and CP or the other strainranges, you immediately determine which is the most damaging and which is the least damaging.

If there are all about equally damaging, I would say that the tests are giving you a very valuable result in that they tell you there will not be a big effect of different types of histories. You can use the lower bound life line, whether is PP, CP or PC, to design in the simplest possible way.

In other words, you apply SRP in connection with that lower bound life and get a life that is probably going to be as accurate as you can ever get, considering material variability in the first place and other complications that come about by attempts to make more quantitative computations.

So, I think you are right in that in connection with nickel-base superalloys, where the life lines are almost about the same, the best use of SRP is to tell you which of those lines is likely to be a lower bound and then design to that. I do however take exception with you, in your comment that other methods have been found to be good. I think that you would be in considerable trouble in trying to apply the time-and-cycle fraction to some of these complex superalloys where we have trouble in applying SRP.

I have personal experience with a few applications in which life values vary by factors of 5 on the unconservative side, and 20 or more on the conservative side, and I would never regard the time-and-cycle fraction to be good approach to the problem.

The other aspect of the nickel-base superalloys is that we obviously have materials in which two other phenomena, that have been brought out at this conference, are important compared to the stainless steels and low alloy steels that we have experience with.

One of them is the separation of the initiation from the propagation phase. For the materials that we have a lot of experience in the past, the AISI 316 and 304, the 2 1/4 Cr and 1 Cr - 1 Mo steels, etc ..., it did not matter very much if we separate initiation from propagation.

We got very good results in establishing the life values. When we consider the nickel-base superalloys which may have a very low fracture toughness, as Dr. HALFORD already mentioned, and where the development of even the tiniest crack may cause the end of the fatigue test, it becomes very important to separate these two phases from each other.

Furthermore, we have not had experience in such problems before, nor have other method had been used to get such experience.

The other problem is the mean stress effect. Again, in other earlier studied materials, mean stress was a relatively minor factor. It did not override the difference of effect of the nature of the strain : CP in AISI 316 stainless is so much more damaging than PC that, even in the presence of a beneficial compressive stress, it still remains the most damaging type of strain.

But for nickel-base superalloys where the SRP lines come closely together, one produces a tensile mean stress and the other produces a compressive mean stress; then, you may get an apparent inversion of life relationship, but not because PC is really more damaging than CP but because PC is associated with a tensile mean stress.

So, to answer D. TALLAN'S request : where do we go from here ? I would say this conference has brought to the floor at least these two major questions that we need to resolve in the future in relation to the type of alloys most applicable in connection with gas turbine applications. But still, a positive note in relation to SRP : once you run the SRP life lines and you establish that there is not much difference among them, I certainly would not try to split hairs; I would design to the lowest of these lines and by-pass the whole problem. So, SRP has told me which one of the life lines is the most damaging and it guided me in making the choice of which should be the design life.

Dr. J. L. CHABOCHE (ONERA, France)

Je voudrais donner quelques détails sur la technique illustrée à la Fig. A0 et développée à l'ONERA de manière à prendre en compte les effets de cumulation non linéaire d'endommagement par fatigue et fluage.

Dans certains cas, la méthode SRP ne permet pas de traduire complètement tous les effets possibles de la contrainte moyenne. Une solution serait donc de les prévoir dès la détermination du modèle d'endommagement par fatigue. Ainsi, la durée de vie en fatigue dépend en partie de la contrainte moyenne, ce qui peut se traduire par un terme qui tient compte de l'effet des contraintes moyenne et maximale .

A titre d'exemple, la fig. 19 de mon exposé montre les résultats d'essais de fatigue pure réalisés, sur l'alliage IN-100, à diverses températures comprises entre 700 et 1000°C et à la fréquence de 5Hz, la contrainte moyenne étant nulle (essais à mise-en-charge alternée) ou non. A partir des courbes donnant le nombre de cycles à rupture en fonction de la contrainte maximale, il est possible de déduire l'influence de la contrainte moyenne pour ensuite l'inclure dans le modèle de fatigue

Par ailleurs, pour illustrer les effets de cumulation non linéaire d'endommagement, nous avons mis en évidence que dans les essais de fatigue à contrainte imposée, l'endommagement évolue plus vite lorsque le niveau de contrainte est plus élevé (Fig. A1). A partir de ces courbes, le schéma de la Fig. A2 montre l'effet de cumulation non linéaire, dans le cas d'essais à contrainte imposée à deux niveaux, le premier niveau de contrainte étant le plus élevé (N1 et N2 sont les nombres de cycles effectués respectivement au 1^o et au 2^o niveau de contrainte)

Au moyen d'une loi d'évolution de l'endommagement, telle que celle illustrée à la Fig.20 de mon exposé, on peut prévoir un tel effet comme le montrent des confrontations avec des essais à deux niveaux, en contrainte alternée (valeur moyenne nulle) ou en contrainte ondulée, c'est à dire en présence d'un effet de "rochet".

CONTINUOUS DAMAGE APPROACH

DAMAGE STATE PARAMETER D:

$D = 0 \longrightarrow$ Undamaged

$D = 1 \longrightarrow$ Rupture (Macroscopic crack)

EFFECTIVE STRESS CONCEPT:

$$\sigma_{\text{eff}} = \frac{\sigma}{1-D}$$

CREEP - FATIGUE SEPARATION

$$dD = f(\sigma, T, D) dt + g(\sigma_M, \bar{\sigma}, T, D) dN$$

↓
CREEP

time dependant

intercrystalline
microcracks

↓
FATIGUE

cycle dependant

transcrystalline
microcracks

Fig. A0 : The continuous Damage approach developed at ONERA

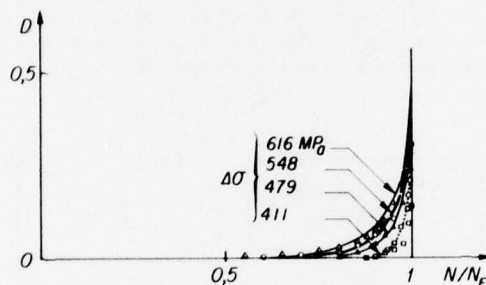


Fig. A1 : Fatigue damage evolution as measured in the pure fatigue tests (5 Hz; load control) for IN-100 at 1000°C

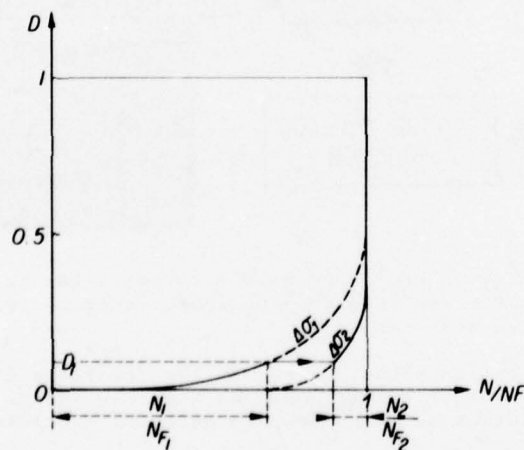


Fig. A2 : Schematic of the non-linear cumulative effect observed in the two-levels fatigue tests (high to low sequence)

Prof. S. S. MANSON

In considering cumulative fatigue damage, I think a very important distinction needs to be made between what happens within a single hysteresis loop and what happens into successive hysteresis loops that are not identical.

Normally, we have repetitive cycling resulting in a single hysteresis loop in which there are creep and plastic strains; what we are concerned with is how to combine those in order to find the total damage within that loop. We are having trouble even with that problem in trying to take into account mean stress effects and separation of the initiation and propagation phases.

If I understand Dr. CHABOCHE's procedure, it really refers to successive cycles in which different levels of stress are imposed. We have run, in the past, similar programmes in cumulative fatigue damage in which a number of cycles of high stress was followed by a number of cycles of low stress, or conversely low stress followed by high stress; and we have got these non-linear cumulative effects. We had in fact applied in the past, at first what we called "separation of the fatigue process into initiation and propagation phases" and, later on, re-interpreted the results as a "double linear damage rule": in essence, drawing two straight lines to represent the curves that Dr. CHABOCHE pointed out. More recently, we have been doing more work along that line to characterize the type of results that he showed, quite accurately, by separating out of process into what we call "Phase I" and "Phase II". They are not definitive processes but we recognize that there are two distinctive processes which, if imagined to be present, can predict the results exactly as they have been observed.

So, I can understand the concept that non-linear cumulative damage be applied to successive cycles of unequal magnitude. But I do not know how one would use, within the same hysteresis loop, the combination of mean stress and strain cycling, and call that non-linear, in the sense that has been proposed, because the problems we are facing are with a single repetitive loop.

Dr. J. L. CHABOCHE

Comme l'illustre la Fig. A3, l'équation d'évolution de l'endommagement est séparée en deux équations partielles déterminées séparément à la suite d'essais d'une part de fluage et d'autre part de fatigue de base (du type PP).

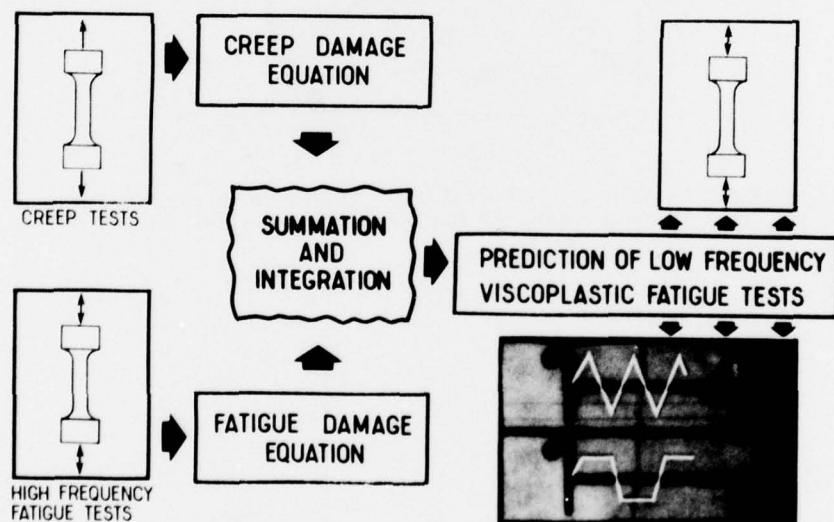


Fig. A3 : Damage summation procedure used to predict the creep-fatigue interaction, under low frequency periodic cycling, from pure creep and pure fatigue test results.

Par intégration, il est possible de prévoir les résultats d'essais de fatigue à cyclage périodique lent (fréquence faible, avec ou sans période de maintien) pour autant que l'on connaisse l'évolution de la contrainte au cours du cycle stabilisé.

La règle de mélange de cumulation conduit à une interaction non-linéaire des termes cumulés de fatigue et de fluage (cfr. Fig. 21 de mon exposé). En fait, l'interaction au cours d'un cycle périodique, est du même type que dans le cas des essais à deux niveaux.

Dans le cas présent, il y a effet de cumulation non-linéaire par suite de la non-unicité des courbes d'évolution du dommage en fonction de t/t_f et de N/N_f ; pour l'alliage IN-100 par exemple, l'évolution en fluage est beaucoup plus rapide qu'en fatigue pure (Fig. A4).

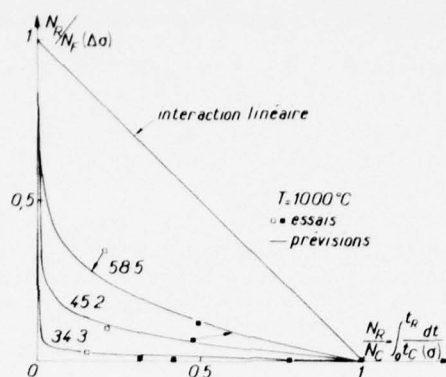


Fig. A4 : The non-linear creep-fatigue interaction observed and predicted for IN-100 at 1000°C.

Dr. G. J. LLOYD (UKAEA, U.K.)

Considering the case of creep-fatigue damage and the question of creep-fatigue interaction, I would like to suggest that the linear damage summation rule is completely inappropriately framed to predict a situation where you have two completely different state variables.

Therefore, from first principles, I think you could imagine that you have quite good grounds for not expecting good predictive or correlation abilities.

In the physical sense, you could understand this because the fatigue process implies the mechanism of crack propagation and the creep part is either dislocation creep or the production of grain boundary cavitations. So, I am suggesting that any agreement between creep-fatigue life and the linear damage summation rule may be fortuitous unless the N/N_f or t/t_f fraction independently approach one but not as a sum.

Dr. J. L. CHABOCHE

Les deux phénomènes de fluage et de fatigue sont distincts mais se manifestent simultanément, ce qui se traduit par la coexistence de fissures inter-et trans-granulaires. Dans notre approche, nous considérons que la fissuration intercrystalline due au fluage interagit avec la fissuration transcrystalline qui correspond surtout à la propagation de fissures le long des joints de grains. Cette interaction entraîne une accélération de la fissuration au cours des cycles successifs.

Je précise bien que cette accélération réciproque est produite par l'addition de deux termes non-linéaires d'endommagement (fatigue et fluage) dans chacun desquels figure explicitement la valeur actuelle de l'endommagement.

Dr. H. NOWACK (DFVLR, Germany)

I would like to ask first what alternative concepts are available to account for the sequence effects and, secondly, is it acceptable to consider that creep and fatigue are somewhat equivalent for nickel-base superalloys, taking into account that the basic SRP curves, plotting the total inelastic strain versus the life, are on one line or in a narrow scatterband?

Mr. M. H. HIRSCHBERG (NASA-LEWIS RESEARCH CENTER, U.S.A.)

As one of the proponents of the SRP method and one of the originators of this AGARD activity, I remind you of the basic objective of this program, namely to determine first, if the SRP method of characterizing the high temperature low cycle fatigue behaviour of materials using simple laboratory specimens can be used to predict the lives of other simple laboratory specimens when subjected to a complex loading cycle. I think that this discussion is now getting into very important but more complex questions. We should eventually discuss them, but I think we have to first address our original objective before we take up these questions.

For example :

- Do you feel this is as good as or a better way for characterizing the low cycle fatigue behaviour of materials at high temperature than you are currently using ?
- Is SRP a good way to correlate low cycle fatigue testing under those conditions ?
- Can SRP be used to extrapolate under those simple conditions on laboratory specimens ?

So, I would suggest we go back to our original objectives in this program and try to address these questions first if we could.

Prof. P. HANCOCK (CIT, U.K.)

We are looking on SRP as a predictive method and obviously what we want to do is some extrapolation. However for the laboratory tests we have done, it is basically interpolation; all the numbers of cycles we are talking about are between 10 and 10^3 - 10^4 and we are actually interpolating within that data. So, I would like to ask, from those who have data from extrapolation, how they find it to work ?

Prof. S. S. MANSON

I did show in this meeting that some data on 2 1/4 Cr - 1 Mo steel, AISI 316 stainless and low alloy steels have been analyzed and in which the 10 to 100 hours data were used to extrapolate to at least of the order of one year, i.e. 8 to 10,000 hours, with relatively good results. So, as much as is available has been looked at and is regarded as quite positive.

In another report I have written for the Oak Ridge National Laboratory, I make an attempt on how to go about predicting cycles by SRP, for hold times that will be very long and in which the life values would be of the order of millions of cycles, i.e. 30 years or more. The procedure is practical but its accuracy has not been established because there are no data.

Prof. P. HANCOCK

Indeed, it has been well demonstrated with solid solution alloys, such as low alloy steels and even hardened stainless steels, where the problem is really one of initiation, that long time predictions are possible.

However, this conference has shown that there are certain differences between the superalloys and the previously studied simpler materials. There is generally a reversal of the SRP lines; the differences may be perhaps between initiation and propagation and in terms of mean stress.

So, I am asking whether anybody has any real extrapolation data for superalloys.

Prof. S. S. MANSON

First, let me add another difference in relation to the question of mean stress. With the PP type of loading for example, you can have zero mean stress, but higher maximum stress than you require for a CC loading. So, let me just mention the additional complication that it is not only mean stress effect but also a maximum stress effect as well. The reason for PP being more damaging than CC or one of the other strainrange types may simply be the fact that, in order to get the same strainrange with PP-type of loading, one must go to a higher stress so that the presence of even a very small crack will already cause the fracture toughness to be exceeded and rapid initiation and onset of fracture.

Now, returning to your question, I doubt that anybody has information of that type. But, let us take a step further since, in this conference, we are evaluating SRP in contrast to other methods :

- Why would other methods not have the same problem ?
- Do they not need to characterize the basic behaviour of the material ?
- Should they not need to know whether the onset of a small crack will cause instantaneous fracture ?
- Do they not need to know everything that we need to know for SRP purposes ?

So, such ambiguities as exist in the application of this method will correspondingly be present in the others and when long time data are available, I am sure they can be used to evaluate alternative methods.

Mr. M.H.HIRSCHBERG

I would like to remind everybody of a secondary objective of this AGARD activity. Besides evaluating SRP, we wanted to generate a reference body of well documented high temperature low cycle fatigue data that others could use for evaluating different predictive methods. For the purpose of aiding in accomplishing this, we designed a data sheet that all the participating laboratories used in order to document the data in the same units and format.

This body of data was collected from each of the laboratories and will be published in the AGARD Report containing all the papers presented at this meeting. For completeness, we are attempting to document for each of the materials tested, the chemical composition, mechanical properties, heat treatment as well as the creep-fatigue including the test parameters such as the frequencies, temperatures, hold times, stresses, strains, and lives.

Dr. H.P. VAN LEEUWEN (NRL, The Netherlands)

I would like to address the question of crack propagation versus crack initiation raised a couple of times during this meeting. I think Prof. MANSON gives an example of the importance of crack propagation in the case of a rather brittle material where even a small crack causes nearly instantaneous fracture.

I would like to take an exception to this statement. It is when crack propagation constitutes a considerable fraction of the total life that you have to consider crack propagation.

In room temperature fatigue, many investigations have been made on crack propagation and many conferences have been held on this topic. Now, we are able to deal with crack propagation at room temperature but with considerable difficulty.

Crack propagation at high temperatures is probably even more difficult to account for but I think there is a way out of this and still you would be able to apply some sort of SRP. Now, a few years ago we have had a High Temperature Fatigue and Creep Conference in Philadelphia, which was repeated at Sheffield, and several papers dealt with crack propagation during high temperature fatigue. It was shown that you could plot crack propagation rate not as a function of the stress intensity factor range but as a function of K^2 minus the square of the threshold value of the same stress intensity factor. This could be interpreted as correlating with the CTOD (Crack Tip Opening Displacement). A similar approach could be made on the basis of the strain at the root of a notch.

Recently, I had an opportunity to look at some work on high temperature fracture and there CTOD had been measured; as you could see, CTOD had an elastic as well as a time-dependent fraction. I think this opens a whole new field of study because now, as soon as you have a crack, you can start to look at CTOD, take out the various portions (the elastic, plastic and creep-dependent fractions) and then try to apply SRP not to the overall strain of the specimen but to the strain at the root of the notch or crack.

Dr. G.R.HALFORD (NASA Lewis Research Center, U.S.A.)

All the experiments reported during this conference have been performed on specimens that can best be called crack initiation specimens and no more than that. They have a small diameter, and the strains across either a diameter, a gage length, or the specimen ends have been controlled. Furthermore, the strain is distributed uniformly through the specimen test zone, the stress has a certain value, and that is what is known about the specimen. Once a crack of a given magnitude begins to generate its own stress field, then that condition can be treated best by fracture mechanics type principles. When a crack grows that large in our small specimens they become useless since we can not control what we would like to control in a fracture mechanics type crack propagation test. I believe the information obtained from specimens of the nature we are working with here can only be considered as crack initiation data.

Dr. H.P. VAN LEEUWEN

In room temperature fatigue, we have a long time ago dropped the notion that we should test smooth specimens because the things we deal with in practice are not smooth. So, I would like to suggest that we drop the idea of testing smooth specimens and to start testing fracture mechanics-sort of specimens. We should start with a notched specimen and apply a Neuber-type of analysis to the strain at the root of the notch and then have the initiation period treated with SRP.

Mr. M.H.HIRSCHBERG

Included in the test data collected from the laboratories, we have on record the total number of cycles to failure, and in some cases, the cycles to a 5 percent drop off in load, as well as the first observation of any indication of crack initiation.

All of the data collected so far indicate a negligible difference between cycles to total failure on these smooth specimens and the initiation as far as it can be identified. Thus, there seems to be a negligible crack growth period in these kinds of tests. However, if we are dealing with notched specimens, we should obviously have to separate initiation and propagation periods since the propagation period occurs under lower stresses and therefore takes a longer time. But, to characterize a material by the SRP method in order to determine what the initiation period is, we believe very strongly that this is best done with smooth specimens.

Dr. G.R. HALFORD

What we are considering to be the definition of crack initiation life does not make a great deal of difference for the specimens we are testing. We can choose almost any convenient event as the crack initiation life. Possibilities are: a) the first sighting of a crack using a microscope; b) the first noticeable drop in load range for strain-controlled tests; c) the life at which the load drops by a fixed percentage from the steady-state load range; d) the life at which the ratio of the tensile load to the compressive load drops by a fixed percentage from the steady-state ratio; e) the life for complete separation of the small laboratory specimens we test; f) or some other event as thought to be of significance for the application at hand.

I contend that, regardless of our choice, we will obtain approximately the same results on a relative basis. That is, if CP type straining is bad by any of these definitions, it will be bad by any of the other definitions as well.

What is chosen as the criteria is not so absolutely important as to choose a criteria that can be used consistently in characterizing the behavior of the material.

If we are going to adopt the concept of a crack initiation stage, which we handle with specimens of this size, and a crack propagation stage, which we handle with a specimen designed for crack propagation studies, then we will have to select some crack length to use as the transition value. The choice is somewhat arbitrary, but should be convenient for the user. If we can only detect a 0.1" crack for the purpose of a crack propagation study, there is no sense in discussing a 0.001" crack. I suspect the important thing is to keep a consistent definition.

Mr. W. WIEMANN (KWU, Germany):

I am a little bit in contradiction to Dr. HALFORD. I have seen from the tabulated data the difference between N_5 and N_f is between 5 and 50% in number of cycles. That can mean that there are certain different definitions used for N_5 as the number of cycles to crack initiation and, on the other hand, that there is different thermo-mechanical behaviour which is responsible for the crack running velocity in the different materials. Therefore, in my opinion, the best would be, that all people have the same definition for crack initiation to the specimens. You are taking here smooth, solid or tubular, specimens and even those both types of specimens may have a certain difference in a crack running velocity from initiation to failure.

Prof. S.Y. ZAMRIK (Penn State University, U.S.A.)

The question of crack initiation and propagation is a confusing issue.

Crack initiation is not well defined, it could be three or four grains deep, 1/8" long, or three inches long. The definition is dependent upon the user.

Therefore, we should avoid debating the issue of crack initiation and propagation. We should concentrate on developing methods that would work in design analysis to prevent failure. For example, in biaxial fatigue it is difficult to determine initiation from propagation; I have seen series of cracks developing in plate under biaxial stress loading, and neither of these visible cracks led to failure.

CAPTAIN JACK HYZAK (AFML/LLN, U.S.A.)

The question still remains as to how does SRP compare to other methods for predicting high temperature LCF. At AFML we are not directly concerned with design; thus, we were not utilizing any other modeling approaches before entering into this committee activity. I am still wondering how some of the participants, especially those directly involved with engine design, feel about SRP. What aspects of SRP are particularly effective and what models are they now using which they feel are more useful? I am particularly interested in the problem of predicting crack initiation in nickel base superalloys.

Dr. G.J. LLOYD

A suggestion enabling to assess the relative role of initiation compared with propagation. If you prepare a normally smooth specimen and a square specimen of the same cross section area, then propagate a crack from that square specimen and measure the rate of

growth. Integration of it gives you the so-called propagation life. This allows you to assess the number of cycles for initiation at the given total strainrange that you apply. Repeat the exercise for a number of strainranges. You could finally derive a smooth specimen endurance curve and the crack propagation curve.

Dr. H.P. VAN LEEUWEN

Under conditions where plasticity is very important, neither of stresses or strains is really descriptive of the problem. What we are really interested in, is the energy dissipation which is not obtained by measuring at notches or cracks but by measuring the displacement at the point of load application.

This is the ultimate goal, that we look at the energy dissipation and one possible approach would be not to look at the width of the hysteresis loop but to look at its area.

Mr. R.M.WALLACE (PWA, GPD, U.S.A.)

With regards to the comments about crack initiation and propagation phases, let us consider the example of IN-100 alloy.

If we start with an inherently clean material, without service-induced cracks, the total fatigue process might incipiently look something like nucleation of dislocations at discontinuities such as MC carbides thus resulting in microcracks. The whole process is a statistical one that we call crack initiation. On our strain-controlled specimens, however, we have found that these microcracks link up forming macrocracks, the growth of which is predictable using linear elastic fracture mechanic techniques. We have shown this in a recent AFML program, on IN-100, at temperature up to 1350°F.

In addition, using a newly developed multiparameter distribution analysis acoustic emission technique, we have found for the IN-100 alloy at temperatures in the 1000 - 1200°F range, particularly at the low strain amplitude level, that the point at which macrocracking occurs can be as low as 40 to 55 % of the total life. For IN-100, under these strain and temperature testing conditions, stress ratio and dwell effects are very important on crack propagation and therefore the dwell effects we are experiencing may be on crack propagation, not crack initiation.

I do not know if this result is generally extendable to an alloy like René 95. As a matter of fact, we intend to pursue our strain-control testing and analysis of other disk alloys, including IN-100, Waspaloy, Astroloy and advanced AF 2 - 1 DA alloy which would be a strong candidate for advanced turbine disk alloys in many of our engines.

At P.W.A., we have developed a LCF prediction system based on total strainrange and mean stress, using notch specimen data. The dwell effect can be beneficial or degrading to the life. For example, testing Waspaloy in the 800°F range generally dwell might perhaps increase life whereas a 1200°F dwell might perhaps degrade life. So, the change of life due to the dwell is assumed to come from changes in the mean stress level at equivalent strain ranges.

Further, during our strain-control testing, we use the acoustic emission technique. Integrating what we see from the acoustic emission results with mechanistic studies, we separate crack initiation and propagation lives and move on to modelling these data. Now, using this crack initiation life criterion, the next step should be to come up with an accurate constant strain-amplitude model, and then to use appropriate statistic for design systems. Certainly, SRP is one of the methods we intend to use in this process.

We will keep the model based on total strainrange and mean stress : we think it is the most powerful crack initiation tool today. However, what we will extract from SRP are better ideas on how to handle several effects such as dwell.

One of the big problems I personally see for high strength alloys, like IN-100 and René 95, is the accurate analytical calculation of the inelastic strain.

Dr. C.J.FRANKLIN, (SULZER BROTHERS LTD, Gas Turbine Division, Switzerland)

I think that SRP is the most promising of the methods that I have studied for fatigue life prediction. It would appear, however, that there is still a long way to go before we can use it for the high temperature nickel base alloys.

I would like to address a few remarks to a number of points that have been raised in the discussion.

First, I think that with SRP, or any other LCF prediction method, we should only attempt to predict crack initiation. The main reason for only predicting initiation is that once we have a crack in a component, that has any significant length, there are often cyclic stresses present which will help to propagate the crack although they were not part of the basic cycle that had initiated it. For example the vibratory

stresses in the case of turbine blades which are normally small in comparison to the strain cycles that initiate thermal fatigue cracks.

Secondly, in support of a remark from Dr. HALFORD, I also think that we should forget that a material contains cracks until one of the cracks attains sufficient length for it to dominate the local stress field. There is, in fact, a stress distribution inside every piece of material; even when the material is loaded uniaxially. This stress distribution is produced because, on the microscopic scale, the material is heterogeneous and has anisotropic properties. So, until a crack has a length where its presence dominates this internal stress field it is just another stress raiser and we should forget that we can see a crack/cracks with the electron microscope.

I think that there is a problem with life prediction by SRP, that we have not touched upon. This problem is particularly difficult in the case of turbine blades. SRP automatically assumes that we have a good knowledge of the stress-strain hysteresis loop for some complex thermal fatigue cycle which has to be analysed. This, however, is not the case and it is, in fact, a very difficult problem to predict the hysteresis loop. A vast amount of material data is needed to determine and define such material properties as: creep curves, stress relaxation, cyclic stress/strain curves etc. The general nature of this problem is such that we do not have constitutive relationships to describe this data accurately or reliably.

There is, of course, the experimental methods of determining stress/strain hysteresis loops in which we first predict the elastic behaviour of the component and then program this into a fatigue machine in order to obtain the real loop experimentally. For cooled turbine blades, however, and I suspect even for uncooled ones, this method is unlikely to give a very accurate knowledge of the stress/strain hysteresis loop. The reason for this is that creep is occurring through-out the structure, at different rates, as a result of the temperature and stress distributions obtaining. Under these conditions the total strain at any point within the blades is a function of the creep strain which is accumulating and the blade is bending and deforming as a whole.

A knowledge of the purely elastic behaviour is not a good starting point for programming a fatigue machine to measure the hysteresis loop because, in the turbine blade, the plastic strain affects the total strain history. One thing that SRP, or any other fatigue life prediction method should tell us, therefore, is how to predict the stress/strain hysteresis loop.

Prof. S.S.MANSON

Several parts of this discussion are not really pertinent to the objectives of the conference. I would like first to address one remark to Dr. VAN LEEUWEN who seems to be in contradiction to something that I have said but did not mean in the way he apparently interpreted it: there is not difference between us as regards the importance of crack propagation in highly brittle materials. I realize that highly brittle materials do not have much of a crack propagation phase; my point was that normally we have a crack propagation in a ductile material; in a brittle material the crack propagation phase may be absent. So when we apply SRP concepts developed on ductile materials which have a crack propagation phase to a brittle material that does not include such crack propagation we must be especially cautious.

Mr. WALLACE's comment that the way in which PWA treats the problem is by total strainrange and mean stress effects is something that I know they have been doing. Their approach uses a power-law formula involving total strainrange and mean stress, rather than considering that the exponent in the power-law for elastic strain is different from the exponent in the power-law for plastic strain. The effect is that their equation cannot be correct at both high and low strains; it is valid only in a limited range where the strainrange/life data have been linearized.

Now, regarding Dr. FRANKLIN's comment that the application of SRP requires an accurate knowledge of the constitutive equations, so that an accurate hysteresis loop can be constructed, and his requirement that SRP provides design engineers with information on how to predict the stress-strain hysteresis loop. First it should be pointed out that SRP is a fatigue fracture theory, not a theory for predicting constitutive equations. Although it would be good for SRP if accurate procedures were available for determining the stress and strain, even separating creep and plasticity components, such a requirement is not a fair one to impose on SRP any more than it would be to impose it on any other method of analysis. All methods would benefit from such a capacity.

However, it is fortunate that such accurate prediction is not really necessary. Rather, what is important to know is the variation of total strainrange and temperature with time. Usually the total strainrange can be estimated fairly accurately using the "principle of elastic strain invariance" which is accurate for thermal stress problems, or by measurement, or by other procedures the designer may have at his disposal. From the knowledge of strain and temperature we can establish the hysteresis loop in a semi-experimental manner by subjecting a uniaxial specimen to such strain and temperature history and noting the stresses developed at each instant of time. The specimen itself,

in other words, acts as the best interpreter of the rheological behaviour, and provides us with as accurate a stress-strain analysis as we can get. Then using procedures we have already described in the literature, we can separate the strainrange components, and apply SRP principles to determine life. The specimen need not be tested to failure, since that might take too long, and invalidate entirely the use of SRP as a predictive approach.

My point is mainly that SRP does not require any more than any other method a knowledge of stresses and strain that are hard to predict by constitutive analysis, and that such requirement as exists, can be satisfied by a semi-experimental approach.

APPENDIX A1

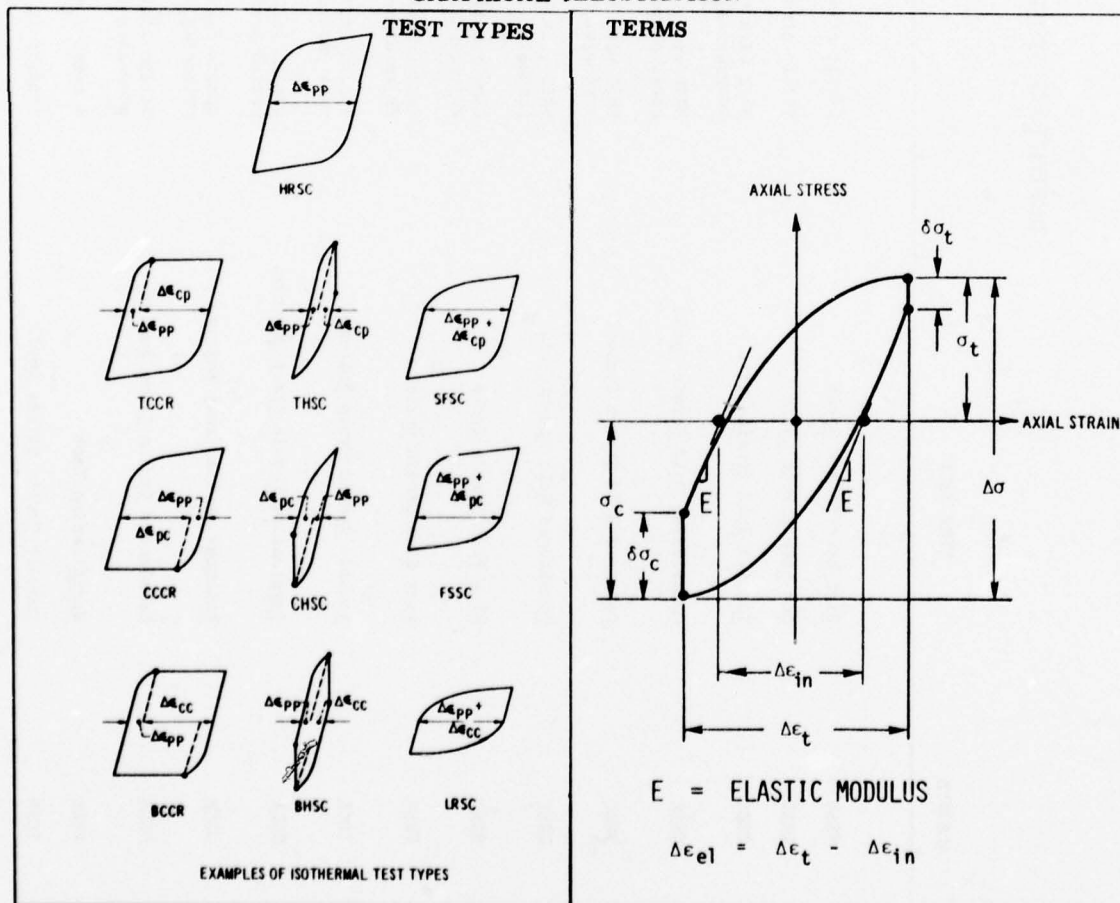
Appendix A1 contains a tabulation of the high-temperature, low-cycle, creep-fatigue results generated by the laboratories participating in the SRP evaluation program. Also contained are the chemical compositions, material processing and heat treatments, and the conventional mechanical properties for each alloy tested. A common creep-fatigue data sheet was used to ensure that pertinent information was reported in a consistent manner. A sample data sheet is shown below along with a graphical illustration of both terms and test types as well as definitions of the most common creep-fatigue cycles employed in the program. The information contained in this appendix was submitted to the NASA-Lewis Research Center where Mr. J.F. Saltsman painstakingly transcribed the information to a computerized format for ease of storage, analysis and retrieval. In this form, it represents an extremely valuable body of creep-fatigue data on engineering alloys. As much of the raw data as possible is included in the tabulations so that future analyses and interpretations can be made with a minimum of effort.

The four tables included in this appendix are titled as follows:

TABLE I ---	Chemical Composition - Wt%
TABLE II ---	Processing & Heat Treatment
TABLE III ---	Mechanical Properties
TABLE IV ---	Creep-Fatigue Data

The results shown in each table are arranged according to the laboratories and the order in which their corresponding papers appear in the body of this volume. Creep-fatigue data from PSU and ORNL are not included in TABLE IV, but do appear in the respective papers.

GRAPHICAL ILLUSTRATION



DEFINITIONS OF TEST TYPES

ACRONYM	TYPE TEST	DESCRIPTION OF TEST
HRSC	<u>H</u> igh <u>R</u> ate <u>S</u> train <u>C</u> ycle	Cyclic strain rate producing 100% PP strainrange.
LRSC	<u>L</u> ow <u>R</u> ate <u>S</u> train <u>C</u> ycle	Cyclic strain rate producing CC and PP strainrange components.
TRSC	<u>T</u> ensile <u>H</u> old <u>S</u> train <u>C</u> ycle	HRSC with hold period at maximum tensile strain producing CP and PP strainrange components.
CHSC	<u>C</u> ompressive <u>H</u> old <u>S</u> train <u>C</u> ycle	HRSC with hold period at maximum compressive strain producing PC and PP strainrange components.
BRSC	<u>B</u> alanced <u>H</u> old <u>S</u> train <u>C</u> ycle	HRSC with hold periods at both maximum tensile and maximum compressive strains producing CC and PP strainrange components.
URSC	<u>U</u> nbalanced <u>H</u> old <u>S</u> train <u>C</u> ycle	HRSC with unequal hold periods at maximum tensile and maximum compressive strains producing CP (or PC), CC, and PP strainrange components.
SFSC	<u>S</u> low <u>F</u> ast <u>S</u> train <u>C</u> ycle	Slow tensile straining rate and fast compressive straining rate producing CP and PP strainrange components.
FSSC	<u>F</u> ast <u>S</u> low <u>S</u> train <u>C</u> ycle	Fast tensile straining rate and slow compressive straining rate producing PC and PP strainrange components.
TCCR	<u>T</u> ensile <u>C</u> yclic <u>C</u> reep <u>R</u> upture	Strain limited cycle with tensile stress hold period and fast compressive straining rate producing CP and PP strainrange components.
CCCR	<u>C</u> ompressive <u>C</u> yclic <u>C</u> reep <u>R</u> upture	Strain limited cycle with fast tensile straining rate and compressive stress hold period producing PC and PP strainrange components.
BCCR	<u>B</u> alanced <u>C</u> yclic <u>C</u> reep <u>R</u> upture	Strain limited cycle with hold periods at equal tensile and compressive stresses producing CC and PP strainrange components.
UCCR	<u>U</u> nbalanced <u>C</u> yclic <u>C</u> reep <u>R</u> upture	Strain limited cycle with hold periods at unequal tensile and compressive stresses producing CP (or PC), CC, and PP strainrange components.
VERF	<u>V</u> erification Test	A complex stress-strain cycle as defined in the author's paper.
TOSD	<u>T</u> ensile <u>C</u> yclic <u>S</u> tress <u>D</u> well	Similar to TCCR, except dwell time is controlled constant instead of strainrange.

SAMPLE DATA SHEET

STRAINRANGE PARTITIONING TEST SUMMARY RECORD			
1			
GENERAL INFORMATION:			
1. Name of laboratory	2. Responsible engineer	3. Date of test	
4. Material designation	5. Material heat number	6. Specimen number	
7. Test type	8. Sketch of strain-time waveform	9. Temperature of test, °C	
(See definitions)			
RATE DATA (Half-Life Values):			
10. Cyclic frequency, Hz	11. Tensile strain rate, %/sec.	12. Compressive strain rate, %/sec.	
13. Tensile hold time, sec.	14. Compressive hold time, sec.	15.	
16.	17.	18.	
STRESSES (Half-Life Values) in units of MPa:			
19. σ_t	20. σ_c	21. $\Delta\sigma$	
22. $\delta\sigma_t$	23. $\delta\sigma_c$		
24. Cyclic strain hardening, _____ % change in stress range from 1st to half-life cycle Cyclic strain softening, _____ % change in stress range from 1st to half-life cycle			
STRAINS (Half-Life Values) in units of %:			
25. $\Delta\epsilon_t$	26. $\Delta\epsilon_{in}$	27. $\Delta\epsilon_{el}$	
28. $\Delta\epsilon_{pp}$	29. $\Delta\epsilon_{pc}$	30. $\Delta\epsilon_{cp}$	
31. $\Delta\epsilon_{cc}$	32.	33.	
FAILURE DATA			
34. No. cycles to first indication of cracking (note method of detection)			
35. N_1 , cycles when ratio of max tensile to max comp. stress decreases 10% from half-life or stabilized value.			
36. N_5 , cycles when stress range decreases by 5% from half-life or stabilized value			
37. N_f , cycles for complete fracture			
38. t_f , test time for complete fracture, hours			

2	
Strain-Time Waveform	Time
Stress-Time Waveform	Time
Temperature-Time Waveform	Time
Hysteresis Loop	Fracture Surface

TABLE I: CHEMICAL COMPOSITION - WT %

LAB	MATERIAL	Al	P	Au	Si	B	S	C	Ta	Co	Ti	Cb	V	Cb+Ta	Cr	Zr	Cu	H2	Fe	O2	Hf	N	Mo	Al+Ti	Mn	Ni
TRW	RENE' 80	2.990	---	---	---	0.015	0.170	9.730	---	---	4.870	---	---	---	13.800	---	---	---	0.130	---	---	---	4.110	---	<0.020	BAL
NASA		---	---	<0.050	---	---	---	---	---	---	---	---	---	3.940	0.043	---	---	---	---	---	---	---	---	---	---	
NASA	IN100	5.450	---	---	0.110	0.016	0.170	15.100	---	---	4.760	0.970	---	---	10.300	---	---	---	---	---	---	---	2.960	---	<0.020	BAL
NASA	IN100	Similar to P8WA IN100																								
P8WA	IN100	4.980	---	---	---	0.020	0.070	18.500	---	---	4.320	0.780	---	---	12.400	---	---	---	---	---	---	---	3.200	---	---	BAL
CHERA	IN100	5.500	---	---	---	0.014	0.180	15.000	---	---	4.700	1.000	---	---	10.000	---	---	---	---	---	---	---	3.000	---	---	BAL
CIT	WAR H 002	5.500	---	---	0.200	0.020	0.150	10.000	---	---	1.500	---	---	---	9.000	0.100	0.050	---	0.500	1.500	---	---	0.500	---	0.200	BAL
NGIE	NIMONIC 90	1.460	---	---	0.380	0.035	0.090	16.200	---	---	2.430	---	---	---	19.450	0.080	0.060	---	0.950	---	---	---	---	---	0.050	BAL
ER	WASPALOY	1.600	0.015	---	0.150	0.010	0.100	15.000	---	---	3.300	---	---	---	21.000	0.100	0.080	---	2.000	---	---	---	5.000	---	0.100	BAL
CEAT	WASPALOY	1.320	0.012	---	0.060	0.009	0.037	13.000	---	---	2.935	---	---	---	20.485	0.006	0.082	---	0.165	---	---	---	3.940	---	0.003	BAL
NPL	IN738LC	3.430	---	---	---	---	0.115	8.200	0.860	---	3.400	---	---	---	15.800	0.045	---	---	---	---	---	---	1.700	---	---	BAL

TABLE II: PROCESSING & HEAT TREATMENT

LAB	MATERIAL	PROCESSING		HEAT TREATMENT	
TRW NASA	RENE' 80	TRW master heat no. BL-5138, bare 6 coated with Codep B-1(aluminide). Individually cast bars(hole bored for tubular specimens). ASTM grain size = 3		1220C-2 hr in vac, inert Q to RT; 1095C-4 hr in vac, inert Q to RT; 1050C-4 hr in vac, FC in 1 hr to 650C, AC to RT (simulates coating cycle); 845C-16 hr in vac, FC to RT. Rough machine before heat treatment, finish grind after.	
NASA	IN100	Cast.		None.	
NASA	IN100	Similar to P&WA.		Similar to P&WA.	
P&WA	IN100	Powder - GATORIZED(TM)		Solution 2050F, Stabilized 1500F and 1800F, precipitation 1200F and 1400F.	
OMERA	IN100	Cast.		Coating heat treatment: vapor phase aluminization at 1150C - 3 hrs.	
CIT	HAR M 002	Cast.		870C for 16 hrs. - furnace cool.	
NGIE	NIMONIC 90	Bar. ASTM grain size = 4		8 hr - 1080C/AC + 16 hr - 700C/AC.	
RE	WASPALLOY	Vacuum melted or electro-flux remelted.		4 hrs.995 - 1035C OQ, 4 hrs 350C AC, 16 hrs 760C AC.	
CEAT	WASPALLOY	Cold rolled bars (35mm dia.) with strain control during cold rolling. ASTM grain size = 7		1030C, 4 hr, WQ; 850C, 4 hr, AC; 760C, 16 hr, AC.	
NPL	IN738LC	Investment cast. Linear intercept grain size = 0.75 mm		2 hr 1120C, air cool + 24 hr 845C, air cool.	

TABLE II - (CONTINUED)

LAB	MATERIAL	PROCESSING		HEAT TREATMENT	
APML	RENE' 95	Forged at 1149C. Duplex structure warm-worked grain size = 75um, recrystallized grain size = 4um		Forge 1100C; partial sol. 1094C, 1 hr, OQ. 760C, 16hr.	
CNR	IN738LC	Cast.		1120C for 2 hr in vac, Q to RT; 845C for 24 hr in vac, Q to RT.	
MARTEST	AMZIRC	Cold drawn to half hard. ASTM grain size = 7		Aged at 420C in cracked natural gas.	
MARTEST	NARLOY Z	Centrifugically cast & forged,		Solution annealed and aged.	
DFVLR	Ti-6Al-4V	Rolled.		As received.	
US	1-Cr-Mo-V	Forged 14 in. cubes.		Soak at 1000C, FC to 690C at 50C/hr. Hold for 70 hr. AC. Reheat to 975C, soak in salt bath. Q into salt bath at 450C. Hold for 5 hr. AC. Reheat in salt bath to 700C for 20 hr after rough machining of specimen to act as tempering heat treatment.	
ORNL	HASTELOY X	Heat 2600-3-4936, Stellite Div, Cabot Corp. ASTM B-435-71, 1/2 in. thick plate. ASTM grain size = 4		Solution anneal.	
ORNL	2 1/4Cr-1Mo	Heat 3P5601, B&W CO. ASME SA-387 Grade D, 1-in. thick plate. ASTM grain size = 5		Isothermal anneal.	
PSU	304 SS	None listed.		None listed.	

TABLE III - (CONTINUED)

LAB	MATERIAL	PROCESS	TEMP C	TENSILE PROPERTIES				CREEP RUPTURE PROPERTIES					
				EX10-3	0.2 YLD	ULT	RA-%	10 HR	100 HR	1000 HR			
				MPA	MPA	MPA	MPA	MPA	MPA	MPA			
APHL	RENE' 95	FORGED	20 650	--- ---	1317.0 1207.0	1613.0 1448.0	11.8 12.4	---	999.0	---	854.0	---	
CNR	IN738LC	CAST	20 850	197.9 149.4	1019.0 723.7	1141.0 806.8	5.5 --	393.0	12.7	310.0	12.7	226.0	12.7
MARTEST	ANZIRC	WROUGHT	20 538	115.3 81.0	336.0 212.5	378.0 216.5	81.5 84.0	---	---	---	---	---	---
MARTEST	NARLOY Z	WROUGHT	20 538	127.0 98.6	198.3 130.0	316.2 152.7	51.0 41.5	---	---	---	---	---	---
DPVLR	Ti-6Al-4V	ROLLED	20 450	106.0 89.1	1046.0 637.0	1069.0 729.0	42.0 49.1	588.0	---	481.0	---	392.0	---
UB	1-Cr-Mo-V	WROUGHT	20 565	203.0 153.0	635.0 400.0	805.0 500.0	64.0 80.0	360.0	50.0	310.0	50.0	240.0	11.0
ORNL	HASTELLOY X	WROUGHT	20 871	199.0 137.0	349.0 161.0	764.0 165.0	59.0 89.0	103.0	---	69.0	---	45.0	---
ORNL	2 1/4Cr-1Mo	WROUGHT	20 538	206.0 158.0	220.0 172.0	482.0 351.0	67.0 78.0	315.0	---	218.0	---	147.0	---
			593	140.0	156.0	265.0	89.0	218.0	---	144.0	---	97.0	---
PSU	304 SS	WROUGHT	20 643	--- ---	189.0 74.0	539.0 254.0	75.6 35.7	---	---	---	---	---	---

1 KSI = 6.895 MPA

LABORATORY: TRW
 MATERIAL: REME 80, UNCOATED
 TABLE IV: CREEP-FATIGUE DATA
 RATE DATA & STRESSES

SPEC NO	TEST TYPE	TEMP-C	FREQ HZ	RATE DATA (HALF-LIFE VALUES)			STRESS-RATE (HALF-LIFE VALUES)			STRESS-RANGE (HALF-LIFE VALUES)			RELAXATION (HALF-LIFE VALUES)			CYCLIC STRAIN (HALF-LIFE VALUES)		
				TEN	STEADY-STATE	COMP	TEN	STEADY-STATE	COMP	TEN	MAX	MIN	TEN	MAX	MIN	TEN	MAX	MIN
110U-PP-25	HSC	25/25	1.0E 00	2.0E 00	2.0E 00	2.0E 00	0	0	0	810.2	900.4	1710.6	0.0	0.0	0.0	0.0	0.0	0.0
99U-PP-14	HSC	25/25	1.0E 00	1.3E 00	1.3E 00	0	0	0	0	628.8	545.4	1174.2	0.0	0.0	0.0	0.0	0.0	0.0
101U-PP-16	HSC	204/204	1.0E 00	1.5E 00	1.5E 00	0	0	0	0	668.8	662.6	1331.4	0.0	0.0	0.0	0.0	0.0	0.0
102U-PP-17	HSC	204/204	1.0E 00	1.5E 00	1.5E 00	0	0	0	0	674.3	712.3	1386.6	0.0	0.0	0.0	0.0	0.0	0.0
1U-PP-1	HSC	538/538	1.0E 00	1.7E 00	1.7E 00	0	0	0	0	664.0	735.6	1399.6	0.0	0.0	0.0	0.0	0.0	0.0
2U-PP-2	HSC	538/538	1.0E 00	1.5E 00	1.5E 00	0	0	0	0	568.2	615.7	1183.9	0.0	0.0	0.0	0.0	0.0	0.0
105U-PP-20	HSC	649/649	1.0E 00	1.6E 00	1.6E 00	0	0	0	0	576.4	589.6	1166.0	0.0	0.0	0.0	0.0	0.0	0.0
107U-PP-22	HSC	649/649	1.0E 00	1.3E 00	1.3E 00	0	0	0	0	495.7	444.8	940.5	0.0	0.0	0.0	0.0	0.0	0.0
104U-PP-19	HSC	760/760	1.0E 00	1.6E 00	1.6E 00	0	0	0	0	536.4	568.2	1104.6	0.0	0.0	0.0	0.0	0.0	0.0
103U-PP-18	HSC	760/760	1.0E 00	1.2E 00	1.2E 00	0	0	0	0	424.1	388.2	812.3	0.0	0.0	0.0	0.0	0.0	0.0
74U-PP-13	HSC	871/871	1.0E 00	2.5E 00	2.5E 00	0	0	0	0	521.2	510.2	1031.4	0.0	0.0	0.0	0.0	0.0	0.0
21U-PP-8	HSC	871/871	1.0E 00	1.7E 00	1.7E 00	0	0	0	0	417.2	413.7	830.9	0.0	0.0	0.0	0.0	0.0	0.0
41U-PP-10	HSC	871/871	1.0E 00	1.3E 00	1.3E 00	0	0	0	0	350.9	357.1	708.0	0.0	0.0	0.0	0.0	0.0	0.0
22U-PP-9	HSC	871/871	1.0E 00	4.8E-01	4.8E-01	0	0	0	0	180.7	156.5	337.2	0.0	0.0	0.0	0.0	0.0	0.0
42U-PP-11	HSC	871/871	1.0E 00	5.9E-01	5.9E-01	0	0	0	0	162.1	222.0	384.1	0.0	0.0	0.0	0.0	0.0	0.0
6U-PP-5	HSC	1000/1000	1.0E 00	2.5E 00	2.5E 00	0	0	0	0	278.6	243.4	522.0	0.0	0.0	0.0	0.0	0.0	0.0
4U-PP-3	HSC	1000/1000	1.0E 00	1.9E 00	1.9E 00	0	0	0	0	279.3	264.8	544.1	0.0	0.0	0.0	0.0	0.0	0.0
109U-PP-24	HSC	1000/1000	1.0E 00	1.2E 00	1.2E 00	0	0	0	0	210.9	192.4	403.3	0.0	0.0	0.0	0.0	0.0	0.0
7U-PP-6	HSC	1000/1000	1.0E 00	1.1E 00	1.1E 00	0	0	0	0	191.0	191.0	382.0	0.0	0.0	0.0	0.0	0.0	0.0
108U-PP-23	HSC	1000/1000	1.0E 00	6.8E-01	6.8E-01	0	0	0	0	156.5	137.9	294.4	0.0	0.0	0.0	0.0	0.0	0.0
5U-PP-4	HSC	1000/1000	1.0E 00	5.5E-01	5.5E-01	0	0	0	0	92.4	84.1	176.5	0.0	0.0	0.0	0.0	0.0	0.0
8U-PP-7	HSC	1000/1000	1.0E 00	4.9E-01	4.9E-01	0	0	0	0	117.2	124.8	242.0	0.0	0.0	0.0	0.0	0.0	0.0
92U-PP-13	CCR	871/871	1.0E-02	--	--	0	0	0	0	553.7	246.1	799.8	0.0	0.0	0.0	0.0	0.0	0.0
26U-PP-9	CCR	871/871	1.4E-02	--	--	0	0	0	0	519.9	231.0	750.9	0.0	0.0	0.0	0.0	0.0	0.0
51U-PP-12	CCR	871/871	1.7E-02	--	--	0	0	0	0	438.5	194.7	633.2	0.0	0.0	0.0	0.0	0.0	0.0
95U-PP-16	CCR	871/871	2.6E-03	--	--	0	0	0	0	390.2	147.6	537.8	0.0	0.0	0.0	0.0	0.0	0.0
25U-PP-10	CCR	871/871	5.3E-02	--	--	0	0	0	0	168.3	29.0	197.3	0.0	0.0	0.0	0.0	0.0	0.0
10U-PP-2	CCR	1000/1000	5.3E-03	--	--	0	0	0	0	478.6	159.3	637.9	0.0	0.0	0.0	0.0	0.0	0.0
12U-PP-4	CCR	1000/1000	4.2E-03	--	--	0	0	0	0	490.2	151.7	641.9	0.0	0.0	0.0	0.0	0.0	0.0
89U-PP-11	CCR	1000/1000	1.1E-02	--	--	0	0	0	0	270.3	103.4	373.7	0.0	0.0	0.0	0.0	0.0	0.0
94U-PP-14	CCR	1000/1000	2.0E-02	--	--	0	0	0	0	239.2	115.2	354.4	0.0	0.0	0.0	0.0	0.0	0.0
9U-PP-1	CCR	1000/1000	3.5E-02	--	--	0	0	0	0	226.8	49.3	275.1	0.0	0.0	0.0	0.0	0.0	0.0
97U-PP-15	CCR	1000/1000	2.0E-02	--	--	0	0	0	0	188.3	72.4	260.7	0.0	0.0	0.0	0.0	0.0	0.0
23U-PP-6	CCR	1000/1000	1.6E-01	--	--	0	0	0	0	176.5	78.6	255.1	0.0	0.0	0.0	0.0	0.0	0.0
26U-PP-8	CCR	1000/1000	1.5E-01	--	--	0	0	0	0	195.9	48.3	244.2	0.0	0.0	0.0	0.0	0.0	0.0
112U-PP-11	CCR	871/871	1.6E-02	--	--	64.0	0	0	0	284.8	519.2	804.0	0.0	0.0	0.0	0.0	0.0	0.0
86U-PP-9	CCR	871/871	1.2E-02	--	--	83.0	0	0	0	216.5	474.3	690.8	0.0	0.0	0.0	0.0	0.0	0.0
30U-PP-5	CCR	871/871	4.1E-02	--	--	24.0	0	0	0	251.0	451.0	702.0	0.0	0.0	0.0	0.0	0.0	0.0
31U-PP-6	CCR	871/871	3.1E-02	--	--	32.0	0	0	0	193.1	402.7	595.8	0.0	0.0	0.0	0.0	0.0	0.0
36U-PP-7	CCR	871/871	1.6E-02	--	--	62.3	0	0	0	128.2	255.9	397.1	0.0	0.0	0.0	0.0	0.0	0.0
14U-PP-1	CCR	1000/1000	6.7E-03	--	--	150.0	0	0	0	201.3	271.2	472.5	0.0	0.0	0.0	0.0	0.0	0.0
111U-PP-10	CCR	1000/1000	2.2E-02	--	--	46.0	0	0	0	128.2	225.1	354.3	0.0	0.0	0.0	0.0	0.0	0.0
35U-PP-8	CCR	1000/1000	1.7E-02	--	--	59.0	0	0	0	98.6	180.0	278.6	0.0	0.0	0.0	0.0	0.0	0.0
16U-PP-3	CCR	1000/1000	2.2E-02	--	--	46.0	0	0	0	128.2	175.2	303.4	0.0	0.0	0.0	0.0	0.0	0.0

TABLE IV: CREEP-FATIGUE DATA (CONTINUED)

 LABORATORY: TRW
 MATERIAL: RENE' 80, UNCOATED

STRAINS & FAILURE DATA

SPEC NO	TOTAL	STRAIN RANGES (HALF-LIFE VALUES) %				FAILURE DATA-CYCLES			
		EL	IN	PE	PC	CP	CC	NO	NI
110U-PP-25	0.979	0.828	0.151	0.151	0.000	0.000	0.000	--	1306
99U-PP-14	0.639	0.568	0.071	0.071	0.000	0.000	0.000	--	6900
101U-PP-16	0.741	0.667	0.074	0.074	0.000	0.000	0.000	--	1574
102U-PP-17	0.769	0.698	0.071	0.071	0.000	0.000	0.000	--	2170
10U-PP-1	0.874	0.773	0.101	0.101	0.000	0.000	0.000	--	1621
20U-PP-2	0.747	0.654	0.093	0.093	0.000	0.000	0.000	--	1950
105U-PP-20	0.784	0.669	0.115	0.115	0.000	0.000	0.000	--	744
107U-PP-22	0.842	0.539	0.103	0.103	0.000	0.000	0.000	--	4402
104U-PP-19	0.792	0.663	0.129	0.129	0.000	0.000	0.000	--	496
103U-PP-18	0.604	0.486	0.116	0.116	0.000	0.000	0.000	--	4216
70U-PP-13	1.262	0.657	0.605	0.605	0.000	0.000	0.000	--	145
21U-PP-8	0.851	0.529	0.322	0.322	0.000	0.000	0.000	--	642
41U-PP-10	0.630	0.451	0.179	0.179	0.000	0.000	0.000	--	1410
22U-PP-9	0.241	0.215	0.026	0.026	0.000	0.000	0.000	--	163533
40U-PP-11	0.296	0.245	0.051	0.051	0.000	0.000	0.000	--	217620
60U-PP-5	1.250	0.363	0.887	0.887	0.000	0.000	0.000	--	103
40U-PP-3	0.544	0.378	0.566	0.566	0.000	0.000	0.000	--	306
100U-PP-24	0.576	0.280	0.296	0.296	0.000	0.000	0.000	--	1240
70U-PP-6	0.561	0.265	0.296	0.296	0.000	0.000	0.000	--	2298
100U-PP-23	0.343	0.204	0.139	0.139	0.000	0.000	0.000	--	5766
50U-PP-4	0.277	0.122	0.155	0.155	0.000	0.000	0.000	--	6302
80U-PP-7	0.247	0.169	0.078	0.078	0.000	0.000	0.000	--	22115
90U-PP-13	1.064	0.510	0.554	0.094	0.460	0.000	0.000	--	41
20U-PP-9	0.856	0.478	0.378	0.095	0.283	0.000	0.000	--	145
91U-PP-12	0.659	0.402	0.257	0.048	0.209	0.000	0.000	--	356
98U-PP-16	0.601	0.343	0.258	0.075	0.183	0.000	0.000	--	396
20U-PP-10	0.330	0.126	0.204	0.040	0.164	0.000	0.000	--	1415
10U-PP-2	1.999	0.443	1.556	0.218	1.338	0.000	0.000	--	13
10U-PP-4	1.809	0.445	1.364	0.109	1.255	0.000	0.000	--	30
80U-PP-11	0.579	0.259	0.319	0.048	0.271	0.000	0.000	--	187
90U-PP-14	0.464	0.246	0.218	0.031	0.187	0.000	0.000	--	418
90U-PP-1	0.544	0.191	0.723	0.038	0.715	0.000	0.000	--	479
90U-PP-15	0.292	0.161	0.111	0.022	0.089	0.000	0.000	--	1978
20U-PP-6	0.386	0.177	0.209	0.015	0.194	0.000	0.000	--	9810
20U-PP-8	0.409	0.169	0.240	0.023	0.217	0.000	0.000	--	10164
112U-CP-11	0.907	0.512	0.335	0.077	0.308	0.000	0.000	--	101
80U-CP-9	0.772	0.440	0.332	0.026	0.306	0.000	0.000	--	147
30U-CP-5	0.736	0.447	0.289	0.035	0.254	0.000	0.000	--	193
30U-CP-6	0.568	0.360	0.208	0.006	0.222	0.000	0.000	--	530
30U-CP-7	0.564	0.253	0.111	0.019	0.092	0.000	0.000	--	3705
140U-CP-1	1.595	0.328	1.287	0.280	0.987	0.000	0.000	--	12
110U-CP-10	0.957	0.246	0.711	0.178	0.533	0.000	0.000	--	75
30U-CP-8	0.436	0.193	0.243	0.016	0.227	0.000	0.000	--	527
16U-CP-3	0.569	0.211	0.378	0.114	0.264	0.000	0.000	--	601

 0.50
 2.00
 0.50
 0.50
 0.50
 0.50
 0.20
 1.30
 0.10
 1.20
 0.04
 0.20
 0.40
 0.00
 53.50
 0.02
 0.10
 0.30
 0.60
 1.50
 1.70
 5.90
 1.10
 2.30
 5.90
 42.80
 1.00
 2.00
 4.30
 5.90
 2.30
 25.30
 16.30
 12.10
 1.30
 2.40
 1.30
 1.30
 4.70
 2.10
 0.50
 1.00
 3.60
 1.50

TABLE IV: CREEP-FATIGUE DATA (CONTINUED)

LABORATORY: TRW MATERIAL: RENE' 80, UNCOATED		RATE DATA & STRESSES									
SPEC NO	TEST	TEMP-C	RATE DATA (HALF-LIFE VALUES)			STRESS (HALF-LIFE VALUES)			STRESS (HALF-LIFE VALUES)		
			FREQ	STRAIN-RATE-K/SEC	HOLD TIME-SEC	TEN	COMP	RANGE	RELAXATION	CYCLES	SPRAIN
17U-CP-4	TCCR	1000/1000	4.5E-02	--	22.0	0	80.0	163.4	243.4	0.0	0.0
71U-CC-7	UCCR	871/871	4.5E-03	--	110.0	110.0	351.0	285.5	636.5	0.0	0.0
73U-CC-8	UCCR	871/871	4.4E-03	--	110.0	110.0	344.7	320.7	665.4	0.0	0.0
76U-CC-9	UCCR	871/871	2.6E-03	--	190.0	190.0	289.0	245.4	534.4	0.0	0.0
120U-CC-12	UCCR	871/871	7.6E-03	--	66.0	66.0	213.0	206.1	419.1	0.0	0.0
79U-CC-10	UCCR	871/871	3.3E-03	--	150.0	150.0	222.7	189.7	412.4	0.0	0.0
119U-CC-11	UCCR	1000/1000	7.4E-03	--	68.0	68.0	186.9	174.5	361.4	0.0	0.0
67U-CC-6	UCCR	1000/1000	2.9E-03	--	170.0	170.0	80.7	53.8	134.5	0.0	0.0
19U-CC-3	UCCR	1000/1000	2.3E-03	--	220.0	220.0	128.9	100.0	228.9	0.0	0.0
40U-CC-5	UCCR	1000/1000	8.7E-03	--	38.0	76.0	100.7	68.3	169.0	0.0	0.0
20U-CC-4	UCCR	1000/1000	3.2E-02	--	16.0	16.0	85.5	56.5	142.0	0.0	0.0

LABORATORY: TRW
MATERIAL: RENE' 80, UNCOATED

STRAINS & FAILURE DATA

SPEC NO	STRAIN RANGES (HALF-LIFE VALUES) %				FAILURE DATA-CYCLES				TIME-HRS	
	TOTAL	EL	IN	PC	NO	NI	NE	NP	IF	IF
17U-CP-4	0.409	0.169	0.240	0.030	0.000	0.210	0.000	0.000	1385	8.60
71U-CC-7	1.368	0.405	0.963	0.241	0.067	0.000	0.655	0.000	25	1.60
73U-CC-8	1.193	0.424	0.769	0.085	0.084	0.000	0.600	0.000	35	2.20
76U-CC-9	0.784	0.340	0.444	0.013	0.031	0.000	0.400	0.000	165	17.60
120U-CC-12	0.622	0.267	0.355	0.071	0.007	0.000	0.277	0.000	181	6.60
79U-CC-10	0.507	0.263	0.244	0.029	0.010	0.000	0.205	0.000	637	53.10
119U-CC-11	0.973	0.251	0.722	0.079	0.029	0.000	0.614	0.000	69	2.60
67U-CC-6	0.599	0.093	0.506	0.101	0.025	0.000	0.380	0.000	257	24.80
19U-CC-3	0.457	0.159	0.298	0.060	0.029	0.000	0.209	0.000	420	51.00
40U-CC-5	0.273	0.118	0.155	0.031	0.008	0.000	0.116	0.000	4783	152.60
20U-CC-4	0.233	0.099	0.134	0.013	0.007	0.000	0.114	0.000	8154	70.50

TABLE IV: CREEP-FATIGUE DATA (CONTINUED)

LABORATORY: TRW
MATERIAL: FENE 80, COATED

RATE DATA & STRESSES

SPEC NO	TEST TYPE	TEMP-C	FREQ HZ	RATE DATA			HALF-LIFE VALUES			STRESS RANGE			HALF-LIFE VALUES			CYCLIC STRAIN HARDENING %
				SEIN	TEIN	COMP	SEC	WSEC	SEC	MAX	MIN	MAX	SEC	WSEC	SEC	
77C-PP-11	HRSC	871/871	1.0E-00	2.0E-00	0.0	2.0E-00	0	0	0	452.3	441.3	893.6	0	0	0	0.0
52C-PP-7	HRSC	871/871	1.0E-00	1.5E-00	0	1.5E-00	0	0	0	409.6	394.4	804.0	0	0	0	0.0
51C-PP-6	HRSC	871/871	1.0E-00	1.3E-00	0	1.3E-00	0	0	0	355.1	355.1	710.2	0	0	0	0.0
54C-PP-8	HRSC	871/871	1.0E-00	8.2E-01	0	8.2E-01	0	0	0	231.0	277.2	508.2	0	0	0	0.0
55C-PP-9	HRSC	871/871	1.0E-00	3.8E-01	0	3.8E-01	0	0	0	112.4	113.1	225.5	0	0	0	0.0
75C-PP-10	HRSC	1000/1000	1.0E-00	1.9E-00	0	1.9E-00	0	0	0	285.5	273.7	559.2	0	0	0	0.0
45C-PP-3	HRSC	1000/1000	1.0E-00	5.8E-01	0	5.8E-01	0	0	0	178.6	177.2	355.8	0	0	0	0.0
47C-PP-4	HRSC	1000/1000	1.0E-00	6.9E-01	0	6.9E-01	0	0	0	128.9	126.2	255.1	0	0	0	0.0
49C-PP-5	HRSC	1000/1000	1.0E-00	4.5E-01	0	4.5E-01	0	0	0	116.5	113.1	229.6	0	0	0	0.0
43C-PP-1	HRSC	1000/1000	1.0E-00	3.0E-01	0	3.0E-01	0	0	0	71.7	74.4	146.1	0	0	0	0.0
90C-PP-7	CCCR	871/871	5.1E-03	---	---	---	0	195.0	0	566.8	233.7	800.5	0	0	0	0.0
59C-PP-4	CCCR	871/871	1.0E-02	---	---	---	0	103.0	0	628.8	210.3	839.1	0	0	0	0.0
93C-PP-9	CCCR	871/871	1.3E-02	---	---	---	0	80.0	0	493.6	233.0	726.6	0	0	0	0.0
61C-PP-5	CCCR	871/871	1.2E-02	---	---	---	0	84.0	0	520.1	232.3	752.4	0	0	0	0.0
88C-PP-6	CCCR	871/871	7.8E-03	---	---	---	0	128.0	0	326.2	193.1	519.3	0	0	0	0.0
56C-PP-1	CCCR	1000/1000	1.5E-02	---	---	---	0	65.0	0	348.2	153.8	502.0	0	0	0	0.0
58C-PP-3	CCCR	1000/1000	1.7E-02	---	---	---	0	59.0	0	297.2	117.2	414.4	0	0	0	0.0
96C-PP-10	CCCR	1000/1000	1.3E-02	---	---	---	0	77.0	0	282.7	133.1	415.8	0	0	0	0.0
57C-PP-2	CCCR	1000/1000	1.3E-02	---	---	---	0	76.0	0	242.0	106.2	348.2	0	0	0	0.0
93C-PP-8	CCCR	1000/1000	4.7E-03	---	---	---	0	215.0	0	304.8	66.2	371.0	0	0	0	0.0
84C-PP-6	TCGR	871/871	5.4E-03	---	---	---	190.0	---	0	358.5	608.1	966.6	0	0	0	0.0
115C-CP-11	TCGR	871/871	2.1E-02	---	---	---	47.0	---	0	340.6	405.7	836.3	0	0	0	0.0
62C-CP-1	TCGR	871/871	1.5E-02	---	---	---	65.0	---	0	275.8	505.4	781.2	0	0	0	0.0
83C-CP-5	TCGR	871/871	1.0E-02	---	---	---	95.7	---	0	198.0	530.9	728.9	0	0	0	0.0
64C-CP-2	TCGR	871/871	1.5E-02	---	---	---	66.5	---	0	240.6	322.0	562.6	0	0	0	0.0
113C-CP-9	TCGR	1000/1000	2.5E-02	---	---	---	40.0	---	0	200.0	330.3	530.3	0	0	0	0.0
66C-CP-4	TCGR	1000/1000	1.8E-02	---	---	---	55.0	---	0	171.0	344.7	515.7	0	0	0	0.0
85C-CP-7	TCGR	1000/1000	8.3E-03	---	---	---	120.0	---	0	145.5	205.4	350.9	0	0	0	0.0
65C-CP-3	TCGR	1000/1000	1.8E-02	---	---	---	55.0	---	0	115.8	293.7	409.5	0	0	0	0.0
87C-CP-8	TCGR	1000/1000	4.3E-02	---	---	---	23.0	---	0	124.1	197.2	321.3	0	0	0	0.0
72C-CC-3	UCGR	871/871	3.7E-03	---	---	---	140.0	---	140.0	446.1	406.8	852.9	0	0	0	0.0
69C-CC-2	UCGR	871/871	5.0E-03	---	---	---	110.0	---	100.0	341.9	317.2	659.1	0	0	0	0.0
78C-CC-4	UCGR	871/871	4.5E-03	---	---	---	110.0	---	110.0	347.5	301.3	648.8	0	0	0	0.0
80C-CC-5	UCGR	871/871	2.6E-03	---	---	---	200.0	---	200.0	333.0	300.6	633.6	0	0	0	0.0
118C-CC-10	UCGR	871/871	4.9E-03	---	---	---	100.0	---	100.0	263.4	232.3	495.7	0	0	0	0.0
68C-CC-1	UCGR	1000/1000	4.3E-03	---	---	---	160.0	---	80.0	208.9	179.3	388.2	0	0	0	0.0
81C-CC-6	UCGR	1000/1000	5.6E-03	---	---	---	90.0	---	90.0	178.6	150.3	328.9	0	0	0	0.0
116C-CC-8	UCGR	1000/1000	5.1E-03	---	---	---	100.0	---	100.0	195.5	148.9	344.8	0	0	0	0.0
117C-CC-9	UCGR	1000/1000	5.2E-03	---	---	---	130.0	---	60.0	150.7	141.4	302.1	0	0	0	0.0
82C-CC-7	UCGR	1000/1000	4.0E-03	---	---	---	120.0	---	120.0	155.2	120.7	275.9	0	0	0	0.0

TABLE IV: CREEP-FATIGUE DATA (CONTINUED)

LABORATORY: TRW
MATERIAL: RENE' 80, COATED

SPEC NO	TOTAL EL	STRAIN RANGES (HALF-LIFE VALUES) %				STRAINS & FAILURE DATA				FAILURE DATA-CYCLES			IP-HRS
		IN	PP	PC	CP	CC	NO	NI	N5	NI	N5	NI	
77C-PP-11	1.011	0.569	0.442	0.000	0.000	0.000	--	--	--	293	--	293	0.10
52C-PP-7	0.742	0.512	0.230	0.000	0.000	0.000	--	--	--	1365	--	1365	0.40
51C-PP-6	0.672	0.452	0.220	0.000	0.000	0.000	--	--	--	1860	--	1860	0.50
54C-PP-8	0.470	0.324	0.086	0.000	0.000	0.000	--	--	--	71982	--	71982	19.40
55C-PP-9	0.191	0.145	0.046	0.000	0.000	0.000	--	--	--	426870	--	426870	114.90
75C-PP-10	0.961	0.388	0.573	0.000	0.000	0.000	--	--	--	233	--	233	0.10
45C-PP-3	0.490	0.247	0.243	0.000	0.000	0.000	--	--	--	2188	--	2188	0.60
47C-PP-4	0.343	0.177	0.166	0.000	0.000	0.000	--	--	--	9412	--	9412	2.50
49C-PP-5	0.225	0.159	0.066	0.000	0.000	0.000	--	--	--	101184	--	101184	27.20
43C-PP-1	0.152	0.101	0.051	0.000	0.000	0.000	--	--	--	206460	--	206460	55.50
90C-PC-7	1.055	0.510	0.545	0.457	0.000	0.000	--	--	--	48	--	48	2.60
59C-PC-4	1.107	0.535	0.572	0.114	0.000	0.000	--	--	--	63	--	63	1.90
95C-PC-9	0.835	0.463	0.372	0.033	0.339	0.000	--	--	--	126	--	126	2.80
61C-PC-5	0.774	0.480	0.294	0.042	0.252	0.000	--	--	--	282	--	282	5.60
88C-PC-6	0.485	0.331	0.154	0.031	0.123	0.000	--	--	--	1855	--	1855	65.00
56C-PC-1	0.819	0.348	0.471	0.132	0.339	0.000	--	--	--	55	--	55	1.00
56C-PC-3	0.581	0.288	0.293	0.038	0.255	0.000	--	--	--	240	--	240	3.90
96C-PC-10	0.585	0.289	0.296	0.044	0.252	0.000	--	--	--	262	--	262	5.50
57C-PC-2	0.450	0.242	0.208	0.019	0.189	0.000	--	--	--	386	--	386	9.20
93C-PC-8	0.424	0.257	0.167	0.025	0.142	0.000	--	--	--	691	--	691	41.20
84C-CP-6	1.145	0.616	0.529	0.096	0.000	0.433	--	--	--	29	--	29	1.50
115C-CP-11	0.907	0.533	0.374	0.034	0.000	0.340	--	--	--	77	--	77	1.00
62C-CP-1	0.995	0.498	0.497	0.040	0.000	0.457	--	--	--	150	--	150	2.70
83C-CP-5	0.709	0.464	0.245	0.035	0.000	0.210	--	--	--	455	--	455	12.10
64C-CP-2	0.490	0.358	0.132	0.016	0.000	0.116	--	--	--	1818	--	1818	33.60
113C-CP-9	1.023	0.368	0.655	0.164	0.000	0.491	--	--	--	45	--	45	0.50
66C-CP-4	0.966	0.358	0.608	0.110	0.000	0.498	--	--	--	66	--	66	1.00
85C-CP-7	0.568	0.244	0.324	0.074	0.000	0.250	--	--	--	134	--	134	4.50
65C-CP-3	0.603	0.284	0.319	0.045	0.000	0.274	--	--	--	251	--	251	3.30
87C-CP-8	0.422	0.223	0.199	0.030	0.000	0.169	--	--	--	950	--	950	6.20
72C-CC-3	1.377	0.543	0.834	0.125	0.050	0.659	--	--	--	33	--	33	2.50
69C-CC-2	1.005	0.420	0.585	0.099	0.059	0.000	--	--	--	108	--	108	6.00
78C-CC-4	0.917	0.413	0.504	0.071	0.085	0.000	--	--	--	109	--	109	5.70
80C-CC-5	0.824	0.404	0.420	0.017	0.000	0.013	--	--	--	171	--	171	18.60
118C-CC-10	0.582	0.316	0.266	0.050	0.016	0.000	--	--	--	544	--	544	31.70
68C-CC-1	1.135	0.269	0.865	0.069	0.060	0.000	--	--	--	17	--	17	1.10
81C-CC-6	0.790	0.228	0.562	0.045	0.133	0.000	--	--	--	76	--	76	3.80
116C-CC-8	0.754	0.239	0.031	0.000	0.026	0.458	--	--	--	77	--	77	4.20
117C-CC-9	0.555	0.210	0.345	0.069	0.017	0.000	--	--	--	225	--	225	12.00
82C-CC-7	0.445	0.191	0.254	0.015	0.016	0.000	--	--	--	621	--	621	42.90

TABLE IV: CREEP-FATIGUE DATA (CONTINUED)

LABORATORY: NASA
MATERIAL: RENE80, UNCOATED, TESTED IN AIR

RATE DATA & STRESSES

SPEC NO	TEST TYPE	TEMP-C	FREQ HZ	RATE DATA (HALF-LIFE VALUES)			STRESS (HALF-LIFE VALUES)			STRESS (HALF-LIFE VALUES) MPA		
				TEN	COMP	SEC	TEN	COMP	SEC	TEN	COMP	SEC
REE205	HRSC	1000/1000	1.0E 00	--	--	--	0	0	0	420.9	420.9	841.8
REE215	HRSC	1000/1000	1.0E 00	--	--	--	0	0	0	370.9	370.9	741.8
REE206	HRSC	1000/1000	1.0E 00	--	--	--	0	0	0	358.2	358.2	716.4
REE204	HRSC	1000/1000	1.0E 00	--	--	--	0	0	0	206.2	206.2	412.4
REE200	CCCR	1000/1000	6.8E-05	--	--	--	0	0	0	467.1	467.1	934.2
REE219	CCCR	1000/1000	7.0E-04	--	--	--	0	0	0	355.0	355.0	710.0
REE213	CCCR	1000/1000	9.9E-04	--	--	--	0	0	0	321.7	321.7	643.4
REE210	CCCR	1000/1000	7.6E-03	--	--	--	0	0	0	183.3	183.3	366.6
REE223	TCCR	1000/1000	6.4E-05	--	--	--	0	0	0	127.7	127.7	255.4
REE208	TCCR	1000/1000	5.4E-04	--	--	--	0	0	0	172.6	172.6	345.2
REE201	TCCR	1000/1000	5.5E-04	--	--	--	0	0	0	172.0	172.0	344.0
REE221	TCCR	1000/1000	4.2E-03	--	--	--	0	0	0	110.4	110.4	220.8
REE220	TCCR	1000/1000	2.2E-02	--	--	--	0	0	0	89.0	89.0	178.0
REE211	BCCR	1000/1000	1.8E-03	--	--	--	0	0	0	244.1	244.1	488.2
REE212	BCCR	1000/1000	6.2E-04	--	--	--	0	0	0	157.8	157.8	315.6
REE217	BCCR	1000/1000	9.2E-03	--	--	--	0	0	0	156.3	156.3	312.6

STRAINS & FAILURE DATA

SPEC NO	STRAIN RANGES (HALF-LIFE VALUES) %			FAILURE DATA-CYCLES			FAILURE DATA			FAILURE DATA		
	EL	IN	PC	CP	CC	NO	NI	N2	N3	NI	N2	N3
REE205	1.525	0.656	0.869	0.869	0.000	--	42	30	42	42	30	42
REE215	1.557	0.578	0.979	0.979	0.000	--	55	27	55	55	27	55
REE206	0.989	0.558	0.431	0.431	0.000	--	177	152	177	177	152	177
REE204	0.410	0.321	0.089	0.089	0.000	--	4890	4890	4890	4890	4890	4890
REE200	2.612	0.504	2.108	0.222	1.866	--	--	--	--	--	--	--
REE219	1.007	0.383	0.624	0.268	0.356	--	--	--	--	--	--	--
REE213	0.916	0.391	0.525	0.258	0.267	--	--	--	--	--	--	--
REE210	0.339	0.237	0.102	0.031	0.071	--	--	--	--	--	--	--
REE223	1.472	0.416	1.056	0.299	0.000	--	--	--	--	--	--	--
REE208	1.098	0.400	0.698	0.218	0.000	--	--	--	--	--	--	--
REE201	0.927	0.350	0.577	0.195	0.000	--	--	--	--	--	--	--
REE221	0.534	0.281	0.253	0.089	0.000	--	--	--	--	--	--	--
REE220	0.354	0.245	0.109	0.055	0.000	--	--	--	--	--	--	--
REE211	2.214	0.381	1.833	0.276	0.000	--	--	--	--	--	--	--
REE212	0.531	0.228	0.303	0.071	0.000	--	--	--	--	--	--	--
REE217	0.461	0.211	0.250	0.067	0.000	--	--	--	--	--	--	--

TABLE IV: CREEP-FATIGUE DATA (CONTINUED)

LABORATORY: NASA				RATE DATA & STRESSES											
MATERIAL: REN80, COATED, TESTED IN AIR															
SPEC NO	TEST TYPE	TEMP-C	FREQ HZ	RATE DATA				HALF-LIFE VALUES				STRESSES			
				STRAIN	RATE	TIME	COEF	TIME	COEF	TIME	COEF	TEN	COMP	RANGE	HAZARDING
				PERCENT	PERCENT	PERCENT		PERCENT		PERCENT		PERCENT	PERCENT	PERCENT	PERCENT
REE322	HRSC	1000/1000	1.0E 00	--	--	--	--	--	--	--	--	481.5	481.5	963.0	0.0
REE317	HRSC	1000/1000	1.0E 00	--	--	--	--	0	0	0	0	394.6	394.6	789.2	0.0
REE310	HRSC	1000/1000	1.0E 00	--	--	--	--	0	0	0	0	440.4	440.4	880.8	0.0
REE304	HRSC	1000/1000	1.0E 00	--	--	--	--	0	0	0	0	375.2	375.2	750.4	0.0
REE306	HRSC	1000/1000	1.0E 00	--	--	--	--	0	0	0	0	298.6	298.6	597.2	0.0
REE300	HRSC	1000/1000	1.0E 00	--	--	--	--	0	0	0	0	239.5	239.5	479.0	0.0
REE323	HRSC	1000/1000	1.0E 00	--	--	--	--	0	0	0	0	198.2	198.2	396.4	0.0
REE311	HRSC	1000/1000	1.0E 00	--	--	--	--	0	0	0	0	176.2	176.2	352.4	0.0
REE312	CCCR	1000/1000	5.0E-04	--	--	--	--	0	0	0	0	365.6	365.6	731.2	0.0
REE301	CCCR	1000/1000	2.2E-03	--	--	--	--	0	0	0	0	323.5	323.5	647.0	0.0
REE303	CCCR	1000/1000	3.4E-03	--	--	--	--	0	0	0	0	234.1	234.1	468.2	0.0
REE328	CCCR	1000/1000	1.3E-01	--	--	--	--	0	0	0	0	210.1	210.1	420.2	0.0
REE315	TCCR	1000/1000	9.1E-04	--	--	--	--	--	--	--	--	169.1	169.1	338.2	0.0
REE305	TCCR	1000/1000	1.1E-03	--	--	--	--	--	--	--	--	152.9	152.9	305.8	0.0
REE308	TCCR	1000/1000	1.9E-03	--	--	--	--	--	--	--	--	100.0	100.0	200.0	0.0
REE302	TCCR	1000/1000	1.1E-03	--	--	--	--	--	--	--	--	90.3	90.3	180.6	0.0
REE309	BCCR	1000/1000	5.4E-04	--	--	--	--	--	--	--	--	203.1	203.1	406.2	0.0
REE316	BCCR	1000/1000	4.9E-04	--	--	--	--	--	--	--	--	169.1	169.1	338.2	0.0
REE313	BCCR	1000/1000	2.6E-03	--	--	--	--	--	--	--	--	115.9	115.9	231.8	0.0
REE314	BCCR	1000/1000	4.8E-02	--	--	--	--	--	--	--	--	103.4	103.4	206.8	0.0

TABLE IV: CREEP-FATIGUE DATA (CONTINUED)

LABORATORY: NASA
MATERIAL: RENE80, COATED, TESTED IN AIR

STRAINS & FAILURE DATA

SPEC NO	TOTAL	STRAIN RANGES (HALF-LIFE VALUES) %				FAILURE DATA-CYCLES				TF-HRS		
		EL	IN	PP	PC	CP	CC	NO	NI			
REE322	1.917	0.751	1.166	1.166	0.000	0.000	0.000	--	43	24	43	0.01
REE317	1.091	0.615	0.475	0.476	0.000	0.000	0.000	--	69	69	69	0.02
REE310	1.399	0.687	0.712	0.712	0.000	0.000	0.000	--	85	58	85	0.02
REE304	1.101	0.585	0.516	0.516	0.000	0.000	0.000	--	93	93	93	0.03
REE306	0.696	0.465	0.231	0.231	0.000	0.000	0.000	--	99	76	650	0.18
REE300	0.515	0.385	0.130	0.130	0.000	0.000	0.000	--	1666	640	1666	0.46
REE323	0.397	0.309	0.088	0.088	0.000	0.000	0.000	--	2228	2228	3820	1.06
REE311	0.324	0.278	0.046	0.046	0.000	0.000	0.000	--	6719	6970	15000	4.28
REE312	2.410	0.424	1.986	0.330	1.656	0.000	0.000	--	--	--	24	13.20
REE301	1.007	0.387	0.620	0.226	0.392	0.000	0.000	--	--	--	159	20.47
REE303	0.387	0.248	0.139	0.063	0.076	0.000	0.000	--	--	--	1200	97.25
REE328	0.312	0.224	0.088	0.044	0.044	0.000	0.000	--	--	--	1900	4.10
REE315	1.369	0.407	0.962	0.238	0.000	0.724	0.000	--	--	--	14	4.25
REE305	1.022	0.392	0.630	0.134	0.000	0.496	0.000	--	--	--	48	11.58
REE308	0.631	0.311	0.320	0.088	0.000	0.232	0.000	--	--	--	432	63.47
REE302	0.337	0.235	0.102	0.058	0.000	0.044	0.000	--	--	--	3928	45.45
REE309	2.133	0.343	1.790	0.342	0.000	0.000	1.448	--	--	--	11	5.52
REE316	0.984	0.261	0.723	0.141	0.000	0.036	0.546	--	--	--	36	20.44
REE313	0.492	0.197	0.295	0.035	0.000	0.000	0.260	--	--	--	620	65.23
REE314	0.266	0.173	0.093	0.011	0.000	0.000	0.082	--	--	--	4457	25.92

TABLE IV: CREEP-FATIGUE DATA (CONTINUED)

LABORATORY: NASA
MATERIAL: IN-100, CAST

RATE DATA & STRESSES

SPEC NO.	TEST TYPE	TEMP C	TENS/COMP	FREQ HZ	RATE DATA (HALF-LIFE VALUES)			STRESS-RANGE			HALF-LIFE VALUES			CYCLIC STRAIN
					STRESS	TIME	TIME-SEC	MIN	MAX	MIN	RELAXATION	MIN	RELAXATION	
INN-2	HRSC	925/925	5.0E-01	--	--	--	0	0	735.0	774.0	1510.0	0.0	0.0	--
INN-32	HRSC	925/925	5.0E-01	--	--	--	0	0	573.6	619.2	1192.8	0.0	0.0	--
INN-3	HRSC	925/925	5.0E-01	--	--	--	0	0	493.0	520.0	1003.0	0.0	0.0	--
INN-17	HRSC	925/925	5.0E-01	--	--	--	0	0	548.7	584.1	1112.8	0.0	0.0	--
INN-18	HRSC	925/925	5.0E-01	--	--	--	0	0	385.3	400.7	786.0	0.0	0.0	--
INN-36	HRSC	925/925	5.0E-01	--	--	--	0	0	224.1	228.2	452.3	0.0	0.0	--
INN-24	HRSC	925/925	5.0E-01	--	--	--	0	0	172.4	172.4	345.9	0.0	0.0	--
INN-12	ECCR	925/925	1.6E-05	--	--	--	--	--	228.2	228.2	456.4	0.0	0.0	--
INN-16	ECCR	925/925	1.4E-04	--	--	--	--	--	171.0	171.0	342.0	0.0	0.0	--
INN-89	ECCR	925/925	3.0E-03	--	--	--	--	--	200.7	200.7	401.4	0.0	0.0	--
INN-99	TCCR	925/925	2.7E-04	--	--	--	0	0	322.7	674.3	997.0	0.0	0.0	--
INN-11	TCCR	925/925	1.0E-04	--	--	--	0	0	169.6	594.3	763.9	0.0	0.0	--
INN-9	TCCR	925/925	1.9E-03	--	--	--	0	0	142.0	360.6	502.6	0.0	0.0	--
INN-74	CCCR	925/925	5.1E-04	--	--	--	0	0	504.7	241.3	746.0	0.0	0.0	--
INN-13	CCCR	925/925	4.4E-04	--	--	--	0	0	486.8	140.6	627.4	0.0	0.0	--
INN-15	CCCR	925/925	7.1E-04	--	--	--	0	0	412.3	141.3	553.6	0.0	0.0	--
INN-73**	VERF	925/925	2.8E-03	--	--	--	6.0	116.0	621.5	655.0	1276.5	28.6	223.2*	--
INN-72**	VERF	925/925	2.8E-03	--	--	--	6.0	116.0	366.1	355.1	721.2	51.4	214.5*	--
INN-47**	VERF	925/925	2.8E-03	--	--	--	6.0	116.0	345.4	259.2	604.6	46.7	113.9*	--
INN-75**	VERF	925/925	2.8E-03	--	--	--	116.0	6.0	436.4	582.6	1019.0	207.8*	54.1	--
INN-68**	VERF	925/925	2.8E-03	--	--	--	116.0	6.0	375.1	462.6	837.7	225.4*	20.0	--
INN-66**	VERF	925/925	2.8E-03	--	--	--	116.0	6.0	247.5	352.0	559.8	101.3*	32.8	--

* STRESS IS SUM OF THREE RELAXATION PERIODS
** VERIFICATION TESTS

TABLE IV: CREEP-FATIGUE DATA (CONTINUED)

LABORATORY: NASA
MATERIAL: IN-100, CAST

STRAINS & FAILURE DATA

SPEC NO	STRAIN RANGES (HALF-LIFE VALUES) %					FAILURE DATA-CYCLES					TIME-HRS	
	TOTAL	EL	IN	EE	PC	SC	NO	NI	NS	NT	TF	TF
INN-2	2.170	0.924	1.246	1.246	0.000	0.000	--	--	--	15	0.01	0.01
INN-32	1.351	0.769	0.582	0.582	0.000	0.000	--	--	--	50	0.33	0.33
INN-3	0.920	0.638	0.282	0.282	0.000	0.000	--	--	--	96	0.35	0.35
INN-17	1.125	0.708	0.417	0.417	0.000	0.000	--	--	--	160	0.11	0.11
INN-18	0.640	0.500	0.140	0.140	0.000	0.000	--	--	--	300	0.17	0.17
INN-36	0.332	0.292	0.040	0.040	0.000	0.000	--	--	--	4015	2.23	2.23
INN-24	0.236	0.222	0.014	0.014	0.000	0.000	--	--	--	51261	23.36	23.36
INN-12	1.208	0.290	0.918	0.108	0.000	0.810	--	--	--	17	301.50	301.50
INN-16	0.650	0.218	0.432	0.039	0.019	0.374	--	--	--	102	203.37	203.37
INN-89	0.402	0.258	0.144	0.045	0.000	0.099	--	--	--	840	73.33	73.33
INN-99	2.300	0.643	1.657	0.365	0.000	1.288	6	6	6	5	6.09	6.09
INN-11	0.899	0.485	0.414	0.182	0.000	0.232	--	--	--	60	163.92	163.92
INN-9	0.414	0.320	0.094	0.047	0.000	0.047	--	--	--	1100	159.32	159.32
INN-74	1.324	0.481	0.643	0.207	0.436	0.000	19	20	20	22	12.02	12.02
INN-13	0.577	0.399	0.178	0.076	0.102	0.000	--	--	--	139	87.31	87.31
INN-15	0.450	0.352	0.098	0.034	0.064	0.000	--	--	--	332	129.11	129.11
INN-73**	1.625	0.823	0.802	0.677	0.107	0.000	--	--	--	17	1.73	1.73
INN-72**	0.822	0.465	0.357	0.219	0.105	0.000	--	--	--	84	8.40	8.40
INN-47**	0.517	0.350	0.127	0.054	0.043	0.000	--	--	--	454	47.11	47.11
INN-75**	1.502	0.657	0.845	0.724	0.000	0.099	--	--	--	15	1.55	1.55
INN-68**	0.866	0.540	0.326	0.181	0.000	0.132	--	--	--	79	7.97	7.97
INN-66**	0.505	0.387	0.118	0.053	0.000	0.044	--	--	--	1400	140.00	140.00

** VERIFICATION TESTS

TABLE IV: CREEP-FATIGUE DATA (CONTINUED)

LABORATORY: NASA
MATERIAL: IN-100, GATORIZED

RATE DATA & STRESSES

SPEC NO	TEST TYPE	TEMP-C	FREQ HZ	RATE DATA (HALF-LIFE VALUES)			STRESS-RANGE			STRESS (HALF-LIFE VALUES)			Cyclic Strain Hardening %
				TEN	COMP	SEC	TEN	COMP	MAX	TEN	COMP	MAX	
9	HRSC	760/760	8.0E-01	--	--	0	0	0	1305.0	1518.0	2823.0	0.0	0.0
17	HRSC	760/760	8.0E-01	--	--	0	0	0	1170.0	1194.0	2364.0	0.0	0.0
19	HRSC	760/760	8.0E-01	--	--	0	0	0	952.0	907.0	1859.0	0.0	0.0
12	HRSC	760/760	8.0E-01	--	--	0	0	0	914.0	914.0	1828.0	0.0	0.0
8	HRSC	760/760	8.0E-01	--	--	0	0	0	670.0	666.0	1366.0	0.0	0.0
18	TCCR	760/760	1.4E-04	--	--	0	--	0	499.0	1279.0	1778.0	0.0	0.0
20	TCCR	760/760	7.0E-04	--	--	0	--	0	560.0	1161.0	1721.0	0.0	0.0
15	TCCR	760/760	7.3E-04	--	--	0	--	0	337.0	1143.0	1480.0	0.0	0.0
23	TCCR	760/760	1.4E-03	--	--	0	--	0	662.0	1205.0	1867.0	0.0	0.0
4	TCCR	760/760	5.8E-03	--	--	0	--	0	553.0	1050.0	1603.0	0.0	0.0
6	CCCR	760/760	2.5E-04	--	--	0	--	0	1117.0	433.0	1550.0	0.0	0.0
13	CCCR	760/760	6.7E-03	--	--	0	--	0	804.0	215.0	1019.0	0.0	0.0
10	CCCR	760/760	4.6E-03	--	--	0	--	0	628.0	434.0	1062.0	0.0	0.0
22	BCCR	760/760	7.1E-04	--	--	--	--	--	670.0	693.0	1363.0	0.0	0.0
3	BCCR	760/760	3.8E-03	--	--	--	--	--	608.0	623.0	1231.0	0.0	0.0
14	BCCR	760/760	1.2E-02	--	--	--	--	--	521.0	521.0	1042.0	0.0	0.0

STRAINS & FAILURE DATA

SPEC NO	TOTAL EL	STRAIN-RANGES (HALF-LIFE VALUES) %			CP	CC	NO	FAILURE DATA-CYCLES			MP	TP-HRS
		EL	IN	PP				NA	NE	NT		
9	3.924	1.637	2.287	2.287	0.000	0.000	--	--	--	--	29	0.01
17	2.305	1.373	0.933	0.933	0.000	0.000	--	--	--	--	63	0.02
19	1.256	1.077	0.179	0.179	0.000	0.000	--	--	--	--	401	0.14
12	1.222	1.057	0.165	0.165	0.000	0.000	--	--	--	--	413	0.15
8	0.845	0.776	0.069	0.069	0.000	0.000	--	--	--	--	3085	1.07
18	2.240	1.029	1.212	0.192	0.000	0.000	--	--	--	--	9	17.75
20	1.633	0.999	0.634	0.204	0.000	0.000	--	--	--	--	12	4.70
15	1.760	0.340	1.140	0.212	0.000	0.000	--	--	--	--	20	7.60
23	1.718	1.082	0.636	0.276	0.000	0.000	--	--	--	--	41	7.98
4	1.299	0.928	0.371	0.091	0.000	0.000	--	--	--	--	259	12.30
6	1.892	0.899	0.993	0.273	0.720	0.000	--	--	--	--	26	23.00
13	0.828	0.591	0.238	0.072	0.166	0.000	--	--	--	--	129	53.70
10	0.736	0.617	0.119	0.083	0.036	0.000	--	--	--	--	502	30.40
22	1.754	0.791	0.973	0.193	0.000	0.044	--	--	--	--	33	12.30
3	1.192	0.715	0.477	0.181	0.000	0.048	--	--	--	--	112	8.26
14	0.755	0.604	0.151	0.022	0.000	0.002	--	--	--	--	652	15.40

LABORATORY: P&WA
 MATERIAL: IN-100, CATERPILAR

TABLE IV: CREEP-FATIGUE DATA (CONTINUED)																
FATIGUE DATA & STRESSES																
SPEC NO	TEST TYPE	TEMP-C	FREQ HZ	EFFECTIVE STRESS (HALF-LIFE VALUES)				STRESS (HALF-LIFE VALUES) MPA				CYCLIC STRAIN				
				PP	PC	CP	CC	TEN	COMP	MAX	RANGE		RELAXATION			
PE-4	+HSC	650/650	5.0E-01	1.0E-00	1.0E-00	1.0E-00	0	0	1137.0	482.0	1619.0	0	0	0.0	0.0	0.0
PE-3	+HSC	650/650	5.0E-01	1.3E-00	1.3E-00	1.3E-00	0	0	1108.0	793.0	1901.0	0	0	0.0	0.0	2.00
00133	+HSC	650/650	5.0E-02	1.5E-01	1.5E-01	1.5E-01	0	0	1106.0	999.0	2105.0	0	0	0.0	0.0	6.00
00134	+HSC	650/650	5.0E-02	1.5E-01	1.5E-01	1.5E-01	0	0	1084.0	944.0	2028.0	0	0	0.0	0.0	0.0
00136A	+HSC	650/650	5.0E-02	1.0E-01	1.0E-01	1.0E-01	0	0	1074.0	421.0	1495.0	0	0	0.0	0.0	0.0
00136	+HSC	650/650	1.7E-02	4.0E-02	4.0E-02	4.0E-02	0	0	935.0	694.0	1629.0	0	0	0.0	0.0	0.0
00136B	+HSC	650/650	3.5E-02	1.4E-01	1.4E-01	1.4E-01	0	0	1143.0	1203.0	2346.0	0	0	0.0	0.0	1.20
00123	+THSC	650/650	5.0E-02	1.5E-01	1.5E-01	1.5E-01	---	---	977.0	1018.0	1995.0	0	19.9	0.0	0.0	6.00
00131	+THSC	650/650	5.0E-02	1.5E-01	1.5E-01	1.5E-01	---	---	1018.0	1027.0	2045.0	0	9.0	0.0	0.0	6.00
00132	+THSC	650/650	5.0E-02	1.5E-01	1.5E-01	1.5E-01	300.0	300.0	981.0	842.0	1823.0	0	68.5	0.0	0.0	2.50
00244	+THSC	650/650	5.0E-02	1.0E-01	1.0E-01	1.0E-01	120.0	120.0	911.0	739.0	1650.0	0	86.0	0.0	0.0	3.60
00145	+THSC	732/732	5.0E-02	1.5E-01	1.5E-01	1.5E-01	3600.0	3600.0	667.0	1121.0	1788.0	0	199.0	0.0	0.0	1.00
00143	+THSC	732/732	5.0E-02	1.5E-01	1.5E-01	1.5E-01	300.0	300.0	834.0	1028.0	1862.0	0	129.0	0.0	0.0	2.50
00144	+THSC	732/732	5.0E-02	1.5E-01	1.5E-01	1.5E-01	1800.0	1800.0	732.0	1019.0	1751.0	0	185.0	0.0	0.0	1.80
00134A	+TCS	650/650	5.0E-02	1.5E-01	1.5E-01	1.5E-01	300.0	300.0	875.0	1009.0	1888.0	0	0	0.0	0.0	3.70
00120	+TCS	650/650	5.0E-02	1.5E-01	1.5E-01	1.5E-01	3600.0	3600.0	963.0	1097.0	2060.0	0	0	0.0	0.0	0.0
00235	+TCS	650/650	5.0E-02	1.5E-01	1.5E-01	1.5E-01	120.0	120.0	886.0	808.0	1694.0	0	0	0.0	0.0	3.40
00233	+TCS	650/650	5.0E-02	1.0E-01	1.0E-01	1.0E-01	120.0	120.0	798.0	940.0	1738.0	0	0	0.0	0.0	4.00
00137	+TCS	650/650	5.0E-02	1.5E-01	1.5E-01	1.5E-01	7200.0	7200.0	935.0	1111.0	2046.0	0	0	0.0	0.0	2.50
00234	+TCS	650/650	5.0E-02	8.5E-02	8.5E-02	8.5E-02	120.0	120.0	985.0	345.0	1330.0	0	0	0.0	0.0	0.0

* = ZERO TO MAX STRAIN CYCLING

STRAINS & FAILURE DATA

SPEC NO	STRAIN RANGES (HALF-LIFE VALUES) %				FAILURE DATA - CYCLES				TIME - HRS	
	TOTAL	EL	IN	PP	NI	NS	NP	NP	FP	FP
PE-4	1.000	0.972	0.028	0.028	0.000	0.000	0.000	2737	1.52	1.52
PE-3	1.250	1.196	0.054	0.054	0.000	0.000	0.000	1098	0.61	0.61
00133	1.500	1.358	0.142	0.142	0.000	0.000	0.000	737	4.09	4.09
00134	1.500	1.372	0.128	0.128	0.000	0.000	0.000	557	3.09	3.09
00136A	1.000	0.981	0.019	0.019	0.000	0.000	0.000	4697	25.09	25.09
00136	1.200	1.163	0.037	0.037	0.000	0.000	0.000	2412	40.20	40.20
00136B	2.000	1.692	0.308	0.308	0.000	0.000	0.000	212	1.58	1.58
00123	1.500	1.239	0.261	0.261	0.000	0.000	0.000	86	86.00	86.00
00131	1.500	1.281	0.219	0.219	0.000	0.000	0.000	236	119.00	119.00
00132	1.500	1.326	0.174	0.174	0.000	0.000	0.000	372	31.00	31.00
00244	1.000	0.964	0.036	0.036	0.000	0.000	0.000	3037	103.60	103.60
00145	1.500	1.149	0.351	0.351	0.000	0.000	0.000	64	80.00	80.00
00143	1.500	1.196	0.304	0.304	0.000	0.000	0.000	188	15.50	15.50
00144	1.500	1.212	0.288	0.288	0.000	0.000	0.000	103	51.50	51.50
00134A	1.500	1.397	0.103	0.103	0.000	0.000	0.000	301	25.10	25.10
00120	1.500	1.243	0.257	0.257	0.000	0.000	0.000	85	85.00	85.00
00235	1.500	1.468	0.032	0.032	0.000	0.000	0.000	2459	81.90	81.90
00233	1.000	0.960	0.040	0.040	0.000	0.000	0.000	1349	44.90	44.90
00137	1.500	1.158	0.342	0.342	0.000	0.000	0.000	67	134.00	134.00
00234	0.850	0.838	0.012	0.012	0.000	0.000	0.000	6559	219.00	219.00

TABLE IV: CREEP-FATIGUE DATA (CONTINUED)

RATE DATA & STRESSES																			
TEST TYPE	SPEC NO	TEMP-C	FREQ HZ	RATE DATA (HALF-LIFE VALUES)				RATE DATA & STRESSES				STRESS (HALF-LIFE VALUES)				STRAIN (HALF-LIFE VALUES)			
				TEN	STR	ENR	COMP	TEN	STR	ENR	COMP	TEN	STR	ENR	COMP	TEN	STR	ENR	COMP
7	HRSC	900/900	5.0E 00	--	--	--	--	0	0	0	515.0	515.0	1030.0	0.0	0.0	--	--	--	--
6	HRSC	900/900	5.0E 00	--	--	--	--	0	0	0	479.5	479.5	959.0	0.0	0.0	--	--	--	--
1	HRSC	900/900	5.0E 00	--	--	--	--	0	0	0	445.0	445.0	890.0	0.0	0.0	--	--	--	--
2	HRSC	900/900	5.0E 00	--	--	--	--	0	0	0	411.0	411.0	822.0	0.0	0.0	--	--	--	--
3	HRSC	900/900	1.0E 01	--	--	--	--	0	0	0	376.5	376.5	753.0	0.0	0.0	--	--	--	--
4	HRSC	900/900	1.0E 01	--	--	--	--	0	0	0	342.5	342.5	685.0	0.0	0.0	--	--	--	--
5	HRSC	900/900	1.0E 01	--	--	--	--	0	0	0	308.0	308.0	616.0	0.0	0.0	--	--	--	--
10	HRSC	900/900	1.0E 01	--	--	--	--	0	0	0	287.5	287.5	575.0	0.0	0.0	--	--	--	--
8	HRSC	900/900	1.0E 01	--	--	--	--	0	0	0	308.0	308.0	616.0	0.0	0.0	--	--	--	--
11	HRSC	900/900	1.0E 01	--	--	--	--	0	0	0	287.5	287.5	575.0	0.0	0.0	--	--	--	--
24	HRSC	1000/1000	5.0E 00	--	--	--	--	0	0	0	308.0	308.0	616.0	0.0	0.0	--	--	--	--
58	HRSC	1000/1000	5.0E 00	--	--	--	--	0	0	0	274.0	274.0	548.0	0.0	0.0	--	--	--	--
25	HRSC	1000/1000	5.0E 00	--	--	--	--	0	0	0	240.0	240.0	480.0	0.0	0.0	--	--	--	--
26	HRSC	1000/1000	5.0E 00	--	--	--	--	0	0	0	205.5	205.5	411.0	0.0	0.0	--	--	--	--
N12	CHSC	900/900	3.0E-03	4.5E-02	4.5E-02	4.5E-02	4.5E-02	--	--	300.0	512.0	295.0	807.0	0.0	0.0	54.0	-6.00	--	--
N10	CHSC	900/900	3.0E-03	3.3E-02	3.3E-02	3.3E-02	3.3E-02	--	--	300.0	420.0	252.0	612.0	0.0	0.0	32.5	-5.00	--	--
N9	CHSC	900/900	1.7E-02	3.3E-02	3.3E-02	3.3E-02	3.3E-02	--	--	30.0	357.0	264.0	621.0	0.0	0.0	31.0	-6.50	--	--
37	CHSC	1000/1000	2.8E-03	5.2E-02	5.2E-02	5.2E-02	5.2E-02	--	--	330.0	336.0	245.0	581.0	0.0	0.0	76.0	-5.50	--	--
N13	CHSC	1000/1000	3.0E-03	4.0E-02	4.0E-02	4.0E-02	4.0E-02	--	--	300.0	336.0	195.0	531.0	0.0	0.0	53.0	-4.00	--	--
39	THSC	900/900	2.8E-03	4.2E-02	4.2E-02	4.2E-02	4.2E-02	330.0	330.0	330.0	302.0	438.0	740.0	0.0	43.0	0.0	-6.50	--	--
N8	THSC	900/900	3.0E-03	3.3E-02	3.3E-02	3.3E-02	3.3E-02	300.0	300.0	300.0	247.0	394.0	641.0	0.0	27.0	0.0	-4.50	--	--
36	THSC	1000/1000	2.8E-03	5.2E-02	5.2E-02	5.2E-02	5.2E-02	330.0	330.0	330.0	257.0	325.0	583.0	0.0	71.0	0.0	-4.50	--	--
N36	THSC	1000/1000	3.0E-03	3.0E-02	3.0E-02	3.0E-02	3.0E-02	300.0	300.0	300.0	185.0	248.0	433.0	0.0	41.0	0.0	-8.00	--	--
N37	THSC	1000/1000	3.0E-03	2.2E-02	2.2E-02	2.2E-02	2.2E-02	300.0	300.0	300.0	135.0	212.0	347.0	0.0	26.0	0.0	-3.00	--	--
44	TCCR	900/900	2.8E-03	--	--	--	--	330.0	330.0	--	342.4	342.4	684.8	0.0	0.0	0.0	--	--	--
45	TCCR	1000/1000	2.8E-03	--	--	--	--	330.0	330.0	--	171.0	171.0	342.0	0.0	0.0	0.0	--	--	--
54	BCCR	900/900	2.8E-03	--	--	--	--	165.0	165.0	165.0	342.4	342.4	684.8	0.0	0.0	0.0	--	--	--
N5	BCCR	900/900	1.4E-02	--	--	--	--	20.0	20.0	20.0	416.0	416.0	832.0	0.0	0.0	0.0	--	--	--
N6	BCCR	900/900	2.6E-03	--	--	--	--	180.0	180.0	180.0	312.0	312.0	624.0	0.0	0.0	0.0	--	--	--
N6	BCCR	900/900	1.7E-02	--	--	--	--	15.0	15.0	15.0	342.4	342.4	684.8	0.0	0.0	0.0	--	--	--
51	BCCF	1000/1000	5.5E-04	--	--	--	--	870.0	870.0	870.0	188.0	188.0	376.0	0.0	0.0	0.0	--	--	--
55	BCCR	1000/1000	2.8E-03	--	--	--	--	165.0	165.0	165.0	171.0	171.0	342.0	0.0	0.0	0.0	--	--	--
N32	BCCR	1000/1000	2.6E-02	--	--	--	--	180.0	180.0	180.0	171.0	171.0	342.0	0.0	0.0	0.0	--	--	--
57	ECR	1000/1000	1.7E-02	--	--	--	--	15.0	15.0	15.0	171.0	171.0	342.0	0.0	0.0	0.0	--	--	--
N35	BCCR	1000/1000	2.6E-03	--	--	--	--	180.0	180.0	180.0	154.0	154.0	308.0	0.0	0.0	0.0	--	--	--
N34	BCCR	1000/1000	1.4E-02	--	--	--	--	20.0	20.0	20.0	154.0	154.0	308.0	0.0	0.0	0.0	--	--	--
40	LRCR	900/900	3.3E-02	--	--	--	--	--	--	--	411.0	411.0	822.0	0.0	0.0	0.0	--	--	--
28	LRCR	900/900	3.3E-02	--	--	--	--	--	--	--	426.0	426.0	852.0	0.0	0.0	0.0	-1.70	--	--
42	LRCR	900/900	3.3E-02	--	--	--	--	--	--	--	342.4	342.4	684.8	0.0	0.0	0.0	--	--	--
49	LRCR	900/900	3.3E-02	--	--	--	--	--	--	--	274.0	274.0	548.0	0.0	0.0	0.0	--	--	--
33	LRCR	1000/1000	3.3E-02	--	--	--	--	--	--	--	295.0	295.0	590.0	0.0	0.0	0.0	-1.50	--	--
27	LRCR	1000/1000	3.3E-02	--	--	--	--	--	--	--	233.0	233.0	466.0	0.0	0.0	0.0	-3.00	--	--
34	LRCR	1000/1000	3.3E-02	--	--	--	--	--	--	--	175.0	175.0	350.0	0.0	0.0	0.0	-4.00	--	--

LABORATORY: ONERA
MATERIAL: IN-100, COATED

TABLE IV: CREEP-FATIGUE DATA (CONTINUED)

SPEC NO	STRAIN RANGES (HALF-LIFE VALUES) %						STRAINS & FAILURE DATA				FAILURE DATA - CYCLES			1P-HRS
	TOTAL EL	EL IN	EL IN	EL IN	EL IN	EL IN	CC	NO	NI	NS	NP	NS	NP	
7	0.771	0.643	0.129	0.129	0.000	0.000	0.000	--	--	--	635	--	635	0.04
6	0.720	0.600	0.121	0.121	0.000	0.000	0.000	--	--	--	900	--	900	0.05
1	0.694	0.556	0.138	0.138	0.000	0.000	0.000	--	--	--	1260	--	1260	0.07
2	0.600	0.513	0.086	0.086	0.000	0.000	0.000	--	--	--	2120	--	2120	0.12
3	0.530	0.470	0.059	0.059	0.000	0.000	0.000	--	--	--	3670	--	3670	0.10
4	0.478	0.428	0.050	0.050	0.000	0.000	0.000	--	--	--	9460	--	9460	0.26
5	0.416	0.385	0.031	0.031	0.000	0.000	0.000	--	--	--	12210	--	12210	0.38
10	0.385	0.359	0.026	0.026	0.000	0.000	0.000	--	--	--	17340	--	17340	0.48
8	0.413	0.385	0.028	0.028	0.000	0.000	0.000	--	--	--	27260	--	27260	0.76
11	0.372	0.359	0.014	0.014	0.000	0.000	0.000	--	--	--	48320	--	48320	1.34
24	0.571	0.419	0.152	0.152	0.000	0.000	0.000	--	--	--	520	--	520	0.03
58	0.468	0.372	0.095	0.095	0.000	0.000	0.000	--	--	--	1520	--	1520	0.08
25	0.371	0.326	0.045	0.045	0.000	0.000	0.000	--	--	--	5450	--	5450	0.30
26	0.297	0.279	0.018	0.018	0.000	0.000	0.000	--	--	--	24380	--	24380	1.35
N12	0.700	0.504	0.196	0.055	0.098	0.000	0.041	--	235	187	250	187	23.00	
N10	0.525	0.420	0.105	0.010	0.025	0.000	0.070	--	744	734	764	734	70.00	
N9	0.490	0.388	0.102	0.011	0.020	0.000	0.071	--	910	888	944	888	15.70	
37	0.785	0.395	0.350	0.200	0.085	0.000	0.105	--	--	--	107	--	107	10.70
N13	0.616	0.361	0.255	0.077	0.107	0.000	0.072	--	253	234	268	234	24.60	
39	0.642	0.462	0.180	0.056	0.000	0.045	0.079	--	190	194	239	194	23.90	
N6	0.480	0.400	0.080	0.008	0.000	0.010	0.062	--	--	1110	1495	--	137.00	
3E	0.788	0.396	0.392	0.210	0.000	0.082	0.100	--	57	48	64	--	6.40	
N36	0.474	0.294	0.180	0.054	0.000	0.038	0.088	--	172	198	243	198	22.30	
N37	0.332	0.236	0.096	0.050	0.021	0.000	0.025	--	500	560	870	560	80.00	
44	0.578	0.428	0.150	0.034	0.000	0.030	0.086	--	--	115	--	115	11.60	
45	0.378	0.232	0.146	0.024	0.000	0.022	0.100	--	--	100	111	100	11.10	
54	0.686	0.428	0.258	0.090	0.000	0.168	0.168	--	--	138	159	138	15.90	
N5	0.715	0.520	0.245	0.085	0.000	0.000	0.160	--	--	--	200	--	200	3.89
N6	0.555	0.350	0.165	0.032	0.000	0.000	0.133	--	--	268	294	268	29.40	
56	0.592	0.428	0.164	0.054	0.000	0.000	0.110	--	--	300	338	300	5.60	
51	0.776	0.256	0.520	0.110	0.000	0.000	0.410	--	--	17	24	--	12.00	
55	0.408	0.233	0.175	0.044	0.000	0.000	0.131	--	--	225	263	225	2.63	
N32	0.406	0.234	0.172	0.036	0.000	0.000	0.136	--	--	505	568	505	61.50	
57	0.344	0.233	0.111	0.023	0.000	0.000	0.088	--	--	720	800	720	13.30	
N35	0.325	0.210	0.138	0.017	0.000	0.000	0.121	--	--	790	954	--	103.40	
N34	0.279	0.210	0.078	0.011	0.000	0.000	0.067	--	--	3040	3109	--	60.40	
40	0.688	0.514	0.174	0.106	0.000	0.000	0.068	--	--	299	299	299	2.50	
28	0.684	0.528	0.156	0.066	0.000	0.000	0.090	--	280	270	300	270	2.50	
42	0.510	0.428	0.082	0.029	0.000	0.000	0.053	--	--	1130	1130	--	9.40	
49	0.384	0.342	0.042	0.009	0.000	0.000	0.033	--	--	4014	4014	--	33.45	
33	0.700	0.400	0.300	0.225	0.000	0.000	0.075	--	269	255	275	255	2.30	
27	0.447	0.307	0.140	0.070	0.000	0.000	0.070	--	--	850	850	--	7.10	
34	0.300	0.234	0.066	0.013	0.000	0.000	0.053	--	2290	2220	2520	2220	21.00	

TABLE IV: CREEP-FATIGUE DATA (CONTINUED)

LABORATORY: CIT
MATERIAL: MAR M002

RATE DATA & STRESSES

SPEC NO	TEST TYPE	TEMP-C TEN/COMP	PREQ HZ	RATE DATA (HALF-LIFE VALUES)				STRESSES (HALF-LIFE VALUES)				CYCLIC STRAIN HARDENING %
				SIGMA-TEN	PRE- COMP	TIME- HOURS	TIME- SECS	TEN MAX	COMP MAX	RANGE MAX	RELAXATION TEN	
9A	HRSC	750/750	6.0E-01	--	--	--	0	753.0	790.0	1543.0	0.0	0.0
7A	HRSC	750/750	6.0E-01	--	--	--	0	656.0	588.0	1244.0	0.0	0.0
8A	HRSC	750/750	6.0E-01	--	--	--	0	607.0	522.0	1129.0	0.0	0.0
6A	HRSC	750/750	6.0E-01	--	--	--	0	520.0	475.0	995.0	0.0	0.0
14	HRSC	850/850	6.0E-01	--	--	--	0	1106.0	1040.0	2146.0	0.0	0.0
13	HRSC	850/850	6.0E-01	--	--	--	0	753.0	678.0	1431.0	0.0	0.0
10	HRSC	850/850	6.0E-01	8.7E-01	6.2E-01	--	0	447.0	533.0	980.0	0.0	0.0
18	HRSC	850/850	6.0E-01	--	--	--	0	420.0	411.0	831.0	0.0	0.0
19	HRSC	850/850	6.0E-01	--	--	--	0	324.0	324.0	648.0	0.0	0.0
1E	HRSC	950/950	1.0E 00	--	--	--	0	461.0	425.0	886.0	0.0	0.0
24	HRSC	1040/1040	1.0E 00	--	--	--	0	443.0	471.0	914.0	0.0	0.0
21	HRSC	1040/1040	1.0E 00	--	--	--	0	320.0	366.0	686.0	0.0	0.0
22	HRSC	1040/1040	1.0E 00	4.0E-01	4.0E-01	--	0	292.0	292.0	584.0	0.0	0.0
25	HRSC	1040/1040	1.0E 00	--	--	--	0	202.0	221.0	423.0	0.0	0.0
10A	CCCR	750/750	--	--	--	--	20.0	613.0	460.0	1073.0	0.0	0.0
32	CCCR	850/850	--	--	--	--	20.0	940.0	645.0	1585.0	0.0	0.0
33	CCCR	850/850	--	--	--	--	20.0	723.0	437.0	1140.0	0.0	0.0
38	CCCR	850/850	--	--	--	--	20.0	574.0	268.0	842.0	0.0	0.0
2B	CCCR	950/950	--	--	--	--	20.0	415.0	137.0	552.0	0.0	0.0
31	CCCR	1040/1040	--	--	--	--	20.0	531.0	285.0	816.0	0.0	0.0
34	CCCR	1040/1040	--	--	--	--	20.0	414.0	196.0	610.0	0.0	0.0
42	CCCR	1040/1040	--	--	--	--	20.0	311.0	107.0	418.0	0.0	0.0
11A	TCCR	750/750	--	--	--	20.0	20.0	429.0	631.0	1060.0	0.0	0.0
29	TCCR	850/850	--	--	--	20.0	20.0	478.0	858.0	1336.0	0.0	0.0
39	TCCR	850/850	--	--	--	20.0	20.0	430.0	770.0	1200.0	0.0	0.0
30	TCCR	850/850	--	--	--	20.0	20.0	377.0	714.0	1091.0	0.0	0.0
37	TCCR	850/850	--	--	--	20.0	20.0	351.0	724.0	1075.0	0.0	0.0
2E	TCCR	1040/1040	--	--	--	20.0	20.0	245.0	433.0	678.0	0.0	0.0
27	TCCR	1040/1040	--	--	--	20.0	20.0	172.0	325.0	497.0	0.0	0.0
40	TCCR	1040/1040	--	--	--	20.0	20.0	160.0	346.0	506.0	0.0	0.0
12A	BCCR	750/750	--	--	--	20.0	20.0	614.0	567.0	1181.0	0.0	0.0
47	BCCR	850/850	--	--	--	20.0	20.0	477.0	448.0	925.0	0.0	0.0
35	UCCR	850/850	--	--	--	20.0	20.0	678.0	584.0	1262.0	0.0	0.0
44	UCCR	850/850	--	--	--	20.0	20.0	467.0	413.0	880.0	0.0	0.0
4B	UCCR	950/950	--	--	--	20.0	20.0	217.0	217.0	434.0	0.0	0.0
36	UCCR	1040/1040	--	--	--	20.0	20.0	310.0	287.0	597.0	0.0	0.0
41	UCCR	1040/1040	--	--	--	20.0	20.0	293.0	283.0	576.0	0.0	0.0
45	UCCR	1040/1040	--	--	--	20.0	20.0	147.0	160.0	307.0	0.0	0.0
46	UCCR	1040/1040	--	--	--	20.0	20.0	141.0	154.0	295.0	0.0	0.0

TABLE IV: CREEP-FATIGUE DATA (CONTINUED)

LABORATORY: CIT
MATERIAL: MAR M002

SPEC NO	STRAINS & FAILURE DATA										FAILURE DATA-CYCLES			IF-HRS
	TOTAL	EL	IN	PP	PC	CP	CC	NO	NI	NS	NI	NS	NI	
9A	0.872	0.768	0.104	0.104	0.000	0.000	0.000	--	--	--	--	327	--	0.20
7A	0.771	0.735	0.036	0.036	0.000	0.000	0.000	--	--	--	--	1515	--	0.80
8A	0.648	0.616	0.032	0.032	0.000	0.000	0.000	--	--	--	--	1977	--	1.00
6A	0.573	0.567	0.006	0.006	0.000	0.000	0.000	--	--	--	--	9613	--	5.40
14	2.020	1.176	0.844	0.844	0.000	0.000	0.000	--	--	--	--	10	--	0.01
13	1.065	0.895	0.170	0.170	0.000	0.000	0.000	--	--	--	--	220	--	0.10
10	0.685	0.646	0.039	0.039	0.000	0.000	0.000	--	--	--	--	825	--	0.40
18	0.544	0.519	0.025	0.025	0.000	0.000	0.000	--	--	--	--	1790	--	0.80
19	0.304	0.300	0.004	0.004	0.000	0.000	0.000	--	--	--	--	10963	--	5.00
1B	0.664	0.549	0.155	0.155	0.000	0.000	0.000	--	--	--	--	511	--	0.15
24	0.977	0.636	0.341	0.341	0.000	0.000	0.000	--	--	--	--	95	--	0.03
21	0.705	0.525	0.180	0.180	0.000	0.000	0.000	--	--	--	--	370	--	0.10
22	0.502	0.435	0.067	0.067	0.000	0.000	0.000	--	1200	930	--	1640	--	0.50
25	0.449	0.405	0.044	0.044	0.000	0.000	0.000	--	--	--	--	1600	--	1.30
10A	0.600	0.585	0.016	0.016	0.008	0.008	0.000	--	--	--	--	1673	--	10.00
32	1.000	0.789	0.211	0.074	0.067	0.143	0.000	--	--	--	--	92	--	0.50
33	0.707	0.633	0.071	0.071	0.028	0.046	0.000	--	--	--	--	408	--	2.50
38	0.487	0.476	0.011	0.011	0.001	0.010	0.000	--	--	--	--	1261	--	7.60
2B	0.423	0.351	0.072	0.041	0.031	0.031	0.000	--	--	--	--	1511	--	8.70
31	0.928	0.413	0.515	0.155	0.155	0.360	0.000	--	--	--	--	53	--	0.30
34	0.550	0.373	0.177	0.046	0.131	0.000	0.000	--	--	--	--	802	--	2.30
42	0.315	0.249	0.066	0.026	0.040	0.000	0.000	--	--	--	--	1985	--	11.60
11A	0.670	0.630	0.040	0.018	0.000	0.022	0.000	--	--	--	--	2173	--	11.30
29	0.996	0.776	0.220	0.066	0.000	0.154	0.000	--	--	--	--	165	--	1.00
39	0.863	0.769	0.094	0.025	0.000	0.068	0.000	--	--	--	--	805	--	4.90
30	0.731	0.639	0.092	0.025	0.000	0.078	0.000	--	--	--	--	1075	--	6.40
37	0.600	0.537	0.063	0.009	0.000	0.053	0.000	--	--	--	--	1895	--	11.20
26	0.724	0.445	0.279	0.075	0.000	0.204	0.000	--	--	--	--	99	--	0.50
27	0.538	0.385	0.153	0.055	0.000	0.098	0.000	--	--	--	--	347	--	2.00
40	0.402	0.278	0.124	0.031	0.000	0.093	0.000	--	--	--	--	451	--	2.60
12A	0.700	0.652	0.048	0.032	0.000	0.000	0.016	--	--	--	--	1377	--	15.80
47	0.586	0.473	0.113	0.029	0.000	0.000	0.084	--	--	--	--	571	--	6.60
35	0.796	0.585	0.211	0.063	0.000	0.033	0.114	--	--	--	--	180	--	2.00
44	0.489	0.437	0.052	0.003	0.000	0.003	0.046	--	--	--	--	1325	--	15.00
4B	0.360	0.274	0.086	0.014	0.000	0.006	0.066	--	--	--	--	1995	--	21.00
36	0.891	0.435	0.456	0.132	0.000	0.004	0.319	--	--	--	--	57	--	0.60
41	0.700	0.350	0.350	0.091	0.000	0.014	0.245	--	--	--	--	119	--	1.40
45	0.398	0.198	0.200	0.024	0.000	0.016	0.160	--	--	--	--	502	--	5.80
46	0.297	0.176	0.121	0.015	0.000	0.016	0.095	--	--	--	--	1237	--	12.00

TABLE IV: CREEP-FATIGUE DATA (CONTINUED)

LABORATORY: NGTE
MATERIAL: NIMONIC 90

RATE DATA & STRESSES

SPEC NO	TEST TYPE	TEMP-C	FREQ HZ	RATE DATA (HALF-PIE-TYPE-VALUES)			STRESS (HALF-PIE-TYPE-VALUES)			RELAXATION			CYCLIC STRAIN		
				TEN	COMP	SHAIN-RATE-K/SEC	TEN	COMP	HOLD-TIME-SEC	TEN	COMP	MAX	TEN	COMP	HARDENING %
2/8/78	HRSC	650/650	4.2E-01	--	--	--	0	0	0	756.0	770.0	1526.0	0.0	0.0	-4.00
85/8/77	HRSC	650/650	4.2E-01	--	--	--	0	0	0	746.0	768.0	1514.0	0.0	0.0	-8.00
84/8/77	HRSC	650/650	4.2E-01	--	--	--	0	0	0	583.0	609.0	1192.0	0.0	0.0	-13.00
3/8/78	HRSC	650/650	4.2E-01	--	--	--	0	0	0	554.0	572.0	1126.0	0.0	0.0	-14.00
8/8/78	HRSC	810/810	4.2E-01	--	--	--	0	0	0	612.0	637.0	1249.0	0.0	0.0	-5.00
31/8/77	HRSC	810/810	4.2E-01	--	--	--	0	0	0	605.0	628.0	1233.0	0.0	0.0	-16.00
39/8/77	HRSC	810/810	4.2E-01	--	--	--	0	0	0	521.0	556.0	1077.0	0.0	0.0	-19.00
32/8/77	HRSC	810/810	4.2E-01	--	--	--	0	0	0	476.0	507.0	983.0	0.0	0.0	-20.00
34/8/77	HRSC	810/810	4.2E-01	--	--	--	0	0	0	482.0	506.0	988.0	0.0	0.0	-17.00
35/8/77	HRSC	810/810	4.2E-01	--	--	--	0	0	0	430.0	481.0	911.0	0.0	0.0	-19.00
30/8/77	HRSC	810/810	4.2E-01	--	--	--	0	0	0	378.0	445.0	923.0	0.0	0.0	-12.00
33/8/77	HRSC	810/810	4.2E-01	--	--	--	0	0	0	251.0	528.0	779.0	0.0	0.0	--
41/8/77	HRSC	810/810	4.2E-01	--	--	--	0	0	0	255.0	353.0	648.0	0.0	0.0	-3.00
62/8/77	HRSC	900/900	4.2E-01	--	--	--	0	0	0	366.0	386.0	752.0	0.0	0.0	-13.00
79/8/77	HRSC	900/900	4.2E-01	--	--	--	0	0	0	348.0	372.0	720.0	0.0	0.0	-13.00
80/8/77	HRSC	900/900	4.2E-01	--	--	--	0	0	0	320.0	348.0	668.0	0.0	0.0	-3.00
87/8/77	HRSC	900/900	4.2E-01	--	--	--	0	0	0	282.0	310.0	592.0	0.0	0.0	-6.00
83/8/77	HRSC	900/900	4.2E-01	--	--	--	0	0	0	270.0	270.0	540.0	0.0	0.0	-2.00
92/8/77	HRSC	900/900	4.2E-01	--	--	--	0	0	0	214.0	269.0	483.0	0.0	0.0	--
45/8/77	CCCR	810/810	1.7E-02	--	--	--	0	0	55.0	899.0	578.0	1427.0	0.0	0.0	14.00
46/8/77	CCCR	810/810	2.5E-02	--	--	--	0	0	35.0	586.0	409.0	995.0	0.0	0.0	-5.00
47/8/77	CCCR	810/810	5.6E-02	--	--	--	0	0	15.0	486.0	271.0	757.0	0.0	0.0	3.00
42/8/77	TCCR	810/810	1.7E-02	--	--	--	55.0	0	0	528.0	808.0	1336.0	0.0	0.0	3.00
43/8/77	TCCR	810/810	3.3E-02	--	--	--	27.0	0	0	376.0	594.0	970.0	0.0	0.0	10.00
44/8/77	TCCR	810/810	5.6E-02	--	--	--	15.0	0	0	318.0	501.0	819.0	0.0	0.0	-1.00
53/8/77	TCCR	810/810	1.3E-01	--	--	--	5.2	0	0	281.0	412.0	693.0	0.0	0.0	-3.00
48/8/77	BCCR	810/810	3.7E-03	--	--	--	110.0	160.0	0	472.0	472.0	944.0	0.0	0.0	-3.00
49/8/77	BCCR	810/810	9.3E-03	--	--	--	36.0	72.0	0	388.0	381.0	769.0	0.0	0.0	--
54/8/77	BCCR	810/810	3.3E-01	--	--	--	1.2	1.8	0	448.0	451.0	889.0	0.0	0.0	-12.00
50/8/77	BCCR	810/810	2.0E-02	--	--	--	12.6	38.0	0	338.0	344.0	682.0	0.0	0.0	-6.00
55/8/77	BCCR	810/810	2.0E-02	--	--	--	20.0	28.0	0	320.0	325.0	645.0	0.0	0.0	-2.00
52/8/77	BCCR	810/810	1.1E-01	--	--	--	3.5	5.4	0	374.0	384.0	758.0	0.0	0.0	-4.00
66/8/77	BCCR	810/810	8.1E-02	--	--	--	6.0	4.5	0	367.0	376.0	743.0	0.0	0.0	-6.00
6/8/78	BCCR	810/810	8.1E-02	--	--	--	6.0	3.6	0	353.0	353.0	706.0	0.0	0.0	-4.00
4/8/78	BCCR	810/810	1.1E-01	--	--	--	3.3	3.6	0	367.0	380.0	747.0	0.0	0.0	--
9/8/78	BCCR	810/810	2.7E-02	--	--	--	17.4	17.4	0	280.0	264.0	544.0	0.0	0.0	-3.00
51/8/77	BCCR	810/810	5.6E-02	--	--	--	8.0	10.0	0	244.0	261.0	525.0	0.0	0.0	-14.00
69/8/77	LRSC	810/810	3.3E-02	--	--	--	--	--	--	--	--	900.0	0.0	0.0	-28.00
7/8/78	LRSC	810/810	3.3E-02	--	--	--	--	--	--	508.0	528.0	1036.0	0.0	0.0	-12.00
10/8/78	LRSC	810/810	3.3E-02	--	--	--	--	--	--	--	--	878.0	0.0	0.0	-15.00
77/8/77	LRSC	810/810	3.0E-03	--	--	--	--	--	--	--	--	841.0	0.0	0.0	-19.00
76/8/77	LRSC	810/810	3.0E-03	--	--	--	--	--	--	--	--	760.0	0.0	0.0	-16.00
76/8/77	LRSC	810/810	3.0E-03	--	--	--	--	--	--	--	--	--	0.0	0.0	-16.00

TABLE IV: CREEP-FATIGUE DATA (CONTINUED)

SPEC NO		TEST TYPE	TEMP C	RATE DATA (HALF-LIFE VALUES)				STRESSES (HALF-LIFE VALUES)				RELAXATION				CYCLIC STRAIN																																																																																																																																																																																																																																																																																																																																																																																																																																																																																																																																																																																																																																																																																																																																																																																																																																																																																																																																																				
				FREQ HZ	STEADY STATE	STEADY STATE	STEADY STATE	STEADY STATE	STEADY STATE	STEADY STATE	STEADY STATE	STEADY STATE	STEADY STATE	STEADY STATE	STEADY STATE	STEADY STATE	STEADY STATE	STEADY STATE	STEADY STATE	STEADY STATE																																																																																																																																																																																																																																																																																																																																																																																																																																																																																																																																																																																																																																																																																																																																																																																																																																																																																																																																																
				TEN	COMP	TEN	COMP	TEN	COMP	TEN	COMP	TEN	COMP	TEN	COMP	TEN	COMP	TEN	COMP	TEN	COMP	TEN	COMP	TEN	COMP	TEN	COMP	TEN	COMP	TEN	COMP	TEN	COMP	TEN	COMP	TEN	COMP	TEN	COMP	TEN	COMP	TEN	COMP	TEN	COMP	TEN	COMP	TEN	COMP	TEN	COMP	TEN	COMP	TEN	COMP	TEN	COMP	TEN	COMP	TEN	COMP	TEN	COMP	TEN	COMP	TEN	COMP	TEN	COMP	TEN	COMP	TEN	COMP	TEN	COMP	TEN	COMP	TEN	COMP	TEN	COMP	TEN	COMP	TEN	COMP	TEN	COMP	TEN	COMP	TEN	COMP	TEN	COMP	TEN	COMP	TEN	COMP	TEN	COMP	TEN	COMP	TEN	COMP	TEN	COMP	TEN	COMP	TEN	COMP	TEN	COMP	TEN	COMP	TEN	COMP	TEN	COMP	TEN	COMP	TEN	COMP	TEN	COMP	TEN	COMP	TEN	COMP	TEN	COMP	TEN	COMP	TEN	COMP	TEN	COMP	TEN	COMP	TEN	COMP	TEN	COMP	TEN	COMP	TEN	COMP	TEN	COMP	TEN	COMP	TEN	COMP	TEN	COMP	TEN	COMP	TEN	COMP	TEN	COMP	TEN	COMP	TEN	COMP	TEN	COMP	TEN	COMP	TEN	COMP	TEN	COMP	TEN	COMP	TEN	COMP	TEN	COMP	TEN	COMP	TEN	COMP	TEN	COMP	TEN	COMP	TEN	COMP	TEN	COMP	TEN	COMP	TEN	COMP	TEN	COMP	TEN	COMP	TEN	COMP	TEN	COMP	TEN	COMP	TEN	COMP	TEN	COMP	TEN	COMP	TEN	COMP	TEN	COMP	TEN	COMP	TEN	COMP	TEN	COMP	TEN	COMP	TEN	COMP	TEN	COMP	TEN	COMP	TEN	COMP	TEN	COMP	TEN	COMP	TEN	COMP	TEN	COMP	TEN	COMP	TEN	COMP	TEN	COMP	TEN	COMP	TEN	COMP	TEN	COMP	TEN	COMP	TEN	COMP	TEN	COMP	TEN	COMP	TEN	COMP	TEN	COMP	TEN	COMP	TEN	COMP	TEN	COMP	TEN	COMP	TEN	COMP	TEN	COMP	TEN	COMP	TEN	COMP	TEN	COMP	TEN	COMP	TEN	COMP	TEN	COMP	TEN	COMP	TEN	COMP	TEN	COMP	TEN	COMP	TEN	COMP	TEN	COMP	TEN	COMP	TEN	COMP	TEN	COMP	TEN	COMP	TEN	COMP	TEN	COMP	TEN	COMP	TEN	COMP	TEN	COMP	TEN	COMP	TEN	COMP	TEN	COMP	TEN	COMP	TEN	COMP	TEN	COMP	TEN	COMP	TEN	COMP	TEN	COMP	TEN	COMP	TEN	COMP	TEN	COMP	TEN	COMP	TEN	COMP	TEN	COMP	TEN	COMP	TEN	COMP	TEN	COMP	TEN	COMP	TEN	COMP	TEN	COMP	TEN	COMP	TEN	COMP	TEN	COMP	TEN	COMP	TEN	COMP	TEN	COMP	TEN	COMP	TEN	COMP	TEN	COMP	TEN	COMP	TEN	COMP	TEN	COMP	TEN	COMP	TEN	COMP	TEN	COMP	TEN	COMP	TEN	COMP	TEN	COMP	TEN	COMP	TEN	COMP	TEN	COMP	TEN	COMP	TEN	COMP	TEN	COMP	TEN	COMP	TEN	COMP	TEN	COMP	TEN	COMP	TEN	COMP	TEN	COMP	TEN	COMP	TEN	COMP	TEN	COMP	TEN	COMP	TEN	COMP	TEN	COMP	TEN	COMP	TEN	COMP	TEN	COMP	TEN	COMP	TEN	COMP	TEN	COMP	TEN	COMP	TEN	COMP	TEN	COMP	TEN	COMP	TEN	COMP	TEN	COMP	TEN	COMP	TEN	COMP	TEN	COMP	TEN	COMP	TEN	COMP	TEN	COMP	TEN	COMP	TEN	COMP	TEN	COMP	TEN	COMP	TEN	COMP	TEN	COMP	TEN	COMP	TEN	COMP	TEN	COMP	TEN	COMP	TEN	COMP	TEN	COMP	TEN	COMP	TEN	COMP	TEN	COMP	TEN	COMP	TEN	COMP	TEN	COMP	TEN	COMP	TEN	COMP	TEN	COMP	TEN	COMP	TEN	COMP	TEN	COMP	TEN	COMP	TEN	COMP	TEN	COMP	TEN	COMP	TEN	COMP	TEN	COMP	TEN	COMP	TEN	COMP	TEN	COMP	TEN	COMP	TEN	COMP	TEN	COMP	TEN	COMP	TEN	COMP	TEN	COMP	TEN	COMP	TEN	COMP	TEN	COMP	TEN	COMP	TEN	COMP	TEN	COMP	TEN	COMP	TEN	COMP	TEN	COMP	TEN	COMP	TEN	COMP	TEN	COMP	TEN	COMP	TEN	COMP	TEN	COMP	TEN	COMP	TEN	COMP	TEN	COMP	TEN	COMP	TEN	COMP	TEN	COMP	TEN	COMP	TEN	COMP	TEN	COMP	TEN	COMP	TEN	COMP	TEN	COMP	TEN	COMP	TEN	COMP	TEN	COMP	TEN	COMP	TEN	COMP	TEN	COMP	TEN	COMP	TEN	COMP	TEN	COMP	TEN	COMP	TEN	COMP	TEN	COMP	TEN	COMP	TEN	COMP	TEN	COMP	TEN	COMP	TEN	COMP	TEN	COMP	TEN	COMP	TEN	COMP	TEN	COMP	TEN	COMP	TEN	COMP	TEN	COMP	TEN	COMP	TEN	COMP	TEN	COMP	TEN	COMP	TEN	COMP	TEN	COMP	TEN	COMP	TEN	COMP	TEN	COMP	TEN	COMP	TEN	COMP	TEN	COMP	TEN	COMP	TEN	COMP	TEN	COMP	TEN	COMP	TEN	COMP	TEN	COMP	TEN	COMP	TEN	COMP	TEN	COMP	TEN	COMP	TEN	COMP	TEN	COMP	TEN	COMP	TEN	COMP	TEN	COMP	TEN	COMP	TEN	COMP	TEN	COMP	TEN	COMP	TEN	COMP	TEN	COMP	TEN	COMP	TEN	COMP	TEN	COMP	TEN	COMP	TEN	COMP	TEN	COMP	TEN	COMP	TEN	COMP	TEN	COMP	TEN	COMP	TEN	COMP	TEN	COMP	TEN	COMP	TEN	COMP	TEN	COMP	TEN	COMP	TEN	COMP	TEN	COMP	TEN	COMP	TEN	COMP	TEN	COMP	TEN	COMP	TEN	COMP	TEN	COMP	TEN	COMP	TEN	COMP	TEN	COMP	TEN	COMP	TEN	COMP	TEN	COMP	TEN	COMP	TEN	COMP	TEN	COMP	TEN	COMP	TEN	COMP	TEN	COMP	TEN	COMP	TEN	COMP	TEN	COMP	TEN	COMP	TEN	COMP	TEN	COMP	TEN	COMP	TEN	COMP	TEN	COMP	TEN	COMP	TEN	COMP	TEN	COMP	TEN	COMP	TEN	COMP	TEN	COMP	TEN	COMP	TEN	COMP	TEN	COMP	TEN	COMP	TEN	COMP	TEN	COMP	TEN	COMP	TEN	COMP	TEN	COMP	TEN	COMP	TEN	COMP	TEN	COMP	TEN	COMP	TEN	COMP	TEN	COMP	TEN	COMP	TEN	COMP	TEN	COMP	TEN	COMP	TEN	COMP	TEN	COMP	TEN	COMP	TEN	COMP	TEN	COMP	TEN	COMP	TEN	COMP	TEN	COMP	TEN	COMP	TEN	COMP	TEN	COMP	TEN	COMP	TEN	COMP	TEN	COMP	TEN	COMP	TEN	COMP	TEN	COMP	TEN	COMP	TEN	COMP	TEN	COMP	TEN	COMP	TEN	COMP	TEN	COMP	TEN	COMP	TEN	COMP	TEN	COMP	TEN	COMP	TEN	COMP	TEN	COMP	TEN	COMP	TEN	COMP	TEN	COMP	TEN	COMP	TEN	COMP	TEN	COMP	TEN	COMP	TEN	COMP	TEN	COMP	TEN	COMP	TEN	COMP	TEN

LABORATORY: CEAT
MATERIAL: WASPALOY

RATE DATA & STRESSES

TABLE IV: CREEP-FATIGUE DATA (CONTINUED)

LABORATORY: CEAT
MATERIAL: WASPALOY

STRAINS & FAILURE DATA

SPEC NO	STRAIN RANGES (HALF-LIFE VALUES) %					NO		FAILURE DATA - CYCLES					TF-HRS	
	TOTAL	EL	IN	EP	PC	CP	CC	NI	NE	NP	TF	TF		
B1-10	1.410	0.350	1.020	1.020	0.000	0.000	0.000	--	140	120	142	0.08		
B1-9	0.981	0.350	0.631	0.631	0.000	0.000	0.000	--	300	235	303	0.17		
B1-6	0.796	0.305	0.491	0.491	0.000	0.000	0.000	--	462	370	470	0.26		
B1-19	0.571	0.261	0.310	0.310	0.000	0.000	0.000	--	1100	960	1109	0.62		
B1-11	0.340	0.223	0.117	0.117	0.000	0.000	0.000	--	3235	3150	3396	1.89		
B1-18	0.280	0.214	0.066	0.066	0.000	0.000	0.000	--	7500	7260	7618	4.23		
B2-8	0.993	0.340	0.653	0.563	0.090	0.000	0.000	--	71	63	72	0.64		
B1-16	1.006	0.332	0.674	0.594	0.080	0.000	0.000	--	122	124	135	1.20		
B2-4	0.792	0.325	0.467	0.400	0.067	0.000	0.000	--	148	144	153	1.36		
B1-2	0.607	0.290	0.317	0.279	0.038	0.000	0.000	--	274	257	305	2.71		
B2-18	0.333	0.272	0.061	0.047	0.014	0.000	0.000	--	740	738	792	7.04		
B2-6	0.270	0.259	0.011	0.005	0.006	0.000	0.000	--	1042	994	1076	9.56		
B2-1	0.594	0.322	0.672	0.598	0.000	0.084	0.000	--	--	--	160	1.42		
B2-9	0.801	0.307	0.494	0.427	0.000	0.067	0.000	--	--	200	210	1.87		
B1-12	0.601	0.241	0.360	0.318	0.000	0.042	0.000	--	361	354	384	3.41		
B2-17	0.335	0.244	0.091	0.067	0.000	0.024	0.000	--	1600	1450	1616	14.36		
B2-7	0.275	0.232	0.043	0.031	0.000	0.012	0.000	--	2655	2325	2679	23.81		
B1-20	0.999	0.224	0.775	0.695	0.000	0.005	0.075	--	135	100	136	2.34		
B1-14	0.796	0.220	0.576	0.517	0.000	0.004	0.055	--	190	162	192	3.30		
B1-17	0.563	0.178	0.385	0.339	0.000	0.008	0.038	--	442	343	450	7.75		
B1-1	0.344	0.183	0.161	0.139	0.000	0.003	0.019	--	880	850	1012	17.43		
B1-15	0.199	0.173	0.026	0.018	0.000	0.000	0.008	--	--	2750	3100	53.38		
B2-3	0.788	0.214	0.574	0.469	0.000	0.045	0.060	--	139	119	140	4.70		
B2-16	0.787	0.215	0.572	0.473	0.000	0.044	0.055	--	150	119	150	5.04		
B2-14	0.791	0.219	0.572	0.473	0.000	0.040	0.059	--	152	119	152	5.11		
B2-2	0.791	0.213	0.578	0.480	0.000	0.041	0.057	--	185	153	189	6.35		
B2-11	0.597	0.214	0.383	0.306	0.000	0.033	0.044	--	201	174	210	7.05		
B2-12	0.591	0.201	0.389	0.306	0.000	0.036	0.047	--	213	182	237	7.96		
B1-21	0.596	0.194	0.402	0.342	0.000	0.025	0.035	--	344	259	351	11.79		

TABLE IV: CREEP-FATIGUE DATA (CONTINUED)

LABORATORY: NPL
MATERIAL: IN738LC

RATE DATA & STRESSES

SPEC NO	TEST TYPE	TEMP-C	RATE DATA (HALF-LIFE VALUES)				STRESSSES (HALF-LIFE VALUES)				CYCLIC STRAIN			
			PREQ HZ	STRAIN-RATE-1/SEC	TEMP	COMP	TEN	COMP	MAX	RELAXATION		TEMP	COMP	HARDENING %
DCH28	HRSC	850/850	8.0E-01	1.3E-00	1.3E-00	0	0	343.0	542.0	885.0	0.0	0.0	0.0	-5.00
DCH42	HRSC	850/850	2.5E-01	1.0E-00	1.0E-00	0	0	892.0	916.0	1808.0	0.0	0.0	0.0	-43.00
DCH79	HRSC	850/850	5.0E-01	1.0E-00	1.0E-00	0	0	427.0	648.0	1075.0	0.0	0.0	0.0	-33.00
DCH65	HRSC	850/850	3.8E-01	1.0E-00	1.0E-00	0	0	751.0	826.0	1577.0	0.0	0.0	0.0	--
DCH41	BCCR	850/850	7.8E-01	7.0E-01	50.0	75.0	0	350.0	350.0	700.0	0.0	0.0	0.0	--
DCH43	BCCR	850/850	6.5E-03	1.0E-00	1.0E-00	75.0	100.0	400.0	400.0	800.0	0.0	0.0	0.0	--
DCH73	BCCR	850/850	1.0E-03	1.0E-00	1.0E-00	250.0	700.0	550.0	550.0	1100.0	0.0	0.0	0.0	--
DCH94	BCCR	850/850	9.6E-03	1.0E-00	1.0E-00	38.0	63.0	450.0	450.0	900.0	0.0	0.0	0.0	--
DCH39	CCCR	850/850	3.6E-03	1.0E-00	1.0E-00	0	275.0	930.0	500.0	1430.0	0.0	0.0	0.0	--
DCH40	CCCR	850/850	8.3E-02	1.0E-00	1.0E-00	0	10.0	690.0	400.0	1090.0	0.0	0.0	0.0	-8.00
DCH45	CCCR	850/850	3.7E-02	7.0E-01	7.0E-01	0	25.0	455.0	300.0	755.0	0.0	0.0	0.0	--
DCH67	CCCR	850/850	6.8E-02	1.0E-00	1.0E-00	0	12.0	731.0	400.0	1131.0	0.0	0.0	0.0	-7.50
DCH46	TCCR	850/850	7.5E-02	8.0E-01	8.0E-01	12.0	0	300.0	710.0	1010.0	0.0	0.0	0.0	-5.00
DCH66	TCCR	850/850	2.1E-02	9.0E-01	9.0E-01	45.0	0	350.0	845.0	1196.0	0.0	0.0	0.0	-3.00
DCH68	TCCR	850/850	9.8E-03	8.0E-01	8.0E-01	100.0	0	190.0	640.0	830.0	0.0	0.0	0.0	-3.00
DCH93	TCCR	850/850	1.7E-03	1.0E-00	1.0E-00	600.0	0	450.0	958.0	1408.0	0.0	0.0	0.0	-3.50

STRAINS & FAILURE DATA

SPEC NO	TOTAL	STRAIN RANGES (HALF-LIFE VALUES) %				CC	NO	FAILURE DATA-CYCLES				IF-HRS
		EL	IN	EP	PC			NI	NI	NI	NI	
DCH28	0.700	0.668	0.032	0.032	0.000	0.000	--	--	6178	19	1.92	0.01
DCH42	2.000	1.160	0.840	0.045	0.000	0.000	--	--	475	45	0.13	0.12
DCH79	1.000	0.920	0.080	0.080	0.000	0.000	200	--	2214	147	22.90	0.68
DCH85	1.300	1.040	0.257	0.257	0.000	0.000	1500	--	147	3	7.70	1.00
DCH41	0.700	0.530	0.168	0.032	0.000	0.000	90	--	15	15	1.56	1.56
DCH43	1.000	0.590	0.410	0.120	0.000	0.000	--	--	105	750	16.00	1.20
DCH73	2.000	0.655	1.345	0.200	0.000	0.000	40	--	1056	92	4.30	4.30
DCH94	1.300	0.726	0.574	0.231	0.000	0.000	--	--	2099	25	48.20	4.60
DCH35	2.000	0.770	1.230	0.430	0.000	0.000	--	--	18	18	--	--
DCH40	1.000	0.730	0.270	0.170	0.100	0.000	115	--	105	750	16.00	1.20
DCH45	0.700	0.640	0.057	0.036	0.021	0.000	850	--	1056	92	4.30	4.30
DCH67	1.300	0.980	0.420	0.250	0.170	0.000	94	--	2099	25	48.20	4.60
DCH46	1.000	0.800	0.197	0.113	0.000	0.084	700	--	1056	92	4.30	4.30
DCH66	1.300	0.830	0.410	0.200	0.000	0.000	65	--	2099	25	48.20	4.60
DCH68	0.700	0.566	0.134	0.087	0.000	0.047	2000	--	1950	18	--	--
DCH93	2.000	0.840	1.160	0.285	0.000	0.875	15	--	18	18	--	--

LABORATORY: APRN
MATERIAL: FENEY 95

TABLE IV: CREEP-FATIGUE DATA (CONTINUED)

RATE DATA & STRESSES

SPEC NO	TEST TYPE	TEMP-C	FREQ HZ	RATE DATA (HALF-LIFE VALUES)				STRESSES (HALF-LIFE VALUES) MPa				CYCLIC STRAIN
				TEN	COMP	WAVE	WAVE	TEN	COMP	WAVE	WAVE	
SPEC NO	TEST TYPE	TEMP-C	FREQ HZ	RATE DATA (HALF-LIFE VALUES)				STRESSES (HALF-LIFE VALUES) MPa				CYCLIC STRAIN
				TEN	COMP	WAVE	WAVE	TEN	COMP	WAVE	WAVE	
21	HRSC	650/650	3.3E-01	1.5E 00	1.5E 00	1.5E 00	1.5E 00	1241.0	1310.0	2551.0	0.0	0.0
17	HRSC	650/650	3.3E-01	1.3E 00	1.3E 00	1.3E 00	1.3E 00	1227.0	1345.0	2572.0	0.0	0.0
18	HRSC	650/650	3.3E-01	1.2E 00	1.2E 00	1.2E 00	1.2E 00	1206.0	1283.0	2489.0	0.0	0.0
224	HRSC	650/650	3.3E-01	1.1E 00	1.1E 00	1.1E 00	1.1E 00	1158.0	1214.0	2372.0	0.0	0.0
22	HRSC	650/650	3.3E-01	1.1E 00	1.1E 00	1.1E 00	1.1E 00	1158.0	1193.0	2351.0	0.0	0.0
240	HRSC	650/650	3.3E-01	1.1E 00	1.1E 00	1.1E 00	1.1E 00	1110.0	1200.0	2310.0	0.0	0.0
26	HRSC	650/650	3.3E-01	9.3E-01	9.3E-01	9.3E-01	9.3E-01	1076.0	1131.0	2207.0	0.0	0.0
27	HRSC	650/650	3.3E-01	8.0E-01	8.0E-01	8.0E-01	8.0E-01	985.0	1007.0	1972.0	0.0	0.0
29	HRSC	650/650	3.3E-01	6.7E-01	6.7E-01	6.7E-01	6.7E-01	800.0	917.0	1717.0	0.0	0.0
30	HRSC	650/650	3.3E-01	6.0E-01	6.0E-01	6.0E-01	6.0E-01	740.0	862.0	1602.0	0.0	0.0
234	HRSC	650/650	3.3E-01	6.0E-01	6.0E-01	6.0E-01	6.0E-01	683.0	923.0	1606.0	0.0	0.0
235	HRSC	650/650	3.3E-01	6.0E-01	6.0E-01	6.0E-01	6.0E-01	684.0	891.0	1574.0	0.0	0.0
239	HRSC	650/650	3.3E-01	5.9E-01	5.9E-01	5.9E-01	5.9E-01	736.0	830.0	1566.0	0.0	0.0
6	CHSC	650/650	1.6E-02	1.2E 00	1.2E 00	1.2E 00	1.2E 00	1230.0	1249.0	2479.0	0.0	103.4
11	CHSC	650/650	1.6E-02	1.1E 00	1.1E 00	1.1E 00	1.1E 00	1120.0	1110.0	2230.0	0.0	108.0
14	CHSC	650/650	1.6E-02	1.1E 00	1.1E 00	1.1E 00	1.1E 00	1220.0	1200.0	2420.0	0.0	73.8
8	CHSC	650/650	1.6E-02	9.3E-01	9.3E-01	9.3E-01	9.3E-01	1140.0	1030.0	2230.0	0.0	42.8
13	CHSC	650/650	1.6E-02	8.0E-01	8.0E-01	8.0E-01	8.0E-01	1080.0	965.0	2045.0	0.0	15.9
241	CHSC	650/650	1.6E-02	7.3E-01	7.3E-01	7.3E-01	7.3E-01	972.0	895.0	1867.0	0.0	9.6
16	CHSC	650/650	1.6E-02	6.7E-01	6.7E-01	6.7E-01	6.7E-01	855.0	848.0	1703.0	0.0	2.8
238	CHSC	650/650	1.6E-02	6.0E-01	6.0E-01	6.0E-01	6.0E-01	880.0	700.0	1580.0	0.0	34.8
222	CHSC	650/650	1.7E-03	9.3E-01	9.3E-01	9.3E-01	9.3E-01	1214.0	1070.0	2254.0	0.0	96.5
41	CHSC	650/650	1.7E-03	8.0E-01	8.0E-01	8.0E-01	8.0E-01	1131.0	807.0	1938.0	0.0	0.0
5	THSC	650/650	1.6E-02	1.2E 00	1.2E 00	1.2E 00	1.2E 00	1180.0	1340.0	2520.0	210.0	0.0
10	THSC	650/650	1.6E-02	1.1E 00	1.1E 00	1.1E 00	1.1E 00	1110.0	1290.0	2400.0	132.0	0.0
7	THSC	650/650	1.6E-02	9.3E-01	9.3E-01	9.3E-01	9.3E-01	1103.0	1317.0	2420.0	51.4	0.0
12	THSC	650/650	1.6E-02	8.0E-01	8.0E-01	8.0E-01	8.0E-01	890.0	1145.0	2035.0	11.0	0.0
39	THSC	650/650	1.6E-02	7.3E-01	7.3E-01	7.3E-01	7.3E-01	745.0	1023.0	2192.0	55.2	0.0
38	THSC	650/650	1.6E-02	6.7E-01	6.7E-01	6.7E-01	6.7E-01	696.0	1021.0	1717.0	33.1	0.0
233	THSC	650/650	1.6E-02	6.7E-01	6.7E-01	6.7E-01	6.7E-01	616.0	1092.0	1708.0	13.1	0.0
33	THSC	650/650	1.6E-02	6.7E-01	6.7E-01	6.7E-01	6.7E-01	571.0	1096.0	1667.0	3.5	0.0
237	THSC	650/650	1.6E-02	6.0E-01	6.0E-01	6.0E-01	6.0E-01	485.0	1047.0	1532.0	8.3	0.0
226	THSC	650/650	1.7E-03	9.3E-01	9.3E-01	9.3E-01	9.3E-01	896.0	1317.0	2213.0	52.1	0.0
40	THSC	650/650	1.7E-03	8.0E-01	8.0E-01	8.0E-01	8.0E-01	745.0	1227.0	1972.0	427.0	0.0
1	BHSC	650/650	8.1E-03	1.2E 00	1.2E 00	1.2E 00	1.2E 00	1250.0	1351.0	2601.0	197.2	149.0
2	BHSC	650/650	8.1E-03	1.1E 00	1.1E 00	1.1E 00	1.1E 00	1172.0	1268.0	2440.0	128.2	96.5
32	BHSC	650/650	8.1E-03	9.3E-01	9.3E-01	9.3E-01	9.3E-01	1034.0	1186.0	2220.0	66.9	49.0
9	BHSC	650/650	8.1E-03	8.0E-01	8.0E-01	8.0E-01	8.0E-01	930.0	1062.0	1992.0	51.7	60.7
15	BHSC	650/650	8.1E-03	6.7E-01	6.7E-01	6.7E-01	6.7E-01	807.0	938.0	1745.0	42.7	35.2
229	BHSC	650/650	8.1E-03	6.0E-01	6.0E-01	6.0E-01	6.0E-01	556.0	883.0	1539.0	0.0	0.0
28	BHSC	650/650	8.3E-04	1.2E 00	1.2E 00	1.2E 00	1.2E 00	1234.0	1331.0	2565.0	376.5	329.0
31	BHSC	650/650	8.3E-04	9.3E-01	9.3E-01	9.3E-01	9.3E-01	1030.0	1180.0	2270.0	338.0	297.2
230	BHSC	650/650	8.3E-04	8.0E-01	8.0E-01	8.0E-01	8.0E-01	980.0	1103.0	2083.0	128.9	104.8

TABLE IV: CREEP-FATIGUE DATA (CONTINUED)

LABORATORY: AFML
MATERIAL: RENE 95

SPEC NO	STRAINS & FAILURE DATA										FAILURE DATA-CYCLES			PP-HRS
	TOTAL	EL	IN	PP	PC	CP	CC	NO	NI	NS	NP			
BASELINE TESTS - PHASE I														
21	2.200	1.450	0.790	0.790	0.000	0.000	0.000	--	--	--	203	0.17		
17	2.000	1.470	0.530	0.530	0.000	0.000	0.000	--	--	--	234	0.19		
18	1.800	1.420	0.410	0.410	0.000	0.000	0.000	--	--	--	307	0.25		
224	1.600	1.350	0.250	0.250	0.000	0.000	0.000	--	--	--	415	0.35		
22	1.600	1.340	0.311	0.311	0.000	0.000	0.000	--	--	--	461	0.38		
240	1.600	1.320	0.285	0.285	0.000	0.000	0.000	--	--	--	463	0.39		
26	1.400	1.260	0.220	0.220	0.000	0.000	0.000	--	--	--	784	0.65		
27	1.200	1.130	0.104	0.104	0.000	0.000	0.000	--	--	--	1629	1.36		
29	1.000	0.980	0.018	0.018	0.000	0.000	0.000	--	--	--	5159	4.30		
30	0.900	0.913	0.012	0.012	0.000	0.000	0.000	--	--	--	16215	13.50		
234	0.900	0.920	0.013	0.013	0.000	0.000	0.000	--	--	--	19160	15.97		
235	0.900	0.900	0.008	0.008	0.000	0.000	0.000	--	--	--	22364	18.54		
239	0.880	0.890	0.013	0.013	0.000	0.000	0.000	--	--	--	28697	23.91		
6	1.800	1.350	0.429	0.370	0.059	0.000	0.000	--	--	--	207	3.50		
11	1.600	1.210	0.468	0.406	0.062	0.000	0.000	--	--	--	209	3.56		
14	1.600	1.340	0.324	0.282	0.042	0.000	0.000	--	--	--	219	3.93		
8	1.400	1.250	0.192	0.168	0.024	0.000	0.000	--	--	--	413	7.30		
13	1.200	1.160	0.098	0.089	0.009	0.000	0.000	--	--	--	846	14.80		
241	1.100	1.060	0.049	0.043	0.005	0.000	0.000	--	--	--	1940	33.95		
16	1.000	0.971	0.010	--	--	0.000	0.000	--	--	--	3093	54.12		
238	0.900	0.900	0.028	0.022	0.005	0.000	0.000	--	--	--	4619	90.83		
222	1.400	1.280	0.136	0.116	0.020	0.000	0.000	--	--	--	224	37.52		
41	1.200	1.050	0.185	0.130	0.055	0.000	0.000	--	--	--	283	47.40		
245	2.000	1.320	0.657	0.537	0.000	0.120	0.000	--	--	--	171	2.99		
5	1.600	1.290	0.522	0.447	0.000	0.075	0.000	--	--	--	255	4.47		
10	1.600	1.350	0.297	0.262	0.000	0.035	0.000	--	--	--	257	4.51		
7	1.400	1.210	0.206	0.175	0.000	0.031	0.000	--	--	--	749	13.09		
12	1.200	1.160	0.089	0.083	0.000	0.006	0.000	--	--	--	1289	23.02		
39	1.100	1.010	0.089	0.070	0.000	0.019	0.000	--	--	--	1781	31.17		
38	1.000	0.978	0.049	0.043	0.000	0.006	0.000	--	--	--	5013	87.72		
233	1.000	0.970	0.060	0.053	0.000	0.007	0.000	--	--	--	6519	114.08		
33	1.000	0.952	0.038	0.036	0.000	0.002	0.000	--	--	--	9609	163.15		
237	0.900	0.870	0.046	0.041	0.000	0.005	0.000	--	--	--	16418	267.31		
228	1.400	1.230	0.185	0.155	0.000	0.030	0.000	--	--	--	441	80.57		
40	1.200	1.100	0.126	0.102	0.000	0.024	0.000	--	--	--	1705	285.58		
1	1.800	1.300	0.550	0.437	0.000	0.028	0.085	--	--	--	156	5.29		
2	1.600	1.270	0.348	0.276	0.000	0.018	0.055	--	--	--	238	9.07		
32	1.400	1.200	0.201	0.163	0.000	0.010	0.028	--	--	--	358	12.13		
9	1.200	1.070	0.122	0.087	0.005	0.000	0.030	--	--	--	959	32.46		
15	1.000	0.952	0.078	0.054	0.000	0.004	0.020	--	--	--	1289	43.65		
229	0.900	0.880	0.024	0.024	0.000	0.000	0.000	--	--	--	5277	173.42		
28	1.800	1.060	0.701	0.486	0.000	0.027	0.188	--	--	--	115	33.41		
31	1.400	0.933	0.497	0.304	0.000	0.023	0.170	--	--	--	199	65.95		
30	1.200	1.060	0.157	0.084	0.000	0.014	0.060	--	--	--	331	110.55		

TABLE IV: CREEP-FATIGUE DATA (CONTINUED)

LABORATORY: APML
MATERIAL: RENE 95

RATE DATA & STRESSES

SPEC	TEST	TEMP-C	RATE DATA (HALF-LIFE VALUES)		TIME-SEC	TEN	STRESSES (HALF-LIFE VALUES)		RELAXATION	CYCLIC STRAIN	
			SIRAIN-RATE-W/SEC	HOLD			COMP	RANGE			
Cyclic Creep Tests - Phase II											
RE-11	HRSC	650/650	6.0E-01	3.5E-00	0	1407.0	1483.0	2896.0	0.0	0.0	
RE-16	HRSC	650/650	4.0E-01	1.3E-00	0	1124.0	1207.0	2331.0	0.0	0.0	
RE-4	CCCR	650/650	3.2E-04	1.2E-01	0	1476.0	1203.0	2676.0	0.0	0.0	
RE-15	CCCR	650/650	1.6E-03	1.8E-01	0	1138.0	862.0	2000.0	0.0	0.0	
RE-20	TCCR	650/650	8.2E-04	1.5E-01	1180.0	1220.0	1510.0	2730.0	0.0	0.0	
RE-14	TCCR	650/650	1.0E-03	1.7E-01	980.0	1027.0	1365.0	2392.0	0.0	0.0	
RE-7	BCCR	650/650	1.2E-04	--	2340.0	1103.0	1103.0	2266.0	0.0	0.0	
RE-13	BCCR	650/650	3.2E-04	--	960.0	1000.0	1000.0	2000.0	0.0	0.0	
RE-10	BCCR	650/650	1.8E-03	--	--	993.0	993.0	1966.0	0.0	0.0	
Validation Tests - Phase III											
227	HRSC	650/650	1.5E-03	9.3E-01	600.0	993.0	1214.0	2227.0	164.1	91.0	
223	HRSC	650/650	1.5E-03	8.0E-01	600.0	814.0	1131.0	1945.0	80.0	36.5	
226	HRSC	650/650	1.5E-03	9.3E-01	60.0	1138.0	1110.0	2248.0	109.6	34.5	
225	HRSC	650/650	1.5E-03	8.0E-01	60.0	1034.0	965.0	1999.0	84.1	73.1	
23*	LRSC	650/650	8.3E-04	7.5E-04	--	1110.0	1248.0	2358.0	0.0	0.0	
24*	LRSC	650/650	8.3E-04	5.8E-04	0	1151.0	1296.0	2453.0	0.0	0.0	
25*	LRSC	650/650	8.3E-04	3.0E-04	0	1000.0	1255.0	2255.0	0.0	0.0	
20*	LRSC	650/650	8.3E-04	4.2E-04	0	1110.0	1234.0	2344.0	0.0	0.0	
34	LRSC	650/650	8.3E-04	2.2E-03	0	945.0	1138.0	2083.0	0.0	0.0	
19*	LRSC	650/650	8.3E-04	1.7E-04	0	807.0	1076.0	1883.0	0.0	0.0	
252	SPSC	650/650	1.7E-03	2.3E-03	9.3E-01	1147.0	1207.0	2354.0	0.0	0.0	
251	PSSC	650/650	1.7E-04	9.3E-01	2.3E-03	1110.0	1220.0	2330.0	0.0	0.0	
247	VERF	650/650	1.6E-02	1.2E-00	60.0	1186.0	1283.0	2469.0	0.0	101.0	
246	VERF	650/650	1.6E-02	1.2E-00	60.0	1172.0	1310.0	2482.0	113.8	0.0	
244	VERF	650/650	1.6E-02	1.1E-00	60.0	1062.0	1248.0	2310.0	68.9	0.0	
242	VERF	650/650	1.6E-02	1.2E-00	60.0	1124.0	1283.0	2407.0	89.6	0.0	

* PLASTIC STRAIN RATES REPORTED

TABLE IV: CREEP-FATIGUE DATA (CONTINUED)

LABORATORY: AFML
MATERIAL: FENEZ 95

SPEC NO	STRAINS & FAILURE DATA										FAILURE DATA-CYCLES			TIME-HRS	
	TOTAL	EL	IN	PE	PC	CE	CC	NO	NI	NE	NI	NE	NI	NE	TIME-HRS
Cyclic Creep Tests - Phase II															
RE-11	2.900	1.650	1.240	1.240	0.000	0.000	0.000	--	--	--	--	--	--	72	0.03
RE-16	1.640	1.330	0.308	0.308	0.000	0.000	0.000	--	--	--	--	--	--	671	0.75
RE-4	2.340	1.530	0.810	0.403	0.407	0.000	0.000	--	--	--	--	--	--	27	23.60
RE-15	1.200	1.140	0.125	0.076	0.049	0.000	0.000	--	--	--	--	--	--	454	78.20
RE-20	2.340	1.560	0.777	0.410	0.000	0.367	0.000	--	--	--	--	--	--	34	11.45
RE-14	1.680	1.370	0.306	0.162	0.000	0.144	0.000	--	--	--	--	--	--	124	38.56
RE-7	2.230	1.260	0.930	0.318	0.000	0.051	0.561	--	--	--	--	--	--	39	79.40
RE-13	1.500	1.140	0.304	0.105	0.000	0.042	0.157	--	--	--	--	--	--	164	143.20
RE-10	1.300	1.130	0.146	0.089	0.000	0.000	0.057	--	--	--	--	--	--	393	60.90
Validation Tests - Phase III															
227	1.400	1.110	0.292	0.198	0.000	0.042	0.052	--	--	--	--	--	--	455	83.80
223	1.200	1.040	0.158	0.113	0.000	0.025	0.021	--	--	--	--	--	--	945	174.03
226	1.400	1.170	0.221	0.158	0.000	0.009	0.054	--	--	--	--	--	--	349	64.27
225	1.200	1.060	0.162	0.114	0.000	0.006	0.042	--	--	--	--	--	--	463	85.45
23*	1.800	1.350	0.450	0.432	0.000	0.000	0.018	--	--	--	--	--	--	113	36.17
24*	1.740	1.400	0.350	--	0.000	0.000	--	--	--	--	--	--	--	159	52.48
25*	1.440	1.290	0.180	--	0.000	0.000	--	--	--	--	--	--	--	282	94.00
20*	1.600	1.340	0.250	--	0.000	0.000	--	--	--	--	--	--	--	301	101.29
34	1.300	1.190	0.120	0.120	0.000	0.000	0.000	--	--	--	--	--	--	525	175.33
19*	1.170	1.070	0.100	0.100	0.000	0.000	0.000	--	--	--	--	--	--	1133	360.94
252	1.400	1.340	0.066	0.058	0.000	0.008	0.000	--	--	--	--	--	--	194	32.23
251	1.400	1.330	0.098	0.086	0.000	0.000	0.000	--	--	--	--	--	--	635	114.64
247	1.800	1.350	0.356	0.298	0.058	0.000	0.000	--	--	--	--	--	--	263	4.60
246	1.800	1.350	0.412	0.347	0.000	0.065	0.000	--	--	--	--	--	--	253	4.43
244	1.600	1.280	0.266	0.227	0.000	0.039	0.000	--	--	--	--	--	--	447	7.81
242	1.800	1.320	0.422	0.371	0.000	0.051	0.000	--	--	--	--	--	--	472	8.28

* PLASTIC STRAIN RATES REPORTED

TABLE IV: CREEP-FATIGUE DATA (CONTINUED)

LABORATORY: CNR
MATERIAL: IN738LC, CAST

RATE DATA & STRESSES

SPEC NO	TEST TYPE	TEMP-C	FREQ HZ	RATE DATA (HALF-LIFE VALUES)				STRESSES (HALF-LIFE VALUES) MPa				CYCLIC STRAIN
				TEN	COMP	SEC	HOLD	TEN	COMP	RANGE	RELAXATION	
SPEC NO	TEST TYPE	TEMP-C	FREQ HZ	RATE DATA (HALF-LIFE VALUES)				STRESSES (HALF-LIFE VALUES) MPa				CYCLIC STRAIN
				TEN	COMP	SEC	HOLD	TEN	COMP	RANGE	RELAXATION	
150C	HRSC	850/850	--	4.6E-01	4.6E-01	0	0	586.0	610.0	1196.0	0.0	0.0
351C	HRSC	850/850	--	4.6E-01	4.6E-01	0	0	685.0	707.0	1392.0	0.0	0.0
183C	HRSC	850/850	--	4.6E-01	4.6E-01	0	0	661.0	703.0	1364.0	0.0	0.0
154C	HRSC	850/850	--	4.6E-01	4.6E-01	0	0	701.0	740.0	1441.0	0.0	0.0
83C	HRSC	850/850	--	4.6E-01	4.6E-01	0	0	798.0	858.0	1656.0	0.0	0.0

STRAINS & FAILURE DATA

SPEC NO	STRAIN RANGES (HALF-LIFE VALUES) %				FAILURE DATA - CYCLES			
	TOTAL	EL	IN	PP	NO	NI	NP	RP
150C	0.874	0.839	0.035	0.035	0.000	--	--	--
351C	1.141	1.010	0.131	0.000	0.000	--	--	--
183C	1.355	1.056	0.297	0.000	0.000	--	137	--
154C	1.591	1.137	0.454	0.000	0.000	--	--	--
83C	2.050	1.289	0.761	0.000	0.000	--	--	--

TABLE IV: CREEP-FATIGUE DATA (CONTINUED)

LABORATORY: MAR-TEST, INC.
MATERIAL: AMTIRC

RATE DATA & STRESSSES

SPEC NO	TEST TYPE	TEMP-C	P FREQ	RATE DATA			HALF-LIFE VALUES			STRESSSES			HALF-LIFE VALUES			CYCLIC STRAIN		
				TEN	COMP	Hz	STRAIN-RATE	W/SEC	HOLD TIME	TEN	COMP	MAX	TEN	COMP	MAX	TEN	COMP	HARDENING %
36	LRSC	538/538	4.0E-03	4.0E-02	4.0E-02	4.0E-02	4.0E-02	4.0E-02	0	0	0	113.0	0.0	0.0	0.0	0.0	0.0	-65.90
39	LRSC	538/538	4.0E-03	4.0E-02	4.0E-02	4.0E-02	4.0E-02	4.0E-02	0	0	0	110.5	0.0	0.0	0.0	0.0	0.0	-65.90
35	LRSC	538/538	1.0E-01	1.0E-01	1.0E-01	1.0E-01	1.0E-01	1.0E-01	0	0	0	227.0	0.0	0.0	0.0	0.0	0.0	-46.80
4	LRSC	538/538	2.0E-02	2.0E-01	2.0E-01	2.0E-01	2.0E-01	2.0E-01	0	0	0	134.5	0.0	0.0	0.0	0.0	0.0	-63.80
42	LRSC	538/538	1.0E-01	1.0E-01	1.0E-01	1.0E-01	1.0E-01	1.0E-01	0	0	0	162.0	0.0	0.0	0.0	0.0	0.0	-58.80
5	LRSC	538/538	2.5E-02	2.0E-02	2.0E-01	2.0E-01	2.0E-01	2.0E-01	0	0	0	131.0	0.0	0.0	0.0	0.0	0.0	-65.40
10	LRSC	538/538	3.6E-02	2.0E-01	2.0E-01	2.0E-01	2.0E-01	2.0E-01	0	0	0	124.0	0.0	0.0	0.0	0.0	0.0	-68.40
11	LRSC	538/538	5.0E-02	2.0E-01	2.0E-01	2.0E-01	2.0E-01	2.0E-01	0	0	0	124.0	0.0	0.0	0.0	0.0	0.0	-69.70
108	LRSC	538/538	3.3E-02	2.0E-01	2.0E-01	2.0E-01	2.0E-01	2.0E-01	0	0	0	115.9	0.0	0.0	0.0	0.0	0.0	-64.10
37	LRSC	538/538	1.4E-02	4.0E-02	4.0E-02	4.0E-02	4.0E-02	4.0E-02	0	0	0	103.5	0.0	0.0	0.0	0.0	0.0	-70.00
2	LRSC	538/538	3.3E-02	2.0E-01	2.0E-01	2.0E-01	2.0E-01	2.0E-01	0	0	0	120.0	0.0	0.0	0.0	0.0	0.0	-67.70
12	LRSC	538/538	5.9E-02	2.0E-01	2.0E-01	2.0E-01	2.0E-01	2.0E-01	0	0	0	130.5	0.0	0.0	0.0	0.0	0.0	-67.60
6	LRSC	538/538	5.0E-02	2.0E-01	2.0E-01	2.0E-01	2.0E-01	2.0E-01	0	0	0	118.5	0.0	0.0	0.0	0.0	0.0	-70.90
13	LRSC	538/538	6.7E-02	2.0E-01	2.0E-01	2.0E-01	2.0E-01	2.0E-01	0	0	0	134.5	0.0	0.0	0.0	0.0	0.0	-68.50
74	LRSC	538/538	1.0E-00	5.2E-00	5.2E-00	5.2E-00	5.2E-00	5.2E-00	0	0	0	179.0	0.0	0.0	0.0	0.0	0.0	-40.90
75	LRSC	538/538	1.0E-00	5.2E-00	5.2E-00	5.2E-00	5.2E-00	5.2E-00	0	0	0	167.0	0.0	0.0	0.0	0.0	0.0	-40.80
40	LRSC	538/538	1.4E-02	4.0E-02	4.0E-02	4.0E-02	4.0E-02	4.0E-02	0	0	0	96.4	0.0	0.0	0.0	0.0	0.0	-72.50
41	LRSC	538/538	3.6E-01	1.0E-00	1.0E-00	1.0E-00	1.0E-00	1.0E-00	0	0	0	125.5	0.0	0.0	0.0	0.0	0.0	-68.60
38	LRSC	538/538	3.6E-01	1.0E-00	1.0E-00	1.0E-00	1.0E-00	1.0E-00	0	0	0	129.0	0.0	0.0	0.0	0.0	0.0	-68.80
107	LRSC	538/538	5.9E-02	2.0E-01	2.0E-01	2.0E-01	2.0E-01	2.0E-01	0	0	0	113.7	0.0	0.0	0.0	0.0	0.0	-66.90
45	LRSC	538/538	4.0E-03	2.0E-01	2.0E-01	2.0E-01	2.0E-01	2.0E-01	0	0	0	131.0	0.0	0.0	0.0	0.0	0.0	-65.40
46	LRSC	538/538	4.0E-03	2.0E-01	2.0E-01	2.0E-01	2.0E-01	2.0E-01	0	0	0	131.0	0.0	0.0	0.0	0.0	0.0	-64.50
69	LRSC	538/538	2.9E-03	1.8E-01	1.8E-01	1.8E-01	1.8E-01	1.8E-01	0	0	0	120.7	0.0	0.0	0.0	0.0	0.0	-63.40
72	LRSC	538/538	3.2E-03	2.0E-01	2.0E-01	2.0E-01	2.0E-01	2.0E-01	0	0	0	115.9	0.0	0.0	0.0	0.0	0.0	-70.10
49	LRSC	538/538	1.4E-02	2.0E-01	2.0E-01	2.0E-01	2.0E-01	2.0E-01	0	0	0	119.0	0.0	0.0	0.0	0.0	0.0	-68.90
50	LRSC	538/538	1.4E-01	2.0E-01	2.0E-01	2.0E-01	2.0E-01	2.0E-01	0	0	0	125.0	0.0	0.0	0.0	0.0	0.0	-67.40
44	LRSC	538/538	4.0E-03	2.0E-01	2.0E-01	2.0E-01	2.0E-01	2.0E-01	0	0	0	131.0	0.0	0.0	0.0	0.0	0.0	-62.60
43	LRSC	538/538	4.0E-03	2.0E-01	2.0E-01	2.0E-01	2.0E-01	2.0E-01	0	0	0	131.0	0.0	0.0	0.0	0.0	0.0	-63.70
67	LRSC	538/538	2.9E-03	2.0E-01	2.0E-01	2.0E-01	2.0E-01	2.0E-01	0	0	0	126.9	0.0	0.0	0.0	0.0	0.0	-62.50
47	LRSC	538/538	1.4E-02	2.0E-01	2.0E-01	2.0E-01	2.0E-01	2.0E-01	0	0	0	107.0	0.0	0.0	0.0	0.0	0.0	-71.80
48	LRSC	538/538	1.4E-03	2.0E-01	2.0E-01	2.0E-01	2.0E-01	2.0E-01	0	0	0	111.0	0.0	0.0	0.0	0.0	0.0	-70.70
68	LRSC	538/538	3.2E-03	2.0E-01	2.0E-01	2.0E-01	2.0E-01	2.0E-01	0	0	0	97.9	0.0	0.0	0.0	0.0	0.0	-74.10
73	LRSC	538/538	1.5E-03	2.0E-01	2.0E-01	2.0E-01	2.0E-01	2.0E-01	0	0	0	124.1	0.0	0.0	0.0	0.0	0.0	-64.20
112	LRSC	538/538	2.7E-02	4.0E-02	4.0E-02	4.0E-02	4.0E-02	4.0E-02	0	0	0	113.0	0.0	0.0	0.0	0.0	0.0	-64.20
109	LRSC	538/538	1.5E-02	4.0E-02	4.0E-02	4.0E-02	4.0E-02	4.0E-02	0	0	0	133.4	0.0	0.0	0.0	0.0	0.0	-63.70
110	LRSC	538/538	2.7E-02	4.0E-02	4.0E-02	4.0E-02	4.0E-02	4.0E-02	0	0	0	126.4	0.0	0.0	0.0	0.0	0.0	-66.20

TABLE IV: CREEP-FATIGUE DATA (CONTINUED)

LABORATORY: MAR-TEST, INC.
MATERIAL: ANZIEC

STRAINS & FAILURE DATA

SPEC NO	STRAIN RANGES (HALF-LIFE VALUES) %				FAILURE DATA-CYCLES				T-F-HRS
	TOTAL	EL	IN	PP	PC	CP	CC	NO	
36	5.000	0.140	4.860	--	0.000	0.000	--	--	234
39	5.000	0.140	4.860	--	0.000	0.000	--	--	238
35	5.000	0.280	4.720	--	0.000	0.000	--	--	245
4	5.000	0.200	4.800	--	0.000	0.000	--	--	366
42	5.000	0.200	4.800	--	0.000	0.000	--	--	462
5	4.000	0.190	3.810	--	0.000	0.000	--	--	552
10	2.800	0.180	2.620	--	0.000	0.000	--	--	1055
11	2.000	0.180	1.820	--	0.000	0.000	--	--	1239
108	3.000	0.140	2.860	--	0.000	0.000	--	950	1310
37	1.400	0.130	1.270	--	0.000	0.000	--	--	1613
2	3.000	0.174	2.826	--	0.000	0.000	--	--	1615
12	1.700	0.190	1.510	--	0.000	0.000	--	--	1770
6	2.000	0.170	1.830	--	0.000	0.000	--	--	2051
13	1.500	0.200	1.300	--	0.000	0.000	--	--	2453
74	2.600	0.220	2.380	--	0.000	0.000	--	--	3132
75	2.600	0.210	2.390	--	0.000	0.000	--	--	3480
40	1.400	0.120	1.280	--	0.000	0.000	--	--	3693
41	1.400	0.155	1.245	--	0.000	0.000	--	--	5215
38	1.400	0.160	1.240	--	0.000	0.000	--	--	5431
107	1.700	0.140	1.560	--	0.000	0.000	--	4500	5780
45	5.000	0.124	4.876	--	0.038	0.000	--	--	253
46	5.000	0.126	4.874	--	0.036	0.000	--	--	262
69	4.620	0.111	4.509	--	0.039	0.000	--	--	948
72	1.400	0.105	1.295	--	0.039	0.000	--	--	1224
49	1.400	0.124	1.276	--	0.023	0.000	--	--	1947
50	1.400	0.130	1.270	--	0.025	0.000	--	--	3180
44	5.000	0.142	4.858	--	0.000	0.047	--	--	190
43	5.000	0.126	4.874	--	0.000	0.041	--	--	211
67	5.000	0.111	4.889	--	0.000	0.046	--	--	218
47	1.400	0.108	1.292	--	0.000	0.025	--	--	1152
48	1.400	0.110	1.290	--	0.000	0.027	--	--	1062
68	1.400	0.074	1.326	--	0.000	0.047	--	--	1156
73	5.000	0.068	4.932	--	0.000	0.000	--	--	234
112	1.400	0.140	1.260	--	--	0.000	--	--	3239
109	2.600	0.170	2.430	--	0.000	--	--	300	387
110	1.400	0.160	1.240	--	0.000	--	--	800	1006

TABLE IV: CREEP-FATIGUE DATA (CONTINUED)

RATE DATA & STRESSES

SPEC NO	TEST TYPE	TEMP-C	FREQ		RATE DATA		HALF-LIFE VALUES		STRESS-RATE		HALF-LIFE VALUES		CYCLIC STRAIN
			Hz	Hz	TEMP	COMP	TEMP	COMP	TEMP	COMP	TEMP	COMP	
17	LRSC	538/538	2.9E-02	2.0E-01	2.0E-01	0	0	293.0	0.0	0.0	0.0	-4.56	
118	LRSC	538/538	7.7E-04	4.0E-03	4.0E-03	0	0	177.0	0.0	0.0	0.0	-23.70	
27	LRSC	538/538	7.7E-03	4.0E-02	4.0E-02	0	0	238.0	0.0	0.0	0.0	-11.50	
24	LRSC	538/538	7.7E-03	4.0E-02	4.0E-02	0	0	248.0	0.0	0.0	0.0	-10.10	
112	LRSC	538/538	6.7E-03	4.0E-02	4.0E-02	0	0	241.0	0.0	0.0	0.0	-12.70	
35	LRSC	538/538	1.7E-01	1.0E-00	1.0E-00	0	0	325.0	0.0	0.0	0.0	4.80	
18	LRSC	538/538	4.0E-02	2.0E-01	2.0E-01	0	0	276.0	0.0	0.0	0.0	-8.00	
114	LRSC	538/538	5.0E-02	2.0E-01	2.0E-01	0	0	279.0	0.0	0.0	0.0	-7.00	
23	LRSC	538/538	1.9E-01	1.0E-00	1.0E-00	0	0	325.0	0.0	0.0	0.0	4.80	
106	LRSC	538/538	1.0E-02	4.0E-02	4.0E-02	0	0	234.0	0.0	0.0	0.0	-13.00	
26	LRSC	538/538	1.9E-01	1.0E-00	1.0E-00	0	0	325.0	0.0	0.0	0.0	3.50	
29	LRSC	538/538	1.0E-00	5.2E-00	5.2E-00	0	0	372.0	0.0	0.0	0.0	0.00	
102	LRSC	538/538	5.0E-02	2.0E-01	2.0E-01	0	0	277.3	0.0	0.0	0.0	-2.50	
30	LRSC	538/538	1.0E-00	5.2E-00	5.2E-00	0	0	374.0	0.0	0.0	0.0	0.00	
105	LRSC	538/538	2.5E-01	1.0E-00	1.0E-00	0	0	309.0	0.0	0.0	0.0	8.00	
117	LRSC	538/538	2.2E-03	4.0E-03	4.0E-03	0	0	173.0	0.0	0.0	0.0	-30.50	
15	LRSC	538/538	8.3E-02	2.0E-01	2.0E-01	0	0	248.0	0.0	0.0	0.0	-12.40	
20	LRSC	538/538	2.2E-02	4.0E-02	4.0E-02	0	0	207.0	0.0	0.0	0.0	-21.90	
13	LRSC	538/538	1.0E-01	2.0E-01	2.0E-01	0	0	245.0	0.0	0.0	0.0	-9.90	
25	LRSC	538/538	2.2E-02	4.0E-02	4.0E-02	0	0	207.0	0.0	0.0	0.0	-18.80	
104	LRSC	538/538	1.0E-02	4.0E-02	4.0E-02	0	0	200.0	0.0	0.0	0.0	-20.60	
101	LRSC	538/538	2.0E-01	2.0E-01	2.0E-01	0	0	242.5	0.0	0.0	0.0	-6.40	
19	LRSC	538/538	1.2E-01	2.0E-01	2.0E-01	0	0	228.0	0.0	0.0	0.0	-15.20	
21	LRSC	538/538	5.5E-01	1.0E-00	1.0E-00	0	0	225.0	0.0	0.0	0.0	-7.60	
16	LRSC	538/538	1.4E-01	2.0E-01	2.0E-01	0	0	220.0	0.0	0.0	0.0	-17.00	
22	LRSC	538/538	5.5E-01	1.0E-00	1.0E-00	0	0	225.0	0.0	0.0	0.0	-7.60	
103	LRSC	538/538	5.0E-01	1.0E-00	1.0E-00	0	0	252.0	0.0	0.0	0.0	0.00	
47	LRSC	538/538	7.2E-01	1.0E-00	1.0E-00	0	0	225.0	0.0	0.0	0.0	-13.60	
42	LRSC	538/538	3.1E-03	2.0E-01	2.0E-01	0	300.0	127.0	138.0	265.0	0.0	-12.30	
41	LRSC	538/538	3.1E-03	2.0E-01	2.0E-01	0	300.0	127.0	138.0	265.0	0.0	-13.70	
43	LRSC	538/538	3.2E-03	2.0E-01	2.0E-01	0	300.0	105.0	105.0	210.0	0.0	-22.80	
45	LRSC	538/538	3.2E-03	2.0E-01	2.0E-01	0	300.0	103.0	111.0	214.0	0.0	-21.30	
40	LRSC	538/538	3.1E-03	2.0E-01	2.0E-01	300.0	0	128.0	143.0	271.0	76.0	-11.70	
39	LRSC	538/538	3.1E-03	2.0E-01	2.0E-01	300.0	0	124.0	143.0	267.0	79.0	-11.90	
38	LRSC	538/538	3.2E-03	2.0E-01	2.0E-01	300.0	0	110.0	122.0	232.0	60.0	-16.80	
37	LRSC	538/538	3.2E-03	2.0E-01	2.0E-01	300.0	0	110.0	117.0	227.0	64.0	--	
110	FSSC	538/538	1.9E-02	1.0E-00	4.0E-02	0	0	166.0	117.0	283.0	0.0	4.00	
108	FSSC	538/538	3.8E-02	1.0E-00	4.0E-02	0	0	148.0	128.0	276.0	0.0	5.35	
114	SFSC	538/538	1.4E-03	4.2E-03	2.5E-01	0	0	114.0	155.0	268.0	0.0	-4.30	
111	SFSC	538/538	1.3E-02	4.0E-02	1.0E-00	0	0	139.0	173.0	312.0	0.0	2.97	
109	SFSC	538/538	1.9E-02	4.0E-02	1.0E-00	0	0	133.0	163.0	295.0	0.0	4.60	
107	SFSC	538/538	3.8E-02	4.0E-02	1.0E-00	0	0	121.0	141.0	262.0	0.0	1.60	
116	SFSC	538/538	1.4E-03	7.0E-04	1.0E-00	0	0	81.0	119.0	200.0	0.0	-13.80	
115	SFSC	538/538	8.0E-03	4.0E-03	1.0E-00	0	0	93.0	119.0	212.0	0.0	-11.30	
113	SFSC	538/538	7.7E-02	4.0E-02	1.0E-00	0	0	105.0	119.0	223.0	0.0	-13.60	

LABORATORY: MAR-TEST, INC.
MATERIAL: MARLOY 2

TABLE IV: CREEP-FATIGUE DATA (CONTINUED)

STRAINS & FAILURE DATA

SPEC NO	TOTAL	STRAIN RANGES (HALF-LIFE VALUES) %			NO	FAILURE DATA - CYCLES			
		MIN	MAX	CP		NO	NO	NO	NO
17	3.500	0.297	3.203	0.000	--	--	--	99	0.36
118	2.600	0.180	2.420	0.000	--	--	--	116	42.00
27	2.600	0.241	2.359	0.000	--	--	75	133	4.90
24	2.600	0.252	2.348	0.000	--	--	--	154	5.60
112	3.000	0.240	2.760	0.000	--	--	115	154	6.40
35	3.000	0.330	2.670	0.000	--	--	159	165	0.27
18	2.500	0.280	2.220	0.000	--	--	--	253	1.76
14	2.000	0.283	1.717	0.000	--	--	--	331	1.34
23	2.600	0.328	2.272	0.000	--	--	--	339	0.53
106	2.000	0.240	1.760	0.000	--	--	260	351	9.75
26	2.600	0.328	2.272	0.000	--	--	--	364	0.53
29	2.600	0.380	2.220	0.000	--	--	--	474	0.13
102	2.000	0.280	1.720	0.000	--	--	380	535	3.00
30	2.600	0.380	2.220	0.000	--	--	--	588	0.16
105	2.000	0.310	1.690	0.000	--	--	550	673	0.75
117	0.900	0.180	0.720	0.000	--	--	650	787	101.00
15	1.200	0.252	0.948	0.000	--	--	--	1126	3.76
20	0.900	0.210	0.690	0.000	--	--	--	1138	14.30
13	1.000	0.248	0.752	0.000	--	--	--	1169	3.25
25	0.900	0.210	0.690	0.000	--	--	--	1196	15.00
104	1.000	0.200	0.800	0.000	--	--	850	1266	17.50
101	1.000	0.250	0.750	0.000	--	--	1600	1948	5.40
19	0.850	0.230	0.620	0.000	--	--	--	2469	5.90
21	0.900	0.259	0.641	0.000	--	--	--	3586	1.90
16	0.700	0.224	0.476	0.000	--	--	--	3601	70.00
22	0.900	0.259	0.641	0.000	--	--	--	3909	1.95
103	1.000	0.250	0.750	0.000	--	--	4700	5022	2.90
47	0.700	0.240	0.460	0.000	--	--	12500	14194	5.50
42	2.600	0.180	2.420	0.086	--	--	--	337	30.50
41	2.600	0.180	2.420	0.085	--	--	--	353	32.00
43	0.900	0.140	0.760	0.073	--	--	--	2981	256.00
45	2.600	0.140	0.760	0.076	--	--	--	3392	291.00
40	2.600	0.200	2.400	0.000	--	--	--	75	5.80
39	2.600	0.190	2.410	0.000	--	--	--	102	9.60
38	0.900	0.170	0.730	0.000	--	--	--	262	22.50
37	0.900	0.170	0.730	0.000	--	--	--	317	27.20
110	2.000	0.290	1.710	--	--	--	280	451	6.50
108	1.000	0.280	0.720	0.000	--	--	1180	2091	15.10
114	3.000	0.270	2.730	0.000	--	--	13	16	3.20
111	3.000	0.320	2.680	0.000	--	--	31	35	0.76
109	2.000	0.300	1.700	0.000	--	--	51	65	0.95
107	1.000	0.270	0.730	0.000	--	--	190	233	1.72
116	0.500	0.240	0.260	0.000	--	--	90	115	23.00
115	0.500	0.220	0.280	0.000	--	--	230	300	10.45
113	0.500	0.230	0.270	0.000	--	--	890	1156	4.20

TABLE IV: CREEP-FATIGUE DATA (CONTINUED)

LABORATORY: DFVLR
MATERIAL: TiAl6V4

RATE DATA & STRESSES

SPEC NO	TEST TYPE	TEMP-C	FREQ HZ	RATE DATA (HALF-LIFE VALUES)				STRESS (HALF-LIFE VALUES)				CYCLIC STRAIN	
				SEPARATION RATE-1/2 SEC HOLD TIME-SEC	TEN	COMP	TIME-SEC	TEN	COMP	MAX	RANGE		
154/06	UCCR	450/450	1.0E-01	5.6E-01	5.6E-01	6.0	9.0	540.0	519.1	1059.1	0.0	0.0	-8.27
190/14	UCCR	450/450	1.0E-01	9.6E-01	8.4E-01	2.0	8.4	590.9	565.2	1160.1	0.0	0.0	-8.32
150/05	UCCR	450/450	1.0E-01	6.3E-01	5.1E-01	15.0	510.0	650.6	545.6	1196.2	0.0	0.0	-5.14
190/01	UCCR	450/450	5.0E-02	7.0E-01	7.0E-01	4.5	19.2	624.6	645.4	1270.0	0.0	0.0	-10.29
154/07	TCCR	450/450	1.0E-01	5.9E-01	5.5E-01	420.0	0	379.8	849.7	1229.5	0.0	0.0	1.03
069/16	TCCR	450/450	1.0E-01	8.2E-01	8.4E-01	990.0	0	567.6	1031.6	1599.2	0.0	0.0	10.29
065/25	TCCR	450/450	1.0E-01	1.6E-00	2.1E-00	59.0	0	672.5	840.7	1513.2	0.0	0.0	-6.54
069/14	TCCR	450/450	1.0E-01	1.6E-00	2.1E-00	122.0	0	674.3	861.0	1535.0	0.0	0.0	-4.52
190/15	CCCR	445/445	1.0E-01	5.9E-01	5.7E-01	0	3.6	557.0	493.0	1050.0	0.0	0.0	-7.77
190/19	CCCR	450/450	1.0E-01	7.0E-01	6.5E-01	0	117.0	633.1	484.0	1117.1	0.0	0.0	-9.59
190/02	CCCR	450/450	1.0E-01	7.5E-01	6.5E-01	0	687.0	671.5	495.9	1167.4	0.0	0.0	-7.38
069/15	CCCR	452/452	1.0E-01	1.3E-00	1.2E-00	0	3000.0	846.3	608.9	1455.2	0.0	0.0	-2.23
069/16	HSC	458/458	3.0E-01	6.3E-01	6.3E-01	0	0	522.1	532.3	1054.4	0.0	0.0	-6.36
069/12	HSC	450/450	3.0E-01	8.2E-01	8.2E-01	0	0	586.1	586.1	1172.2	0.0	0.0	-5.90
190/09	HSC	453/453	3.0E-01	1.1E-00	1.1E-00	0	0	625.3	639.8	1265.1	0.0	0.0	-2.99
069/23	HSC	459/459	3.0E-01	2.2E-00	2.2E-00	0	0	674.2	728.2	1402.4	0.0	0.0	--
190/08	HSC	452/452	3.0E-01	5.6E-01	5.6E-01	0	0	502.9	412.6	915.5	0.0	0.0	-2.56
194/01	HSC	455/455	3.0E-01	5.4E-01	5.4E-01	0	0	476.2	494.5	970.7	0.0	0.0	-9.80
194/05	HSC	450/450	3.0E-01	6.9E-01	6.9E-01	0	0	557.3	554.7	1112.0	0.0	0.0	-5.17
194/09	HSC	452/452	3.0E-01	6.1E-01	6.3E-01	0	0	503.6	549.9	1053.5	0.0	0.0	-5.53
150/17	TCCR	454/454	1.0E-01	5.9E-01	6.7E-01	168.0	0	384.2	658.3	1042.5	0.0	0.0	-6.17
194/04	TCCR	452/452	1.0E-01	6.1E-01	4.9E-01	300.0	0	305.8	835.0	1140.9	0.0	0.0	-4.56
150/16	BCCR	450/450	1.0E-01	5.7E-01	5.7E-01	6.0	10.2	503.6	470.1	973.7	0.0	0.0	-3.80
195/06	UHSC	449/449	1.0E-01	9.0E-01	9.6E-01	1356.0	0.8	532.5	864.9	1397.4	0.0	0.0	2.96
195/17	UHSC	447/447	1.0E-01	9.6E-01	9.6E-01	1080.0	0.5	573.7	867.2	1440.9	0.0	0.0	1.94
195/07	UHSC	450/450	1.0E-01	7.9E-01	7.9E-01	1800.0	0.6	455.2	856.2	1321.4	0.0	0.0	2.57

TABLE IV: CREEP-FATIGUE DATA (CONTINUED)

LABORATORY: DPULR
 MATERIAL: TiAl6V4

STRAINS & FAILURE DATA

SPEC NO	STRAIN RANGES (HALF-LIFE VALUES) %				FAILURE DATA - CYCLES				F-F-RS
	TOTAL EL	EL	IN	PE	PC	CP	CC	NO	
194/06	1.103	0.874	0.229	0.149	0.000	0.009	0.071	1410	1639
190/14	1.637	1.009	0.618	0.478	0.013	0.000	0.127	500	583
190/05	1.638	0.998	0.640	0.389	0.013	0.000	0.238	290	401
190/01	2.680	1.088	1.585	1.178	0.000	0.090	0.317	168	213
194/07	1.308	0.945	0.263	0.147	0.000	0.116	0.000	1120	1889
069/16	2.215	1.304	0.911	0.445	0.000	0.453	0.000	223	272
069/25	4.244	1.323	2.921	1.523	0.000	1.398	0.000	74	106
069/14	4.205	1.286	2.919	1.558	0.000	1.361	0.000	53	81
190/15	1.067	0.882	0.205	0.154	0.051	0.000	0.000	1300	1665
190/15	1.304	0.944	0.360	0.231	0.129	0.000	0.000	520	698
190/02	1.505	1.025	0.480	0.324	0.156	0.000	0.000	327	420
069/15	2.391	1.206	1.085	0.617	0.470	0.000	0.000	124	142
069/18	0.920	0.847	0.073	0.073	0.000	0.000	0.000	3500	5393
069/12	1.190	1.091	0.180	0.180	0.000	0.000	0.000	1725	2765
190/09	1.450	1.016	0.434	0.434	0.000	0.000	0.000	550	765
069/23	2.438	1.256	1.182	1.182	0.000	0.000	0.000	306	357
190/08	0.903	0.850	0.053	0.053	0.000	0.000	0.000	14600	18140
194/01	0.864	0.825	0.039	0.039	0.000	0.000	0.000	8732	13700
194/05	0.952	0.720	0.232	0.232	0.000	0.000	0.000	1500	2750
194/09	0.937	0.839	0.098	0.098	0.000	0.000	0.000	3500	6005
190/17	1.067	0.896	0.179	0.105	0.000	0.074	0.000	2250	4225
194/04	1.100	0.908	0.192	0.085	0.000	0.107	0.000	1760	3388
190/18	1.105	0.893	0.212	0.109	0.000	0.000	0.000	2400	2994
195/06	2.434	1.325	1.109	0.477	0.000	0.426	0.103	85	137
195/17	2.418	1.198	1.220	0.549	0.000	0.437	0.234	89	150
195/07	1.976	1.177	0.799	0.287	0.000	0.351	0.161	195	215

TABLE IV: CREEP-FATIGUE DATA (CONTINUED)

LABORATORY: UNIV OF BRISTOL
MATERIAL: 1CR NO V STEEL

SPEC NO	TEST TYPE	TEMP-C TEN/COMP	FREQ HZ	RATE DATA (HALF-TYPE VALUES)				RATE DATA & STRESSES				STRESSES (HALF-TYPE VALUES)				CYCLIC STRAIN HARDENING %			
				TEN	COMP	TEN	COMP	TEN	COMP	TEN	COMP	TEN	COMP	TEN	COMP	TEN	COMP	TEN	COMP
99	HRSC	565/565	5.8E-02	4.0E-01	4.0E-01	0	0	415.0	0	415.0	0	830.0	0	0.0	0.0	-19.10			
92	HRSC	565/565	8.0E-02	4.0E-01	4.0E-01	0	0	390.0	0	390.0	0	780.0	0	0.0	0.0	-21.40			
70	HRSC	565/565	1.7E-01	4.0E-01	4.0E-01	0	0	350.0	0	350.0	0	700.0	0	0.0	0.0	-22.20			
82*	HRSC	565/565	2.1E-01	4.0E-01	4.0E-01	0	0	340.0	0	340.0	0	680.0	0	0.0	0.0	-20.90			
A300	CHSC	565/565	5.5E-03	4.0E-01	4.0E-01	1.0	173.0	380.5	173.0	380.5	173.0	762.5	0	159.0	0.0	-20.40			
A304	CHSC	565/565	5.8E-04	4.0E-01	4.0E-01	1.0	1727.0	369.7	1727.0	369.7	1727.0	729.9	0	217.0	0.0	-21.50			
28	CHSC	565/565	6.0E-04	4.0E-01	4.0E-01	1.0	1727.0	378.0	1727.0	378.0	1727.0	756.8	0	180.0	0.0	-19.70			
A234	CHSC	565/565	5.7E-03	4.0E-01	4.0E-01	1.0	173.0	383.6	173.0	383.6	173.0	753.6	0	130.0	0.0	-17.10			
25	CHSC	565/565	6.0E-04	4.0E-01	4.0E-01	1.0	1727.0	365.1	1727.0	365.1	1727.0	737.4	0	154.5	0.0	-21.90			
A237	CHSC	565/565	5.7E-03	4.0E-01	4.0E-01	1.0	173.0	362.6	173.0	362.6	173.0	701.6	0	109.5	0.0				
160	TCCR	565/565	--	4.0E-01	4.0E-01	2100.0	1.0	325.0	1.0	325.0	1.0	674.4	0	0.0	0.0	--			
27	TCCR	565/565	--	4.0E-01	4.0E-01	2100.0	1.0	345.6	1.0	345.6	1.0	673.2	0	0.0	0.0	--			
26	TCCR	565/565	--	4.0E-01	4.0E-01	2100.0	1.0	284.4	1.0	284.4	1.0	594.8	0	0.0	0.0	-16.50			
BERK (2)	THSC	565/565	--	--	--	57600.0	12.0	315.0	12.0	315.0	12.0	666.0	167.0	0.0	0.0	-21.10			
BERK (1)	THSC	565/565	--	--	--	10330.0	1.0	280.0	1.0	280.0	1.0	595.0	118.0	42.0	0.0	--			
135	THSC	565/565	1.0E-04	4.0E-01	4.0E-01	10330.0	1.0	367.0	1.0	367.0	1.0	800.0	217.0	0.0	0.0	--			
133	THSC	565/565	1.0E-04	4.0E-01	4.0E-01	10330.0	1.0	360.0	1.0	360.0	1.0	800.0	165.0	0.0	0.0	--			
110	THSC	565/565	6.0E-04	4.0E-01	4.0E-01	1727.0	1.0	355.0	1.0	355.0	1.0	770.0	170.0	0.0	0.0	-20.00			
109	THSC	565/565	6.0E-04	4.0E-01	4.0E-01	1727.0	1.0	370.0	1.0	370.0	1.0	816.0	145.0	0.0	0.0	--			
176	THSC	565/565	6.0E-04	4.0E-01	4.0E-01	1727.0	1.0	263.0	1.0	263.0	1.0	620.0	73.0	0.0	0.0	--			
136	THSC	565/565	5.0E-04	4.0E-01	4.0E-01	1727.0	1.0	365.0	1.0	365.0	1.0	730.0	230.0	170.0	0.0	--			
95	UHSC	565/565	5.0E-04	4.0E-01	4.0E-01	1727.0	1.0	355.0	1.0	355.0	1.0	710.0	180.0	145.0	0.0	--			

TABLE IV: CREEP-FATIGUE DATA (CONTINUED)

LABORATORY: UNIV OF BRISTOL
MATERIAL: 1CR MO V STEEL

SPEC NO	TOTAL	STRAIN RANGES (HALF-LIFE VALUES) %				STRAINS & FAILURE DATA				FAILURE DATA-CYCLES			
		EL	IN	EF	FC	CF	CC	NO	NI	NE	NF	TF-HRS	
99	3.470	0.540	2.930	2.930	0.000	0.000	0.000	--	--	--	138	--	
92	2.360	0.510	1.850	1.850	0.000	0.000	0.000	--	--	--	300	--	
70	1.154	0.458	0.696	0.696	0.000	0.000	0.000	--	--	880	--	--	
82*	0.964	0.444	0.520	0.520	0.000	0.000	0.000	--	--	--	--	--	
A300	2.000	0.479	1.521	1.371	0.150	0.000	0.000	--	--	362	--	19.30	
A304	1.530	0.420	1.110	0.945	0.165	0.000	0.000	--	--	320	--	173.70	
28	2.040	0.465	1.575	1.400	0.126	0.000	0.000	--	--	506	--	--	
A234	1.440	0.491	0.949	0.372	0.119	0.000	0.000	--	--	562	--	--	
25	1.236	0.415	0.621	0.577	0.144	0.000	0.000	--	--	850	--	--	
A237	0.853	0.424	0.429	0.325	0.104	0.000	0.000	--	--	42	--	23.30	
160	2.576	0.640	1.936	0.216	0.000	1.720	0.000	--	--	--	65	35.30	
27	1.570	0.577	0.993	0.189	0.000	0.804	0.000	--	--	--	79	46.50	
26	1.300	0.560	0.740	0.154	0.000	0.586	0.000	--	--	--	73	1169.30	
BERK (2)	1.380	0.292	1.088	0.960	0.000	0.128	0.000	--	--	--	208	3330.00	
BERK (1)	0.620	0.345	0.275	0.182	0.000	0.055	0.037	--	--	--	97	--	
135	2.590	0.381	2.209	2.067	0.000	0.142	0.000	--	--	--	--	--	
133	1.086	0.415	0.671	0.563	0.000	0.108	0.000	--	--	150	--	--	
110	2.016	0.392	1.624	1.513	0.000	0.111	0.000	--	--	158	--	--	
109	1.050	0.439	0.611	0.516	0.000	0.095	0.000	--	--	229	--	--	
176	0.533	0.357	0.176	0.128	0.000	0.048	0.000	--	--	435	--	--	
136	2.600	0.220	2.380	2.380	0.000	0.039	0.111	--	--	215	--	--	
95	1.840	0.251	1.589	1.470	0.000	0.023	0.095	--	--	230	--	--	

* TEST STOPPED DUE TO SPECIMEN BUCKLING, 1110 CYCLES COMPLETED

REPORT DOCUMENTATION PAGE			
1. Recipient's Reference	2. Originator's Reference	3. Further Reference	4. Security Classification of Document
	AGARD-CP-243	ISBN 92-835-0220-5	UNCLASSIFIED
5. Originator	Advisory Group for Aerospace Research and Development North Atlantic Treaty Organization 7 rue Ancelle, 92200 Neuilly sur Seine, France		
6. Title	CHARACTERIZATION OF LOW CYCLE HIGH TEMPERATURE FATIGUE BY THE STRAINRANGE PARTITIONING METHOD		
7. Presented at	the 46th Meeting of the AGARD Structures and Materials Panel held in Aalborg, Denmark on 11-12 April 1978.		
8. Author(s)	Various		9. Date
			August 1978
10. Author's Address	Various		11. Pages
			362
12. Distribution Statement	This document is distributed in accordance with AGARD policies and regulations, which are outlined on the Outside Back Covers of all AGARD publications.		
13. Keywords/Descriptors	<div style="display: flex; justify-content: space-between;"> <div> Fatigue (materials) High temperature tests Life (durability) </div> <div> Mechanical properties Strains </div> </div>		
14. Abstract	<p> This Specialists' Meeting brought together the principal participants in a cooperative testing programme aimed at the evaluation of the strainrange partitioning approach to the analysis and prediction of low cycle high temperature fatigue life. A number of laboratories in several countries participated in this programme, each testing its own materials of interest under its own laboratory conditions to ensure that the results obtained would provide validation for a wide range of aerospace materials and to ensure maximum usefulness to each participating laboratory. </p>		

<p>AGARD Conference Proceedings No. 243 Advisory Group for Aerospace Research and Development, NATO CHARACTERIZATION OF LOW CYCLE HIGH TEMPERATURE FATIGUE BY THE STRAINRANGE PARTITIONING METHOD Published August 1978 362 pages</p> <p>This Specialists' Meeting brought together the principal participants in a cooperative testing programme aimed at the evaluation of the strainrange partitioning approach to the analysis and prediction of low cycle high temperature fatigue life. A number of laboratories in several countries participated in this programme, each testing its own materials of interest under its</p> <p>P.T.O.</p>	<p>AGARD-CP-243</p> <p>Fatigue (materials) High temperature tests Life (durability) Mechanical properties Strains</p>	<p>AGARD Conference Proceedings No. 243 Advisory Group for Aerospace Research and Development, NATO CHARACTERIZATION OF LOW CYCLE HIGH TEMPERATURE FATIGUE BY THE STRAINRANGE PARTITIONING METHOD Published August 1978 362 pages</p> <p>This Specialists' Meeting brought together the principal participants in a cooperative testing programme aimed at the evaluation of the strainrange partitioning approach to the analysis and prediction of low cycle high temperature fatigue life. A number of laboratories in several countries participated in this programme, each testing its own materials of interest under its</p> <p>P.T.O.</p>	<p>AGARD-CP-243</p> <p>Fatigue (materials) High temperature tests Life (durability) Mechanical properties Strains</p>
<p>AGARD Conference Proceedings No. 243 Advisory Group for Aerospace Research and Development, NATO CHARACTERIZATION OF LOW CYCLE HIGH TEMPERATURE FATIGUE BY THE STRAINRANGE PARTITIONING METHOD Published August 1978 362 pages</p> <p>This Specialists' Meeting brought together the principal participants in a cooperative testing programme aimed at the evaluation of the strainrange partitioning approach to the analysis and prediction of low cycle high temperature fatigue life. A number of laboratories in several countries participated in this programme, each testing its own materials of interest under its</p> <p>P.T.O.</p>	<p>AGARD-CP-243</p> <p>Fatigue (materials) High temperature tests Life (durability) Mechanical properties Strains</p>	<p>AGARD Conference Proceedings No. 243 Advisory Group for Aerospace Research and Development, NATO CHARACTERIZATION OF LOW CYCLE HIGH TEMPERATURE FATIGUE BY THE STRAINRANGE PARTITIONING METHOD Published August 1978 362 pages</p> <p>This Specialists' Meeting brought together the principal participants in a cooperative testing programme aimed at the evaluation of the strainrange partitioning approach to the analysis and prediction of low cycle high temperature fatigue life. A number of laboratories in several countries participated in this programme, each testing its own materials of interest under its</p> <p>P.T.O.</p>	<p>AGARD-CP-243</p> <p>Fatigue (materials) High temperature tests Life (durability) Mechanical properties Strains</p>

<p>own laboratory conditions to ensure that the results obtained would provide validation for a wide range of aerospace materials and to ensure maximum usefulness to each participating laboratory.</p> <p>Papers presented at the 46th Meeting of the AGARD Structures and Materials Panels held in Aalborg, Denmark on 11-12 April 1978.</p> <p>ISBN 92-835-0220-5</p>	<p>own laboratory conditions to ensure that the results obtained would provide validation for a wide range of aerospace materials and to ensure maximum usefulness to each participating laboratory.</p> <p>Papers presented at the 46th Meeting of the AGARD Structures and Materials Panels held in Aalborg, Denmark on 11-12 April 1978.</p> <p>ISBN 92-835-0220-5</p>
<p>own laboratory conditions to ensure that the results obtained would provide validation for a wide range of aerospace materials and to ensure maximum usefulness to each participating laboratory.</p> <p>Papers presented at the 46th Meeting of the AGARD Structures and Materials Panels held in Aalborg, Denmark on 11-12 April 1978.</p> <p>ISBN 92-835-0220-5</p>	<p>own laboratory conditions to ensure that the results obtained would provide validation for a wide range of aerospace materials and to ensure maximum usefulness to each participating laboratory.</p> <p>Papers presented at the 46th Meeting of the AGARD Structures and Materials Panels held in Aalborg, Denmark on 11-12 April 1978.</p> <p>ISBN 92-835-0220-5</p>

B55
4

AGARD

NATO  OTAN

7 RUE ANCELLE · 92200 NEUILLY-SUR-SEINE
FRANCE

Telephone 745.08.10 · Telex 610176

**DISTRIBUTION OF UNCLASSIFIED
AGARD PUBLICATIONS**

AGARD does NOT hold stocks of AGARD publications at the above address for general distribution. Initial distribution of AGARD publications is made to AGARD Member Nations through the following National Distribution Centres. Further copies are sometimes available from these Centres, but if not may be purchased in Microfiche or Photocopy form from the Purchase Agencies listed below.

NATIONAL DISTRIBUTION CENTRES

BELGIUM

Coordonnateur AGARD - VSL
Etat-Major de la Force Aérienne
Quartier Reine Elisabeth
Rue d'Evere, 1140 Bruxelles

CANADA

Defence Scientific Information Service
Department of National Defence
Ottawa, Ontario K1A 0Z2

DENMARK

Danish Defence Research Board
Østerbrogades Kaserne
Copenhagen Ø

FRANCE

O.N.E.R.A. (Direction)
29 Avenue de la Division Leclerc
92 Châtillon sous Bagneux

GERMANY

Zentralstelle für Luft- und Raumfahrt-
dokumentation und -information
c/o Fachinformationszentrum Energie,
Physik, Mathematik GmbH
Kernforschungszentrum
7514 Eggenstein-Leopoldshafen 2

GREECE

Hellenic Air Force General Staff
Research and Development Directorate
Holargos, Athens, Greece

ICELAND

Director of Aviation
c/o Flugrad
Reykjavik

ITALY

Aeronautica Militare
Ufficio del Delegato Nazionale all'AGARD
3, Piazzale Adenauer
Roma/EUR

LUXEMBOURG

See Belgium

NETHERLANDS

Netherlands Delegation to AGARD
National Aerospace Laboratory, NLR
P.O. Box 126
Delft

NORWAY

Norwegian Defence Research Establishment
Main Library
P.O. Box 25
N-2007 Kjeller

PORTUGAL

Direcção do Serviço de Material
da Força Aérea
Rua da Escola Politecnica 42
Lisboa
Attn: AGARD National Delegate

TURKEY

Department of Research and Development (ARGE)
Ministry of National Defence, Ankara

UNITED KINGDOM

Defence Research Information Centre
Station Square House
St. Mary Cray
Orpington, Kent BR5 3RE

UNITED STATES

National Aeronautics and Space Administration (NASA)
Langley Field, Virginia 23365
Attn: Report Distribution and Storage Unit

THE UNITED STATES NATIONAL DISTRIBUTION CENTRE (NASA) DOES NOT HOLD STOCKS OF AGARD PUBLICATIONS, AND APPLICATIONS FOR COPIES SHOULD BE MADE DIRECT TO THE NATIONAL TECHNICAL INFORMATION SERVICE (NTIS) AT THE ADDRESS BELOW.

PURCHASE AGENCIES

Microfiche or Photocopy

National Technical
Information Service (NTIS)
5285 Port Royal Road
Springfield
Virginia 22161, USA

Microfiche

Space Documentation Service
European Space Agency
10, rue Mario Nikis
75015 Paris, France

Microfiche

Technology Reports
Centre (DTI)
Station Square House
St. Mary Cray
Orpington, Kent BR5 3RF
England

Requests for microfiche or photocopies of AGARD documents should include the AGARD serial number, title, author or editor, and publication date. Requests to NTIS should include the NASA accession report number. Full bibliographical references and abstracts of AGARD publications are given in the following journals:

Scientific and Technical Aerospace Reports (STAR)
published by NASA Scientific and Technical
Information Facility
Post Office Box 8757
Baltimore/Washington International Airport
Maryland 21240, USA

Government Reports Announcements (GRA)
published by the National Technical
Information Services, Springfield
Virginia 22161, USA



Printed by Technical Editing and Reproduction Ltd
Harford House, 7-9 Charlotte St, London W1P 1HD

ISBN 92-835-0220-5